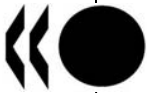


Unclassified

NEA/CSNI/R(2009)5



Organisation de Coopération et de Développement Économiques
Organisation for Economic Co-operation and Development

17-Dec-2009

English text only

**NUCLEAR ENERGY AGENCY
COMMITTEE ON THE SAFETY OF NUCLEAR INSTALLATIONS**

**NEA/CSNI/R(2009)5
Unclassified**

STATE-OF-THE-ART REPORT ON NUCLEAR AEROSOLS

JT03276300

Document complet disponible sur OLIS dans son format d'origine
Complete document available on OLIS in its original format

English text only

THE GROUP HAVING PREPARED THIS SOAR CONSISTED OF

Hans-Josef Allelein (Chairman)	GRS, Germany
Ari Auvinen	VTT, Finland
Joanne Ball	AECL, Canada
Salih Guntay	PSI, Switzerland
Luis Enrique Herranz	CIEMAT, Spain
Akihide Hidaka	JAEA, Japan
Alain V. Jones	formerly JRC Ispra, EC
Martin Kissane	IRSN, France
Dana Powers	SNL, USA
Gunter Weber	GRS, Germany

ANNOTATION ON THE REFERENCES

The reader will find a list of references at the end of each sub-chapter. The advantage of this is close connection between written text and the quoted reference, the disadvantage is that some references are listed more than once in the whole report.

The authors hope the advantage will outweigh the disadvantage.

EXECUTIVE SUMMARY

Background

Nuclear aerosol investigations began in the late 1960s and early 1970s. The progress made both in experimental studies and in code development is attested to by the publication of three CSNI-sponsored State-of-the-Art Reports (SOAR) on nuclear aerosols since 1979. Initially, fast reactor safety was the main concern of the work, as reflected in the content of the first aerosol SOAR. The TMI accident in 1979 motivated an interest in LWR source terms and resulted in the production of a supplement to the first SOAR which concentrated on LWR aerosol issues. In contrast to the fast reactor situation, the large quantity of steam present in the LWR containment atmosphere following an accident tends to make aerosol particles more compact, reducing the modelling problem of defining shape factors. On the other hand, two new effects had to be modelled: deposition due to steam condensation onto surfaces (diffusiophoresis) and particle growth by steam condensation onto the particles themselves.

The second SOAR dealt with primary-system fission-product release and transport. This SOAR included a survey of the models available in the literature for homogeneous and heterogeneous nucleation, for vapor condensation on aerosols, and for aerosol agglomeration, and noted that these and other models had been incorporated in circuit codes.

The last workshop on aerosols organised by the OECD was held in Cologne in June 1998. One recommendation made at this workshop was to prepare a SOAR on aerosol behaviour in both the primary circuit and in containment.

Objectives

Following the recommendation of the Cologne workshop, the CSNI mandated the preparation of a SOAR with four main objectives:

- To assess the status of existing experimental data and analytical capabilities required for predicting aerosol source terms from LWR accidents
- To address the strengths and weaknesses of the codes used to predict aerosol behaviour in the reactor coolant circuit and containment, and provide validation results and uncertainties, in particular for plant applications,
- To summarise findings from recent ISP exercises on nuclear aerosols and related thermal-hydraulic behaviour in the reactor coolant circuit and containment.
- To identify safety-relevant pending issues and to propose research activities that will reduce gaps in the understanding of relevant processes and deficiencies in modelling capabilities.

Scope

The Nuclear Aerosol Writing Group met several times over a three-year period from 2003 to 2006 to prepare the current SOAR, which provides a survey of issues surrounding the prediction of nuclear aerosol behaviour in the primary system and containment. It should be noted that the subject matter of the report is

limited to nuclear aerosols and does not extend to other LWR accident source term topics that do not have a direct bearing on aerosol behaviour.

The structure of this SOAR is in line with the objectives listed above. The introduction is followed by a background chapter discussing the fundamentals of aerosol behaviour with bibliography of the pertinent literature. Chapter 3 is devoted to the topics of aerosol formation/growth, transport, and retention and release. Chapter 4 provides descriptions of codes for modelling circuit and containment aerosol behaviour, and Chapter 5 describes the experiments used for their validation. Chapters 6 and 7 provide examples of validation results, and plant applications of source term calculations. Chapter 8 summarises the findings of the Cologne Workshop and progress made since, and provides recommendations for future work.

Results and their significance

The theoretical, experimental and modelling studies presented in this SOAR summarise the status and current understanding of a wide range of nuclear aerosol topics. The significance of these results is that they allow for the identification of existing gaps in code capability and experimental data that prevent accurate predictions of the source term. A general conclusion from this document is that there still exist a number of items for which additional work is required. However, the status of aerosol codes and experimental data-bases has improved substantively since the publication of previous SOARS.

At the time when the 1994 SOAR on circuit aerosols was written, plant analysis codes, (as distinct from special-purpose research tools) were relatively crude, and their validation base was largely confined to tests using simulant materials. Now, while these codes still use lumped-parameter descriptions of the thermal hydraulics that can place some constraints on the accuracy of their predictions, they include a more complete calculation of gas-phase chemistry, interactions with particles and surfaces in the primary circuit, and a better treatment of coupling between aerosol dynamics and thermal hydraulics in the containment. Models are also available for aerosol interactions with engineered safety features such as suppression pools in BWRs, and complex structures such as steam generators in PWRs.

The experimental database for development and validation of aerosol codes has benefited from more accurate and extensive instrumentation to measure a wider range of phenomena (e.g., the ability to measure airborne water). Numerous analytical tests have been performed, and are continuing, to address specific phenomena such as resuspension, revaporisation, and trapping in complex structures. Large-and small-scale containment aerosol experiments have also been performed and analysed in international programmes, notably the KAEVER and VANAM tests. Perhaps the most significant advance on the experimental side is the availability of integral experiments in the PHÉBUS facility on fission product and structural material release and transport. These tests demonstrate the complex inter-linkage between different phenomena and have refined our understanding of nuclear aerosols, particularly in the circuit, where we are now able to refer to measured particle sizes and compositions. PHÉBUS has also provided information on specific phenomena such as revaporisation. The PHÉBUS integral experiments are now complete but post-test analyses and interpretation of the results continues. Data from aerosol-related experimental programmes such as ARTIST and THAI also still require analysis.

A large number of Probabilistic Safety Analyses (PSA2) plant studies have been performed around the world, frequently involving aspects of aerosol behaviour. This report provides some examples, including sensitivity studies that demonstrate the impact of aerosol-related processes, however few such analyses have been published. The aerosol community is therefore not always fully briefed on the risk-relevance of the numerous phenomena currently under study. The question of risk significance deserves a more concerted effort, in aerosol physics as in other relevant fields. This will require additional probabilistic analysis for new plant designs and evaluation of their sensitivity to various models and parameters.

It is expected that increasingly stringent safety standards and new power reactor designs will generate aerosol-related safety questions that will require experimental capabilities, analytical tools, and the expertise to use both intelligently. Aerosol-related computational and modelling capability is now being utilised to address industrial problems, and major environmental issues such as climate change are producing a body of knowledge that should be integrated with that developed within the reactor safety community. The CSNI structure appears well suited to developing structures and mechanisms for stimulating such cross-fertilisation.

Conclusions and recommendations

A number of conclusions and recommendations have been made throughout the text of this document. The most important are summarised briefly below subdivided into three categories

Generic Issues

Code-users' workshop on plant analysis: The CSNI workshop recommended in 1998 that a meeting on the use of severe-accident codes in plant calculations for source term estimation, including codes used by utilities, be held. More than eight years after formulation of this recommendation it has still not been acted upon. There remains a need to harmonise user practices with respect to plant analyses in order to reduce divergence in results. The objective would ideally be to produce online "best practice" guidelines for the major codes.

Shape factors: Models describing aerosol dynamics generally assume spherical, fully dense particles but nuclear aerosols are often neither, particularly those originating from core melt sequences, or accident scenarios in which large parts of containment have low humidity. The importance of shape factors has been demonstrated in uncertainty and sensitivity analyses. Although such parametric studies can be performed for accident scenarios, the difficulty is in knowing what constitutes a "reasonable" variation of the shape factors for representative conditions. At the minimum, it is recommended that measurements of two diameters (e.g., aerodynamic and volume-equivalent diameter) of aerosols from prototypical integral experiments be obtained to determine the dynamic shape factor.

Reactor Coolant System Issues

Analytical support by the use of CFD Codes: CFD treatment of coupled aerosol/flow phenomena is not universal because of the complexity of the phenomena and geometries, and the effort required for implementation. At present, efforts are being made to simulate particle transport and deposition in complex reactor structures with CFD, however more work needs to be done this treatment becomes satisfactorily accurate.

Mechanical Resuspension: Existing models are inadequate to evaluate the safety impact of aerosol resuspension in the primary circuit, which is both design- and scenario-dependent. Experiments are required for the development and validation of models to: a) account for the porosity of a deposit, which affects the mass and size distribution of resuspended material and b) simulate the effect of shock and vibrations (alone and in combination with flow increases) on resuspension. There is also limited work on the resuspension of wet deposits or wet deposits which have dried in situ. It is recommended that scoping calculations be performed to assess the potential impact of this behaviour on the source term. Finally, it has to be said that the consequences for a severe accident of a light-water reactor due to resuspension from the RCS varies depending on the scenario, i.e., bypass or non-bypass sequences. For non-bypass sequences, the influence of this resuspension on the potential source term may well be insignificant within a few hours. However, improvement of resuspension modelling with respect to bypass sequences is clearly very desirable.

Deposition in singularities and complex structures: No significant advances appear to have been made since 1998 in the experimental investigation or the modelling of deposition in singularities such as changes in cross section or bends. Some code improvements have been made by including the best-available models from published literature.

Significant progress has been made with respect to deposition in steam generators (SGs). Most probabilistic risk assessments (PRAs) and severe accident codes assume that a significant fraction of fission products flowing through a non-isolated break in a SG escapes to the environment. This may not be the case however, as demonstrated in several recent experimental programmes. SGTR was the first European project (2000-2002) to improve understanding in a systematic way of possible retention mechanisms in tubes and in the complex structures of the secondary side of a SG. In particular, the PSAERO and HORIZON experiments from Finland were conducted to study in-tube retention whereas retention in the SG bundle has been investigated in PECA-SGTR and the ongoing ARTIST experiments (respectively in Spain and Switzerland). In addition, certain modelling efforts to develop a correlation for the retention in the bundle were initiated. Thorough interpretation of the data from the above experiments is incomplete and modelling efforts continue. It is expected that the main issues regarding SGTR will be answered after termination of these activities.

Particle break-up in highly turbulent flows: Highly turbulent flow inside a tube may induce break-up of particles due to (i) impaction on the walls, (ii) strong shear in the flow or (iii) the vena contracta and shock wave at the tube exit. This phenomenon was observed, e.g., in Phase I of the ARTIST tests as well as in supplementary experiments. However, to determine whether aerosol particles may break up in severe accidents would require more information on the structure and the nature of the bonding forces between primary particles for severe accident aerosols as well as for the TiO₂ agglomerates used in ARTIST Phase I. In Phébus tests, which produced more prototypical aerosols, SEM micrographs showed fairly compact, sintered agglomerate structures unlike the ARTIST TiO₂ particles. Consequently, intra-particle forces can be expected to be higher in reality than in these TiO₂ agglomerates. Nevertheless, the issue is of some importance since the generation of submicron particles from supramicron ones leads to less-efficient retention of the aerosols concerned. In the first instance, accident sequences other than SGTR inducing highly-turbulent flows need to be identified; comparison of plant calculations without and with (assumed) break-up for SGTR and the other pertinent sequences would then allow evaluation of the risk relevance of the break-up phenomenon. If the risk impact is significant then, in the absence of relevant data for severe accident aerosols, data for prototypical particles are needed in highly-turbulent accident-relevant conditions.

Impact of Chemistry: The fundamental importance of chemistry to prediction of source terms arising from potential severe accidents is well established. Nuclear safety codes model chemical reactions using the thermodynamic equilibrium approach, which relies on having thermodynamic data for each chemical species covered. Unfortunately, the uncertainties associated with some of these data are often large and divergence between data series originating from different sources can be considerable. It is recommended (as is being done for the ASTEC code) that the thermo-chemical data used by codes be thoroughly verified and that key sources of uncertainty be identified. Moreover, while the thermodynamic approach is pragmatic, it is of limited value when addressing accident scenarios in which slow chemical kinetics precludes achievement of thermodynamic equilibrium (e.g. secondary-side, cold-leg and containment conditions). In this context it is recommended to:

- Assess the value of the simplistic approach (taken in ASTEC/SOPHAEROS and VICTORIA codes) of assigning user-defined cut-off temperatures below which chemical reactions in the RCS do not occur. Use of PHÉBUS FP results with respect to iodine in the RCS should prove helpful;
- Follow closely experimental programmes that are investigating reaction rates for iodine species (e.g., the French CHIP series).

- Assess whether FP species other than iodine, which may reach the containment in the vapor phase, require kinetic modelling (especially important for hot-leg and high-pressure sequences where vapor fractions at the RCS breach will be significant).
- Lastly, the effects of radiolysis in the RCS are unknown. Radiolysis may have little impact in the core region (temperatures being so high that only simple atomic and radical species exist), but may be important in cooler regions of the RCS involving significant deposits (high local dose rate) such as in a cold-leg sequence. In terms of direct consequences for aerosols, one effect will be reduction of the threshold super-saturation at which vapors nucleate since a high density of electrically-charged condensation nuclei will form. In terms of consequences for the source term, the meagre state of knowledge renders even qualitative evaluation difficult.

Revaporisation of deposits: Although significant progress has been made regarding studies on revaporisation from several projects (Phébus FP, the EC 4th Framework Programme projects RVP and REVAP-ASSESS and the EXSI project), experimental work on revaporisation remains scarce; further theoretical and experimental developments are necessary to understand the revaporization process. In addition, the safety relevance ought to be further demonstrated by assessing, conceivably, the impact of a weak source of fission products from the reactor coolant system for some hours after the main release-from-core phase.

Containment Issues

Charge effects: Small deposits of aerosols on the outer walls of the 10 m³ containment vessel in the PHÉBUS test FPT0 could not be explained by electrophoretic effects. However, even if charge effects on aerosol deposition are not seen to be significant in test facilities (with or without a radiation field) there is no firm evidence that this effect would be negligible in an accident. At present there is no consensus among experts on whether further investigations of charging effects are necessary or not.

Mixed aerosols in condensing atmospheric conditions: Although there has been considerable progress in modelling aerosol deposition as a function of relative humidity, a comparison of the adequacy of code results from ISP 37 and ISP 44 indicate that there is still some work to be done to ensure satisfactory coupling between thermal hydraulic and aerosol models so that these capture correctly aerosol behaviour in most environments. An additional uncertainty in modelling aerosol behaviour in the containment in humid conditions arises from determining the hygroscopicity associated with a mixture of aerosols of different compositions. Finally, there is some uncertainty regarding the density of multi-component aerosols, and whether this parameter is important for accident conditions with a wide variety of aerosol components. Both the PHÉBUS tests and the KAEVER experiments suggest that an average aerosol particle composition and size might be attained in containment. The KAEVER experiments further suggest that this average particle would behave like the most hygroscopic of its individual components. Confirmation of these findings, in a large- or intermediate-scale experiment performed under saturated conditions might significantly simplify modelling aerosol behaviour in wet conditions.

Mechanical Resuspension: Compared with deposits in the primary system, deposits in containment will have significantly lower particle loadings, and be distributed over larger areas. Resuspension of such deposits is possible as a consequence of a breach of containment and/or a hydrogen burn. It is recommended that experimental studies be performed on resuspension of real or simulated deposits at containment-typical loadings, particularly during flow disturbances, as a function of the deposit composition and history (dry, wet, wet then dried in situ etc.) and as the result of hydrogen deflagrations. In addition, probabilistic studies should be undertaken to evaluate the safety significance of containment resuspension.

Re-entrainment in the Containment: Re-entrainment of particulate fission products will occur at several water and core melt pools during a severe accident. The release rates of radiological materials are relatively small but the sources are persistent. A significant contribution to the source term by re-entrainment is possible in the late accident phase. However, reliable analytical investigations including risk relevant aspects do not exist yet. With a few exceptions, there are only a few codes able to simulate the FP release from boiling or flashing sumps.

Up to now all re-entrainment tests including ThAI have been made on ideal systems with appropriate concentrations of soluble and insoluble materials but without surfactants or impurities. Additional experiments are required to evaluate entrainment under realistic conditions. After improvement and validation of re-entrainment models for realistic conditions is achieved reliable accident calculations to quantify the effect of re-entrainment from boiling pools on the source term will be possible. In the light of these results it may be desirable to investigate measures reducing the release of fission products by re-entrainment.

Pool scrubbing: Some BWR and PWR severe accident scenarios involve transport of radioactive aerosols through pools of water where particles can be retained. This phenomenon, known as pool scrubbing, has the potential to reduce the source term. Results provided by both stand-alone and integral code models indicate satisfactory agreement with simple experiments for integral retention. However, a systematic experimental database is required for validation purposes. Particular attention should be given to removal of aerosols during formation and subsequent disintegration and coalescence of bubbles, and the effects of submerged structures and contaminants (surfactants).

Removal by sprays: This issue has been extensively investigated by the French organisations CEA and IRSN using specific apparatuses and the CARAIDAS, MISTRA and TOSQAN test facilities. The data should be made accessible to the nuclear community, at least the OECD partners. Validated modelling based on these experimental investigations has been implemented in the codes ASTEC and TONUS. The ASTEC model can be found in the open literature. Further work on containment sprays is low priority for countries that have access to this data but in other countries and for certain advanced designs it remains important to establish effective removal by spray systems and both experimental and analytical efforts continue.

Influence of recombiners: Phenomenological experiments have demonstrated that there is a potential for the operation of Passive Autocatalytic Recombiners (PARs) to generate volatile molecular iodine by thermal decomposition of metal-iodide containment aerosols. Scoping calculations indicate that this conversion process might be a significant contribution to the molecular iodine in the containment atmosphere. It has also to be recognised that iodine may not be the only fission product concerned, e.g., some formation of the highly volatile species ruthenium tetroxide might be possible in the conditions expected within PARs though no investigation of this has been performed. Further experimental investigations in realistic conditions (mixed-aerosol and mixed-atmosphere composition) are necessary.

Hydrogen-burn effects on suspended aerosols: Heat release by hydrogen burns may have a strong effect on aerosol characteristics and could possibly liberate volatile forms of iodine. Experiments in the ThAI facility demonstrate that there is a clear effect of hydrogen-combustion-induced flows on resuspension of already deposited CsI aerosol. These findings have to be expanded to consider other types of relevant aerosol species and other plant applications. However, chemical effects on iodine-containing aerosols have not been studied; information from the ongoing investigation of the impact of recombiners on aerosols may be relevant.

Release from MCCI pool: The behaviour of aerosols formed after the release from a molten corium concrete pool was investigated in the 1990s in the ACE phase C and BETA tests and more recently in the

OECD-MCCI and EC Framework Programmes (LPP and MP projects). However, efforts to further aerosol code development and validation from these experiments has been limited. As there is currently little known activity in this area it is recommended that the following steps be initiated in the near future:

a)

- Recalculation of the old test results to evaluate the thermodynamic basis of the present models by comparing concrete erosion processes and aerosol nucleation due to vaporization from the free upper surface and into gas bubbles in the corium concrete pool,
- Obtain information on the characterization of concrete-based aerosols; conventional (non-nuclear) knowledge about concrete aerosols may be a good starting point;
- Evaluate information from the EC projects MP and LPP from the specific view of fission products release due to MCCI;

Penetration of aerosols through leak paths: From a review of available data and models including recent research in SARNET on dry aerosol transport in cracks, the recommendation can be made that additional separate effects and integral tests are required:

- Separate effect tests should provide a detailed characterization of the scenarios and the phenomena necessary for model development and validation of individual depletion mechanisms;
- Integral tests should focus on measuring overall process variables such as mass retained to provide a data base for checking the overall model performance.

The boundary conditions (hydraulic diameter, curvature of the path, fluid composition pressure drop, wall temperature, and aerosol size) for these experiments should, obviously, be as close as possible to those postulated under accident conditions.

For wet aerosols, it is recommended that additional experiments be performed to characterise aerosol transport through sequential expansion and contraction regions representative of the leak path from containment to the outside atmosphere and to evaluate the extent of leak-path plugging.

Fire aerosols: Little is known about the properties or amounts of aerosols produced from fires, and how mixing of flaky fire aerosol with nuclear aerosol particles would impact on the aerosol depletion rate in containment. There is a need for further experimental investigation of fire aerosols especially from cable fires. This could be done in a future step of the OECD PRISME and/or the Sandia CAROLFIRE projects. The aerosol production rate, the particle size distribution and the shape factors are of main concern. It is recommended that existing multi-component aerosol models be extended in order to simulate the interaction of fire aerosols with a pre-existing nuclear aerosol.

TABLE OF CONTENTS

EXECUTIVE SUMMARY	5
TABLE OF CONTENTS	13
1. INTRODUCTION	19
2. GENERAL PHENOMENA	21
2.1 Aerosol Physics in Reactor Accident Analyses	21
2.2 Aerosol Formation	23
2.3 Growth of Aerosol Particles	25
2.3.1 Growth by coagulation	25
2.3.2 Growth by condensation	28
2.4 Aerosol Growth as a Result of Hygroscopicity	30
2.5 Fractal Nature of Aerosols	31
2.6 Aerosol Deposition	31
2.6.1 Gravitational settling and diffusion	32
2.6.2 Inertial deposition of aerosol particles	33
2.6.3 Phoretic deposition processes	35
2.7 Resuspension of Deposited Particles	36
2.8 Aerosol Removal by Engineered Safety Systems	37
2.8.1 Steam suppression pools	40
2.8.2 Fan coolers	41
2.9 Aerosol Removal by Filtered Vents	41
2.10 Computer Modelling of Aerosols	43
2.11 Annotated Bibliography	43
3. ACCIDENT PHENOMENOLOGY	49
3.1 Formation and Growth	49
3.1.1 Phenomena considered and state of knowledge	49
3.1.2 Particle formation in the primary system	52
3.1.3 Containment aerosols	55
3.2 Impact of Thermal Hydraulics	57
3.2.1 Impact of thermal hydraulics on aerosol behaviour in the primary circuit	57
3.2.2 Impact of thermal hydraulics on aerosol behaviour in the containment	59
3.3 Fission-Product Transport and Deposition	64
3.3.1 Introduction	64
3.3.2 Synopsis of RCS phenomena and their modelling	64
3.3.3 Agglomeration of aerosols	66
3.3.4 Deposition of aerosols	67
3.3.5 Containment	70
3.4 Aerosol Behaviour in Complex Structures of Steam Generator Secondary Site	73
3.4.1 Issue and status	73
3.4.2 Theoretical background on possible aerosol removal in the steam generator	76
3.4.3 Inertial impaction and interception in the separator and dryer sections	79
3.4.4 Other processes	79

3.5	Resuspension	82
3.5.1	Resuspension in primary circuit	82
3.5.2	Resuspension in containment	85
3.6	Pool Scrubbing	87
3.7	Re-Entrainment	92
3.8	Aerosol Formation during High Pressure Melt Expulsion from the Reactor Coolant System	96
3.9	Aerosols from MCCI	100
3.10	Aerosols from Fire	108
3.11	Spray Systems	111
3.12	The Impact of Catalytic Hydrogen Recombiners	121
3.13	Filters	123
3.14	Two Phase Flashing Jets and Water Aerosol Behaviour	127
3.15	Penetration Leakages	130
3.15.1	Introduction	130
3.15.2	Current modelling and experimental studies	131
3.15.3	Measurement of the retention of wet aerosols	132
4.	MODELLING APPROACHES IN CODES (INCLUDING BASIC VALIDATION)	137
4.1	Integral Codes	137
4.1.1	MELCOR	137
4.1.2	ASTEC (SOPHAEROS and CPA)	142
4.1.3	MAAP4	147
4.1.4	THALES 2	149
4.1.5	ECART	155
4.1.6	APROS SA	157
4.2	Circuit	161
4.2.1	VICTORIA	161
4.2.2	ATHLET-CD	168
4.3	Containment	169
4.3.1	CONTAIN	169
4.3.2	COCOSYS	175
4.3.3	ART/REMOVAL	181
4.3.4	SMART	183
4.3.5	GOTHIC	184
4.3.6	KUPOL	185
5.	RECENT VALIDATION WORK	187
5.1	Integral Experiments	187
5.1.1	The PHÉBUS fission product programme	187
5.1.2	ISP-46 (PHÉBUS FPT1)	190
5.2	Circuit	193
5.2.1	Revaporization in the FPT0, FPT1 and FPT2 circuits	193
5.2.2	FALCON (Including ISP-34)	194
5.2.3	STORM (Including ISP-40)	197
5.2.4	WIND	204
5.3	Containment Experiments	207
5.3.1	DEMONA	207
5.3.2	MARVIKEN-V	209
5.3.3	LACE	211
5.3.5	VANAM (including ISP-37)	217
5.3.6	KAEVER (including ISP-44)	222

5.3.7	AHMED	228
5.3.8	VICTORIA.....	232
5.4	Aerosol Release in the Course of MCCI (ACE-C).....	236
5.5	REST, REVENT, ThAI Re-Entrainment Tests	237
5.6	Pool Scrubbing Tests.....	239
5.7	Resuspension Tests.....	242
5.7.1	Continuous flow experiments.....	242
5.7.2	Transient flow experiments.....	243
5.8	Spray Systems (French Tests)	244
5.9	Containment Venting Filters	247
5.9.1	International efforts for qualification of containment venting filters	248
5.9.2	CCI containment venting filter.....	255
5.9.3	Removal of iodine by the containment venting filters	258
5.9.4	International status of use of containment venting filters	258
5.10	Ongoing Tests.....	258
5.10.1	Aerosol behaviour in steam generators	258
5.10.2	EVAN.....	264
5.10.3	Penetration leakage tests	265
5.10.4	ThAI aerosol tests.....	266
5.10.5	Impact of catalytic hydrogen recombiners	269
5.10.6	Aerosol growth under saturated conditions (Canadian tests).....	272
6.	EXAMPLES FOR VALIDATION.....	273
6.1	Comparison of MELCOR Predictions to Experiments	273
6.2	CONTAIN for PHÉBUS FPT1	277
6.3	Example for Uncertainty and Sensitivity Analyses of Two Aerosol Calculations.....	283
7.	SOURCE TERM CALCULATIONS IN PLANT APPLICATIONS	287
7.1	MELCOR Calculation for a US American PWR (Station Blackout Scenario).....	287
7.2	ASTEC Calculation for a German PWR (MB LOCA Scenario)	294
7.3	Aerosol-Related Uncertainties in the Prediction of Severe Accident Source Terms	304
8.	IDENTIFIED OPEN ISSUES (INCLUDING RECOMMENDATIONS).....	307
8.1	Introductory Remarks	307
8.2	Generic Issues.....	308
8.2.1	Code-users' workshop on plant analysis	308
8.2.2	Shape factors	308
8.2.3	Computational fluid dynamics codes	309
8.3	Reactor Coolant System Issues	309
8.3.1	Mechanical resuspension.....	309
8.3.2	Deposition in singularities and complex structures.....	310
8.3.3	Particle break-up in highly turbulent flows	311
8.3.4	Influence of chemistry.....	311
8.3.5	Revaporisation of deposits	312
8.4	Containment Issues.....	313
8.4.1	Charge effects.....	313
8.4.2	Mixed aerosols in condensing atmospheric conditions.....	313
8.4.3	Mechanical resuspension.....	313
8.4.4	Re-entrainment from pools.....	314
8.4.5	Pool scrubbing.....	314
8.4.6	Removal by sprays	315

8.4.7	Influence of recombiners.....	315
8.4.8	Hydrogen-burn effects on suspended aerosols.....	315
8.4.9	Release from MCCI pool	316
8.4.10	Penetration through leak paths	317
8.4.11	Fire aerosols	317
8.5	Concluding Remarks	318
9.	APPENDIX 1: Characteristics of Aerosols under LWR Severe Accident Conditions.....	323
9.1	Context	323
9.2	Review of Available Information.....	323
9.2.1	Aerosols in the RCS	324
9.2.2	Aerosols in the containment.....	329
9.3	Discussion	331
9.3.1	Uranium contribution	331
9.3.2	Tin contribution.....	331
9.3.3	Silver contribution.....	331
9.3.4	Cadmium contribution.....	331
9.3.5	Indium contribution.....	331
9.3.6	Fission product contribution.....	332
9.3.7	Size, shape and structure	332
9.3.8	Variability.....	333
9.3.9	Other considerations.....	333
9.4	Conclusion.....	334
10.	APPENDIX 2: Aerosol Shape Factors.....	337
10.1	Fundamentals.....	337
10.2	Dynamic and Collision Shape Factors	338
11.	APPENDIX 3: Spray Modelling Developed from Recent Analytical Work	345
11.1	Relaxation of Droplets.....	345
11.2	Droplet Coalescence.....	346
11.3	Coupling of Droplet Relaxation and Coalescence.....	347
11.4	Evolution of the Atmosphere Conditions	349
11.5	Aerosol Removal Modelling	350
11.5.1	Inertial capture.....	350
11.5.2	Interception.....	351
11.5.3	Brownian diffusion.....	352
11.5.4	Phoretic capture.....	352
11.6	Gaseous Iodine Removal by Sprays	353
12.	APPENDIX 4: Overview of Filtration Devices.....	357
12.1	Nuclear Aerosol Filtration.....	357
12.1.1	Development of the high-efficiency particulate air (HEPA) filter	357
12.1.2	Challenges for test procedures	359
12.1.3	Demonstrated safety by the use of HEPA filters.....	359
12.1.4	Deep-bed sand and glass fibre filters	359
12.1.5	Brief history of gas adsorption	360
12.2	Type of Filters in Use.....	361
12.3	Normal Operation and Design Basis Accidents	361
12.4	Brief Review on Mechanisms of Filtration	363
12.5	Characterisation of Filter Performance.....	365

12.6	Cut Diameter Method.....	367
12.7	Fibrous Filter	368
12.8	Granular Beds.....	370
12.9	Sand Beds.....	373
12.10	Gravel Beds.....	374
12.11	Venturi Scrubbers.....	376
12.12	Water Pools	379
13.	APPENDIX 5: Point-by-Point Review of Issues Identified at the 1998 Aerosol Workshop.....	385

1. INTRODUCTION

The prediction of nuclear aerosols behaviour associated with postulated accidents in nuclear power plants is necessary for the assessment of the radiological consequences of these accidents and hence is an important aspect of reactor safety evaluation. The nature and behaviour of nuclear aerosols can potentially influence both the course and the consequences of reactor accidents. For example, nuclear aerosols can affect the performance of engineered safety systems (e. g. air cleaning systems) as well as the magnitude, dispersion and effects of the radioactive source term leaked to the atmosphere. As a result of the extreme conditions for nuclear aerosols in case of an accident, they exhibit very dynamic mostly physical, but also chemical behaviour and pose special analytical and experimental problems different from those associated with aerosols found under industrial and ambient conditions.

Following a LWR severe accident, the overall radionuclide retention in form of aerosol, both in reactor coolant system and containment, is the result of three processes: transport, deposition and release from dry or wet surfaces (resuspension) or (boiling) water pools (re-entrainment).

Approximately a 30 years tradition in the preparation of state-of-the-art reports on nuclear aerosols and the proceedings of workshops concerning the aerosol issue (summarised in chronological order at the end of this chapter [1 - 8]) demonstrate the substantial work performed by the nuclear community and the progress made in this period of 30 years.

Nevertheless at the last workshop in Cologne, 1998, some important issues were identified, where knowledge did not seem to be sufficient for reliable predictions. Following the recommendations of this workshop the CSNI decided to prepare a state-of-the-art report with three main objectives:

- to summarise the present experimental and analytical knowledge on nuclear aerosols
- to give some examples for validation results and in particular for plant applications, both including uncertainties
- to identify safety relevant still unresolved issues

Nevertheless, it should be understood that the subject matter of the report is nuclear aerosols, and the report does not purport to cover the whole field of radioactive source terms for severe LWR accidents. For example, there is no detailed discussion of fission product chemistry processes that do not have a direct bearing on aerosol behaviour, such as iodine solution chemistry and organic iodine production.

Finally the authors of this report wish to acknowledge significant contributions from a large number of colleagues, which have increased the quality of the report considerably.

References

- [1] NEA Group of Experts, Nuclear Aerosols in Reactor Safety , A state-of-the-art report by a group of experts of the NEA committee on the safety of nuclear installations, June 1979
- [2] CSNI Specialist Meeting on Nuclear Aerosols in Reactor Safety in Gatlinburg, April 1980

- [3] CSNI Group of Experts on Nuclear Aerosols in Reactor Safety, March 1983
- [4] CSNI Specialist Meeting on Nuclear Aerosols in Reactor Safety Workshop Karlsruhe, September 1984
- [5] NEA Group of Experts, Nuclear Aerosols in Reactor Safety - Supplementary Report NEA / OCDE / OECD, Paris 1985
- [6] Nuclear Engineering Applications Section Species to Aerosols - Workshop on Water-Cooled Reactor Aerosol Code Evaluation and Uncertainty Assessment, Brussels, September 1987
- [7a] OECD / NEA, Aerosol behaviour and thermal-hydraulics in the containment (2nd workshop Brussels 1987, Technical Summary), NEA/CSNI/R(92)1, Fontenay-aux-Roses, 1990
- [7b] OECD / NEA Aerosol behaviour and thermal-hydraulics in the containment (2nd workshop Brussels 1987, Proceedings) NEA/CSNI/R(92)1, Fontenay-aux-Roses, 1990
- [8] Third OECD Specialist Meeting on Nuclear Aerosols in Reactor Safety GRS-166, NEA/CSNI/R(98)4, ISBN 3-931995-31-3, Cologne, June 1998

2. GENERAL PHENOMENA

This chapter provides background and introductory information and is directed primarily at those readers with an interest in being reminded of the fundamentals of aerosol behaviour under severe reactor accident conditions. In addition, there is an annotated bibliography that will introduce the reader to the pertinent research literature.

2.1 Aerosol Physics in Reactor Accident Analyses

Most of the radioactive material that can escape from a nuclear power plant during a severe reactor accident will do so in the form of aerosols. Much of reactor accident analysis is the prediction of the behaviour of these radioactive aerosols. Aerosols are very small solid particles or liquid droplets suspended in a gas phase. The suspended solid or liquid particles typically have a range of sizes. Particles may range in size from 0.01 μm to 20 μm . Aerosol concentrations in reactor accident analyses are typically less than 100 g/m^3 and usually less than 1 g/m^3 . At these concentrations, the aerosol particles little affect the gas hydrodynamics, but the gas dynamics profoundly affect the behaviour of the suspended particles. The behaviours of the larger aerosol particles are described usually by continuum mechanics. The smallest particles have diameters less than the mean free path of gas phase molecules and the behaviour of these particles can often be described well by free molecular physics. The vast majority of aerosol particles arising in reactor accident analyses have behaviours in the very complicated regime intermediate between the continuum mechanics and free molecular limit. In this regime, aerosol behaviour must be described using some approximate solution of the Boltzmann equation.

The mechanical regimes of aerosol behaviour are usually categorised in terms of the Knudsen number, Kn , which is the ratio of the mean free path of gas molecules, λ , to the particle diameter D_p :

$$\text{Kn} = \frac{2\lambda}{D_p}$$

Continuum behaviour is approached for $\text{Kn} < 0.1$ and free molecular flow is approached for $\text{Kn} > 10$. These regimes vary with temperature and pressure which affect the mean free path. At atmospheric pressure and room temperature the mean free path of air is about 0.06 μm .

The number density of aerosol particles in a gas phase can be huge - exceeding $10^{13}/\text{m}^3$. It is quite impossible to predict aerosol behaviour by calculating the dynamics of individual particles. Instead aerosols must be considered in a collective sense and the aerosol is taken to have some continuous distribution of particle sizes. Given sufficient time in a quasi-steady state environment with no continued injection of aerosol into the gas phase, an aerosol subjected to particle growth by agglomeration and gravitational deposition onto surfaces will develop a size distribution that is approximated well by a log-normal distribution. The probability density for particles having sizes in the interval D_p to $D_p + dD_p$ is:

$$\text{pdf}(D_p) = \frac{1}{\sqrt{2\pi \ln \sigma}} \exp \left[- \left(\frac{\ln D_p / \mu}{\sqrt{2 \ln \sigma}} \right)^2 \right] d \ln D_p$$

where:

μ = mean particle size

σ = geometric standard deviation of the size distribution

It is common to report aerosol size data in terms of the parameters of the lognormal size distribution (μ and σ) whether or not the aerosol satisfies the criteria for the lognormal distribution being a good approximation of the actual size distribution. Example size distribution for the case of a very narrow size distribution ($\sigma = 1.8$) and for the case of a broad distribution ($\sigma = 3$) are shown in Fig. 2.1-1.

When there are continuing sources of aerosol to the gas phase or when there are complicated processes involving engineered safety features much more complicated size distributions develop. It is not uncommon for aerosols in reactor containments to have bimodal size distributions at least for some significant periods of time early in an accident.

Salient features of aerosol physics under reactor accident conditions that will affect the nature of the aerosols are:

- formation of aerosol particles
- growth of aerosol particles
- shape of aerosol particles
- deposition of particles on surfaces
- resuspension of aerosol particles

Introductory or background information on these and other aspects of nuclear aerosols are provided in the subsections of this chapter that follow. This chapter is concluded with a brief description of the numerical methods used to model the important aerosol phenomena.

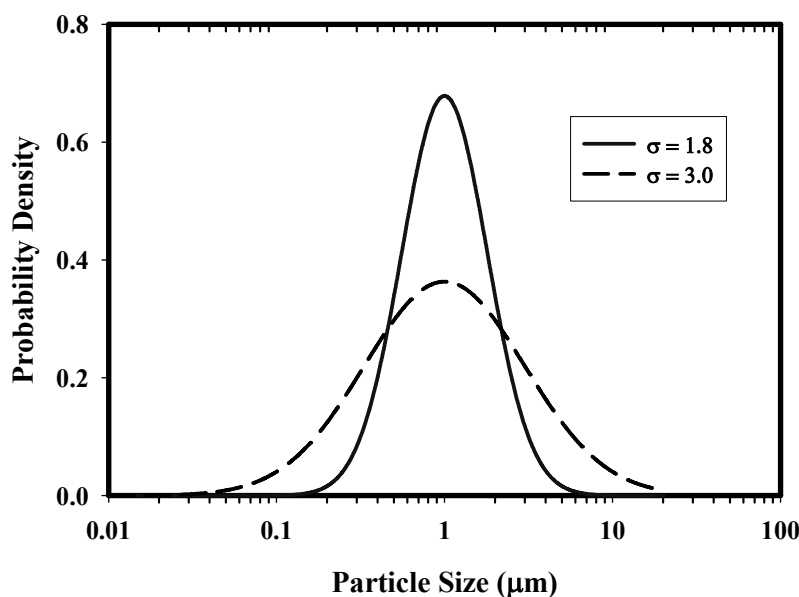


Fig. 2.1-1 Comparison of log normal distributions with different geometric standard deviations, σ , and the same mean, μ

2.2 Aerosol Formation

Aerosol particles can be formed by the mechanical comminution of materials or by the condensation of vapors. Mechanical processes that produce aerosol particles in reactor accidents include:

- entrainment of solids or liquid droplets in high velocity gas flows,
- expulsion of droplets by gases bubbling through liquids,
- shock waves such as those produced in energetic interactions of molten materials with coolants, and
- high pressure melt ejection from the reactor coolant system.

Mechanical processes seldom produce very fine particles that can remain suspended in the gas phase for protracted periods of time. Typically, mechanical processes will not produce particles smaller than about 1-2 μm . Furthermore, most mechanical processes that can produce aerosols are not of prolonged duration and are, thus, not enduring sources of aerosols through large periods of an accident. An exception is the production of aerosols by the bursting of bubbles of gas sparging through liquids. But, the bubble burst source is not an especially intense source of aerosol particles. Aerosol production by mechanical processes is largely ignored in most reactor accident analyses.

Nucleation of particles from supersaturated vapors is the more important source of aerosols in reactor accidents and certainly the source given the most attention in reactor accident analysis computer codes. Vapors rich in radioactive materials are formed from high temperature core debris materials. The vapors become supersaturated as they are transported from the vicinity of the core debris to cooler regions. These supersaturated vapors can nucleate aerosol particles.

Vapor nucleation is a very complicated physical process even when the vapor consists of a single condensable species. Nucleation can occur homogeneously from the vapor when the supersaturation ratio

(ratio of the actual partial pressure of condensable species divided by the equilibrium partial pressure of that species) exceeds a value of 4 - 10. Nucleation is a kinetic process and there is not a sharp onset to this process. Nucleation is usually taken to be occurring when the rate of particle production exceeds one particle per cubic centimeter per second. The supersaturation necessary for any particular vapor to nucleate is a sensitive function of the surface energy of the condensed phase (surface tension in the case of a liquid being produced from the vapor). The rate of tin vapor nucleation is shown in Fig. 2.2-1 as a function of temperature for a vapor initially saturated at 1800 K. It can be seen from this example that nucleation occurs whenever the gas is saturated, but nucleation is quite slow until a substantial supersaturation develops. That is, the vapor has to cool well below saturation for detectable nucleation to be observed. Detectable nucleation (Rate > 1 particle/cm³-s) of the tin aerosol occurs rather abruptly over a narrow temperature range at a temperature over 100 K lower than the temperature at which the vapor becomes saturated. The enormous nucleation rates predicted at still lower temperatures are difficult to realise in practice because heat liberated by nucleation cannot be dissipated from the system.

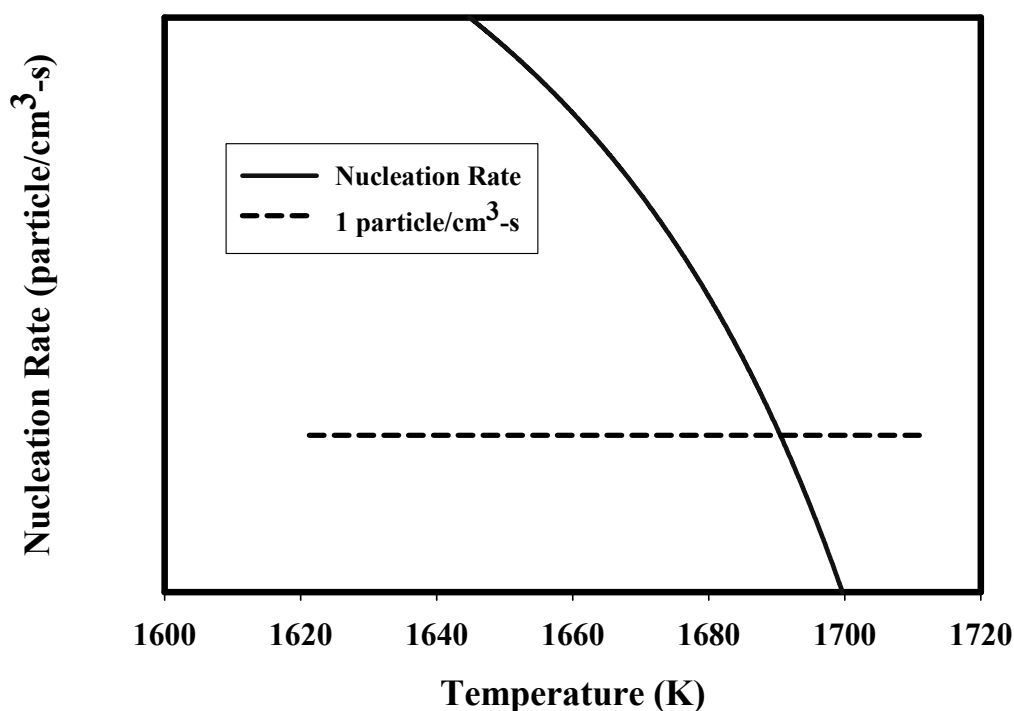


Fig. 2.2-1 Nucleation kinetics of tin vapor initially saturated at 1800 K

Heterogeneous nucleation of vapor on ions in the gas phase can occur at supersaturations that are lower than those needed to drive homogeneous nucleation. The gas phase in a nuclear reactor accident will be intensely irradiated so there will be relatively high concentrations of ions to act as sites for nucleation. Some heterogeneous nucleation of vapors will occur. But, supersaturation ratios that will develop when high temperature vapors escape the regions of core debris into cooler regions can exceed 10^4 . Since nucleation is kinetic in nature, it is quite likely that both homogeneous nucleation and heterogeneous nucleation will occur simultaneously.

The theory of nucleation of complex vapors produced in reactor accidents is vastly more complicated than the theory for single pure vapors outlined above. Indeed, a general theory of nucleation for complex vapors has not yet been developed. The qualitative features of nucleation from complex vapor mixtures are expected to be similar to those of pure vapor nucleation although quantitative features may differ and calculation of these features will involve vapor and condensed phase properties that are not readily

available. Consequently, when nucleation phenomena are considered in accident analyses, approximate models based on nucleation of single vapors are used. The upper and lower bound models of Reiss, Katz and Cohen are quite popular.

It is more common especially in the so-called “lumped node” computer models of reactor accidents to omit mechanistic modeling of nucleation processes. Particle formation is simply assumed to occur when the vapor reaches saturation. The omission is justified by the rapid development of supersaturation in the gas flowing into ever cooler environments and the rapid growth of particles that are nucleated from the vapor. This sudden growth of the nucleated particles can obscure any effects of the details of nucleation kinetics at the “lumped node” level of approximation. Recently, mechanistic treatments of vapor nucleation have been included in computational fluid dynamics models of flows during reactor accidents. In some cases, these models are showing unexpected complexity in the aerosol deposition because of the spatial variations in the supersaturation along a flow path. These findings are, of course, subjects of continued research.

2.3 Growth of Aerosol Particles

2.3.1 Growth by coagulation

Aerosol particles grow by continued condensation of vapor on the nucleated particles and by the coagulation of these particles. Vapor condensation on nucleated particles is limited by the rate at which heat liberated by condensation can be removed. Interior to a cloud of nucleating vapor, only conduction can remove this heat. Velocity differences between the gas phase and the particles are too small to promote much convective heat transport and optical paths for radiation heat transfer are effective only near the perimeter of the cloud. Though some continued vapor condensation will occur, coagulation is the dominant mechanism of particle growth following nucleation. Coagulation greatly affects the size and consequently the mobility of aerosol particles, so the aerosol particles quickly develop a size distribution. The evolution of this size distribution is described by the integrodifferential equation:

$$\begin{aligned} \frac{\partial n(v)}{\partial t} = & \frac{1}{2} \int_0^v K(u, v-u) n(v-u) du \\ & - n(v) \int_0^\infty K(u, v) n(u) du \\ & - R(v) n(v) + S(v) \end{aligned}$$

where:

- $n(v)$ = number density of particles of volume v to $v + dv$ (particles/cm³)
- $K(u, v)$ = collision kernel for particles of volume v and volume u (s⁻¹)
- $R(v)$ = rate constant for deposition of particles of volume v on surfaces (s⁻¹)
- $S(v)$ = source rate of particles (particles/cm³-s)

The first integral on the right-hand side of this equation is the coagulation of particles of volume u and $v-u$ to form a particle of volume, v . The second integral is the coagulation of particles of volume v with particles of any volume to form a particle that is no longer in the v to $v + dv$ volume interval.

Particles coagulate because they cross stream lines of flow to come into contact. There are a variety of mechanisms that can cause particles to cross stream lines. Each of these mechanisms is characterised by a distinct collision kernel, $K(u, v)$. The more common collision kernels recognised in models of aerosol growth during reactor accidents are:

- **Gravitational** - larger particles sweep out smaller particles as they fall under the force of gravity

$$K_g(u, v) = \frac{2\pi}{9} \left(\frac{3}{4\pi} \right)^{4/3} \frac{\gamma^2 g \rho_p}{\chi \mu_g} \epsilon_0(u, v) (v^{1/3} + u^{1/3})^2 |C(v) v^{2/3} - C(u) u^{2/3}|$$

where:

- γ = collision shape factor
- χ = dynamic shape factor
- g = gravitational acceleration
- ρ_p = material density of the particle
- μ_g = gas viscosity

$$\epsilon_0 = \frac{\beta v^{2/3}}{(u^{1/3} + v^{1/3})^2}$$

- β = 0.5 or 1.5
- $C(v)$ = Cunningham slip correction factor for a particle of volume v

- **Brownian diffusion** - fluctuations in molecular bombardment drive particles across streamlines of flow to contact other particles.

$$K_B(u, v) = \frac{2kT}{3\mu_g} (v^{1/3} + u^{1/3}) \left(\frac{C(v)}{v^{1/3}} + \frac{C(u)}{u^{1/3}} \right)$$

where:

- k = Boltzmann constant = 1.38066×10^{-16} ergs/K
- T = absolute temperature (K)

- **Turbulent diffusion** - turbulent eddies carry particles across streamlines to contact other particles

$$K_{TD}(u, v) = \frac{3Z}{4\pi} (v^{1/3} + u^{1/3})^3 \left(\frac{\epsilon_T \rho_g}{\mu_g} \right)^{1/2}$$

where:

- ϵ_T = turbulent energy dissipation rate
- $1.29 \leq Z \leq 5.65$

- **Turbulent inertia** - particles expelled from turbulent eddies impact other particles

$$K_{TI}(u, v) = Z' (v^{1/3} + u^{1/3})^2 |u^{2/3} - v^{2/3}| \frac{\rho_p}{\mu_g} \left(\frac{\epsilon_T^3 \rho_g}{\mu_g} \right)^{1/4}$$

where:

$$0.188 \leq Z' \leq 0.204$$

The Cunningham slip correction factor, $C(v)$, that arises in these various expressions for the collision kernels to account for deviations from continuum mechanics is empirically derived from data for spherical particles. Many different expressions have been given for this correction factor. A commonly used one is:

$$C(v) = 1 + Kn(1.142 + 0.588 \exp(-0.999 / Kn))$$

$$Kn = \frac{2\lambda}{\left(\frac{6v}{\pi}\right)^{1/3}}$$

The collision kernels and the slip correction factor are shown in Fig. 2.3-1 and Fig. 2.3-2 as functions of particle size for a particular set of circumstance (pressure, temperature, etc.).

In many circumstances, one of the mechanisms of coagulation is dominant. There are other circumstances in reactor accident analyses in which several coagulation mechanisms act with similar magnitudes. This gives rise to the issue of addition of kernels. Often kernels are simply added. In other cases more complicated summations are used such as:

$$K_{\text{total}}(u, v) = K_B(u, v) + K_g(u, v) + \sqrt{K_{\text{TD}}^2(u, v) + K_{\text{TI}}^2(u, v)}$$

Research in aerosol physics includes efforts to develop more defensible descriptions of the combined effects of simultaneous coagulation mechanisms.

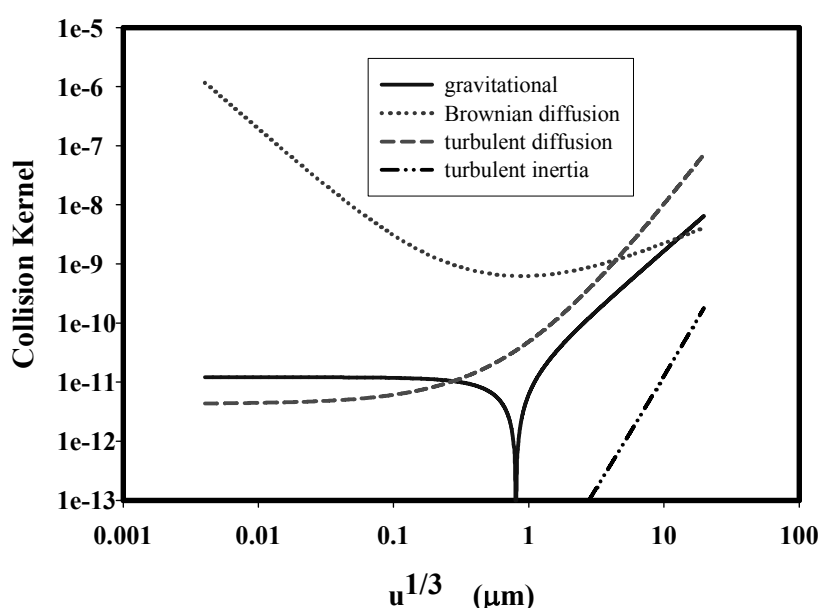


Fig. 2.3-1 Example collision kernels for various mechanisms of coagulation

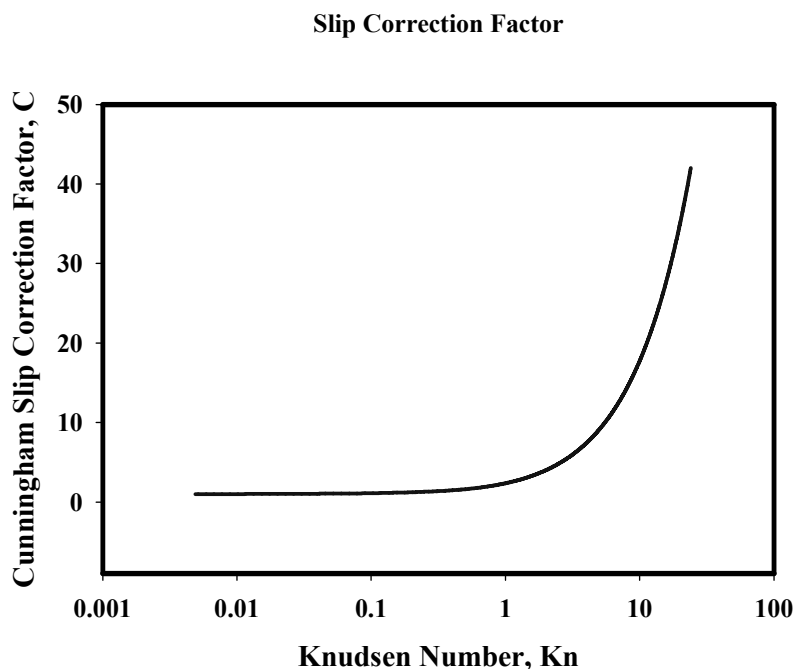


Fig. 2.3-2 Cunningham slip correction factor as a function of Knudsen number

Other coagulation mechanisms can be identified, such as laminar shear. These are not often included in coagulation models for nuclear aerosols. One of the additional coagulation mechanisms of current research interest is coagulation effects of electrostatic charging of aerosol particles. In most aerosol analyses, it is assumed that the average charge on aerosol particles is zero and the distribution of charges on particles is a Boltzmann distribution with zero mean. Certainly, this is what is expected in most laboratory tests including those used to validate aerosol behaviour models. But, in the highly radioactive environment of a reactor accident, there can be net charging of aerosol particles. The charging takes place because of the intense radiation field that produces ions in the atmosphere. The irradiation of the atmosphere produces equal amounts of positively and negatively charged ions. But, positive and negative ions have different mobilities. In air, negative ions are more mobile than positive ions. Consequently, aerosol particles in air are bombarded with higher fluxes of negative ions and can develop a net negative charge. The actual value of the charge depends on the particle size. The charge is also dynamic. The net charge on any given particle fluctuates with time. Strong, long-range electrostatic forces between particles with net charge could have a dramatic effect on coagulation. These effects under accident conditions are elements of current research.

2.3.2 *Growth by condensation*

The two principal mechanisms of aerosol growth, as opposed to aerosol formation, are condensation upon an initially existing particle, and agglomeration/coagulation. The former process usually takes place on a faster timescale than the latter except for the situation following homogenous nucleation, when particle sizes are small but number densities are very high.

The aerosol growth mechanism of condensation on existing particles is sometimes referred to as gas phase conversion. It includes both heterogeneous nucleations, where the initial seed particles are comparable in size to but energetically favoured over the embryos of homogeneous nucleation, as well as condensation upon larger particles, such as takes place in cooler parts of the reactor circuit and in the containment. Chemical reaction between the gas phase and the particle surface is also possible but is not considered

here. A formula frequently used in safety codes to calculate the condensation rate on existing particles is that due to Fuchs and Sutugin [7], which covers both the high and low-Knudsen number ranges:

$$F = 2\pi D d_p (n_0 - n_d) \left(\frac{1 + K_n}{1 + 1.71 K_n + 1.333 K_n^2} \right) \quad (5)$$

where F is the number of molecules condensing on the surface of the particle of diameter d_p in unit time, D is the diffusion coefficient, n_0 and n_d are the molecular concentrations of the condensing species in the bulk gas and at the particle surface respectively, and Kn is the Knudsen number. When the particle is small the effect of the curvature upon the effective saturation pressure at the droplet surface must be taken into account. A rearrangement of equation (2), applied to particles of size other than the critical droplet size, yields for the difference between the vapor pressure over a curved surface and that over a plane surface (the Kelvin effect)

$$p_{drop} = p_{sat} \exp \left(\frac{4\sigma v_{liq}}{k_B T d_p} \right) \quad (6)$$

where v_{liq} is the liquid specific volume and σ the surface tension. This formula can be used to calculate the bulk saturation ratio necessary to induce condensation on droplets of a given size. Smaller droplets are seen to require higher saturation ratios in order to grow by condensation.

For the case of heterogeneous nucleation, where the initial particle radius r_p is of the same order as the critical droplet radius r_{crit} it can be shown from the above equations that the rate of condensation is proportional both to $(S-1)$, where S is the saturation ratio, and to $r_p - r_{crit}$. Hence condensation takes place preferentially to the larger seed particles.

Depending on the deposition process it is possible for a given class of particles to derive expressions for the rate of particle growth. Friedlander [8], for instance, tabulates growth laws for particles of a given diameter depending on the condensation mechanism (diffusion, surface reaction etc.). Such growth laws may then be applied to calculate e.g. the lifetime of a droplet drying out in an unsaturated atmosphere of saturation ratio $S < 1$. The Langmuir equation for the lifetime t of a droplet shrinking from an initial diameter d_i to a final diameter d_f is

$$t = \frac{\rho R T (d_i^2 - d_f^2)}{8 D M p_{sat} (1 - S)} \quad (7)$$

where M is the molecular weight of the condensing species. Such lifetimes are usually short compared with the timescales typical of containment analysis.

While particle translation is strongly damped by viscous forces for small particles, and thus has little effect on condensation, heat transfer is an important consideration in particle growth by mass transfer. Condensation on particles adds thermal energy, raising the particle temperature and hence the saturation pressure. The increasing saturation pressure then acts to limit the condensation rate. Mason [9] proposed a correction factor f_M to equation (5) to account for heat transfer limitation of the condensation rate. It is widely used in safety codes and is calculated from

$$f_M = \left(1 + \frac{p_{sat}}{kT} L D \left(\frac{LM}{RT} - 1 \right) \right)^{-1} \quad (8)$$

where k is the gas phase thermal conductivity and L is the latent heat of condensation.

The specific case of hygroscopic particles in a humid containment atmosphere is considered in more detail in a separate subchapter of this report.

2.4 Aerosol Growth as a Result of Hygroscopicity

Aerosol particles can also grow as a result of water adsorption. All aerosol materials exhibit some amount of hygroscopicity. That is, they can absorb water vapor from the ambient atmosphere. For many aerosol materials, this hygroscopicity amounts to the absorption of little more than a monomolecular layer of water on the surfaces of primary particles that have coagulated to form a larger aerosol particle. Some materials, those with high water solubility such as CsI and CsOH, are much more hygroscopic. They are, in fact, 'deliquescent' and will absorb and dissolve in water until the equilibrium vapor pressure of the solution is equal to the partial pressure of water vapor in the ambient atmosphere. This water absorption causes the particles to grow and the growth can be quite dramatic in the case of pure CsOH or CsI particles. An example calculation of the growth of a CsOH particle initially $2.0\ \mu\text{m}$ in diameter to its equilibrium size, $D_p(\text{eq}) = 8.83\ \mu\text{m}$, is shown in Fig. 2.4-1. What is noteworthy in this figure is the time for growth of the particle. Particle growth to the equilibrium size can occur in seconds. Because of the so-called hygroscopic growth, such particles will settle more rapidly in a humid environment than would be otherwise expected based on their initial sizes and growth by coagulation.

The difficulty encountered in taking hygroscopic growth of particles into account in reactor accident analyses is that seldom are there any aerosol particles that are purely deliquescent in nature. CsOH, CsI, and other very hygroscopic materials will be co-agglomerated with other far less hygroscopic materials. They may, in fact, make up only a small fraction of the mass of any aerosol particle and be buried deep within a matrix of primary particles that have little ability to absorb water. Water absorbed in these composite particles may affect shape factors by filling voids in the composite particle, but may not amount to sufficient growth of the particle to greatly affect deposition and settling characteristics.

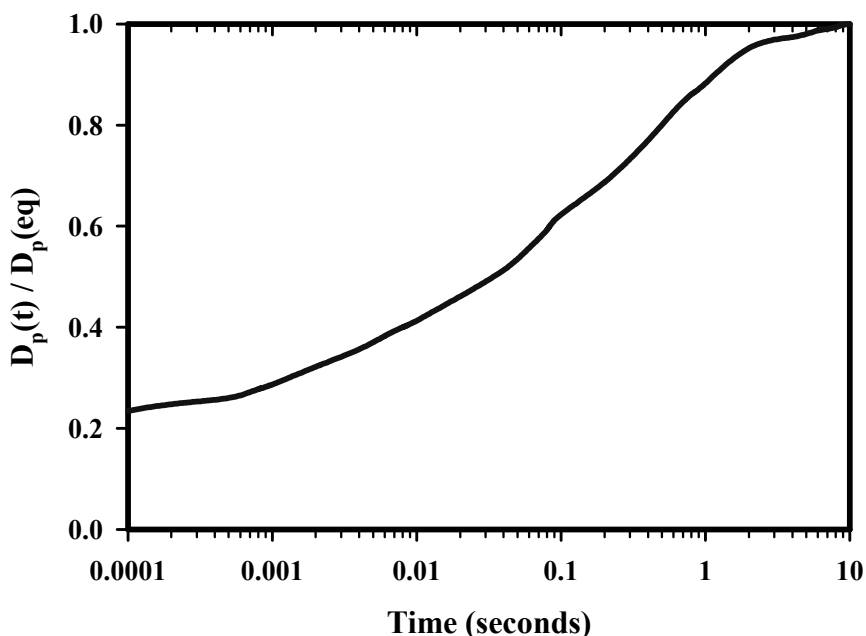


Fig. 2.4-1 Hygroscopic growth of a CsOH particle initially $2\ \mu\text{m}$ in diameter in an atmosphere with relative humidity of 99 % at 363 K

2.5 Fractal Nature of Aerosols

Aerosol particles are quite small and a substantial fraction of the atoms or molecules that make up an aerosol particle are on the particle surface. As a consequence, aerosol particles are quite reactive chemically. When two particles encounter one another, Van der Waals forces and even chemical reactions between particles make it quite likely that the particles will adhere. There typically are not opportunities for multiple encounters among two particles so when the particles adhere, they do not necessarily adopt a minimum energy configuration. In fact, agglomeration of aerosol particles leads to composites that have fractal geometries. That is, the particle sizes are not proportional to the cube root of the volume of material making up the composite. Under conditions of predominantly coagulation by Brownian diffusion, particle dimensions are often found to be proportional to about the square root of the volume of the composite. As the composites age and sinter, the proportionality evolves toward the usual cube root proportionality.

An important element of current aerosol research is the prediction of fractal characteristics of aerosol particles. Interest in the fractal geometry arises because it can affect particle behaviour. The equations of aerosol coagulation (and as discussed later aerosol deposition) have been derived for perfectly dense spherical particles. Since the real particles do not have this geometry and are not perfectly dense, correction factors have to be introduced into the equations. Two correction factors, called shape factors, are commonly introduced:

χ = dynamic shape factor

γ = collision shape factor

The dynamic shape factor accounts for the higher drag of a nonspherical, porous particle. The collision shape factor accounts for the greater spatial extent of a nonspherical particle. When the envelope of a particle is spherical, but the particle is not perfectly dense, the dynamic shape factor and the collision shape factor are equal but not necessarily equal to one. Aerosols in humid environments such as those expected in reactor containment do tend to have spherical envelopes. In the reactor coolant system, such spheroidization of the particles cannot be anticipated and the dynamic and collision shape factors can be quite different.

It is difficult now to predict shape factors for particles. Often test data are used to 'back calculate' shape factors. This is usually done assuming that the shape factors will be independent of particle size which is known not to be the case. There is no assurance that the shape factors derived in this way will be applicable to the analysis of reactor accidents.

2.6 Aerosol Deposition

The natural attenuation of radioactive material available for release from nuclear power plants during accidents occurs because aerosol particles will deposit on surfaces in the reactor. Aerosols deposit on surfaces because they cross stream lines of flow over the surfaces or because they extend far enough to intercept the surface even when the particle center of mass is following a streamline. Van der Waals forces, surface tension forces and even chemical reactions between particles and the surfaces can bind particles to the surfaces when the velocity of impact is sufficiently low, as it usually is.

The rates of aerosol deposition on surfaces are often characterised in terms of 'deposition velocities' which are coefficients that relate the particle flux to the particle concentration in the gas phase:

$$\frac{1}{A} \frac{dN(v)}{dt} = V_d(v)n(v)$$

where:

$\frac{1}{A} \frac{dN(v)}{dt}$ = flux of particles of volume v to a surface

$V_d(v)$ = deposition velocity of particles of volume v

$n(v)$ = number concentration of particles of volume v in bulk gas phase

Processes that can lead to particle deposition include:

- gravitational settling
- diffusion to surfaces
- turbulent deposition
- inertial deposition
- phoretic processes

2.6.1 *Gravitational settling and diffusion*

Gravitational settling and diffusion nearly always affect aerosols. Gravitational settling affects the larger particles most:

$$V_g(v) = \frac{\rho_p g C(v) \left(\frac{6v}{\pi} \right)^{2/3}}{18\mu_g \chi}$$

$V_g(v)$ = gravitational deposition velocity (cm/s)

μ_g = gas viscosity (g/cm•s)

g = gravitational acceleration (cm/s²)

ρ_p = particle material density (g/cm³)

Of course, gravitational deposition only occurs on the upward projections of surfaces.

Diffusion affects the smaller particles the diffusion coefficient for aerosol particles is:

$$D(v) = \frac{C(v) k T}{3\pi\mu_g \left(\frac{6v}{\pi} \right)^{1/3} \chi}$$

The diffusive deposition velocity depends, of course, on geometry and flow conditions. Van der Vate suggests for stagnant enclosures:

$$V_{dif} = 0.22 D^{0.735} \quad (\text{cm / s})$$

where D is in units of cm^2/s . Gravitational deposition velocities and diffusive deposition velocities are shown in Fig. 2.6-1 as functions of the equivalent spherical particle diameter. Clearly, when these two deposition processes are summed, there will be a particle size range of minimum deposition velocity. This is quite characteristic of aerosol deposition when two or more deposition processes are operative. The particle size corresponding to the minimum total deposition velocity is often called the “maximum penetration particle size”. The consequence of having such a minimum in the deposition velocity is that particle deposition can not only reduce the total aerosol concentration, it can also affect the size distribution of particles that remain in the gas phase. Deposition preferentially removes larger and smaller particles, so the size distribution is narrowed around the maximum penetration particle size.

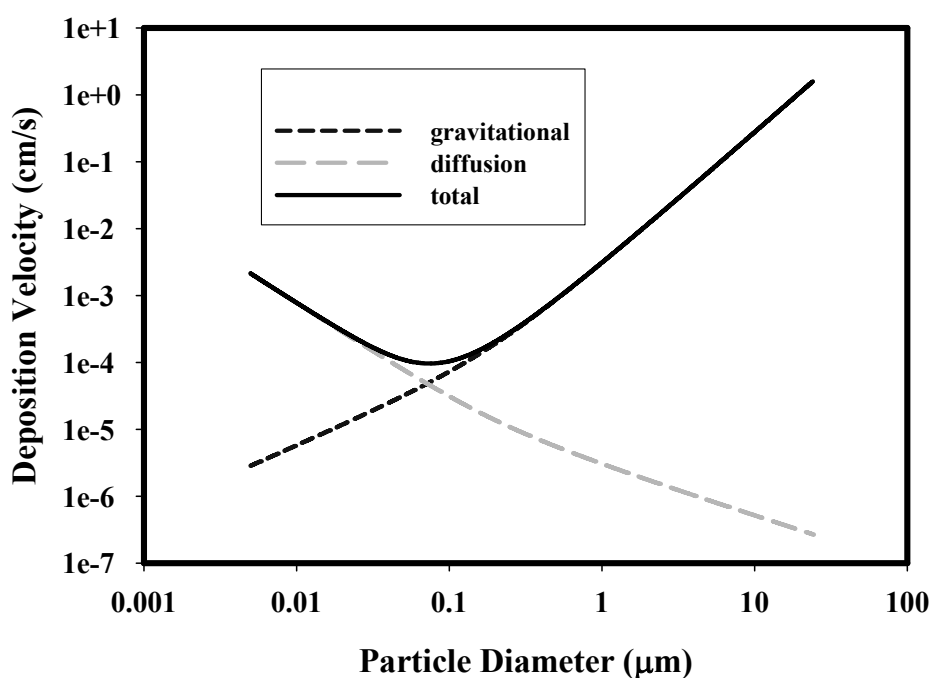


Fig. 2.6-1 Comparison of deposition velocities for particular circumstances

Convection and especially turbulent convection can greatly enhance particle deposition. Turbulent deposition velocities used in reactor accident analysis models are nearly all based on empirical correlations of data. The most notable use of empirical correlations for turbulent deposition is deposition of aerosol in straight pipe flow.

2.6.2 *Inertial deposition of aerosol particles*

Aerosol-laden flows especially in the reactor coolant systems follow tortuous pathways. Whereas the gas phase responds promptly to the accelerations caused by obstacles like bends, contractions and expansions in the flow path, the responses of aerosol particles are delayed by inertia. Time is required for the velocity of the particle in the direction of an obstacle to be arrested and the particle accelerated in the new direction of gas flow. When particles are too massive to do this, they impact and presumably adhere to the obstacle surface. This is often called 'inertial particle deposition'.

Flow patterns in the vicinity of an obstacle can be quite complicated especially under turbulent flow conditions. It has been common, then, to use correlations of experimental data to account for inertial particle deposition in bends, contractions and expansions of flow paths. The independent variable in the

correlations is usually the Stokes number which is the ratio of the distance required to arrest the motion of a particle in the direction of the obstacle to some characteristic dimension of the flow path:

$$\text{Stk} = \frac{C(v) \rho_p D_p^2 v_g}{9 \mu_g L \chi}$$

where:

- Stk = Stokes number (-)
- C(v) = Cunningham slip correction factor (-)
- ρ_p = particle material density (g/cm³)
- D_p = particle diameter (cm)
- v_g = gas velocity (cm/s)
- μ_g = gas viscosity (g/cm•s)
- L = characteristic dimension of flow configuration (cm)

The dependent variable in the correlations can be either the fraction of particles of a specified size that deposit in the flow field, $\eta(D_p)$, or the fraction that successfully negotiate the path through the change in the flow field. Some notable correlations are:

- Correlation of deposition efficiency in turbulent flow through a bend:

$$\log_{10} [1 - \eta(D_p)] = -0.963 \text{ Stk}$$

where the Stokes number is defined in terms of the hydraulic diameter of the pipe.

- Deposition efficiency in a contraction of the flow path from a diameter D_i to a diameter D_o :

$$1 - \frac{\sqrt{\eta(D_p)}}{1 - \left(\frac{D_o}{D_i}\right)^2} = 1.721 - 8.557x + 2.227x^2$$

$$x = \sqrt{\text{Stk}} \left(\frac{D_o}{D_i}\right)^{0.31}$$

- Deposition efficiency from a vena contracta:

$$\eta(D_p) = \left[1 - \left(\frac{D_o}{D_i}\right)^2 \right] \left\{ 1 - \left[1 + \text{Stk} + 0.617 \left(\frac{D_o}{D_i}\right)^2 \text{Stk} \right]^{-1} \right\}$$

for $0.18 < \text{Stk} < 2.03$

$$0.17 < \left(\frac{D_o}{D_i}\right)^2$$

There has been a major dependence in reactor accident analyses on experimental determinations of deposition velocities. Mass transfer to heat transfer analogies are very difficult to justify for aerosols because of the very high Schmidt numbers for aerosols of interest. Recently, a major thrust of aerosol research has been to analyse turbulent aerosol deposition in great detail using computation fluid dynamics techniques. Often these studies are done for turbulent deposition along with other deposition mechanisms. The studies do, no doubt, contribute greatly to the understanding of aerosol behaviour. Unfortunately, the computational labour associated with these detailed models is incompatible with most accident analysis codes. Indeed, even replicating published calculations would entail more labour than is usually available to support improved aerosol modelling in reactor accident analysis codes. It would be most useful if investigators exploring the details of aerosol deposition would correlate their findings into simplified expressions that were similar to the correlations now used in the accident analysis models. Then, results of these detailed analyses could be incorporated into accident analysis models promptly.

2.6.3 *Phoretic deposition processes*

A final, important category of aerosol deposition process is made up of the phoretic processes - usually thermophoresis, which is particle movement in a thermal gradient, and diffusiophoresis, which is particle movement in the flux of a condensing vapor such as steam. Both of these phoretic effects arise because the gas impinging on one side of the particle imparts more momentum than that impinging on the other side. Thermophoresis arises because of temperature differences between the gas phase and the surfaces exposed to aerosol-laden gases. Such temperature differences can be quite large in the coolant system of a reactor during a severe accident. Very hot aerosols and gases emerge from the core region of the reactor and encounter large areas of cool surface. The thermophoretic deposition of aerosols on these surfaces was vigorously researched thirty years ago. From this research emerged what has come to be called the Talbot interpolation formula for the thermophoretic deposition velocity:

$$V_{\text{therm}} = - \frac{\frac{2\mu_g C_s(v)}{\rho_g \chi} \left(\frac{k_g}{k_p} + C_t \text{Kn} \right)}{(1 + 3C_m \text{Kn}) \left(1 + \frac{2k_g}{k_p} + 2C_t \text{Kn} \right)} \nabla \ln T$$

where:

$$C_s = 1.128$$

$$C_m = \frac{(2 - \alpha_m)}{\alpha_m}$$

$$C_t = \frac{15(1 - \alpha_t)}{8 \alpha_t}$$

α_m = momentum accommodation coefficient

α_t = thermal accommodation coefficient

k_g = thermal conductivity of the gas phase

k_p = thermal conductivity of the aerosol particles

The thermophoretic deposition velocity is not an especially strong function of particle size. It does depend on the thermal conductivity of the aerosol particles relative to the thermal conductivity of the gas phase.

Seldom is this particle thermal conductivity well known relative to the ability to estimate the thermal conductivity of the gas phase. Usually bulk material thermal conductivities are used though it is recognised that this may be quite in error. The thermophoretic deposition velocity also depends on accommodation coefficient for gas impinging on particle surfaces. There does not appear to be much of a useful data base on such accommodation coefficients and there are not readily accessible theories for estimating accommodation coefficients. Fortunately, the velocity is not especially sensitive to accommodation coefficients in the plausible range of possible values.

Recently, there has been a renewed interest in thermophoresis. Researchers have obtained detailed solutions of approximate forms of the Boltzmann equation to assess thermophoretic deposition of particles. Their numerical analyses do identify ranges where particles will move up rather than down the thermal gradient. This is called 'negative thermophoresis'. Their numerical results show excellent agreement with data taken in regimes predicted to be challenging to the theory. It is unlikely, however, that such detailed analyses will ever find their ways into accident analysis computer codes. The Talbot interpolation formula also shows good agreement with the available experimental data though the formula will not predict the negative thermophoresis found possible in the more detailed analyses of thermophoresis.

Diffusiophoresis is not usually encountered in the reactor coolant system during a reactor accident since large amounts of vapor are not condensing on surfaces in the reactor coolant system. Diffusiophoresis can arise in the containment of a reactor under accident conditions. It is an especially important aerosol removal process in the AP600 reactor where the steel containment is cooled by water on the outside. The usual form of the diffusiophoretic deposition velocity is:

$$V_{\text{phor}} = - \left(1 + \frac{C(v)}{\chi} \sigma_{12} \left(1 - \frac{P_{\text{H}_2\text{O}}}{P_{\text{Total}}} \right) \right) \frac{D(\text{H}_2\text{O})}{P_{\text{Total}} - P_{\text{H}_2\text{O}}} \nabla P_{\text{H}_2\text{O}}$$

where:

- V_{phor} = diffusiophoretic deposition velocity
 σ_{12} = scattering kernel
 $P_{\text{H}_2\text{O}}$ = partial pressure of the condensing vapor which is usually steam
 $D(\text{H}_2\text{O})$ = diffusion coefficient of the condensing vapor

A variety of expressions for the scattering kernel have been proposed. Williams has formulated a very general expression for the kernel to account for diffuse, specular, Lambert and backward reflection of molecules impinging on the particle surface. Others have considered both momentum and energy accommodation in the formulation of the scattering kernel. Unfortunately, the nature of the scattering of gases from aerosols in reactor accidents is not well known and such sophisticated models are seldom found in reactor accident analysis codes.

2.7 Resuspension of Deposited Particles

Aerosol particles deposited on surfaces can be resuspended in the gas phase. Resuspension can occur when there is:

- a sudden increase of gas flow over the surface
- shock or vibration of the deposition surface

Experimental data on resuspension shows that increased gas flow and shock or vibration of the deposition surface can act synergistically to cause accentuated resuspension.

Events are expected in reactor accidents that lead to resuspension of deposited particulate. These events include:

- sudden generation of steam when core debris relocates from the core region to the lower plenum of the reactor vessel,
- steam generation associated with attempts to quench the core,
- rupture of the reactor pressure vessel,
- violent fuel-coolant interactions such as steam explosions, and
- hydrogen combustion events.

Experimental investigations of resuspension phenomena have focused on the effects of sudden increases in gas flow. These studies have shown that gas flow increases produce a significant initial resuspension followed by a longer term, much lower rate of particle resuspension. The studies also show that the aging of aerosol particles on surfaces makes resuspension more difficult.

The first models of resuspension were based on a balance between the forces holding particles to a surface (Van der Waals forces, surface tension, chemical bonding, etc.) and lift forces from the flowing gas. Such models could predict the initial, intense resuspension, but these early models could not predict the longer term, low intensity resuspension. More recent models have approached modeling resuspension in two ways:

- turbulent eddies are predicted to penetrate the laminar boundary layer to the surface and scour deposited particles from a surface region approximately the size of the penetrating eddy,
- particles vibrate in a potential well created by the adhesive forces. Episodic fluctuations in the vibrations put particles in a state where lift forces can overcome the weakened adhesive forces.

Even more recently, resuspension research has focused on the potential for depositing particles to impart sufficient momentum to already deposited particles to cause resuspension.

2.8 Aerosol Removal by Engineered Safety Systems

The natural aerosol deposition processes discussed above will eventually cleanse the gas phase of particulate. These processes often operate over a longer time scale than the progression of reactor accidents. Fortunately, engineered safety systems, installed in reactor containments to reduce pressure during design-basis loss of coolant accidents, are very effective also at removing aerosol from the containment atmosphere. Important engineered safety features are:

- containment sprays
- steam suppression pools
- fan coolers

Sprays

Sprays flood the containment atmosphere with water droplets. The size distribution of water droplets from a type of spray nozzle commonly found in pressurised water reactor is shown in Fig. 2.8-1. The spray rates

can be quite high so the number of density of water droplets is high. After an initial transient when spray droplets condense excess steam in the containment atmosphere, spray droplets remove aerosol particles from the atmosphere by a combination of three processes - diffusion, interception and impaction. The capture of particles by falling spray droplets is usually expressed in terms of capture efficiency. This efficiency is the ratio of particles actually captured to the number of particles in the droplet path:

$$\epsilon(D_d, d_p) = \frac{4\Delta N(d_p)}{\pi D_d^2 n(d_p) L}$$

where:

$\epsilon(D_d, d_p)$ = capture efficiency for droplet of diameter D_d and particles of diameter d_p

$\Delta N(d_p)$ = number of particles of diameter d_p captured

L = droplet path length

Impaction describes the impact on droplets by particles that cannot follow the streamlines around the droplet. Of course, it is the larger aerosol particles that cannot follow these streamlines. A commonly used expression for the capture of these large particles is:

where:

$$Re_D = \frac{U_T \rho_g D_d}{\mu_g}$$

U_T = droplet terminal velocity

$$Stk = \text{Stokes number} = \frac{C(v) d_p^2 \rho U_T}{9 \mu_g D_d \chi}$$

δ = 0.25 to 0.75

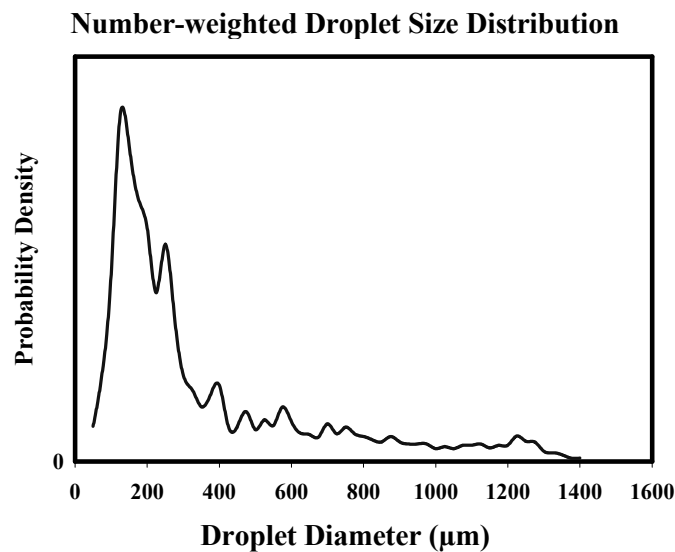


Fig. 2.8-1 Number-weighted droplet size distribution for a common containment spray

Interception occurs when the center of mass of a particle is following a streamline closer to the droplet surface than the particle radius. A common expression for the efficiency of interception is:

$$\begin{aligned}\epsilon(\text{int}) &= \frac{\epsilon(\text{int, visc}) + \text{Re}_D \epsilon(\text{int, pot})/60}{1 + \text{Re}_D/60} \\ \epsilon(\text{int, visc}) &= \frac{1.5(\gamma d_p / D_d)^2}{(1 + \gamma d_p / D_d)^{1/3}} \\ \epsilon(\text{int, pot}) &= \frac{3\gamma d_p}{D_d}\end{aligned}$$

A variety of expressions are available for estimating the collection efficiency due to diffusion. An example is:

$$\epsilon(\text{diffusion}) = \frac{4}{\text{Re}_D \text{Sc}} (2 + 0.557 \text{Re}_D^{1/2} \text{Sc}^{3/8})$$

where:

$$\begin{aligned}\text{Sc} &= \text{particle Schmidt number} = \frac{\mu_g}{\rho_g D_p} \\ D_p &= \text{particle diffusion coefficient} = \frac{C(v)kT}{3\pi\mu_g d_p \chi}\end{aligned}$$

The aerosol capture mechanisms are not entirely independent. A common expression for the combined effects of the three mechanisms is:

$$\epsilon(\text{total}) = 1 - [1 - \epsilon(\text{impaction})][1 - \epsilon(\text{interception})][1 - \epsilon(\text{diffusion})]$$

Total aerosol capture efficiencies for 1000 μm and 200 μm droplets as functions of aerosol particle size are shown in Fig. 2.8-2. The capture efficiency passes through a minimum for both droplet sizes. This, of course, means that spray droplets both remove particles and narrow the size distribution. The minimum varies in location with the size of the spray droplet. Accurate calculation of the effects of spray removal requires that the size distribution of the spray droplets be considered. This is not often done because it requires that the coagulation of the spray droplets during flight be calculated as well. Alternative mechanistic modelling has been developed based on recent analytical work; this modelling is described in Appendix 3.

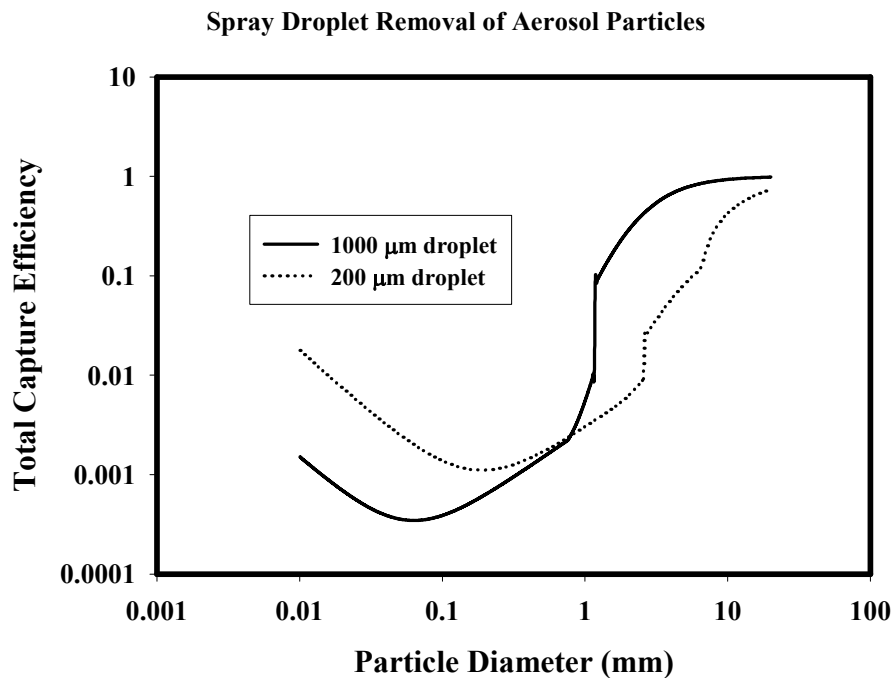


Fig. 2.8-2 Comparison of the capture efficiencies of 1000 and 200 μm droplets

2.8.1 Steam suppression pools

Calculation of the aerosol removal by steam suppression pools is quite involved. Much aerosol removal occurs during the formation of the bubble when diffusiophoresis occurs as steam condenses and impaction occurs at the stagnation of the flow against the growing bubble envelop. Once the bubble detaches and begins to rise in the pool, further aerosol removal can occur by diffusion and gravitational settling within the bubble. Diffusion within the bubble is resisted by expansion of the bubble as pressure head is lost during bubble rise. Vapor flow into the bubble when the water pool is near the boiling point can resist particle removal. Gases within the bubble circulate during bubble rise, so there can be aerosol removal by inertial deposition as aerosols are unable to follow streamlines of flow in the ellipsoidal bubble. Other removal mechanisms can arise. For instance, oscillation of the bubble can remove particles because of delay in the response of particles to changes in bubble shape.

Aerosol removal from gas bubbles sparging through water depends on the depth of the water, but can produce substantial decontamination. The decontamination is usually expressed in terms of the decontamination factor, DF:

$$DF = \frac{\text{aerosol mass concentration initially}}{\text{aerosol concentration in gas emerging pool}}$$

Decontamination factors calculated for gases sparging through the so-called 'T' quenchers in the steam suppression pools of boiling water reactors are shown in Fig. 2.8-3. Even a pool as shallow as about one meter will remove over 90 % of the particulate in the gas stream. It is to be emphasised that the removal also narrows the size distribution of the remaining aerosol around the maximum penetration aerosol particle size. This narrowing of the particle size distribution around a small particle size that is inefficiently removed by the combination of diffusion, gravitational settling and impaction mechanisms makes subsequent filtration processes for the residual aerosol much less efficient than would be expected based on the size distribution of the aerosol entering the suppression pool.

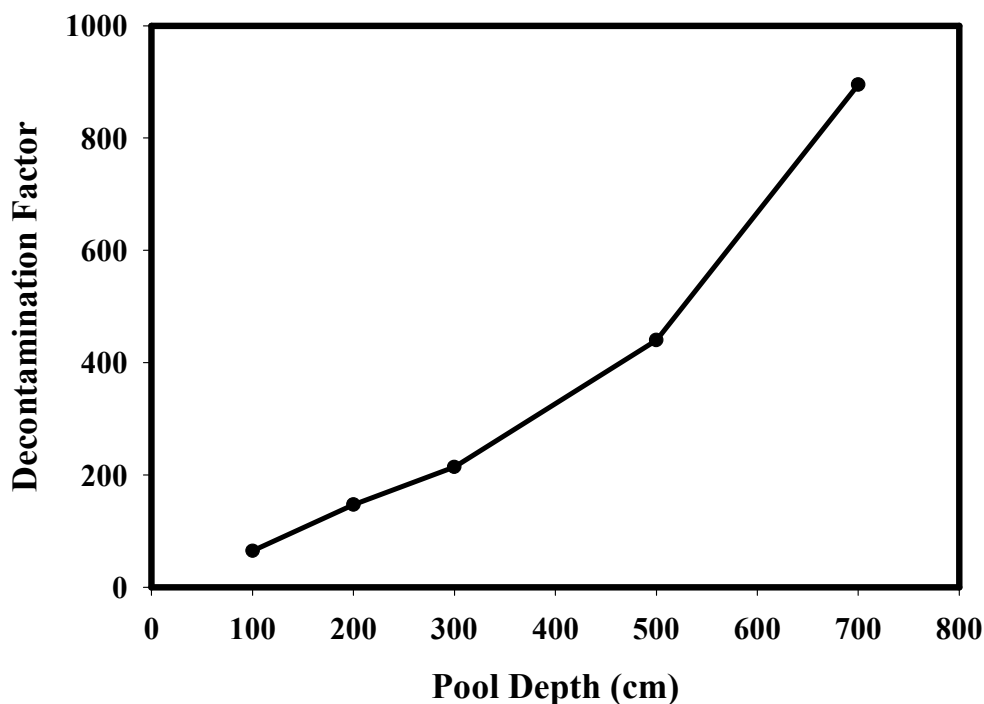


Fig. 2.8-3 Aerosol removal by sparging through a water pool

2.8.2 Fan coolers

Fan coolers can remove aerosol by thermophoresis and by the impaction of particles on rotating fans. Thermophoretic removal decreases with time as the depositing aerosol develop an insulating layer on the cool surfaces.

2.9 Aerosol Removal by Filtered Vents

A final protection against radioactive material released from reactors under accident conditions is to filter the gas stream. Three types of filters are commonly used:

- fibre filters used to protect particular locations such as the control room
- venturi scrubbers
- gravel bed filters

Fiber filters remove particles by trapping them. The overall penetration of a fresh fiber filter, i. e. before it is loaded with particles, can be expressed by:

$$P_f = \exp\left(-\frac{4\alpha L}{\pi(1-\alpha)d_f}E_{tot,f}\right)$$

- P_f = fraction of aerosol penetrating fiber filter
 α = volume fraction of fibers in filter, i.e. 1.0 - porosity
 L = thickness of fiber bed
 d_f = fiber diameter
 $E_{tot,f}$ = total efficiency of a single fiber at particle trapping

The efficiency of a fibre at trapping particles is calculated considering the mechanisms:

- gravitational settling
- inertial impaction
- interception
- diffusion
- thermophoresis
- diffusiophoresis

Electrostatic charging of the filter and particles can also be considered especially for radioactive aerosols. The filter collection efficiency η and the decontamination factor DF are related to the overall penetration by

$$\eta = 1 - P$$

respectively

$$DF = \frac{1}{P}$$

The overall penetration, the collection efficiency and the DF depend strongly on the particle size. The characteristics of the filter, like collection efficiency and pressure drop, change as mass is collected and reduces the porosity of the filter.

Venturi scrubbers precondition the aerosol by injecting water (about 1 liter of water per cubic meter of gas) along with gas through a constricting throat. Gas velocities can be as high as 120 m/s. The liquid water is “atomised” into small droplets at the high velocities. Water droplets can coagulate with the aerosol or otherwise capture the aerosol particles so that they are more efficiently removed by a subsequent filtration system which might be a water pool or a gravel bed.

Gravel beds remove particles by deposition onto the large surface area provided by the gravel. Submerged gravel beds use water to wash away deposited materials from the gravel.

Mechanistic models for the gravel bed filtration efficiency are based on the single grain capture efficiency, extended to a bed of particular size. The penetration of a fresh granular bed filter is given by

$$P_g = \exp\left(-\frac{3\alpha H}{2d_g} E_{tot,g}\right)$$

- P_g = fraction of aerosol penetrating gravel bed
- α = volume fraction of grains in filter, i.e. 1.0 - porosity
- H = gravel bed depth
- d_g = grain diameter
- $E_{tot,g}$ = total efficiency of a single grain at particle trapping

$E_{tot,g}$ for a single grain is comparable to the single fibre-capture efficiency used for fibrous filters. The particles are captured mainly by a combination of particle diffusion, interception and impaction.

2.10 Computer Modelling of Aerosols

The aspect of aerosol modelling that does pose computational challenges is the solution of the dynamic equation to describe the evolution of the aerosol size distribution as a result of particle coagulation. As discussed near the beginning of this chapter, the evolution of the size distribution is described by a complicated integrodifferential equation.

In the 1970's at the time of the Reactor Safety Study, this differential equation was solved using what were called "moment's methods". These methods involved hypothesizing a particle size distribution with undetermined parameters. Typically the lognormal size distribution was hypothesized. The mean and geometric standard deviation of the distribution were then determined through the solution of the differential equation consistent with conservation of mass. These methods were found through an extensive effort of experimental and analytical research to yield inadequate results during periods when aerosols were being injected into a pre-existing aerosol with a different chemical composition. This situation gave rise to multi-modal size distributions for the aerosol that could not be easily described by a single distribution with limited numbers of parameters.

Today, most accident analysis models solve the aerosol dynamic equation using what are called 'sectional methods'. Sectional methods were introduced in MAEROS and NAUA models for the first time. These methods divide the aerosol size distribution into a set of contiguous intervals. Each interval is characterised by a representative particle size. The differential equations are solved for these representative sizes. The methods do suffer from numerical diffusion that can be controlled to some extent by the judicious choice of the size bins. The sectional methods are not especially powerful in situations where vapors and steam are condensing on the aerosol particles. Williams and Loyalka (see Bibliography) provide further critique of these methods. For vapors and steam condensation fixed grid and moving grid methods were developed. The MGA (Moving Grid Analysis) is successfully applied in combination with the MAEROS model through a variety of tests. MAEROS/MGA are incorporated in codes like ASTEC, COCOSYS, CONTAIN and MELCOR.

2.11 Annotated Bibliography

This introduction has not been intended to be comprehensive and the literature cited in this bibliography is similarly incomplete. The works cited here are selected to provide an introduction to the field of aerosol physics pertinent to the issues of reactor accident analyses. Annotations are provided to assist the reader in the selection of documents of interest.

General aerosol physics

The classic reference in the field is:

- N.A. Fuchs, **The Mechanics of Aerosols**, Pergamon Press, 1964

Readers may find:

- S.K. Friedlander, **Smoke, Dust and Haze: Fundamentals of Aerosol Behaviour**, J. Wiley and Sons, 1977.

more readily digested. For a work with much greater mathematical sophistication, see:

- M.M.R. Williams and S.K. Loyalka, **Aerosol Science Theory and Practice with Special Applications to the Nuclear Industry**, Pergamon Press

These texts will provide an introduction to the topics discussed in this chapter as well as other topics not listed in this bibliography.

Nucleation

A good review of the experimental and analytical modeling of the nucleation of pure vapors is provided in:

- E. Honatan, **Theoretical and Experimental Research on Homogeneous Nucleation Phenomena, A State of the Art Report**, Catedra de Tecnologia Nuclear E.T.S. de Ingeniero Industriales, Madrid, 1991.

The upper and lower bounds on the rates of pure vapor nucleation are modelled in:

- H. Reiss, J.I.Katz, and E.R. Cohen, **J. Chem. Phys.**, **48** (1968)5553.

Aerosol hygroscopicity

An account of aerosol growth by water adsorption is found in:

- J. Jokiniemi, 'The Growth of Hygroscopic Particles During Severe Core Melt Accidents', **Nuclear Technology**, **83** (1988) 16.

Details on the derivation of models of hygroscopic growth of pure particles by water absorption including both mass and heat transfer are provided in:

- F.R. Newbold and N.R. Amundson, 'A model for Evaporation of a Multicomponent Droplet', **American Institute of Chemical Engineers, Journal**, **19** (1973) 22.

Fractal nature of aerosols

A modern discussion of fractal dimensionality of aerosols that will provide an introduction to a growing literature base is:

- M. Kostoglou and A.G. Konstandopoulos, 'Evolution of aggregate size and fractal dimension during Brownian coagulation', **J. Aerosol Science**, **32** (2001) 1399.

Cunningham slip correction factor

A recent derivation of the expression for the Cunningham slip correction factor from the Milliken oil drop experimental data and a discussion of other expressions is presented in:

- M.D. Allen and O.G. Raabe, **Aerosol Science and Technology**, **4** (1985) 269.

A more theoretical expression for the slip correction factor is provided by:

- W.F. Phillips, **Physics of Fluids**, **18** (1975) 1069.

Electrostatic charging of an aerosol in a radiation field

Radioactivity of the aerosol material and the presence of an intense radiation field is what makes nuclear aerosols different from aerosols encountered in other fields. The potential of electrostatic charging of aerosols by the radiation field is discussed in:

- C.F. Clement and R.G. Harrison, Enhance Localised Charging of Radioactive Aerosols, **J. Aerosol Science**, **31** (2000) 363.

Diffusive deposition in enclosures

- J.F. van der Vate, **Investigations into the Dynamics of Aerosols in Enclosures Used for Air Pollution Studies**, ECN-86, Netherlands Energy Research Foundation, Petten, The Netherlands, July 1980.

Turbulent deposition of aerosol

The classic study of aerosol deposition in smooth pipes is:

- B.Y.H. Liu and J.K. Agarwal, **J. Aerosol Science**, **5** (1974) 145.

Deposition in rough pipes is discussed in:

- L.A. Hahn, J.J. Stukel, K.H. Leong and P.K. Hopke, 'Turbulent Deposition of Submicron Particles on Rough Walls', **J. Aerosol Science**, **16** (1985) 81.

Inertial deposition of aerosols

Aerosol deposition in bends is discussed in:

- R.I. Crane and R.L. Evans, **J. Aerosol Science**, **8** (1977) 161.
- D.Y. Pui, F. Romay-Novas, and B.Y. Lui, 'Experimental Study of Particle Deposition in Bends of Circular Cross Section', **Aerosol Science and Technology**, **7** (1987) 301.
- C-J. Tsai and D.Y.H. Pui, 'Numerical Study of Particle Deposition in Bends of a Circular Cross-Section-Laminar Flow Regime', **Aerosol Science and Technology**, **12** (1990) 813.

Aerosol deposition in sudden contractions and expansions of the flow path is discussed in:

- G. Ahmadi and Q. Chen, 'Dispersion and Deposition in Turbulent Pipe Flow with Sudden Expansion', **J. Aerosol Science**, **29** (1998) 1097.
- Y.Ye and D.Y. H. Pui, 'Particle Deposition in a Tube with an Abrupt Contraction', **J. Aerosol Science**, **21** (1990) 29.

Aerosol deposition in a *vena contracta*:

- S.P. Belyaev and L.M. Levin, 'Investigation of Aerosol Aspiration by Photographing Particle Tracks Under Flash Illumination', **Aerosol Science**, **3** (1972) 127.

Thermophoresis

The Talbot interpolation formula is described in:

- L. Talbot, R.K. Cheng, R.W. Schefer and D.R. Willis, **J. Fluid Mechanics**, **101** (1980) 737.

Modern analyses that show instances of negative thermophoresis are:

- K. Yamamoto and Y. Ishihara, 'Thermophoresis of a spherical particle in a rarefied gas of a transition regime', **Physics of Fluids**, **31** (1988) 1421.
- S. K. Loyalka, 'Thermophoretic force on a single particle - 1. Numerical solution of the linearized Boltzmann equation', **J. Aerosol Science**, **23** (1992) 291.

Comparison of models to experimental data on thermophoresis is presented in:

- F. Zheng and E.J. Davis, 'Thermophoretic force measurement of aggregates of microspheres', **J. Aerosol Science**, **32** (2001) 1421.

Diffusiophoresis

The classic references on diffusiophoresis are:

- L. Waldmann and K. H. Schmitt, 'Thermophoresis and Diffusiophoresis' Chapter VI in **Aerosol Science**, C.N. Davies, editor, Academic Press, 1966.
- P. Goldsmith and F.G. May, 'Diffusiophoresis and Thermophoresis in Water Vapor Systems', Chapter VII in **Aerosol Science**, C. N. Davies, editor, Academic Press, 1966.

The scattering kernel in the expression for the diffusiophoretic deposition velocity is discussed in:

- M.M.R. Williams, **Z. Naturforsch.**, **27** (1972) 1798 and 1804.

Resuspension

An overall review of resuspension modeling and experiments is provided in:

- G. Ziskind, M. Fichman and C. Gutfinger, 'Resuspension of Particulates from Surfaces to Turbulent Flows - Review and Analysis', **J. Aerosol Science**, **26** (1995) 613.

A recent review of the issues of resuspension is:

- L. Biasi, A. de los Reyes, R.W. Reeks, and G.F. de Santi, 'Use of a simple model for interpretation of experimental data on particle resuspension in turbulent flows', **J. Aerosol Science**, **32** (2001) 1175.

The issue of resuspension caused by the impaction of other aerosol particles is addressed in:

- W. John, D.N. Fritter and W. Winklmayr, 'Resuspension induced by impacting particles', **J. Aerosol Science**, **22** (1991) 723.

Spray removal of aerosol

- D.A. Powers and S.B. Burson, **A Simplified Model of Aerosol Removal by Containment Sprays**, NUREG/CR-5966, Sandia National Laboratories, Albuquerque, NM, June 1993.

Decontamination of aerosol by steam suppression pools

- D.A. Powers, **A Simplified Model of Decontamination by BWR Steam Suppression Pools**, NUREG/CR-6153, Sandia National Laboratories, Albuquerque, NM, May 1997.

Computer modelling of aerosol coagulation

Some of the complexities of the aerosol dynamic equation are described in:

- R.L. Drake, 'A General Mathematical Survey of the Coagulation Equation', in **Topics in Current Aerosol Research**, Volume 3, G.M. Hidy and J.R. Brock, editors, Pergamon Press, 1972.

The sectional method for calculation of aerosol coagulation is described in:

- F. Gelbard and J.H. Seinfeld, 'Simulation of Multicomponent Aerosol Dynamics', **J. Colloid Interface Science**, **78** (1980) 485.

For a comparison of moments methods, sectional methods and other methods, see:

- C. Seigneur, A.B. Hudshwekyj, J.H. Seinfeld, K.T. Whitby, E.R. Whitby, J.R. Brock, and H.M. Barns, 'Simulation of aerosol dynamics: a comparative review of mathematical models', **Aerosol Science and Technology**, **5** (1986) 205.

An attempt to overcome the problems of numerical diffusion is discussed in:

- T.H. Tsang and A. Rao, 'Comparison of different numerical schemes for condensational growth of aerosols', **Aerosol Science and Technology**, **9** (1988) 271

3. ACCIDENT PHENOMENOLOGY

3.1 Formation and Growth

3.1.1 Phenomena considered and state of knowledge

Successive stages in core degradation during a severe accident in a PWR or BWR result in the release of both vapors and aerosol particles which differ in composition depending on their dominant source, be it control rod and fuel burst events, cladding oxidation, fuel heat-up accompanied by geometric changes, molten pool formation, or reflooding of the degraded core. Temperatures in the core region are generally considerably higher than those in the plenum above the core, which in turn are higher than those in the primary circuit. Concentrations are also highest in the core region, and hence the vapor/aerosol mixture carried by the steam/hydrogen stream from the core to the assumed breach in the primary system and out into the containment vessel or the environment undergoes a succession of cooling transients which induce both condensation of vapors upon existing aerosols (heterogeneous nucleation) and the formation of new particles (homogeneous nucleation). Competing with the former process is condensation upon structures, which serves to remove material from the carrier stream, at least temporarily. The two processes mentioned do not alter the elemental content of the carrier stream, but instead affect removal by vapor condensation further downstream and also the mass, size distribution and chemical composition of the suspended aerosol and thus its deposition behaviour. The size distribution of the aerosol is also strongly affected by agglomeration, and in a simulation of fission product transport during a severe accident it is necessary to take into account all the formation and growth processes mentioned.

3.1.1.1 The state-of-the-art report, 1994

At the time of writing of the State of the Art report on Primary System Fission Product Release and Transport [1] physically-based models of all these processes were already available. The SOAR included a survey of the models available in the literature for homogeneous and heterogeneous nucleation, for vapor condensation on aerosols, and for aerosol agglomeration, and noted that these and other models had been incorporated in circuit codes such as VICTORIA, which were being applied both to separate-effect test series e.g. FALCON and to reactor sequences. In the absence of substantial experimental data on the formation and growth of nuclear aerosols during transport under severe accident conditions the SOAR could only detail the competing or reinforcing processes at work in such formation and growth without being able to come to firm conclusions on their relative importance and combined effect under given thermal-hydraulic conditions.

Concerning growth through **Vapor interaction** with aerosols the SOAR concluded that while safety importance (in the circuit) was high, understanding was incomplete. *There is a clear need for vapour-aerosol interaction data. Vapor-surface interaction tests may need to be done with more complex FP species. Data on appropriate species will hopefully come from PHÉBUS FP tests.* There is nothing more about this topic in Chapter 5 of the SOAR, but in the appropriate section of Chapter 4, Section 4.6, we read “Interactions of fission product vapors with primary circuit surfaces and aerosols can substantially modify the magnitude and nature of the source term to the containment. However, the relative importance of the processes is uncertain: while the extensive surface area of the aerosol surfaces indicates that vapor-aerosol interactions should predominate, heat and mass transfer limitations can considerably affect the balance. ... few studies have addressed vapor interactions with suspended aerosols.

Consideration of timescales indicates that the latter processes will be governed by diffusion limitations rather than chemical kinetics. Lack of data on the diffusion of fission product vapors through reactor gases prevents accurate prediction of condensation phenomena. (Representative) data (e.g. from PHÉBUS FP) should guide the requirement for separate-effects studies and the development of more sophisticated models to treat these processes (vapor condensation on suspended aerosols and on deposits)."

Aerosol nucleation and growth, on the other hand was judged by the writers of the SOAR to be of medium safety importance. Concerning the state of knowledge, existing data appeared to be adequate but further modelling or review/consolidation of data was required. *The need for detailed nucleation/growth modelling in the codes has not been clearly established.* Chapter 4 provided more detail and recommended further assessment. *The importance of mechanistically modelling aerosol nucleation has not been assessed. At issue is whether ad hoc treatments of nucleation phenomena are adequate for the purposes of reactor safety analyses. We recommend that coordinated efforts be initiated to determine the importance of aerosol nucleation ... to RCS fission product transport analyses. These assessments would provide the basis for determining if experiments are needed in addition to those already performed or planned.*

In another section the SOAR writing group offered a more general comment on the impact of thermal-hydraulic and core-degradation uncertainties on FP release and RCS transport: *We view these issues as sufficiently important to be considered regarding release and transport analyses and experimental design.* The following sections of this sub-chapter will attempt to review the progress made since the appearance of [1] in the understanding and prediction for nuclear safety purposes of aerosol formation and growth, including vapor condensation on aerosols, nucleation and agglomeration. A final section on containment aerosols will highlight the similarities and differences between the formation and growth of such aerosols and of those in the primary circuit, in the light of PHÉBUS FP results and those of ISPs such as ISP-37 and ISP-44. The subchapter ends with conclusions and some proposed recommendations.

3.1.1.2 Theory of formation and growth

This section presents some of the principal equations used to model the formation and growth aerosols for nuclear safety purposes, together with remarks on their physical basis and applicability. A number of references in the open literature are also included. For further details on the practical calculation of the formation and growth processes considered in safety evaluations the theoretical manuals of the most widely used codes may also be consulted.

Formation

Aerosol particles may be formed by a wide range of processes such as gas-phase chemical reactions, attrition of solids, resuspension etc. Here we will consider the theoretically and practically important topic of homogeneous nucleation, the formation of gas-borne particles by condensation of a supersaturated vapor. Binary and ternary nucleation, in which several vapor species condense together, is important eg in atmospheric science, but is not normally considered in nuclear safety. Vapor condensation onto existing seed particles of another material, termed heterogeneous nucleation when the seed particles are sufficiently small, is considered subsequently.

In homogeneous nucleation a thermally activated first-order transition takes place from the metastable vapor phase to form local concentrations of the vapor molecules which may be considered the precursors of fully formed liquid drops. The liquid phase has a lower chemical potential, but there is a free energy "cost" through the formation of a phase boundary with its corresponding surface energy. Clusters of a certain critical radius r_{crit} or greater will tend to grow still larger, while those of smaller size will tend to lose molecules and hence shrink. The classical theory of nucleation considers that the probability of

attaining a cluster of a given size is exponentially related to the energy necessary to form it [2]. This energy is the difference between a volume term proportional to the logarithm of the saturation ratio S of the free vapor, S being defined by

$$S = p_{\text{vap}}/p_{\text{sat}} \quad (1)$$

where p_{sat} is the saturation pressure, and a surface term proportional to the surface tension σ . The free energy reaches a maximum when the droplet radius takes the value r_{crit} , leading to the following equation for the critical radius:

$$r_{\text{crit}} = \frac{2\sigma v_{\text{liq}}}{k_B T \ln S} \quad (2)$$

where v_{liq} is the specific volume of the liquid. Classical nucleation theory [3] proceeds to calculate the nucleation current J , i.e. the rate of liquid formation per unit volume, assuming a population of clusters with a size distribution determined by the free energy of formation, the single-molecule arrival rate being calculated from kinetic theory. Its final result is the following equation for the nucleation rate per unit volume:

$$J_{\text{CNT}} = \frac{n_{\text{vap}}^2}{n_{\text{liq}}} \left(\frac{2\sigma}{\pi M} \right)^{\frac{1}{2}} \exp \left(\frac{-16\pi\sigma^3}{3n_{\text{liq}}^2 (k_B T)^3 (\ln S)^2} \right) \quad (3)$$

where n_{vap} and n_{liq} are the bulk vapor and liquid number densities respectively and M is the molecular weight.

Some comments are in order. The numerical predictions of classical nucleation theory are usually not very accurate (they are to within 5-10 orders of magnitude in most cases) but it successfully predicts the isothermal variation of the nucleation rate with saturation ratio. However it overpredicts the variation of the nucleation rate with temperature. Numerous attempts have been made to ameliorate the theory (for a review see [4]), improving on the assumption that there is no free energy cost in forming a cluster consisting of a single molecule or taking into account such matters as the curvature-dependence of the surface tension or the translational invariance of the nucleation process, which contributes to the energy via the entropy of mixing. Disappointingly, efforts to render classical nucleation theory more self-consistent in these and other ways have not generally improved its predictions.

This may not matter greatly in nuclear safety evaluations, since for sufficient supersaturations all theories in current use for that purpose predict the rapid formation of a very large number of very small primary particles. The nucleation theorem [5] as extended by Ford [6] provides a formula for the number of molecules in the critical droplet nucleus, n_{crit} in terms of the nucleation rate J_{nuc} :

$$n_{\text{crit}} = \left[\frac{\partial \ln J_{\text{nuc}}}{\partial \ln S} \right]_{V,T} - 1 \quad (4)$$

from which it may be calculated that a critical nucleus contains 30 - 50 molecules. In situations of safety interest where homogeneous nucleation occurs the resulting tiny droplets or embryos rapidly agglomerate to form particles in the 100 - 1000 nm range, referred to in atmospheric science as the accumulation mode,

and the precise sizes, number densities and rates of formation of the original embryos which give rise to them may not be of significance.

Agglomeration and coagulation

Agglomeration usually refers to the formation by collisions of loosely-packed assemblages of primary particles, often highly irregular in shape, such as certain fire aerosols [10]. If the aerosol so formed includes a liquid component its constituents may rearrange to produce roughly spherical particles, and the process is then termed coagulation. As an example, the particles found in the hotter portions of the PHÉBUS circuit are agglomerates of primary particles, whereas those found in the containment vessel are more rounded and compact as a result of water adsorption. Chapter 2 of this report gives the main mechanisms of aerosol agglomeration, as well as appropriate formulae for the individual agglomeration kernels to be used in the General Dynamic Equation. That chapter also supplies a recipe for computing the kernel when several agglomeration processes act simultaneously.

More detailed information for the circuit is given in chapter 3.3.

3.1.2 Particle formation in the primary system

3.1.2.1 PHÉBUS FP tests

The information subsequent to the SOAR of 1994 on particle formation comes largely from the PHÉBUS FP tests, mainly PHÉBUS FPT1, which was the subject of ISP-46, but also test FPT0 [13] and test FPT2, which is currently under analysis. All three tests have the great advantage of working with prototypical materials, and in the latter two tests, used fuel rods of moderate irradiation. They also feature sections of the test circuit operating at temperatures and concentrations characteristic of the degrading core, in-vessel volumes, hot primary circuit elements (1000 K), steam generator tubes and the PWR containment respectively. Both high-steam and high-hydrogen conditions have been investigated, however, tests have been performed with and without boric acid in the coolant stream, and in test FPT3 which was executed in 2004, but is not yet finally analysed, the silver-indium-cadmium control rod of previous tests was replaced by a control rod of boron carbide clad in steel. These tests are considered the best available for the integral investigation of the combined processes governing aerosol growth and vapor condensation. The remarks below are based on PHÉBUS tests FPT0, FPT1 and FPT2.

3.1.2.2 Particle composition

Concerning particle formation, it is found that the particles sampled from the simulated upper plenum and hot leg components are largely composed of silver, together with other elements in proportions which vary depending on the stage of the degradation scenario reached at the time of sampling. During the period of zircaloy oxidation in FPT1, for instance, the particle composition (weight percent) is approximately Ag: 30, Sn: 20, In: 20, Cd: 10, with fission products such as Cs and Mo making up the remainder. All the elements cited arise from the control rod apart from Sn, released from the zircaloy cladding on its oxidation. During the subsequent phase in a typical PHÉBUS transient, where heat-up due to decay heating in a reactor core is simulated by increasing the driver core power to compensate for lateral heat losses from the fuel bundle, the particles, while still predominantly silver, contain significant proportions of the fission products Cs and Mo, whereas during the late phase where a molten pool is formed which then relocates to the bottom of the test section the particles remain silver-rich but contain proportions of uranium and the less volatile fission products as well as the more volatile ones seen in previous phases. In mass terms, silver accounted for the majority of the total release, Cd, Sn and In for 25 %, Cs and Mo together for another 9 % and the remaining fission products including Te, Rb, Tc and I amounted to less than 5 %. “Structural materials”, mainly silver, thus formed the aerosol stream on which the radiologically interesting

fission products were carried as inclusions or condensates, and the location and fate of the latter may largely be deduced by modelling the transport of the structural materials and the interaction of fission products with them. The above remarks refer largely to the results of PHÉBUS tests FPT0 and FPT1. The release of control materials was high in these tests, but in an accident it will depend on the degradation scenario. In PHÉBUS test FPT2 it was found that there was little silver release until the control materials relocated to lower portions of the bundle. The early fission product releases thus took place when silver was in short supply in the primary circuit. The consequences for particle composition in this test are still under investigation.

Chemically the state of the structural materials remains relatively simple. Silver is present as the metal, In and tin as oxides. The chemical form of cadmium is less easy to determine.

3.1.2.3 Particle morphology

The particles from the hot portion of the PHÉBUS circuit have an AMMD of $1.5 - 2 \mu$ and as noted above are principally composed of metallic silver. When examined under a microscope they are seen to consist of agglomerates of primary particles of diameter $< 200 \text{ nm}$. The agglomerates appear fairly solid in nature, with no sign of the hollow spheres typical of fly ash, for instance. The size range observed is too small for the primary particles to have been created by droplet fragmentation or other mechanical means, and too large for the particles to be the direct result of homogeneous condensation, and it is most likely that they are formed through a multistage process in which different formation and growth mechanisms dominate at different stages.

3.1.2.4 Formation and growth of primary particles in the core and pressure vessel

Although some seed particles will be present in the flow channels of the core and in the pressure vessel during fission product release, it appears most probable that the first stage in the creation of the primary particles of silver which provide the backbone and building material for particle transport arise through homogeneous nucleation [14, 15]. The particle mass concentration in the portion of the PHÉBUS installation where temperatures in the right range prevail (3000 to 1500 K, [1]) is most representative in test FPT2, and takes a value of the order of 5 g.m^{-3} of silver. Although considerably higher values may be found during surges in silver release these densities are always much less than the saturation density of silver at the higher end of this temperature range, implying that the rate of transfer from liquid to silver vapor is subject to kinetic, heat transfer or other limitations. The unsaturated carrier stream from the core then cools in the upper plenum region and homogeneous nucleation of silver droplets occurs. The formation of metal aerosols at high temperature through rapid cooling is well-known in metallurgy, volcanology etc., and it is generally accepted that rapid cooling favours homogeneous over heterogeneous condensation, resulting in droplets with sizes in the 10 nm range [16, 17]. As mentioned above the primary particles seen in PHÉBUS tests are ten times larger than this, implying either that the droplets must coalesce before freezing or that rapid condensation of silver takes place on the homogeneously nucleated silver droplets, causing their growth to the size observed. Possibly both processes occur. Further cooling then produced the solid silver “primary particles” seen in the PHÉBUS tests.

3.1.2.5 Effect of pressure

The formation scenario described is based on PHÉBUS measurements made at pressures of the order of 2 bars. Early studies of severe accidents frequently included scenarios, e.g. station blackout, where the system pressure remained high throughout, of the order of 100 - 150 bars, but it is now generally assumed that during such events partial depressurisation will be applied as an accident management measure, reducing the operating pressure during the in-vessel release phase. Such pressure reduction is limited by the accumulator set-points and in PWRs the reduced pressure is of the order of 40 bars. At intermediate

pressures of this order the coolant stream moves an order of magnitude more slowly through the vessel and primary circuit than at low (near-atmospheric) pressure, implying lower cooling rates, while concentrations of released fission products are higher. In this case, for which few experimental data are available, heterogeneous nucleation may play a greater role in the vessel, while the droplets/particles produced by homogeneous nucleation will tend to be larger. Information on these aspects of aerosol physics may become available as a result of Japanese elevated pressure fission product release and transport experiments using simulants.

3.1.2.6 Formation of particles > 1 μ

Independent of the pressure, the extremely numerous primary particles produced in the core and upper plenum region agglomerate to a considerable extent within the vessel and continue to do so in the primary circuit. All agglomeration mechanisms are expected to be active in different degrees depending on the particle size and local conditions within the primary system. Note that agglomeration may take place between chemically dissimilar particles, as occurs in PHÉBUS. The shape of the agglomerates, as shown by SEM photographs, is by no means spherical, a fact which is known to affect both agglomeration and removal processes. Non-spherical shape is usually modelled by the use of shape factors, but it appears extremely difficult to predict a priori the correct shape factors to be used in circuit calculations, particularly as particles of the same mass and composition may have different shapes. The shape factors in turn influence thermophoretic and gravitational deposition rates, as well as agglomeration rates. Sensitivity studies could usefully be performed to evaluate the impact of shape factor variation upon the transmission of fission products through the primary circuit.

3.1.2.7 Vapor condensation on particles

Simultaneously with agglomeration of primary particles fission product and other vapors condense both on the primary particles and on the larger particles resulting from their agglomeration. In PHÉBUS, despite the over-large ratio of pipe surface to particle surface area about half the Te, for instance, is transported in particle form through the hot portion of circuit, and in reactor scenarios one can expect fission product transport as condensate on particles to dominate over vapor condensation on structures [18].

More detailed information for the circuit is given in chapter 3.3.

3.1.2.8 Considerations of chemistry

The similarity of the primary circuit to a tubular reactor has been noted many times [1]. A wide variety of elements and isotopes arise from the degrading core where they react chemically with the carrier gas and with each other, and the resulting maze of active reaction pathways represents a severe challenge to understanding and to the modeller. The reactions continue along the circuit as temperatures drop and elements are selectively removed by deposition processes. Availability of an element for further reaction will depend not only on the chemical compound of which it currently forms a part, but also on the physical phase in which it has become segregated - vapor, surface deposit, condensed layer on aerosol particle or particle matrix. Particles of the same overall composition may have different chemical characteristics depending on whether they are well-mixed or layered. Most important for the prediction of transport behaviour appears to be the element's volatility, a function of both temperature and chemical speciation. Modern codes such as VICTORIA and SOPHAEROS [19] attempt a full equilibrium calculation to determine the speciation of all elements point by point, without prior assumptions. This is a valid general approach, but the calculated speciation is sensitive to uncertainties in the thermochemical properties of the compounds involved, and it has been suggested that chemical kinetics may also play a role under low temperature and pressure conditions, e.g. in the speciation of iodine [20]. The radiologically important element iodine has a volatility which varies along the circuit in a manner which is hard to predict without

positive identification of the species responsible, and indeed the chemical nature of the volatile fraction detected in PHÉBUS in the cold part of the circuit remains a matter for considerable speculation and research. Some fixed data are now available to guide and correct the modeller, however, such as the metallic nature of the silver, the dominance of oxides for the elements In, Sn, U, Cd and Mo, and the probable dominance of the hydroxide for Cs. It is also known from PHÉBUS FPT2 that boric acid in the PWR coolant has only a minor effect on circuit chemistry, aerosol growth and fission product transport.

3.1.2.9 Revaporisation in the primary circuit

Revaporisation is the subject of a separate contribution to this Report. Here it is appropriate to note that there is evidence for the revaporisation of Cs after shutdown in PHEBUS test FPT1 and late in the transient of FPT2. The Cs is released either in the bundle region or in the hot portion of the circuit and on cooling produces a fine aerosol, presumably through homogeneous nucleation, there being little suspended material present at the time to act as seeds for heterogeneous nucleation. The fine aerosol behaves differently from the rest of the aerosol population in the containment, causing Cs to display different deposition behaviour from the other elements (see next section).

3.1.3 Containment aerosols

The removal time for containment aerosols is generally longer than the transient of aerosol release from the degrading core, so that one may expect some averaging of aerosol composition and properties to take place in the containment building. Such averaging is observed to be active in PHÉBUS, despite its rather short removal time, in that the composition of the aerosol is found to be almost constant, consisting largely of Ag metal and the oxides of Sn and In, independent of particle size. All fission products appear to be incorporated in or deposited on this single aerosol “species”, and are removed from the containment atmosphere at the same rate. The sole exception is found to be Cs. Possibly the Cs aerosol resulting from revaporisation (see above) does not deposit on the much larger particles of the main aerosol but maintains an independent existence. A further caveat regarding the “single aerosol” picture of the containment suspended mass must be mentioned: in post-test analyses the solubility of aerosol particles sampled from the containment was found to vary with the stage in the release transient reached at the time of sampling, implying a different composition of the surface layer. This may in turn imply differing hygroscopic behaviour for aerosols of differing genesis.

Particle size and morphology

The process of agglomeration continues within the containment, resulting in an AMMD in PHÉBUS which at 3.5–4 μ is somewhat larger than the values seen in the cold part of the circuit (the geometric standard deviation remains 2.0). The distribution is found to be log-normal, again suggesting a possible simplification in the modelling as for the circuit. The impactor measurements refer to the wet aerosol, with an uncertain amount of adsorbed water, some of which may have been lost in the sampling lines. However the measured removal times are consistent with the AMMD stated. Furthermore, the size distribution is found to remain almost constant throughout a containment transient lasting tens of hours. Compensation appears to be taking place between the competing processes of agglomeration and preferential removal of the larger particles by settling. This finding suggests that a drastic simplification of containment aerosol codes might be made, but it should be recalled that the PHÉBUS containment atmosphere was rather dry, with relative humidities normally less than 80 %. A different behaviour might be seen with higher humidities, with differentiation of the aerosol population according to size and hygroscopicity, as occurred in the KAEVER tests of ISP-44. The topic of aerosol behaviour in a humid containment environment is considered further in a separate chapter of this report.

References

- [1] A.L. Wright et al., Primary System Fission Production Release and Transport NEA/CSNI/R(94)2 (1994)
- [2] J.Frenkel Kinetic theory of liquids, Dover, New York, Chapter 7, 1955
- [3] Y.B. Zeldovich, On the theory of new phase formation: Cavitation J. Exp. Theor. Phys.12, 525, 1942
- [4] Laaksonen, V. Talanquer, D.W. Oxtoby Nucleation: measurements, theory and atmospheric applications Ann. Rev. Phys. Chem. 46, 489, 1995
- [5] D. Kaschiev On the relation between nucleation work, nucleus size and nucleation rate J. Chem. Phys. 76, 5098, 1982
- [6] I. Ford Nucleation theorems, the statistical mechanics of molecular clusters, and a revision of classical nucleation theory Phys. Rev. E., 56, 5615, 1997
- [7] N.A. Fuchs, A.G. Sutugin High dispersed aerosols in Topics in Current Aerosol Research, Vol II; Hindy, G.M. and Brock, J.R. Eds. Pergamon, Oxford, 1971
- [8] S.K. Friedlander, Smoke, Dust and Haze Fundamentals of Aerosol Behaviour. Wiley, New York, 1977
- [9] B.J. Mason The Physics of Clouds Clarendon Press, Oxford, 1971
- [10] I. Colbeck Introduction to aerosol science in Physical and Chemical Properties of Aerosols. Colbeck, I. Blackie Academic and Professional (Chapman and Hall), London, 1998
- [11] M.W. Williams, S.K. Loyalka Aerosol theory and practice Pergamon Press, Oxford, 1991
- [12] W. Koch, S.K. Friedlander The effect of particle surface coalescence on the surface area of a coagulating aerosol J. Coll. Interface Sci., 140, 419-427, 1990
- [13] B. Clement, N. Hanniet-Girault, G. Repetto, D. Jacquemain, A.V. Jones, M.P. Kissane, P. von der Hardt LWR severe accident simulation: synthesis of the results and interpretation of the first PHÉBUS FP experiment FPT0 Nucl. Engrg. and Design 226 5-82, 2003
- [14] C.T.R. Wilson, Condensation of water vapor in the presence of dust-free air and other gases Phil. Trans. Roy. Soc. London 189: 265-307, 1897
- [15] E. Hontanón Theoretical and experimental research on homogeneous nucleation phenomena CTN-67/91, Catedra de Tecnologia Nuclear E.T.S. de Ingenieros Nucleares 2000
- [16] D.W. Oxtoby, Nonclassical nucleation theory for the gas-liquid transition J. Chem. Phys. 89(12): 7521-30, 1988
- [17] D.W. Oxtoby, Homogeneous nucleation: theory and experiment J. Phys. Condensed Matter 4: 7627-7650, 1992
- [18] R.D. Spence, A.L. Wright The importance of fission product/aerosol interactions in reactor accidents Nucl. Technol. 77, 150, 1987
- [19] H.-J. Allelein, K. Neu, J.P. Van Dorsselaere, K. Mueller, P. Krostka, M. Barnak, P. Matejovic, A. Bujan, J. Slaby European validation of the integral code ASTEC (EVITA) Nucl. Eng. and Desn. 221 95-118, 2003

- [20] L. Cantrel, E. Krausmann Reaction kinetics of a fission product mixture in a steam-hydrogen carrier gas in the PHÉBUS primary circuit Nuclear Technology 144(1): 1-15, 2003

3.2 Impact of Thermal Hydraulics

3.2.1 *Impact of thermal hydraulics on aerosol behaviour in the primary circuit*

Introduction

In nuclear safety evaluations thermal-hydraulic behaviour must be determined as a precondition for the calculation of the transport and deposition of released materials, whether in vapor or in aerosol form, from the degrading core through the primary circuit to the postulated breach and into the containment or into the auxiliary building in the case of bypass sequences. In certain special situations such as pool scrubbing or steam generator tube rupture thermal-hydraulics and material transport are intimately coupled and are usually calculated together. More normal is the situation in which the coupling is considered to be looser and the thermal-hydraulics are calculated as a separate issue, with feedbacks to and from the aerosol/vapor transport calculations. Thermal-hydraulics is a general term, including the evaluation of the velocity field of the carrier (usually a single-phase gas), the determination of the temperature field, including structural temperatures which are required as boundary conditions, calculation of the pressure field, and evaluation of the concentrations of the various components of the carrier gas, normally steam and hydrogen, and of the transported materials. Each of these fields affects the aerosol behaviour, as described below, and in some circumstances the aerosol behaviour has a substantial influence on the thermal-hydraulics.

The flow field

The flow field provides the carrier velocity at every point in the primary circuit. It therefore determines the residence time of the aerosol-laden gas stream within each component of the circuit, and hence the magnitudes of the fractional removal of the aerosol by the various deposition processes, e.g. settling, impaction, thermophoresis. The flow is also important in determining the particle size spectrum. For instance, a fast flow through the circuit will provide little time for agglomeration to occur, resulting in a smaller average particle size. It can normally be expected that the calculated thermal-hydraulics will conserve mass, so that the mass transfer rates from one volume to another can be considered reliable. Details of the flow are not usually determined explicitly, although they may be important to the aerosol physics. As an example, the turbulent energy dissipation, which is difficult to evaluate in practical situations, is an essential parameter in the theory of turbulent agglomeration and in eddy impaction. The streamlines of the flow also play a role in determining the concentration of fission products available at a particular point of the circuit at a particular time. Thermal-hydraulic models used in association with fission product transport codes normally assume a sequence of well-mixed connected volumes, in which streaming, recirculation and other effects of the detailed flow field are ignored.

As mentioned elsewhere in the report, another important thermal-hydraulic parameter is the thickness of the boundary layer in transition or turbulent flow, and this is supplied in the one-dimensional codes only through the use of correlations based on fully-developed flow. When the flow is transient or is developing e.g. downstream of a change of section, the calculated boundary layer can be incorrect with consequences for the calculated deposition rate by thermophoresis, for instance.

The role of the flow in remobilising deposits through resuspension is treated elsewhere in this report.

Temperature effects

Thermal-hydraulic calculations determine not only the flow velocity, but also the gas temperature and (when coupled with heat transfer calculations for structures) the local temperature difference between

surface and bulk gas. Both quantities are involved in the determination of the material properties of the gas (thermal conductivity, diffusivity etc.), themselves employed in the calculation of aerosol deposition rates. The gas and wall temperatures also play an essential role in determining the rates of any vapor condensation on existing aerosols, of homogeneous nucleation, and of condensation of vapors on structural surfaces. Sensitivity of aerosol deposition to calculated temperatures varies considerably depending on the scenario, and needs to be determined case by case. The local temperature is important in the chemistry of the transported materials (and that of the carrier), determining reaction rates and chemical equilibria.

Pressure effects

Pressure differences within the primary circuit are not usually large except in special situations such as bypass sequences where critical flow can develop. Of more interest is the overall system pressure. Pressure effects upon core degradation and fission product release are outside the scope of this article. It should be noted however that for a given release the fission product concentrations are higher for higher system pressures. The impact of pressure upon formation and growth was considered in Chapter 3.1. The pressure is also an important factor in determining the Knudsen number, which features in a wide range of processes in aerosol dynamics. Perhaps of most importance is the effect of pressure on the condensation temperature of the carrier gas, usually steam. At high system pressures combined with moderate temperatures condensed water can be formed within the primary circuit, affecting the thermal-hydraulics, which becomes two-phase, and introducing the powerful aerosol deposition mechanism of diffusiophoresis. Transport of fission products in liquid water, revaporisation by evaporation of liquid deposits and other phenomena will then occur, not seen in experiments or scenarios with only single-phase flow in the circuit.

Concentration and composition

The composition of the carrier stream and of the released materials carried within it depends greatly on the core geometry, the degradation model, and assumptions concerning the supply of steam or water and the generation of hydrogen and other gases. Hydrogen being much lighter than steam and its molecule much smaller, carrier gas properties are highly dependent on the steam-hydrogen ratio, and hence so are the calculated aerosol removal rates, local temperatures etc. Non-homogeneous concentrations are likely in many situations, but are generally not considered in aerosol transport codes.

Boundary conditions

Circuit thermal-hydraulics plays a decisive role in fission product transport, deposition and remobilisation, including the formation and dynamics of aerosols. Conversely, fission products and other released materials can affect the thermal-hydraulics. The mass loading of the carrier gas stream by fission products is generally insufficient to have a significant effect on its gas dynamics or on the gas thermal properties, and the thermal energy released by fission product decay during transport is usually comparatively small during the main flow transient. However, fission products deposited on surfaces, whether as aerosols or through sorption, can have significant effects. Mechanical effects include changes in the geometry available for the flow, up to and including plugging of flow paths, and increases in surface roughness. Thermal effects become important when sufficient quantities of self-heating deposit have built up to provide a local heat source. Such a heat source can provoke subsidiary flows, including recirculating flows, can be a cause of revaporisation, and in extreme scenarios can lead to loss of geometry through structural failure.

Modelling aspects

As has been mentioned, the circuit thermal-hydraulics calculated to drive the aerosol transport calculations in severe accident codes is usually relatively unsophisticated. A pipe flow or parallel-channel geometry is combined with one-dimensional fluid dynamics to produce the required velocities, concentrations and temperatures. For reasons connected with the resolution of the aerosol size spectrum the number of volumes cannot be very large, resulting in rather a coarsely discretised resolution of the flow and temperature fields. Numerical experiments show sensitivity of the calculated aerosol processes to the thermal-hydraulic model. The location of wall condensation is particularly sensitive. The application of material transport models in combination with CFD is currently at an experimental stage in nuclear safety evaluations.

Conclusion

Good thermal-hydraulic data are essential for the correct calculation of aerosol and vapor transport processes in the primary circuit. Investigations into calculating more accurate and detailed thermal-hydraulics than current severe accident codes can provide continue. Meanwhile, it is prudent in safety evaluations to determine sensitivities to the thermal-hydraulic side of the calculational route adopted.

3.2.2 *Impact of thermal-hydraulics on aerosol behaviour in the containment*

Introduction

In a severe accident the particulate fission product source term is not only governed by the aerosol processes but depends also on the thermal hydraulic conditions prevailing in the containment. The main interrelations between thermal hydraulics and aerosol physics are

- Transport processes
- Condensation processes
- Fission product decay heat processes

Fig. 3.2-1 shows schematically the most important interrelations in the containment.

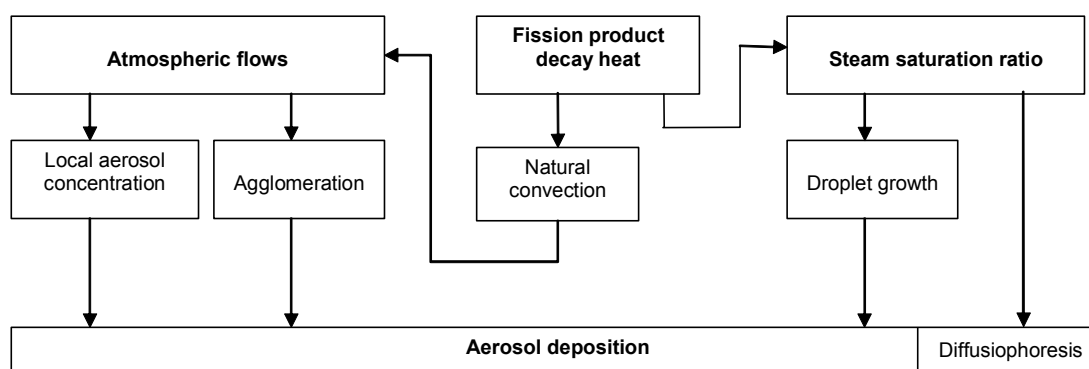


Fig. 3.2-1 Interactions between thermal hydraulics and aerosol behaviour in a LWR-containment

Transport processes

The core melt aerosol entering the containment atmosphere through a leak in the coolant system or from the cavity is distributed in the containment by atmospheric flows. The atmospheric transport is mainly accomplished by pressure balancing flows in the early accident phase and by natural convection in the later phase. In a LWR containment stratifications with the lighter steam at the top and the heavier colder air below are likely. Parts of the containment may be excluded from atmospheric mixing due to such a stratification or to a hindered atmospheric access, e. g. into a dead-ended room. An inhomogeneous aerosol distribution is the consequence.

In the VANAM and the older CSE tests aerosol concentration differences between different compartments in the vessel of approximately two orders of magnitude were measured. In a LWR containment the differences are expected to be higher.

The particle growth by agglomeration as well as the aerosol deposition depend on the local concentration. The aerosol concentration in vicinity of a source is usually higher than in the rest of the containment. Surfaces of containment areas which are not reached by the aerosol, e. g. because of an atmospheric stratification, are ineffective for the global aerosol depletion. In case of a small containment leak the local aerosol concentration around the leak determines the aerosol source term.

Condensation processes

The aerosol behaviour is mainly influenced by two condensation processes: volume and wall condensation. Steam condenses on the aerosol (volume condensation) when the relative humidity in the containment atmosphere has the tendency to exceed saturation conditions. For aerosols of hygroscopic materials volume condensation occurs even at conditions somewhat below saturation conditions. The particle growth by volume condensation accelerates aerosol settling significantly. Fig. 3.2-2 shows the depletion of an insoluble SnO_2 aerosol under dry and condensing conditions [1]. In general volume condensation occurs locally differently in the containment. Predominantly volume condensation takes place around steam sources and close to cold structures. If the atmospheric mixing is poor large aerosol concentration differences may develop between regions with and without volume condensation. An example is the aerosol distribution in the VANAM tests [2].

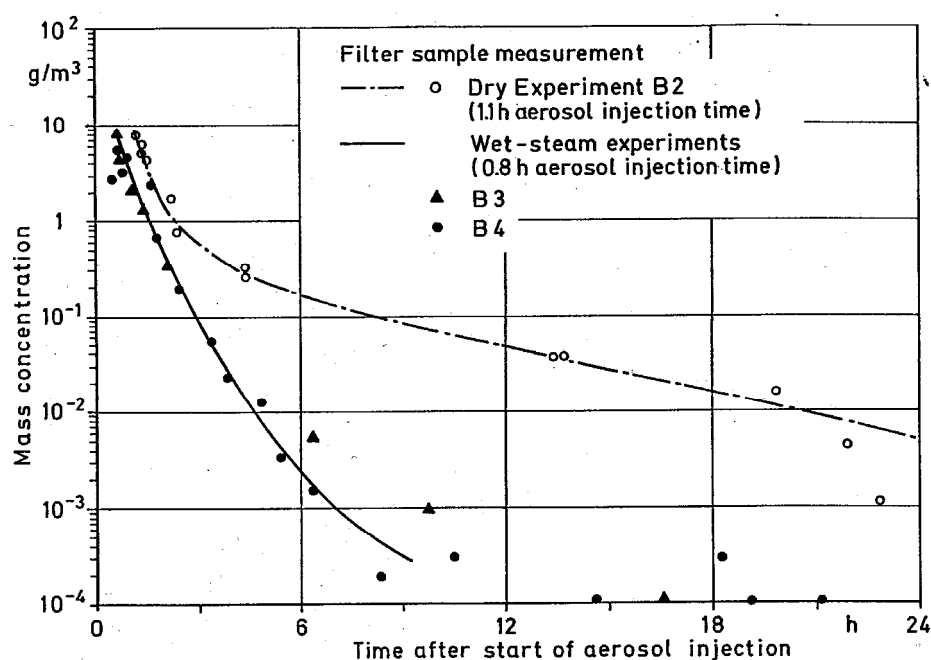


Fig. 3.2-2 Aerosol depletion measured in three DEMONA tests under dry and wet conditions [1]

Fig. 3.2-3 shows the aerosol depletion in test M2. In the outer annular room the aerosol concentration is significantly higher than in the rest of the containment.

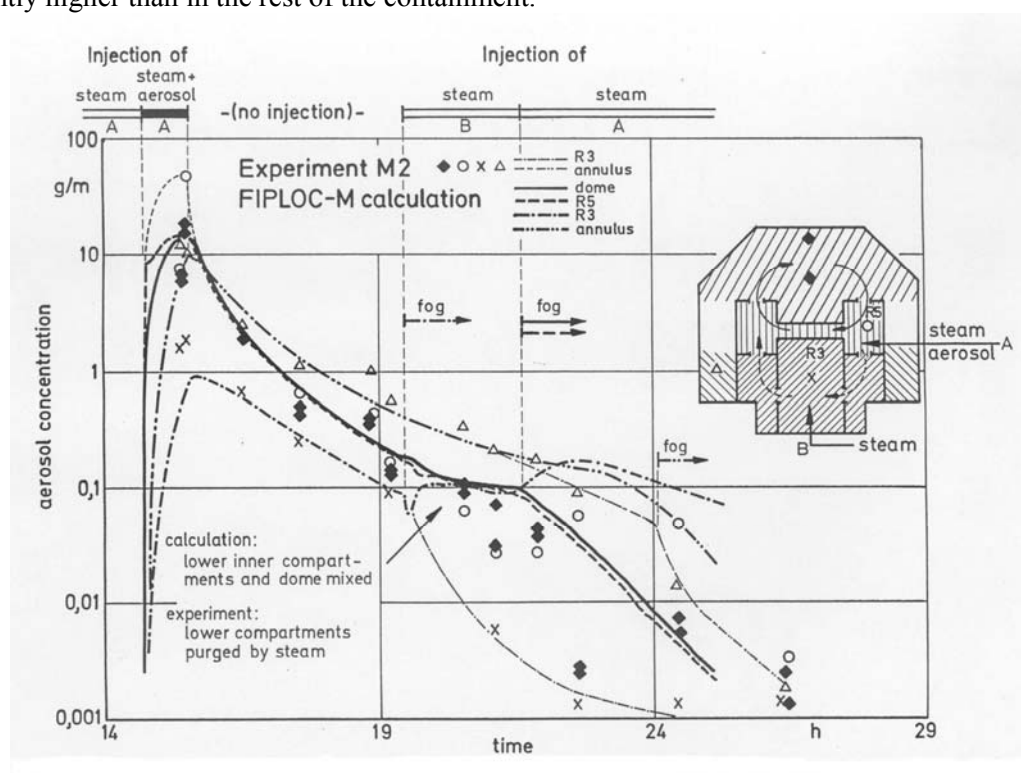


Fig. 3.2-3 Measured and calculated aerosol depletion in the test VANAM M2 [3]

With wall condensation aerosol is deposited by diffusiophoresis onto the wall. Among others wall condensation depends on the steam saturation ratio in the atmosphere and the temperature difference between bulk and wall. Dry and wet walls at the same time and even in the same compartment are possible. In general diffusiophoresis contributes less than sedimentation to the global aerosol depletion. But the AP 1000 and AP 600 reactors are exceptions to this. The used external shell cooling leads to an accentuation of diffusiophoresis to the deposition of aerosol within the containment.

FP decay heat processes

The fission product (FP) decay heat carried by aerosols has a strong feedback on thermal hydraulics. Airborne and deposited radioactive fission products hosted by aerosols present a considerable source of heat. This heat is released partly into the atmosphere and partly into the structures and the sump. The heat-producing gases are distributed in the atmosphere whereas the heat-producing aerosols will be found predominantly on the floors and in the sump.

The decay heat released has a pronounced impact on the relative humidity, the wall and volume condensation rates, and on the natural convection flows within the containment. The decay heat released into the atmosphere reduces the relative humidity and the decay heat released to the sump promotes evaporation which increases the relative humidity. At certain conditions the sump will come even to boil.

All described interaction processes have to be considered in a comprehensive and accurate aerosol source term analysis.

Modelling aspects

Interrelation phenomena can only be examined in code systems where the individual models are numerically coupled. In such couplings parameters of one model are provided for one or several other models. The transfer parameters have to be updated in time. The tightness of the numerical coupling has to be chosen according to the strength and velocity of the physical interrelation.

The modeling of aerosol transport processes requires a moderate coupling of the aerosol and thermal hydraulic models and a multi-compartment representation of the containment. The characteristic period of time of the aerosol processes and the atmospheric transport processes are comparable. The same applies to the modeling of the decay heat feedback.

More complicated is the coupling for the condensation processes. Volume condensation and evaporation are rather fast processes which require more sophisticated coupling methods, like the moving grid technique used in several codes.

In most of the well known containment code systems (ASTEC, COCOSYS, CONTAIN, MELCOR) all mentioned interrelation processes are modeled. Fig. 3.2-4 illustrates the interrelations treated in the CONTAIN code [4]. Sometimes simplifying assumptions are made, e.g. the Kelvin-effect which appears with volume condensation cannot be considered in multi-compartment calculations.

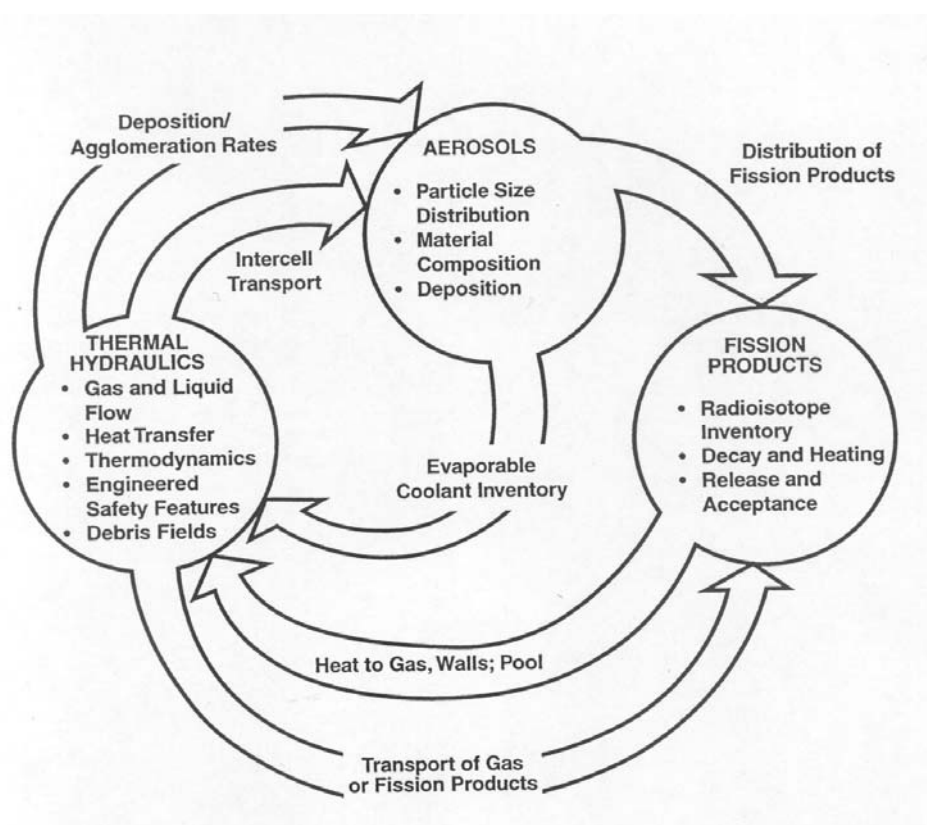


Fig. 3.2-4 Illustration of feedback mechanisms treated in the CONTAIN code [4]

As a consequence of the modeled interrelations the uncertainty of some thermal hydraulic parameters has a very pronounced impact on the uncertainty of the calculated aerosol source term. In the conclusions of the ISP-37 [5] the following is stated:

“However, the aerosol source term to the environment is overestimated in general. The largest uncertainty concerning the aerosol results is caused by a limited number of thermal hydraulic variables like relative humidity, volume condensation rate and atmospheric flow rate.”

The findings of this international study emphasise the importance of aerosol interrelation processes for reliable source term analyses. A few years later the ISP-44 [6] concluded that there is still a need to improve the quality of some thermal hydraulic parameters which have a strong impact on the aerosol results.

References

- [1] T. Kanzleiter DEMONA-Versuche Abschlußbericht, Final Report BLeV-R65.523-01 (1987)
- [2] T. Kanzleiter Versuche zum Verhalten von Kernschmelzunfall-Aerosolen in einer Mehrraum-Containment-Geometrie ("VANAM-Versuche") Abschlussbericht BLeV-R67.098-01 (1995)
- [3] H.-J. Allelein, K.O. Fischer, T. Kanzleiter, S. Schwarz, G. Weber The VANAM Experiments M1 and M2 – Test Results and Multi-Compartmental Analysis European Aerosol Conference AEC '91, Karlsruhe, 16 – 20 Sept. 1991
- [4] K. K. Murata et al. Code Manual for CONTAIN 2.0: A Computer Code for Nuclear Reactor Containment Analysis NUREG/CR-6533 (1997)
- [5] M. Firnhaber, T. F. Kanzleiter, S. Schwarz, G. Weber International Standard Problem ISP-37 VANAM M3 - A Multi Compartment Aerosol Depletion Test with Hygroscopic Aerosol Material GRS-137, OECD/GD (97) 16 (1996)
- [6] M. Firnhaber, K. Fischer, S. Schwarz, G. Weber International Standard Problem ISP-44 KAEVER-Experiments on the Behaviour of Core-melt Aerosols in a LWR Containment OECD/NEA/CSNI/R (2003) 5 (August 2002)

3.3 Fission-Product Transport and Deposition

3.3.1 Introduction

During a severe accident in a nuclear power plant (NPP), fission products (FPs), actinides and structural materials are released as gases or vapors from the degrading core into the reactor coolant system (RCS). These are then swept, in general, by a steam-hydrogen gas mixture towards the breach in the RCS. A number of important physico-chemical processes occur between the point of release from the core and release via the breach of still-suspended materials into the containment (or into the auxiliary building in the case of a containment-bypass sequence). Not only do the phenomena occurring in the RCS reduce the quantity of material released into the containment, they also condition its physico-chemical form; the formation of highly-volatile chemical species leading to vapor-phase contributions to the source into the containment is of particular concern. The importance of the different phenomena in conditioning the source from the RCS varies in terms of the accident sequence, e.g., gravitational settling of aerosols is very minor for a hot-leg break sequence since horizontal surfaces seen by the transported aerosols are limited, much radioactive material remains in the vapor phase due to the relatively high temperatures between core and breach, and transport times through the RCS are short due to the short distance travelled before release into the containment and the high flow rates. Hence, below, a list of phenomena is presented representing the principal phenomena arising beyond that of convection of gases and aerosols by the steam-hydrogen flow and are briefly discussed in Chapter 3.

3.3.2 Synopsis of RCS phenomena and their modelling

The starting point here is a mixture of gases and vapors at a given temperature where this input is assumed along with thermal-hydraulic boundary conditions for a particular RCS geometry.

Homogeneous nucleation of vapors

Even in an unsaturated vapor, molecular clusters exist but they are unstable. Once supersaturation is established for a vapor it is ready to become aerosol or condense on a structural surface. It can be broadly considered that homogeneous nucleation only occurs in conditions of extreme supersaturation in the absence pre-existing aerosol. This is because the high surface energy of the small particles formed by homogeneous nucleation constitutes a greater barrier than that due to condensation on existing surfaces (aerosol or structural).

Nevertheless, it must be remembered that in the present context, the high radiation field reduces this resistance by providing abundant ionic nucleation sites.

In general, therefore, if aerosols are not being produced by mechanical phenomena (e.g., bursting and spraying of control-rod alloy or a steam explosion in the reactor vessel), moving downstream from the point of release, the first aerosols are produced by homogeneous nucleation of the most refractory species. This may be, for example, silver vapor or, in a later stage of the core degradation process, uranium dioxide (or, more likely, uranium trioxide vapor non-congruently reverse-subliming to uranium dioxide). The molecular clusters, or embryo particles, that form then quickly agglomerate while being simultaneously the target of further condensation of the initial nucleating vapor as well as other supersaturating low-volatility species. The picture may well be more complicated since more than one species may supersaturate and, rather than unary nucleation, binary or even ternary nucleation will occur.

Beyond the vapor pressure itself, models require fundamental properties including chemical activities, surface tensions and densities. In nuclear-safety computer codes the phenomenon is simplified.

Condensation of vapors on aerosols and structural surfaces

It should firstly be noted that the process of heterogeneous condensation onto existing aerosols and onto surfaces can be considered a critical phenomenon: in the accident context it is fundamental to the quantities of volatile species reaching the containment in aerosol form rather than being retained on RCS surfaces. The volatile species concerned, i.e., those more volatile than the more refractory species creating the first aerosols, comprise the majority of the most important FPs radiologically, e.g., cesium iodide.

Heterogeneous condensation occurs when a vapor supersaturates and a surface (aerosol or structure) is available. The phenomenon is mainly governed by mass-transfer limitations where, in the RCS, such limitations usually constitute considerably lower resistance to condensation than that of homogeneous nucleation. It must also be remembered that while a vapor may be subsaturated in the bulk flow, it can be supersaturated with respect to a structural surface exhibiting a cooler temperature where (as computer codes assume) aerosols are at the same temperature as their surroundings, i.e., their minuscule heat capacity and large surface-to-volume ratio mean that thermal equilibration with the surrounding gas is always fast. Hence, condensation on a wall can arise without competition from aerosol formation or condensation on aerosols. Once a vapor supersaturates in the bulk flow and aerosols are already present, condensation onto these aerosols is efficient since a small amount of aerosol (in terms of mass) represents a large surface area¹.

Heterogeneous nucleation onto aerosols including the significant negative feedback from warming of the particle due to latent-heat release by the condensing species has been correctly understood for many years. Nevertheless, three complications exist. One arises from an aerosol particles' considerable surface curvature which, combined with the inherent surface tension of the condensed species, induces an increase

¹ To consider a representative situation, given an aerosol loading of the flow of 5g.m^{-3} , assuming aerosols to be spherical with a uniform diameter of $1\mu\text{m}$ and a material density of 3000 kg.m^{-3} , the aerosol surface area is 10m^2 per cubic metre of the flow.

in effective vapor pressure at the liquid surface formed on the aerosol. This so-called Kelvin effect can both reduce total condensation and considerably bias it towards larger particles in an aerosol population (such particles inducing lower surface curvature of the liquid phase). A second complication arises when the particle size is smaller than or of a similar order to the mean free path between molecular collisions (i.e., large Knudsen number). If this is the case consideration of the particle in a continuum regime breaks down and the condensation rate must be corrected [1]. A third complication arises from the probable heterogeneous nature of the aerosol surface affecting sites for condensation: this introduces considerable greater complexity to the condensation phenomenon [2].

Chemisorption of vapors

Chemisorption of certain vapors, i.e., their chemical reaction with structural materials, is a well-known phenomenon but for which little data is available. Some cesium and tellurium species react with metal alloys and empirical chemisorption rates as a function of temperature have been derived for CsOH, CsI, Te (and by extension, to SnTe) for stainless steel and Inconel surfaces.

There are also data for a handful of other species with respect to specific materials such as Zircaloy.

However, it can be said that this is a poorly investigated area where a vast amount of experimental work would be required to provide rates for the species likely to be affected. At present the influence of vapors chemisorption cannot be quantified.

3.3.3 Agglomeration of aerosols

Agglomeration occurs due to particle collisions arising from their differing velocities. Particle motion is induced by Brownian diffusion, sedimentation and turbulence (shear and inertial effects) where other influences such as electrical forces and acoustic influences are less relevant in the present context. Particles combine due to Van der Waals forces, changes in surface free-energies and/or chemical reactions where codes generally assume that the sticking efficiency is unity (i. e., colliding particles always stick together). In the RCS, it is the Brownian mechanism which is of most importance since, once embryo particles have formed, this phenomenon will rapidly lead to larger (and fewer) particles. Once the aerosols have grown to a greater size the other agglomeration mechanisms (properly termed kinematic agglomeration) will come into play. However, the generally short residence times of aerosols and turbulent conditions in the RCS mean that sedimentary agglomeration is usually insignificant.

A particular point that should not be overlooked is that if agglomeration is a significant mechanism then the numerical treatment of the aerosol population is critical in reproducing what the models intend. If a fixed-grid scheme is used then a high number (50 or more) of size bins is usually required to avoid significant spurious diffusion in the re-sizing scheme: a newly-formed particle will not find a size in the discretized scheme that suits it perfectly and fractioning is needed between two adjacent size classes. The coarser the discretization the worse the spurious diffusion.

Probably the most important uncertainty in this area is related to particle shape. As explained in Chapter 2, it is common to associate two shape factors with an aerosol particle, one affecting its mobility (or dynamic) properties, the other its collision properties. Spheres are the most compact particle form possible and so any deviation from this has some impact on the resistance to movement and the probability of colliding with another particle. Particles in the presence of high steam humidity tend to collapse to compact forms under the influence of water surface tension. However, RCS conditions are generally highly superheated and compaction due to steam is only likely to occur near the breach for particular sequences producing saturated or near-saturated conditions in this region (cold-leg break or in the steam-generator tube in the case of a steam-generator tube rupture). Nevertheless, perhaps other condensing species are abundant

enough to cause a compacting effect since there is evidence from representative experiments that particles are, in fact, fairly compact despite superheated steam conditions. This means that high values for the shape factors, such as for chain-like agglomerates, can probably be excluded. Nevertheless, the shape factors and their evaluation remain a significant uncertainty. Evaluation techniques are often empirical where, in relation to an arbitrary particle, there are no reliable analytical techniques for estimating the appropriate values for use in an agglomeration model. Nonetheless, it is desirable that review of the most representative experiments is undertaken with the objective of proposing more realistic values for the shape factors, these values becoming the default values (rather than unity as is now assumed) in nuclear-safety computer codes.

Brownian agglomeration is most significant for small particles where the free-molecular regime (Knudsen number $\gg 1$) and transition regime (Knudsen number of the order of 1) must be considered. The mobility of small particles is very large but this effect is tempered by the reduced target area that they present. Brownian agglomeration is most effective between very small and larger particles. In general, models derive from Brownian diffusion theory with correction factors for the free molecular regime and non-spherical particles.

Gravitational agglomeration is most clearly understood in terms of particle terminal velocities showing the phenomenon to be proportional to the difference in the velocities of the two particles and the sum of their projected areas (the target). Disparity arises in a factor termed the collision efficiency (see [3, 4]), where this constitutes a correction from the ideal situation in which the larger particle sweeps and collects with perfect efficiency all the smaller particles in its projected cylinder during free fall. The correction reduces the efficiency due to hydrodynamic effects where smaller particles tend to flow around the larger particles allowing some to avoid collection. In the RCS, the limited impact of gravitational agglomeration mean that exploration of the different efficiencies is not required here [5].

Turbulent agglomeration arises due to the relative particle velocities induced by the shearing flow field and particle drift relative to the flow arising from inertial differences. This latter contribution is zero for particles of the same size and turbulent agglomeration reaches a minimum in this case. The present modelling is affected by rather high uncertainties.

3.3.4 Deposition of aerosols

Aerosol deposition will occur in the RCS due to Brownian diffusion, thermophoresis, diffusiophoresis, electrophoresis, sedimentation (gravitational settling), inertial impaction (projection onto surfaces by flow-geometry changes and turbulent eddies) and pool scrubbing. Among these phenomena, not all are certain to be significant since they can be considered scenario dependent. Brownian deposition will be significant if particles, once formed, remain small. Pool scrubbing phenomena, the subject of a separate Chapter in this report, may occur in the pressuriser (e.g., high-pressure sequence such as station black-out) or the steam-generator secondary side (steam-generator tube rupture). Probably only thermophoresis can be guaranteed to produce significant deposition whatever the accident sequence.

Deposition due to diffusion

Diffusional deposition is most relevant to the RCS zone where the first vapors nucleate and particles remain small, i.e., within the reactor vessel. For laminar flows, use of the classic Brownian-diffusion approach (Fick's law) is only appropriate in the limit of stagnation. Hence, deposition from a laminar flow due to diffusion is often based on empirical models where that of Gormley and Kennedy [6] is used. A key parameter in this model is the length over which diffusion occurs: in ASTEC/Sophaeros, for example, a fixed value of 10^{-4} m is used. For turbulent flows, the phenomenology changes where the turbulence brings particles close enough to the wall for diffusion to become the dominant transport mechanism and lead to

particle deposition [7]. Diffusional deposition, affecting above all highly-submicron particles, is usually such a small contribution to overall deposition that the modelling approximations do not matter.

Deposition due to thermophoresis

Thermophoresis is a phenomenon which, unusually, does not depend strongly on particle size though is larger for submicron particles. As a result of imbalanced collisions between gas molecules and aerosol particles, particles in a temperature gradient experience a force directed towards cooler temperatures (countered by the hydrodynamic drag force). Highly-conducting (e.g., metallic) particles are less affected by thermophoresis than are particles of more insulating materials. For larger particles a thermal gradient may be established in the particle introducing considerable complexity. Correction for slip due to the greater ease of transport for particles in the free-molecular regime must also be accounted for.

A number of models exist for this phenomenon though it is common to use the Brock formula with numerical coefficients provided by Talbot et al. [8] that allow good agreement with experimental data over the free-molecular, transition and continuum regimes. This modelling would seem to be reliable (well validated) though recent work shows some controversy concerning the validity of the approach in the case of very high temperature gradients, [9, 10]. It is desirable to follow this work in case of any changes required to nuclear-safety computer codes since the aspect of high temperature gradients is relevant.

Deposition due to diffusiophoresis

Diffusiophoresis occurs as particles are entrained by a net flow of a vapor species (steam) towards a surface where the vapor condenses. The flow of the condensing vapor is characterised by its Stefan velocity, a key parameter for the aerosol diffusiophoresis. In the RCS, only certain accident sequences lead to steam condensation on surfaces, those involving lower temperatures such as cold-leg break or steam-generator tube rupture. In fact, diffusiophoresis never occurs alone but must necessarily be accompanied by thermophoresis so we actually observe thermo-diffusiophoresis. Once the thermal-hydraulic problem of determining the Stefan velocity of the condensing steam is resolved, the diffusiophoretic velocity of aerosols is proportional to this velocity but must be corrected as a function of the gas composition (involving not just steam but incondensable gases) and the particle flow regime (Knudsen number): this is complex and the most generally valid model is that of Loyalka [11]. The much simpler model of Waldman [12] is valid in the free-molecular regime only. This modelling has benefited from broad validation and cannot be considered at present a priority for further attention.

Deposition due to electrophoresis

Deposition may be enhanced due to electrophoresis, a complex process dependent on aerosol decay activity, size, concentration and confining geometry. Radioactive aerosols self-charge electrically where, broadly, due to the dominance of α decay (this event generally stripping out more electrons from the particle than the two positive charges it carries away) and β^- decay, a positive charge develops though very small particles can develop a small negative charge – see the relevant theoretical [13] and experimental [14] work. However, the theoretical work indicates that particle charging is very sensitive to two factors: in the RCS the small size of the particles should considerably limit their capacity to self-charge while their high number concentration should reduce their self-charging by facilitating diffusive combination with gas-phase ions. Then again, it must be acknowledged that, as predicted in [13], confinement of the aerosols such as in the RCS may aid charging by lowering ion concentrations. In summary, the theoretical work implies limited self-charging in these conditions except, perhaps, for regions of particularly confined flow.

At present, nuclear-safety computer codes do not take account of this effect. If this is justified or not, can only be shown by a proper assessment of its impact on the fission product source term to the environment.

Deposition due to sedimentation

Particles settle under the influence of gravity where the settling (or terminal) velocity is broadly proportional to the square of the radius. In a turbulent flow particles fall across the boundary layer whereas in a laminar flow the aerosols of the whole flow are concerned. Gravitational settling is not particularly significant in the RCS due to the usually limited size of particles (small settling velocities) and their short residence time before release to the containment. Corrections must be introduced to the situation of a perfectly laminar flow around the particle (Stokes regime) for the cases of slip of small particles and the extra drag on larger particles where flow is no-longer perfectly laminar and wake effects can be induced. Nuclear-safety computer codes do not take this latter effect into account though, as already stated, the settling mechanism most often has a limited impact which may well mean that modelling approximations have little effect on predictions of the source term to the containment. Further work in this area is not a priority.

Deposition due to inertial impaction

Particles can be projected onto surfaces by flow-geometry changes where, due to their inertia, they deviate from the mean flow direction to come into contact with confining walls or obstructions. Such geometries are common in the RCS but most can be generally considered as bends, contractions, expansions or combinations of these. The impaction phenomenon clearly comes in to play as particle size increases where, in general, submicron particles are not concerned being more influenced by other deposition mechanisms. Models for simple geometry changes do exist in the literature but have received little validation in reactor-relevant conditions, particularly highly turbulent flows. Furthermore, there are empirical models for these geometries as well as models for specific complex geometries encountered in reactors such as the components of the steam-generator secondary side.

In turbulent flow, eddies act to project particles towards surfaces where sufficient momentum is imparted to the particles that they can cross the boundary layer and come into contact with the wall. The phenomenon is highly sensitive to particle mass, or more strictly the relaxation time of the particle. A number of theoretical models exist but with varying degrees of agreement with respect to data. Hence, more empirical models are often used such as that derived from the careful experiments of Liu and Agarwal [15]. Since few particles usually become quite large (supramicron) in RCS conditions, this phenomenon is not a dominant mechanism.

One phenomenon which is overlooked in nuclear-safety computer codes which is associated with inertial impaction phenomena is that of particle bounce. The sticking efficiency of particles is not perfect especially for the higher impact velocities. It is possible for impacting particles to bounce, to disintegrate and/or to dislodge particles already on the surface. Significant data requirements are apparent since the models of particle sticking often involve parameters such as the Hamaker constant. What is certain is that for high velocity flows in dry (super-heated steam) conditions with hard (salt, ceramic and metal) particles, bounce will occur. The present understanding on particle bounce is summarised in [16].

References

- [1] S.K. Loyalka, J.W. Park "Aerosol growth by condensation: a generalization of Mason's formula" J. Colloid Interface Sci. 125, 712-716 (1988)
- [2] L.J. Willett et al. "Adsorption on heterogeneous regular surfaces" J. Colloid Interface Sci. 238, 296-309 (2001)
- [3] I.H. Dunbar, J. Fermandjian "Comparison of sodium aerosol codes" CEC report EUR 9172 (1984)

- [4] R.L. Buckley, S.K. Loyalka "Implementation of a new model for gravitational collision cross sections in nuclear aerosol codes" Nucl. Tech. 109, 346-356 (1995)
- [5] H.R. Pruppacher, J.D. Klett "Microphysics of Clouds and Precipitation" Reidel, New York (1978)
- [6] P.G. Gormley, M. Kennedy "Diffusion from a stream flowing through a cylindrical tube" Proc. Roy. Irish Academy, 52, 163 (1949)
- [7] C.N. Davies "Aerosol Science" Academic Press (1966)
- [8] L. Talbot, R.K. Cheng, R.W. Schefer, D. R. Willis "Thermophoresis of particles in a heated boundary layer" J. Fluid Mech., 101, 737-758 (1980)
- [9] R. Muñoz-Bueno, E. Hontañón, M.I. Rucandio "Deposition of fine aerosols in laminar tube flow at high temperature with large gas-to-wall temperature gradients" J. Aerosol Sci. 36(4), 495-520 (2005)
- [10] C. Housiadas, Y. Drossinos "Thermophoretic deposition in tube flow" Aerosol Sci. Tech. 39, 304-318 (2005)
- [11] S.K. Loyalka "Velocity slip coefficient and diffusion slip velocity for a multicomponent gas mixture" Physics of Fluids, 14 n°12, 2599-2604, (1971)
- [12] L.Z. Waldmann "On the motion of spherical particles in non-homogeneous gases" *Rarefied Gas Dynamics*, Academic Press, New York (1961)
- [13] C.F. Clement, R.G. Harrison "Enhanced localised charging of radioactive aerosols" J. Aerosol Sci. 31, 363-378 (2000)
- [14] F. Gendarmes, D. Boulaud, A. Renoux "Electrical charging of radioactive aerosols - comparison of the Clement-Harrison model with new experiments" J. Aerosol Sc. 32, 1437-1458 (2001)
- [15] B.Y. Liu, S.K. Agarwal "Experimental observation of aerosol in turbulent flow" J. Aerosol Sci., 5, 145-155 (1974)
- [16] Special Issue of Aerosol Science and Technology Volume 22, Issue 1 (1995)

3.3.5 *Containment*

During a severe reactor accident nuclear aerosols composed of fission products, actinides and structural material are released into the reactor containment at different locations and at different times. The aerosols enter through a leak in the reactor coolant system (RCS) and after the vessel failure they are released from the molten core in the cavity. Resuspension processes give further nuclear aerosol sources. At a H₂-deflagration deposited aerosol is resuspended and aerosols are re-entrained from flashing or boiling water pools.

The amount of aerosol released by the different sources as well as the particle size distribution varies considerably. During core degradation several 100 kg of aerosol are expected to be swept through the RCS leak. During this release in general the aerosol concentration in the containment ($> 1 \text{ g/m}^3$) reaches the highest values in the accident sequence. The aerosol release with re-entrainment is comparatively small but

it represents a persistent source in the late accident phase. At this time most of the aerosol from other sources has already been deposited.

Especially in the lower part reactor containments are subdivided by structures into compartments of different sizes. The thermal hydraulic conditions within the compartments can vary significantly. The parameters most relevant for the aerosol behaviour are the gas temperature, the relative humidity, the wall and the volume condensation rates and the local atmosphere flow velocity. Locally different thermal hydraulic conditions will be established when atmospheric mixing in the containment is weak or one or several compartments are excluded from mixing. This happens with atmospheric stratifications when a gas with lower density lies above gas with higher density or with dead-end rooms. Thus it is possible that in a part of the containment wet conditions with volume condensation occur increasing aerosol depletion while the other part stays dry.

Transport

The containment atmosphere is mainly mixed by natural convection driven by locally different gas densities. Lowly situated steam and heat sources enhance natural convection. Only in relatively short periods forced convection appears in the containment as during the blow-down phase or with H₂-deflagrations.

From the locations of release the aerosols are distributed within the containment by atmospheric flows. In general the aerosol particles are carried with the gas velocity. Only large particles like condensate droplets have a noticeable slip in the gas. This slip causes an aerosol transport in direction of settling. This additional transport is relevant in stagnant atmospheres.

Deposited aerosols are transported by condensate flows. The aerosols are washed down from the walls and transported by the condensate flows to the sump. Soluble aerosols are washed down more completely than insoluble aerosols. The aerosol wash down process determines the fission product and the decay heat distribution between surfaces and sump. The decay heat released to the gas and to the dry walls heats the atmosphere and reduces the relative humidity. Decay heat released in the sump increases the steam production and the relative humidity.

Aerosol transport and deposition in multi-compartment containment geometries were investigated in the experimental series DEMONA (test A9 only) [1], VICTORIA [2], and VANAM [3]. The VANAM tests were the most comprehensive ones. They were carried out in a large-scale model containment structured into nine compartments. The aerosol concentration measured in the compartments differed by up to two orders of magnitude. The highest concentration was measured in compartments in which the conditions were dry throughout the entire test. In a real containment leaks in the shell are likely to occur in this area. Details are described in chapter 5.3.5. The VANAM tests impressively demonstrated the need of multi-compartment accident analyses. Simple single volume calculations with implicitly well-mixed conditions do not necessarily deliver conservative source term estimations.

Condensation

Particle growth by volume condensation of steam can increase aerosol depletion considerably. In general the particle growth is described by the Mason-equation [4]. Small particles with a strong curvature can be excluded from the condensation process (Kelvin-effect), stay dry and deposit only slowly. In accident calculations the Kelvin-effect is often not treated because of numerical problems. On hygroscopic aerosols condensation already occur at slightly superheated atmospheres (relative humidity < 100 %). Hygroscopic nuclear aerosol materials are CsOH, CsI, Sr(OH)₂ and others. Particles mixed from hygroscopic and non-soluble materials and in droplets where the soluble material is dissolved in water have a reduced

hygroscopic effect. The KAEVER tests [5] demonstrate the impact of the hygroscopic effect on the depletion of single component aerosols and mixed aerosols. The hygroscopic materials employed were CsI, CsOH, and the insoluble materials Ag, SnO₂ (see Chapter 5.3.6).

Volume condensation occurs in a saturated atmosphere, which has a tendency to supersaturation. Equilibrium volume condensation rates are calculated by thermal hydraulic models with the assumption of thermal equilibrium between the steam and the water droplets. Volume condensation appears in compartments with a steam source and certain conditions like cold walls, the presence of non-condensable gas (air), etc. [6]. Up to about 7 % of the released steam may condense in the volume. Decay heat released to the atmosphere reduces volume condensation. The impact of decay heat is investigated analytically since no tests with realistic decay heat releases are available. Even in the PHEBUS FP tests the decay heat was significantly lower than estimated for a severe accident. In general volume condensation occurs locally but the fog droplets are distributed by the atmospheric flows. In other parts of the containment the droplets may dry and shrink again.

Agglomeration

Agglomeration causes a growth of the aerosol particles, a reduction of the particle number, and a mixing of chemically different aerosol materials within the growing particles. The following processes are relevant in the containment: Brownian agglomeration, gravitational agglomeration, and agglomeration by turbulent inertia and turbulent diffusion. In general Brownian agglomeration will prevail. Gravitational agglomeration becomes important when the particle size distribution is broad with pronounced fractions of small and large particles. Agglomeration is only effective at relatively high aerosol concentrations ($> 1 \text{ g/m}^3$).

In multi-component aerosols where the components are not well mixed in each particle the components can deposit with different velocities. Multi-component models have some model restrictions, e.g. the material density for all components, and are only partly validated. A multi-component treatment is necessary when the deposition behaviour of the components is rather different and the aerosol concentration is not very high ($< 1 \text{ g/m}^3$).

Deposition

The deposition of aerosols on the containment surfaces depends on the geometry, the aerosol parameters like particle size distribution, density of the aerosol material, shape of the particles, and thermal hydraulic conditions etc. Aerosol deposition takes place due to the processes sedimentation, diffusion, diffusiophoresis, thermophoresis, and electrophoresis (s. chapters 2.6 and 3.3.1). Here only containment specific aspects on the deposition process including condensation on particles and agglomeration are treated.

In general sedimentation is the most effective depletion mechanism in the containment. Particle growth by agglomeration and volume condensation can increase settling considerably. If condensation is involved the largest uncertainty in the calculated deposition rate is given by uncertain thermal hydraulic parameters like the relative humidity and the volume condensation rate. In the dry case a main uncertainty comes from uncertain shape factors.

Small particles have considerable deposition by diffusion. This process can be essential e. g. for fine/disperse aerosol from re-entrainment processes which especially occur in the late accident phase. The largest modelling uncertainty comes from the boundary layer thickness, which is an input parameter in most models.

Diffusiophoresis is the only important phoresis process in a LWR-containment. Deposition due to diffusiophoresis is nearly independent from the particle size. The local wall condensation rate may differ significantly in the compartments and has to be determined by the thermal hydraulic model. Thermophoresis is only significant with strong temperature gradients in the atmospheric boundary layer along cold walls. This may be the case near the hot corium pool or with fires in the containment.

All important aerosol transport and natural deposition processes relevant in severe accidents are well investigated and modelled. Most accident codes allow a multi-compartment representation of the containment. Additionally aerosol behaviour and thermal hydraulic models are tightly coupled in order to simulate the important interrelation phenomena.

References

- [1] J.O. Liljenzin, J. Collén, W. Schöck, F.J. Rahn Report from the MARVIKEN / DEMONA / LACE Workshop Proceedings of the OECD/NEA Workshop on Aerosol Behaviour and Thermal-Hydraulics in the Containment, Fontenay-aux-Roses (France), 26-28 Nov. 1990, CSNI Report No 176
- [2] J.M. Mäkinen et al. Experimental and Modelling Studies on Containment Aerosol Behaviour in the Victoria Facility 3rd OECD-Specialist Meeting on Nuclear Aerosols in Reactor Safety, Cologne, 15-18 June, 1998
- [3] T. Kanzleiter Versuche zum Verhalten von Kernschmelzunfall-Aerosolen in einer Mehrraum-Containment-Geometrie ("VANAM-Versuche") Battelle-Institut e. V., Frankfurt/Main Abschlußbericht BleV-R67.098-01 (1995)
- [4] J. B. Mason The Physics of Clouds Clarendon Press, Oxford (1971)
- [5] G. Poss, D. Weber Versuche zum Verhalten von Kernschmelzaerosolen im LWR-Containment-KAEVER Fachbericht BF-R-67863, Battelle Ingenieurtechnik GmbH, Mai 1997
- [6] G. Weber Calculation of Local Equilibrium Fog Formation Rates with a Multi-Compartment Containment Code Proceedings of the OECD/NEA Workshop on Aerosol Behaviour and Thermal-Hydraulics in the Containment, Fontenay-aux-Roses (France), 26-28 Nov. 1990, CSNI Report No 176

3.4 Aerosol Behaviour in Complex Structures of Steam Generator Secondary Site

3.4.1 Issue and status

Steam Generator (SG) reliability and performance are serious concerns in the operation of pressurised water reactors. In particular, SG tubing is subject to a variety of degradation processes that can lead to tube cracking, wall thinning, and potential leakage or rupture. However, over the last decade considerable efforts have been spent to understand these degradation processes and to develop improved modes of operation, preventative and corrective measures. Nonetheless the SG tube leakage incidents occurred in the past (see Table 3.4-1) proved that such occurrence can not be completely ruled out. Even if they are design basis events and plants are designed to cope with them it cannot be excluded, that such an event escalates into a severe accident with a significant radioactive release to the environment.

Table 3.4-1 A summary records of steam generator tube rupture accidents

Plant	Date	Leak Rate (lpm)	Break Type and location	Plant status and cause of the rupture
Point Beach Unit 1	February 26, 1975	470	2 adjacent ruptured bulges, each ~20 mm long and wide, hot leg side, above tube sheet, in the sludge pile region	Full power, Wastage
Surry Unit 2	September 15, 1976	1250	Top of U-bend, 114.3 mm long axial crack	Full power, PWSCC in U-bend
Doel Unit 2	June 25, 1979	510	Top of U-bend, 100 mm long axial crack	Heated to normal conditions, PWSCC in U-bend
Prairie Island 1	October 2, 1979	1270	Fish mouth, 76 mm above tube sheet, 38 mm long, 13 mm wide	Full power, Loose parts
Ginna Unit 1	January 25, 1982	2900	Fish mouth, 50 mm above tube sheet, 150 mm long	Full power, Loose parts and tube wear
Fort Calhoun	May 16, 1984	425	Horizontal run at the top, 32 mm long cracks, yielding small fish mouth break of 6 mm long	Plant start-up, ODSCC at a crevice
North Anna Unit 1	July 15, 1987	2410	Top of the 7 th upper tube support plate on cold leg side, 360° circumferential crack	Full power, High cycle fatigue in a U-bend
McGuire Unit 1	March 7, 1989	1900	95 mm axial crack with 9.5 mm wide at the maximum	Full power, ODSCC in the free span
Mihama Unit 2	February 9, 1991	2600	Top of the 7 th upper tube support plate on cold leg side, 360° circumferential crack	Full power, High cycle fatigue
Palo Verde Unit 2	March 14, 1993	910	Freespan region between 8 th and 9 th tube support plate, 65 mm long fish mouth in a 250 mm long axial crack	98 % full power, ODSCC
Indian Point Unit 2	February 15, 2000	564	A low row U-bend	Full power, PWSCC in U-bend
<p>Legend for degradation mechanisms identified below by stressor: Fretting, Wear – flow induced vibration, aggressive chemicals</p> <p>High cycle fatigue – high mean stress level and flow induced vibration, initiating defect (crack, dent, pit, etc.)</p> <p>ODSCC – tensile stresses, impurity concentrations, and sensitive materials</p> <p>PWSCC – temperature, residual tensile stresses, sensitive materials (low mill anneal temperature) Wastage – phosphate chemistry, chloride concentration, resin leakage</p>				

A leakage of radionuclides from the primary circuit into the secondary side negates the effectiveness of the containment. Under certain conditions high release of radionuclides to the environment is possible during postulated severe accidents. Risk assessment studies generally consider two types of severe accidents:

- An operational event or design basis fault that causes a SG tube rupture which then results in core damage;
- A core damage sequence, which might impose prevailing pressure and temperature conditions, could lead to SG tube rupture.

Failure of one or a few tubes can spontaneously happen as a result of any degradation process. However, multiple SG tube failures can only be induced by a very large pressure difference between the primary and the secondary side of the steam generator following occurrence of one of many foreseeable scenarios. A steam line break, turbine trip with a stuck open secondary side safety valve, loss of feed water, ATWS without turbine trip, station black out with a stuck open secondary side safety valve, etc., are examples of such scenarios. Several studies have provided insight into the tube failure mechanisms and conditions leading to tube failure. Conditions necessary to preserve core cooling were identified. These studies also estimated the containment bypass frequencies with a core melt if the latter cannot be avoided.

Most probabilistic risk assessments (PRAs) and severe accident codes assume that a significant fraction of fission products flowing through an unisolated break in a SG escapes to the environment. For example, in NUREG 1150, the median estimate of the fraction of the core inventory of iodine released to the environment was 27%, and the 95th percentile estimate was 80 %. This estimate was based on an expert elicitation panel since none of the specific features of the retention mechanisms in the secondary side of a SG as modelled in severe accident codes were assessed against any experimental data; nor was it possible to quantify the uncertainty involved in the code predictions.

The SGTR project of the 5th Framework Programme of Euratom is the first European project (2000 - 2002) started generating understanding in a systematic way for possible mechanisms for retaining aerosol particles in tubes and in the complex structures of the secondary side of a SG. In particular, PSAERO and HORIZON experiments from Finland were conducted for studying in-tube retention, whereas the retention in the bundle region was investigated in the ARTIST and PECA-SGTR experiments, respectively from Switzerland and Spain. In addition, certain modelling efforts to develop a correlation for the retention in the bundle were initiated.

International cost share project ARTIST (AeRosol Trapping In a Steam GeneraTor), run and coordinated by PSI, (2003-2007) studies aerosol behaviour in tubes of a western design inverted u-tube SG, in the vicinity of the tube break where a transition from a very high to low flow velocities occurs, the far field stages of the bundle, the separator and dryer. A wide range of operational conditions of the components (namely, dry, wet and transition), and thermal-hydraulic and aerosol parameters are addressed. Additionally the droplet behaviour in the separator and dryer is systematically investigated. An extensive interpretation of the data and modelling efforts has accompanied the experimental program.

The SARNET (Network of Excellence for a Sustainable Integration of European Research on Severe Accident Phenomenology) project of the 6th Framework Programme of Euratom (2004 - 2007) provides a further forum where additional efforts are coordinated to understand the complex aerosol-phenomena and to model the available data within the SARNET project.

3.4.2 *Theoretical background on possible aerosol removal in the steam generator*

The main components of a SG are the inlet and outlet plenums, tube bundle, droplet separator and steam dryer. The western design SGs are vertically built and the bundle is composed of straight tubes or inverted u-tubes connecting the inlet and outlet plenums. The Russian VVER designs utilise a horizontal bundle.

As a result of large variations of the flow velocity, and the differences in the geometry of these main components, the important processes are introduced in the following subsections depending on their physical location in the SG.

The following subsections focus on the aerosol removal processes in a vertical SG bundle with an inverted U-bend. Tentative values of various magnitudes important for aerosol behaviour are provided in the following subsections in order to give the reader a feel about their significance. The values are based on a break flow estimated by assuming that there is only one ruptured tube and the ratio of the primary to the secondary pressure is about 5.

3.4.2.1 *Turbulent deposition inside the broken tube*

For any size of the tube break, the flow out of the broken tube is choked because the pressure ratio between the primary and the depressurised secondary side is bigger than two. This produces velocities inside the tube, which are on the order several 100 m/s. At these velocities, turbulent deposition is the dominant aerosol removal mechanism. Turbulent deposition is an eddy diffusion-driven mechanism that becomes important whenever the flow is highly turbulent. Earlier studies [1] indicate that turbulent deposition at these conditions is important and is almost solely a function of tube dimensions (L/D) for particles of interest ($> 0.3 \mu\text{m}$). On the other hand, resuspension may also become important at these high velocities, and somewhat cancel the retention to a degree yet to be investigated. If the break is located in the downstream side of the bend at the cold leg side of the bundle, relatively higher aerosol deposition can be expected in the bend. However, such deposition can cause gradual increase in the pressure drop, which might in turn cause a rapid flushing of deposits. Other possibility for an additional deposition is the fission product vapor condensation in the tubes if the aerosol-laden gas flowing into the inlet plenum from the hot leg is at a temperature of $>900 \text{ K}$, a level at which a certain fraction of volatile fission product mass is still in vapor form. This vapor will then condense on the inner surface of tubes as well as on the airborne particles as the gas cools off due to heat transfer. However, any increase in pressure drop in the broken tube could easily cause flow redistribution among the other intact tubes. Such induced flow redistribution will definitely contribute to retaining aerosols and fission product vapors in the intact tubes. The very dynamic nature of these complex processes of coupled aerosol deposition/resuspension-flow hydrodynamics requires very detailed and simultaneous treatment of the flow and aerosol dynamics and thermodynamics that is not yet attempted.

3.4.2.2 *Inertial and turbulent deposition on the secondary structures in the bundle*

Inertial and turbulent deposition in the break stage

The break stage is the section of the bundle between two support plates (the first could be also the tube sheet) where the aerosol-laden gas is discharged from the ruptured tube. The flow at the break location will be sonic, and local velocities are expected to be on the order of several 100 m/s. The aerosol retention by a single cylinder in turbulent cross flow has been investigated by Douglas [2, 3]. The collection efficiency was correlated as a function of the Stokes number, which is defined by:

$$Stk = \frac{\rho_p d_p^2 U C_s}{18 \mu D} \equiv \frac{\tau U}{D}$$

where ρ_p is the particle density, d_p the particle geometric diameter, U the gas velocity, C_s the slip factor, μ the gas viscosity, D the cylinder diameter, and τ the particle relaxation time. Douglas [2] found that the collection efficiency varied between 2 % to about 30% when the Stokes number was varied between 0.004 and 0.06. For full nominal flow rate (about 900 kg/h), it is expected that the velocity will decrease from a couple of 100 m/s at the break to 10 m/s over the distance spanned by a few tube rows. Table 3.4-2 below illustrates the expected Stokes numbers and particle relaxation time for three different aerosol particle sizes at two representative flow velocities.

Table 3.4-2 Stokes numbers for break stage velocities

AMMD μm	τ s	Stk U= 300 m/s -	Stk U= 10 m/s -
1	5.8 10 ⁻⁶	0.09	0.003
3	4.6 10 ⁻⁵	0.72	0.024
10	3.8 10 ⁻⁴	6.0	0.200

In the actual case the retention is a function of many multiple and dynamic parameters:

- Break type and orientation induced velocity distribution,
- Aerosol characteristics (size distribution, stickiness, etc.),
- Gas and wall temperatures, heat-up of the structures,
- Transport and condensation of fission product vapor, if available.
- Deagglomeration of aerosol agglomerates due to high shear forces produced by the expansion, if it occurs, which might modify the aerosol size distribution,
- Many different aerosol deposition processes, aerosol growth by vapor condensation, removal by interception and impaction, etc.

Inertial impaction on the support plates

Away from the break, the flow will spread and move upwards towards the support plate. As a result the velocity will decrease considerably compared to the sonic speed at the break point. The flow exits the break stage through passages in the support plate. The passages are narrow enough that there exists a potential for inertial impaction on the plate surface. The aerosol retention at a contraction is a function of flow and aerosol characteristics [4] as measured by the Stokes number. For flow at contractions, the aerosol retention has traditionally been correlated as a function of velocity in the far field and the diameter of the contraction. The mean velocity U in the bundle can be obtained from the following relationship:

$$\dot{m} = \rho U A$$

where \dot{m} is the flow rate out of the break, ρ the gas density, and A the free flow area in the bundle. At a typical secondary temperature of 400 °C and pressure of 1 bar, the gas density is 0.32 kg/m³, and thus the mean velocity U in the bundle space is 0.2 m/s for the nominal full flow rate. For an effective diameter of each hole in the support plate of about 8 mm, Stokes numbers as a function of particle diameter at a mean velocity of 0.2 m/s are shown in the Table 3.4-3 below:

Table 3.4-3 Stokes numbers for far field mean velocity of 0.2 m/s

AMMD μm	τ s	Stk -	$(\text{Stk})^{1/2}$ -
1	$5.8 \cdot 10^{-6}$	$1.5 \cdot 10^{-4}$	0.012
2	$4.6 \cdot 10^{-5}$	$1.1 \cdot 10^{-3}$	0.033
10	$3.8 \cdot 10^{-4}$	$9.6 \cdot 10^{-3}$	0.098

In the experiments [4] investigating deposition on the upstream face of a critical orifice, it is found that there is no aerosol retention below $\text{Stk}^{1/2}$ of 0.3. Similarly, in the experiments [4] on aerosol collection in membrane filters, very little retention was found for values of $\text{Stk}^{1/2}$ below 0.2. Simple extrapolation of these results to SG tube support plate might result in expectation of little aerosol deposition on the support plate. However, since the geometry of the holes in the support plate and the flow field underneath or just above the tube support plate are quite complex, the extent of validity of this extrapolation is in question.

Flow expansion at the top surface of the support plate can induce recirculation that could easily alter the deposition pattern of the aerosols. Such details require an in depth analysis of local flow fields in detail and particle tracking.

Inertial impaction on the tubes in the far field stages and on U-bends

Beyond the break stage the flow will be mainly in the vertical direction, and little retention by inertial impaction on the tube structures is expected at a gas mean velocity of in the order of 0.2 m/s. On the U-bend region, the velocity would remain quite small and the retention, based on the Stokes number, can be estimated from the cross-flow data of Douglas [2]. The Stokes numbers are shown for different aerosol sizes in Table 3.4-4 for a flow velocity U of 0.2 m/s and the tube diameter D of 19 mm. The results from Douglas indicate very insignificant retention for Stokes number below $4.0 \cdot 10^{-3}$, which means that for particles under 10 μm the retention should be insignificant if the inertial impaction is the only mechanism.

Table 3.4-4 Stokes numbers for U -bend section

AMMD μm	Stk -
1	$6.2 \cdot 10^{-5}$
3	$4.8 \cdot 10^{-4}$
10	$4.0 \cdot 10^{-3}$

Although the aerosol removal by inertial impaction alone on the surfaces of the straight tubes and on the U-bend can be small, however, expected enhanced recirculation especially in the bend region might

modify the retention process considerably. An experimental and analytical database on the latter is currently not available.

If the break location is within the U-bend section, depending on the number of tube rows that the flow cross through until it reaches the free space below the separator inlet, the retention processes introduced under 'break stage' also apply here.

3.4.3 *Inertial impaction and interception in the separator and dryer sections*

Separators and dryers, due to their complex geometry produce very complex and changing flow patterns and velocities. Inertial impaction, interception, turbulence initiated particle agglomeration are the main processes that can have a role on the particle size dependent aerosol removal. The swirl vane, cyclones and the lid (which hinders water up flow in the normal operation) are the main components of any PWR separators that modify the flow pattern and hence interact with the motion of the particles. The retention efficiency of these components under normal power operation for removing large size water droplets in the order of several 10 µm is very high. However, due to relatively small flow rate and hence gas velocity and the micron-sub-micron aerosol size expected under severe accident conditions, the removal efficiency of these components at full power conditions cannot be applicable to the severe accident conditions.

3.4.4 *Other processes*

Agglomeration

If the aerosol concentration and residence time in the secondary side are large enough, agglomeration occurs and shifts the original size distribution. The aerosol concentration in the secondary side of a PWR can be on the order of 10 g/m³. Assuming spherical aerosols with a density of 2 g/cm³, the number concentration for 1 µm aerosols is in the order of 3·10⁷ particles/cm³. Based on the theory of monodispersed agglomeration [5], the number concentration as a function of time is given by

$$N(t) = \frac{N_0}{1 + N_0 K t}$$

where

$N(t)$ = number concentration at time t

N_0 = number concentration at time 0

K = rate constant = 3.5 10⁻¹⁰ cm³/s (for diameters greater or equal to 1 µm)

t = time in seconds

Assuming an average residence time of about 60 s based on an estimated break flow of 900 kg/h from a broken tube (about 45 s in the bundle, 10 s in the separator, 10 s in the space between the separator and dryer), one has:

$$N(t) = 0.64 N_0$$

Thus, the number concentration drops by about one third in the SG, assuming no other retention mechanism enters into play. The diameter of the particles is given by

$$d(t) = d_0 \left(\frac{N_0}{N} \right)^{1/3} = 1.16 \times d_0$$

Thus, in the course of the 60 seconds, agglomeration would cause an increase of 16 % in the original diameter. If the flow rate is smaller then the residence time will be increased linearly.

The turbulence-initiated agglomeration can take place in various locations as a result of change in the geometry, shape of the hardware causing interferences. As an example to the first is the small flow passages around the tubes in the support plates, which cause contraction and expansion and hence creation of certain turbulences on the top surface of the support plates, the zigzag shape and the pockets of dryer panels for the second. The quantification of the effect of turbulence requires detailed coupled analyses of flow hydrodynamics and the particle tracking, which is still in its research and development phase.

Gravitational settling

Settling velocities as a function of particle diameter is given in Table 3.4-5 below. Even for a large 10 μm particle, the settling velocity is only 18 cm/min, meaning that gravity settling in the secondary side of a SG is negligible for a residence time of the order of 1 minute, shown earlier to be the case.

Table 3.4-5 Settling velocities for different AMMD's

AMMD μm	Settling velocity cm/min
1	0.21
3	1.8
10	18.3

Thermophoresis

Following an accident with dry SG secondary side, the incoming gas is hot (300 °C - 900 °C) while the tube structures have temperatures of about 300 °C, thus deposition by thermophoresis is possible. The thermophoretic velocity depends primarily on the temperature gradient and is a mild function of particle size [5]. Typical velocity values per unit temperature gradient are given in Table 3.4-6 below.

Table 3.4-6 Thermophoretic velocities per unit temperature gradient

AMMD μm	Thermophoretic velocity for unit gradient (1 °C/cm) cm/s
1	$1.3 \cdot 10^{-4}$
3	$1.0 \cdot 10^{-4}$
10	$7.8 \cdot 10^{-5}$

For the purposes of quantifying the possible effect of thermophoretic deposition, the maximum temperature difference between the gas and the structure can be assumed to be 500°C. Given that the distance between the flow centreline and the tube wall is 1 cm, the temperature gradient is of the order of 500 °C/cm. Thus the maximum expected thermophoretic velocity is as given in Table 3.4-7 below:

Table 3.4-7 Thermophoretic velocities for expected temperature gradient

AMMD μm	Thermophoretic velocity cm/s
1	0.065
3	0.050
10	0.040

Since the residence time in a far-field stage is of the order of 6 seconds (1.1 m height and 0.2 m/s velocity), one can see from the above table that the horizontal displacement due to thermophoresis is of the order of 0.3 cm in a stage. Given that less than 1 cm separates the flow centreline from the tube wall, it is concluded that thermophoresis can lead to measurable deposition in dry SG tube rupture conditions.

Aerosol removal in flooded bundle

For accident management purposes, water injection in the dry secondary side may be an option in order to re-establish heat removal and provide a pool where the incoming aerosols can be scrubbed. The POSEIDON [6] pool scrubbing experiments conducted by PSI provided a database on the aerosol removal efficiency of hot pools. The data indicated for example that for a high carrier gas steam fraction (70 %), and a jet injection regime, the decontamination factor (DF) can be higher than 10 even for a shallow pool of 0.3 m submergence. In the context of SG tube rupture, the DF can be expected to be even more significant in view of the high velocity of the jet, the potentially deeper pool, and the presence of dense structures, which can easily disintegrate the incoming jet into a multitude of smaller bubbles with a greater potential for scrubbing than regular pools.

The gas-pool interactions can be analysed in three regions:

- The immediate injection zone characterised by the formation of a gas jet or globule depending on the gas flow rate;
- The break-up zone where the jet or large globule disintegrates into smaller bubbles;
- The bubble rise zone, where individual bubbles rise through the pool stages with a terminal velocity, and periodically squirt out from the support plate narrow constrictions.

Beyond the break-up zone (typically 10 globule diameters away from the injector), the bubbles are oblivious of the details of the injection process, and thus the carrier gas injection rate has no effect on decontamination in the bubble rise zone.

When a jet enters a pool, some of the incoming steam condenses almost instantaneously, with a corresponding scrubbing of a fraction of the aerosols. The extent of condensation depends on the temperature of the water pool. If the pool is close to boiling, which is likely in the long term because of the hot structures and continued steam input, little condensation is to be expected. Hence, the main aerosol removal mechanisms in the hot pool would be inertial in nature: i.e.

- Jet impaction at the injection point;
- Centrifugal impaction and gravitational settling during bubble rise.

The first mechanism depends on the injection flow rate. This supposes that the jet momentum would be locally dissipated because of the dense structures as well as the buoyancy of the bubbles. In addition past experience [6] indicates that the jet is fairly confined near the injection point where most of the removal takes place.

References

- [1] B.Y.H. Liu and J.K. Agarwal, "Experimental Observation of Aerosol Deposition in Turbulent Flow", J. Aerosol Sci., Vol. 5, pp. 145-155, 1974
- [2] P. Douglas and S. Ilias "On the Deposition of Aerosol Particles on Cylinders in Turbulent Cross Flow", J. Aerosol Sci., Vol. 19, No.4, pp. 451-462, 1988
- [3] D. Leaver, J. Li, R. Sher "New Design Applications of Natural Aerosol Deposition in Nuclear Plant Accident Analysis", OECD-CSNI Meeting, June 1998
- [4] Y. Ye and D.Y.H Pui "Particle Deposition in a Tube with and Abrupt Contraction", J. Aerosol Sci., Vol. 21, No.1, pp. 29-40, 1990
- [5] W. Hinds Aerosol Technology, John Wiley & Sons, 1982.
- [6] A. Dehbi, D. Suckow, S. Gntay The Effect of Liquid Temperature on Pool Scrubbing of Aerosols", J. of Aerosol Science, Vol. 28, Suppl. 1 pp. S707-S708, 1997

3.5 Resuspension

3.5.1 Resuspension in primary circuit

Introduction

Particles deposited on the surfaces of the primary coolant circuit may resuspend back to the gas stream. Such phenomenon can take place, if the removal forces affecting the particles are greater than forces that adhere them to the surface. Usually resuspension is caused by sudden increase in the gas flow rate. In a severe accident this may happen, if the rate of steam generation increases for example because of core quench or relocation of molten material. Also either intentional or accidental depressurization of the circuit would significantly increase the flow rate. A very high gas flow rate causes particles to resuspend, even if the flow rate is constant.

Resuspension decreases retention of radionuclides into the circuit. The phenomenon is especially important in by-pass sequences, in which the radionuclides may be released directly to the environment. In these sequences the flow rates may also be very high.

ISP-40, which was based on test SR11 of the STORM series, was the first modeling exercise to address aerosol resuspension in LWR explicitly. The outcome of the exercise was that concerning resuspension none of the participants succeeded in coming close to the experimental results. There was disagreement even on which are the important parameters that affect resuspension [1].

Particle adhesion

In order to calculate particle resuspension it would be important to have an estimate of the forces that bonds particles to the surface. It is known that the most important adhesion force for dry particles is van der Waals force. Other electrostatic forces also bond particles to the surface, but their effect is much

weaker [2]. If there is liquid material in the deposit, surface tension may become the dominant adhesion force. In addition to these, sintering and chemical bonding may further increase the strength of the deposit layer.

In principle it is possible to calculate the strength of the van der Waals force for spherical smooth particles, when Hamaker constant for the material is known and the deformation of the surfaces has been taken into consideration. The calculated results have matched atomic force microscope (AFM) measurements closely [3]. However, the adhesion force is very sensitive to the shape of the particles and to surface roughness. Experimentally the adhesion force has been observed to decrease by an order of magnitude, when the roughness of the surface has been increased from 0.2 nm to 0.7 nm [4]. For this reason direct calculation of the adhesion force is not feasible in reactor safety applications.

In practice adhesion force is always randomly distributed between the particles. Experimentally the adhesion force distribution of single particles on the surface has been observed to approximately follow a log-normal distribution. Log-normal approximation has also been used, when particle resuspension both from monolayer [5, 6] and multilayer [7, 8, 9] deposits has been modeled. It should be noted however, that the adhesion force distribution of a thick deposit layer has not been directly measured.

In a thick deposit layer the number of contacts between particles should greatly influence the strength of the adhesion force. The number of contacts increases as the porosity of the deposit decreases. Experimentally it has been verified that resuspension is much easier from high porosity deposits as from low porosity deposits formed of the same material. Also the difference between PARESS and STORM experiments was explained by the difference in porosities between the deposits [8]. According to the study the main deposition mechanism in PARESS experiments was settling. The resulting deposit layer was highly porous and easily resuspended. In STORM experiments the deposit was formed by thermophoresis, which resulted in a much denser and stronger particle layer, because polydisperse aerosol form a stronger deposit with lower porosity than monodisperse particles. This was shown in a study by Biasi, in which the results from several experimental series were compared [9]. When modeling resuspension, parameters affecting the porosity should thus be included. These would include at least the size distribution and the velocity of the particles depositing on a surface. Hardness of the deposited particles as well as the fraction of liquid material on the deposit layer would also be parameters, which could be relatively easily included in the integral codes.

Removal forces

Forces that cause particle resuspension can be divided to lift forces affecting normal to the surface and drag forces, which tend to move particles parallel to the surface. When the particles are within the viscous sublayer of turbulent flow, the lift forces should be several orders of magnitude weaker than the adhesion forces [10]. Drag forces are not only much stronger, but in experiments done with a centrifuge it has been found out that parallel force required for particle detachment are approximately 1/100 of the required normal force [11]. Parallel forces need to provide energy only to overcome deformation of particles, whereas normal forces have to move the particles out of the range of conservative forces.

Therefore, particles have been observed to move on the surface always before they are resuspended to the gas stream [10]. Because incipient motion on the surface decreases the contact area between particles and the surface, even a relatively weak lift force may resuspend the particles. Experimental observations also show that particles detach from surfaces in discrete events, occurring at random intervals. These observations relate the resuspension to the burst-sweep events taking place in the laminar sublayer of turbulent flows. First resuspension model by Cleaver and Yates assumed that resuspension depends on the frequency, force and area of these events [12].

In some studies it has been claimed that only long term resuspension would be related to turbulent bursts. According to these studies, the rapid resuspension following the increase in the flow rate would be related to the increase in the average drag force. However, in his experiments Wu showed that even short term resuspension during the flow acceleration was significantly decreased, when only the large scale turbulence was dampened [13]. In other studies it was found out that increasing the flow acceleration increases the resuspension rate in short term but substantially decreases it in the long term. These studies strongly support the conclusion that short and long term resuspension are based on the same phenomenon and can not be treated separately.

The diameter of the deposited particles is also an important parameter in many resuspension models. As evident from studies with monolayer deposits, the flow rate needed to cause resuspension decreases as the particle size increases. In these experiments the drag force affecting particles increases with their size. However, particles resuspend as agglomerates from a thick deposit layer. Therefore the primary size of the particles can not be directly used as a parameter, when resuspension is modeled.

In addition to turbulent gas flow also impaction of particles can cause already deposited aerosol to detach from the surface. Erosion has been observed to remove particles efficiently from the surface in jet flows although a pure gas flow did not have the same effect. This was explained by the fact that the momentum of a particle is approximately three orders of magnitude greater than the momentum of gas with the same volume [14]. In her experiments Theerachaisupakij found that gas flow containing at least micron sized particles was substantially more efficient in causing resuspension than pure gas flow. Resuspension from a pipe surface was enhanced as the size of the impacting particles was increased. Submicron particles did not increase the resuspension rate [15]. In PSAERO experiments only a small fraction of particles resuspended from the pipe inlet into pure gas flow. The fraction of resuspended particles increased towards the outlet of the pipe as the concentration of particles in the flow increased. The mass median diameter of particles in these experiments was 3 μm and their density was 9 g/cm^3 [16]. Erosion is an especially efficient process, if the gas flow rate is so high that particles impacting on the surface bounce back to the gas stream. Whether the particles bounce depends on their size and velocity as well as their elasticity and the angle with which they hit the surface [17]. Particle erosion is likely to be an important process in a severe accident. Especially during core relocation the size of the aerosol particles is probably large and their mass concentration in the gas flow is high.

Resuspension dynamics

The adhesion force distribution of deposited particles changes due to resuspension. The average adhesion force in a deposit layer tends to increase, because loosely adhered particles are likely to be the first to resuspend [8, 18, 19]. The increase in the average adhesion force and the discrete random nature of the turbulent bursts also explains why the resuspension rate measured in a number of studies decreases exponentially after the flow rate has been increased [1, 7, 16, 20].

A fact receiving less attention is that resuspension is a continuous process in a turbulent flow as particles are depositing on the surface. Because of resuspension, the adhesion force of a deposit increases as the flow rate during the deposition phase increases. In PSAERO experiments flow rate during the deposition phase was a major parameter influencing the resuspension rate. If the flow rate was lower than during the deposition phase, particles did not significantly resuspend even if the flow was pulsed [16]. Resuspended particles may also deposit back to the surface in the turbulent flow. When they do, they adhere to the surface on average more strongly than before resuspension.

The history of the flow rate during the deposition phase as well as the deposition mechanisms influence the adhesion force distribution. Because of this memory effect, resuspension has to be modeled dynamically. The state of the deposit on the surface has to be also tracked. In addition to adhesion force distribution, the

model should contain frequency, force and area of the turbulent bursts. Erosion caused by depositing particles could be calculated using a similar frequency distribution. Most deposition mechanisms are already adequately modeled for the purpose of predicting resuspension. However, large uncertainties remain in the estimation of turbulent eddy impaction. Obtaining a realistic model for eddy impaction is especially important, because the same mechanisms that carry particles to the surface also cause resuspension.

3.5.2 *Resuspension in containment*

A large fraction of the fission products released from the reactor cooling circuit into the containment is bound to aerosol particles. The aerosol concentration is expected to be high in the early phase of an accident scenario. Later on the aerosol concentration decreases due to sedimentation of aerosols into liquid pools or onto solid surfaces. Atmospheric air currents inside the containment are able to re-release already sedimented aerosol material from solid surfaces into the containment atmosphere. This effect is called dry resuspension. Possible reasons for such heavy air currents can be hydrogen deflagrations or steam explosions. For the determination of the aerosol source term a detailed balance of the release, the sedimentation, and the resuspension of aerosols is necessary.

The detachment of the aerosol particles from the surface is a very complicated process that depends on many unknown parameters. The particles are bound to the surface due to different physical effects that are gravitational forces, Van-der-Waals forces, and electrostatic forces, if the particles carry a small electrical net charge. In the presence of humidity liquid bridges retain the particles on the surfaces. In a multilayer particle bed agglomeration of the particles occurs and a dense particle layer is formed. The aerodynamic forces that lift the particle up into the atmosphere are very hard to determine. It is agreed in literature that the air current must be turbulent, if resuspension occurs. It is distinguished between different mechanisms of resuspension. Erosion describes the steady release of aerosol particles from the surface layer by layer over a longer period of time, while denudation describes the abrupt release of larger amounts of aerosol material in a fraction of a second. The latter effect occurs only, when the velocity above the particle bed is increased suddenly. Further resuspension appears under the impaction of suspended aerosol particles onto a deposition bed. Important parameters are the wall shear stress of the airflow over the surface and the size of the aerosol particles deposited. The influences of these parameters define different ranges of the particle size, in which different adhesive and aerodynamic forces dominate. These influences are theoretically described by Phillips [21].

Most models describe the resuspension under the condition of a constant airflow over a longer period in time of at least several minutes and the particles are removed layer by layer on the basis of erosion. Such conditions are expected during the transport of aerosol in the primary cooling system. In these models the particle bed is completely submerged in a laminar boundary layer that is damaged by randomly occurring bursts. Under these bursts aerodynamic forces act on the particles and lift them up into the atmosphere. A bursting frequency n is assumed that determines how often a burst occurs. The quantity of the removed aerosol mass under a single burst is gained from a criterion that compares the magnitude of the acting aerodynamic and adhesive forces. Such force balance models are developed by Fromentin [18], Braaten et al. [22] and de los Reyes et al. [23] for instance. Reeks [11] has chosen another approach and developed an energy cumulation model. In this model the particles oscillate on the surface and perform a rolling movement. With every burst the particle absorbs energy and oscillates with a higher frequency until it gains enough energy to leave the surface and is entrained by the airflow current. Different versions of such models have been built into severe accident codes and a benchmark has been performed on ISP40 consisting of a combined deposition and resuspension experiment in the STORM programme (de los Reyes et al. [1]).

In contrast to the erosion the process of the denudation is very little modelled. It is expected to be the dominating effect, if an air current lasts only a short period in time. These conditions are fulfilled by hydrogen deflagrations or steam explosions in the containment. A model on the basis of the resuspension model of Fromentin was built into the GRS containment code COCOSYS (Nowack et al. [24]). The advantage of the Fromentin model in comparison to other erosion models is that it describes a multi-layer particle bed. In the modified version for transient events the aerosol particles are not detached layer by layer in different time steps, but a single event can resuspend multiple particle layers at once. The strength of the airflow is only characterised by a maximum velocity and the duration of the current is limited to a few seconds. These changes better fit the conditions found under transient air currents generated by hydrogen deflagrations or steam explosions.

References

- [1] A. de los Reyes, J.A. Capitão, G.F. De Santi, G.F. International Standard Problem 40 - Aerosol deposition and resuspension Final comparison report. Joint Research Centre of the European Communities Report: EUR 18708 EN, NEA/CSNI/R(99)4, Ispra, February 1999
- [2] D.S. Rimal, L.P. Demejo, R.C. Bowen Particle adhesion: Recent advances and current challenges Mittal Festschrift (eds.) W. J. Van Ooij, Anderson Jr., H. R., p. 161-178, 1998
- [3] S. Eichenlaub, C. Chan, S.P. Beaudoin "Hamaker Constants in Integrated Circuit Metalization" Journal of Colloid and Interface Science 248: 389-397, 2002
- [4] Y.I. Rabinovich, J.J. Adler, M.S. Esayanur, A. Ata, R.K. Singh, B.M. Moudgil "Capillary forces between surfaces with nanoscale roughness" Advances in colloid and interface science 96: 213-230, 2002
- [5] M.W. Reeks, J. Reed, D. Hall "On the resuspension of small particles by a turbulent flow" Journal of Phys. D: Appl. Phys. 21: 574-589, 1988
- [6] G. Wen, H.Y.a.K. "On the kinetics of particle reentrainment from surfaces" Journal of Aerosol Science 20(4): 483-498, 1989A
- [7] A. Fromentin "Time dependent particle resuspension from a multi-layer deposit by turbulent flow" Journal of Aerosol Science 20(8): 911-914, 1989B
- [8] H. Friess, G. Yadigaroglu Inclusion of Structural Parameters in the Modeling of Aerosol Resuspension 3rd OECD Specialist Meeting on Nuclear Aerosols in Reactor Safety, 15-18.6.1998, Cologne, Germany, 1998
- [9] L. Biasi, A. de los Reyes, M.W. Reeks, G.F. de Santi "Use of a simple model for the interpretation of experimental data on particle resuspension in turbulent flows" Journal of Aerosol Science 32: 1175-1200, 2001
- [10] A. Ibrahim, R. Brach, P. Dunn "Microparticle detachment from surfaces exposed to turbulent air flow: microparticle motion after detachment" Journal of Aerosol Science 35: 1189-1204, 2004
- [11] M.W. Reeks, D. Hall Kinetic models for particle resuspension in turbulent flows: theory and measurement In: Journal of Aerosol Science 32, p. 1-31, 2001
- [12] J.W. Cleaver, B. Yates "Mechanism of detachment of colloidal particles from a flat substrate in a turbulent flow" Journal of Colloid Interface Science 44: 464-474, 1973

- [13] Y.-L. Wu, C. Davidson, A. Russell “A Stochastic Model for Particle Deposition and Bounceoff” *Aerosol Science and Technology* 17(4): 231-244, 1992B
- [14] W. John, D.N. Fritter, W. Winklmayr “Resuspension induced by impacting particles” *Journal of Aerosol Science* 22: 723-736, 1991
- [15] W. Theerachaisupakij, S. Matsusaka, Y. Akashi, H. Masuda. “Reentrainment of deposited particles by drag and aerosol collision” *Journal of Aerosol Science* 34: 261-274, 2003
- [16] A. Auvinen, J. Jokiniemi, T. Renvall Aerosol Resuspension Experiments in Horizontal SG Tube. EC Report: SAM-SGTR-D025, VTT Processes report: PRO3/P9/03, Espoo, February 2003
- [17] X. Li, P.F. Dunn, R.M. Brach “Monte Carlo Analysis of Polydisperse Microparticle Impacts with Surfaces” *Aerosol Science and Technology* 33(4): 376-385, 2000
- [18] A. Fromentin Particle Resuspension from a Multi-Layer Deposit by Turbulent Flow Paul Scherrer Institut (PSI 38), 1989
- [19] S. Matsusaka, H. Masuda “Adhesive strength distribution of particles deposited on a wall surface” *Journal of Aerosol Science* 32 S1: S937-S938, 2001
- [20] H.Y. Wen, G. Kasper, R. Udischas “Short and long term particle release from surfaces under the influence of gas flow” *Journal of Aerosol Science* 20(8): 923-926, 1989B
- [21] M. Phillips A force balance model for particle entrainment into a fluid stream In: *Journal of Physics D: Applied Physics* 13, p. 221–233, 1980
- [22] D.A. Braaten, U.K.T. Paw, R.H. Shaw Particle resuspension in a turbulent boundary layer-observed and modelled In: *Journal of Aerosol Science* 21, No. 5, S. 613–628, 1990
- [23] A. de los Reyes, E. Hontañón, R. Arias, J.A. Capitão The CÆSAR model for particle resuspension in turbulent flows In: *Journal of Aerosol Science* 28 Suppl. 1 (1997), p. 327-328, 1997
- [24] H. Nowack, M. Dapper, H.-J. Allelein, M.K. Koch Aerosol resuspension phenomena in the containment In: *Annual Meeting on Nuclear Technology*, Aachen, 2006

3.6 Pool Scrubbing

Scenario description and characterisation

Pool scrubbing or wet scrubbing is the removal of aerosol particles in gas bubbles rising in a water pool. The pool thus acts as a filter. Pool scrubbing has applications in various industrial fields where aerosol particle laden gas cleaning is required. The following deals only with aerosols scrubbing; vapor scrubbing is out of its scope.

Pool scrubbing is a very relevant issue in the nuclear safety since it provides a means to reduce source term to the environment during hypothetical severe accidents. Several severe accident scenarios involve the transport paths of fission product aerosols which include passages through stagnant pools of water where pool scrubbing can occur. In Boiling Water Reactors (BWR's) pressure suppression pools (“wetwell”), are such pools although they are primarily designed to avoid over pressurization of the wetwell space. Pool scrubbing in such pools has been given credit as an engineering safety feature capable of mitigating the source term and hence associated risk posed by accidents. Nonetheless, the pool scrubbing scenario is not

BWR specific. Some Pressurised Water Reactor (PWR) sequences may also involve transport paths where pool scrubbing can occur. As an example: A V-Sequence, involving release of radioactivity through safety injection piping (either due to a break or malfunctioning check valves) directly into a tank containing water located in the auxiliary building. Fission products can be scrubbed if the transport path involves a full pressuriser and a stuck open safety relieve valve. During Steam Generator Tube Rupture (SGTR) accidents concurrent with the stuck-open safety relief valve, a good potential for aerosol scrubbing is provided if the secondary side is filled with water. Another scenario common to any type of reactor is a severe accident with vessel breach in which the molten material falls into the reactor pit or drywell and attacks concrete. Corium concrete interaction causes release of medium and low volatile fission products as well as the production of large amounts of concrete aerosols. The gas generated in the interaction will transport the aerosol particles. If the corium is overlaid by a water pool with a certain height it the latter also acts as an aerosol scrubber which attenuates the aerosol particle release to the containment atmosphere. Containment venting filter systems employing water pools utilise also the pool scrubbing to reduce the activity level out of a containment below limits defined by the regulatory bodies.

Several fundamental processes take place during aerosol pool scrubbing: diffusiophoresis, thermophoresis, inertial impaction at the nearby of gas injection, gravity settling, centrifugal deposition and diffusion during bubbles rise, Brownian diffusion, etc. Aerosol characteristics, i.e., size, hygroscopicity, etc, are the key factors for the effectiveness of these removal processes. Gas hydrodynamics plays an essential role determining key variables for pool scrubbing such as bubbles size and surface/volume ratio. In addition, other parameters like pool depth water sub-cooling, carrier gas composition and temperature and velocity, injection mode, water composition, etc., heavily influence individual pool scrubbing processes. In Table 3.6-1 and Table 3.6-2 the ranges of some of these key variables during relevant severe accident sequences [1, 2] are shown.

Table 3.6-1 Pool scrubbing boundary conditions in BWRs

Sequence	Particle AMMD (μm)	Submergence (m)	Injection velocity (cm/s)	Mass % of steam	Temperature
SBO HP-ST	< 3 ("Quencher")	2 – 5 ("Quencher")	25-3000 / 1-15	10-97	subcooled pool
SBO HP-LT			25-3000		
SBO LP-ST	0.2 – 1.5 (downcomer)	1 (downcomer)	3000-9000		
SBO LP-LT			100-25000 / 1-15		

Table 3.6-2 Pool scrubbing boundary conditions in PWRs

Sequence	Particle AMMD (μm)	Submergence (m)	Injection velocity (cm/s)	Mass % of steam	Temperature
SGTR	---	< 12	40 – 5000	10-90	saturated
RHR		0.75 – 2	100 - 250	3 - 97	saturated

Traditionally, the scrubbing efficiency has been expressed in terms of a Decontamination Factor (DF), which is defined by the ratio of the aerosol mass flow rate entering (m^{in}) and the leaving (m^{out}) the pool:

$$DF = \frac{m^{\text{in}}}{m^{\text{out}}}$$

Based on the different nature of hydrodynamic- and aerosol phenomena, the path of aerosols along the pool height is usually split into three regions [3]: injection, rise and pool surface. Consistently, the overall Decontamination Factor is a multiplication of individual Dfs of the three regions of the pool:

$$DF = DF_{\text{inj}} \cdot DF_{\text{rise}} \cdot DF_{\text{sur}}$$

The injection and surface decontamination processes are considered instantaneous whereas it is assumed that several continuous aerosol scrubbing mechanisms are active during bubble rise which can be described by:

$$DF = DF_{\text{inj}} \cdot \exp \left[\left(\frac{1}{V} \sum_n \int_A v_n(r) \cdot dA \right) \cdot \frac{S}{u_{\text{rise}}} \right] \cdot DF_{\text{sur}}$$

The depletion velocity of each individual mechanism is represented by v_n and the time of the bubble in the rise zone is the ratio of water height (S , submergence) and the bubble rise velocity (u_b).

Injection zone

At the injection zone in the pool, the mechanical as well as the thermal gas-liquid interaction determine the scrubbing process.

The gas injection velocity is a key variable in this region. The inlet gas regime is usually classified according to the non-dimensional Weber number:

$$We = \frac{\rho_\ell \cdot D_{\text{inj}} \cdot v_{\text{inj}}^2}{\sigma}$$

as either jet regime ($We \geq 10^5$) or globule regime ($We < 10^5$). Under the jet regime a steady jet cone attached to the injection orifice is formed. Inside the cone a transition from pure gas flow to a churn-turbulent two-phase flow occurs. Intermediated steps in the transition are the bubbly flow and entrained droplet flow. Aerosol impaction on liquid surfaces, either at the cone gas-liquid interface or at surfaces of entrained

droplets, can effectively remove particles from the incoming gas flow. At moderate or low gas velocities characterising the globule regime, other depletion mechanisms such as diffusion, sedimentation and centrifugal deposition could become important. The latter process accounts for the removal of big particles which cannot follow internal gas streamlines and eventually strike the gas-pool surface. Primary bubble oscillations would also enhance aerosol scrubbing. In Fig. 3.6-1 [4] the globule (bubble) and jet regimes for various relevant accident sequences as characterised by a Weber number range are displayed.

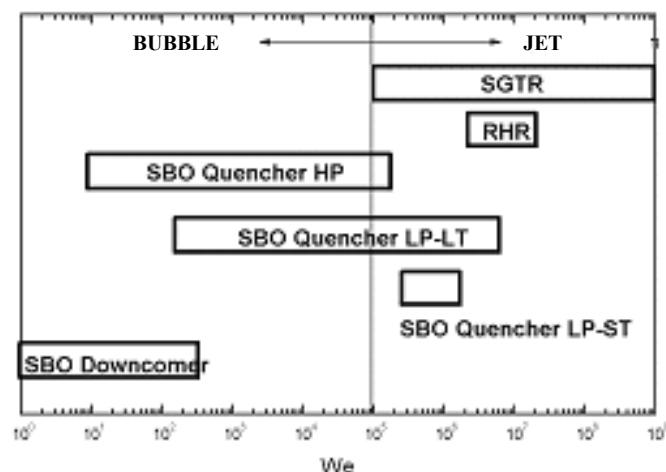


Fig. 3.6-1 Weber range of relevant accident sequences

The thermal interaction between gas and liquid is determined by the temperature difference between both phases and by the gas composition as well. Any temperature difference between gas and water will initiate heat exchange. In the case where gas is hotter than water, particles would be carried to the gas-water interface by thermophoresis. If the gas contains steam and the water temperature is at lower than the saturation temperature the mass transfer as a result of condensation will initiate aerosol removal by diffusiophoresis.

Bubble rise zone

As in the injection zone, the bubble hydrodynamics is closely linked to the scrubbing efficiency. The primary bubble is usually not stable and splits to form a swarm of smaller bubbles. Gas dynamics is quite intense during the bubble rise and a combination of many processes defining bubble size and the distribution will occur. Bubble splitting, growth by vapor flux into the bubble (by hydrostatic pressure decrease) and coalescence coexist. Some key hydrodynamic variables in the aerosol scrubbing are the bubble size distribution and shape and the rising velocity. Small bubbles are usually spherical (i.e., the largest surface-to-volume ratio), which enhances decontamination. However, larger bubbles, either ellipsoidal or cap-shaped, can become more easily deformed, which also contributes to aerosol removal. The bubble residence time (i.e., S/u_{rise}) or gas holdup ultimately determines the final aerosol mass being removed.

Regardless of the shape of the bubbles the major pool scrubbing mechanisms are the diffusion, sedimentation and centrifugal deposition. The combined action of these mechanisms would lead to a minimum of decontamination efficiency at particle aerodynamic diameters around $0.1 \mu\text{m}$. In addition to the main aerosol removal processes, change in the particle size directly affects the pool scrubbing. Particles could grow, if the conditions prevail, because of agglomeration and/or steam condensation and/or hygroscopicity. Agglomeration can be ignored due to short bubble residence time. The effect of condensation becomes more significant if the particles are hygroscopic. Until the bubbles reach a thermal

equilibrium and depending on the steam content, and the temperature gradient diffusiophoresis and thermophoresis could contribute to the aerosol depletion process during bubble rise.

Pool surface zone

At the pool surface bubbles rupture causing production of many micro-droplets (from the fragmented bubble skin). Some of these droplets can be entrained by the gas flow and the others fall back due to their size by the gravity. These entrained droplets transport the very fine aerosol particles as well as dissolved fission products and hence cause accumulation of the activity in the gas space. The amount of droplet entrainment depends primarily on the bubble size distribution reaching the water surface and the gas velocity.

In addition a minor experimental programme was intended to assess the effect of water impurities in the pool scrubbing process [3].

Major outcome of most recent investigations

- On theoretical basis, independent investigations have shown that decontamination by bubble formation and equilibration in a water pool can be significant, both in BWR's and PWR's risk relevant sequences. Under such scenarios carrier gas composition and flow rate are the key variables determining the decontamination efficiency. For shallow pools, the relative significance of the bubble formation and equilibration processes in determining the decontamination can be even larger than that by the decontamination process during the bubble rise through the pool height.
- A peer review of hydrodynamic models in different codes showed that they are remarkably different in both their bases and results. Given their significance in decontamination, bubble size and shape are particularly relevant. No less important, several hydrodynamic phenomena are missing in codes despite they could notably influence particle retention: jet injection, primary bubble rupture, churn-turbulent flow and bubble oscillations and deformations.
- The DF displays an inverted Gaussian type of trend as a function of particle diameter with a minimum at about 0.1 μm .
- Uncertainties in the particle size distribution at the inlet can largely influence DF estimates. The effect of pool scrubbing on the particle size distribution is narrowing towards the particle size yielding the minimum scrubbing efficiency.
- Experiments under different conditions have confirmed that steam condensation at the injection point, particle size, carrier gas flow rate and composition affect significantly the DF, even under hot conditions.
- DF increases smoothly and exponentially with submergence. Increased gas residence time through the pool efficiently raises the DF.
- The decontamination factor of hot water pools is notably larger than 1, a value which was assumed in the past safety studies evaluating the source term from BWRs. This is the case even for small sizes of aerosols with AMMD's on the order 0.2-0.3 μm .

References

- [1] D.A. Powers, J.L. Sprung A Simplified Model of Aerosol Scrubbing by a Water Pool Overlying Core Debris Interacting with Concrete NUREG/CR-5901, SAND92-1422, 1993
- [2] R.M. Bilbao, J.M. Fernández-Salgado, J.A. Fernández-Benítez, A. Alonso-Santos, J.V. López-Montero Severe Accident Phenomenology in BWRs and the Role of PHÉBUS-FP. EUR 15297 EN, 1993
- [3] K. Fischer Modelling of Retention Processes in Water Pools Battelle Ingenieurtechnik, December 1998
- [4] V. Peyrés, L.E. Herranz Programa de Investigación SAC-PS: Influencia de sustancias Contaminantes en la Retención de Aerosoles en Lechos Acuosos. DFN/SN-06/SP-00, 2000

3.7 Re-Entrainment

This chapter describes the re-entrainment process in general, its occurrence in reactor accidents, and the status of analytical and experimental work. Actually re-entrainment processes are modelled in accident codes in a very incomplete way. Proposals are made to reduce this deficit.

Re-entrainment process

When gas is flowing through a pool, droplets are formed at the pool surface and transported with the rising gas flow into the atmosphere. Together with the droplets soluble and insoluble fission products are released in aerosol form to the atmosphere. This process is called re-entrainment or wet resuspension because the released material comes in general from aerosols deposited earlier.

Droplet generation depends essentially on the superficial velocity of the gas flow through the pool. At low superficial velocities the gas flow consists of single bubbles rising through the pool (bubbly flow) and bursting at the surface. Each bursting bubble produces several hundred small so-called film droplets and a small number of larger so-called jet droplets.

At high superficial velocities bubbles of different sizes and shapes rise in a turbulent way (churn turbulent flow). Droplet formation results from a direct momentum exchange between gas flow and liquid. Hollow columns of liquid, whose upper part rapidly disintegrates into droplets due to surface tension, erupt at the pool surface.

Under the accident conditions in a boiling reactor sump the transition from bubbly to churn turbulent flow occurs at a superficial gas velocity of some cm/s. At this transition the droplet formation process changes fundamentally. Therefore different models are required for each regime.

The re-entrainment E is the ratio of the liquid (droplet) mass flux \dot{m}_l to the gas mass flux \dot{m}_g rising through the pool surface. It can also be defined in terms of the density ρ and the superficial velocity j for the liquid and the gaseous phases:

$$E = \frac{\dot{m}_l}{\dot{m}_g} = \frac{\rho_l \cdot j_l}{\rho_g \cdot j_g} \quad (\text{Eq. 1})$$

For bubbly and turbulent flows the re-entrainment increases with an increasing gas velocity. Additionally a strong dependence of E on the bubble size exists for the bubbly flow regime. The re-entrainment is much larger with small gas bubbles than with large ones.

Re-entrainment processes in reactor accidents

In a reactor accident re-entrainment processes can occur in the circuit and the containment at different pools and in different accident phases (Table 3.7-1).

Fission product (FP) re-entrainment takes place on boiling sumps in PWR as well as BWR core melt scenarios. Sumps can boil in case of an extreme decay heat release, or at contact with core melt. Another case is sump flashing during rapid containment depressurization as consequence of a containment leak. With controlled venting the pressure transient is smaller and re-entrainment will be reduced. Venting filters may be loaded additionally by the released aerosol and its decay heat.

Moreover, all pool scrubbing processes, e.g. in a BWR suppression system, are accompanied by re-entrainment phenomena. On the one hand aerosol particles are efficiently scrubbed by the pool water but on the other hand a fraction of the aerosol material retained is re-entrained. Similar re-entrainment processes occur in the suppression systems of the Russian-type reactors WWER-440/213 and RBMK 1000 and 1500.

Re-entrainment also occurs in core melt pools agitated by rising gases from the molten core concrete interactions (H_2O , H_2 , CO_2 , CO , etc.). Together with the melt droplets non-volatile fission products are released.

A discussed accident management strategy is to cool the spread melt by a water layer on top. However, the decay heat of the melt can make the water boil which causes re-entrainment.

Table 3.7-1 Re-Entrainment processes in LWR accidents

Reactor type	Design basis and degraded core accidents	Core melt accidents
PWR	<ul style="list-style-type: none"> • RPV during LOCA, core partly dried out • Pressuriser and pressuriser relief tank at pressuriser leak • Steam generator pipe break 	<ul style="list-style-type: none"> • Boiling sump by FP heat release • Boiling sump at venting • Flashing Sump at containment leak • Core melt agitated by gas • Water on top of core melt pool (EPR)
WWER-440	<ul style="list-style-type: none"> • Wet condenser during LOCA 	
BWR	<ul style="list-style-type: none"> • Discharge into suppression pool • PPV during LOCA 	<ul style="list-style-type: none"> • Boiling sump due to FP heat release • Core melt agitated by gas
RBMK	<ul style="list-style-type: none"> • Accident localisation system at LOCA 	

The aerosol and fission product release rates by re-entrainment are relatively small compared to those of other aerosol generation mechanisms, e.g. by evaporation/condensation processes during the core melt down. Nevertheless re-entrainment can contribute significantly to the radioactive source term in the late accident phase because the process is long lasting. At that time aerosols from other sources have already been depleted to a large extent.

Modelling

In all accident codes re-entrainment is modelled in a very incomplete way as summarised in Table 3.7-2. Very simple approaches which cannot describe this complex process sufficiently, e.g. constant re-entrainment rates, are not considered in the table.

Table 3.7-2 Re-entrainment processes modelled in accident codes

Accident codes		Re-entrainment model for		
		Boiling or flashing sump	Suppression pool with pool scrubbing	Agitated core melt pool
Containment codes	COCOSYS	no	yes	no
	CONTAIN	no	no	yes
Integral codes	ASTEC	no	yes	no
	MAAP	for iodine only	no	no
	MELCOR	no	no	yes

Re-entrainment from boiling or flashing sumps, the most important process in source term analyses, is modelled only in MAAP and for iodine species only. In MAAP the re-entrainment of iodine droplets (CsI , IO_3^- , HOI) for bubbly flows is calculated by the oscillation model of Azbel [1]. For churn turbulent flows the semi-mechanistic correlations of Rozen and Kataoka-Ishii are applied [2]. The Rozen correlation is used with low superficial velocities. It delivers a higher re-entrainment than the correlation of Kataoka-Ishii [3].

In COCOSYS [4] and ASTEC [5] as well as in the circuit code ATHLET-CD re-entrainment is only treated in connexion with pool scrubbing. Re-entrainment is calculated by the module RECOM [6] coupled to the pool scrubbing model SPARC [7]. RECOM uses an oscillation model with critical lamina thickness based on Azbel. For the jet droplet re-entrainment, results of the highly mechanistic code RESUS are taken [6]. RESUS solves the Navier-Stokes equations numerically by use of a finite difference approach. The calculated number and size of the jet droplet is used in RECOM. In the churn turbulent flow regime the re-entrainment is calculated by Kataoka-Ishii. For film droplets and the droplets generated under churn turbulent flow conditions the droplet size distribution has to be given in the input.

In CONTAIN re-entrainment is modelled only for core melt pools [8]. In the module CORCON/VANESA the Azbel model is used for bubbly flow regime and the Kataoka-Ishii correlation for the churn turbulent flow regime [9]. The same applies to MELCOR [10] which also uses CORCON.

With all accident codes the re-entrainment from water as well as core melt pools is calculated by the oscillation model of Azbel for bubbly flows and by the correlation of Kataoka-Ishii for churn turbulent

flows. Only in MAAP the correlation of Rozen for low velocities in the churn turbulent flow regime is applied additionally [11]. Only in the module RECOM used in COCOSYS, ASTEC and ATHLET-CD the jet droplet formation is explicitly treated. Some of the correlations have been modified compared to the original versions.

Especially the re-entrainment models for boiling water pools need several improvements concerning the following items:

- Film droplet formation and dependence on bubble size distribution
- Enrichment of insoluble material in re-entrained droplets
- Re-entrainment spike at onset of boiling
- Size distribution of re-entrained droplets

Conclusions

During a severe accident in a PWR or a BWR re-entrainment of fission products can occur at several water and core melt pools. The release rates are relatively small but the sources are long lasting. Thus a significant contribution to the source term by re-entrainment is likely in the late accident phase. However, thereto no recent analytical investigations are available. One reason is the very incomplete modelling of re-entrainment processes in accident codes.

Out of five codes only one is able to simulate the FP release from boiling or flashing sumps. In general re-entrainment is modelled in the bubbly flow regime based on the oscillation model of Azbel and in the turbulent flow regime by the semi-mechanistic correlation of Kataoka-Ishii. The largest uncertainties come from the film droplet generation model and especially from the uncertain assumptions for the bubble size distribution. Only in RECOM the jet droplet generation is explicitly considered. Only in a few experiments (REST, REVENT, and ThAI re-entrainment tests) re-entrainment has been investigated under LWR accident typical conditions.

References

- [1] D. Azbel and A.L. Liapis Mechanisms of Liquid Entrainment Handbook of Fluids in Motion Ann Arbor Science, Michigan (1983)
- [2] I. Kataoka and M. Ishii Mechanistic Modelling of Pool Entrainment Phenomenon Int. J. Heat Mass Transfer, Vol. 27, No. 11, pp 1999 – 2014 (1984)
- [3] T. Ginsberg Aerosol Generation by Liquid Breakup Resulting from Sparging of Molten Pools of Corium by Gases Released During Core/Concrete Interactions Nucl. Sci. and Eng.: 89, 36 – 48 (1985)
- [4] W. Klein-Heßling, S. Arndt, G. Weber COCOSYS V 1.2 User Manual GRS-P-3/1 (July 2000)
- [5] F. Jacq, H.-J. Allelein ASTEC V0. 2 General Overview, Rev. 0 ASTEC-V0 /DOC/99-09 (April 2000)
- [6] M.K. Koch et al. Radionuclide Re-entrainment at Bubbling Water Pool Surfaces J. Aerosol Sci. Vol. 31, No. 9, pp 1015 – 1028 (2000)

- [7] P.C. Owczarski, K.W. Burk SPARC-90: A Code for Calculating Fission Product Capture in Suppression Pools NUREG/CR – 5765 (1991)
- [8] K.K. Murata et al. Code Manual for CONTAIN 2.0: A Computer Code for Nuclear Reactor Containment Analysis Sandia National Laboratories NUREG/CR-6533 (1997)
- [9] D.R. Bradley et al. CORCON-MOD3: An Integrated Computer Model for Analysis of Molten Core-Concrete Interactions NUREG/CR-5843 (1993)
- [10] R.O. Gauntt et al. MELCOR Computer Code Manuals Vol. 1: Users' Guide for Version 1.8.5 NUREG/CR-6119 Rev.2 (2000)
- [11] D.L.Y. Louie and D.J. Osetek MAAP-IMPAIR Interface for Analysis of Iodine Behaviour in Advanced Reactor Accidents (Phase II) DOE/ID-10466 (March 1994)

3.8 Aerosol Formation during High Pressure Melt Expulsion from the Reactor Coolant System

The accident at Three Mile Island demonstrated that substantial core degradation and core debris relocation to the lower head of the pressure vessel could occur while the reactor coolant system remained at elevated pressure. Prior reactor accident analyses had assumed that depressurization would occur early in the course of an accident, perhaps as part of the accident initiating event. The Three Mile Island accident raised the possibility that molten core debris could penetrate a pressurised reactor vessel and be dispersed throughout the containment.

Safety concerns associated with the pressurised expulsion of core debris from the reactor vessel focused on issues of containment integrity. Initial concerns were that dispersed debris could heat the atmosphere to the point containments failed by overpressure. This is the so-called “direct containment heating” scenario. Further investigations suggested melt expulsion and dispersal might trigger hydrogen combustion events that threatened containment integrity. These concerns prompted several experimental investigations. A cross section of the multinational experimental efforts is reported in a CSNI state of the art report [1]. Following preparation of this state of the art report, several scaled tests were undertaken to support analyses of the containment threats [2]. To a significant extent the concerns over prompt containment failure associated with pressurised expulsion of core debris have been resolved favorably for large dry and subatmospheric containments [3].

Though investigations of high pressure melt expulsion and direct containment heating were focused on the containment loads, there were some early efforts to examine aerosol production associated with the expulsion and dispersion processes [4, 5]. A sequence of frames from an open air test of high pressure melt expulsion is shown in Fig. 3.8-1.

It is apparent that a very large amount of aerosol is produced. Efforts were made to identify aerosol formation mechanisms and to characterise the aerosol produced in tests contained within the Surtsey test facility (a 110 m³ containment vessel). As might well be expected, all of the tests were done with simulant materials rather than real core debris. Usually the simulants were mixtures of molten iron and aluminum oxide produced by a thermitic reaction within a vessel pressurised with nitrogen or steam. Consequently, it is not readily apparent how applicable the aerosol characterization results are to the analysis of reactor accidents. It is thought that the aerosol formation mechanisms are, at least, qualitatively applicable.

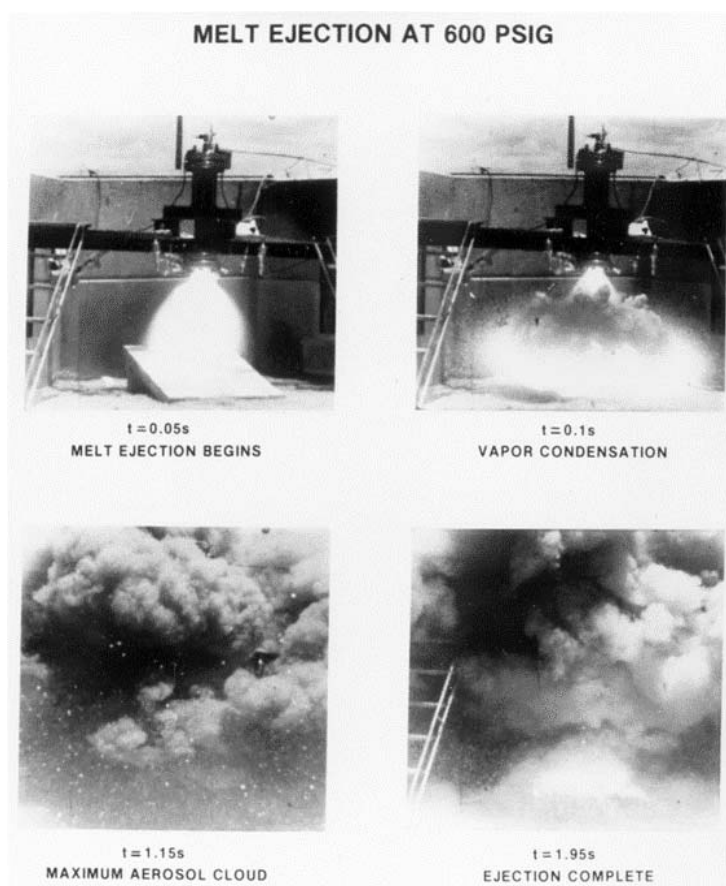


Fig. 3.8-1 Open air test of melt expulsion from a vessel pressurised to 41.3 bar with nitrogen

Three mechanisms of aerosol formation were identified:

- Vaporization from surfaces of high temperature melts,
- Droplet formation by the effervescence of gas from the melt as it emerges from the pressurised vessel, and
- Comminution of melt droplets as they impact surfaces within containment models.

The three mechanisms produce characteristically different aerosol particles. Examples of these particles are shown in Fig. 3.8-2. Vapors evolving from the high temperature melt rapidly transport to cooler environments where they nucleate extremely fine primary particles. More detailed views of these fine aerosol particles are provided in Fig. 3.8-3 and Fig. 3.8-4. It is suspected that the cooling of the vapor is so fast and supersaturations so high that homogeneous nucleation is a predominant path for vapor condensation rather than condensation on either structural surfaces or surfaces of mechanically produced particles. There also appears to be a tendency for the primary particles to coagulate in chains and these chains either fold or agglomerate to form very low density particles.

The second mechanism of aerosol production arises because gases including steam and hydrogen are soluble at high pressure in molten materials. When the melt emerges from the pressure vessel, the solubility drops dramatically and bubbles nucleate in the melt. Frid demonstrated using x-rays to monitor the melt as it emerged from the pressure vessel that gas effervescence was sufficient to completely disrupt the stream of melt emerging from the pressure vessel. As each bubble bursts at the surface of the melt it

cases off droplets in the size range of a few microns. These droplets are small enough that they remain airborne until they have cooled to solidify as very nearly spherical particles.

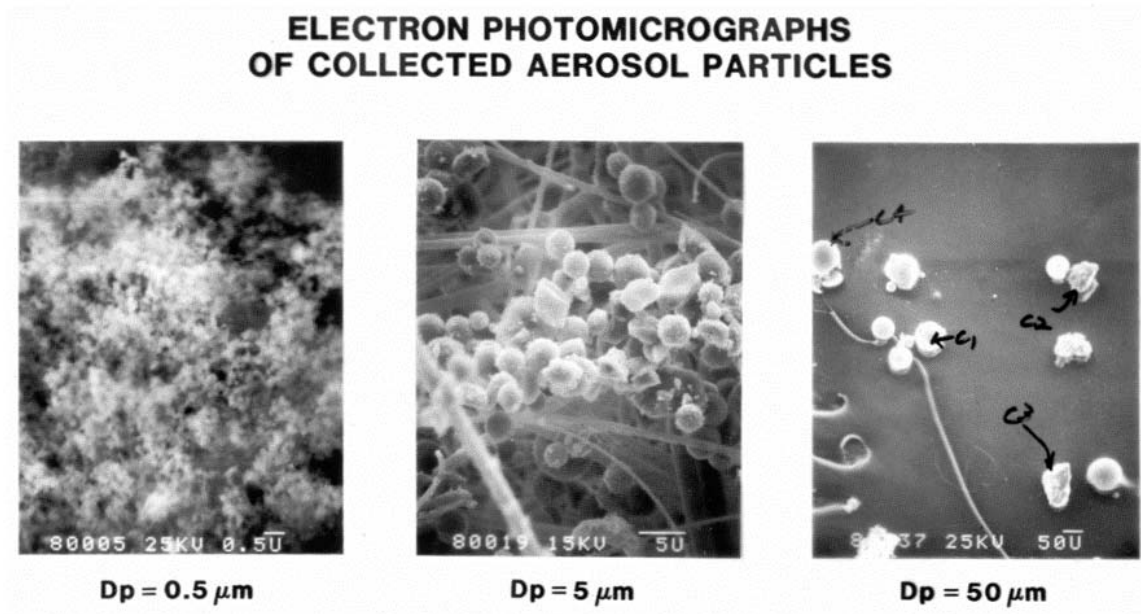


Fig. 3.8-2 Examples of the qualitatively different types of aerosol produce in a high pressure melt expulsion event

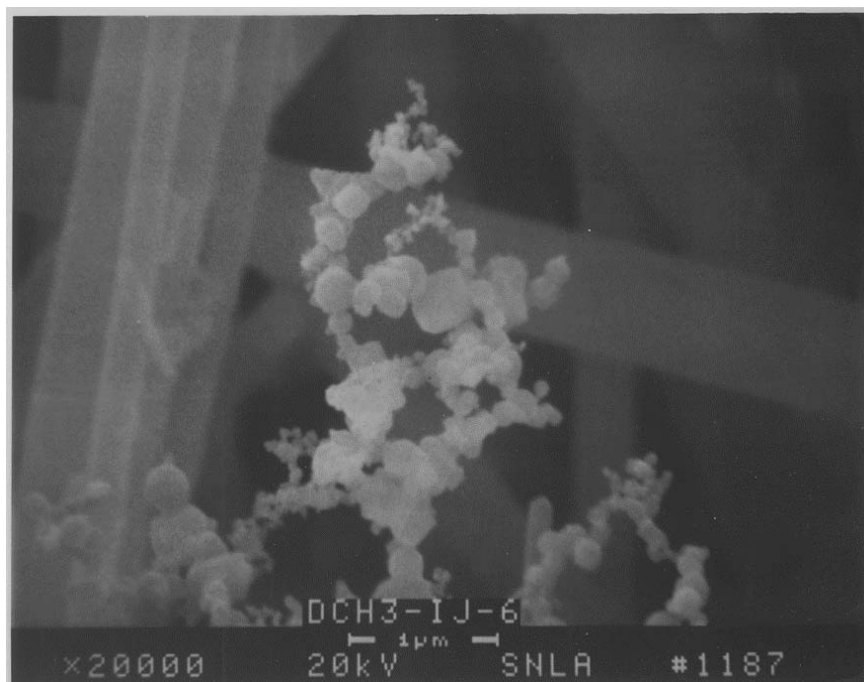


Fig. 3.8-3 Electron micrograph of very fine aerosols produced by vapor nucleation during a high pressure melt expulsion experiment

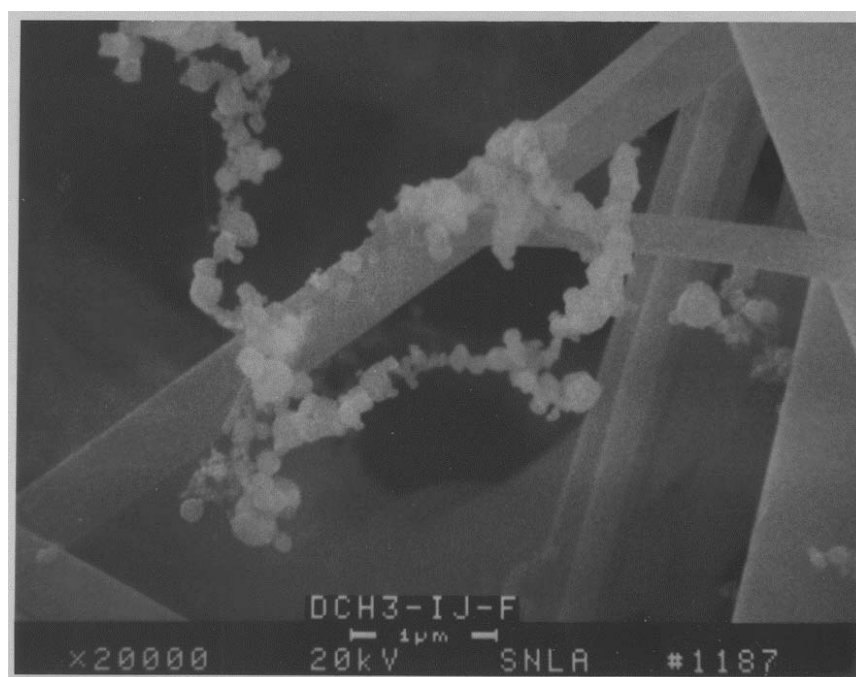


Fig. 3.8-4 Electron micrograph of fine aerosols produced by vapor nucleation during a high pressure melt expulsion experiment. Note the apparent tendency to form chain agglomerates

Larger particles (10-100 μm) are produced by a combination of aspiration and comminution. As melt is expelled from a pressure vessel, the hole in the pressure vessel enlarges. Part way through the expulsion process, the hole is enlarged to the point that the pressurizing gas penetrates the liquid pool and two phase expulsion takes place. The high velocity gas entrains melt droplets. Furthermore, gas also entrains melt previously expelled from the vessel. Droplets accelerated in the gas phase disintegrate until a critical Weber number of about 12 is reached. Further distintegration of the melt droplets can occur as they impact surfaces at very high velocities.

About 1 % of the melt mass expelled from a pressurised vessel is thought to be converted to aerosol. This can produce a substantial aerosol loading of the containment atmosphere. But, if the aerosol production is not coincident with containment failure, the aerosol rapidly agglomerates and sediments so it may not contribute significantly to the risk associated with reactor accidents.

Following resolution of concerns about the containment loads produced by pressurised melt ejection, little effort has been devoted to further characterizing the associated aerosol production. Interest has been further attenuated as accident management measures have been introduced to depressurise reactor coolant systems during accidents involving core degradation. Most accident analysis codes do not include models of aerosol formation associated with core debris expulsion from the reactor coolant system.

References

- [1] Fauske and Associates and Sandia National Laboratories, State-of-the-Art Report (SOAR) on HPME and DCH, OECD, 1996

- [2] T.K. Blanchat, M.M. Pilch, M.D. Allen, Experiments to Investigate Direct Containment Heating Phenomena with Scaled Models of the Calvert Cliffs Nuclear Power Plant, NUREG/CR-6469, Sandia National Laboratories, Albuquerque, NM, January 1997, and references therein
- [3] M.M. Pilch, M.D. Allen, B.W. Spencer, K.D. Bergeron, K.S. Quick, D.L. Knudson, E.L. Tadios, and D.W. Stamps, The Probability of Containment Failure by Direct Containment Heating in Surry, NUREG/CR-6109, Sandia National Laboratories, Argonne National Laboratory, Idaho National Engineering Laboratory, May 1995, and references therein
- [4] J.E. Brockmann and W.W. Tarbell, Nuclear Science and Engineering, 88 (1984)342
- [5] J.E. Brockmann, Progress in Nuclear Energy, 19 (1987) 478

3.9 Aerosols from MCCI

An important source of aerosol input to reactor containment during an unarrested severe reactor accident comes from the interactions of core debris with structural concrete. Classic reactor accident sequences envisage a point at which core debris will penetrate the reactor pressure vessel and fall into the reactor cavity (see Fig. 3.9-1). The core debris will be a mixture of molten uranium dioxide fuel, zirconium dioxide and zirconium metal from the fuel cladding, structural steel and fission products. Much of the core debris will be molten when it penetrates the reactor pressure vessel. If the core debris is not quenched as it emerges from the vessel, it will thermally attack the structural concrete in the reactor cavity. If the core debris is quenched but the quenched debris is not coolable, core debris will reheat and eventually become hot enough to thermally attack the concrete.



Fig. 3.9-1 Photograph of a high temperature melt interacting with calcareous concrete and the associated aerosol production

Aerosol production comes about during core debris interactions with concrete because the core debris is sufficiently hot to produce significant vapor pressures of some core debris constituents and the constituents of ablated and melted concrete. Aerosol production can become significant (see Fig. 3.9-2.) because the gaseous products of concrete decomposition sparge through the core debris. Three mechanisms are usually considered in the analysis of aerosol production during core debris interactions with concrete [1]:

- vaporization from the free, upper surface of core debris,
- vaporization into gas bubbles sparging through molten core debris, and
- mechanical aerosol production when bubbles burst at the surface of molten core debris.

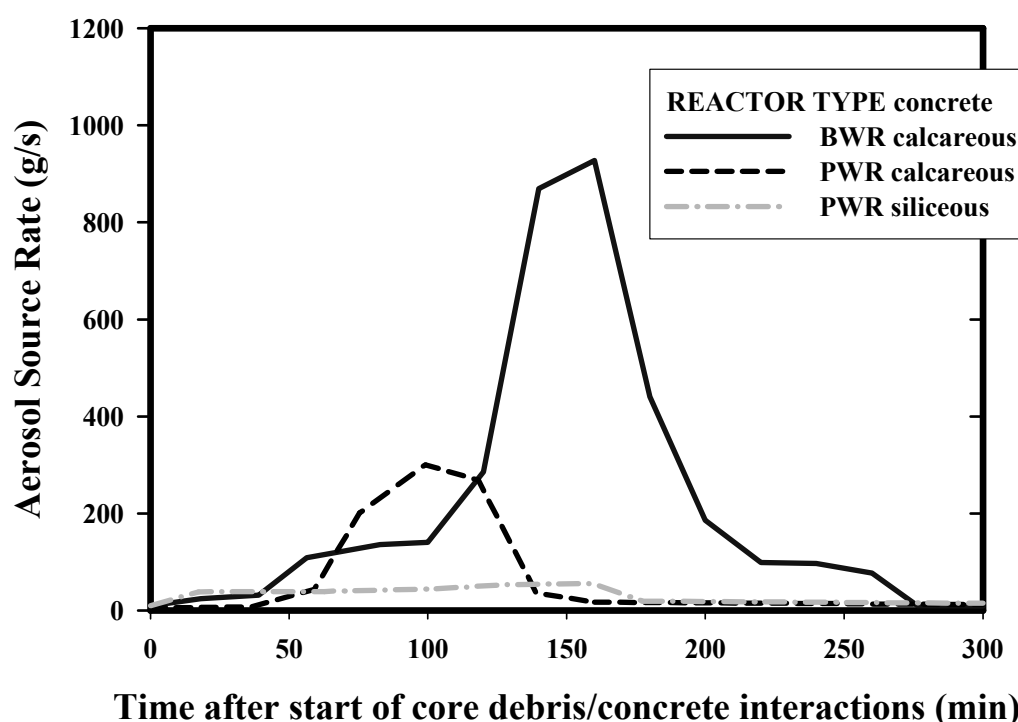


Fig. 3.9-2 Comparison of predicted aerosol production rates during core debris interactions with concrete at different reactors with various concretes

The first of these mechanisms is usually found to be small in comparison to the second if the core debris is molten.

Concretes used in the structural elements of nuclear power plants are typically classed as either calcareous concretes that use limestone (CaCO_3) or dolomite ($\text{CaMg}(\text{CO}_3)_2$) as aggregate or siliceous concretes that use basalt, granite or other silica-rich materials largely free of carbonates as aggregate. Chemical compositions of three representative types of concrete found in nuclear power plants [2] are shown in Table 3.9-1. Clearly, the distinction between calcareous and siliceous concretes is the large amounts of carbon dioxide that can be liberated in the thermal decomposition of calcareous concretes. The other gaseous product of concrete decomposition is water vapor. All concretes have a significant amount of water vapor. About half the water (often called 'free water') is present in the concrete as water in the pore structure of concrete and water of crystallization. The rest of the water (bound water) in the concrete is in the form of calcium hydroxide ($\text{Ca}(\text{OH})_2$) which is the binding agent that holds together the aggregate. At sufficiently high temperature, this calcium hydroxide decomposes to produce calcium oxide and water

vapor. Temperature ranges over which the various gaseous concrete decomposition products are released are [3]:

- Free water: ambient to 230 °C
- Bound water: 300 to 450 °C
- Carbon dioxide: 600 to 1100 °C

Table 3.9-1 Chemical compositions of some representative concretes at nuclear power plants²

Chemical Constituent	Mildly Siliceous Concrete* (weight %)	Calcareous Concrete (weight %)	Limestone/ Common Sand Concrete (weight %)
SiO ₂	54.7	3.6	35.7
CaO	8.8	45.4	31.2
Al ₂ O ₃	8.3	1.6	3.6
MgO	6.2	5.67	0.5
Fe ₂ O ₃	6.2	1.2	1.4
K ₂ O	5.4	0.7	1.2
TiO ₂	1.0	0.15	0.2
Na ₂ O	1.8	0.08	0.8
MnO	0.4	0.01	0.03
Cr ₂ O ₃	0.2	0.004	0.014
H ₂ O	5.0	4.1	4.8
CO ₂	1.5	35.7	22.0

* Siliceous aggregates are quite variable in composition and may contain much higher concentrations of silicon dioxide than basaltic aggregate.

Siliceous concretes melt at temperatures somewhat above 1100 °C and calcareous concretes melt at temperatures from 1200 to 1600 °C. During thermal attack on concrete, there are fronts of gas generation propagating through the concrete ahead of the ablating interface between concrete and the core debris.

The gases liberated from the concrete are observed to pass relatively easily through substantial heads of molten core debris. The oxidizing gases from the concrete, CO₂ and H₂O, react with the metallic constituents of core debris, predominantly Zr and Fe, to form CO and H₂. The very exothermic reaction of the oxidizing gases with zirconium metal in the core debris can be a significant source of heat that sustains

² Note that in addition to these chemical constituents of concrete, structural concrete at nuclear power plants contains about 0.25 g/cm³ reinforcing steel which is mostly iron

high temperatures for protracted periods in the core debris. Such high temperatures, as well as the reactive nature of the gases mean that constituents of the melt will vaporise into the bubbles of gas sparging through the liquid. When these vapor-laden bubbles escape the core debris, the vapors are released into a cooler environment and they condense to form aerosol particles.

Gases sparging through the core debris at sufficiently high velocities can entrain molten material in the form of droplets [4] that have dimensions small enough to be considered aerosol ($< 20 \mu\text{m}$). At lower gas generation rates, gases sparging through the core debris emerge as bubbles that burst at the surface. The bursting of these bubbles imparts very high accelerations to the liquid films ($\sim 10,000 \text{ g}$). Such high accelerations can launch small liquid droplets into the gas flow as drinkers of carbonated beverages well know.

Aerosol production during core debris interactions with concrete, then, depends on the composition of the core debris, especially the zirconium metal content, and the amount of gas that can be produced by the thermal decomposition of the concrete. Comparisons of the aerosol production rates predicted to occur in reactor accidents of different types are shown in Fig. 3.9-3. The highest aerosol production rates occur soon after core debris accumulates in the reactor cavity. The greatest production of aerosol occurs in the case of the boiling water reactor with calcarous concrete. Aerosol production is extremely high in this type of accident because of the large inventory of zirconium metal in a boiling water reactor much of which is not oxidised at the time core debris penetrates the reactor vessel.

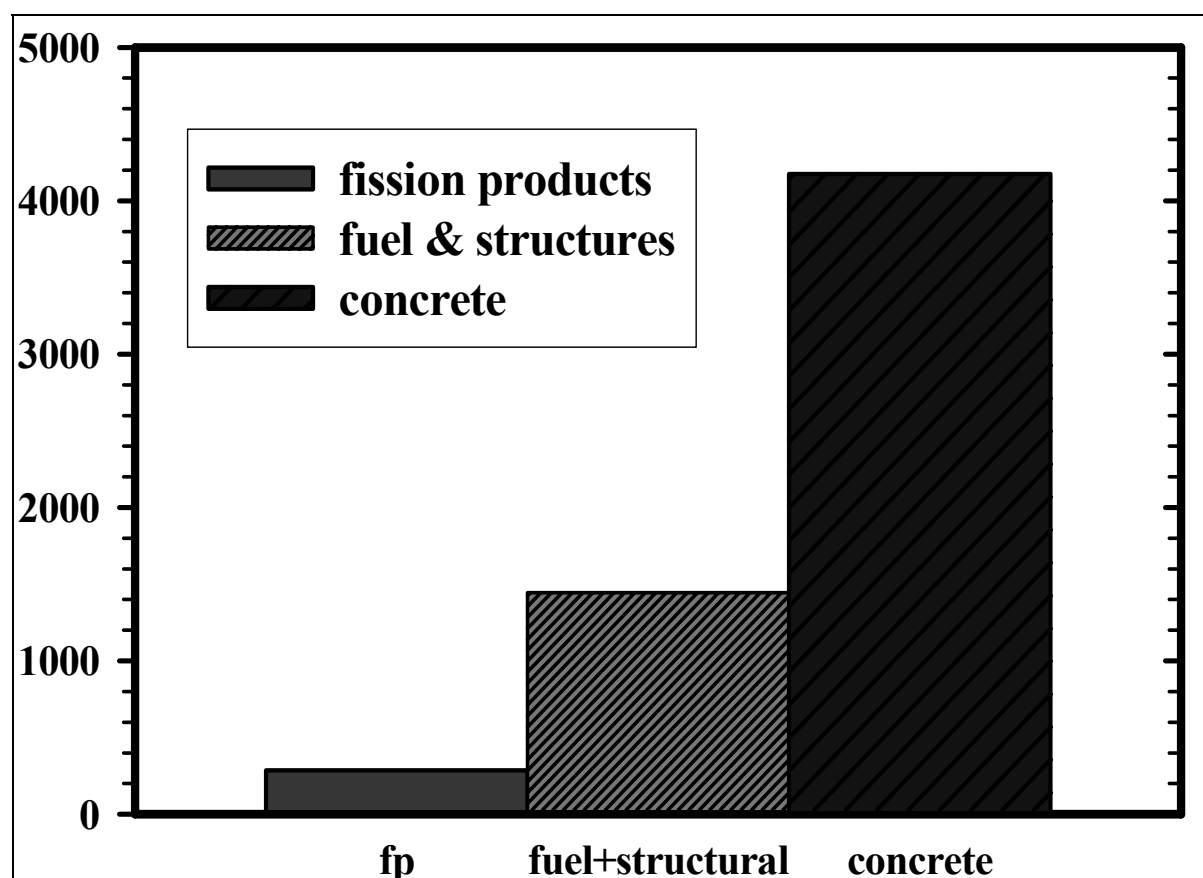


Fig. 3.9-3 Sources of aerosolised materials during core debris interactions with concrete [in kg]

Without this large inventory of zirconium metal in the core debris, aerosol production predicted for an accident at a pressurised water reactor with calcareous concrete is much attenuated though still significant. Aerosol production when pressurised water reactor core debris interacts with siliceous concrete is smaller still.

Aerosol production is persistent during core debris interactions with concrete. Even after the core debris has solidified, temperatures are sufficiently high that concrete decompositions continues and the gaseous products of decomposition sweep vapors of the more volatile species into cooler environments where they condense to form aerosol particles.

Much of the aerosol produced during core debris interactions with concrete is nonradioactive material. Most comes from constituents of concrete and structural materials as is shown by the comparisons in Fig. 3.9-3 for an accident involving boiling water reactor core debris interacting with calcareous concrete. Nevertheless, significant releases of radionuclides can occur during core debris interactions with concrete. Release fractions for various classes of radionuclides derived from tests and model predictions of core debris interactions with concrete and used for regulatory analyses in the USA [6] are shown in Table 3.9-2. But recent investigations lead to the assumption that the release of the volatile radionuclides (halogens, alkali metals and to a less extent Te) are not coming from the MCCI. They are in-vessel release from fuel remaining in the RPV, but being released during the ex-vessel phase of the accident.

Table 3.9-2 Radionuclide release fractions associated with core debris concrete interactions at BWRs and PWRs

	Boiling Water Reactor	Pressurised Water Reactor
Radionuclide Release Duration (hr)	3.0	2.0
Fraction of Initial Core Inventory of Radionuclide Released During Core Debris/Concrete Interactions		
Halogens (I, Br)	0.30	0.25
Alkali Metals (Cs, K)	0.35	0.35
Tellurium	0.25	0.25
Ba, Sr	0.10	0.10
Ru, Mo, Pd	0.0025	0.0025
Ce	0.005	0.005
La	0.005	0.005

Releases of nonradioactive isotopes of important fission product elements observed in the ACE tests [5] are shown in Fig. 3.9-4. Only the relative releases can be compared to results of accident analyses since total release is quite dependent on details of melt composition and the accident scenario. Surprising features of the tests are the measured releases of Mo and Ru which are not predicted by the computer models of fission product release during core debris interactions with concrete. This has been attributed to improper modeling of the partitioning of fission products between the oxide and metal phases of core debris interacting with concrete.

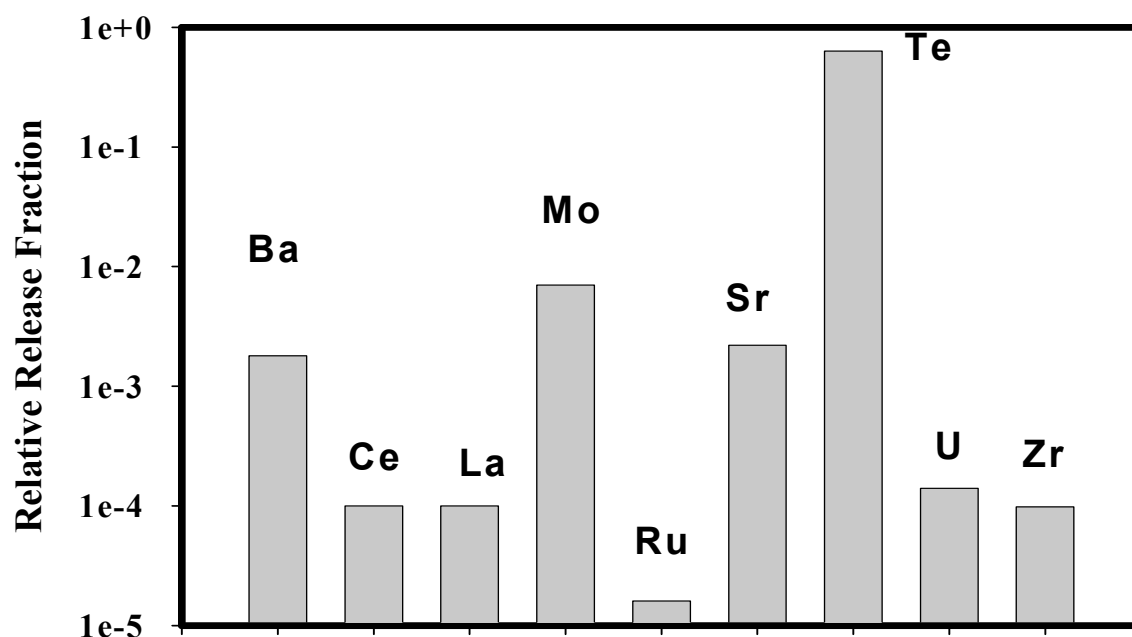


Fig. 3.9-4 Relative release fraction observed in the ACE L6 test

Some attempts have been made to characterise the particle size distribution of aerosols evolved during core debris interactions with concrete [7]. Much of this effort has been directed at determining the fraction of aerosol formed by entrainment and the fraction formed by the condensation of vapors. In general, aerosols produced by entrainment are expected to be larger than those produced by vapor condensation. Furthermore, the aerosol particles produced by entrainment should have compositions much like the bulk melt whereas aerosol particles produced by vapor condensation should have compositions reflecting the relative vapor pressures of the melt constituents. It is, however, difficult to get reproducible data immediately above the melt where the environment is very dynamic and farther from the site of melt interactions with concrete, coagulation of the aerosol obscures differences in aerosol produced by mechanical and vaporization processes.

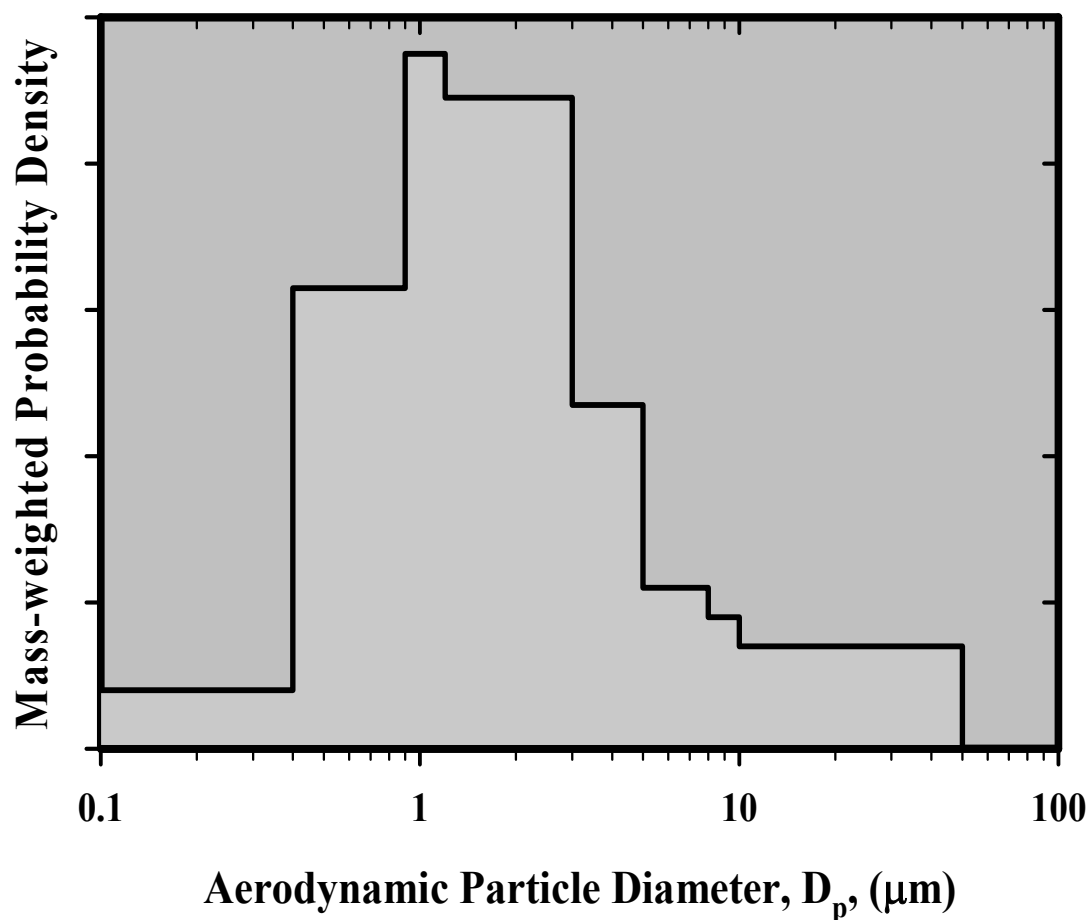


Fig. 3.9-5 Typical aerosol size distribution derived from impactor data taken during core debris interactions with concrete

A typical mass-weighted aerodynamic particle size probability density function produced from data collected by aerosol impactors during melt interactions with concrete is shown in Fig. 3.9-5. Aerodynamic mass mean particle sizes are typical around 1 μm . The geometric standard deviation values are variable exceeding 3 when interactions are very vigorous. This breadth of the aerosol particle size distribution when melt/ concrete interactions are vigorous is attributed to multiple mechanisms of aerosol production being operative. As interaction vigor subsides, aerosol size distributions are typically found to be narrower with geometric standard deviations sometimes less than 2. There is some evidence of compositional variability across the size distribution, but it is not especially pronounced.

A common accident management strategy is to provide water to cover any core debris that escapes to the reactor cavity. Though it has not been demonstrated that the water will quench core debris in a reactor cavity and prevent interactions with concrete, it has been shown that a water pool overlying core debris can attenuate aerosol production rather significantly. Attenuation of the aerosol production during core debris interactions with an overlying water pool is thought to occur by two processes. The water pool will typically cause a crust to form over the core debris that interferes with or filters aerosol produced by the entrainment of molten core debris in the gas flow and aerosol production by bubble bursting. Vapors can also condense as they pass through the crust. The water body will also scrub aerosol and vapors from bubbles emerging from the core debris and sparging through the water much as does a steam suppression

pool. That is, aerosols are removed from bubbles by a combination of diffusion, inertial impaction and sedimentation. As little as 30 cm deep pools of saturated water have been observed to reduce aerosol production during tests of core debris interactions with concrete by a factor of up to 15 [8].

Models of aerosol production during core debris interactions with concrete

Most of the important accident analysis codes have some modeling of aerosol production during core debris interactions with concrete. The most thoroughly documented of these models is the VANESA model [1] that is now part of the MELCOR computer code [9]. The models of aerosol production have to be coupled with a model of core debris attack on concrete such as the CORCON model [10] in MELCOR. The models of core debris attack on concrete provide melt temperatures, melt compositions, gas production rates and geometrical data for the aerosol production models. All of the models estimate the vapor pressures of important melt constituents and the mass transport of these vapors into bubbles of the gas sparging through the molten core debris. Correlations are based largely on data obtained for bubbles sparging through water or similarly conventional liquid [4]. Some of the models account for the mechanical production of aerosol by entrainment or bubble bursting. Entrainment modeling is usually based on data obtained for gas sparging through water. Typically, the detailed behaviour of vapors released from the core debris via the sparging gases is not modeled. It is more typical for the vapor mass to be assumed to nucleate particles that populate the smallest bin in an sectional representation of the aerosol size distribution in the reactor containment atmosphere. The subsequent coagulation and deposition of these aerosols along with aerosols from other sources are modeled using the aerosol physics models in the accident analysis codes.

References

- [1] D.A. Powers, J.E. Brockmann, and A.W. Shiver, VANESA: A Mechanistic Model of Radionuclide Release and Aerosol Generation During Core Debris Interactions With Concrete, NUREG/CR-4308, Sandia National Laboratories, Albuquerque, NM, July 1986
- [2] D.A. Powers and F.E. Arellano, Large-scale Transient Tests of the Interaction of Molten Steel with Concrete, NUREG/CR-2282, Sandia National Laboratories, Albuquerque, NM, January 1982
- [3] D. A. Powers, "Empirical Models for the Thermal Decomposition of Concrete", Transactions of the American Nuclear Society 26, (1977) 401
- [4] I. Kataoka and M. Ishii, International Journal of Heat and Mass Transfer, 27 (1984) 1999
- [5] J.K. Fink, D.H. Tompson, D.R. Armstrong, B.W. Spencer, and B.R. Sehgal, High Temperature and Materials Science, 33 (1995) 51
- [6] L. Soffer, S.B. Burson, C.M. Ferrell, R.Y. Lee, J.N. Ridgely, Accident Source Terms for Light-Water Nuclear Power Plants, NUREG-1465, U.S. Nuclear Regulatory Commission, Washington D.C., February 1995
- [7] J.E. Brockmann, Progress Nuclear Energy, 19 (1987) 7
- [8] R.E. Blose, J. Gronager, A. Suo-Antilla, D. Bradley, and J.E. Brockmann, SWISS: Sustain Heated Metallic Melt Concrete Interaction with an Overlying Water Pool: Experiments and Analyses, SAND85-1546, Sandia National Laboratories, Albuquerque, NM, 1985

- [9] R.O. Gauntt, R.K. Cole, C.M. Erickson, R.G. Gido, R.D. Gasser, S.B. Rodriguez, and M.F. Young, MELCOR Computer Code Manuals, NUREG/CR-6119, Rev.2, Sandia National Laboratories, Albuquerque, NM, December 2000
- [10] D.R. Bradley and D.R. Gardner, CORCON-Mod3: An Integrated Computer Model for Analysis of Molten Core Concrete Interactions: Users Manual, NUREG/CR-5843, Sandia National Laboratories, Albuquerque, NM, 1992

3.10 Aerosols from Fire

Fire is a hazard that can afflict all nuclear power plants. On average, a plant will have a reportable fire about once every two years. In most cases, these fires are readily suppressed and extinguished using the fire protection features of the plant. Occasionally fires of such magnitude that they threaten the safety of the plant. Of course, the most famous of the threatening fires was that at the Browns Ferry nuclear station [1] in 1975. Many enhancements to fire protection were made at nuclear plants following the incident at Browns Ferry. Still, significant fires occur [2]. Risks of fires leading to core damage have been assessed by all operating nuclear plants in the USA [3]. As shown in Fig. 3.10-1, the risk of fire leading to core damage is typically commensurate with the risk that other, internal plant events more familiar in accident analyses will lead to core damage. The risk analyses have shown that the major types of fires at nuclear power plants include combustion of hydrogen used to cool turbines, lubricating oil fires, and cable fires. Of these, cable fires are of the most safety concern. The cables of interest include power cables, control cables and instrumentation cables. Combustion of the insulation on these cables can lead to electrical shorts that can cause spurious operation of equipment, loss of safety functions and misleading control room information.

Cable fires can be the source of an enormous amount of aerosol. A photograph of smoke coming from a cable fire at a non-nuclear power plant is shown in Fig. 3.10-2. Fire and smoke from the burning of a transformer at a nuclear power plant substation is shown in Fig. 3.10-3. The smoke from cable fires is known to be quite corrosive and often contains substantial hydrochloric acid. There is a concern, then, that smoke produced in any fire, but especially smoke from cable fires, could damage equipment in plants. Because of aerosol transport, the equipment damage by deposited, corrosive aerosol particles could occur at locations well removed from the site of the fire. The effects of smoke from burning cable insulation on digital circuits that might be used in nuclear power plants have been investigated [4]. Their investigations identified types of circuits that were susceptible to smoke damage. There is, then, safety reasons to want to understand the behaviour and transport of aerosol produced by cable fires aside from interest in the interaction of fire aerosol with radioactive aerosol from a core degradation accident.

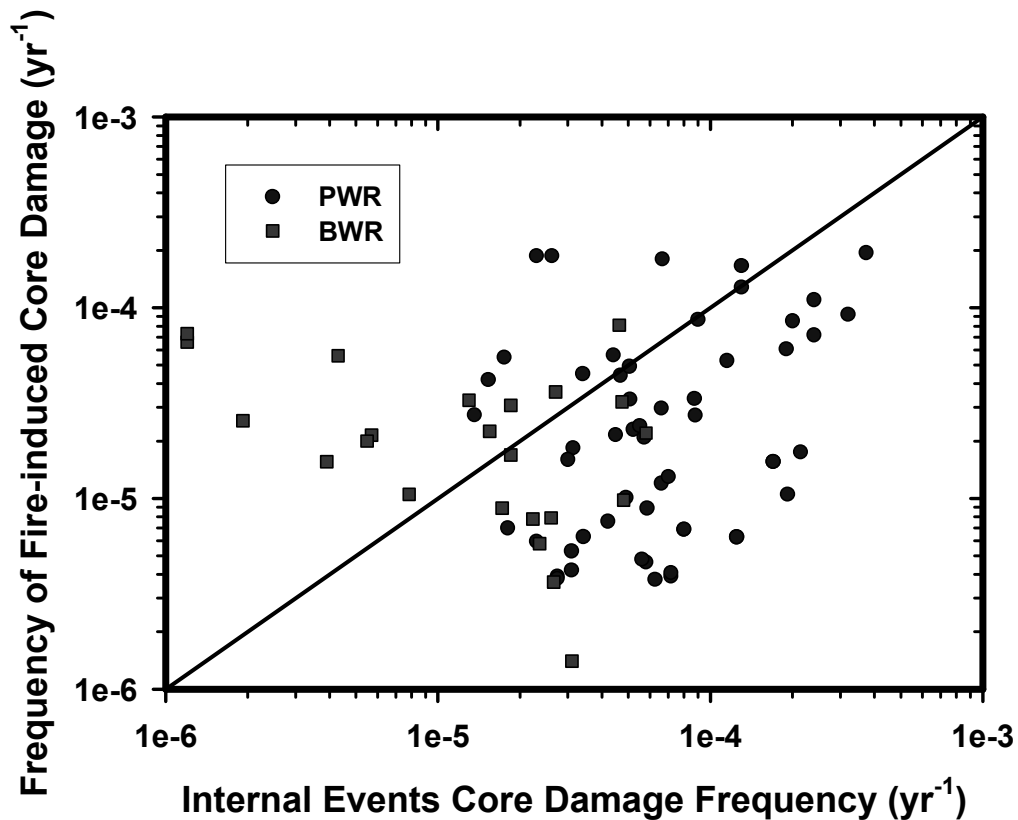


Fig. 3.10-1 Frequency of core damage caused by fire plotted against the expected frequency of core damage caused by all other credible events during plant operations for US nuclear power plants. Points are shown for US boiling water reactors (BWR) and US pressurised water reactors (PWR). Points above the diagonal black line indicate plants with greater risk from fire than from other internal initiators of plant damage. In all cases, the fire risk is commensurate with risk from other internal events.



Fig. 3.10-2 Smoke from a cable fire at a non-nuclear power plant



Fig. 3.10-3 Fire and smoke produced during a substation fire

Whereas much is known about smoke and soot aerosols produced in hydrocarbon fires, relatively little is known about the aerosol generated when cable insulation burns. The extinction coefficient of aerosol was measured in smoke tests with digital equipment [4]. Also the relative amounts of aerosol deposition on horizontal and vertical surfaces in a 92x92x123 cm test chamber were measured. Examples of these results are shown in Fig. 3.10-4 and Fig. 3.10-5. Otherwise, no quantitative information has been found about the characteristics of cable fire aerosols such as size distribution, shape factors and production rates. There are plans in ongoing cable fire tests being sponsored by the US Nuclear Regulatory Commission to collect some limited amounts of information about cable fire aerosol.

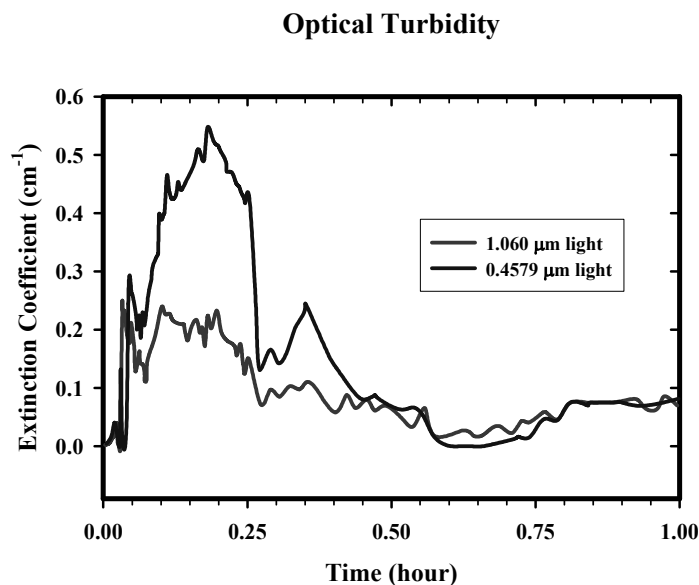


Fig. 3.10-4 Optical extinction coefficient of aerosol-laden gas phase during test of digital equipment in a cable fire. Extinction coefficient was measured at two different wave lengths each over path lengths of 1.9 and 3.2 cm to correct for the deposition of aerosols on lens surface

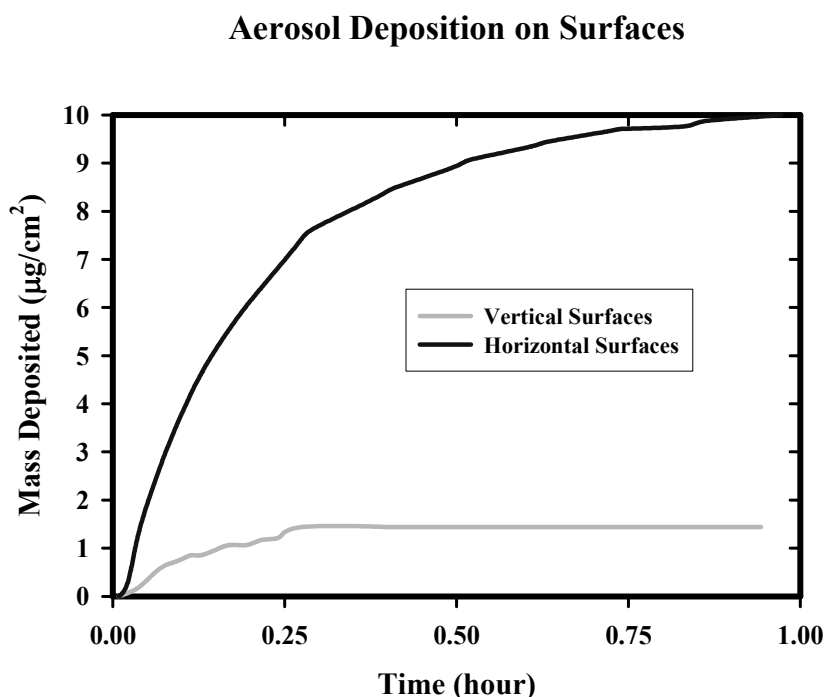


Fig. 3.10-5 Deposition of cable fire aerosols on vertical and horizontal surfaces during test of digital equipment

References

- [1] R.L. Scott "Browns Ferry Nuclear Power Plant Fire on March 22, 1975" Nuclear News, 17 (1976) 592
- [2] S.P. Nowlen, M. Dazarians, F. Wyant Risk Methods Insights Gained From Fire Incidents, NUREG/CR-6738, Sandia National Laboratories, Albuquerque, NM, September 2001
- [3] Division of Risk Analysis and Application, Office of Nuclear Regulatory Research, Perspectives Gained From the Individual Plant Examination of External Events (IPEEE) Program, NUREG-1742, Volumes 1 and 2, U.S. Nuclear Regulatory Commission, Washington, DC, April 2001
- [4] T.J. Tanaka, S.P. Nowlen, and D.J. Anderson, Circuit Bridging of Components by Smoke, NUREG/CR-6476, Sandia National Laboratories, Albuquerque, NM, October 1996, and references therein

3.11 Spray Systems

The reactor containment buildings of most pressurised water reactors and the drywells of most boiling water reactors are equipped with water spray systems. These spray systems were installed to condense steam and reduce the pressure threat to containment or drywell integrity in the event of a design-basis, large break in the reactor coolant system. Sprays are also very effective at removing aerosol particles from the containment or drywell atmospheres during severe reactor accidents [1, 2].

Spray systems consist of a large number of spray nozzles oriented differently near the top of the containment or drywell. These nozzles discharge large numbers of water droplets that fall along ballistic trajectories through the atmosphere and sweep out aerosol particles. Some characteristics of two spray nozzles commonly used in US reactors are shown in Fig. 3.11-1 and Fig. 3.11-2. The Whirljet spray nozzle

discharges water through multiple orifices over a circular pattern when directed downward so that at a distance of 3.35 m from the nozzle, 65 % of the water flow is relative uniformly dispersed over a region 3.35 m in diameter and the remaining 35 % of the flow is over an annular region with inner diameter 3.35 m and outer diameter 5.2 m. The Sprayco Model 1713-A nozzle discharges water droplets through a single nozzle. The diameter of the sprayed region is 2.58 m at 3.05 m from the nozzle, 3.60 m at 4.57 m from the nozzle and 5.8 m at a distance of 30.5 m from the nozzle. The water distribution over the sprayed region is not entirely uniform even at large distances from the nozzle as shown in Fig. 3.11-3. To achieve more uniform droplet distribution over the sprayed volume of a containment or drywell, spray patterns are overlapped.

Spray droplets remove aerosol particles from the containment or drywell atmospheres by several mechanisms:

- **Diffusiophoresis:** Steam condensing on the droplets sweeps aerosol particles into the droplet.
- **Impaction:** Aerosol particles unable to follow streamlines of flow around a droplet collide with the droplet.
- **Interception:** Because of their finite dimensions, aerosol particles with centers of mass moving along streamlines of flow contact and adhere to the droplets.
- **Diffusion:** Brownian motion carries particles across streamlines of flow into contact with falling droplets.

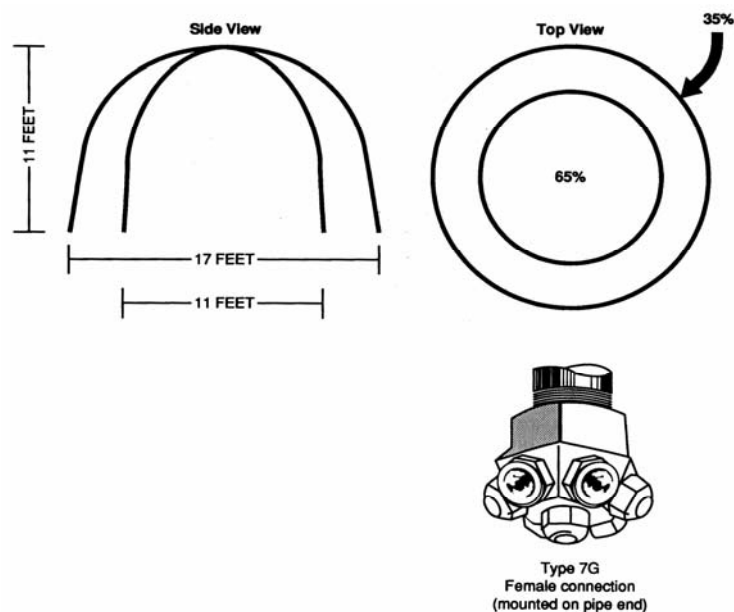


Fig. 3.11-1 Characteristics of a whirljet spray nozzle

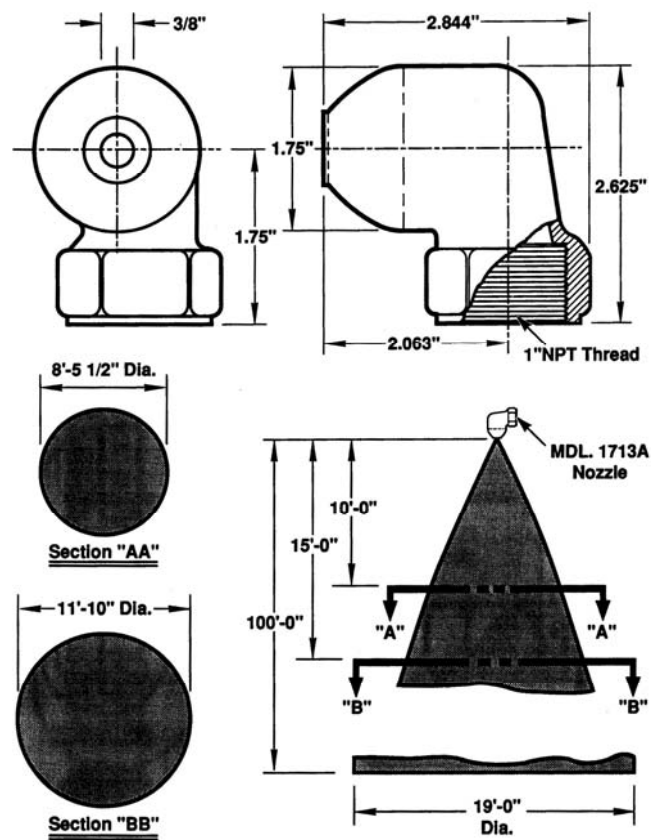


Fig. 3.11-2 Characteristics of a sprayco model 1713-A spray nozzle

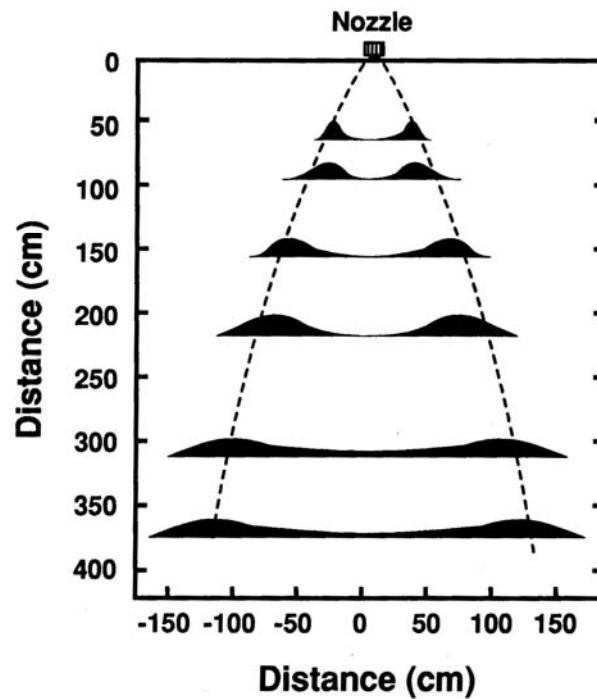


Fig. 3.11-3 Nonuniformity of spray droplet distribution from a sprayco model 1713-A spray

The diffusiophoresis mechanism is only important early in an accident when the atmosphere is steam rich and aerosol concentrations are quite low. Consequently, this mechanism is not usually considered in the analysis of the steady state effectiveness of aerosol removal by sprays.

Water droplets falling through a gas are approximately oblate ellipsoids. The droplet presents a cross-section characterised by an effective diameter $D_d(e)$ as it falls through the gas. Were the aerosol particles fixed, the water droplet would sweep out aerosols within the volume defined by the droplet cross-sectional area times the length of its trajectory. Aerosol removal would be independent of particle size. In actuality, the aerosols will try to follow the streamlines of flow around the falling droplets. Because some particles will flow around the falling droplet, there is an inefficiency in the aerosol removal by falling droplets relative to removal of fixed aerosol particles. The efficiency of aerosol removal by impaction, interception and diffusion is expressed as the ratio of the number of particles actually removed from the atmosphere by a particular mechanism to the number of fixed particles that would be removed by a droplet along the same trajectory.

$$\epsilon(i) = \frac{4N^*(i)}{\pi D_d(e)^2 n(i)L}$$

where:

- $\epsilon(i)$ = removal efficiency of particles of size class i
- $N^*(i)$ = actual number of particles of size class i removed
- $D_d(e)$ = effective droplet diameter
- $n(i)$ = concentration of particles of size class i in the atmosphere
- L = pathlength of droplet trajectory

Because the hydrodynamics of flow around a droplet, especially in a field of other droplets, can be complicated, there are different descriptions of the particle collection efficiency especially for impaction and interception mechanisms. Some commonly used expressions are [3]:

- **Impaction**

$$\epsilon(\text{impaction}) = \frac{\epsilon(\text{viscous}) + Re_d \epsilon(\text{potential})/60}{1 + Re_d/60}$$

where:

- $\epsilon(\text{impaction})$ = efficiency of particle removal by impaction

$$\epsilon(\text{potential}) = \begin{cases} 0 & \text{for } \text{Stk} \leq 0.08334 \\ \left(\frac{\text{Stk}}{\text{Stk} + \delta} \right)^2 & \text{for } \text{Stk} \geq 0.2 \\ 8.57 \left(\frac{\text{Stk}}{\text{Stk} + \delta} \right)^2 (\text{Stk} - 0.08334) & \text{for } 0.08334 < \text{Stk} < 0.2 \end{cases}$$

$$\epsilon(\text{viscous}) = \begin{cases} 0 & \text{for } \text{Stk} \leq 1.214 \\ \frac{1}{\left(1 + \frac{0.75 \ln(2\text{Stk})}{\text{Stk} - 1.214} \right)^2} & \text{for } \text{Stk} > 1.214 \end{cases}$$

$$\text{Stk} = \text{Stokes number} = \frac{C d_p^2 \rho_g U_T}{9 \mu_g D_d(e) \chi}$$

$$\text{Re}_d = \text{droplets Reynolds number} = \frac{U_T \rho_g D_d(e)}{\mu_g}$$

- d_p = aerosol particle diameter
- $D_d(e)$ = effective droplet diameter
- U_T = terminal velocity of the falling droplet
- δ = uncertain constant $0.25 < \delta < 0.75$
- μ_g = gas viscosity
- ρ_g = gas density
- χ = dynamic shape factor for aerosol particle

- **Interception**

$$\epsilon(\text{int}) = \frac{\Psi(\text{viscous}) + \text{Re}_d \Psi(\text{potential}) / 60}{1 + \text{Re}_d / 60}$$

where:

$$\Psi(\text{potential}) = 3I$$

$$\Psi(\text{viscous}) = (1 + I)^2 \left[1 - \frac{1.5}{(1 + I)} + \frac{0.5}{(1 + I)^2} \right]$$

$$I = \frac{\gamma d_p}{D_d(e)}$$

and γ is the collision shape factor of the aerosol particles. Gieseke and Lee [4] have discussed the complications and approximations involved in these particle removal efficiencies for the interception mechanism.

- **Diffusion**

Many expressions have been developed for the removal of aerosol particles by water droplets by diffusion. Among these are:

$$\epsilon(\text{diffusion}) = \frac{4}{Pe} (1 + 0.557 Re_d^{1/2} Sc^{3/8})$$

$$\epsilon(\text{diffusion}) = \frac{3.18}{Pe^{2/3}}$$

$$\epsilon(\text{diffusion}) = \frac{1}{\sqrt{2 Pe D_d(e)}}$$

$$\epsilon(\text{diffusion}) = \frac{2.18}{\sqrt{Pe}} \quad \text{for } \frac{d_p}{D_d(e)} < \frac{0.3}{\sqrt{Pe}}$$

where:

$$Pe = \text{Peclet number} = Sc Re_d$$

$$Sc = \text{Schmidt number} = \frac{3\pi\mu_g^2 d_p}{\rho_g C k T}$$

k = Boltzmann constant

C = Cunningham slip correction factor

These expressions are based on the collection by diffusion to an isolated sphere. Of course water droplets are neither spherical nor isolated. It is known [5] that the mass transport to a sphere is affected by the presence of another spherical collector.

Terminal water velocities and drag coefficients on water droplets falling through air are discussed in conventional sources [6] and include the model [7]:

$$\ln Re_T = -3.126 + 1.01 \ln N_D - 0.01912 [\ln N_D]^2$$

$$2.4 < N_D < 10^7 \quad 0.1 < Re_T < 3550$$

where:

$$Re_T = \text{terminal Reynolds number} = U_T \rho_g D_d(e) / \mu_g$$

$$N_D = \text{Best number} = 4 \rho_g (\rho_\ell) g D_d(e)^3 / 3 \mu_g^2$$

$$C_D = \text{drag coefficient} = N_D / Re_T^2$$

The combined effects of impaction, interception and diffusion on the removal of aerosol are modeled either additively:

$$\epsilon(\text{total}) = \epsilon(\text{impaction}) + \epsilon(\text{int}) + \epsilon(\text{diffusion})$$

or with a compound model:

$$\epsilon(\text{total}) = 1 - [1 - \epsilon(\text{impaction})][1 - \epsilon(\text{int})][1 - \epsilon(\text{diffusion})]$$

The removal efficiency is highly dependent on both the particle size and the effective droplet diameter. Diffusion is effective at the removal of very small aerosol particles ($<0.1 \mu\text{m}$). Impaction affects mostly aerosol particles larger than about $5 \mu\text{m}$. Interception affects particles in the size range of 0.5 to $2 \mu\text{m}$. Consequently, as shown in Fig. 3.11-4, there is a minimum in the total aerosol removal efficiency when plotted against aerosol particle size. This minimum depends on the droplet diameter. For droplets on the order of $1000 \mu\text{m}$, this minimum is in the vicinity of 0.1 to $0.2 \mu\text{m}$. For smaller droplets, the minimum shifts to larger particle sizes. The effect of the minimum in the aerosol capture efficiency is that sprays not only reduce the amount of aerosol present in the containment atmosphere, they also sharpen the size distribution of the aerosol around the size of minimum removal efficiency. This effect is shown for an example calculation in Fig. 3.11-5. For this example calculation, an initial aerosol with a mean diameter near $1 \mu\text{m}$ and a broad size distribution evolves under the action of a spray to become an aerosol with a much narrower size distribution centered round about $0.3 \mu\text{m}$.

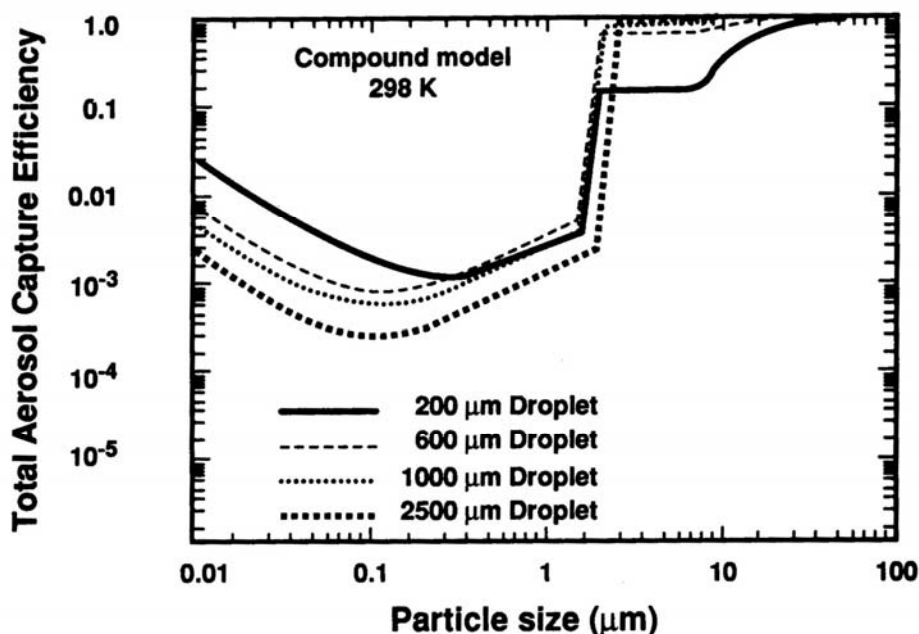


Fig. 3.11-4 Overall aerosol removal efficiency by a spray droplet as a function of particle size and droplet size. Note that the aerosol particle size least efficiently removed by spray droplets varies with the size of droplet

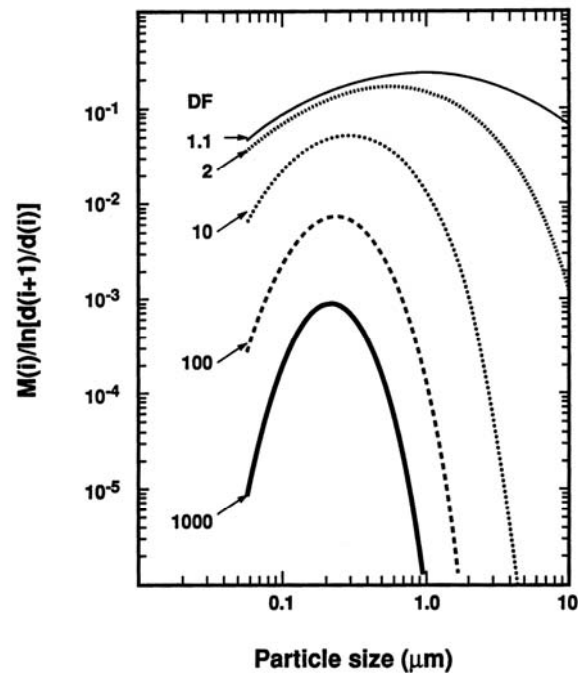


Fig. 3.11-5 Evolution of the aerosol size distribution and mass concentration during spraying. Curves are labeled by the total decontamination achieved by the spray. Note both the attenuation of the aerosol as well as the shift and narrowing of the size distribution

Many models of the effects of spray on aerosol in reactor accident consider only a single droplet size and often predict a persistent residual aerosol concentration that is only very slowly removed from the atmosphere. In fact, spray nozzles produce a distribution of droplet sizes. The number distribution of droplets from two types of spray nozzles are shown in Fig. 3.11-6 and Fig. 3.11-7. The number distributions are not simple, but they are peaked for reasonably small droplets. On the other hand, the mass weighted distribution of the spray droplet sizes are peaked in both cases above 1000 μm .

Whirljet Spray Head

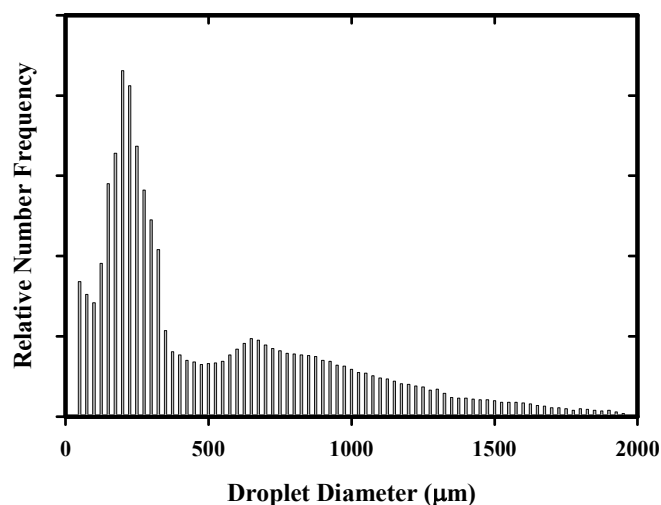


Fig. 3.11-6 Number distribution of spray droplet sizes for a whirljet spray head

To avoid an artificial prediction of a persistent aerosol in a sprayed atmosphere, it is necessary to account for the distribution of spray droplets sizes. A complication in doing this is that spray droplets collide with each other. A commonly used expression for the efficiency of droplet-droplet interactions is:

$$\epsilon_{ij}(\text{droplet} - \text{droplet}) = \frac{D_d^2(i)}{[D_d(i) + D_d(j)]^2} \quad \text{for } D_d(i) > D_d(j)$$

Experimental evidence suggests that this expression over estimates the interactions of droplets with other droplets of similar size. A more empirical expression consistent with available experimental data is [8]:

$$\epsilon_{ij}(\text{droplet} - \text{droplet}) = \begin{cases} 1 - \frac{D_d(j)}{D_d(i)} & \text{for } \frac{D_d(j)}{D_d(i)} < \frac{1}{8} \\ 0 & \text{otherwise} \end{cases}$$

Sprayco Model 1713-A

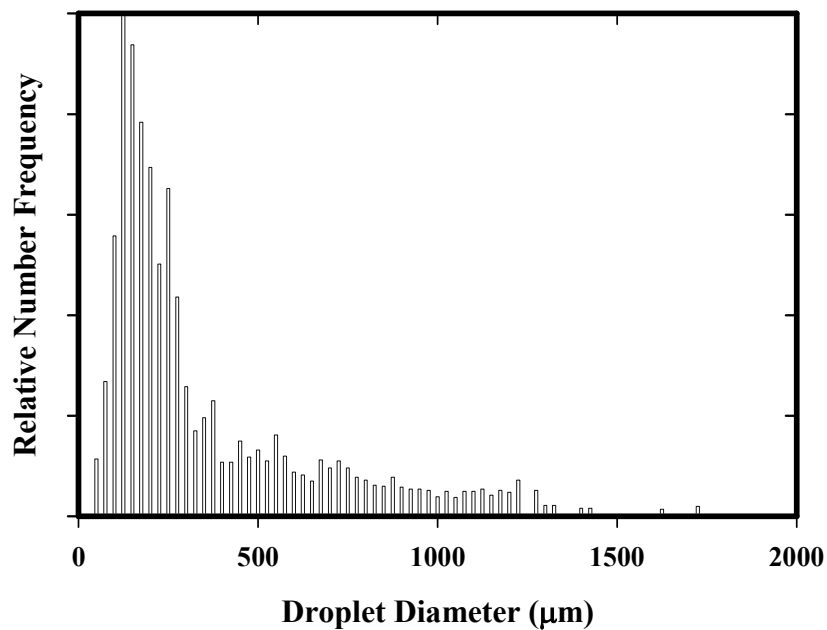


Fig. 3.11-7 Number distribution of spray droplet size for a sprayco model 1713-A nozzle

The evolution of the spray droplet size distribution as a function of fall distance is shown in Fig. 3.11-8. The effect of droplet-droplet interactions is to remove from the distribution the smaller droplets which are more effective at trapping aerosol particles.

There has not been a great incentive to improve models of spray removal of aerosol particles since sprays are enormously effective at decontaminating a atmosphere. Reductions in the aerosol concentration by a factor of 10 can initially be achieved in a time on the order of one hour. Further reductions in the aerosol concentration are slower because the action of the spray alters the size distribution of the aerosol so that particles are less efficiently removed. Nevertheless, decontamination factors in excess of 1000 are practically achieved.

Watanabe *et al.* [9]. have reported integral tests to validate the modeling of spray removal of aerosols in the MELCOR accident analysis model. The tests were done in a facility 18 m tall with a volume of 12.2 m³. CsI particulate were used in the test. Other tests in the effort used latex particles. The investigators were able to obtain good agreement between test results and model predictions.

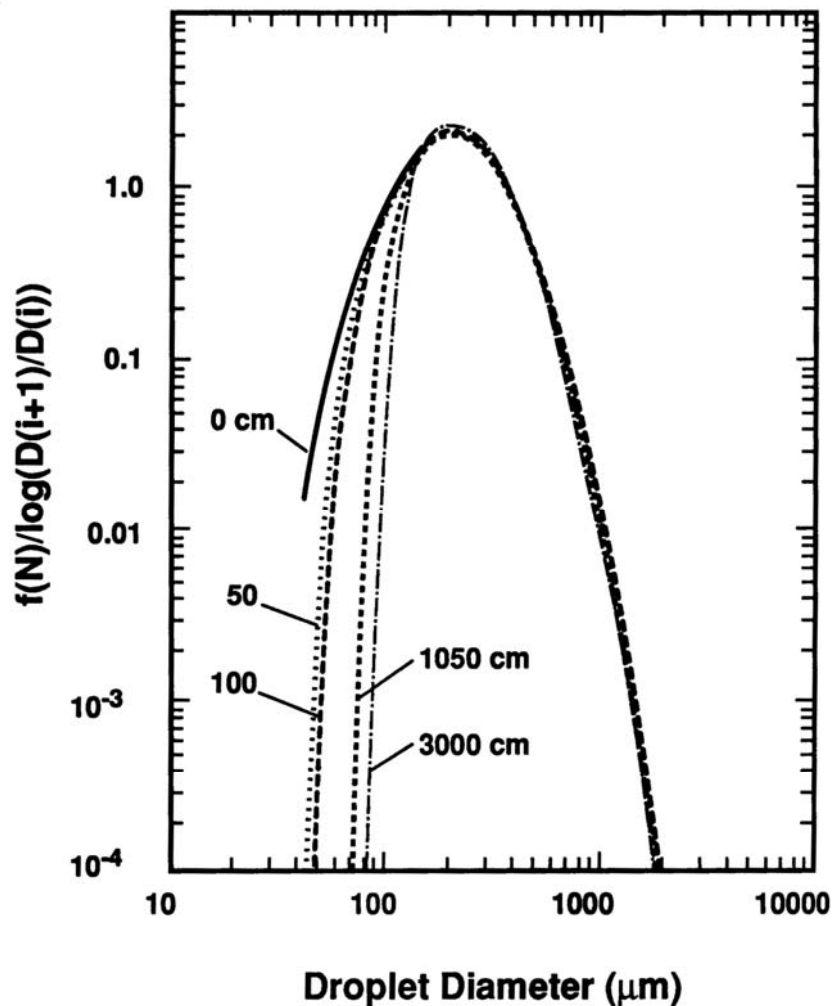


Fig. 3.11-8 Evolution of droplet size distribution as a function of fall distance based on the empirical model of droplet-droplet interactions

References

- [1] R.K. Hilliard, et al Nuclear Technology, 10 (1971) 499
- [2] M. Tanaka, et al Nuclear Technology, 54 (1981) 54
- [3] D.A. Powers and S.B. Burson A Simplified Model of Aerosol Removal by Containment Sprays, NUREG/CR-5966, Sandia National Laboratories, Albuquerque, NM, June 1993
- [4] K.W. Lee and J.A. Gieseke J. Aerosol Sci., 11 (1980) 335

- [5] A.R.H. Cornish Trans. Institute of Chemical Engineers, 43 (1965) 332
- [6] R. Clift, J.R. Grace and M.E. Weber Bubbles, Drops and Particles, Academic Press, 1978
- [7] C.S. Pemberton J. Air Pollution, 3 (1960) 168
- [8] N. Arbel and Z. Levin Pure and Applied Geophysics, 115 (1977) 869
- [9] A. Watanabe, H. Nagasaka, S. Yokooori, and M. Akinaga
http://www.nupec.or.jp/database/paper/paper_11/

3.12 The Impact of Catalytic Hydrogen Recombiners

Background

Passive hydrogen re-combiners have been studied for many years as a means of preventing accumulation of hydrogen in the containment of a water-cooled reactor following a design-basis or severe accident [1, 2]. Their installation is now an established and sometimes mandatory measure. Back-fitting of such devices on existing nuclear power plants has been performed or is in progress in many countries while Generation III reactor designs (AP600, EPR, etc.) are already equipped with them.

Passive autocatalytic recombiners (PAR) are usually based on palladium and/or platinum dispersed on some substrate medium. A PAR comprises a vertical conduit with the catalytically-active part near the bottom. If hydrogen is present in the containment, the hydrogen molecules making contact with the noble-metal catalyst react with the oxygen of the containment atmosphere producing steam and heat. The reaction heat provokes heating up of the catalytic elements inducing natural convection which draws more of the containment atmosphere into the PAR from below. The effect is not only to recombine hydrogen with oxygen as it passes through the catalytic elements but to mix the containment atmosphere eliminating any pockets where hydrogen concentrations may be elevated. We note also that carbon monoxide is oxidised on the catalysing surface. While the operating principle of PARs is well understood, there remains some progress to be made before it can be said that a thorough understanding exists of the sensitivity of PARs to the conditions expected to be produced by design-basis or severe accidents. It should be noted, however, that while little information is in the public domain (e.g., see [2, 3]) much more probably remains proprietary. There are a number of companies marketing PARs, e.g., Atomic Energy of Canada Limited, AREVA/ Framatome-ANP, Nuklear Ingenieur Service mbH, Electrowatt-Ekono AG, and each design is different having its own operating characteristics.

There is a potential problem with the use of PARs in relation to aerosol particles suspended in the containment atmosphere. As these pass through the catalytic elements they will be heated up along with the gases and this will inevitably lead to partial evaporation of volatile species from the aerosols. Peak temperatures of the catalytic elements varies according to the manufacturer but is in the range 500 - 900 °C, i. e., high enough to evaporate many fission-product species. These fission-product vapors may well interact chemically with each other and/or with the gases of the atmosphere (in general a combination of nitrogen, oxygen, steam, carbon monoxide and carbon dioxide), especially oxygen. There is therefore the possibility that reactions in PARs could lead to formation of more volatile forms of fission-product species aggravating the source term by converting easily-filtered aerosol material into more troublesome vapors and gases.

Current knowledge

Only a single series of experiments, known as RECI, has been performed to investigate the thermal decomposition of fission-product species in conditions related to those of a severe accident [4, 5]. The

objective of the RECI experiments was measurement of any creation of more volatile forms of iodine, viz. I_2 , HOI and HI, from metal-iodide species expected in severe accidents, viz. AgI, InI, CdI_2 and CsI. Two of these species, cesium iodide or cadmium iodide, in an atmosphere of humidified air were injected as aerosols into a heated tube in tests both with and without the presence of a catalysing surface. The experiments comprised separate tests for aerosols of each of the two pure substances. The peak temperature of the heated tube was varied between 500 and 950 °C. The gas-phase iodine species were not measured in the heated tube but downstream where temperature had once again become ambient. It was found that thermal decomposition producing molecular iodine could occur even for the more stable of these species, cesium iodide, where the presence of a catalyst increased the iodide to iodine conversion by a factor of two to three. At the highest temperatures, conversion rates of more than 10 % were measured for cesium iodide. Conversion rates for cadmium iodide were significantly greater. Sensitivity to parameters such as particle size and transit time through the heated zone was checked where longer transit times and smaller particles led to higher conversion rates. A further effect of the partial evaporation of the aerosols was to produce a population of small particles as the vapor(s) re-condensed during cooling downstream of the heated tube. This new population resulting from homogeneous nucleation was significantly smaller than any of the source particles injected into the heated tube.

A potential effect of the molecular iodine production would be to poison the catalyst with respect to hydrogen conversion. However, in separate tests, this poisoning was found to be very limited [3].

Initial analysis of the RECI tests [6] supports the idea that the kinetics of the chemical reactions downstream of the heated zone is the key to understanding the conversion rates. In other words, if a thermodynamic approach to chemistry is assumed (i.e., equilibrium chemistry) as the flow cools then the volatile species convert back to less volatile forms and conversion is virtually zero. Furthermore, the conversion rates calculated at the peak temperature, i.e., in the heated tube, are close to those measured at ambient temperature implying almost complete quenching of chemical reactions once they left the heated tube.

It should be understood that these experimental results are simply a confirmation of the potential for iodine species from containment aerosols to convert to more volatile species while in transit through a PAR. A number of representativity aspects prevent these results from being extrapolated to the reactor case. In the first instance, the aerosols investigated were pure substances: the consequences of using prototypical mixed-substance aerosols will necessarily alter the gas-phase chemistry produced in the PARs. In addition, the presence of mixed aerosols with refractory kernels will perhaps facilitate re-condensation of evaporated species during cooling onto existing aerosols rather than formation of new ones, i. e., heterogeneous rather than homogeneous nucleation. The gas mixture used in these tests was humidified air where, in the containment, at least during a severe accident, a less-oxidizing mixture containing a higher steam fraction as well as hydrogen will be present: it is known that reducing conditions are thermodynamically less favourable to formation of volatile iodine species. Finally, the cool-down characteristics of the flow leaving the PARs have not been reproduced in the RECI tests: this is crucial to the propensity for vapors to re-convert as they cool where more rapid cooling will not favour this re-conversion to a gas-vapor-aerosol mixture closer to that at equilibrium at ambient temperature.

References

- [1] F. Fineschi, G. Koroll, J. Rohde "Mitigation of hydrogen hazards in water cooled power reactors", IAEA-TECDOC-1196 (2001)
- [2] E. Bachellerie, F. Arnould, M. Auglaire, B. de Boeck, O. Braillard, B. Eckardt, F. Ferroni, R. Moffett "Generic approach for designing and implementing a passive autocatalytic recombiner PAR-system in nuclear power plant containments" Nucl. Eng. Des. 221(1-3), 151-165 (2003)

- [3] F. Morfin, J.-D. Sabroux, A. Renouprez “Catalytic combustion of hydrogen for mitigating hydrogen risk in case of a severe accident in a nuclear power plant: study of catalysts poisoning in a representative atmosphere”, *Applied Catalysis B: Environmental* 47, 47-58 (2004)
- [4] F. Deschamps, J.-C. Sabroux “Etude de la production d’iode gazeux par un aerosol d’iodure de césium soumis à des températures élevées dans l’air humide” *Proc. 18th French Aerosol Conference*, Paris, 11-12 Dec. 2002, ASFERA (2002)
- [5] F. Deschamps, J.-C. Sabroux “Particulate iodide to gaseous iodide conversion in a passive autocatalytic hydrogen recombiner” *J. Aerosol Sci.* 34, S1087-S1088 (2003)
- [6] N. Baltzer, M.P. Kissane private communication (2005)

3.13 Filters

Type of filters in use

The requirements for the design of a filter system in removing the fission products depend on the thermal hydraulic conditions (temperature, pressure, humidity level or steam condensation, flow rate through the filter system) and concentration of the fission products in gaseous and aerosol form. The severity of the conditions imposed by the normal operational conditions or accidents (design basis or severe accidents involving core damage) produce the challenge for the design of the systems.

Normal operation and design basis accidents

During operational conditions containments are normally kept sub atmospheric in order to avoid any accidental release of even small activity into the environment. Ventilations systems, depending on the design and regulatory requirements, may contain parallel trains of filtration systems. A typical filter train contains the following sequential components: (1) a moisture separator to remove entrained water droplets, (2) a heater to control relative humidity (RH) when the RH of the air entering the carbon adsorber exceeds nominally 70 %, (3) prefilters, (4) HEPA filters, (5) a charcoal adsorber, (6) HEPA filters downstream of the adsorbers, and (7) a fan. Fig. 3.13-1, adopted from [1], displays a typical filtration unit. Ducts, valves, and dampers are also included for system isolation and flow control, as well as related instrumentation. When the moisture and dust loads are low for all credible operating modes, the prefilter and moisture separator may not be required.

The source of activity in the containment originates from the release of dissolved activity (e.g., iodine) in the primary coolant water as a result of a leak from the circuit. The source of the activity in the circuit could be due to leaking fuel elements or due to iodine spiking. The maximum permissible activity level in the circuit and in the containment is defined by regulations.

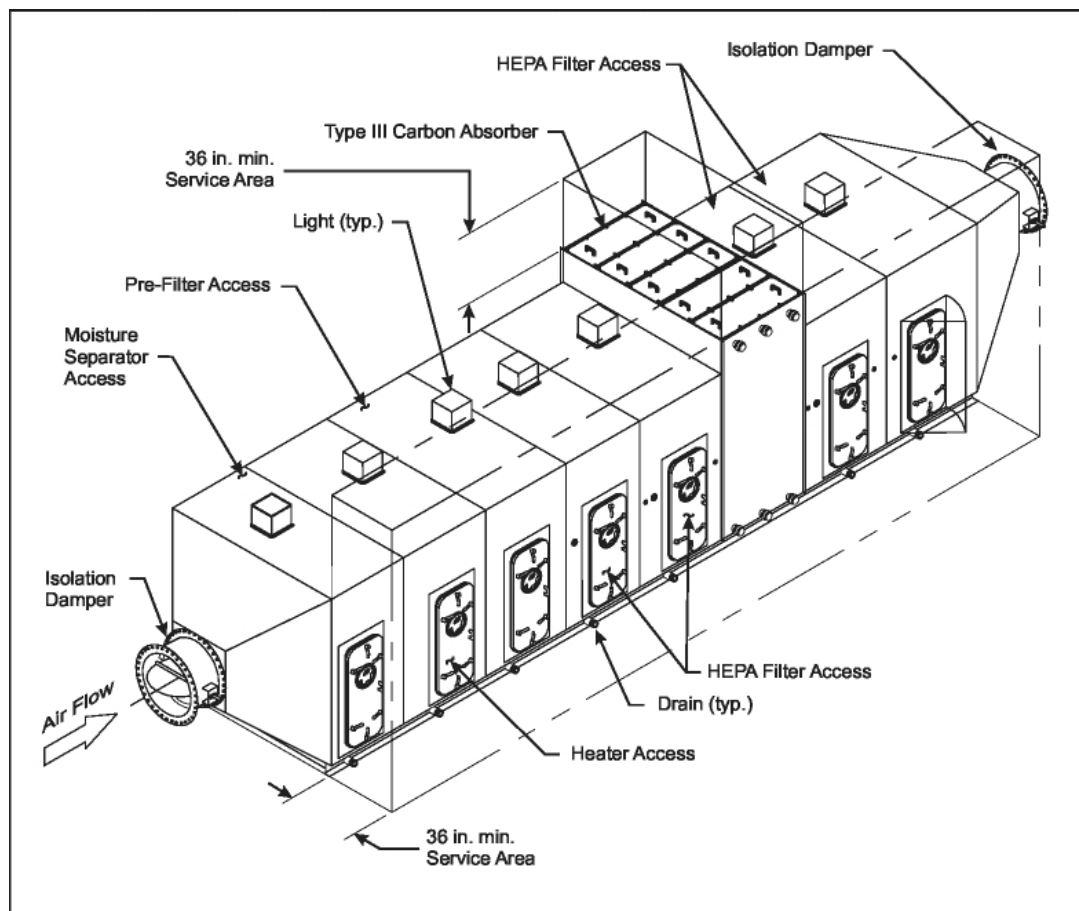


Fig. 3.13-1 A typical air cleaning system [1]

By definition design basis accidents (DBA) involving loss of coolant foresee rupture of cladding of certain number of fuel rods, which then causes the release of fuel cladding gap inventory into the primary coolant water. The inventory is mostly composed of noble gases, and volatile fission products (iodine, cesium). The release of the primary coolant water into the containment causes the activity release into the containment. If the accident is a containment by-pass accident then the activity is released directly either into the auxiliary/reactor building (V-sequence) or through the broken steam generator tube(s) (SGTR) into the steam generator secondary side and after some scrubbing in the secondary water, eventually directly into the environment. Loss of coolant accidents due to SGTR with few tube failure normally do not cause any fuel cladding failure, but a certain fraction of the dissolved activity in the primary circuit at the time of the accident may be released into the environment in a combination of gas and in water dissolved form. Release of water droplets or continuous water flow will be the transport media for the dissolved activity out of the steam generator secondary side. The break location determines the extent of each of such release.

Containment or auxiliary (reactor) building filtration systems are designed to avoid any substantial release of activity transported by aerosol particles and gaseous iodine. Of course the main assumption at the background of this statement is that the containments are isolated and there are no uncontrolled leak paths.

Severe accidents

Severity of the conditions during severe accidents varies depending on the success of the accident management measures attempted. However, anticipated conditions: high temperature, high pressure, high

steam concentrations, hydrogen burns or detonations, high aerosol and gaseous fission product concentrations, and resulting high activity levels, are very much depending on the accident progression driven by the status of the hardware as well as the accident management efforts. Contrary to the operational or design basis accident conditions the anticipated severe accident conditions cannot be used as the design parameters for the conventional filtration systems within the practical limitations. However, as a result of the emerging new regulatory requirements for the severe accidents, which can not be 'normally' fulfilled by the conventional filtration systems new filtration concepts were developed in 1980s to backfit the current operating reactors in some countries. The main emphasis in the new regulatory requirements is to keep the pressure in the containment under the design limits in order to avoid catastrophic containment failures by relieving the pressure by venting through a containment venting filter, which should at the same time remove the aerosol particles and molecular gaseous iodine with certain efficiencies.

Some of the new developed systems by various vendors at that time were tested by an international project, Advanced Containment Experiments (ACE) Phase A, 1988-1992 [2]. The following section summarises the filter concepts and the results achieved from the ACE experiments. Another containment venting filter unit developed and tested in Switzerland is also introduced.

Characterisation of filter performance

There are several parameters currently in use to describe the effectiveness of a filtration device. These are, however, all based on the mass of material injected to a device, m_{in} , and the mass of material exhausted, m_{out} . In the nuclear industry the most commonly used parameter is the Decontamination Factor, DF, which is defined as the ratio of the injected to exhausted mass:

$$DF \equiv \frac{m_{in}}{m_{out}}$$

Intimately related to the DF is the penetration, P_t , which is defined as the ratio:

$$P_t \equiv \frac{m_{out}}{m_{in}}$$

This is just the inverse of the DF. The collection efficiency, η , is defined the ratio of the collected to the injected mass. This can be written in terms of the injected and exhausted masses as:

$$\eta \equiv 1 - \frac{m_{out}}{m_{in}}$$

For most filtration devices, the efficiency of collection depends strongly on the particle size. Hence it is useful to introduce the concept of a "fractional efficiency" where the definitions above apply for particular particle size ranges. This definition introduces a difficulty for processes where the particles change size within the filtration device. For example, hygroscopic particles can grow substantially [3] in wet scrubbers. In this situation, the amount of exhausted mass in a particular size range must be based on the inlet size distribution. Unfortunately, this is impossible to do experimentally, where only inlet and outlet size distributions are measured, but the inlet and outlet particle concentrations in each size range cannot be related. The only ways to determine this information are to either use aerosols, which do not grow, or less ambiguously, inject only monodisperse aerosols.

The penetration can be quantified on the basis of a one dimensional filtration model as illustrated in Fig. 3.13-2

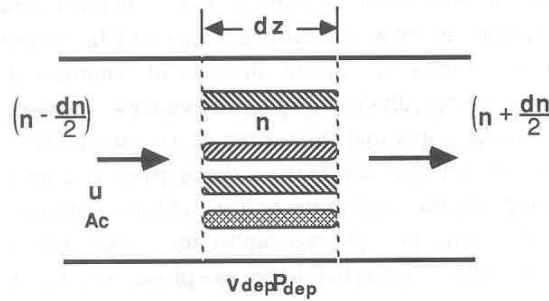


Fig. 3.13-2 Scheme of a one-dimensional filtration model

If the flow of aerosols through a control volume of length dz is considered and additionally a deposition velocity v_{dep} and a deposition area of $P_{dep}dz$ are postulated, a mass conservation equation for aerosols can be written as:

Aerosols in $\left(n - \frac{dn}{2}\right) u_g A_c$	- Aerosols out $\left(n + \frac{dn}{2}\right) u_g A_c$ $=$ $-\frac{dn}{n} =$	= Aerosols deposited $n v_{dep} P_{dep} dz$ $\frac{v_{dep} P_{dep}}{Q_g} dz$
--------------------------------------------------------	---------------------------------------------------------------------------------------	------------------------------------------------------------------------------------

and after the integration as:

$$P_t \equiv \frac{1}{DF} \equiv 1 - \eta \equiv \frac{n_{out}}{n_{in}} = \exp\left\{-\frac{v_{dep} A_{dep}}{Q_g}\right\}$$

$$= \exp\left\{-\frac{v_{dep} A_{dep} \tau}{V_g}\right\}$$

These expressions for overall penetration or efficiency apply to all the filters considered.

Nomenclature

Latin Symbols

A_c	Cross sectional flow area
A_{dep}	Deposition area
DF	Decontamination factor
m_{in}	Mass of aerosol particles injected to filtration system
m_{out}	Mass of aerosol particles exhausted from filtration system
m_p	Particle mass
n	Aerosol particle number

n_{in}	number of particles entering in the filter
n_{out}	number of particles leaving the filter
P_{dep}	Deposition area in the vertical surface of a filter slice along the integration direction
P_t	Penetration
Q_g	Volumetric flow rate of gas
u_g	Gas velocity
v_{dep}	Deposition velocity
z	Axial distance along venturi from the water injection point

Greek Symbols

η	Overall collection efficiency
--------	-------------------------------

References

- [1] DOE handbook, nuclear air cleaning handbook, DOE Technical Standards, DOE-HDBK-1169-2003, November 2003
- [2] M. Merilo, I.B. Wall "Containment Filtration Systems Tests, Summary Report" Electric Power Research Institute, ACE Phase A, TR-A22, February 1992
- [3] M.S. Hoseyni, A.T. Wassel "Growth of Aerosol Particles in a Steam Environment and its Effect on Removal", Nuclear Eng. & Des, Vol. 97, 103 - 109, (1986)

3.14 Two Phase Flashing Jets and Water Aerosol Behaviour

The scenario for generation of a two-phase flashing jet in a reactor accident involves pressurised coolant upstream of a break being released into a region of lower temperature and pressure. The value of the superheat (T_{sh}) for the pressurised water depends upon its initial temperature, and the saturation temperature of the atmosphere to which it is released, $T_{sat}(P_{\infty})$. If the saturation temperature is less than the initial temperature of the liquid, then the release is defined to be superheated, with the degree of superheat equal to $T_{sh} = T_0 - T_{sat}(P_{\infty})$. If the liquid is released into standard atmospheric conditions, this simply represents the amount the initial temperature exceeds the normal boiling point of that liquid ($T_{sh} = T_0 - T_b$). The initial state of the water is termed sub-cooled. If there is a break in the heat transport system, and the water remains subcooled at the exit of the break, it would emerge as a single-phase homogeneous jet that would disintegrate through mechanical processes. If downstream conditions lie below the liquid/vapor phase line, ($T_{sh} > 0$), the liquid pressure in the vicinity of the break may drop below the local saturated vapor pressure, and the process known as flashing begins. The flashing process would be expected to be the dominant mechanism for formation of water droplet aerosols after breaks in the high-pressure primary-heat transport system (HTS).

Most current jet dispersion codes divide the process of atomisation or flashing of superheated jets into two possible outcomes governed by mechanisms that operate independently, and whose relative importance depend on the degree of superheat of the liquid: the first is termed mechanical break-up, the second flashing break-up. However, there is no consensus regarding the relative contributions of these two processes to the droplet size distribution from a flashing jet.

The behaviour of the two-phase (water-droplet and steam) jet has important implications for reactor accident safety analyses. High enthalpy coolant flashing can cause the containment pressure to rise above atmospheric, thereby increasing the potential for airborne fission products to leak out of containment. The water droplets generated in the jet can "wash" previously released airborne aerosols and gaseous fission

products out of the atmosphere. The jets themselves are also a primary means by which fission products enter containment. Water droplets formed by the jet discharge can coalesce to form larger droplets, settle to the floor of the discharge room, impinge upon containment walls and structural surfaces, or remain suspended, where they could be carried to the atmosphere through containment leaks, or to another room in containment. Consequently, evaluation of the radiological consequences of nuclear reactor accidents requires models for two phase flashing jets.

Water droplet aerosols generated by two-phase flashing jets are subject to the same aerosol removal processes that are modelled routinely for dry aerosols in atmospheric aerosol codes (see Chapter 2). However, the large momentum of the jets from an HTS break can result in inertial impaction becoming a uniquely dominant removal mechanism if there are any obstacles in the jet path [1, 2]. The combination of processes such as inertial impaction and turbulent deposition (see Chapter 2) that act to remove water droplets after jet-obstacle interaction is referred to as impingement. The solid surface acts as an aerosol collection device, with a collection efficiency³ that depends on droplet thermophysical and transport properties (size, angle of incidence, velocity), and surface roughness.

Aerosol collection efficiencies for inertial impaction are generally correlated to the droplet Stokes number (St_d), defined as the ratio of particle stopping distance, or inertial range (τ) at a given velocity, to the nozzle (or jet) radius (see Chapter 2). Assuming that the velocity and droplet size distribution are known at the region where jet impaction takes place, and that correlations between collection efficiency and droplet Stokes number hold, jet impingement could be modelled using the same correlations. However all of the data correlating collection efficiencies to Stokes numbers was obtained at Reynolds numbers of less than 1×10^4 , [3, 4, 5] whereas Reynolds numbers for inertial impaction from 10 MPa discharges could be more than an order of magnitude higher [Chiang, 1998]. There are no studies of impactor collection efficiencies at high Reynolds numbers.

A large body of data on the behaviour of flashing liquid propane is available from a European Union funded program performed by the CEA in Grenoble [7, 8]. The propane release behaviour was examined as a function of orifice diameter and initial storage pressure. The experiments measured the void-fraction, pressure and temperature data within the blowdown vessel. Droplet size and velocity measurements were taken at 3 downstream axial locations, and the distributions have been described as well-behaved functions that could be adequately represented by general size distribution functions such as the lognormal or Rosin-Rammler⁴ [9]. Unfortunately, there are very few experiments suitable for validating models on the behaviour of flashing jets from high temperature, high pressure water releases, and even fewer for validation of processes such as impingement⁵.

The WALE facility experiments [1, 2] represent the largest collection of data on flashing water jet releases, and are the only intermediate scale studies performed on droplets generated by flashing and removed by impingement on obstacles. The studies were performed in a 19 m³ cylindrical pressure vessel, with discharge of liquid water at 1 to 10 MPa, and various degrees of sub-cooling. The effects of nozzle geometry (size, length to diameter ratios), impingement plate characteristics (size, orientation with respect to the jet and distance from break) were examined. Droplet velocities and size were also measured, although experimental difficulties were encountered with measurement of the former. In general, the data

³ defined as the ratio of the mass of droplets or particles deposited on the solid surface per unit time to the total mass of droplets or particles moving with the jet per unit time.

⁴ The weight-size distribution proposed by Rosin and Rammler in 1933 is where $M(>\ell)$ is the cumulative mass of all particles of mass greater than size ℓ , M_T is the total mass of the distribution, Φ is a size related to the average size of the distribution, and the exponent k is a free parameter. [10]:

⁵ Small-scale studies published by [11] have been used to correlate liquid collection efficiency for a two-phase jet impinging normally on a flat surface.

showed that, for the entire range of conditions studied, more than 99 % of the water droplets were removed from the vessel by various mechanisms.

The behaviour of flashing jets, including their production of water droplets, is reasonably well understood qualitatively. However, there is no consensus in the literature regarding the prediction of water aerosol droplet sizes from these jets, and very little data with which to validate models for aerosol removal from this high temperature, high pressure flashing jet releases.

References

- [1] R.J. Fluke, K.R. Weaver, G.L. Ogram, L.N. Rogers, C.F. Forrest The Water Aerosol Leakage Experiments: Programme Description and Preliminary Results In Proceedings of the Second International Conference on Containment Design and Operation, Toronto, 1990A
- [2] R.J. Fluke, G.L. Ogram, L.N. Rogers, K.R. Weaver Aerosol Behaviour in the Water Aerosol Leakage Experiments In Proceedings of the Second International Conference on Containment Design and Operation, Toronto, 1990B
- [3] V.A. Marple A Fundamental Study of Inertial Impactors. Ph.D. Thesis, University of Minnesota, Minneapolis, MN, 1970
- [4] V.A. Marple, B.Y.H. Liu Characteristics of Laminar Jet Impactors Environmental Science and Technology, 8, 648, 1974
- [5] V.A. Marple, K.L. Rubow Theory and Design Guidelines In Cascade Impactor Sampling and Data Analysis, American Industrial Hygiene Association Monograph, J.P. Lodge and T.L. Chan (editors), 1986
- [6] H.W. Chiang A Model for the Removal of Water Droplet Aerosols from a Flashing Jet Impinging onto a Plate In Proceedings of an OECD/CSNI Workshop on Nuclear Aerosols in Reactor Safety, Cologne Germany, NEA/CSNI/R(98)4, 1998
- [7] E. Hervieu, T. Veneau Experimental Determination of the Droplet Size and Velocity Distributions at the Exit of the Bottom Discharge Pipe of a Liquefied Propane Storage Tank During a Sudden Blowdown J. Loss Prev. Ind., 9, No. 6, 413-455, 1996
- [8] S. Vandroux-Koenig, G. Berthoud Modelling of a Two-Phase Momentum Jet Close to the Breach, in the Containment Vessel of a Liquefied Gas J. Loss Prev. Ind., 10, No. 1, 17-29, 1997
- [9] H.W.M. Witlox, P.J. Bowen Flashing Liquid Jets and Two-Phase Dispersion a Review Health and Safety Executive (HSE) Contact Research Report 403. St Clements House, 2-16 Colegate, Norwich, UK, 2002
- [10] W.K. Brown, H.K. Wohletz Derivation of the Weibull Distribution Based on Physical Principles and Its Connection to the Rossin-Rammler and Lognormal Distributions Journal of Applied Physics 78, No. 4, 2758-2763, 1995
- [11] N.A. Fuchs, C.N. Davis (editors) The Mechanics of Aerosols Pergamon Press, Oxford England, 1964

3.15 Penetration Leakages

3.15.1 Introduction

An understanding of the aerosol-removal and transport in containment leak paths is important both from the perspective of calculating the amount of airborne activity released into the environment and in estimating the doses to containment for equipment qualification and habitability assessment.

In the event of a reactor accident in which the containment envelope becomes pressurised, there is a potential for aerosol and gas leakage to the outside atmosphere through a variety of paths that can be categorised as belonging to one of three general types:

- valves and seals
- concrete joints, cracks and penetration gaps (e.g., process and control wiring and piping), and
- pores in intact concrete.

Leakage past seals and valves in containment would involve a sudden change in the flow cross-sectional area and short path lengths relative to those of the other flow paths. Leak paths along concrete-penetration gaps, joints and cracks are more tortuous and significantly longer. Finally, leak paths through concrete pores are characterised by small diameter cross-sectional areas, long and complex flow channels and high flow resistances. Depending upon the temperature of and flow through these paths, and the size of the aerosols, significant aerosol retention might be expected. However, many safety analyses still assume that aerosol release rates and gas release rates are identical.

Most experimental investigations on aerosol retention in leak paths [1, 2, 3, 4] have focused on small leaks and capillaries of diameters ranging from few microns to few millimetres, submitted to pressured differences up to several bars. However, large scale experiments were conducted in the Containment System Experiments (CSE) programme which used a one-fifth linear scale model of a typical 1000 MWe PWR [5]. The CSE results indicated aerosol decontamination factors from 10 to 100 under dry conditions (15 for iodine and 100 for cesium), and complete retention under wet conditions. More recently, [6] performed large-scale experiments on actual containment penetrations of BWR containments and they found decontamination factors for CsI under dry conditions ranging from 10 to 1000.

Some theoretical developments have been also undertaken. [7] proposed a broadly accepted correlation (Equation 1) that relates the total aerosol mass, m (g), leaked before reaching a complete plugging of the crack to duct of diameter D (cm³),

$$m = k \cdot D^3 \quad (1)$$

where k (30 ± 20 g/cm³) is an empirical constant determined by fitting data obtained from straight and smooth ducts 20 μ m to 26.5 cm in diameter with circular cross sections, submitted to pressure differences ranging from 0.3 kPa to 0.7 MPa.

The theoretical basis for aerosol penetration in cracks was reviewed by [8]. However, a mechanistic model based upon this theory would be too complex to be implemented in current safety analyses codes. Intermediate approaches between empirical correlations and mechanistic models look to be the most promising. Anyway, whatever modelling nature, models used in containment codes must be validated over a range of conditions (e.g., leak path geometries, temperatures, pressures etc.) that may be reactor and accident specific. Presently, existing models are not mature enough and a sound, reliable and representative database against which to validate them is still missing.

The first subchapter presents the status of current modelling and experimental studies on aerosol leakage. The first summary describes work being carried out within the Severe Accident Research NETwork (SARNET) project of the 6th Framework Programme of the European Commission, and it is based on a recent paper presented at the International Conference on Nuclear Energy for New Europe 2005 by [9]. The second subchapter is CANDU specific work being performed at AECL to characterise wet aerosol leakage through containment leak path geometries.

3.15.2 *Current modelling and experimental studies*

The factors influencing aerosol retention in a leak path have been identified and classified as follows:

- **Thermo-hydraulics;** the most important variables are the pressure inside the containment, the gas composition, the pressure drop and the wall temperature along the crack. Factors which influence steam condensation onto crack surfaces will be particularly relevant.
- **Crack geometry;** the important parameters are primarily the crack path length and hydraulic diameter; crack section shape (likely flat) and curvature are also very important.
- **Aerosol characteristics;** the reference parameters would be in-containment average composition, concentration and size distribution.

It is worth noting that variables considered highly uncertain at the time the leak path initiates (like composition and morphology of aerosols), have been disregarded. Otherwise, accurate models relying on those variables would not yield reliable estimates.

The values of these variables should encompass two bounding scenarios: the “short term scenario”, in which energetic phenomena, such as hydrogen deflagrations and/or steam explosions might result in an early containment impairment; and the “long term scenario” where steam and gas released from the molten core-concrete interaction would cause containment over-pressurization. In the former, the in-containment aerosol concentration could reach high values (1-10 g/m³) and size distribution would be shifted toward particles of the order of some microns. In the latter, the aerosol concentration would be lower and the size distribution would be weighed more heavily in the range of sub-micron particles. According to experimental data available, the maximum interest from a safety point of view should be placed on particles around 0.1 µm (since they would undergo the lowest retention).

Table 3.15-1 Some variables influencing the aerosol retention inside containment cracks

Crack path	≥ wall thickness (1.0 – 1.4 m)
Crack cross section and shape	<< 2-3 cm ² - flat, in the case of long term scenario
Containment internal pressure	5 – 10 bar
Crack surface temperature	room to containment gas temperature
Atmosphere composition	depending on accident scenario and evolution
Aerosol size distribution	0.1 – 5 µm

Two different approaches are being used to model aerosol retention: Eulerian and Lagrangian. A brief description is given next. In-crack flow dynamics and heat transfer studies [10, 11], even though highly important for aerosol behaviour, are not reported here.

An experimental programme on aerosol retention within concrete cracks is being conducted by IRSN [12, 13]. Reinforced concrete samples (128 cm x 75 cm x 10 cm) are being subjected to shear stresses up to 645 kN. The resulting cracked wall is placed between two identical sealed boxes. Fluorescein particles are injected in the upstream box and their mass concentration is measured in both upstream and downstream boxes. Particles having diameters of 1 μm and 4 μm in dry atmospheres have been tested so far, and it is planned to conduct tests with 50 nm-particles. The maximum pressure drop across the wall has been 80 mbar.

Fig 3.15-1 is a scheme of the IRSN facility.

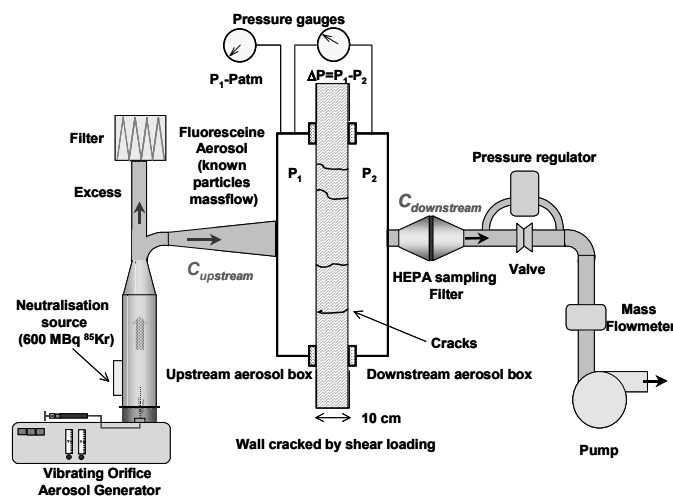


Fig. 3.15-1 IRSN facility to investigate aerosol retention in containment cracks

Total retention of aerosol particles was observed for 4 μm particles under all the velocities tested. However, only a fraction of the 1 μm aerosols was retained. The main retention mechanisms involved were diffusion, sedimentation and impaction (at the crack inlet). Experiments with air-steam mixtures are planned to study the effect of wet conditions in the crack decontamination factor.

Presently, another experimental facility, named COLIMA (CEA), is being considered as a future candidate in which to conduct experiments since it has appealing characteristics like the ability to generate prototypical MCCI aerosols, design pressure and temperature of 5 bar and 140 °C, respectively, and the capability of producing steam.

3.15.3 Measurement of the retention of wet aerosols

Wet aerosols (droplets containing suspended or dissolved fission products) are more prevalent than dry aerosols in most postulated design basis CANDU accident scenarios. However, the published literature on aerosol behaviour in containment leak paths is predominantly for dry aerosols, as are the empirical correlations used to describe the behaviour. Although some empirical deposition models may be applicable to wet aerosol behaviour, aerosol characteristics such as particle shape, and deposit characteristics (fluid rather than solid) could cause somewhat different behaviour in potential leak paths. Over the past few years, experiments and modelling studies have been performed at AECL to characterise wet aerosol leakage through containment leak path geometries. The following section describes experiments on aerosol droplet deposition and transport through paths that are representative of seals and valves in containment.

Flow paths and conditions

As described earlier, aerosol leakage through valves and airlock-door seals in containment will be characterised by an abrupt change in the cross-sectional flow area, where gas and aerosol flows move from a high pressure (containment) region, through small gaps resulting from seals or valves being improperly seated, to a lower pressure region. A diagram of the generalised leak path through a single contraction is shown in Fig. 3.15-2. Note that the leak path from containment to the environment through airlock door seals and isolation valves generally involves more than one such abrupt contraction.

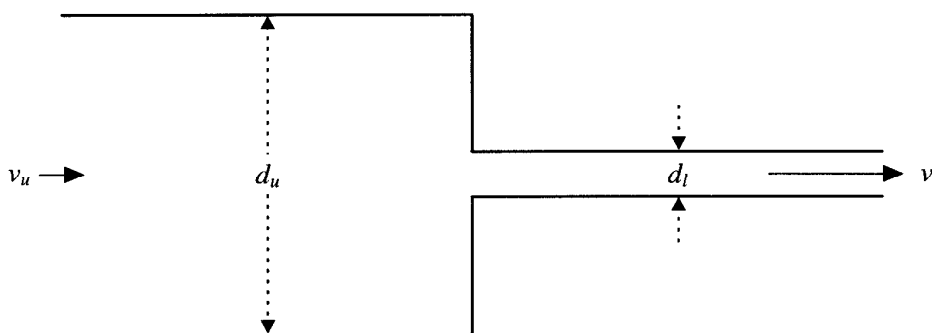


Fig. 3.15-2 Diagram of a generalised leak path

The abrupt change in flow area for a pressurised flow is expected to lead to aerosol leakage occurring under choked-flow (or sonic) conditions at the contracted portions of the leak paths. The flow through an opening of a given diameter increases with increasing pressure differential until a pressure wave, created within or near the exit of the orifice, results in sonic flow. A further reduction in downstream pressure cannot increase the velocity through the opening, and the gas velocity through the hole will be maintained at the speed of sound⁶. A choked-flow condition results in a constant mass-flow rate, at the speed of sound, through a nozzle or an opening. The criterion for choked flow is a downstream absolute pressure of less than 53 % (for air) of the upstream absolute pressure [14].

An experimental benefit resulting from a choked-flow condition is that the leak paths are self-regulating to ensure a constant flow rate. Choked-flow conditions can be achieved by either pressurising the upstream side of the leak paths or by maintaining a sufficiently low pressure downstream of the leak paths to ensure that the downstream-to-upstream pressure ratio is lower than 0.53⁷. The latter choice was selected because it was expected to adequately simulate aerosol leakage from containment, but without the experimental difficulties associated with a design in which the upstream chamber would be at an elevated pressure.

Experiments

Experiments on aerosol leakage were performed in a cubic plexi-glass chamber fitted with an aerosol characterization port and a pair of filtration ports. The filtration ports are shown schematically in Fig. 3.15-3. A deflector was installed above each port to prevent collection of surface runoff from the vertical surface in to the port entrance. The constricted leak path portion of an isolation-damper valve was simulated using commercially available copper tubing, with diameters and lengths representative of

⁶ The sonic velocity U_{sonic} ($\text{m}\cdot\text{s}^{-1}$) for a gas is: where: R = gas constant ($=287 \text{ m}\cdot\text{N}\cdot\text{kg}^{-1}\cdot\text{K}^{-1}$), T_u = upstream temperature (K) and γ = specific heat ratio ($=1.4$) [15].

⁷ The atmospheric (101 kPa) to containment (225 kPa) pressure ratio following an accident is estimated to be 0.45 in CANDU reactors.

damper valve leak paths possible in CANDU stations. The simulated constricted flow path of the airlock-door seals was fabricated in-house, using cylindrical copper tubing of much smaller dimensions.

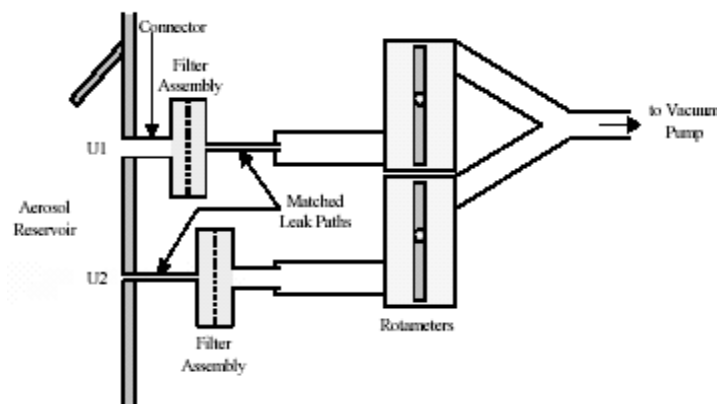


Fig. 3.15-3 Schematic of filtration sampling lines

The filtration assembly shown in Fig. 3.15-3 consisted of two separate flow lines (U1 and U2) containing matched leak paths. The U1 line consisted of a high efficiency filter assembly to collect water droplets, upstream of the prototypical leak path, whereas in the U2 line, the filter assembly was positioned downstream of the leak path. Each line was connected to a rotameter through a valve to measure the flow; the valves were used to match the flow rates through the U1 and U2 lines. A vacuum pump was connected to the downstream port of the rotameters to maintain low pressures and ensure choked-flow conditions through the leak path.

A Cyclone Fogger (Curtis Dyna-Fog[®], Model 3000) containing a solution of an uranine dye in water was used for aerosol generation. The uranine (sodium fluorescein) dye fluoresces at a characteristic wavelength and concentrations of the uranine-water retained on the filter assemblies and in the leak paths were determined using fluorescence spectrophotometry. In a typical experiment, the vacuum pump was started, and the flow valves for each line were adjusted so that the rotameter reading on each line was the same. The fogger was switched on to inject aerosols into the cubic reservoir, and a phase-Doppler anemometer (PDA) focused through the aerosol characterisation port was used to measure the mean (average) diameter of wet aerosols. The mean droplet size generated for these experiments was 9.7 μm . Droplet mass concentration was not measured, but can be estimated from the ratio of the aerosol injection rate and the volumetric flow rate through the filtration port to be around 5 $\text{g}\cdot\text{m}^{-3}$ for the isolation damper valve experiments. The experiments described here were performed at ambient temperatures.

Filters and leak path assemblies were removed after each experiment and washed thoroughly with known quantities of distilled water, to re-dissolve the deposited uranine dye. Samples of the filter and leak path washes were then submitted for fluorescence analysis to determine the uranine concentration. The aerosol-penetration and aerosol-deposition efficiencies were estimated directly from the measured uranine concentrations. The method has been adapted from one reported by [16].

Results in Table 3.15-2 show that for the simulated damper-valve leak paths, the average penetration efficiency,, is 36 % \pm 5 % (1σ), and the average deposition efficiency,, is 64 % \pm 6 % (1σ). There is no significant effect of tube length on the deposition efficiency. For airlock-door seal leak paths, the average penetration efficiency,, is 80 % \pm 2 % (1σ), and the average deposition efficiency,, is 20 % \pm 2 % (1σ).

Table 3.15-2 Retention and transmission efficiency in an idealised isolation-damper valve contraction

Test No.	η_p^I (%)	η_d^I (%)
<i>(a) 9-cm long tube</i>		
D9R1	46	54
D9R2	26	74
D9R3	37	63
<i>(b) 6-cm long tube</i>		
D6R1	44	56
D6R2	36	64
D6R3	34	66
<i>(c) 3-cm long tube</i>		
D3R1	34	66
D3R2	35	65
D3R3	31	69
Average	36	64

Table 3.15-3 Retention and transmission efficiency in an idealised airlock-door seal leak contraction

Test No.	η_p^{II} (%)	η_d^{II} (%)	$\eta_p^{II} + \eta_d^{II}$ (%)	η_p^I (%)	η_d^I (%)
<i>0.6-cm long tube</i>					
A6R1	113	33	146	77	23
A6R2	69	17	86	80	20
A6R3	85	18	103	82	18
Average	89	23	112	80	20

Leak path plugging

From earlier measurements of depressurisation tests performed with a simulated isolation-damper valve leak paths, it was shown that the post-accident elevated pressure in a CANDU containment building would level off (from 140 kPa(g) to zero) in about 15 minutes. Hence, tests were performed to monitor aerosol flow through the U2 lines for the same duration of time to examine whether leak path plugging would occur. The experiments indicated that there would be no leak path plugging during containment overpressurization for an aerosol mass density of about $5 \text{ g}\cdot\text{m}^{-3}$.

References

- [1] C.T. Nelson, R.P. Johnson Aerosol leakage tests -Status of Technology for Radiological Consequence Assessment of postulated Accidents in LMFBR's, ERDA-56, Springfield, USA, 1975
- [2] S.L. Sutter Depleted Uranium Dioxide Powder Flow Through Very Small Openings NUREG/CR-1099, PNL-3177, 1979
- [3] J.P. Mitchell, R.T. Edwards, H.M.E. Ball The Penetration of aerosols Through Fine Capillaries Journal of Radioactive Materials Transport (RAMTRANS), n. 3, 5-17, 1992
- [4] D.A.V. Morton, J.P. Mitchell Aerosol Penetration through Capillaries and Leaks: Experimental Studies on the Influence of Pressure Journal of Aerosol Science, n. 26, pp 353-367, 1995
- [5] R.K. Hilliard, A.K. Postma Large-Scale Fission Product Containment Tests Nuclear Technology, Vol. 53, n. 2, pp 163-175, 1981
- [6] A. Watanabe, T. Hashimoto, M. Osaki Fission Product Aerosol Trapping Effects in the Leakage Path of Containment Penetration under Severe Accident Conditions in Proc. 3rd OECD Specialist Meeting on Nuclear Aerosols in Reactor Safety, Cologne, Germany, 1998
- [7] E.U. Vaughan Simple Model for Plugging of Ducts by Aerosol Deposits Trans. Am. Nucl. Soc., 28, 507, 1978
- [8] C.F. Clement Aerosol Penetration through Capillaries and Leaks: Theory Journal of Aerosol Science, 26, 369, 1995
- [9] F. Parozzi, S. Paci ECART Code Integrated Approach for Thermal-Hydraulic-Source Term Analysis, Proc. 4th International Conference on Nuclear Option in Countries with Small and Medium Electricity Grids, 16-20 June, 2002, Dubrovnik, Croatia, 2002
- [10] H. Simon, N. Coulon, R. Tomassian, G. Nahas A model for two-phase flow through small opening cracks 4th European Thermal Sciences Conference, 29-31 March 2004, Birmingham, UK, 2004
- [11] H. Simon, N. Coulon, R. Tomassian, G. Nahas Air-steam leakage through cracks in concrete walls. NURETH-11, 2-6 October, 2005, Avignon, France
- [12] T. Gelain, F. Gensdarmes, J. Vendel Experimental study on aerosol penetration through cracked concrete wall, Congress EAC 2004 Budapest, September 6-10, 2004
- [13] T. Gelain, J. Vendel Détermination de modèles de dépôt d'aérosols dans un réseau de fissures, Congrès français sur les aérosols (CFA) Paris 14-15 décembre 2005
- [14] H.C. Hinds Aerosol Technology: Properties, Behaviour, and Measurement of Airborne Particles, John Wiley & Sons, Toronto, 1982
- [15] V.L. Streeter, E.B. Wylie Fluid Mechanics, McGraw-Hill Book Co., New York, 1979
- [16] J.K. Agarwal Aerosol Sampling and Transport Ph.D. Thesis, University of Minnesota, 1975

4. MODELLING APPROACHES IN CODES (INCLUDING BASIC VALIDATION)

4.1 Integral Codes

4.1.1 MELCOR

4.1.1.1 Introduction

MELCOR [1] is a systems-level model for the prediction of the progression of accidents in light water nuclear power reactors and other nuclear facilities. It was developed initially by the U.S. Nuclear Regulatory Commission (NRC) as a model to support the quantitative estimation of risk to the public associated with nuclear facilities and especially nuclear power plants. This initial thrust of code development has been augmented, and MELCOR has become a tool for the mechanistic analysis of reactor accidents. MELCOR has become the repository used by the NRC for the preservation of knowledge and understanding of severe accidents developed in a variety of experimental and analytical research efforts. For the purposes of reactor accident analyses, the code is intended to predict accident progression from the initiating event, to the point of core uncover, through vessel failure and the expulsion of core debris into the containment, to the point of containment failure and the prolonged escape of radioactive materials into the nuclear power plant environment. The MELCOR code provides input to a companion code, MACCS, for the analysis of radioactive material dispersion in the environment and the consequences of this dispersion.

The MELCOR code has a substantial, world-wide community of users. The code has a rather flexible architecture so that it can be used to predict accident progression in many different types of nuclear reactors. MELCOR is also applied to the prediction of accident progression in facilities for processing of nuclear materials especially for accidents involving fires.

The MELCOR code was developed initially as a systems-level analysis code and was not intended for the analysis of experiments. Instead, it was envisaged that the code would adopt and adapt essential features though not all the detailed features of computer codes used for the analysis of major experiments. This has been done in many cases as will become apparent in the discussion below of the major “packages” in the MELCOR code. There has been, however, an increasing willingness to use the systems-level code directly for the analysis of major experiments. It is a statement concerning the flexible architecture of the code that such analyses are possible. It is also a statement concerning the increase in capabilities of routinely available computational devices that the MELCOR code continues to be developed in the direction of ever more detailed descriptions of accident phenomena. The MELCOR code has become, consequently, an important tool in the drive to make the safety regulation of nuclear power plants based ever more on realistic rather than overly conservative depictions of accident phenomena.

4.1.1.2 Major MELCOR “packages”

The MELCOR computer code consists of a number of “packages” that address particular aspects of reactor accident analyses. The more important of these packages are listed in Table 4.1-1. Most of the packages in MELCOR are associated with the analysis of reactor core and structure degradation. The RN package is devoted to the prediction of radionuclide behaviour under accident conditions. The RN package will be the focus of the discussions in this brief description of the MELCOR computer code.

Table 4.1-1 Pertinent 'packages' in the MELCOR computer code for reactor accident analysis

Symbol	Package Name	Description
EXEC	Executive Package	Responsible for overall execution control of the calculations
BUR	Burn Package	models the combustion of gases in control volumes
CAV	Cavity Package	Models the attack on the basemat concrete by hot or even molten core materials
CND	Condenser Package	Models the effects of Isolation Condenser Systems and Passive Containment Cooling Systems found in some boiling water reactors
CF	Control Function Package	Allows users to modify the modeling in MELCOR by defining functions of variables in the MELCOR database and make the values of these functions available to other MELCOR packages
COR	Core Package	Calculates the thermal response of the reactor core, the lower plenum internal structures, core internal support structures and the reactor vessel lower head.
CVH	Control Volume Hydrodynamics Package	Modeling of the thermal-hydraulic behaviour of liquid water, water vapor and gases in control volumes
DCH	Decay Heat Package	Models the decay heat power from fission products
FCL	Fan Cooler Package	Models the heat and mass transfer associated with operation of fan coolers in the reactor containment
FDI	Fuel Dispersal Package	Models fuel expulsion from the reactor vessel to the reactor cavity. This includes modeling high pressure melt ejection and the dispersal of core debris over several volumes
FL	Flow Path Package	Description of interconnection of volumes and the condensation or evaporation of water along flow paths.
HS	Heat Structures Package	Models energy transfer to and within structures
MP	Material Properties Package	Models thermophysical properties of materials needed in the modeling done in other packages
NCG	Noncondensible Gas Package	Models noncondensible gases as ideal gases.
PAR	Passive Autocatalytic Hydrogen Recombiner Package	Calculates the removal of hydrogen from the containment atmosphere caused by the operation of passive hydrogen recombiners
RN	Radionuclide Package	Models release, transport and behaviour of radionuclides
SPR	Containment Spray Package	Models heat and mass transport between spray droplets and the containment atmosphere

The MELCOR code categorises radionuclides and other pertinent materials into elemental classes that exhibit similar chemistry. The default classes are listed in Table 4.1-2. Users of the code can define additional classes to track particular materials more exactly. The behaviours of all the materials in a class are tracked based on the predicted behaviour of a particular representative of the class. The representatives of the default classes are also shown in Table 4.1-2.

Table 4.1-2 Material classes in MELCOR

Class	Name	Representative	Member Elements
1	Noble Gas	Xe	He, Ne, Ar, Kr, Xe, H ₂ and N ₂
2	Alkali Metals	Cs	Li, Na, K, Rb, Cs, Fr, Cu
3	Alkaline Earths	Ba	Be, Mg, Ca, Sr, Ba, Ra, Es, Fm
4	Halogens	I	F, Cl, Br, I At
5	Chalcogens	Te	O, S, Se, Te, Po
6	Platinoids	Ru	Ru, Rh, Pd, Re, Os, Ir, Pt, Au, Ni
7	Early Transition Elements	Mo	V, Cr, Fe, Co, Mn, Nb, Mo, Tc, Ta, W
8	Tetravalents	Ce	Ti, Zr, Hf, Ce, Th, Pa, Np, Pu, C
9	Trivalentes	La	Al, Sc, Y La, Ac, Pr, Nd, Pm, Sm, Eu, Gd, Tb, Dy, Ho, Er, Tm, Yb, Lu, Am, Cm, Bk, Cf
10	Uranium	U	U
11	More Volatile Main Group	Cd	Cd, Hg, Zn, As, Sb, Pb, Tl, Bi
12	Less Volatile Main Group	Sn	Ga, Ge, In, Sn, Ag
13	Boron	B	B, Si, P
14	Water	H ₂ O	H ₂ O
15	Concrete	-	-
16	Cesium iodide	CsI	CsI

The MELCOR code treatment of radionuclides includes:

- Release of radionuclides from intact fuel and from core debris,
- Transport and deposition of radionuclide vapors and aerosols through the reactor coolant system,
- Behaviour of radionuclides and radioactive aerosols in the reactor containment, and
- Effects of engineered safety systems on the amount of radioactive material that can be released from the reactor containment.

Each of these aspects of the code is discussed in subsections that follow.

Radionuclide release from fuel

MELCOR considers radionuclide release from fuel both within the reactor vessel and when reactor fuel has been expelled from the reactor coolant system into the containment. Radionuclide release from fuel within the reactor vessel can be calculated using one of three closely related models:

- CORSOR,
- CORSOR-M, and
- CORSOR-Booth

All three of these models have an empirical relationship to tests of fission product release from fuel heated usually out of pile. Most users now prefer the CORSOR-Booth model. Diffusion coefficients in this model have been upgraded to match well more recent tests such as those being done as part of the PHÉBUS-FP project.

Ex-vessel release of radionuclides is done with the VANESA model [2] developed based on experimental data explicitly for this purpose. The model considers fission product release by vaporization into bubbles of gas sparging through core debris attacking structural concrete. It also considers the mechanical formation of aerosols due to the bursting of bubbles at the surface of molten core debris. Radionuclide release can be retarded substantially by the presence of a water pool over the surface of the core debris. Modeling of this attenuation of the ex-vessel release is akin to that used in MELCOR to model decontamination of aerosol-laden gas flows through steam suppression pools.

Aerosol nucleation from vapors

MELCOR does not explicitly model the nucleation of aerosols from vapors that cool once they escape core debris. Extensive numerical experimentation has shown that the details of nucleation are quickly obliterated by the rapid coagulation of fine particles as predicted by the model of aerosol dynamics discussed below. Consequently, once vapor reaches saturation, saturation is relieved by condensation on surfaces and nucleation of particles that are assumed to be in the smallest size bin of the aerosol dynamics model. Water vapor is allowed by the MELCOR code to form aerosols called ‘fog’ in the code. These water droplets can interact with other types of aerosol particles.

Aerosol dynamics

Modeling of the agglomeration and deposition of aerosol particles is done in MELCOR using the MAEROS model. The MAEROS model was developed by Gelbard [3] and is one of the earliest models to use the sectional method for the prediction of aerosol behaviour in a control volume. MAEROS is both multisectional and multicomponent. A model for hygroscopicity effects is available in MELCOR. Each size class considered in MAEROS can have a different chemical composition. Deposition mechanisms considered in MAEROS are:

- Gravitational settling,
- Diffusion,
- Thermophoresis, and
- Diffusiophoresis

MELCOR does not currently treat inertial deposition processes.

Vapor deposition

MELCOR considers vapor deposition by condensation. There is also the capability to model vapor chemisorption onto surfaces. This aspect of the modeling is undergoing re-examination in comparison to the more comprehensive vapor deposition modeling found in the VICTORIA code which is described elsewhere in this report.

Engineered safety features

The MELCOR code considers the effects of engineered safety features on aerosols. Specific features that are modeled include decontamination by:

- Steam suppression pools
- Sprays
- Ice beds
- Filters
- Fan coolers

Decontamination by steam suppression pools is done with the SPARC90 model [4] developed for the NRC. This model calculates removal of both aerosol and iodine gas from gases sparging through suppression pools. The spray model allows a distribution of droplet sizes but does not now mechanistically calculate droplet-droplet interactions. Models for decontamination by filters and fan coolers are rather simple and have not received a great deal of attention.

4.1.1.3 Code status

The MELCOR code is widely used for both regulatory and safety analysis purposes. The code is finding increased use for the safety analysis of non-reactor nuclear facilities in addition to continued use for analysis of reactor accidents. The code is still being actively maintained and developed. A new version of the code was released in 2005. A FORTRAN 95 version of the code is expected in 2006. Following release of the FORTRAN 95 code version, much of the development effort will be devoted to an extensive comparison of code predictions to test results and documentation of the validation status of the code. Because of the flexibility of the MELCOR design and the component nature of the package architecture, it is felt that the MELCOR code will be adaptable to the assessment of future reactor designs.

References

- [1] R.O. Gauntt, R.K. Cole, C.M. Erickson, R.G. Gido, R.D. Gasser, S.B. Rodriguez, and M.F. Young, MELCOR Computer Code Manuals, NUREG/CR-6119, Volumes 1-3, Sandia National Laboratories, Albuquerque, NM, December 2000
- [2] D.A. Powers, J.E. Brockmann, A.W. Shiver, VANESA: A Mechanistic Model of Radionuclide Release and Aerosol Generation during Core Debris Interactions with Concrete, NUREG/CR-4308, Sandia National Laboratories, Albuquerque, NM, July 1986
- [3] F. Gelbard MAEROS User Manual, NUREG/CR-1391, Sandia National Laboratories, Albuquerque, NM, December 1982
- [4] P.C. Owczarski and K.W. Burk, SPARC-90: A Code for Calculating Fission Product Capture in Suppression Pools, NUREG/CR-5765, Pacific Northwest Laboratory, Richland, WA, October 1991

4.1.2 *ASTEC (SOPHAEROS and CPA)*

4.1.2.1 *An overview of the ASTEC/SOPHAEROS code*

Introduction

The ASTEC/SOPHAEROS code, developed by IRSN as part of the IRSN-GRS ASTEC integral code [1], models radionuclide transport in the reactor coolant system (RCS). The main features of the code in its current version (v1.2) are described here along with an outline of validation activities and development work. The principal use of ASTEC/SOPHAEROS arises from the following applications:

- IRSN has performed a Probabilistic Safety Analysis level 2 for French 900 MWe PWRs using ASTEC and is set to start a PSA level 2 for 1300 MWe PWRs using ASTEC v1.3;
- SOPHAEROS-IST 2.0 (corresponding to SOPHAEROS v2.0 with some generic and CANDU-specific improvements implemented by AECL) is the Canadian Industry Standard Toolset code for analysing FP transport in the RCS of CANDU reactors [2];
- ASTEC/SOPHAEROS was used and validated in a European context through the EVITA project [3], part of the European Commission's 5th Framework Programme;
- The ASTEC V1 code has been distributed internationally in the context of the SARNET network of excellence, part of the European Union's 6th Framework Programme.

Overview of modelling

The basic element of ASTEC/SOPHAEROS modelling is the control volume where the RCS must be described as a sequence of volumes, each comprising one or several freely-oriented truncated cones. Arbitrary geometries can be dealt with involving, e. g., bifurcations, closed loops, etc. Within each control volume, the modelled vapor and aerosol phenomena are summarised in

Table 4.1-3 where the associated literature source and/or a brief description for each model is provided.

A chemical element is partitioned among its possible chemical species via the use of an independent thermochemical database. ASTEC/SOPHAEROS v1.2 operates with a comprehensive database covering 65 elements generating 747 compounds. Recent restructuring of the numerical solver for ASTEC/SOPHAEROS v1.2 allows this database to be used routinely (a reduced database exists which was once of interest in reducing calculation time by covering just over 100 chemical species but can now be considered obsolete). Each chemical species can exist in one of five physical states: vapor; vapor condensed on a wall; vapor sorbed on a wall; aerosol and deposited aerosol. The fraction of a species converted into condensed or deposited states no longer participates in the chemistry where this chemical inactivation is permanent unless revaporization occurs. Aerosol phenomena are handled by discretizing the (arbitrary, freely evolving) size distribution over a user-determined, logarithmic grid of up to 50 size classes. Use of a large number of size classes is particularly important in situations where homogeneous nucleation, heterogeneous nucleation, or agglomeration is important. SOPHAEROS is supplied with thermal-hydraulic conditions via coupling to the ASTEC/CESAR module.

Table 4.1-3 Phenomena modelled in ASTEC/SOPHAEROS v1.2

	Mechanism		Literature source and/or brief description
V P a h p e o n u o r m e n a	vapor-phase chemistry		Equilibrium; comprehensive database (800 species).
	homogeneous nucleation		[4] for condensation rate.
	heterogeneous nucleation (reversible)		Brownian-diffusion-limited mass transfer onto a sphere, inclusion of Mason effect [5].
	sorption on metal-alloy surfaces		Empirical velocities as a function of temperature.
	condensation on surfaces (reversible)		Chilton-Colburn analogy [6]; laminar, $Nu=3.66$ (cylinder); turbulent [7]
A P e h r e o n s o o m l e n a	sedimentation		Stokes' velocity with Cunningham correction.
	turbulent (eddy) impaction		[8]
	diffusion	laminar (Brownian) turbulent	[9] laminar; [10] turbulent.
	thermophoresis		[11]
	diffusiophoresis		Based on Stefan velocity [17]; [14] for free-molecular regime; option [15,16] more general.
	inertial impaction in bends		Hybrid model based on [18] for laminar flow, [19] for turbulence; option of centrifugal model.
	inertial impaction in geometrical contractions		[23] or [24] depending on contraction angle
	agglomeration	Brownian, gravit-ational, turbulent	[20] continuum regime, [12] free-molecular regime; [21] gravitational; [22] turbulent.
	mechanical resuspension		Semi-empirical resultant-force model devised for the ECART code, retuned by GRS [25]; optional model based on [26].

Numerical method

The mass-balance equations resulting from the intra-volume phenomena combined with inter-volume transport produce a non-linear system solved numerically by a Newton-Raphson method. To illustrate how the code deals with the diverse phenomenology involved in the transport process, we take the aerosol state (state 2 in SOPHAEROS, hence suffix 2 below) entailing the following mass-conservation equation for a given aerosol size class i :

$$\frac{dm_{2,i}}{dt} = s_{2,i} + (\tau_{f,i}^{up} m_{2,i}^{up} - \tau_{f,i} m_{2,i}) + \dot{m}_{agg,i} + \dot{m}_{cond,i} - \tau_{d,i} m_{2,i} + \tau_{r,i} m_{4,i} + \delta_{1,i} \sum_{n=1}^{vapours} J_n$$

where, taking each right-hand-side term successively,

s is an aerosol source rate,

τ_f are flow-dependent transport rates into and out of the volume,

$\dot{m}_{agg,i}$ is a compound term representing particle agglomeration into and out of size class i ,

$\dot{m}_{cond,i}$ is a compound term representing heterogeneous nucleation onto smaller particles bringing mass into size class i and evaporation from class i particles taking mass away,

τ_r is the mechanical resuspension rate of class i deposited aerosols (state 4, hence suffix 4),

J_n is the mass rate of formation of aerosols due to homogeneous nucleation of vapor species n where the Dirac delta is zero except for $i=1$, i.e., vapors seed into the smallest size class only.

Further details of the numeric method can be found in the theoretical manual for SOPHAEROS where, notably, a full description of a number of matrix optimizations used to accelerate the solution scheme are described.

Validation

A wide variety of data sources is employed for validation. Table 4.1-4 shows the currently-used experiments where a full reassessment of the experimental database is underway (i.e., some cases may be abandoned while others will be added).

Table 4.1-4 Current validation matrix

Test Type	Project	Character	Tests Used	Main Phenomena
aerosol phenomena	LACE <i>consortium</i>	aerosol, large-scale, semi-analytical	1 LA3B	<ul style="list-style-type: none"> • eddy impaction • 90°-bend impaction
	TUBA-T <i>IRSN</i>	aerosol, SGT-scale, single-effect	9 TT14,22,24-31	<ul style="list-style-type: none"> • thermophoresis
	TUBA-D <i>IRSN</i>	aerosol, SGT-scale, analytical	12 TD01-TD12	<ul style="list-style-type: none"> • diffusiophoresis • thermophoresis
	TRANSAT <i>IRSN</i>	aerosol, large-scale, semi-analytical	7 TR1, 2, 4-8	<ul style="list-style-type: none"> • eddy impaction • 90°-bend impaction • settling
	DEPAT <i>IRSN</i>	aerosol, large-scale, analytical	6 DEPAT01-03 DEPM01-03	<ul style="list-style-type: none"> • eddy impaction

Test Type	Project	Character	Tests Used	Main Phenomena
	ADPFF <i>AEA Tech.</i>	aerosol, full-scale, analytical	15 WT10-23, 25	<ul style="list-style-type: none"> • eddy impaction • 90°-bend impaction • settling
	STORM <i>CEC-ENEL</i>	aerosol, large-scale, semi-analytical	SD 04, ISP 40 SR (in progress)	<ul style="list-style-type: none"> • thermophoresis • eddy impaction • mechanical resuspension
vapor & mixed phenomena	DEVAP <i>IRSN-CEA</i>	vapor, small-scale, analytical	7 8,13-15, 17, 18, 20	<ul style="list-style-type: none"> • chemisorption • condensation
	AERODEVAP <i>IRSN-CEA</i>	aerosol/vapor small-scale, semi-analytical	3 01, 02, 04	<ul style="list-style-type: none"> • heterogeneous nucleation • condensation • vapor-aerosol interaction
	Falcon <i>AEA Tech.</i>	simulant fuel, small-scale, semi-analytical	4 Fal-17, 18, 19, 20	<ul style="list-style-type: none"> • vapor chemistry • condensation • vapor-aerosol interaction
	REVAP-ASSESS <i>4th Framework</i>	vapor, small-scale, analytical	3 2 VTT tests, Fal-25	<ul style="list-style-type: none"> • revaporization
integral	VERCORS HT IRSN-EDF-CEA	irradiated fuel, small-scale, integral	3 HT1, 2, 3 (in progress)	<ul style="list-style-type: none"> • full range
	HCE COG	irradiated fuel, small-scale, integral	1 3 (in progress)	<ul style="list-style-type: none"> • full range
	BTF COG	irradiated fuel, in-pile, integral	1 104 (in progress)	<ul style="list-style-type: none"> • full range
	PHÉBUS-PF IRSN-CEC-EDF	irradiated fuel, in-pile, integral	3 FPT0, 1, 2, 4 (in progress)	<ul style="list-style-type: none"> • full range

Development

Future work is determined essentially on the basis of applications requirements and the feedback from validation activities. Hence, in the shorter term, this work will include implementing models for more complex geometries (e.g., steam generator secondary side as part of the ARTIST project, [12]) as well as retention by water volumes that arise in the RCS, e.g., [13]. In addition, verification of all the thermochemical data and completion of the species considered is in progress where the first stage of this work was to compare the list of species used by SOPHAEROS (originating mainly from the SGTE database [14]) with species included in other database collections. The 65 elements dealt with have been prioritised

in terms of importance and the process of data verification is now well advanced. In the longer term, development of physical models may address limited gas-phase chemical kinetics; this need arose from feedback from PHEBUS analyses leading IRSN to prepare the CHIP experiments studying gas-phase chemistry for key iodine reactions. In the context of improved accident-analysis capabilities, the study of cold-leg break sequences requires that steam condensation onto aerosols be examined.

References

- [1] J.P. Van Dorsselaere, F. Jacq, H.-J. Allelein, B. Schwinges “ASTEC code status and applications” US NRC CSARP meeting, Bethesda, USA, 5-7 May 2003 (2003)
- [2] L.W. Dickson, R.S. Dickson “Fission-product transport and retention in the PHTS under accident conditions”, 20th Annual Conference of the Canadian Nuclear Society, 30 May-2 June 1999, Montreal, Canada, ISBN 0-919784-80-1 (1999)
- [3] H.-J. Allelein, K. Neu, J.P. Van Dorsselaere, K. Müller, P. Kostka, M. Barnak, P. Matejovic, A. Bujan, J. Slaby “European validation of the integral code ASTEC (EVITA)” Nucl. Eng. Des. 221, 95-118 (2003)
- [4] S.L. Girshick, C.P. Chiu, P.H. McMurray “Time dependent aerosol models and homogeneous nucleation rates”, Aerosol Sci. Tech. 13, 465-477 (1990)
- [5] B.J. Mason “The physics of clouds (2nd ed.)” Clarendon Press, Oxford (1971)
- [6] T.H. Chilton, A.P. Colburn “Mass transfer (absorption) coefficients” Industrial and Engineering Chemistry 26, 1183–1187 (1934)
- [7] P.W. Dittus, L.M.K. Boelter “Heat transfer in automobile radiators of the tubular type” Univ. Calif. Pub. Eng. 2 (13), 443–461 (1930) (re-published in Int. J. Comm. Heat and Mass Transfer 12, 3-22 (1985))
- [8] B.Y. Liu, S.K. Agarwal “Experimental observation of aerosol in turbulent flow” J. Aerosol Sci., 5, 145-155 (1974)
- [9] P.G. Gormley, M. Kennedy “Diffusion from a stream flowing through a cylindrical tube”, Proc. Roy. Irish Academy, 52, 163 (1949)
- [10] C.N. Davies “Aerosol Science” Academic Press (1966)
- [11] L. Talbot, R.K. Cheng, R.W. Schefer, D.R. Willis “Thermophoresis of particles in a heated boundary layer” J. Fluid Mech., 101, 737-758 (1980)
- [12] S. Guentay, D. Suckow, A. Dehbi, R. Kapulla “ARTIST: introduction and first results”, Nucl. Eng. Des. 231(1), 109-120 (2004)
- [13] B.M. Schmitz “Pool scrubbing module SPARC-B/98 for Sophaeros v2mod0_1- model description” GRS Technical Notice TN-SMZ-00-1 (2000)
- [14] Landolt-Börnstein “Numerical data and functional relationships in Science and Technology, Group IV: Physical Chemistry”, Volume 19: Thermodynamic properties of inorganic materials compiled by SGTE, Subvolume A, Pure Substances’, Springer (1999)

4.1.2.2 *ASTEC-CPA*

The aerosol behaviour inside the containment is modelled in the ASTEC module CPA (Containment Part of ASTEC), which is almost identical with the main COCOSYS modules THY and AFP. For the description see chapter 4.3.2.

4.1.3 *MAAP4*

4.1.3.1 *Brief description*

The Modular Accident Analysis Program (MAAP) Version 4 is a computer code that simulates the response of light water and heavy water moderated nuclear power plants, during severe accident sequences. MAAP4 is an integrated code with capabilities to calculate the thermal-hydraulic response of the core, the Reactor Coolant System (RCS), the containment and the auxiliary buildings, as well as the fission product release, transport and deposition during postulated severe accident conditions [1]. MAAP4 is used in a wide range of plant evaluations including design basis evaluations, Level 1 and Level 2 success criteria for probabilistic risk assessments, radiological source term assessments, and accident management guidance evaluations. MAAP4 also includes a graphical interface, MAAP4-GRAAPH, enabling the user to interactively interface with the code during execution, to modify the status of on-site power, pumps, valves, etc., as well as, to directly observe the results [2].

4.1.3.2 *Status*

MAAP has been developed and maintained by Fauske & Associates Incorporated (FAI), since the beginning of the code in 1981, under the sponsorship of the Electric Power Research Institute (EPRI) and the MAAP Users Group (MUG). The code continues to be developed and maintained by FAI. Recent versions include MAAP4-CANDU, that extend MAAP4 applicability to CANDU power plants. It should be noted that the CANDU specific versions do not involve any changes to the previous fission product / aerosols transport capabilities. Validation of MAAP4 was performed against HDR experiments, CORA tests, TMI-2 accident, CSTF tests, FEBUS FPT0 test, ORNL VI test series, SFD tests at INEL, AP600 OSU tests, and LOFT experiments [3].

4.1.3.3 *Modelling*

	Brief Description / Literature Source
Reactor Components Modelled	<ul style="list-style-type: none"> • Reactor Core • Reactor Cooling System (RCS) • Containment • Reactor auxiliary buildings
Geometry Idealization	<ul style="list-style-type: none"> • A network of nodes inter-connected by flow paths
Inter-nodal Transport	<ul style="list-style-type: none"> • Transport of corium, water and gases including aerosols through flow paths
Thermal hydraulics	<ul style="list-style-type: none"> • Modelled by mass and energy equations • Flow rates are determined from quasi-steady momentum balances • Pressure, temperature and miscellaneous thermodynamic properties are determined from mass and energy of gaseous components in a node.
Fission Product Transport	<ul style="list-style-type: none"> • Fission products can exist in the solid, liquid, and vapor forms. • Twelve fission product compounds and three chemical compounds

Aerosol Transport	<p>which affect the pH value in the water pool [4] are tracked by the code.</p> <ul style="list-style-type: none"> • In the primary system, fission products are not dissolved in the water and hence are not transported by water, but only by carrier gas. • In the containment, the dissolution of fission products in water pools is modelled, and hence they are transported by both water and carrier gas. • Fission product vapor - aerosol condensation/evaporation is modelled by maintaining phase equilibria [1]. • Vapor - surface condensation / evaporation is modelled by diffusion [1]. • Simultaneous aerosol growth by agglomeration and removal by a number of aerosol deposition mechanisms are modelled by empirical correlations specially developed for the code, based on a principle of similarity and scaling [1, 5, 6,]. This empirical approach differs from the traditional, time-consuming, detailed calculations involving a solution of the Smoluchowski equation for the evolution of particle size distribution, but results in reduced computational time. The empirical approach considers the Brownian and gravitational agglomeration and the aerosol removal mechanisms listed below: <ul style="list-style-type: none"> • Sedimentation • Diffusiophoresis • Thermophoresis • Inertial impaction
--------------------------	----------------------------------------------------------------------------------------------------------------------------------------------------------------------------------------------------------------------------------------------------------------------------------------------------------------------------------------------------------------------------------------------------------------------------------------------------------------------------------------------------------------------------------------------------------------------------------------------------------------------------------------------------------------------------------------------------------------------------------------------------------------------------------------------------------------------------------------------------------------------------------------------------------------------------------------------------------------------------------------------------------------------------------------------------------------------------------------------------------------------------------------------------------------------------------------------------------------------------------------------------------------------------------------------------------------------------------------------------------------------------------------------------------------------------------------

References

- [1] R.E. Henry, C.Y. Paik, M.G. Plys, "MAAP4 – Modular Accident Analysis Program for LWR Power Plant - Code Structure and Theory, Computer Code Manual" Fauske & Associates Inc., prepared for: Electric Power Research Institute (EPRI), Volume 2, May 1994
- [2] R.E. Henry, C.Y. Paik, M.G. Plys, "MAAP4 – Modular Accident Analysis Program for LWR Power Plant – MAAP4-GRAAPH, Volume 4, Rev 0.0 / 0.1, May 1994 (Some Rev 0.1 updates to June 1995)
- [3] R.E. Henry, C.Y. Paik, M.G. Plys, "MAAP4 – Modular Accident Analysis Program for LWR Power Plant – Major Benchmarks" Fauske & Associates Inc., Volume 3A, Rev0.0 and 0.1, May 1994
- [4] FAI Internal Memo from C.D. Wu to R. J. Hammersley, "Implementation of pH Model in MAAP4", October 8, 1993
- [5] "Technical Support for Issue Resolution" Fauski and Associates Incorporated Report 85.27, July, 1985
- [6] M. Epstein, P.G. Ellison, and R. E. Henry "Correlations of Aerosol Sedimentation" J. Colloid Interface Sci., Vol. 113, No:2, October, 1986

4.1.4 THALES 2

The THALES-2 code [1] is an integrated severe accident analysis code developed at the Japan Atomic Energy Research Institute (JAERI) in order to simulate the accident progression and transport of radioactive materials for probabilistic safety assessment (PSA) of a nuclear power plant (NPP).

In 1982, JAERI developed, as a first step, the computer code system THALES [2] (Thermal-Hydraulic Analysis of Loss of Coolant Emergency Core Cooling and Severe Core Damage) for the analysis of accident progression. In 1988, the code was combined with the ART (Analysis of Radionuclide Transport) code [3] developed also by JAERI and the THALES/ART code system started. After that, the code system was improved by coupling the radionuclide transports models with the thermal hydraulic ones and a prototype of single code, namely, the THALES-2 code [1, 4] was completed in 1991. Then, the abbreviation THALES was changed to the Thermal Hydraulics and radionuclide behaviour Analysis of Light water reactor to Estimate Source terms under severe accident conditions.

The code has also been validated through analyses of experiments [5] and comparison with other computer codes [6, 7]. The THALES-2 code currently consists of BWR and PWR versions. Since the development of BWR version [8] advances compared with the PWR version, the outlines of BWR version are described below.

4.1.4.1 Overview of THALES-2 BWR

Accident progression

The THALES-2 BWR code [1, 7, 8] calculates various physical phenomena such as thermal-hydraulics, melt progression and radionuclide behaviour under the severe accident conditions. While progression of core meltdown accidents are markedly different depending on the initiating event and the operability of safety features, the THALES-2 BWR code postulates the accident progression such as described below.

1. Either the direct release of the primary coolant due to a break at system boundary or the coolant boil off ascribed to insufficient cooling during a transient causes decrease of the primary coolant inventory. When no cooling function such as those by Emergency Core Cooling System (ECCS) is unavailable, core will be uncovered.
2. Fuel rods begin heatup when they are exposed to the steam over the mixture level. When the temperature of a fuel rod rises high enough for activating Zr-H₂O reaction, cladding oxidation occurs and hydrogen is generated. Since this reaction is exothermic, it accelerates the core heatup. Further heatup of the core results in core meltdown; fuel rods lose their own shape by melting or fragmentation, and slump into lower part of the core. These slumping debris boil off the water remaining in the lower part of the pressure vessel and heat up the support plate and the bottom head. Heated up support plate and bottom head lose their strength and finally the bottom head melt-through occurs. After pressure vessel melt-through, corium-core debris together with structure materials drops into the reactor cavity.
3. Containment pressure and temperature rise with blowdown of the primary coolant, gas generated by concrete decomposition and hydrogen burning. After the reactor vessel failure, the molten material falls down into the reactor cavity and core/concrete interaction is initiated. During the core/concrete interaction, non-condensable gases are produced by the core/concrete interaction and the pressure in the containment atmosphere begins to increase. When the sufficient cooling with the engineered safety features such as the containment spray is unavailable, containment failure will occur and the gases in the containment are released to the environment.

Environment of THALES-2 BWR

THALES-2 BWR code requires information for a configuration of a plant including geometrical data, accident sequence (operational conditions of ECCS and operator actions), initial conditions of thermal-hydraulics and so on. THALES-2 BWR code gives trends of thermal-hydraulic condition, mass distribution of radionuclides, timing of events such as containment failure, and source terms.

THALES-2 is a highly modularised code system. The main part is supported by the subroutines, LOGIC1, UCL2 and SPLPACK. The UCL2 is for unit conversion, which enables the user to prepare input data with any unit, and the LOGIC1 for modeling the control circuit of safety-related system and for event control which defines the accident sequence. The SPLPAC is used to support graphic functions of THALES-2.

Structure of THALES-2 BWR

In the THALES-2 BWR code, calculations of thermal-hydraulics, release of radionuclide from fuel, radionuclide deposition and transport are performed at a given infinitesimal time increment δt . Fig. 4.1-1 shows data transfer inside the code. Firstly, thermal-hydraulic calculations are performed including the melt-relocation. After that, release of radionuclides from fuel and molten materials are calculated. By using these results, deposition and transport of radionuclide are calculated. Based on the results of radionuclide distribution, decay heat in each phase in the volume are calculated and delivered to the thermal-hydraulic calculation at the next time step $t + \delta t$.

THALES-2 uses three kinds of time increments for: 1) thermal-hydraulic in the containment system, 2) thermal-hydraulic in the reactor coolant system, and 3) radionuclide behaviour calculation. These three time increments are automatically determined in the code.

4.1.4.2 Plant Model in THALES-2 BWR

Multiple-volume presentation of BWR plant

The multiple volumes representation is used in the THALES-2 BWR code to describe the mass/energy transport radionuclide behaviour in LWRs plants. In this method, the primary and the containment systems are divided into many volumes. Fig. 4.1-2 shows a typical configuration of volumes for a BWR with a Mark-I containment

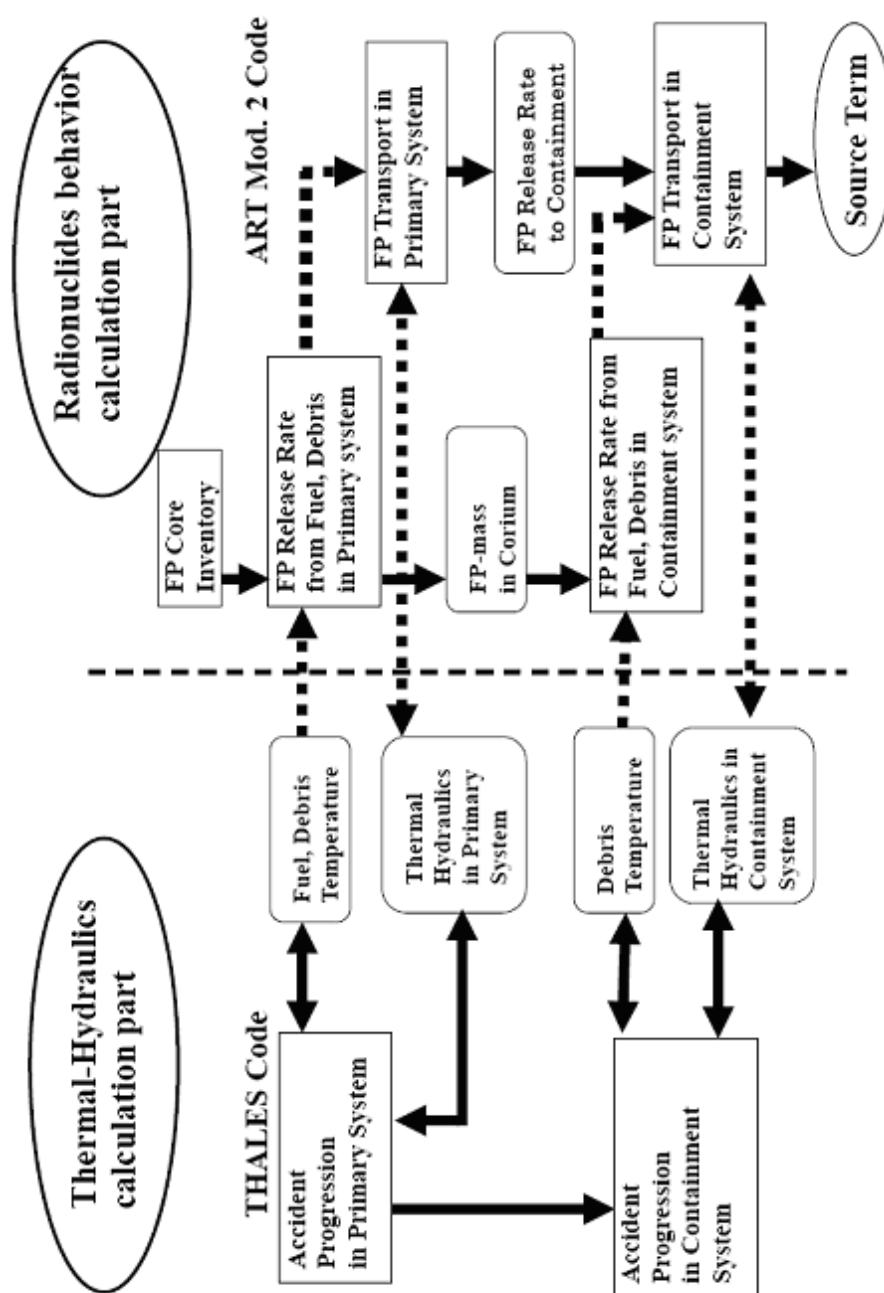


Fig. 4.1-1 Data transfer in THALES-2 BWR code system

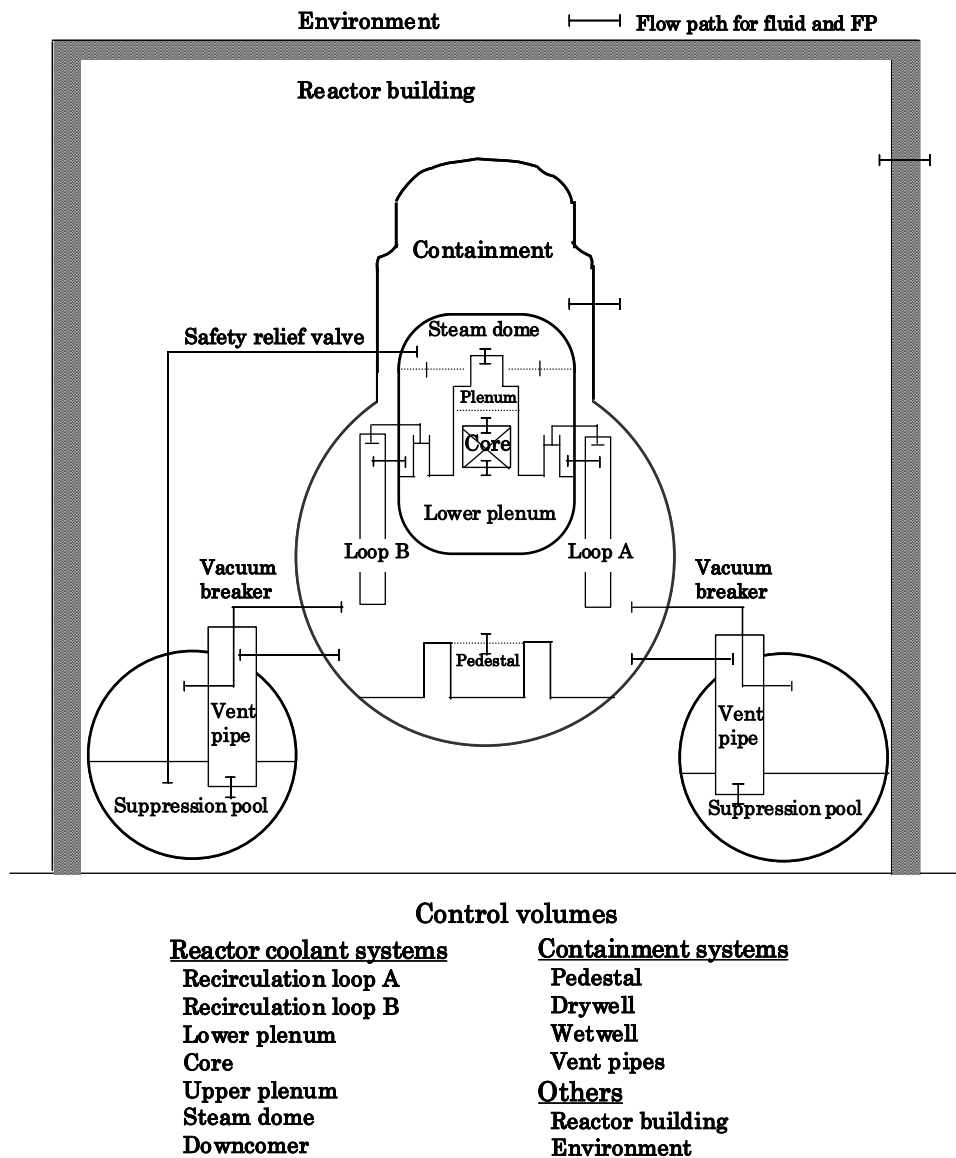


Fig. 4.1-2 An example of multi-volume representation of a BWR/MARK-I plant

Concept of system, volume, junction and path

In the multiple-volume presentation, a plant is represented by a combination of 'system', 'volume', 'tank', 'path' and 'junction' which are briefly described below.

Volume: A unit of region such as recirculation loops, upper plenum and core,

System: A set of volumes, which have the same pressures are connected by junctions

Tank: A region in which coolant inventory changes such as condensate storage tank,

Junction: A model element to calculate mass/energy transport among volumes,

Path: A model element to calculate mass/energy transport among systems.

A concept of 'system' and 'volume' was introduced to realise fasten running capability without losing accuracy. The system consists of volumes, which are combined by junctions and have the same pressure.

Some of 'system's and 'volume's in the THALES-2 BWR code are fixed to get fast running capability as follows:

<u>System</u>	<u>Volume</u>
Reactor Coolant System	Downcomer (DC), Lower Plenum (LWPL) Core (CORE), Upper Plenum (UPPL) Steam Dome (STMD), Loop A (LOPA), Loop B (LOPB)
Drywell System	Drywell (DRYW), Pedestal (CAVI) Vent Pipe (VENT)
Wetwell System	Wetwell (WETW)

User can define additional systems and volumes by input data. Each volume is further divided into a gas region and a liquid region by a mixture level. The geometry of a volume maybe represented by several cylindrical segments to calculate the correct mixture level.

Coolant sources outside systems such as the condensate storage tank are modeled by 'tank' which treats only coolant inventory change. Fluid flow at a system boundary such as coolant injection by ECCS, break flow and coolant release through safety and relief valves are modeled by 'path' which connects a volume within a system and a tank outside a system. The path flows are used as a boundary condition of the hydraulic calculation within a system, while the junction flow rates are given as a result of the hydraulic calculation within the system.

As for radionuclide in volumes, six phases are defined to describe mass distribution of radionuclides as follows:

- Phase 1: Radionuclide of vapor form in gas region
- Phase 2: Radionuclide of aerosol form in gas region
- Phase 3: Radionuclide in liquid region or on the floor
- Phase 4: Radionuclide of condensed form at structure surface
- Phase 5: Radionuclide of aerosol form at structure surface
- Phase 6: Radionuclide of absorbed form at structure surface

4.1.4.3 Outlines of radionuclide behaviour models

Radionuclide group

In the THALES-2 BWR, 20 radionuclides are classified into several groups (maximum 10) in terms of their chemical characteristics. Typical elements or compounds of each group are Kr-Xe, CsI, CsOH, Te, Sr, Ru, La and other particulates. An aerosol form is assumed in the code for Sr, Ru and La because their vapor pressures are very low in severe accident conditions.

Total mass of radionuclides in the core are implemented by table data in the code for typical BWR plant. The core inventory of plant concerned is given by a ratio of thermal power and inventory. In the THALES-2 BWR code, a core region is represented by the groups of fuel assembly (maximum 5) and vertical nodes (maximum 25). Distribution of radionuclide inventory in the core region is automatically allocated to each core region in the code.

Radionuclide release from fuel

For radionuclide release from fuel before the reactor vessel failure (in-vessel), the CORSOR model and the new model with pressure effect proposed by the VEGA program [9] are applied to calculate release rates of radionuclides. After the vessel failure (ex-vessel release), the empirical model proposed by W.Murfin is used to calculate generation rates of aerosols of concrete components during core/concrete interaction. In addition, the CORSOR model is also applied to calculate release rates of radionuclides during the ex-vessel release.

Radionuclide behaviour

The radionuclide transport models are illustrated in Fig. 4.1-3. In this code, radioactive materials can take the form of gas, aerosol, deposit on structure walls and floors, and solution in water. The code solves the governing equations for multi-component aerosol, taking into account the size growth by agglomeration and condensation/evaporation of steam and volatile materials on the aerosol. Models are provided for various transport processes, including the condensation/evaporation and chemical absorption of the gas species at structure surfaces, deposition of aerosol to walls and floors, removal by sprays and filters, scrubbing by water pools, and convection by liquid as well as gas flow.

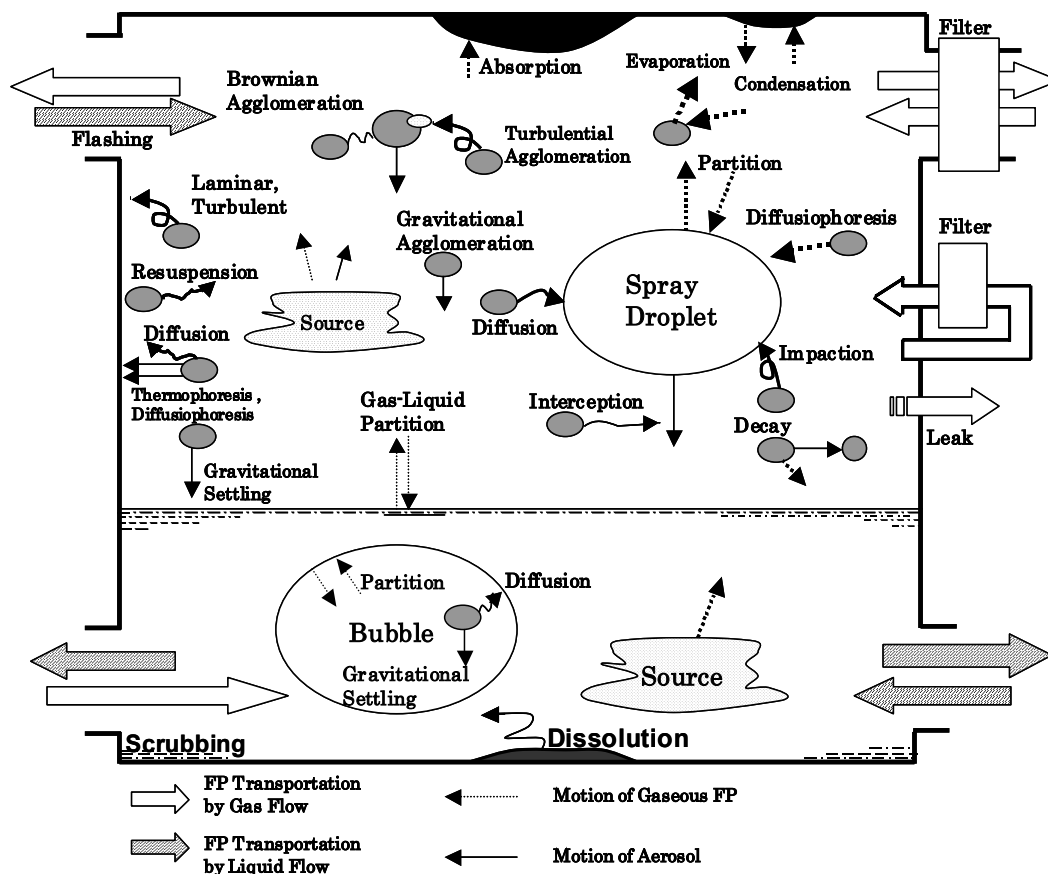


Fig. 4.1-3 Radionuclide transport models in THALES-2 BWR

References

- [1] M. Kajimoto et al. "Development of THALES-2, A Computer Code for Coupled Thermal-Hydraulics and FP Transport Analyses for Severe Accident at LWRs and Its Application to Analysis of FP Revaporization Phenomena" Proc. Int. Topical Mtg. on Safety of Thermal Reactors, Portland, pp. 584-592 (1991)
- [2] K. Abe et al. "Overview of Development and Application of THALES Code System for Analyzing Progression of Core Meltdown Accident of LWR's" Proc. 2nd Int. Symp. on Nucl. Power Plant Thermal Hydraulics and Operations, Tokyo (1986)
- [3] T. Ishigami et al. "User's Manual of ART Code for Analyzing Fission Product Transport Behaviour during Core Meltdown Accident" JAERI-M 88-093 (1988) (in Japanese)
- [4] K. Muramatsu et al. "Modeling Improvement and Application of the Integrated Severe Accident Analysis code THALES-2 for Assessment of Accident Management Strategies" Proc. Int. Conf. on Probabilistic Safety Assessment Methodology and Applications (PSA'95), pp. 216-221, Korea, (1995)
- [5] A. Hidaka et al. "Comparative Study of FP Deposition in WIND Project by ART and VICTORIA" Proc. Int. Conf. on Probabilistic Safety Assessment Methodology and Applications (PSA'95), pp. 241-246, Korea, (1995)
- [6] S. Kondo et al. "Comparison of Analytical Models and Calculated Results of Source Term Evaluation Codes" OECD/CSNI PSA Workshop, NUREG/CP-0115, pp. 273-287 (1990)
- [7] A. Hidaka et al. "Comparative Study of Source Terms of a BWR Severe Accident by THALES-2, STCP and MELCOR" Proc. 1992 National Heat Transfer Conf., HTC-Vol. 6, pp. 408-416 (1992)
- [8] J. Ishikawa et al. "Systematic Source Term Analyses fro Level 3 PSA of a BWR with Mark-II Type Containment with THALES-2 Code" 10th Int. Conf. on Nucl. Eng. (2002)
- [9] A. Hidaka et al. "Proposal of Simplified Model of Radionuclide Release from Fuel under Severe Accident Conditions Considering Pressure Effect" J. Nucl. Sci. Technol. 41(12), pp. 1192 - 1203 (2004)

4.1.5 ECART

ECART (ENEL Code for the Analysis of Radionuclide Transport) is an integrated primary circuit and containment code, originally created in 1989 for nuclear power plant severe accident analysis, but now also applied to fusion plants, industrial fires etc. The utilities ENEL and EdF contributed to its initial development, while its wider application for risk analysis is being carried forward by CESI. The code calculates the two-phase thermal-hydraulics for both the primary system and the containment and for material transport calculates aerosol and vapor transport together with chemical equilibrium and specific reactions between the gaseous phase and important structural surfaces. The principal models used are listed in Table 4.1-5.

An interesting feature of the code useful in experimental analysis is its ability to accept incomplete thermal-hydraulic data e.g. data specified only at certain junctions or boundaries, and then to use its internal calculation capabilities to complete the thermal-hydraulic conditions required by the aerosol and chemistry sections of the code. Validation studies have used data from the ATT-Marviken V, LACE, DEMONA, VANAM, STORM and PHÉBUS programmes. Recent applications of ECART have been to

aerosol resuspension and chemical reactions in PWR circuits, the safety analysis of IRIS, and transient analyses of the fusion experiment ITER.

Table 4.1-5 Circuit and containment models

	Mechanism	Literature source and/or brief description
Thermal-hydraulics	Transport of carrier gas/liquid mass, momentum, energy	Control volumes, each with a liquid and a gas volume in equilibrium 1-d and 2-d connection of volumes Bulk and wall condensation split
	Exchanges with structures	Included
	Vapor/gas transport	Secondary gases e.g. nobles, accounted for
	Sprays and sprinklers	Ad-hoc Lagrangian model accounting for droplet size distribution and injection speed
	Pool scrubbing	Included within control volume
	Gas combustion (hydrogen and others)	Accounted for through equilibrium chemistry
	Fires and explosive aerosol clouds	Models of pyrolysing solid surfaces, pool fires and detection of explosible aerosol clouds
	Radiative heat transfer from flames	View factors among flames and structures calculated with Montecarlo method Aerosol cloud absorption accounted
	Decay heat	13 most powerful elements accounted for
Vapor phenomena	Vapor-phase chemistry	Equilibrium with 126 reacting species (including carrier gases)
	Homogeneous nucleation	Not modelled (source seed required)
	Heterogeneous nucleation	Not modelled (source seed required)
	Sorption on surfaces (one-way)	Selected species/surface combinations e.g. irreversible sorption of I, I ₂ , HI, CsOH, Te and Te ₂ vapors on steel
	Condensation/Evaporation onto/from surfaces and aerosol particles	Calculated by diffusion equations
Aerosol phenomena	Transport	Well-mixed within each volume. Corrections for components with concentration gradients e.g. long pipes Discretised size distribution; simplified multi-component description (composition accounted for each size bin in each volume, for both airborne and deposited particles)
	Aerosol shape	Aerodynamic and collision shape factors
	Particle growth	Includes hygroscopic behaviour, Kelvin effect
	Settling	Stokes and non-Stokes regimes
	Turbulent impaction	Liu-Agarwal data

	Diffusion	Davies, Gormley-Kennedy
	Thermophoresis	Brock correlation with Talbot coefficients
	Diffusiophoresis	Schmidt-Waldmann
	Bend impaction	Stokes and non-Stokes regimes; size-dependent trapping in narrow bends
	Agglomeration	Brownian (Smoluchowski) Gravitational Turbulent (Saffman and Turner)
	Mechanical resuspension	Modelled through experimental correlation [1]
	Aerosol fall-back	Accounted for
	Scrubbing in water sumps	Lagrangian model accounting aerosol depletion within rising bubble - [2]

References

- [1] F. Parozzi A fast-running model for physical aerosol resuspension accounting for STORM experimental results Int. Mtg. "Best-Estimate" Methods in Nuclear Installation Safety Analysis (BE-2000), Washington Dc, USA, November 2000
- [2] F. Parozzi, S. Paci ECART code integrated approach for thermal-hydraulic source term analysis 4th Int. Conf. on Nuclear Option in Countries with Small and Medium Electricity Grids, Dubrovnik, Croatia, June 2002

4.1.6 APROS SA

4.1.6.1 Introduction

APROS (Advanced PROcess Simulator) is a multifunctional advanced process simulation software developed by Fortum and the Technical Research Centre of Finland. It is used for process and automation design, developing operation procedures and training at nuclear power plants, as well as for the full spectrum of the transient and accident analyses. APROS has passed an extensive validation programme.

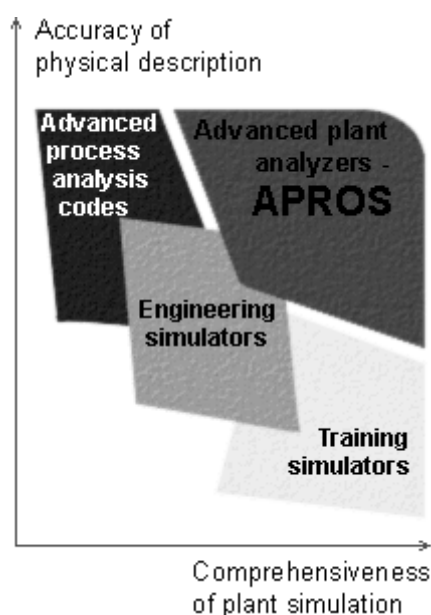
Most accident analyses for the new operating license of Loviisa NPP at uprated reactor power are made using APROS. The recent versions of APROS include components for detailed containment analysis, as well.

APROS software is applicable also in engineering and operator training of thermal power plants.

The versatile APROS simulation software suits as well for purposes of building engineering or training simulators and plant simulation models.

4.1.6.2 Severe accident extension

During the implementation of SAM for the Loviisa NPP, a tool for simulating severe accident phenomena was seen necessary. Specific phenomena, as in-vessel retention and hydrogen mitigation and



fission product behaviour in an ice condenser containment, were to be introduced into the system. The selection of using APROS software as a platform for the severe accident was a natural choice for Fortum.

The development of APROS SA [1] aims at a severe accident simulator for the Loviisa NPP that is capable of calculating the severe accident sequences faster than real time. The necessary phenomena are the core relocation, molten pool formation, core slumping into the lower plenum, in-vessel retention of the molten pool, hydrogen formation and fission product release from the overheating core, hydrogen mitigation with passive autocatalytic recombiners in the ice condenser containment, fission product retention in the RCS and in the containment, as well as in the long narrow pipelines in the containment bypass routes. In addition, the radiation levels at the plant site are to be included into the simulator.

The visualisation of the calculation results plays an important role in training the severe accident phenomena. In Fig. 4.1-4 can be seen an example of temperature profile in the Loviisa NPP ice condenser containment at two situations.



Fig. 4.1-4 Temperature distribution in Loviisa NPP ice condenser containment at 0 s (left) and 3 s, (right) after a 500 cm² break in cold leg calculated by APROS SA. (Color gradient is from blue to red to yellow with blue corresponding 20 °C, red 60 °C and yellow 100 °C) [1]

4.1.6.3 Aerosol modelling

The aerosol modelling in APROS SA is based on fixed, user defined aerosol size classes, where no aerosol growth is assumed. Each fission product group acts as individual substance with their own aerosol material densities. Currently, for each FP group there are three different aerosol size groups, one group for gaseous species, and one for deposited mass. The deposited mass can be either on the dry surfaces of a simulation node or dissolved in the water within the node. The FPs are transported between the nodes along with the flowing gas or water.

The fission product groups in APROS SA are:

- Noble gases (Kr, Xe)
- Iodine (I, Br)
- Cesium (Cs, Rb)
- Tellurium (Te)
- Metallic compounds (not released from the core)
- Oxidic compounds (not released from the core)

The TH condition calculated by the other models in APROS or APROS SA are used for FP calculation, and the FP calculation gives the decay power distribution as input to the other models. The distribution of metallic and oxidic compounds not released from the reactor core is used for the decay power distribution calculation between the metallic and oxidic molten pools at the bottom of the RPV lower head.

The fission product release from the reactor core is based on the CORSOR-M model [2], and the released FPs (other than noble gases) are instantaneously in form of aerosol after the release. This means that the vapor phase chemistry in the RCS is not considered.

The aerosol processes in the APROS SA are those that play the most important role in the case of the Loviisa NPP:

- Sedimentation
- Thermophoresis (Talbot correlation; independent of aerosol particle size)
- Diffusiophoresis (independent of aerosol particle size)
- Turbulent (eddy) impaction in the RCS and bypass pipelines (modified model to meet the coupling with the resuspension model by [3])
- Revaporisation
- Resuspension [3]
- Spray droplet washout (impaction, interception, diffusion)
- Inter-volume aerosol fall to lower levels (similar to sedimentation)

The FP calculation has no other effect on the other parts of calculation than through providing the decay power distribution. Iodine chemistry is modelled as simple equilibrium calculation with fixed water pool pH and temperature dependent partitioning of gaseous iodine (I_2). The formation of organic iodine is not accounted for.

The limitation of the FP modelling is that it cannot be used for detailed analyses on FP behaviour. The essential information from the APROS SA fission product calculation is qualitative data with a reasonable accuracy for training purposes of severe accident simulations and usage of EOPs for SAM.

The aerosol models have been validated against different experimental data. The revaporisation and deposition in the pipe systems have been verified against the data from the RCS part in the ISP-46 from the PHÉBUS FPT1 (see Fig. 4.1-5) [4]. The aerosol behaviour in the containment has been compared with the results from the VICTORIA facility (a scale model of the Loviisa ice condenser containment) [5, 6]. The

resuspension model validation is currently under work, and the results are to be compared with the results from the Horizon [7] and PSAERO [8] facilities.

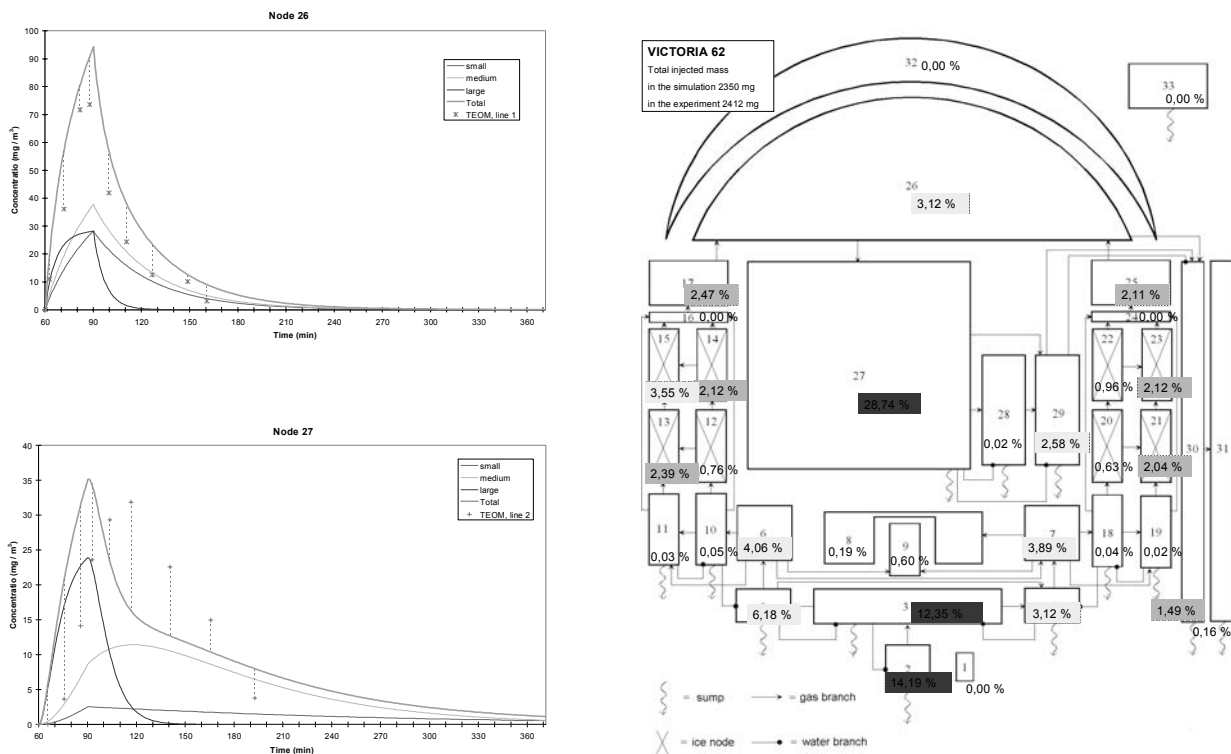


Fig. 4.1-5 Comparison of APROS SA aerosol calculation with VICTORIA experimental results [6]

4.1.6.4 Future plans

In future, the models for aerosol size distribution in the RCS calculated from the aerosol mass concentration are to be implemented, which probably accelerates the calculation speed significantly. There is a very high number of calculation nodes in a typical simulation environment in a detailed plant model, and therefore a reduction of individually calculated aerosol groups is foreseen.

The radiation level calculation from the FP distribution is one essential part of a severe accident simulator, as it provides information for simulation of radiation measurement device used during accidents. The essential information on the coefficients to calculate the radiation levels from the activities is to be implemented rather in the user interface of APROS SA than directly into the FP calculation.

References

- [1] E. Raiko, K. Salminen, P. Lundström, M. Harti, T. Routamo Severe accident training simulator APROS SA. Proceedings of NURETH-10 The 10th International Topical Meeting on Nuclear Reactor Thermal Hydraulics, October 5-11, 2003, Seoul, Korea, 2003
- [2] M. Silberberg, J.A. Mitchell, R.O. Meyer, C.P. Ryder Reassessment of the Technical Bases for Estimating Source Terms Final Report. U.S. Nuclear Regulatory Commission, Office of Nuclear Regulatory Research, Washington, July 1986. NUREG-0956

- [3] A. Auvinen, J.K. Jokiniemi Modelling resuspension of particle layer in an internal tube flow Presented in the European Aerosol Conference (EAC04), September 6-10, 2004, Budapest, Hungary
- [4] V. Karttunen Validation of a fission product revaporization model Helsinki University of Technology, Master's thesis, Espoo, January 10, 2005. 81 p. + Apps, 2005a
- [5] V. Karttunen APROS SA fission product validation in containment nodes with CsOH Fortum Nuclear Services Ltd, Report 24.1.2005. TERMO-435, 2005b
- [6] V. Karttunen APROS SA fission product validation in containment nodes with Ag Fortum Nuclear Services Ltd, Report 25.4.2005. TERMO-466, 2005c
- [7] T. Routamo, J. Jokiniemi, J. Mäkynen Aerosol Deposition in Horizontal Steam Generator Tubes in Severe Accident Conditions Proceedings of NURETH-10 - The 10th International Topical Meeting on Nuclear Reactor Thermal Hydraulics, October 5-11, 2003, Seoul, Korea, 2003
- [8] A. Auvinen^a, J.K. Jokiniemi^a, A. Lähde^a, T. Routamo^b, P. Lundström^b, H. Tuomisto^b, J. Dienstbier^c, S. Güntay^d, D. Suckow^d, A. Dehbi^d, M. Sloodman^e, L. Herranz^f, V. Peyres^f, J. Polo^f, "SG tube rupture (SGTR) scenarios" Nuclear Engineering and Design 235 (2005) 457–472
^a VTT Processes, Biologinkuja 7, P.O. Box 1602, VTT Espoo 02044, Finland
^b Fortum Nuclear Services, Vantaa, Finland
^c Nuclear Research Institute Rez plc, Czech Republic
^d Paul Scherrer Institute, Villigen-PSI, Switzerland
^e Nuclear Research and Consultancy Group, Arnhem, Netherlands
^f Centro de Investigaciones Energeticas, Medioambientales y Tecnologicas, Madrid, Spain

4.2 Circuit

4.2.1 VICTORIA

The VICTORIA computer code [1, 2] attempts to predict the behaviour of radionuclides in the reactor coolant system under severe accident conditions. It addresses the release of radionuclides, the chemical forms adopted by the radionuclides, as well as the formation, growth and deposition of aerosol particles. The computer code was not intended for the routine analysis of severe reactor accidents. The idea for the development of a mechanistic treatment of radionuclide behaviour in the reactor coolant system arose in the aftermath of the accident at Three Mile Island. It had become obvious that simplistic treatment of the radionuclide releases during core degradation in terms of noble gases, gaseous iodine and general particulate could not lead to results of adequate accuracy. At the same time, a wealth of experimental evidence of chemical interactions of radionuclides in the reactor coolant system environment under accident conditions was coming available from research programs in the USA, UK, and France. Simply "patching" existing radionuclide transport models with *ad hoc* chemical models became increasingly unsatisfactory. Experimental results, though quite significant, were obtained for limited conditions and selected species. A broader analytic approach was needed that could account for experimental findings and extrapolate these findings to more drastic conditions expected to develop in some classes of risk-significant accidents and even to other chemical systems that had not received individual study. The VICTORIA model was developed to address this need. It was intended to be used to interpret experiments and to extrapolate the results to accident conditions. The objective of the detailed mechanistic analyses was to determine important phenomena that had to be represented in systems level accident analysis models such as MELCOR.

VICTORIA is a lumped computational node computer code. Computational nodes can be quite small in comparison to those used in systems-level reactor accident analysis codes. Key elements of the VICTORIA computer code are models of:

- Fission product release from degrading reactor fuel and precious metal control rods
- Chemical speciation of radionuclides and other materials vaporized during reactor core degradation
- Formation and growth of aerosol particles
- Deposition of vapors on surfaces along the flow paths through the reactor coolant system
- Deposition of aerosols on surfaces along the flow paths through the reactor coolant system
- Resuspension of deposited aerosol
- Revaporisation of radionuclides on surfaces in the reactor coolant system

The VICTORIA computer code does not attempt to predict the inventories of radionuclides in reactor fuel at the start of an accident. These inventories are usually obtained using the ORIGEN [3] computer code. The VICTORIA computer code does not try to predict the flows through the reactor coolant system or the temperatures of the structures along the flow paths. These are obtained from other models such as MELCOR.

Synoptic descriptions of the models in VICTORIA are presented in the sections that follow.

Radionuclide release from the fuel

The VICTORIA model was not originally intended to address issues of radionuclide release from the fuel. Other models like CORSOR [4] exist for making such predictions. It was found, however, convenient to include release models into the computer code. Still this is an area that has received the least model development attention.

The code considers two configurations of the reactor fuel for the purposes of estimating radionuclide release:

- intact fuel in rod geometry that may or may not have cladding still in place
- rubble that may be molten produced as the core loses its geometry

The distinct models of radionuclide release in these configurations are discussed in subsections below.

Release from intact fuel

For the purposes of estimating release from fuel in rod-like geometry, VICTORIA originally had two models. One was a very mechanistic model patterned after the FASTGRASS [5] model developed at Argonne National Laboratory. The other was the more empirical model based on the well-known Booth solution to the diffusion problem and parameterised based on results of tests of radionuclide release from irradiated fuel done at Oak Ridge National Laboratory. It was found that the mechanistic model required input that is not routinely available. Furthermore, the model was not especially reliable. Based on a recommendation of a peer review group the very mechanistic release model was deleted from the VICTORIA computer code.

The Booth-type modeling of fission product release has been replaced in the more recent version of VICTORIA by a more mechanistic model that considers:

- diffusive release of fission products from fuel grains
- transport of fission product vapors through the pore network of the fuel
- transport of fission product vapors through the gap between the fuel pellets and the cladding to a break in the cladding when the cladding is present
- mass transport of fission product vapors away from the break in the cladding or other free surface.

Diffusion coefficients for fission products in fuel grains are taken from Matzke [6]. Gas phase diffusion coefficients are calculated based on the well-known Chapman Enskog expression for binary diffusion coefficients assuming a Lennard-Jones intermolecular potential. Binary diffusion coefficients are combined to define effective diffusion coefficients for multicomponent gaseous mixtures. The assumption of Lennard-Jones intermolecular potentials is a common one for computer codes like VICTORIA. Two issues are associated with this assumption. First, the Lennard-Jones intermolecular potential is not precisely applicable to the vapor species of interest since many are polyatomic and many are either radicals or have permanent dipole moments. Most consider this to be an issue of modest importance. More difficult is that reliable estimates of the parameters for the potential, collision diameter and energy well depth, are not available. Parameters used in the modeling can be considered no more than educated guesses.

The advantages of the current release modeling in VICTORIA include accounting for the effects of both ambient pressure and ambient gas composition as well as temperature on the releases of fission products from the fuel.

Release from fuel debris

It is assumed in the VICTORIA computer code that relocation of fuel yields a rubble bed. Modeling of fission product release from the rubble bed is based on the assumption that the rubble is composed of fuel cylinders with lengths and diameters specified by the user to adequately reflect the surface to volume ratio of real debris. Fission products diffuse through grains and pores of the fuel cylinders much as they do in intact fuel. Mass transport of vapors that reach the geometric surfaces of the fuel cylinders is modeled. The VICTORIA code does have a model of fission product release from a molten pool. There have not been many opportunities to evaluate and refine this model.

Release of control rod material

Vapors and aerosol are produced when silver-indium-cadmium control rods found in pressurised water reactors fail during reactor accidents. These vapor and aerosol materials can interact with radionuclide vapors and aerosols produced by core degradation and affect reactor accident source terms. VICTORIA models the production of vapor and aerosols produced by the failure of silver-indium-cadmium control rods. The production is considered to involve two phases - a burst failure when the control rod cladding fails because the internal pressure exceeds the pressure in the reactor coolant system and a continued vaporization release from the molten control rod alloy.

The burst release involves the venting of vapors from the control rod and the entrainment of 2 % of the control rod alloy above the failure location. The entrained aerosol is taken to have a geometric mean particle size of 0.5 μm with a geometric standard deviation of 1.8.

Vaporization of the Ag-In-Cd alloy is done by either fixing the location of the alloy or allowing the alloy to "candle" or drain downward. Vaporization is calculated for material that is candling.

There is not now in VICTORIA a model of vapor and aerosol production from boron carbide control blades degradation during boiling water reactor accidents.

Chemical speciation of released material

The essential model in VICTORIA is a prediction of the chemical speciation of the materials vaporized from the reactor core. The model is applied in each of the computational nodes of the model so the evolution of the speciation is taken into account. The model is based on the assumption of chemical equilibrium at the local temperature and constant volume rather than the more common condition of constant pressure. The computational method for finding the equilibrium speciation was specially developed for the VICTORIA code, but is akin to the well-known NASA method.

The chemical equilibrium analysis considers the elements Ag, Ar, B, Ba, Cd, Cr, Cs, Eu, Fe, H, He, I, In, Kr, Mn, Mo, Ni, O, Ru, Sb, Sn, Sr, Te, U, Xe, Zr. The equilibrium calculation considers 288 chemical species. Chemical species considered in the equilibrium model were chosen from species with readily available thermodynamic data. The species are primarily from binary M-O, M-H, M-Te and M-I systems where M designates a metal or electropositive species. Very few mixed oxide vapor species are considered. Certainly, the speciation has not been optimised for the high temperature conditions encountered in severe reactor accidents. There has not been an aggressive attempt to include vapor species not addressed in conventional compilations of thermodynamic data.

Multiple condensed phases can be predicted to form in the equilibrium calculation. VICTORIA considers all condensed phases to form ideal solutions of one type or another. Three types of condensed phase solutions are recognised: metallic, oxidic, and metal iodides. This is, at best, an approximate treatment since many important solid species even within a given class of species recognised by VICTORIA are not mutually soluble in the solid state.

A great deal of attention has been devoted to making the chemical equilibrium solver in VICTORIA execute both reliably and quickly. The routine is called multiple times in each computation node and in each time step as is discussed below in connection with vapor deposition.

Aerosol formation and growth

The VICTORIA computer code does not make a mechanistic prediction of aerosol particle nucleation from supersaturated vapors. Rather, it assumes that aerosol is formed promptly when the vapor reaches a point of saturation of one or more of its constituents as predicted with the chemical speciation model. Neglect of nucleation modeling was based on calculational exercises that showed details of the aerosol size distribution produced by mechanistic nucleation processes were promptly obscured by the coagulation of the product aerosol particles.

The implementation of the approximate treatment of aerosol formation depends on the results obtained from the chemical speciation model. When chemical speciation calculations indicate that a condensed phase is formed or more mass is transferred to the condensed phase, this mass is placed in the smallest size bin of aerosol considered in the aerosol modeling (See below).

The aerosol growth is calculated based on a conventional master equation using the CHARM [7] code. CHARM uses a sectional method to solve the master equation. That is, the aerosol size distribution is divided into a set of bins.

The solution is achieved using a finite interval collocation method. The coagulation kernel considers coagulation of aerosol particles by:

- gravitation settling
- Brownian diffusion
- turbulent inertia
- turbulent diffusion

Aerosol growth as a result of hygroscopicity is not considered in VICTORIA since temperatures arising in typical analyses exceed the critical temperature of water.

Vapor deposition and revaporization

As vapors pass through and out of the core region, they cool. A temperature is reached eventually where the equilibrium chemical speciation will include some condensed phases. That is, the vapor will condense or react with surfaces. Vapor condensation can involve deposition on surfaces, deposition on aerosol particles and nucleation on particles. On the other hand, changes in temperature or chemical conditions along the flow path or with time can cause previously deposited materials to vaporize.

The VICTORIA computer code has an involved method for the description of the condensation and evaporation so that the processes are fully reversible. The equilibrium speciation of the bulk gas phase at constant volume and temperature and including any aerosol present is calculated. Another equilibrium speciation calculation is done for surfaces adjacent to the flowing gas which might be at quite different temperatures than the bulk gas phase. Differences in the vapor pressures at the surface and in the gas phase define the driving force for either vaporization or vapor deposition. The partitioning of vapor among structural surfaces, aerosol surfaces and new aerosol is found through mass transport considerations. The competitive mass transport to structural surfaces and to suspended aerosol is evaluated. Any additional condensation (or evaporation) necessary to relieve disequilibrium in the system is apportioned to nucleated aerosol that is assumed to appear in the smallest aerosol "bin".

Aerosol deposition

Aerosol deposition is considered in the VICTORIA computer code to occur as a result of:

- gravitational settling
- Brownian diffusion
- turbulent deposition
- thermophoresis
- inertial deposition from flow in
 - bends
 - flow path contractions
 - *vena contracta*

A specialised model for inertial deposition in the separators and dryers of boiling water reactors is also included in the VICTORIA modeling.

Diffusiophoretic deposition is not considered in VICTORIA. There is not usually condensing water in the reactor coolant system under severe accident conditions and the condensing fluxes of vapor to structural surfaces within the system are too small to significantly affect aerosol deposition rates.

Conventional models are used for gravitational settling and Brownian diffusion (see Chapter 2).

Turbulent deposition modeling is based on particle size. For submicron particles, turbulent deposition is based on a model by Davies [8]:

$$V_d = \frac{Sc^{-2/3} v_g}{14.5 \left[\frac{1}{6} \ln \left(\frac{(1+\Phi)^2}{1-\Phi+\Phi^2} \right) + \frac{1}{\sqrt{3}} \tan^{-1} \left(\frac{2\Phi-1}{\sqrt{3}} \right) + \frac{\pi}{\sqrt{3}} \right]}$$

and for larger particles, turbulent deposition is based on a model by Sehmel [9]:

$$V_d = 3.69 \times 10^{-8} \rho_p^{1.01} \left(\frac{d_p}{d_h} \right)^{2.1} Re^{3.02} v_g$$

where:

V_d = particle disposition velocity (cm/s)

v_g = gas velocity (cm/s)

ρ_p = particle material density (g/cm³)

d_p = particle diameter (cm)

d_h = hydraulic diameter of flow path (cm)

Re = Reynolds number (-)

Sc = Schmidt number

$$\Phi = \frac{Sc^{1/3}}{2.9}$$

Thermophoretic deposition is based on the Talbot [10] interpolation expression.

Inertial deposition in bends is based on the Pui [11] correlation. Deposition as a result of contractions in the flow is based on the Ye and Pui [12] correlation. Deposition produced by a *vena contracta* is calculated from a correlation by Belyaev and Levin [13]. These correlations are discussed in Chapter 2 of this report.

4.2.1.1. Aerosol resuspension

VICTORIA uses an outdated model of resuspension based on a curve fit to experimental data [14]:

$$\frac{dF}{dt} = \begin{cases} 0 & Re < 2300 \\ 0.05 (U^*)^2 / t^{1.25} & Re > 2300 \end{cases}$$

where:

- F = fraction of deposit remaining
- Re = Reynolds number
- U * = friction velocity (m/s)
- t = time from point at which Re became greater than 2300

This model is applicable only to aerosol that is present on surfaces as dry dust and should not apply to deposited aerosols that have interacted chemically with the surface or with other deposited materials. It does not account for any aging of the deposited material which will usually reduce the propensity for resuspension. There is no consideration of surface vibration or shock waves on the ability to resuspend deposited materials.

4.2.1.2 Status

Development and use of the VICTORIA computer code is no longer supported. Currently underway is an effort to evaluate the findings obtained with VICTORIA in the analyses of a variety of experiments to identify improvements needed in the fission product modeling in the MELCOR computer code.

References

- [1] N.E. Bixler VICTORIA 2.0: A Mechanistic Model for Radionuclide Behaviour in a Nuclear Reactor Coolant System under Severe Accident Conditions NUREG/CR-6131, Sandia National Laboratories, Albuquerque, NM, 1998
- [2] T.J. Heames et al. VICTORIA: A Mechanistic Model of Radionuclide Behaviour in the Reactor Coolant System Under Severe Accident Conditions NUREG/CR-5545, Sandia National Laboratories, Albuquerque, NM, December 1992
- [3] A.G. Croff ORIGEN2: A versatile computer code for calculating the nuclide composition and characteristics of nuclear materials Nuclear Technology, 62 (1983) 335
- [4] M.R. Kuhlmann, D.J. Lehmicke and R.O. Meyer CORSOR User's Manual NUREG/CR-4173, BMI-2122, Battelle Memorial Institute, Columbus, Ohio, March 1985
- [5] J. Rest and S.A. Zawadzki FASTGRASS: A Mechanistic Model for the Prediction of Xe, I, Cs, Te, Ba and Sr Release from Nuclear Fuel Under Normal and Severe Accident Conditions: User's Guide for Maintenance, Workstation and Personal Computer Applications NUREG/CR-5840, Argonne National Laboratory, Argonne, IL, 1992
- [6] H. Matzke A Diffusion in Ceramic Oxide Systems Advances in Ceramics, 17 (1986) 1
- [7] C.J. Wheatley CHARM: A Model for Aerosol Behaviour in Time-Varying Thermal Hydraulic Conditions NUREG/CR-5162, Sandia National Laboratories, Albuquerque, NM, 1988
- [8] C.N. Davies Aerosol Science Academic Press, 1966
- [9] G.A. Sehmel J. Geophys. Res., 75 (1970) 1766
- [10] L. Talbot, T.K. Cheng, R.W. Schefer and D.R. Willis J. Fluid Mechanics 101 (1980) 737
- [11] D.Y. Pui, R. Fomay-Novas and B.Y. Liu Aerosol Science and Technology, 7 (1987) 301

- [12] Y.Ye and D.Y. Pui J. Aerosol Science, 21 (1990) 29
- [13] S.P. Belyaev and L.M. Levin J. Aerosol Science, 3 (1972) 127
- [14] A.L. Wright, W.L. Patterson and J.Y. King TRAP-MELT Validation Tests: Series 2 Aerosol Resuspension Test Data Summary Report, Letter Report to the US Nuclear Regulatory Commission, Oak Ridge National Laboratory, Oak Ridge, TN, 1984

4.2.2 *ATHLET-CD*

The system code ATHLET-CD (Analysis of Thermal-Hydraulics of Leads and Transients with Core Degradation [1]) is designed to describe the reactor coolant system thermal-hydraulic response, core damage progression, fission products and aerosol behaviour during severe accidents, to calculate the source term for containment analyses, and to evaluate accident management measures [2]. It is being developed by GRS in cooperation with the Institut für Kernenergetik und Energiesysteme (IKE), University of Stuttgart. ATHLET-CD also includes the aerosol and fission product transport code SOPHAEROS (see chapter 4.1.2), which is being developed by the French Institut de Radioprotection et de Sûreté Nucléaire (IRSN).

The ATHLET-CD structure is highly modular in order to include a manifold spectrum of models and to offer an optimum basis for further development. It contains the original ATHLET models for a comprehensive simulation of the thermal-hydraulics in the reactor coolant system. The ATHLET code [3] comprises: (a) a thermo-fluid-dynamic module, (b) a heat transfer and heat conduction module, (c) a neutron kinetics module, (d) a general control simulation module, and (e) the general solver of differential equation systems FEBE (Forward Euler - Backward Euler [4]). The thermo-fluid-dynamic module includes two different fluid-dynamics equation systems: (a) a six-equation model, with fully separated balance equations for liquid and vapor, complemented by mass conservation equations for up to 5 different non-condensable gases and by a boron tracking model, and (b) a five-equation model, with a mixture momentum equation and a full-range drift-flux formulation for the calculation of the relative velocity between phases. Specific models for pumps, valves, steam separators, mixture level tracking, critical flow, etc. are also available in ATHLET.

The rod module ECORE consists of models for fuel rods, absorber rods (AIC and B₄C) and for the fuel assembly including BWR canister and absorber. The module describes the mechanical rod behaviour (ballooning), zirconium and boron carbide oxidation (Arrhenius type rate equation), Zr-UO₂ dissolution, as well as melting of metallic and ceramic components. The melt relocation (candling model) is simulated by rivulets with constant velocity and cross section, starting from the node where rod failure is predicted to occur. The model accounts for oxidation, freezing, re-melting, re-freezing and melt accumulation due to blockage formation. The feedback to the thermal-hydraulics considers steam starvation and blockage formation [5]. Besides the convective heat transfer, energy can also be exchanged by radiation between fuel rods and to surrounding core structures.

The release of fission products is modeled by rate equations or by a diffusion model within the module FIPREM [6]. The transport and retention of fission products and aerosols in the reactor coolant system are simulated by the code SOPHAEROS [7].

For the simulation of debris bed a specific model MESOCO [8] is under development, with its own thermal-hydraulic equation system, coupled to the ATHLET fluid-dynamics on the outer boundaries of the debris bed. The transition of the simulation of the core zones from ECORE to MESOCO depends on the degree of degradation in the zone. The code development comprises also late phase models for core slumping, melt pool behaviour and vessel failure.

The code system ATHLET/ATHLET-CD can be coupled to the containment code system COCOSYS (see chapter 4.3.2), and it is the main process model within the German nuclear plant analyser ATLAS. The ATLAS environment allows not only a graphical visualization of the calculated results but also an interactive control of the simulation.

The code validation is based on integral tests and separate effect tests, as proposed by the CSNI validation matrices [9], and covers thermal-hydraulics, bundle degradation as well as release and transport of fission products and aerosols.

References

- [1] K. Trambauer, C. Bals, J.-D. Schubert, H. Austregesilo ATHLET-CD Mod 2.1 - Cycle A User's Manual Gesellschaft für Anlagen- und Reaktorsicherheit (GRS) mbH, GRS-P-4, Vol. 1., 2006
- [2] V. Teschendorff, K. Trambauer
Simulation of severe accidents with detailed thermal hydraulic models Kerntechnik, 63, 18-24, 1998
- [3] H. Austregesilo, C. Bals, A. Hora, G. Lerchl, P. Romstedt ATHLET Mod 2.0 Cycle A - Models and Methods Gesellschaft für Anlagen- und Reaktorsicherheit (GRS) mbH, GRS-P-1, Vol. 4., 2003
- [4] E. Hofer An $A(\alpha)$ -Stable Variable Order ODE-Solver Topical Meeting on Advances in Math. Methods, Munich, April 1981
- [5] K. Trambauer Coupling methods of thermal-hydraulic models with core degradation models in ATHLET-CD In: Proceedings of the 6th International Conference on Nuclear Engineering, ICONE-6368, San Diego, USA, May 10-15, 1998
- [6] K.D. Hocke, A. Paller, A. Schatz Modelling and Code Development for the improved Description of FP and Aerosol release during LWR Core Heat-up and Degradation CL-NA-15210-EN-C, European Commission, 1994
- [7] C. Fiche User's manual of SOPHAEROS V2.2, IRSN N.T. SEMIC 2004/13, 2004
- [8] M. Bürger, M. Buck, W. Schmidt, G. Pohlner, W. Widmann Ausbau und Verifikation der Spätphasenmodelle und des Gesamtmodells zum Kernschmelzen in KESS und ATHLET-CD IKE 2-145, Universität Stuttgart, 2001
- [9] K. Trambauer, T.J. Haste, B. Adroguer, Z. Hózer, D. Magallon, A. Zurita In-Vessel Core Degradation Code Validation Matrix - Update 1996-1999 OECD Nuclear Energy Agency, NEA/CSNI/R(2000)21, 2000

4.3 Containment

4.3.1 *CONTAIN*

Introduction

The CONTAIN 2.0 computer code is a modular and integrated analysis tool used for predicting physical conditions, chemical compositions, and distributions of radiological materials inside a containment building following the release of material from the primary system in a light-water reactor accident [1]. It can also predict the source term to the environment. Interactions among thermal-hydraulic phenomena, aerosol behaviour and fission product behaviour are taken into account. The code includes atmospheric

models for steam/air thermodynamics, inter-cell flows, condensation/evaporation on structures and aerosols, aerosol behaviour, and gas combustion. It also includes models for reactor cavity phenomena such as core-concrete interactions and coolant pool boiling. Heat conduction in structures, fission product decay and transport, radioactive decay heating, and the thermal-hydraulic and fission product decontamination effects of engineered safety features are also modeled. For those phenomena affected by significant uncertainty, CONTAIN 2.0 is provided with the capability of introducing user-specified input parameters in order to perform sensitivity studies.

Status

CONTAIN was developed at Sandia National Laboratories under the sponsorship of the US Nuclear Regulatory Commission (USNRC) for analyzing containment phenomena under severe accident and design basis accident conditions. The first version was released in 1984 [2]. A detailed history of CONTAIN code release can be found in the CONTAIN 2.0 code manual [1]. This note refers to the third major release of the code (CONTAIN 2.0).

An extensive independent review of the CONTAIN code was done in the mid 90s [3]. At that time, the Peer Review Committee judgement was extremely positive and stated that the code could be applied to both selected design basis accidents and severe accidents for both current reactors and advanced light water reactors. In this regard, the CONTAIN code was assessed against data concerning the passive containment cooling system of the AP600 Westinghouse reactor [4].

Even though in the revised severe accident code strategy of USNRC the role of CONTAIN for source term analyses is de-emphasised, aerosol and fission product models are in many cases state-of-the-art and suitable for many types of source term analyses.

Extensive validation of the CONTAIN code modeling has been carried out. A good example is the thermo-hydraulics, inter-cell flow and hydrogen combustion models that have been compared against more than 20 tests [5]. In the particular case of aerosol modeling, recent validation exercises have been carried out in the frame of OECD/CSNI against experiments like VANAM-M3 [6], KAEVER [7], PHÉBUS-FPT1 [8]. In addition, further CONTAIN-to-data comparisons are set on individual bases [9, 10].

Aerosol modelling

The basic aerosol modeling in CONTAIN comes from the MAEROS code [11] together with some enhancements. The major generic features are:

- Size distribution can be described by 10-20 classes.
- Chemical composition can be detailed by using 8 material components.
- Steam condensation onto particles is tightly coupled with thermal-hydraulics.

As shown in the Table below, two methods are available in CONTAIN to model condensation/evaporation of water onto/from particles: fixed- and moving-grid.

CONTAIN 2.0 is provided with two aerosol injections into the containment: the primary circuit and the core-concrete interaction. The former is given through the code input deck, whereas the latter is a result of the VANESA module in CORCON-Mod3.

Some relevant hypotheses assumed in the aerosol treatment are:

- The size interval over which aerosol distribution extends is partitioned geometrically.
- The particle volume in a class *i* is at least twice the one in the previous smaller class.
- The aerosol material density is assumed to be the same for all components.
- The aerosol shape (considered through dynamic and agglomeration shape factors) is independent of aerosol composition.
- The medium in which the aerosol processes are assumed to occur has fixed composition and is taken to be air.
- Gas properties appearing in equations for deposition rates are evaluated by-default for bulk conditions.
- The degree of turbulent agglomeration is fixed throughout the problem (input deck).
- Thermal conductivity ratio between air and aerosol is not composition-dependent.

INTERACTION MECHANISMS			
Agglomeration	Brownian diffusion		Friedlander
	Differential gravitational settling		MAEROS code (Fuch's collision efficiency)
	Turbulent shear		Saffman and Turner (Collision efficiency set to 1.0)
	Turbulent acceleration in eddies		Saffman and Turner (Fuch's collision efficiency)
Steam condensation	Moving-grid	Solute effect Kelvin effect	Mason equation
	Fixed-grid (default model)	None of above effects modeled	
NATURAL DEPOSITION MECHANISMS			
Gravitational settling			MAEROS code
Diffusiophoresis			Waldmann & Schmidt
Thermophoresis			Talbot
Diffusion			MAEROS code
ESF DEPOSITION MECHANISMS			
Sprays	Diffusion Diffusiophoresis Thermophoresis Impaction Interception	[12]	
Ice condensers	Gravitational settling Diffusion Diffusiophoresis Thermophoresis Impaction Interception	ICEDF code [13]	
Fan coolers	Diffusiophoresis	Waldmann & Schmidt	
Pools	Core-concrete interactions	VANESA (SCRUB) [14]	
	BWR suppression pools	SPARC (85) [15]	

Processes and systems with impact on aerosols

	DESCRIPTION	TREATMENT
Atmosphere/Pool Thermal-Hydraulics & Intercell Flow	<p>Atmosphere bulk fluid:</p> <ul style="list-style-type: none"> – Non-condensable gas – Coolant vapor – Homogeneously dispersed liquid coolant <p>Pool bulk fluid</p> <ul style="list-style-type: none"> – Coolant 	<ul style="list-style-type: none"> – The cell fluids are stagnant and well-mixed – Flow occurs through flow paths – Flow is controlled by a fluid slug with an effective length. – Flow paths are not repositories
Lower Cell and Cavity	<p>Core-concrete interactions(with/without overlying coolant):</p> <ul style="list-style-type: none"> – Basemat ablation – Production of gases and steam (H₂, CO, CO₂, H₂O) and ablation products 	<ul style="list-style-type: none"> • CORCON-MOD3 (the VANESA code is integrated): – Gas generation – Convective or boiling heat transfer – Aerosol generation <p>Aerosols are scrubbed if there is a coolant pool on the core debris upper surface. or, alternatively,</p> <ul style="list-style-type: none"> • A one-dimensional system of material layers
Direct Containment Heating	Molten debris ejection (under high pressure) as a finely dispersed collection of particles into the containment	<ul style="list-style-type: none"> • Standard containment models (intercell flow, two-phase atmosphere and coolant thermodynamics, heat transfer to structures, radiative heat transfer, hydrogen transport and combustion, ...) and • A suite of DCH-specific models (transport and trapping of multiple dispersed core-debris fields, debris droplets chemistry, convection and radiation heat transfer from the debris, ...).
Fission Product Behaviour		<ul style="list-style-type: none"> – Fission product assigned to repositories (hosts): atmosphere gas, suspended aerosols, coolant pool, and structure surface. – Fission product transfer between hosts feasible.

	DESCRIPTION	TREATMENT
		<ul style="list-style-type: none"> – Two alternate ways of representing fission product decay
Combustion	<ul style="list-style-type: none"> – Deflagration of premixed gas – Diffusion flame burning of jets – Bulk spontaneous recombination 	<ul style="list-style-type: none"> – Modified HECTR 1.8 – Parametric model (dynamics of the diffusion flame not modeled – Parametric model (user provides recombination threshold temperature and time constant)
Heat & Mass Transfer	<p>In-containment heat and mass absorption of the thermal energy entering containment during a reactor accident.</p> <ul style="list-style-type: none"> – Natural and forced convection – Condensation mass and heat transfer – Condensate film mass transfer – Radiative heat transfer – Boiling heat transfer – Heat conduction 	<ul style="list-style-type: none"> – State of the art correlations – Heat/Mass transfer analogy – Fixed film thickness (structure-pool) and film tracking model (structure-structure) – Net enclosure model and direct radiation model – Adapted model from CORCON – The solving method uses finite difference techniques
Other models	<ul style="list-style-type: none"> – BWR suppression pool vent discharge – Safety relief valve (SRV) discharge – Fan cooler – Ice condenser – Sprays – Liquid transport system components 	

Computational considerations

Overall, CONTAIN solves the aerosol equations by an explicit Runge-Kutta algorithm.

Steam condensation/evaporation onto/from particles is numerically handled in a different way depending on the approach adopted (i.e., fixed- or moving-grid methods).

The fixed grid model models the condensation of water vapor onto aerosols and the evaporation of water from them. Condensation is taken into account within the Runge-Kutta integration of the integro-differential equation that describes aerosol evolution. Two solution methods are used for evaporation. For high superheat, when aerosol water evaporation is insufficient to keep the atmosphere saturated, a method of characteristics is employed. For evaporation under nearly saturated conditions, the Runge-Kutta method is used.

The moving-grid model uses an algorithm based on the method of characteristics. After the effects of condensation are calculated over a system timestep, the aerosol is remapped onto the fixed grid. This remapping is performed by approximating the particle mass distribution as being constant with respect to the logarithm of particle diameter.

The moving-grid method has the computational advantage of reducing numerical diffusion compared to the fixed-grid one. However, this could result in an order-of-magnitude larger amount of computer time. In addition, the fixed-grid method is more robust.

References

- [1] K.K. Murata, D.C. Williams, J. Tills, R.O. Griffith, R.G. Gido, E.L. Tadios, E.J. Davis G.M. Martínez, K.E. Washington "Code Manual for CONTAIN 2.0: A Computer Code for Nuclear Reactor Containment Analyses" NUREG/CR-6533, SAND97-1735, June 1997
- [2] K.D. Bergeron K.D. User's Manual for CONTAIN 1.0, A Computer Code for Severe Nuclear Reactor Accident Containment Analysis NUREG/CR-4085, SAND84-1204, Sandia National Laboratories, Albuquerque, NM, May 1985
- [3] B.E. Boyack "CONTAIN Independent Peer Review" LA-12866, Los Alamos National Laboratory, Los Alamos, NM, 1995
- [4] R. Vijaykumar, M. Khatib-Rahbar "Applicability of the CONTAIN Code Heat and Mass-Transfer Models to Asymmetrically Heated Vertical Channels" Nuclear Technology 128,3, 313-326, 1999
- [5] NEA "SOAR on Containment Thermalhydraulics and Hydrogen Distribution" NEA/CSNI/R(1999)16
- [6] M. Firnhaber, T.F. Kanzleiter, S. Schwarz, G. Weber "VANAM-M3: A Multi Compartment Aerosol Depletion Test with Hygroscopic Aerosol Material" NEA/CSNI/R(96)26, 1997
- [7] M. Firnhaber, K. Fischer, S. Schwarz, G. Weber "ISP-44 (KAEVER tests): "ISP-44 - Comparison and Interpretation Report - Final", NEA/CSNI/R(2003)5, 2003
- [8] B. Clement, T. Haste "Comparison Report on International Standard Problem ISP-46 (FPT1)" Note Technique SEMAR 03/021, 2003
- [9] I. Kljenak, B. Mavko "Simulation of FPT1 Test Containment Phase with the CONTAIN computer Code" IJS-DP-8614 rev. 1, Dec. 2002
- [10] L.E. Herranz, L. Del Prá C., A.M. Rincón "CIEMAT Contribution to the PHEBEN-2 Project: Interpretation of the PHÉBUS-FPT1 Experiment" CIEMAT 1025, Sept. 2003

- [11] F. Gelbard “MAEROS User Manual” NUREG/CR-1391, SAND80-0822, Sandia National Laboratories, Albuquerque, NM 1982
- [12] N.A. Fuchs “The Mechanics of Aerosols”, Pergamon Press, 1964
- [13] W.K. Winegardner, A.K. Postma, M.W. Jankowski “Studies of Fission Product Scrubbing with the Ice Compartments” NUREG/CR-3248, PNL-4691, Richland, WA, 1983
- [14] D.A. Powers, J.E. Brockmann, A.W. Shiver “VANESA: A Mechanistic Model of Radionuclide Release and Aerosol Generation during Core Debris Interactions with Concrete” NUREG/CR-4308, SAND85-1370, NM 1986
- [15] P.C. Owczarski, R.I. Schrenk “Technical Bases and User’s Manual for the Prototype of a Suppression Pool Aerosol Removal Code” NUREG/CR-3317, WA 1985

4.3.2 *COCOSYS*

Brief overview

The **CO**ntainment **CO**de **SY**stem **COCOSYS** [1, 2] has been developed for the comprehensive simulation of severe accidents in light-water reactor containments. The aim is to simulate all relevant phenomena, processes and conditions that may occur inside the containment during such accidents. **COCOSYS** is also able to simulate design basis accidents. One focus of **COCOSYS** is on the extensive consideration of interactions between the various developing phenomena, such as thermal hydraulics, hydrogen combustion, and aerosol and nuclide behaviour.

The structure of **COCOSYS** is shown in Fig. 4.3-1. The thermal hydraulic main module **THY** simulates the thermodynamic of the steam/air atmosphere, atmospheric flows, hydrogen distribution, heat and mass transfer to walls, heat conduction and storage in structures, H_2 deflagration, and pyrolysis processes. In the aerosol and fission product main module **AFP** the transport and deposition behaviour of aerosols, the behaviour of fission products including the decay heat release, and chemical reactions especially those of iodine are treated. The core concrete interaction main module **CCI** describes the physical and chemical behaviour of the core melt, the concrete erosion, and the fission product release from the corium concrete pool. Apart from the three main modules further programs are coupled to **COCOSYS**, namely **DET3D** for the simulation of H_2 detonation, the commercial CFD code **CFX** for special fluid dynamic problems, and the in-house-developed **LAVA** code for melt relocation from one room to a neighbouring one and spreading. The data can be visualised both online and offline with the **ATLAS** programme. For the purpose of complete sequence calculations **COCOSYS** has been coupled to the primary circuit code **ATHLET-CD** which simulates core degradation.

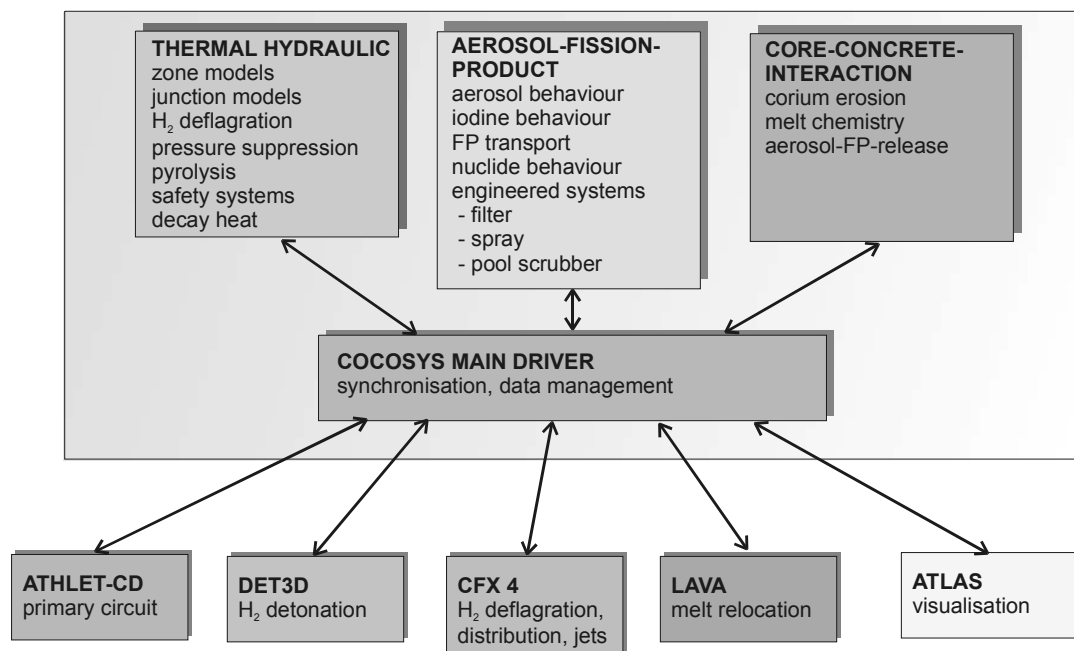


Fig. 4.3-1 Modular structure of COCOSYS

Aerosol modelling

The aerosol module AERIKA in the main module AFP describes the behaviour and the transport of a multi-component polydisperse aerosol in a multi-compartment containment geometry. The aerosol may be composed of up to eight chemically different aerosol components and the size distribution is discretised into a number of size classes. All essential agglomeration and deposition processes are treated. The growth of non-soluble and hygroscopic aerosol particles by volume condensation is modelled. The aerosol retention by engineered systems like granular and fibrous filters, by water pools (pool scrubbing) and by containment sprays is also modelled. Furthermore, all essential interactions with other containment processes like the aerosol intercompartmental transport by gas and water flows, the condensation/evaporation to/from aerosol particles, the depletion of aerosols carrying iodine, and the decay heat release from airborne and deposited aerosols are treated.

The FIPHOST [3] module calculates the transport of the fission products within the containment. It differentiates between the atmosphere, the aerosol and the sump water as fission product carriers. The fission products can be deposited on surfaces in the atmosphere and in the sump. They are transported together with the mobile carriers by the prevailing atmosphere and water flows. All relevant transfers between the carriers are considered: aerosol deposition by natural processes or aided by technical systems such as filters and spray systems, washing-off from walls, and the carrier change due to radioactive decay.

The module FIPISO [4] calculates the decay, the dynamic behaviour and the transport of fission product inventory in the containment and the release to the environment. Generally, between 400 and 600 different nuclides are considered in the calculation. The decay heat release in the individual zones and on the individual carriers is taken into account in the THY main module.

Aerosol dynamics in a control volume

Within the module AERIKA in each control volume the aerosol dynamics are calculated by the model MAEROS, developed by Sandia National Laboratories, USA [5], which is also used in other codes like CONTAIN and MELCOR. The agglomeration kernel is determined by a two-dimensional integration over particle size and the deposition coefficients by a one-dimensional integration. Owing to this accurate method, a comparably low number of maximum 20 particle classes is sufficient. The aerosol coefficients are calculated for various thermal hydraulic states at the beginning of a COCOSYS run and do not have to be re-calculated anew for each time step. The first order ODE system for the aerosol concentration is solved by FEBE (Forward Euler, Backward Euler) either implicitly or explicitly.

The way the coefficients for a multi-component system are calculated bring with it the following restrictions: (1) aerosol material density is the same for all aerosol components (max. 8), all particles in a certain size class have the same composition of materials, and (3) the dynamic and the agglomeration shape factors are independent of the aerosol composition.

Particle growth by condensation is calculated by the moving-grid method, Moving Grid Analysis (MGA) [6]. In contrast to the conventional fixed-grid method in MGA the grid of the particle size classes is apparently moved. By this the numerical diffusion, which is an uncontrolled smearing of aerosol mass over several size classes, is reduced. The Kelvin effect and the solubility effect for hygroscopic aerosols are included in MGA.

Table 4.3-1 gives an overview on the natural aerosol phenomena modelled in COCOSYS-AERIKA.

Table 4.3-1 Modelling of natural aerosol processes in COCOSYS

Phenomenon	Mechanism	Modelling (reference and/or short description)
Agglomeration	Brownian	MAEROS [5]
	Gravitational	MAEROS; optional collision efficiencies: (1) Fuchs [7], (2) Pruppacher Klett [8], and (3) Pruppacher Klett truncated
	Turbulent shear	MAEROS
	Turbulent inertial	MAEROS; same collision efficiencies as for gravitational agglomeration
Steam condensation	Condensation on non-soluble aerosol	Mason equation including Kelvin effect; Moving-grid-method (MGA) [6]
	Condensation on hygroscopic aerosol	Mason equation including solubility and Kelvin effects; Moving-grid-method (MGA)
Natural deposition	Sedimentation	Stokes velocity with Cunningham correction
	Diffusion	Brownian (laminar) diffusion
	Thermophoresis	MAEROS
	Diffusiophoresis	Waldmann und Schmitt [9]
Resuspension	Dry resuspension by transient gas flows	Extension of semi-empirical Fromentin model [10]
	Re-entrainment; droplet production by bubble bursting	RECOM [11]

Aerosol interactions with other containment phenomena

An essential characteristic of COCOSYS is the fact that all important interactions between different containment phenomena are taken into account. In Table 4.3-2 the modelled interactions between thermal hydraulics, fission product behaviour and aerosol behaviour are summarised.

Table 4.3-2 Main aerosol - thermal hydraulic interactions modelled in COCOSYS

Interaction	Modelled process	Remarks
Thermal hydraulics → aerosol behaviour	Aerosol transport by gas flows	
	Aerosol transport by water flows	
	Diffusiophoresis	
	Particle growth by condensation	
	Dry resuspension by hydrogen deflagration	Modelling not completed
	Re-entrainment (wet resuspension) from boiling sump	
Aerosol → thermal hydraulics	FP aerosol decay heat releases into atmosphere, walls and sump	
	Contribution of aerosol to the atmosphere density	

The modelled interaction processes take place with various strengths respectively velocities. This is considered in COCOSYS by an adaptation of the numerical coupling of the models to the strength of the prevailing interaction. In general tight couplings are used for fast interaction processes and loose ones for slow processes.

The interactions were also thoroughly examined in two uncertainty and sensitivity analyses on a “dry” and a “wet” aerosol case. In the first application the dry aerosol behaviour in the test VANAM M2 was investigated [12]. The test was carried out in a nine-compartment geometry. 179 uncertain aerosol and thermal hydraulic parameters were identified and analysed. The second application was on LACE test LA4 with a two-component aerosol under wet conditions, i.e. with steam condensation on the aerosol, in a single volume geometry [13]. 58 uncertain parameters were selected.

The uncertainty of the aerosol results was found to be significantly larger in the wet case than in the dry case. The main contributors identified were uncertain input parameters (dynamic and agglomeration shape factors, diameter of injected particles), and the model option with/without Kelvin effect for condensation calculation. The results revealed also the importance of uncertainties in thermal hydraulic boundary conditions (atmosphere flows, volume condensation rate) for the calculated aerosol behaviour.

In another uncertainty and sensitivity study the modelling of the volume condensation rate was investigated for a multi-compartment application [14]. The study shows that the uncertainty of the total volume condensation rate in the entire containment is moderate and the local volume condensation rate in certain compartments is large in parts, causes mainly by uncertainties in the calculated gas flows.

Engineered safety system

In AFP three engineered aerosol retention systems are modelled:

- Filters (fibrous and granular)
- Spray
- Pool scrubber

In Table 4.3-3 the modelling of these systems is briefly described:

Table 4.3-3 Modelling of engineered aerosol retention systems in COCOSYS

System	Retention mechanism	Modelling (reference and/or short description)
Fibrous filter	Diffusion	Semi-empirical model [15, 16], use of Kuwabara-factor [17]
	Interception	
	Impaction	
	Gravitation	
Granular filter	Diffusion	[18]
	Interception	
	Impaction	[19]
	Gravitation	[20]
Spray	Impaction	Based on [7]
	Interception	
	Diffusion	Based on model in CONTAIN 2.0 [21]
	Diffusiophoresis	
	Thermophoresis	
Pool scrubber	Brownian	SPARC-B [22], an extended version of SPARC-90 [23]
	Gravitational	
	Turbulent shear	
	Turbulent inertial	

Validation

The aerosol modelling in COCOSYS has been continuously validated on experiments of the most important containment projects within the last 20 years. Some older tests were calculated with the COCOSYS precursor code FIPLOC. Table 4.3-4 gives an overview on the validation work performed. For detailed descriptions of the tests mentioned see chapter 5.1.2 and 5.3.

Table 4.3-4 Validation work on the aerosol modelling in COCOSYS

Project	Test	Remarks
DEMONA	B2	
LACE	LA4	Uncertainty and sensitivity analysis with FIPLOC
VANAM	M1, M2, M2*, M3, M4	International Standard Problem ISP-37 (VANAM M3)
AHMED	NaOH tests	CSNI benchmark exercise
KAEVER	K90, K106, K123, K148, K151, K156, K159, K186, K187, K188	ISP-44 (KAEVER tests),
VICTORIA	61, 62	With FIPLOC
PHÉBUS	FPT0, FPT1	ISP-46 (PHÉBUS FPT1)

Status

Aerosol modelling in COCOSYS has been completed except for the processes dry resuspension and re-entrainment. The modelling of the Kelvin-effect is not yet satisfactory because of numerical instabilities occurring especially with multi-compartment applications.

References

- [1] W. Klein-Heßling, S. Arndt, G. Weber COCOSYS V 1.2 User Manual GRS-P-3/1, 2000
- [2] H.-J. Allelein, S. Arndt, W. Klein-Heßling, S. Schwarz, C. Spengler, G. Weber COCOSYS: Status of Development and Validation of the German Containment Code System Technical Meeting on Severe Accident and Accident Management for NPP, Japan, March 2006
- [3] S. Arndt, G. Weber FIPHOST - A Module to Calculate the Fission Product Transport in a LWR Containment GRS-A-2553, April 1998
- [4] U. Hesse FIPISO-98, ein Rechenmodell zum Nuklidverhalten in einem Raumzellensystem nach einem Reaktorstörfall GRS-A-2750, 1998
- [5] F. Gelbard MAEROS User Manual NUREG/CR-1391, 1982
- [6] F. Gelbard Modeling Multicomponent Aerosol Particle Growth By Vapor Condensation Aerosol Science and Technology 12:399-412, 1990
- [7] N. A. Fuchs The Mechanics of Aerosols Pergamon Press, Oxford, 1964
- [8] H. R. Pruppacher, J. D. Klett Microphysics of Clouds and Precipitation Reidel, New York, 1978
- [9] C. N. Davies Aerosol Science Academic Press, 1966

- [10] A. Fromentin Particle Resuspension from a Multi-Layer Deposit by Turbulent Flow Paul Scherrer Institute, Würenlingen, Bericht Nr. 38, 1989
- [11] A. Voßnacke Untersuchung zur Tropfenbildung an Oberflächen gasdurchströmter Flüssigkeiten bei Störfällen in kerntechnischen Anlagen Dissertation, Ruhr-Universität Bochum, Bochum, 1999
- [12] E. Hofer, B. Krzykacz, L. Langhans, G. Weber Uncertainties and Sensitivities in Aerosol Calculations-An Analysis of a FIPLOC-M Application to the Experiment VANAM M2 PSAM II-Conference, San Diego, 20 – 25 March 1994
- [13] J. Langhans, H.G. Friederichs, E. Hofer, B. Krzykacz, B.M. Schmitz, G. Weber Unsicherheits-und Sensitivitätsanalyse zum Aerosolmodell in FIPLOC-M, Teil 2: Nasses Aerosolverhalten im LACE-Experiment LA4 GRS-A-2217, 1994
- [14] G. Weber, E. Hofer, B. Krzykacz Uncertainty and Sensitivity Analysis of Fog Formation Rates Calculated with the Containment Code FIPLOC-M J. Aerosol Sci., Vol.23, Suppl., pp S 269 - S 272, 1992
- [15] K. W. Lee, B. Y. H. Liu Experimental Study of Aerosol Filtration by Fibrous Filters Aerosol Sci. Technol., 1:35-46, 1982
- [16] K. W. Lee, B. Y. H. Liu Theoretical Study of Aerosol Filtration by Fibrous Filters Aerosol Sci. Technol., 1:47-62, 1982
- [17] S. Kuwabara The forces experienced by randomly distributed parallel circular cylinders or spheres in viscous flows at small Reynolds numbers J.Phys.Soc.Japan 14(4):527-532, 1959
- [18] C. Gutfinger, G. I. Tardos Theoretical and Experimental Investigation on Granular Bed Dust Filters Atm. Environment, 13:853-867, 1979
- [19] T. D'Ottavio, S. L. Goren Aerosol Capture in Granular Beds in the Impaction Dominated Regime Aerosol Sci. and Technol., 2:91-108, 1983
- [20] G.I. Tardos et al. Experiments on Aerosol Filtration in Granular Sand Beds J. Colloid and Interface Science, 71(3):616-621, 1979
- [21] K.K. Murata et al. Code Manual for the CONTAIN 2.0: A Computer Code for Nuclear Reactor Containment Analysis\NUREG/CR-6533, 1997
- [22] K. Fischer Modellierung von Abscheidevorgängen in Wasservorlagen Battelle Ingenieurtechnik GmbH, Eschborn BF-R68.411-1, 1998
- [23] P.C. Owczarski, K.W. Burk SPARC-90: A Code for Calculating Fission Product Capture in Suppression Pools NUREG/CR-5765, 1991

4.3.3 ART/REMOVAL

4.3.3.1 ART code

The ART (Analysis of Radionuclide Transport) code [1] has been developed at JAERI as a module of the source term analysis code, THALES-2 [2] to analyse the behaviour of fission products (FP) in reactor coolant system and containment during LWR severe accidents. The thermal-hydraulic condition needs to

be given as a function of time. The code can consider FP transport and removal by natural deposition and by engineered safety features such as spray systems. As for the FP aerosol deposition, the code can treat gravitational settling, thermophoresis, diffusiophoresis, Brownian diffusion and resuspension. For the gaseous FP, the code can deal with condensation, chemisorption and revaporization. The code also considers the aerosol growth by gravitational, Brownian and turbulent agglomeration and condensation or revaporization of gaseous FP at the aerosol surface. Major physical models in ART were verified through analyses of the international standard problems and JAERI's WIND/WAVE experiments [3].

4.3.3.2 *REMOVAL code*

The REMOVAL (REMOval of Volatile fission products and Aerosol in an LWR containment) code [4] was developed at JAERI to analyse the fission products behaviour in the containment of LWR during a severe accident. Physical models considered in the code are

- a) agglomeration due to Brownian, gravitational and turbulent motion,
- b) Brownian diffusion
- c) thermophoresis
- d) diffusiophoresis
- e) spray removal by gravity and collision
- f) steam condensation onto aerosol particle
- g) entrainment from flashing pool.

In the analysis, the containment is divided into several compartments and the behaviour of the aerosol, iodine and noble gas is analysed for each compartment assuming the uniformity inside the compartment. Thermal-hydraulic condition should be given for each compartment as a function of time.

4.3.3.3 *ART/REMOVAL (ART combined with REMOVAL model)*

In order to participate in the ISP-44 (International Standard Problem No.44)⁵⁾, the hygroscopicity model based on the Mason's equation in REMOVAL code was tentatively combined with ART code because ART does not treat it and the development of REMOVAL finished in early 1990's [5]. It is noted that present ART does not include the related REMOVAL model due to numerical problems. For calculation of aerosol growth by steam condensation, the relative humidity at aerosol surface in Mason's equation is reevaluated taking into account the Kelvin's effect and the Raoult's law. Then, the equilibrium aerosol size is calculated by iteration until the growth rate becomes zero. Since it usually takes much CPU time for iteration calculation, REMOVAL calculates the equilibrium radius of aerosol by assuming the aerosol surface temperature equal to atmospheric temperature and uses the calculated value during the iteration to reduce computation time.

References

- [1] T. Ishigami et al. "User's Manual of ART Code for Analyzing Fission Product Transport Behaviour during Core Meltdown Accident" JAERI-M 88-093 (1988)
- [2] M. Kajimoto et al. "Development of THALES-2, A Computer Code for Coupled Thermal-Hydraulics and FP Transport Analyses for Severe Accident at LWRs and Its Application to Analysis of FP Revaporization Phenomena" Proc. Int. Topical Meeting on Safety of Thermal Reactors, Portland, pp.584-592 (1991)

- [3] A. Hidaka et al. "Experimental Analyses of Iodine Behaviour under Severe Accident Conditions with ART" J. Nucl. Mater. 248, pp. 226-232 (1997)
- [4] K. Muramatsu, K. Abe, M. Ida, N. Watanabe, K. Soda, N. Yamano "Sensitivity Study on BWR Source Terms using the THALES/ART and REMOVAL" Proceedings of the International ENS/ANS Conference on thermal reactor safety, Vol. 6, pp.2407-2416 (1988)
- [5] M. Firnhaber et al. "International Standard Problem ISP44 KAEVER Experiments on the Behaviour of Core-melt Aerosols in a LWR Containment Comparison Report TABLE OF CONTENTS" NEA/CSNI/R(2003)5 (2002)

4.3.4 *SMART*

Brief theoretical description

SMART is a code that models containment aerosol and iodine behaviour. Fission products are assumed to enter into containment in one of two physical forms, either as gases or dissolved or suspended in small water aerosols generated by a primary heat transport system break discharge. The initial droplet size distribution is considered to be log-normal and is characterised by two parameters: the geometric mean diameter and the geometric standard deviation. In SMART, the geometric mean diameter is considered to be equal to the critical diameter, where the critical diameter is defined as a diameter when the drag force on the droplet exceeds the surface tension forces. Currently SMART does not model aerosol release during a steam-only discharge, however this capability is being incorporated into the code.

SMART assumes that aerosol is transported within containment by bulk gas flows. Within a particular node or a room, the liquid aerosol droplets undergo coagulation and also deposit on walls and floors due to various natural phenomena (e.g., gravitational settling). To model the coagulation and removal processes mathematically, the continuous aerosol size spectrum is divided into a finite number of intervals, and within each interval, the aerosol size is assumed to be constant. The initial mass distribution of the fission products in the aerosol size classes are provided by upstream analysis, while the changes in the fission product masses in the size classes due to radioactive decay and build-up, coagulation and deposition in containment are calculated in SMART.

	Brief Description
Reactor Components Modelled	<ul style="list-style-type: none"> • Containment only • Emergency Filtered Air Discharge System (EFADS), models aerosol removal by HEPA filters and iodine removal by charcoal filters • Dousing (models water droplet aerosol formation by operation of dousing systems) • Moderator (for removal of aerosols by moderator scrubbing)
Geometry Idealization	<ul style="list-style-type: none"> • A network of nodes inter-connected by flow paths • Up to 200 nodes possible, nodalization must be consistent with the thermalhydraulics containment model.
Inter-nodal Transport	<ul style="list-style-type: none"> • Flow paths modelled as a fictitious pipe with convective flow of gas mixtures, aqueous solutions, and water droplet aerosols (containing dissolved or suspended fission products).

Thermalhydraulics	<ul style="list-style-type: none"> • Interfaces with a containment thermalhydraulic model (GOTHIC) to obtain transient thermalhydraulic properties • Gases, fission products and aerosols in a node are assumed to be perfectly mixed • Fission product and aerosol processes do not contribute to mass, momentum or energy exchange (e.g. no feedback to thermalhydraulics code)
Fission Product Transport	<ul style="list-style-type: none"> • Convective flow through links of fission products dissolved in water droplet aerosols, bulk liquid or in the gaseous phase • Solid (dry) fission products are not modelled • Break or other discharge sources into a room • Convective flow out of holes to the external atmosphere • Removal by sinks (EFADS, adsorption of iodine on walls, aerosol deposition on walls and floor) • Generation from precursors in radioactive decay-build up processes • Removal by decay • Iodine species alone can be transported and tracked between different phases in each node (bulk water, condensing films, gas, suspended water droplets, adsorbed on surfaces) <p>See fission product transport mechanisms above. Aerosol processes modelled are</p>
Aerosol Transport	<ul style="list-style-type: none"> • Generation of aerosols by break discharge or dousing • Aerosol agglomeration <ul style="list-style-type: none"> • Brownian • Gravitational • Turbulent-Inertial and Turbulent-Shear • Removal by Impingement (inertial impac • Moderator Washout • Gravitational Settling • Turbulent Deposition • Stefan flow • Thermophoresis

Reference

Private communication between J. Ball and the Chairman.

4.3.5 GOTHIC

The containment thermohydraulics code GOTHIC has the potential to be developed into a code with aerosol modelling capabilities, since it contains models to generate, entrain and transport small water droplets while tracking these droplets. However, the current GOTHIC release (GOTHIC 7.2a) does not contain aerosol modeling capabilities.

GOTHIC solves conservation equations for mass, momentum and energy for multi-component, multi-phase flow and these equations are solved for up to three primary fields (Steam/gas mixtures, continuous liquid, liquid droplet), and up to two secondary fields (mist, liquid components).

There are a few options available in GOTHIC to generate, entrain and transport small water droplets. Droplets can be formed either by operations such as flashing (break discharge), by dousing, or by the user specifying that droplets should be formed when the atmosphere becomes supersaturated with steam. For example, the spray nozzle component is used to model containment sprays, ice condenser drain flows into the lower containment and vessel spray systems. The nozzle model converts liquid flow through a flow path, network link or 3D connector from the continuous liquid phase to the droplet phase with the fraction of the liquid converted into droplets and the drop diameter specified as functions of time.

For modeling volume condensation, the user has the option of choosing a fog model, in which very small drops are created when the atmosphere becomes supersaturated or the “mist” option, in which mist is created when the atmosphere becomes supersaturated. In the fog model, the droplets can be tracked, however, when small drops are combined with the large drops from a break or spray, the average drop size is not representative of either population, resulting in possible excessive heat and mass transfer at the drop surfaces. The mist phase is not combined with the drop phase and is assumed to move with the vapor phase. When the mist concentration exceeds the user specified limit, the excess mist is either converted to drops or is deposited in the liquid phase, depending on the user specification for the drop diameter from excess mist. If the drop diameter from excess mist is set to zero, then the excess mist is deposited in the liquid phase. Otherwise, new drops are created at the specified diameter (default is 200 μm).

Despite the potential for modeling some aerosol phenomena (wet aerosol) in GOTHIC, the code does not currently allow fission product transport in any other component except the vapor phase. Incorporation of aerosol phenomena to simulate fission product transport and deposition in containment would require significant effort.

There is a GOTHIC development task, approved by the GOTHIC Advisory Group, to implement a drop field distribution model into the next release of GOTHIC (7.3, not expected to be released for at least 2 years). This will allow GOTHIC to calculate a distribution of droplet diameters for each lumped control volume and cell within a subdivided control volume. However, modeling fission product transport in these aerosol droplets, or from dry aerosols, is not currently being considered for future development.

Reference

Private communication between J. Ball and the Chairman.

4.3.6 KUPOL

An aerosol model was implemented into the Russian thermal-hydraulic code KUPOL-M [1]. This coupled version allows to simulate aerosol transport in a subdivided containment. For a lumped-parameter model a complete kinetic equation of aerosol transport is the Liouville equation for a size distribution function. It takes into account processes of condensation, sedimentation, convective exchange, diffusional, turbulent and thermophoretic deposition as a source form and coagulation process as a collision integral form. We will only consider the processes of condensation and evaporation onto and from aerosol particles and aerosol coagulation. So, we write the equation in such a way:

The last term on the left-hand side of the equation represents steam condensation onto droplets with mass. The first and the second terms on the right-hand side of the equation describe coagulation mechanism,

taking into account particle arrival into the given size space from the smaller ones and particle removal from the given size space into the larger ones.

The accepted coagulation models use the coagulation kernels, simulating mechanisms of gravitational coagulation, Brownian coagulation, turbulent and diffusional coagulation and turbulent shear one.

The differential equation of aerosol transport is solved by a fractions method [2]. The collision integrals are expressed as a source form in each fraction.

References

- [1] A.D.Efanov, A.A.Loukianov, N.N.Shangin, Yu.S.Yuriev, A.A.Zaitsev, S.L.Soloviev, L.I.Zaitchik Development of a containment code KUPOL-M for a substantiation of the VVER's accident localization system functions Proc. of ICON10, #22281, Arlington, VA, April 14–18, 2002
- [2] A.G. Godizov, A.D. Efanov, A.A. Lukianov, O.V. Supotnitskaya Simulation of processes of water aerosol coagulation-condensation growth using a combination of methods of groups and fractions Proc. of NURETH-11, Paper: 224, Popes' Palace Conference Center, Avignon, France, October 2-6, 2005

5. RECENT VALIDATION WORK

5.1 Integral Experiments

5.1.1 *The PHÉBUS fission product programme*

Introduction

Since the TMI2 accident in 1978, an important international effort has been made on research on severe accidents, involving integral experiments, separate-effect tests and model developments. The PHÉBUS-FP programme has played and is still playing an important role in this landscape. A number of lessons have been learned from the analysis of the results – see e.g. [1, 2] - and from their use for source term assessment studies, [3]. As a result, increasingly better-qualified assessment tools have been developed but remaining uncertainties have been evidenced. For reducing them IRSN, CEA and EDF have launched a new International Source Term Programme comprising a series of separate-effect experiments, [4].

The international PHÉBUS FP programme, initiated in 1988 and supported by the European Commission, is one of the major research programmes on severe accidents for light-water reactors. Regarding the interpretation of PHÉBUS, an international co-operation has been established for more than ten years, particularly helpful for the improvement and common understanding of severe accident phenomena. After a short description of the facility and of the test matrix, below the main outcomes and results of the first four integral tests are provided and analysed. Several results were unexpected and some are of importance for safety analyses, particularly concerning fuel degradation, cladding oxidation, chemical form of some fission products, especially iodine, effect of control rod materials on degradation and chemistry, iodine behaviour in the containment. Prediction capabilities of calculation tools have largely been improved as a result of this research effort.

Description of the facility and test matrix

The PHÉBUS FP programme is investigating key phenomena involved in LWR severe-accident sequences through a series of five in-pile integral experiments. The facility provides prototypic reactor conditions which allow the study of basic phenomena governing core degradation through to its late phase (melt pool formation), hydrogen production, FP release and transport, circuit and containment phenomena, and iodine chemistry. The phenomena studied take place (i) in the core region simulated by a 1-m long bundle of 20 irradiated fuel rods and a control rod, (ii) in the primary system components for which a steam generator is simulated by a single inverted U-tube, (iii) in the containment building simulated by a 10 m³ tank including a sump, the atmosphere and painted wet and dry surfaces. All three of these components are scaled down by roughly 1/5000 as compared with a French 900 MWe power plant. This is illustrated in Fig. 5.1-1. A more comprehensive description can be found in, e.g., [5, 6].

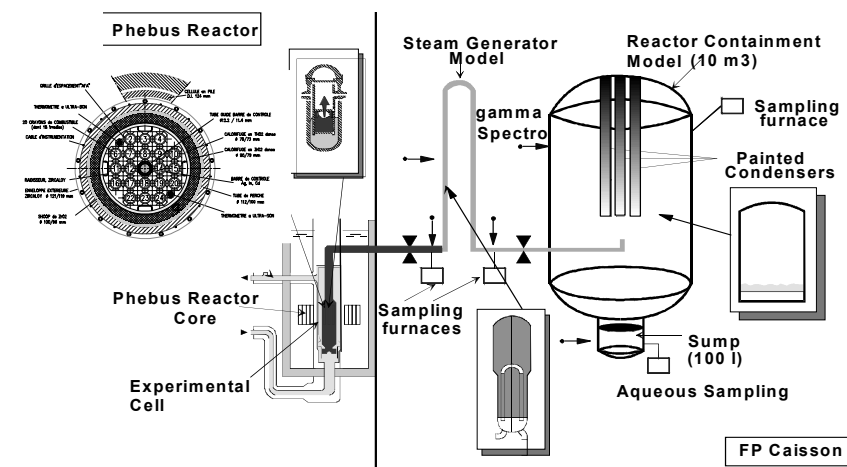


Fig. 5.1-1 The PHÉBUS-FB facility

The test matrix is given in Table 5.1-1. The first two tests were performed in similar conditions except for fuel burn-up (FPT-0 used trace-irradiated fuel whereas FPT-1 fuel had been irradiated to 24GWd/tU): bundle including a silver-indium-cadmium control rod subjected to a steam-rich environment, hot leg heated up to 700 °C, cold leg at 150 °C, acidic and cold sump water. For FPT-2, the bundle was subjected to a steam-poor environment and the sump water was alkaline and evaporating at the end of the test. For FPT-3, the silver-indium-cadmium control rod was replaced by a boron carbide one, other test conditions being close to those of FPT-2. The FPT-4 test was of a different nature as it investigated the release of low-volatility fission products and actinides from a debris bed made of fuel pellet fragments and oxidised cladding shards heated up to the formation of a molten pool.

Table 5.1-1 PHÉBUS-FP test matrix

Test n°	Type of fuel	Fuel Degradation	Primary Circuit	Containment	Date
FPT-0	Fresh Fuel 1 Ag-In-Cd rod 9 days pre irradi.	Melt Progression & FP release in steam-rich environment	FP chemistry and deposits in non-condensing steam generator	Aerosol deposition Iodine radiochemistry at pH5	Dec. 2 1993
FPT-1	BR3 fuel \approx 23 GWd/tU 1 Ag-In-Cd rod Re irradiation	As FPT-0 with irradiated fuel	As FPT-0	As FPT-0	July 26 1996
FPT-2	As FPT-1 BR3 fuel \approx 32 GWd/tU	As FPT-1 under steam poor conditions	As FPT-1 with effect of boric acid	PH9 evaporating sump	Oct. 12 2000
FPT-3	As FPT-1 with B4C instead of Ag-In-Cd BR3 fuel \approx 24 GWd/tU	As FPT-2	As FPT-0	PH5 evaporating sump recombiner coupons	Nov. 18 2004
FPT-4	EDF fuel 38 GWd/tU no reirradiation	Low volatile FP& actinide release from $\text{UO}_2\text{-ZrO}_2$ debris bed up to melting	Integral filters in test device Post-test analyses on samples		July 22 1999

Main outcomes with respect to FP transport

The release of volatile fission product is generally well calculated even if some codes using the CORSOR approach tend to overestimate the kinetics at the beginning of the transient, [7, 8]. Semi-empirical models, though not modelling all the processes, are able to do well using a consistent set of parameters for separate-effect tests and PHÉBUS-FP integral experiments. The situation is more contrasted for less volatile elements for which chemistry plays a major role. A better understanding of the underlying phenomena has been gained using mechanistic models [8].

In the particular case of FPT-0, using trace-irradiated fuel, the early release of volatile fission products can only be explained by taking into account fuel dissolution during the cladding oxidation phase. Barium release is much smaller in the PHÉBUS tests performed in a bundle geometry than in separate-effect annealing tests. This difference is attributed to interactions of fuel with the cladding material and maybe iron which greatly reduce the volatility of barium, [9]. These two observations illustrate the strong coupling between fuel degradation and fission-product release phenomena.

The release from the silver-indium-cadmium control rod is often not well enough calculated by certain codes, especially for silver which has an important impact on iodine chemistry. The governing phenomena are well understood but a modelling effort is still needed mainly concerning the coupling between degradation and release.

Fission-product transport in the RCS is characterised by two zones of significant deposition coinciding with sections in which temperatures dropped rapidly. These were the vertical section of the hot leg above the bundle where the gas cooled from temperatures as high as 1600 °C down to 700 °C and in the steam generator (SG) riser where temperatures cooled from 700 °C to 150 °C. For the first two tests, FPT-0 and FPT-1, marked differences in volatility were seen for different elements where iodine and cadmium barely deposited at all in the hot leg of the circuit with significant deposition only in the SG. Cesium deposition, in contrast, was significant and nearly the same in both cooling zones; completing the range of volatilities, others elements such as molybdenum and silver deposited primarily in the vertical hot leg with relatively little additional deposition downstream.

Recent analyses performed applying a standard version of the ASTEC/Sophaeros code show that the code is able to reproduce some important aspects of the FPT-0 and FPT-1 tests, principally vapor/aerosol behaviour and total retentions, [10]. As for fission-product speciation, it is worth noting that cesium was condensed in the hot leg of the circuit, thus not being transported as CsOH as often assumed in the past. Calculation results indicate that cesium molybdate and iodide are the main species. Though the overall retention in the circuit is well calculated, the deposition in the vertical hot leg is underestimated. This is largely accounted for by the effect of simultaneously-developing flow characterised by much higher temperature gradients and mass transfer to the wall than in the case for developed flow. The deposition in the steam generator is generally overestimated by a factor of about two. A number of hypotheses have been explored in relation to this discrepancy [10] and 2D particle-tracking calculations performed [11], but no conclusive explanations have been so far obtained.

In the containment, thermal-hydraulics was mainly governed by the balance between the incoming steam and its condensation. Simple lumped-parameter codes using a coarse noding (1 or few volumes) are able to reproduce the measured phenomena. Most of the aerosol mass was deposited on the bottom of the containment and most of the remainder on the condensing surfaces. A small fraction was observed on the containment walls. The first two kinds of deposits are generally well captured by lumped-parameter codes using classical models for gravitational settling and diffusiophoretic deposition [12] although some had difficulties to reproduce the split between deposition on the bottom and on the condensing surfaces. A

mechanism based on turbulence damping in the boundary layer has been identified to account for the small deposit (2 %) on the walls in FPT-1.

Generally speaking, the simulation by calculation codes of thermal-hydraulics and aerosol behaviour in the PHÉBUS FP containment is satisfactory.

References

- [1] M. Schwarz, B. Clément, A.V. Jones “Applicability of PHÉBUS FP results to severe accident safety evaluations and management measures”, Nucl. Eng. Des. 209, 173-181 (2001)
- [2] J. Birchley, T. Haste, H. Bruchertseifer, R. Cripps, S. Güntay, B. Jäckel “PHÉBUS-FP: Results and significance for plant safety in Switzerland” Nucl. Eng. Des. 235, 1607-1633 (2005)
- [3] J.M. Evrard, C. Marchand, E. Raimond, M. Durin “Use of PHÉBUS FP experimental results for source term assessment and level 2 PSA” Proc. 5th Technical Seminar on the PHÉBUS FP Programme, Aix-en-Provence, France, 24-26 June 2003
- [4] B. Clément “Towards reducing the uncertainties on source term evaluations: an IRSN/CEA/ EdF R&D programme” Proc. Eurosafe Forum, Berlin, Germany, 8-9 Nov. 2004
- [5] M. Schwarz, G. Hache, P. von der Hardt “PHÉBUS FP: a severe accident research programme for current and advanced light water reactors” Nucl. Eng. Des. 187, 47-69 (1999)
- [6] B. Clément, N. Hanniet-Girault, G. Repetto, D. Jacquemain, A.V. Jones, M.P. Kissane, P. von der Hardt “LWR severe accident simulation: synthesis of the results and interpretation of the first PHÉBUS FP experiment FPT0” Nucl. Eng. Des. 226, 5-82 (2003)
- [7] B. Clément, T. Haste “ISP-46 – PHÉBUS FPT1”, NEA/CSNI/R(2004)18, August 2004
- [8] R. Dubourg, H. Faure-Geors, G. Nicaise, M. Barrachin “Fission product release in the first two PHÉBUS tests FPT0 and FPT1” Nucl. Eng. Des., article in press
- [9] R. Dubourg, P. Taylor “A qualitative comparison of barium behaviour in the PHÉBUS FPT0 test and analytical tests” J. Nucl. Mat. 294, 32-38 (2001)
- [10] M.P. Kissane, I. Drosik “Interpretation of Fission-product transport behaviour in the PHÉBUS FPT0 and FPT1 tests” Nuclear Eng. Des. 236, 1210-1223 (2006)
- [11] C. Housiadas, K. Müller, J., Carlsson, Y. Drossinos “Two-dimensional effects in thermophoretic particle deposition: the PHÉBUS-FP steam generator” J. Aerosol Sci.32, pp. S1029-S1040 (2001)
- [12] I. Kljenak, B. Mavko “Simulation of containment phenomena during the PHÉBUS FPT1 test with the CONTAIN code” Proc. Nuclear Energy for New Europe 2002, Kranjska Gora, Slovenia, 9-12 Sept. 2002

5.1.2 ISP-46 (PHÉBUS FPT1)

Introduction

The objective of this ISP is to assess the capability of computer codes to reproduce an integral simulation of the physical processes taking place during a severe accident in a pressurised water reactor, i.e. including

fuel degradation and associated hydrogen production and fission product release, fission product and structural material transport in the primary circuit, aerosol behaviour in the containment and iodine radiochemistry.

The ISP was conducted as an open exercise, with all the relevant experimental results being available to the participants. It was divided into four phases:

- Fuel degradation, hydrogen production, fission product and structural material release ('bundle', phase 1);
- Fission product and aerosol transport in RCS ('circuit', phase 2);
- Thermal-hydraulics and aerosol physics in containment ('containment', phase 3);
- Iodine chemistry in containment ('chemistry', phase 4).

The emphasis was on integral calculations (all phases). The aim was not to carry out interpretation work, but to use the codes as in plant studies, i.e. with standard models/options as far as possible, representing the facility in a similar level of detail; this constituted the mandatory 'base case' calculation. A more detailed 'best-estimate' sensitivity study could also optionally be performed.

Fifteen different codes were used: ASTEC, ATHLET-CD, COCOSYS, CONTAIN, ECART, FEAST, IMPACT/SAMPSON, ICARE/CATHARE, IMPAIR, INSPECT, MAAP4, MELCOR, SCDAP/RELAP5, SCDAPSIM and SOPHAEROS, of these 4 are integral codes (ASTEC, IMPACT/SAMPSON, MAAP4 and MELCOR). For the base case, 47 calculations were received, with 21 for the optional best-estimate version. Of the base case calculations, 14 were integral (at least 3 phases calculated).

For the base case, a nodding scheme was recommended in the specification report. The bundle is divided into 11 axial nodes and typically 3-5 radial rings, with normally 1 or 2 thermal hydraulic flow channels. The circuit is divided into 11 nodes, this being the minimum considered necessary for an adequate calculation of deposition. The containment model is simple, with 1 node for the main volume and 1 for the sump, taking advantage of the well-mixed conditions. For best-estimate calculations, often only nodding density was increased by typically a factor 2 or more, at the choice of the user.

The results were analysed in detail, comparing the results amongst each other and with the FPT1 data. There was considerable scatter amongst the results obtained from each code by different users, the 'user effect'. To minimise this effect, representative cases were selected where necessary, taking into account the quality of key output variables, completeness and accuracy of the technical reports, and including code developers where possible. This analysis led to an assessment of the main models in each of the four areas considered. Here only phases 2 and 3 dealing with aerosols are summarised below. There was on the whole little significant difference between the base and best-estimate cases, with at most a small improvement only in the results of the latter cases, so conclusions could be drawn on the basis of the former.

Assessment of codes and models

The following phenomena/parameters are in general well simulated by the codes:

- Bundle – thermal response (given adjustment of input nuclear power and shroud thermal properties within experimental uncertainties), hydrogen production (including oxidation of relocated melt), bundle final state material distribution (given suitable reduction of the bulk fuel relocation temperature from the ceramic value, in the longer term a more mechanistic model is desirable), total release of volatile fission products;

- Circuit – total retention of fission products and structural materials (but after cancellation of errors);
- Containment – thermal hydraulic behaviour (as exemplified by average gas temperature, pressure, relative humidity and condensation rate), depletion rates;
- Chemistry – models of the Ag/I reaction in the liquid phase are adequate for FPT1 (this cannot be extended to other cases where the Ag is not so much in excess with respect to I; due to the large excess of silver, in the experiment, radiolytic production of gaseous iodine and dissociation of silver iodide did not play an important role in the overall iodine behaviour).

The following phenomena/parameters were reasonably well simulated, but some modelling improvement is desirable:

- Bundle – outlet coolant temperatures (overprediction), time dependence of volatile FP release (generally too fast a release at low temperatures, e.g. for CORSOR-type approaches);
- Circuit – distribution of deposition in the circuit (underestimation in the upper plenum where vapor condensation and thermophoresis are the dominant mechanisms, overestimation in the steam generator hot leg where the mechanisms are thermophoresis for all elements + vapor condensation for I and Cd), noting that too coarse a noding leads to underestimation of deposition;
- Containment – relative importance of the two main depletion processes (diffusiophoresis and gravitational settling), but it is hard to make firm conclusions owing to the variability in the results;
- Chemistry – no items identified.

The following phenomena/parameters were not well simulated and substantial model development is necessary:

- Bundle – release of medium and low volatiles (e.g. tendency to calculate low for Mo, very high for Ba, reasonable order of magnitude for Ru and U but considerable scatter), and of structural materials (Ag/In/Cd from the control rod where the basic process of evaporation from a molten AIC pool is not captured, tin from the Zircaloy cladding);
- Circuit – iodine speciation and physical form;
- Containment – no items identified;
- Chemistry – gas phase reactions, organic iodine reactions, including production and destruction through radiolytic processes (definition of optimum parameters for the modelling codes such as adsorption velocity and desorption rate on/from painted surfaces, and the facility to input the gaseous iodine fraction at containment entrance, are recommended).

Concerning the circuit, the overestimation of bundle outlet temperature cannot fully explain the upper plenum results; its main effect is to displace the zone where vapors nucleate. For some elements, part of the discrepancy in the deposition pattern is due to the wrong prediction of the chemical form, and thus of its volatility; Cs is generally calculated as a vapor at 700 °C, whereas it was condensed in the experiment. However, this is also not enough to explain the underestimation in the upper plenum and overestimation in the steam generator rising line. Finding explanations is presently part of the work performed in the frame of the interpretation of PHÉBUS-FP tests.

Care is needed in extrapolating the rather good results for the containment directly to the reactor case, as the PHÉBUS containment thermal hydraulics are relatively simple, and the role of gravitational settling is overscaled, with a shorter residence time of aerosols in the atmosphere and probably less effect of agglomeration than for real plants.

Concerning the *source term*, the accuracy of containment calculations in integral treatments is sensitive, often highly, to results of previous stages (propagation of uncertainties). Key features are the calculation of FP release from the bundle, and of the structural materials Ag, In, Cd and Sn (the kinetics of release of these and of FPs are as important as the final amounts); the temperatures at the entrance to the circuit, which strongly influence the deposition pattern; while for those codes which calculate the chemistry, the speciation is influenced by the calculated release. The release of structural materials was often undercalculated or not calculated at all, leading to undercalculation of total mass of aerosols, but this had only a weak impact on overall retention in the reactor coolant system (RCS) and depletion in the containment. Iodine speciation and physical form in the circuit was poorly predicted - no code reproduced the observed gaseous iodine fraction in the RCS.

5.2 Circuit

5.2.1 *Revaporization in the FPT0, FPT1 and FPT2 circuits*

The following is a review of information concerning chemical revaporization of deposits in the circuits of the FPT0, FPT1 and FPT2 tests. The information comes from γ -spectrometry at the instrument station known as Point C with corroborating data from γ -spectrometry of the steam generator located a little further downstream. Some speculation on the mechanism affecting deposited cesium is included (after [1]).

The results of the FPT0 and FPT1 circuits were reviewed by Kissane [1]. Firstly, it must be said that no evidence can be found of revaporization during FPT0 because the relevant spectrometer signals were saturated for much of the test. Even so, if the apparent revaporization of hot-leg deposits seen in FPT1 and 2 (see below) also occurred in FPT0, it would probably not have been detectable. This is because the initial inventory of fission products was quite low and the hot leg was, at the measuring station of Point C, a low-deposition region of the circuit. For FPT1, evidence of revaporization is clear since about 40 % of the Cs deposited at Point C (a zone of very light deposition, as in FPT0) was observed to relocate to the SG riser following termination of the bundle transient - see Figure below. Indeed, this relocation appears only to stop when isolation of the containment from the circuit occurred, i.e., steam flow stopped. No other fission product (FP) was observed to relocate implying that relocation was not the result of mechanical resuspension. Furthermore, the fact that the cesium species released from the deposit involved no other (measurable) FP significantly limits the possible candidates for the revaporizing species.

For FPT2, at the 21st meeting of the CCIC Zabiego presented in some detail the current status of results from sequential samples and on-line gamma-spectrometry measurements [2]. The findings are more complex than for FPT1. Significant deposition was observed along the hot leg during the steam-starvation phase. Deposits at Point C were then seen to lose some cesium (50 %), iodine (80 %), indium and rubidium when the steam-starvation phase ended. Given that the flow regime at this location was laminar throughout the test, mechanical resuspension would seem an unlikely explanation despite the relocation of a number of FPs (though it would still be prudent to check that a refractory species such as silver was unaffected). The results support the idea of partial re-vaporization of cesium, iodine, indium and rubidium from hot-leg deposits when reducing conditions switched to oxidizing conditions. The shut-down phase also produced loss of cesium from the Point C deposits as observed in FPT1. Coincidentally, downstream in the steam generator, significant Cs deposition occurred after the core was shut down.

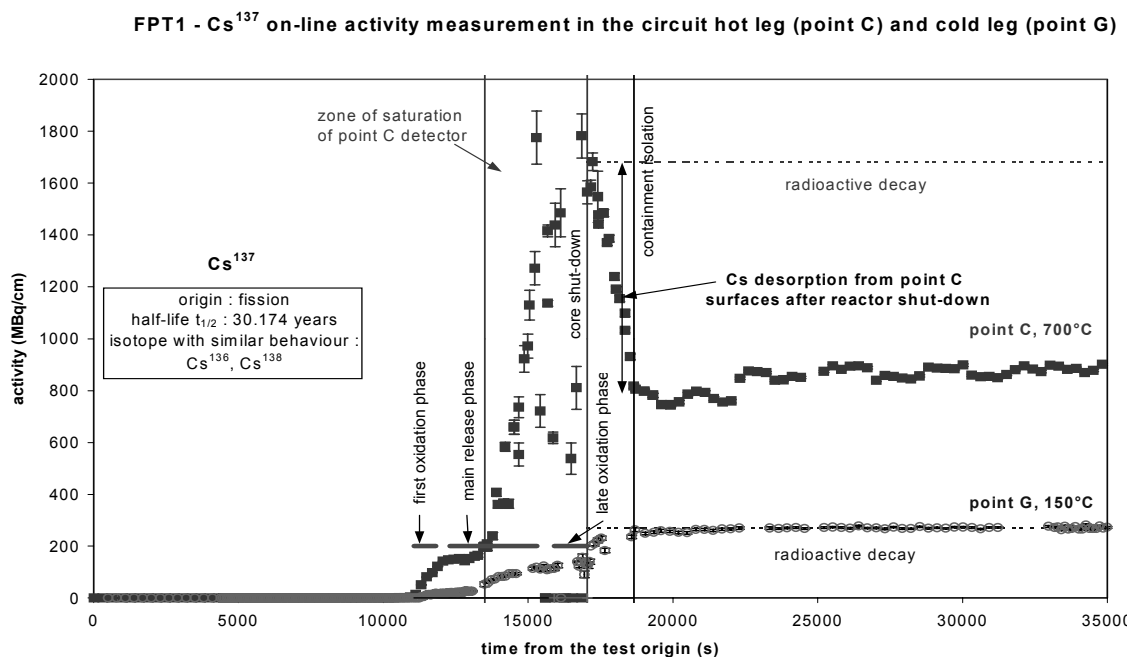


Fig. 5.2-1 (Figure 22 from [1]; Figure 5.2-18 of the FPT1 Final Report): FPT1 experimental data on Cs activity at Point C (upper line in red) showing the drop in activity following core shutdown that continued until steam injection stopped

Concerning the remobilization of Cs, it is well known that some Cs species tend to chemisorb on alloy surfaces such as Inconel with “trapping” of a fraction of the Cs. The mechanism involves penetration of Cs into the substrate and reaction with silica, present as an impurity. The trapping appears accentuated by surface corrosion, longer times and higher temperatures. While the PHÉBUS hot leg was hot enough for the effect to be very significant, crucially it did not have a pre-corroded surface. Furthermore, there were revaporization experiments carried out in the RVP project on pipe samples cut from the vertical section of the FPT1 hot leg. Though not directly comparable to Point C conditions, the sample zone most closely resembling Point C shows a large fraction being easily resuspended in pure steam at 630 °C with only a smaller fraction trapped in a low-volatility form. Indeed, despite the mixed nature of the deposit, the revaporization rate was analogous to that of CsOH measured in control tests. Hence, revaporization of largely untrapped Cs as CsOH from Point C fits the FPT1 observations and is compatible with some code analyses.

References

- [1] M.P. Kissane, “Interpretation of PHÉBUS tests FPT0 and FPT1: synthesis of analyses of fission-product behaviour in the circuit”, Note Technique SEMAR 03/96, Oct. 2003
- [2] M. Zabiego, L. Pantera, “FPT2 Data Analysis” in N. Girault, “Containment Chemistry Interpretation Circle”, IRSN Compte Rendu de Réunion DPAM/SEMIC/2004-70, April 2004

5.2.2 FALCON (Including ISP-34)

5.2.2.1 Objectives and procedure

The FALCON small-scale experiments were performed at AEA Winfrith in 1992-3 and were intended as a preparation for the PHÉBUS FP series of in-pile tests. Their primary purpose was to provide information

on the influence of fission product chemistry on circuit transport and containment deposition. Also investigated were multi-component aerosol effects and vapor-aerosol interactions. In each experiment one to six simulant fuel samples were heated by an induction furnace in a silica vessel. The samples contained concentrations of non-radioactive fission product elements typical of high burnup fuel in a UO_2 matrix. These included CsI, CsOH, Te, SrO, BaO and MoO. The pellets were clad in Zircaloy-4. Depending on the experiment control rod alloy materials could also be included, clad in stainless steel. The temperatures were increased sufficiently to burst the fuel and control rod pellets. Heating was then continued up to 3000 K to produce a continuous release of materials, transported by a carrier gas through the model circuit. The carrier gas was mainly helium admixed with low concentrations of steam and/or hydrogen. Optionally boric acid could be injected above the heated region.

5.2.2.2 *Model circuit and experimental details*

The circuit consisted of a thermal gradient tube of length 480 mm followed in the primary circuit experimental series by a straight stainless steel pipe 800 mm long. In the containment series this pipe was replaced by a stainless steel circuit with several bends followed by a steel box modelling the containment. Analysts have largely considered the data from the thermal gradient tube to be of most interest [1] and this component and the experimental data obtained from it will now be described in more detail. The geometry of the thermal gradient tube varied during the test series. In the earlier tests, including FAL-17 and FAL-18 the first section of length 100 mm had a diameter of 35 mm, while for the remaining 380 mm the diameter was reduced to 25 mm. In subsequent tests, including FAL-19 and FAL-20 the diameter was 25 mm throughout. A series of five independently heated zones, each of length approx. 60 mm, allowed a wall temperature profile to be maintained. A uniform temperature gradient was generally imposed, from 1100 K to 400 K approximately. Both wall and gas temperatures were measured at selected points along the tube. The tube was lined with stainless steel foil, which could be removed after the test for analysis. Bulk deposits were examined with ICPOES, atomic absorption spectrometry, and colorimetry. Iodine was collected in Maypacks and examined with X-ray fluorescence spectroscopy. Individual particles were measured using energy dispersive spectroscopy with a scanning electron microscope, and particle characterisation was also applied to obtain size and morphology data. Speciation was studied through powder X-ray diffraction and X-ray photoelectron spectroscopy.

5.2.2.3 *FALCON tests and ISP 34*

As part of the ongoing series of code validation problems promoted by the CSNI [2] International Standard Problem 34 was based on four tests of the FALCON series, FAL-17 to FAL-20 [3, 4, 5, 6]. The first two were primary circuit tests while the latter two used a circuit including a containment vessel. However as far as circuit phenomena are concerned this made little difference. We here focus attention on the thermal gradient tube. The sources differed in the materials injected into the carrier gas stream, as follows:

	FAL-17	FAL-18	FAL-19	FAL-20
He (l/min)	10	10	4	4
Steam (cm^3/min at 20 °C)	0.21	0.21	3.1	0
H ₂	5 % of H ₂ O	5 % of H ₂ O	5 % of H ₂ O	5 % of He
Boric acid (ppm)	2000	0	2000	0

The experimental results offered for comparison with analyses were the deposition profiles for a specified series of elements.

5.2.2.4 Analyses

The ISP proved popular, attracting 50 submissions from 12 countries, using the system or circuit codes in use at the time, including MELCOR VICTORIA and RAFT. The final report was issued in December 1994 [7, 8]. It was concluded that several chemistry issues of aerosol and fission product behaviour required further code improvements, and that there was a strong user effect. It also appeared that revaporisation might have been important in determining the final deposition profiles. Non-representative aspects of the experiments identified included laminar flow conditions throughout and a high surface to volume ratio. There were also uncertainties in the mass release rates.

[1] pointed out that for constant wall temperatures and carrier gas conditions (obtaining during most of each experiment analysed) the percentage of a given element deposited at a specified location was independent of the instantaneous release rate. These authors were thus able to treat thermal gradient tube deposition in FALCON as a steady flow problem. They also noted that the deposition profiles for vapors were qualitatively different from those for aerosols, the former showing a threshold dependent on the condensation temperature. They used this finding plus correlations between the deposition profiles of different elements to obtain information on speciation. It was concluded that

- The results show that speciation is important, and can vary with the carrier gas composition
- In the presence of excess boric acid Cs is predominantly in the form of cesium borate. In the concentrations present in FALCON the borate condenses at a temperature 250 K higher than the hydroxide
- The iodine data are ambiguous; possibly in FAL-18 the dominant species was CsI, but the volatility of iodine varied between tests, suggesting differing speciation
- Molybdenum was more volatile in the boric acid tests
- Cadmium showed similar behaviour in all tests
- Silver was an aerosol in the test in reducing conditions, but entered the thermal gradient tube as a gas in the other experiments
- The deposition velocities of aerosol particles (deposited mostly by thermophoresis) appeared to be largely independent of the aerosol composition

5.2.2.5 Status

Currently there are no ongoing analyses of the FALCON tests. The thermal gradient tube data from this series are however of good quality, despite uncertainties in the timing and magnitude of the releases from the simulant source, and might usefully be revisited to help shed light on the circuit data from PHÉBUS FP, which are copious but not always easy to interpret.

References

- [1] I.M. Shepherd, Y. Drossinos, C.G. Benson Modelling fission product vapor transport in the FALCON facility Nuclear Technology 110,181-197, 1995
- [2] CSNI: CSNI International Standard Problems (ISP) Brief description (1975-1999). NEA/CSNI/R(2000)5. May 2000
- [3] A.M. Beard, P.J. Bennett Data report 23, Integral test 17, FAL/P(92)77 Winfrith Technology Centre, May 1992

- [4] A.M. Beard, P.J. Bennett FALCON data report 24, Integral test 18, FAL/P(93)83 Winfrith Technology Centre, Jan 1993
- [5] A.M. Beard, P.J. Bennett FALCON data report 26, Integral test 19, FAL/P(93)90 Winfrith Technology Centre, Feb 1993
- [6] A.M. Beard, P.J. Bennett FALCON data report 27, Integral test 20, FAL/P(93)94 Winfrith Technology Centre, May 1993
- [7] D.A. Williams OECD International Standard Problem No. 34, FALCON code comparison report. AEA RS 3394, AEA Winfrith (June 1994)
- [8] D.A. Williams OECD International Standard Problem No. 34 FALCON fission product experiments FAL-ISP-1 and FAL-ISP-2 Comparison Report. NEA/CSNI/R(94)27 December 1994

5.2.3 **STORM (Including ISP-40)**

5.2.3.1 *Recent analyses of the STORM deposition and resuspension experiments (ISP-40)*

The STORM series of experiments was performed at the European Commission's Joint Research Centre, Ispra (Italy) in the period 1996-97. Each experiment was divided into two phases. In the deposition phase a SnO_2 simulant aerosol carried by a steam-air-nitrogen mixture through a 63 mm diameter horizontal pipe of length 5000 mm built up a layer of deposit, mostly by thermophoresis and eddy impaction, while in the resuspension phase a higher-velocity nitrogen flow mechanically resuspended and relocated a fraction of the deposit. The international standard problem ISP-40 was based on the two phases of STORM test 11 [1], and is described elsewhere in Section 5.1.5.1. Subsequent to the publication of the ISP-40 Final Report a number of teams have continued to analyse tests of the STORM series with the aim of providing further support and validation to resuspension models, judged to be inadequate in the conclusions of the ISP.

Most of the information available on recent STORM analyses is to be found in the Final Report of the EVITA project [2, 3] and concerns Test SR11. There has also been some work on STORM test SR09 [4], the essential differences of which from SR11 are as follows. The deposition phase used the same simulant aerosol SnO_2 and a similar steam-nitrogen-air mix as carrier gas, but took place at the slightly lower temperature of 340 °C. The temperature difference between the test section wall and the gas stream was 50 °C, as compared with 100 °C in SR11. The carrier velocity was higher, 24.9 m/s versus 18 m/s in the later test. This combination was expected to result in more deposition by impaction and relatively less by thermophoresis. The deposited mass was similar in the two tests. The resuspension phase of SR09 took place in a single step, at a nitrogen velocity of 52.3 m/s. As in SR11, to minimise thermophoresis during this phase the gas and wall temperatures had the same value, 340 °C.

A team at VEIKI has re-analysed test SR11 using the SOPHAEROS module of the integral code ASTEC v0.3. The test section was divided into 11 longitudinal sections, and the aerosol size distribution was divided into 20 logarithmically equal size bins, ranging from 2 nm to 40 µm. These analysts found that nearly all the deposition was by thermophoresis, and succeeded in calculating the mass deposited to within 30 %. The profile of the deposit along the tube was nearly flat in the calculations, although in the test an estimated 30 % reduction in surface density of aerosol was seen from inlet to outlet. The calculated deposit was then used in the resuspension phase. The resuspension rate calculated by the semi-empirical model used in the code was found to be constant during each velocity step, and with default values for the adhesive force and resuspension rate parameters matched the total mass resuspended rather well for the earlier steps. As carrier gas velocities exceeded 60 m/s, however, the resuspended mass became

underpredicted, by a factor of two at the end of the final velocity step. Significantly, redeposition of resuspended aerosol by impaction was predicted towards the outlet of the test section.

The JRC team and collaborators have continued the analysis of experiments of the STORM series, including the deposition tests SD04, SD05, SD07, SD08, SR09, SR11, SR12 and the resuspension tests SR09 and SR11 as well as SR12, again using SOPHAEROS. The deposition phase of SR10 was similar to that of SR09 but with a lower carrier velocity, and the velocity during the resuspension phase was double that in SR09. The deposition phase of STORM SR12 was identical to that of SR11, while the resuspension phase had three steps with carrier velocities increasing from 90 to 110 m/s. Like the VEIKI team the JRC reseearchers were able to achieve good prediction of the deposition phase in SR11, and their results for the resuspension phase are similar.

The SOPHAEROS model [5] decides whether particles of a given size will resuspend on the basis of a balance of adhesive and aerodynamic forces, the rate of the subsequent resuspension being calculated by a semi-empirical model originally used in ECART. Predominant among the adhesive forces in the STORM tests is the cohesive force, proportional to a user-specified cohesive force coefficient. With the default value of this coefficient the predicted resuspension rate in SR09 is too great, but the JRC team found that good agreement with the data, including the final profile of the deposit, could be achieved with a cohesive force coefficient ten times the default value. The JRC team has also analysed tests SR10, SR11 and SR12 using the SOPHAEROS implementation of the Reeks-Biasi rock'n'roll model (see below). It has been found that the rock'n'roll model underestimates the final resuspended fraction in all the tests analysed. The time-dependence of the resuspension behaviour is also different from that observed. Nearly all the resuspension is predicted to occur within a very short time, whereas the experimentally observed resuspension has a duration of some 25 s.

The JRC analysis also points up the importance of the deposition mode in determining the resuspension behaviour. In test SR10 a lower temperature difference between pipe wall and carrier gas resulted in a significant contribution from eddy impaction to the total deposition, accompanied by an increased aerosol mass median diameter. During the resuspension phase resuspension began at a lower fluid velocity than in tests where the deposition was predominantly by thermophoresis (80 m/s in SR09 compared to 100 m/s in SR12).

The use of semi-empirical models with adjusted coefficients is not very satisfactory, and a less empirical resuspension model has been developed by [6] which is claimed to account for the resuspension behaviour observed in several STORM tests, in preceding test series which were reviewed in the SOAR on circuit aerosol behaviour [7] and in other experiments available in the literature, without becoming too complex for use in engineering safety codes. The model assumes a log-normal distribution of adhesive forces, and includes correlations for the geometric mean and standard deviation of the adhesive force distribution. It has been found that the effective adhesion is much less than for particles in smooth contact with the pipe surface, consistent with an effect of surface roughness, and that sub-micron particles are more tightly bound when a deposit already exists than when there is less than a mono-layer of deposit present. The Biasi model has been implemented in SOPHAEROS.

It should be noted however that in STORM and in other tests e.g. the VTT PSAERO [8] tests, the resuspension rate for a given gas velocity declines with time, and there is also a contribution apparently due to gas acceleration [9] effects not currently accounted for (see chapter 3.5.1). Gas velocities favouring resuspension also favour turbulent impaction, the models for which are not fully validated, and in resuspension experiments the two processes are likely to occur simultaneously. Compounding of model uncertainties may therefore occur during their analysis. A further point is that essentially all the data considered in ISP-40 and in subsequent related developments refer to dry aerosols, and separate-effect tests to provide data on the resuspension of wetted and semi-liquid deposits do not appear to have been

performed. There is thus no great incentive at present for the development of models treating resuspension from such deposits.

References

- [1] P. Dilara, A. Krasenbrink, R. Hummel STORM test SR-11: ISP-40 Quick Look Report Technical Note, Joint Research Centre, Ispra (Italy), March 1998
- [2] H.-J. Allelein, K. Neu, J.P. Van Dorsselaere, K. Mueller, P. Kostka, M. Barnak, P. Matejovic, A. Bujan, J. Slaby European validation of the integral code ASTEC (EVITA). *Nucl. Eng. and Desn.* 221 (2003) 95-118
- [3] H.-J. Allelein, K. Mueller et al. European validation of the integral code ASTEC (EVITA) Final Report, Parts 1&2. European Commission report (2004)
- [4] P. Dilara, A. Krasenbrink, R. Hummel, J. Area Capitao STORM test SR-09: Deposition of SnO₂ in Partially Insulated Pipes with Steam and Resuspension of SnO₂ from Partially Insulated Pipes with N₂ Quick Look Report. Technical Note, Joint Research Centre, Ispra (Italy), February 1998
- [5] M. Missirlian, N. Alpy, M.P. Kissane "ASTEC V0 SOPHAEROS code version 2.0. Fission product analysis in PWR circuits Theoretical manual, Rev 0", ASTEC-V0/DOC/00-06. NT/SEMAR/01/98, December 2001
- [6] L. Biasi, A. de los Reyes, M. Reeks, G. de Santi Use of a simple model for the interpretation of experimental data on particle resuspension in turbulent flows *Journal of Aerosol, Science* 32,1175-1200 (2001)
- [7] A.L. Wright et al. Primary System Fission Production Release and Transport NEA/CSNI/R(94)2 (1994)
- [8] A. Auvinen^a, J.K. Jokiniemi^a, A. Lähde^a, T. Routamo^b, P. Lundström^b, H. Tuomisto^b, J. Dienstbier^c, S. Güntay^d, D. Suckow^d, A. Dehbi^d, M. Slootman^e, L. Herranz^f, V. Peyres^f, J. Polo^f, "SG tube rupture (SGTR) scenarios" *Nuclear Engineering and Design* 235 (2005) 457–472
^a VTT Processes, Biologinkuja 7, P.O. Box 1602, VTT Espoo 02044, Finland
^b Fortum Nuclear Services, Vantaa, Finland
^c Nuclear Research Institute Rez plc, Czech Republic
^d Paul Scherrer Institute, Villigen-PSI, Switzerland
^e Nuclear Research and Consultancy Group, Arnhem, Netherlands
^f Centro de Investigaciones Energeticas, Medioambientales y Tecnologicas, Madrid, Spain
- [9] N. Ardey, F. Mayinger Aerosol resuspension by highly transient containment flow: insights by means of laser optical methods *Kerntechnik*, 68-75 (1998)

5.2.3.2 ISP-40: aerosol deposition and resuspension

Uncertainty in the modelling of aerosol resuspension had been mentioned as a problem in the SOAR of 1994 [1], although it was found difficult to ascertain its safety import. International Standard Problem ISP-40 was set up to address aerosol deposition and resuspension phenomena in the reactor cooling system and was based on test SR11 of the STORM series performed at the European Commission's Joint Research Centre, Ispra (Italy) in 1997 [2]. The scenario was one of nuclear aerosol deposition in the relief lines of a PWR during a steam blackout followed by resuspension of the deposits by the steam surge resulting from a core slump. Like other STORM tests the experiment upon which this ISP was based took place in two

phases. In the deposition phase SnO_2 simulant aerosol was transported through a horizontal test section (diameter 63 mm, length 5000.5 mm) by a carrier gas consisting of a mixture of steam, N_2 , air, Ar and He. The constant gas velocity was approx. 18 m/s, and while the gas temperature was approx 370 °C the wall temperature was 100 °C cooler so that deposition took place largely by eddy impaction and by thermophoresis. The aerosol had a GMD of 0.43 μm and a GSD of 1.7, and the deposition phase continued long enough to build up 162 g of deposit.

The test section and its deposit were then kept at 370 °C for a period of about 24 hours, during which the following phase of the test was prepared. In this resuspension phase, nitrogen gas was passed through the test section in a series of mass flow rate plateaux, and the mass resuspended during each phase and its size distribution were measured by downstream sampling stations. Velocities up to 127 m/s were investigated.

Fig. 5.2-2 shows the mass flow rates for the various steps as well as the mass remaining in the deposit after each step. A feature of the STORM tests is that the mass distribution of the deposit along the pipe could be measured by a radioactive tracer, and such profile data were collected in test SR11 for comparison with predictions.

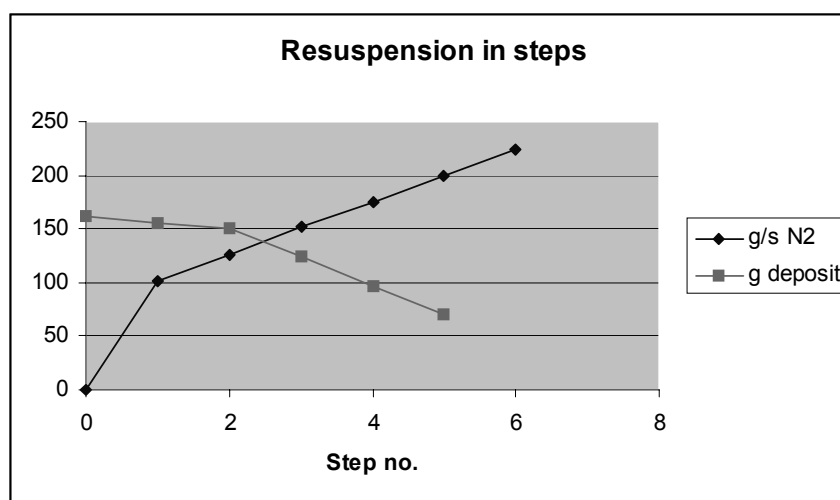


Fig. 5.2-2 Mass flow rate and mass remaining in the deposit

The ISP attracted 18 participants, who could choose to calculate one or both of the experimental phases. The deposition phase was run blind, while for the resuspension phase participants were supplied with the size distribution of the resuspended mass for each step in the gas flow. Contributions were collated in January 1998. It was subsequently found that the steam flow during deposition had been given incorrectly. More importantly, the sizes of the resuspended aerosols had been overstated by a factor of two. Working now with open conditions, participants were invited to recalculate their submissions. Sensitivity studies were also produced by some participants, and the final report of the ISP [3] was based on all submissions received, taking due account of the data available to the participants at the time each calculation was made.

The final report came to the following conclusions:

1. Modelling of thermophoretic deposition is adequate
2. There are problems with the modelling of deposition due to turbulent flows

3. Aerosol deposition and resuspension need to be treated together
4. Aerosol retention depends strongly on the thermal-hydraulic conditions
5. One-dimensional bulk parameter modelling is generally adequate to calculate aerosol retention in fully developed flow in straight pipes
6. The particle tracking codes used in this ISP are still in a preliminary phase of their development and, while having a stronger physical basis, generally require the knowledge of parameters which are not generally known
7. In terms of the results obtained, there was a tendency of almost all codes to overpredict aerosol deposition in the test pipe
8. Aerosol resuspension can significantly affect the source term in the case of dry aerosol deposits in turbulent flows
9. Experimental data is needed for resuspension of aerosol mixtures with different liquid fractions
10. Present aerosol resuspension models are inadequate
11. The potential for resuspension depends strongly on the characteristics of the deposit
12. Deposition models should give an indication of the state of the deposit, not only of the mass deposited
13. Separate effects tests are needed to relate the characteristics of the deposit to their chemical composition and to the mechanisms by which the deposit was formed
14. Mono-layer resuspension models are only a step towards the development of multi-layer models

Modelling and code effects

It is of interest for the appreciation of the impact of uncertainties in resuspension modelling to quantify the variation in model predictions seen in the ISP-40 submissions.

Fig 5.2-3 shows the calculated masses of aerosol resulting from the deposition phase, and compares them with the experimental value. With the exception of those from MELCOR users and the particle tracking code MARIE predictions are similar, and may be considered acceptable. Note that the result marked Pisa-2 is produced by allowing resuspension to take place simultaneous with deposition. The predicted very low net deposited mass is a result of too much resuspension.

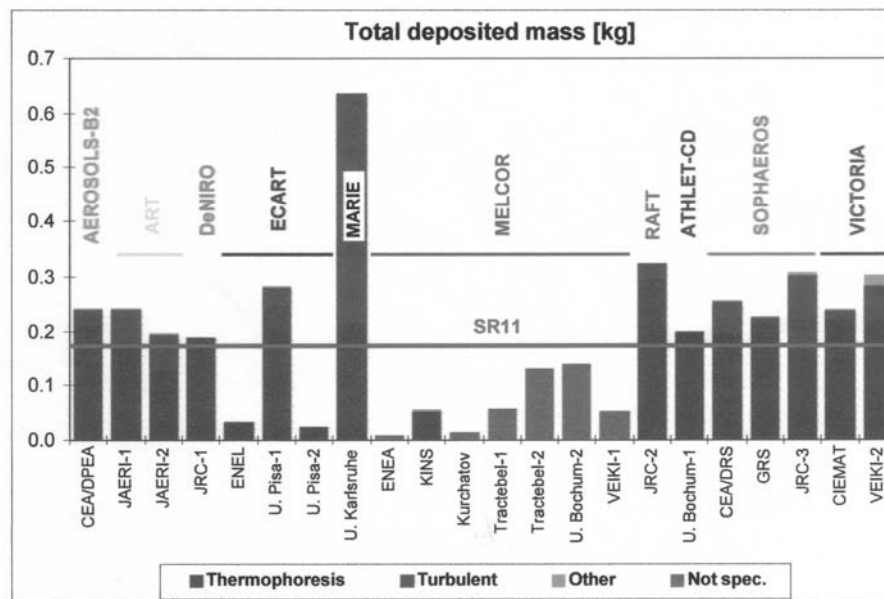


Fig. 5.2-3 Total deposited mass

The situation is less encouraging for the resuspension calculations. Fig. 5.2-4 provides the fractions of deposited mass remaining after each step of the resuspension part of the test, as calculated by each code but normalised to the same total deposited mass to compensate for differences in calculations of the deposition phase. The column corresponding to the experimental data is marked SR11. Very wide variations in predicted resuspension behaviour with increasing gas flow can be observed, quite apart from the differences in predicted total resuspended mass. For instance, ART predicts near-total resuspension at the first velocity step, whereas one of the SOPHAEROS predictions has over 65 % of the deposit still present after the final step with highest gas flow. The substantial user effect also visible (see the pairs of calculations made using CAESAR, ECART, SOPHAEROS or VICTORIA) arises from uncertainties in the parameters of the particular resuspension model implemented in each code. In addition, most codes experienced difficulty in calculating the time-dependence of resuspension during each step. In the experiment most of the resuspension took place over a relatively short time at the beginning of the step, whereas a number of models calculated a constant resuspension rate for given thermal-hydraulic conditions.

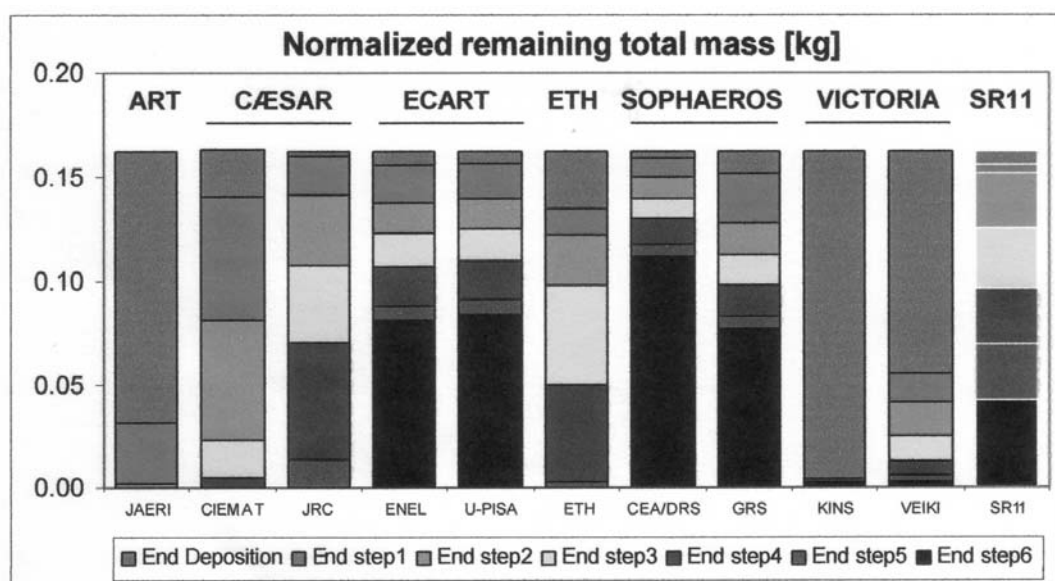


Fig. 5.2-4 Aerosol mass remaining in the deposit

Besides the resuspended masses participants were also invited to reproduce the measured size distribution of resuspended aerosol. It was found in the test that increasing gas flow resuspended progressively smaller particles, and this trend was broadly reproduced in the submitted calculations. However, the absolute sizes varied very widely (see Fig. 5.2-5) and the trend mentioned was nearly absent in some calculations but exaggerated in others.

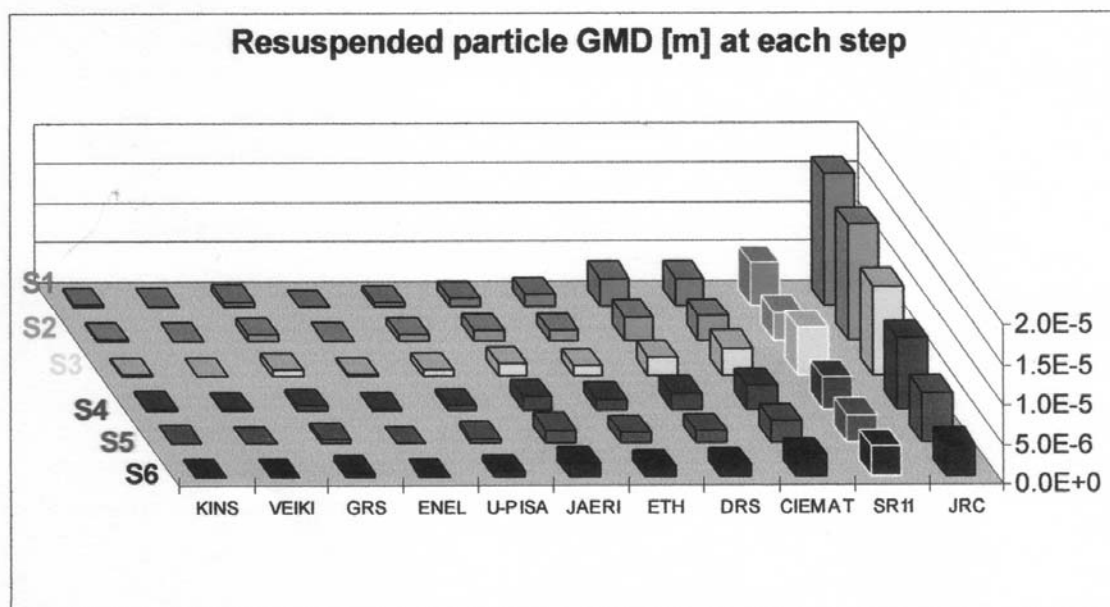


Fig. 5.2-5 Geometric mean diameter of the particle at the outlet of the test pipe

References

- [1] A.L. Wright et al. Primary System Fission Production Release and Transport NEA/CSNI/R(94)2 (1994)
- [2] P. Dilara, A. Krasenbrink, R. Hummel STORM test SR-11: ISP-40 Quick Look Report Technical Note, Joint Research Centre, Ispra (Italy), March 1998
- [3] A. de los Reyes Castelo, J.A. Capitão, G. de Santi International Standard Problem 40 – Aerosol Deposition and Resuspension Final Comparison Report, Joint Research Centre, EUR 18708 EN, OECD NEA/CSNI/R(99)4 February 1999

5.2.4 *WIND*

WAVE experiments

Small-scale basic tests have been performed with the WAVE (Wide range Aerosol model Verification) facility [1] at JAERI to investigate the cesium iodide (CsI) deposition onto the inner surface of a pipe under typical severe accident conditions. In the tests, a crucible including the CsI powder was placed at upstream part of the electrically heating test pipe and generated CsI vapor or aerosol was delivered to the downstream pipe by nitrogen gas. Several coupons made of SUS304 were set in the test pipe and the deposited mass on them were measured after the tests.

The tests with a horizontal straight pipe showed that a relatively large amount of CsI was deposited on the upstream floor (bottom) of the pipe and at the downstream ceiling (top) of the pipe [1]. Analyses of the experiments have also been conducted with the three-dimensional thermal-hydraulic code and the radionuclide transport analysis code, ART [2, 3]. The experimental results were reproduced well with ART by using a peripherally subdivided pipe cross section and associated representative thermal-hydraulic information from the thermal-hydraulic code prediction. These experiments and analyses indicate that the major deposition mechanisms for the chemical form of CsI are thermophoresis and condensation, both of which depend on the thermal gradient in the gas.

Moreover, several tests using a quartz glass pipe with a 90 degree bend have been performed to investigate the CsI aerosol behaviour at the bend and the effect of pipe orientation after the bend on aerosol behaviour [4]. Three tests with horizontal, upward, and downward pipe orientation after the bend showed enhancement of CsI deposition in the upward vertical pipe due to a transition from laminar to turbulent flow. The flow regime in the horizontal and downward pipes was kept at laminar flow in spite of the same flow velocity. The reason for turbulent flow only in the upward pipe is that the downward flow near the low-temperature pipe surface is opposite to the direction of main stream. The ART calculation which considers the thermal-hydraulics of only the main stream reproduced well the thermophoretic deposition in the horizontal and downward pipes but underpredicted the deposition for the upward vertical pipe by one order of magnitude. To precisely predict the deposition in the upward oriented pipe, the flow regime should be evaluated carefully by taking into account the natural circulation in the pipe as well as the main stream.

These studies showed that the coupling of the radionuclide behaviour and the detailed fluid-dynamic phenomena was essential to accurately predict the CsI deposition at a bend or at a vertical pipe as well as in a horizontal straight pipe. Little attention has been paid to such coupling in previous studies.

WIND experiments

The piping of reactor coolant system could be heated by high temperature gases from the reactor core region and the decay heat of the deposited fission products (FP). Under such conditions, the integrity of the reactor piping would be threatened by this temperature increase together with the high system pressure. The WIND (Wide range piping Integrity Demonstration) project [5, 6] was initiated in 1993 to evaluate the integrity and safety margin of reactor piping under severe accident conditions. The WIND project consists of tests and analyses related to aerosol behaviour and piping structural integrity.

A schematic diagram of the WIND facility is shown in Fig. 5.2-6.

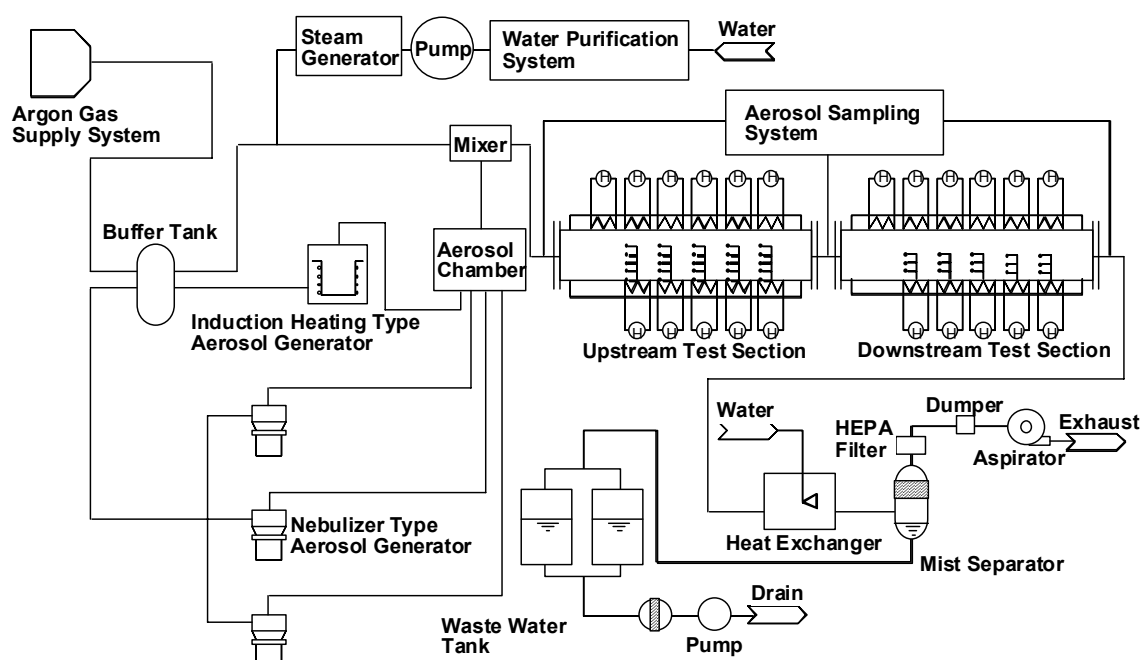


Fig. 5.2-6 Schematic diagram of the WIND facility

In the aerosol deposition tests, cesium iodide (CsI) aerosol was introduced into two horizontal test sections connected in series. These sections consist of straight stainless steel pipes with an inner diameter of approximately 10 cm and a length of 2 m. Argon or a mixture of argon and superheated steam was used as a carrier gas to suspend and transport the aerosol into the test sections. Temperature gradients with the maximum temperature of 1273 K and 973 K were developed in the test sections. The deposition density of cesium onto the upstream test section in WAV1-D is shown in Fig. 5.2-7. The test results on the spatial distribution of the aerosol deposition and the thermo-fluiddynamic analysis with the WINDFLOW code [7] showed that the formation of a natural convective secondary flow of gases resulted in the deposition of CsI onto the ceiling and side wall areas of the test sections and that the dominant deposition mechanisms were the condensation of vapor and the thermophoresis of CsI aerosol [8]. No remarkable decomposition of CsI was observed in the tests with environments of argon and superheated steam. The results obtained from the aerosol deposition tests have been applied for the validation of the ART code, which is used for a detailed analysis of the FP behaviour during a severe accident.

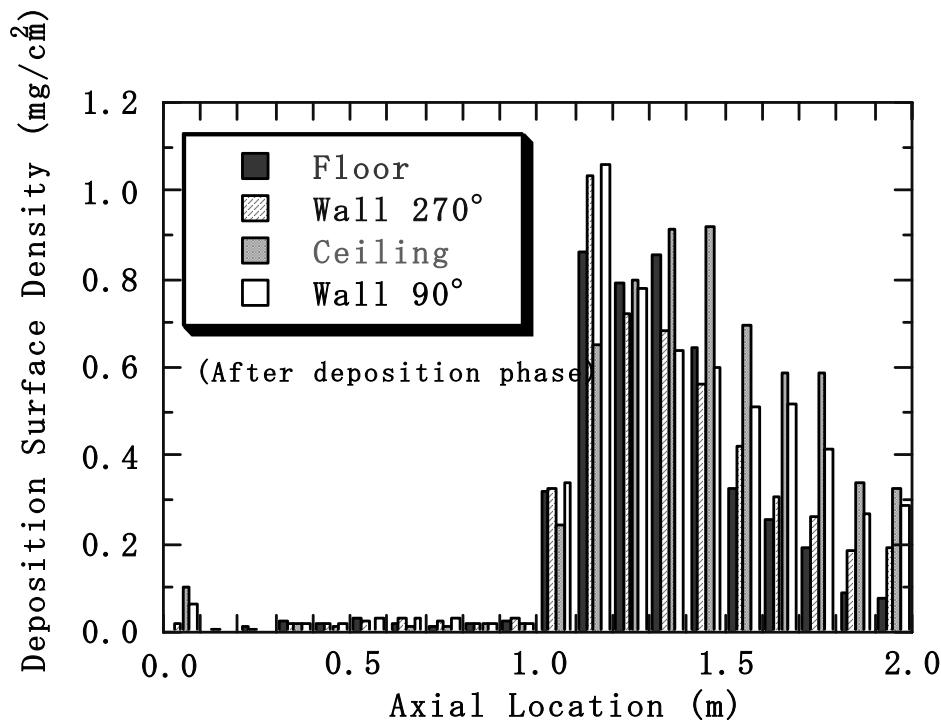


Fig. 5.2-7 Deposition density of cesium onto the upstream test section in WAV1-D

References

- [1] A. Hidaka, et al. "Experimental and Analytical Study on the Behaviour of Cesium Iodide Aerosol/Vapor Deposition onto Inner Surface of Pipe Wall under Severe Accident Conditions" J. Nucl. Sci. Technol. 32 (10), pp.1047-1053 (1995)
- [2] T. Ishigami et al. "User's Manual of ART Code for Analyzing Fission Product Transport Behaviour During Core Meltdown Accident" JAERI-M 88-093 (1988).
- [3] M. Kajimoto et al. "Development of THALES-2, A Computer Code for Coupled Thermal-Hydraulics and FP Transport Analyses for Severe Accident at LWRs and Its Application to Analysis of FP Revaporization Phenomena" Proc. Int. Topical Meeting on Safety of Thermal Reactors, Portland, pp.584-592 (1991)
- [4] A. Hidaka, et al. "Deposition of Cesium Iodide Particles in Bends and Sections of Vertical Pipe under Severe Accident Conditions" J. Aerosol Sci., 31(9), pp.1045-1059 (2000)
- [5] K. Hashimoto, et al. "Current Status of WIND Project" JAERI-Conf 99-005, pp.161-164 (1999)
- [6] A. Hidaka, et al. "Experimental and Analytical Study on Aerosol Behaviour in WIND Project" Nucl. Eng. and Des., Vol.200, pp.303-315 (2000)
- [7] Y. Maruyama et al. Vapor Condensation and Thermophoretic Aerosol Deposition of Cesium Iodide in Horizontal Thermal Gradient Pipes J. Nucl. Sci. Technol., 36(5), pp. 433-442 (1999)
- [8] H. Shibasaki et al. Revaporization of CsI Aerosol in a Horizontal Straight Pipe in a Severe Accident Condition Nucl. Technol., 134, pp. 62-70 (2001)

5.3 Containment Experiments

5.3.1 DEMONA

The DEMONA tests were performed to investigate the natural aerosol removal in a PWR containment under core melt accident conditions. Their main objective was to demonstrate the validity of the aerosol code NAUA. From 1983 to 1986 nine large-scale tests were carried out in the Battelle model containment in Frankfurt/Main [1, 2]. The programme was sponsored by the German Federal Minister for Research and Technology (BMFT) and the USNRC.

The 630 m³ model containment was made of reinforced concrete and had roughly the shape of a German PWR containment. The interior was subdivided into several compartments (Fig. 5.3-1).

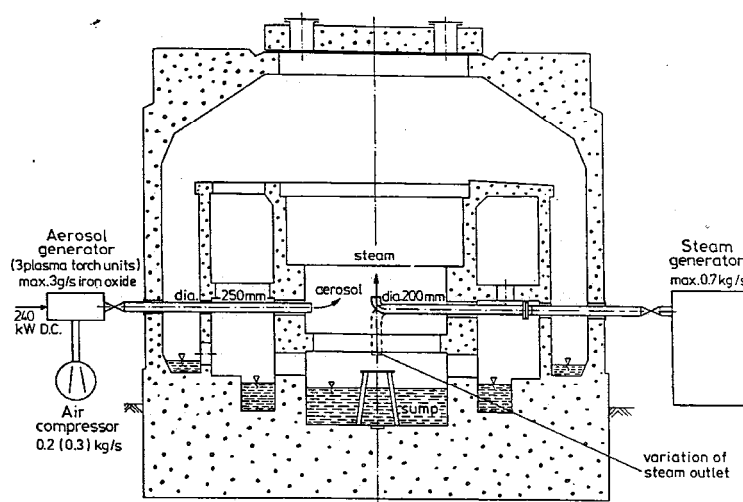


Fig. 5.3-1 Battelle model containment for DEMONA tests

In each test the containment structures were heated up by steam releases first. Then the test aerosol generated by three plasma torches was injected up to a maximum concentration of about 10 g/m³. Aerosol material and composition as well as the thermal hydraulic conditions varied in each test (Table 5.3-1). Except for test A9 a single room configuration of the containment was used.

Table 5.3-1 DEMONA programme test matrix

Test	Aerosol material	Description
A1	SnO ₂	Thermal hydraulic test without aerosol
B2	SnO ₂	Dry test without volume condensation
B3	SnO ₂	Base test with volume condensation
B4	SnO ₂	Base test, repetition
B5	SnO ₂	Test with delayed volume condensation
B6	Ag + MgO	Test with low concentration and delayed volume condensation
A7	Fe ₂ O ₃	Base test, repetition with iron oxide aerosol
A8	Fe ₂ O ₃ + SnO ₂	Test with mixed aerosol
A9	Fe ₂ O ₃ + SnO ₂	Multi-compartment test with mixed aerosol and delayed volume condensation

The base test B3 simulated a scenario with a late overpressure failure of the containment. After the SnO_2 -aerosol release the atmospheric pressure was kept constant by a steam injection near the bottom which guaranteed a well mixing of the containment atmosphere. During the aerosol depletion phase a moderate volume condensation took place accelerating the aerosol settling (Fig. 5.3-2).

A9 was the only DEMONA Test with a multi-compartment configuration. A four-room-geometry was formed by closing several flow openings. The mixed aerosol injection was followed by a dry and a wet depletion phase. The aerosol was inhomogeneously distributed with generally higher concentrations in the lower compartments than in the upper ones (Fig. 5.3-3). Because of the limited number of aerosol sampling stations it was not possible to measure spatial aerosol distribution in detail.

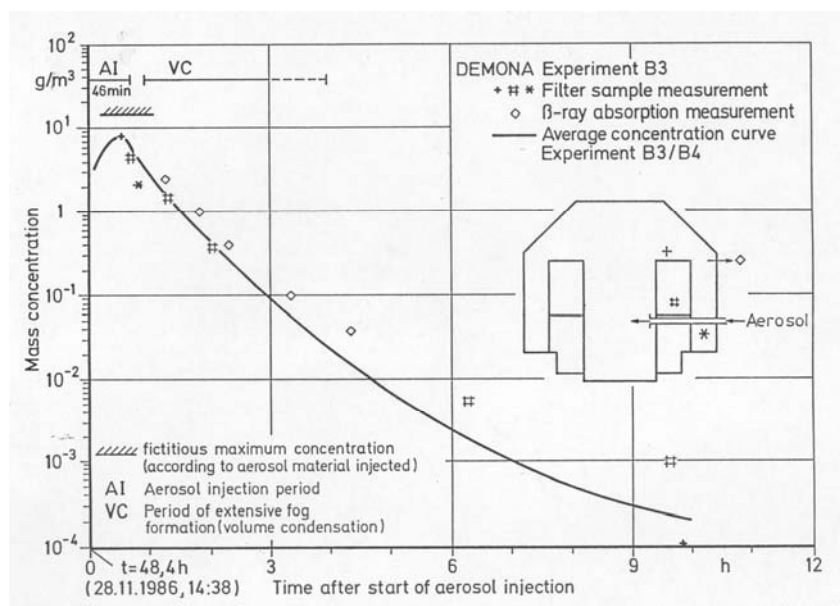


Fig. 5.3-2 Aerosol depletion in DEMONA base test B3

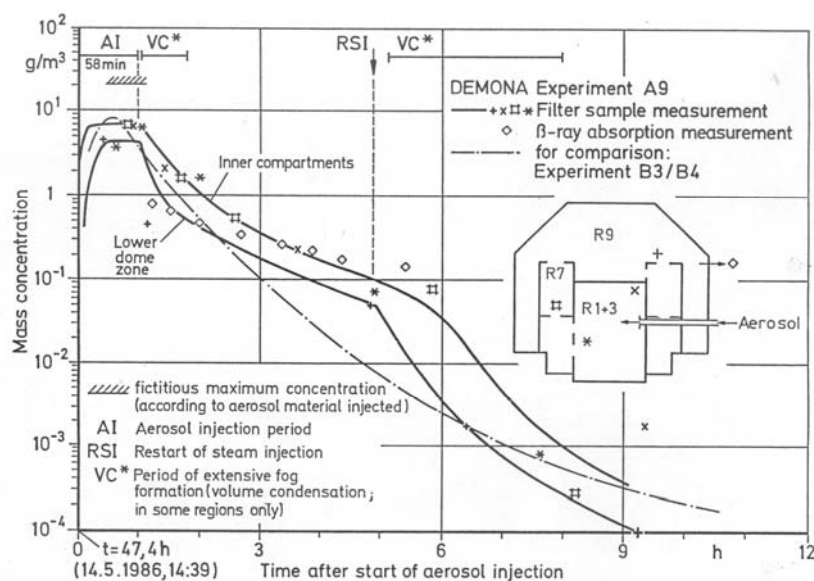


Fig. 5.3-3 Aerosol depletion in the DEMONA multi-compartment test A9

Calculations with the aerosol code NAUA showed a good agreement with the measured aerosol behaviour in the dry DEMONA tests but had some deficits for the wet tests. The multi-compartment effects measured in test A9 could not be considered by the single volume code NAUA. DEMONA test B3 was the subject of a code comparison study initiated by the CEC [3].

References

- [1] T. F. Kanzleiter DEMONA-Versuche Abschlussbericht, Final Report; BleV-R65.523-01 (1987)
- [2] W. Schöck, H. Bunz, R.E. Adams, M.L. Tobias, F.J. Rahn Large-Scale Experiments on Aerosol Behaviour in Light Water Reactor Containments Nuclear Technology 81, pp 139 - 157 (1988)
- [3] W. Schöck Assessment of the outputs from the various computer codes used in Member States to study the behaviour of aerosols in LWR containments in case of severe accidents Final Report to the, CEC, ECI-1413-B7210-85-D, KfK Karlsruhe (1987)

5.3.2 MARVIKEN-V

In the large-scale MARVIKEN-V tests (1982 to 1985) the transport and deposition of aerosols and volatile species were measured in a simulated LWR primary circuit [1]. The reactor vessel, the pressuriser, and the relief tank were the main components interconnected by pipes (Fig. 5.3-4). In five tests performed the circuit geometry and the test conditions were varied. The effects of different temperature ranges (25 °C to 1200 °C), superheated steam, condensing steam, and water were studied. Non-radioactive materials were used for fission product simulants (CsOH, CsI, Te) and core structure simulants (Ag, Mn). The materials were vaporized by separate plasma torches forming condensation aerosols. The aerosol concentrations in the tests lay between 36 and 132 g/m³.

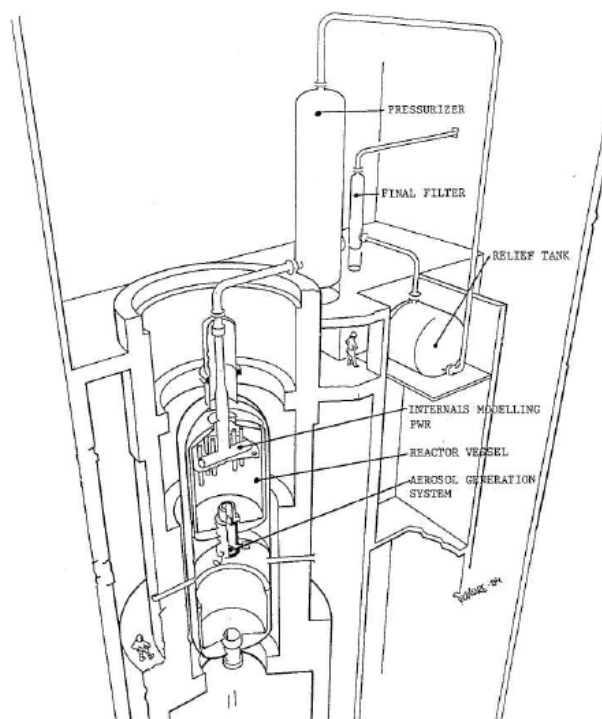


Fig. 5.3-4 Sketch of the MARVIKEN-V test facility

Table 5.3-2 shows the test matrix. In the first three tests only the part of the circuit downstream of the reactor vessel was used and thermal hydraulic conditions were varied. In tests 4 and 7 the whole circuit was integrated and sequences with simultaneous core damage with fission product release and structural aerosol release were measured. Table 5.3-3 summarises the results showing the aerosol retention in the components and pipes measured in the five tests. The retention in the circuit ranged from 15 % in test 2A to 74 % in test 4. Sedimentation and inertial impaction were the dominant deposition phenomena observed. The data show also the high aerosol removal efficiency of the relief tank when filled with water. There are some indications that the fission and corium aerosols were not well-mixed in the reactor vessel. The MARVIKEN –V experiments demonstrated that LWR primary circuits have some aerosol retention capability. The generated data have been used for code validation.

Table 5.3-2 MARVIKEN-V test matrix

Test	Geometry	Conditions	Aerosol
1	Pressuriser	High temperatures Relief tank dry	Fissium
2A	↓ Pipe	Low temperature	
2B	↓ Relief tank	Condensation in piping Water in relief tank	
4	Reactor vessel PWR internals	High aerosol concentration Water in relief tank	Fissium + Corium
7	↓ Pipe ↓ Pressuriser ↓ Pipe ↓ Relief tank	High aerosol concentration Water in relief tank	Fissium

Fissium: simulated by a mixture of CsOH, CsI, Te;

Corium: simulated by a mixture of Ag, Mn

Table 5.3-3 MARVIKEN-V, Aerosol concentration and retention in different components (in %)

Test	1	2A	2B	4	7
Aerosol concentration g/m ³	35	62	51	132	52
Retention, %					
Reactor vessel	-	-	-	30	11
Piping to pressuriser	-	-	-	8	3
Pressuriser	32	14	45	25	6
Piping to relief tank	4	1	5	11	20
Relief tank	10	85	49	26	59
Scrubber	41				
Final filter	0.3	0.1	0.04	0.1	0.2

Reference

- [1] J.O. Liljenzin, J. Collén, W. Schöck, F.J. Rahn Report from the MARVIKEN-V / DEMONA / LACE Workshop Proceedings of the OECD/NEA Workshop on Aerosol Behaviour and Thermal-Hydraulics in the Containment, Fontenay-aux-Roses (France), 26-28 Nov. 1990 CSNI Report No. 176

5.3.3 LACE

The LACE tests [1-4, 6] were sponsored by an international consortium in the later half of the 1980's when the understanding and identification of issues concerning aerosols in nuclear reactor accidents were still developing. These tests investigated the behaviour of aerosols in high velocity gas flows and in large models of containment buildings. Four LA tests were conducted. One of these tests, LA3, consisted of three phases denoted by LA3A, LA3B, and LA3C. These LA tests were supplemented by three tests of aerosol behaviour in high velocity gas flow through pipes called the 'Containment Bypass' or CB tests [5].

The facility used in the LA and CB tests is shown in Fig. 5.3-5. It consists of a piping system connected to an 852 m³ volume used variously to simulate an auxiliary building or a reactor containment building. In tests of aerosol behaviour in high velocity gas flows, only the piping system of the facility was used.

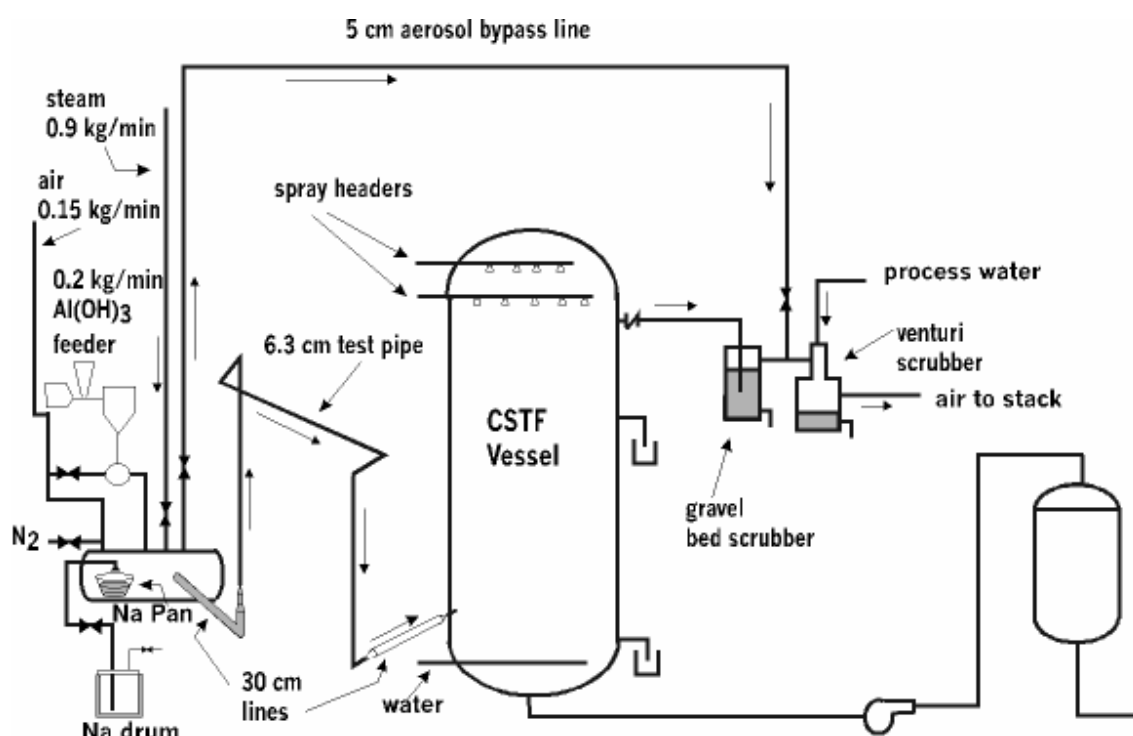


Fig. 5.3-5 Schematic diagram of the facility used for the LACE tests

For the LA tests, the piping system was a 6.3 cm diameter, about 28 m long pipe with six 90° bends, two vertical sections and four horizontal sections. In the CB tests, the 6.3 cm pipe connected to a 30 cm diameter pipe and then to a scrubber.

Some of the details of the LA tests are shown in Table 5.3-. Test objectives and the qualitative results of the tests are:

- **LA-1:**

The LA-1 test was intended to simulate a containment bypass accident sequence with aerosol passing through the reactor coolant piping system into a reactor auxiliary building vented to the air. The aerosol used in this and other LA tests was a mixture of water-soluble CsOH and insoluble MnO. More than 98 % of the aerosol was retained in the piping system. The aerosol behaviour in the auxiliary building model is shown in Fig. 5.3-6. Revaporization of deposited aerosol was not investigated in the test.
- **LA-2:**

The LA-2 test examined the leakage from a containment volume with relatively large leaks at elevations of 26.5 and 4.0 meters. The test was to explore the possibility of density stratification of the aerosol-laden gas phase in the containment model much as had been suggested by results of the DEMONA tests. About 38 % of the injected aerosol mass was allowed to leak from the containment volume. No significant differences were observed in the mass escaping through high and low leaks and it was concluded that no significant stratification of the gas phase in the containment volume occurred.
- **LA-3:**

The LA-3 test examined aerosol behaviour in high velocity flows through the piping system only. The 3 phases of the test examined the effects of the gas velocity and the ratio of soluble, liquefied, aerosol and insoluble, solid aerosol. In general, 70 % or more of the aerosol material was retained in the piping system. Again, revaporization of the deposited aerosol was not studied in the LACE program.
- **LA-4:**

The LA-4 test examined the behaviour of aerosol in a containment. Cesium hydroxide aerosol was injected for 50 minutes after the start of the test. MnO aerosol injection was started after 30 minutes and continued for 50 minutes. During aerosol injection, the pressure in the containment model increased to about 3 bar. It was held at this pressure for 200 minutes and, then, the containment model was depressurised to simulate containment failure.

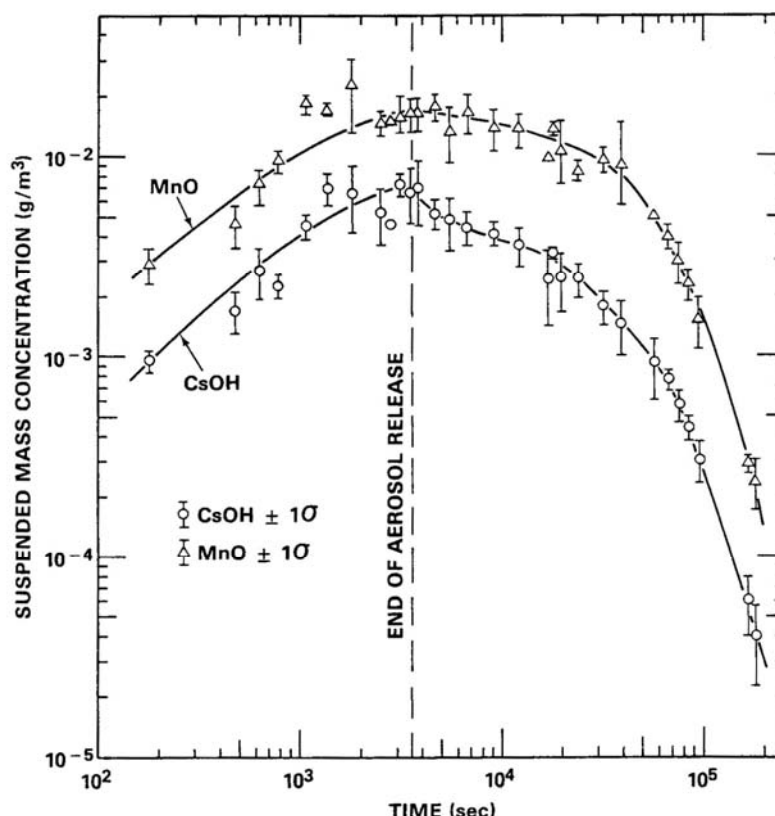


Fig. 5.3-6 Aerosol behaviour in the auxiliary building model during the LA-1 test

The CB tests examined aerosol behaviour in high velocity gas flows and were conducted much like the LA-1 test though there were some differences in the piping system. Features of the tests are shown in Table 5.3-5. The tests showed that large quantities of aerosol can be retained in the piping system. The dispositions of aerosol following the tests are shown in Table 5.3-6. The variations in the amounts of materials retained in the piping system in these tests strongly suggest that very hygroscopic aerosol such as NaOH particles behave quite differently than aerosol materials like $\text{Al}(\text{OH})_3$ that are much less hygroscopic. The pertinence of this observation to reactor accidents depends critically on the chemical forms of materials released as aerosol during the accidents.

References

- [1.] F.J. Rahn Summary of the LWR Aerosol Containment Experiments (LACE) Program - Interim Report LACE TR-012, Electric Power Research Institute, Palo Alto, CA, January 15, 1987
- [2] R.K. Hilliard, L.D. Muhlestein, T.J. Albiol, Final Report of Experimental Results of LACE Test LA2 - Failure to Isolate Containment LA-TR-007, Westinghouse Hanford Company, Richland, WA, June 1987
- [3] D.R. Dickinson, R.K. Hilliard, L.D. Muhlestein D.C. Mecham, G. Carraro Aerosol Behaviour in LWR Containment Bypass Piping - Results of LACE Test LA3 LACE TR-011, July 1987

- [4] J.D. McCormack, R.K. Hilliard, J.M. Slgado Final Report of Experimental Results of LATE Test LA4 - Late Containment Failure with Overlapping Aerosol Injection Periods LACE-TR-025, October 1987
- [5] G.R. Bloom, R.K. Hilliard, J.D. McCormack, L.D. Muhlestein Aerosol Behaviour Under LWR Containment Bypass Conditions - Results of Tests CB-1, CB-2, and CB-3 LACE TR-001, Westinghouse Hanford Company, Richland, WA, November 1986
- [6] T.A. Allbiol, J.D. McCormack, L.D. Muhlestein Instrumentation and Measurement Techniques Used in the LACE Program LACE TR-006, Hanford Engineering Development Laboratory, Richland, WA, June 1987

Table 5.3-4 Features of the LA tests

Test	CsOH input rate (g/s)	MnO input rate (g/s)	input gas velocity* (m/s)	aerodynamic mass median diameter (µm)	geometric standard deviation	Auxiliary building temperature (K)
LA-1	1.8	2.3	97	1.64	1.91	388 P = 1.1 bar
LA-2	0.63	0.68		1.7	1.7	P varies 1.1 to 2.2 bar
LA-3						
-3A	0.11	0.51	75	1.4	2.0	not used
-3B	0.10	0.76	24	2.4	2.0	not used
-3C	0.34	0.56	23	1.9	2.1	not used

* velocity at the start of the piping system. Because of pressure drop through the piping system, velocity increases along the piping system.

Table 5.3-5 Features of the CB tests

Test	Aerosol Composition	Aerosol input rate (g/s)	Aerodynamic Mass Median Diameter (μm)	Geometric Standard Deviation	Input Gas Velocity (m/s)	Gas Temperature (K)	Auxiliary Building Temperature (K)
CB-1	100 % NaOH	3.0	3.9	2.9	100	459	358
CB-2	67 % NaOH 33 % $\text{Al}(\text{OH})_3$	0.9	3.1	2.6	91	384	354
CB-3	100 % $\text{Al}(\text{OH})_3$	2.0	4.3	2.5	97	433	351

Table 5.3-6 Disposition of aerosol in the CB tests and the LA-1 test

Test	Retained in Pipes* (%)	Auxiliary Building		
		horizontal surfaces (%)	walls (%)	vented (%)
CB-1	58	26.9	7.1	8.0
CB-2	48	33.8	9.9	8.3
CB-3	14	46.4	5.2	34.4
LA-1	98	<1	-	<1

5.3.4 ACE-B: large scale combined effects experiment

One large scale experiment was conducted at the Containment Systems Test Facility (CSTF) located at the Hanford site in the USA. The CSTF, shown in Fig. 5.3-7 was consisted of an aerosol generation facility, a test vessel (volume 852 m^3) and associated equipment. The internal surface of the test vessel was painted with the same epoxy coating as used in the RTF or laboratory scale ACE experiments. The purpose of the large scale experiment was to evaluate the effectiveness of volatile iodine sinks (i.e., bulk aerosols, painted surfaces, steam condensation and water reservoirs). Fig. 5.3-8 shows various phases of the experiment. CsOH and MnO aerosol particles were fed in the test vessel in the first two phases. In addition, HI , in the first phase, and I_2 , in the second phase, were injected. Steam was continuously fed in order to keep the vessel wall at 100°C for duration about 4.5 days. The pH value of the sump was kept at 5.6 until the I_2 injection, during which it was simultaneously increased to 8.5. The thermal-hydraulic parameters, temperatures, pressure, wall condensation rate, pool water amount, were measured and the deposition coupon samples were collected.

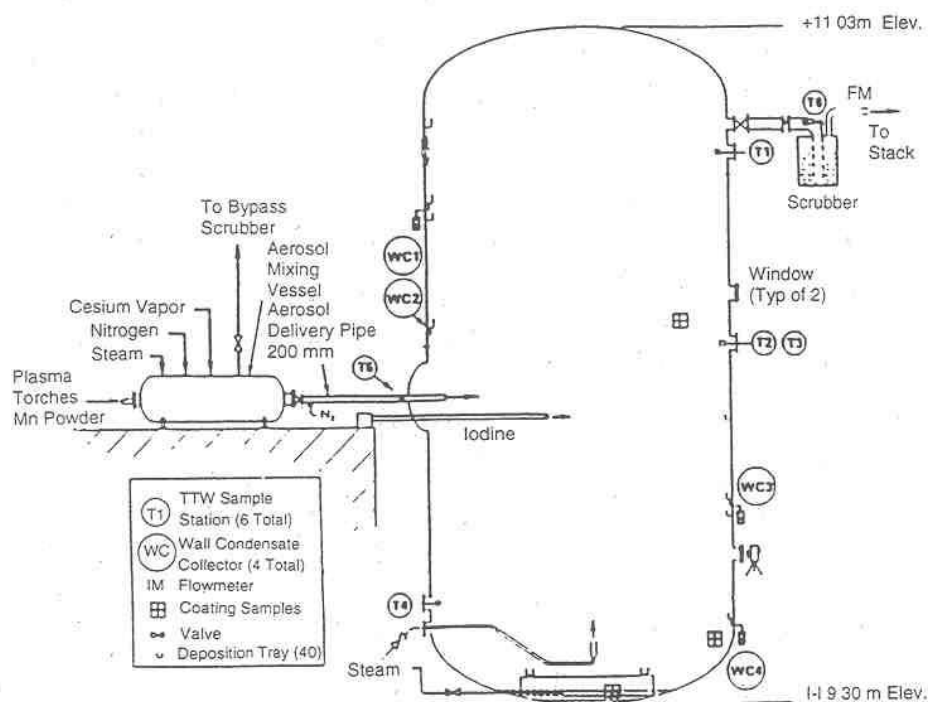


Fig. 5.3-7 Diagram of the CSTF test arrangement

The major output of the experiment was that both forms of iodine, HI and I₂, were removed from the atmosphere at the same rate as the aerosol material. The aerosol material (CsOH) had experienced significant particle growth due to its hygroscopic nature which then enhanced the removal rate by sedimentation. Airborne organic iodine constituted only 0.2 % of the initially introduced iodine after the major species had been removed from the atmosphere by settling or deposition. Fig. 5.3-9 shows the total iodine and particulate iodine concentration measured in the test vessel atmosphere during the experiment.

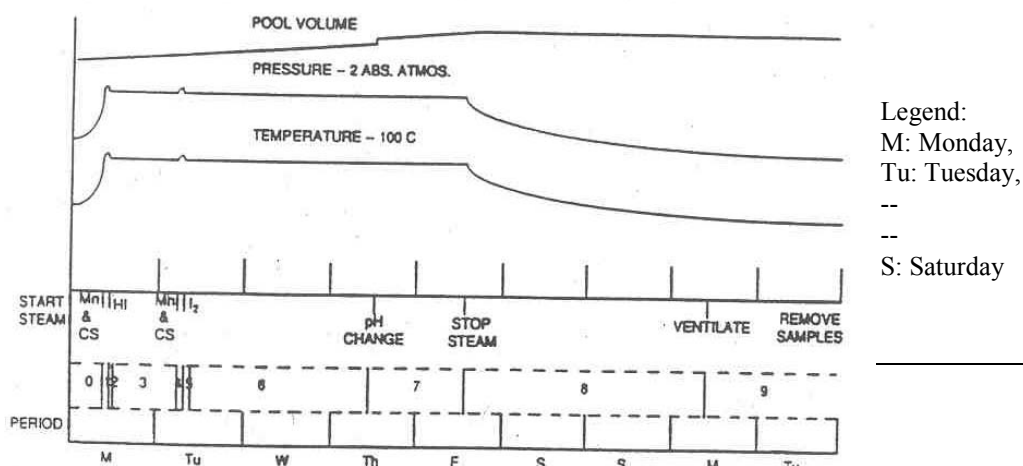


Fig. 5.3-8 The CSTF iodine experiment test sequence

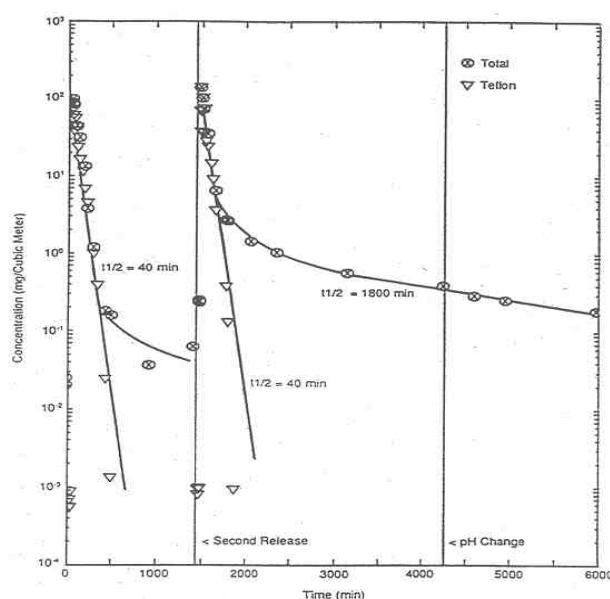


Fig. 5.3-9 Total iodine and particulate iodine concentration measured during the CSTF experiment

5.3.5 VANAM (including ISP-37)

The VANAM tests (1988 – 1993) provided relevant experimental data for the validation of coupled thermal hydraulic and aerosol codes for accident analyses [1]. Five large-scale tests were carried out in the 626 m³ Model Containment of the Battelle Institut in Frankfurt/Main. The main features of the VANAM tests were:

- Multi-compartment geometry with locally different thermal hydraulic conditions
- Local volume condensation and its effect on aerosol depletion
- Behaviour of insoluble and hygroscopic aerosol materials in saturated and super-saturated steam-air atmospheres
- Impact of a hydrogen deflagration on aerosol behaviour (dry resuspension)

Table 5.3-7 gives an overview of the five VANAM tests. In test M4 the dry resuspension of settled aerosol by a hydrogen deflagration was measured. Although the deflagration was rather mild a significant resuspension effect was observed.

Table 5.3-7 Overview of the VANAM tests

Test	Aerosol Material	Description
M1	SnO ₂	Dry aerosol depletion period followed by a wet depletion period with weak volume condensation
M2	SnO ₂	Dry aerosol depletion period followed by a wet depletion period with strong volume condensation
M2*	SnO ₂	Dry aerosol depletion period followed by a further aerosol injection and a wet depletion period
M3	NaOH	Dry aerosol depletion period followed by a further hygroscopic aerosol injection and a wet depletion period; Subject of ISP-37
M4	SnO ₂ + NaOH	Dry aerosol depletion period followed by a hydrogen-air-detonation with aerosol resuspension (Scoping Test)

The VANAM test M3 was subject of the International Standard Problem (ISP) No. 37 which dealt with thermal hydraulics and aerosol behaviour in a LWR containment following a severe accident with core melt down [2]. Only this test is described in more detail here.

The Battelle Model Containment (BMC) was made of reinforced concrete and consisted of nine individual compartments interconnected by vent openings (Fig. 5.3-10). In the first test phase the BMC was heated up by steam injected into compartment R5, representing the blowdown of the primary circuit over the pressuriser quench tank. Then in test M3 a hygroscopic NaOH aerosol generated by three plasma torches was injected into the steam-air-atmosphere during two separate periods. During and after the first injection the non-condensing containment atmosphere was stratified causing an inhomogeneous NaOH aerosol distribution. In the dome and in the upper compartments the NaOH concentration was significantly higher than in the lower compartments. The depletion of the hygroscopic NaOH aerosol was somewhat faster than the depletion of the insoluble SnO_2 in test M2* under similar conditions (r.h. approx. 90 %) because of the hygroscopic water take up.

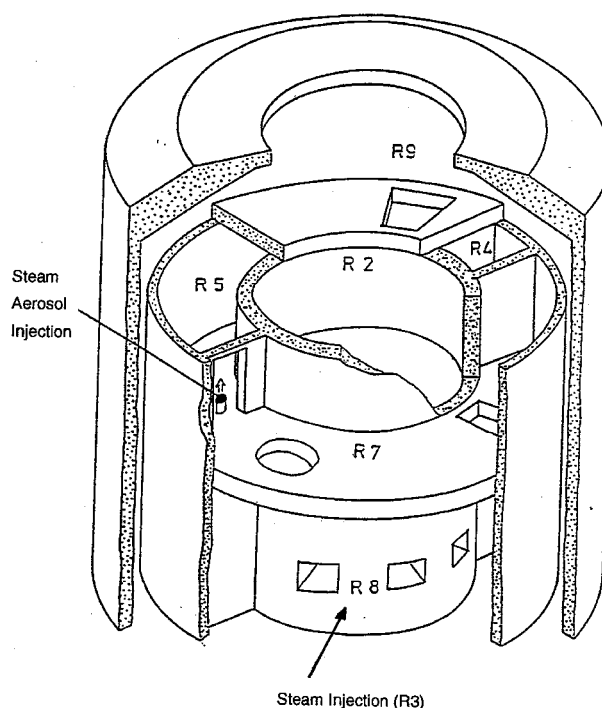


Fig. 5.3-10 Battelle Model Containment in the configuration for VANAM M3

After the second NaOH aerosol injection representing the aerosol release from the core concrete interaction steam was injected into the central bottom compartment. This steam production was corresponding to a contact of core melt to sump water and induced a natural convection which mixed the atmosphere in large parts of the containment. In most compartments the rising steam content caused volume condensation which increased the aerosol depletion significantly. Only in the annular part of R9 no volume condensation occurred and the measured NaOH concentration there was for many hours up to two orders of magnitude higher than in the other compartments (Fig. 5.3-11).

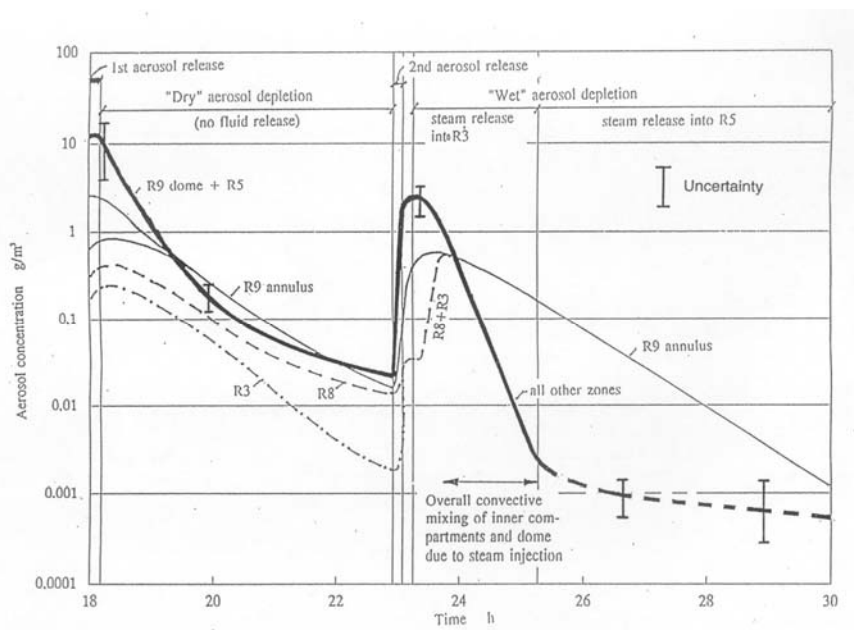


Fig. 5.3-11 Measured NaOH aerosol concentration in test VANAM M3

The ISP-37 consisted of a thermal hydraulic and an aerosol part. Main objective of the aerosol part of the open exercise (the participants knew all relevant test results) was to calculate the inhomogeneous distribution and the depletion of the NaOH aerosol. Representatives of 22 organisations from 9 OECD member countries, two non-OECD countries and the CEC submitted a total of 23 thermal-hydraulic and 22 aerosol calculations. They used the codes CONTAIN, ECART, FIPLOC (a precursor of COCOSYS), and MELCOR for coupled thermal-hydraulic and aerosol calculations, and MACRES, MOSAIC and REMOVAL for stand alone aerosol calculations.

Fig. 5.3-12 to Fig. 5.3-14 show the results of the predominantly used codes. In the MELCOR standard version the solubility effect was not modelled. The user's influences on the CONTAIN and FIPLOC results are high.

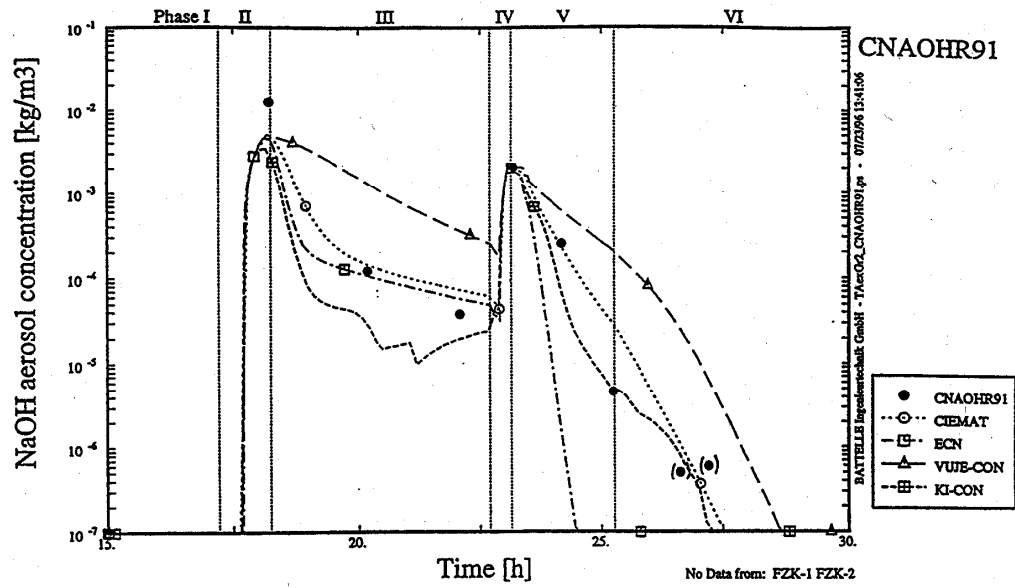


Fig. 5.3-12 ISP-37; NaOH aerosol concentration in the dome (CONTAIN)

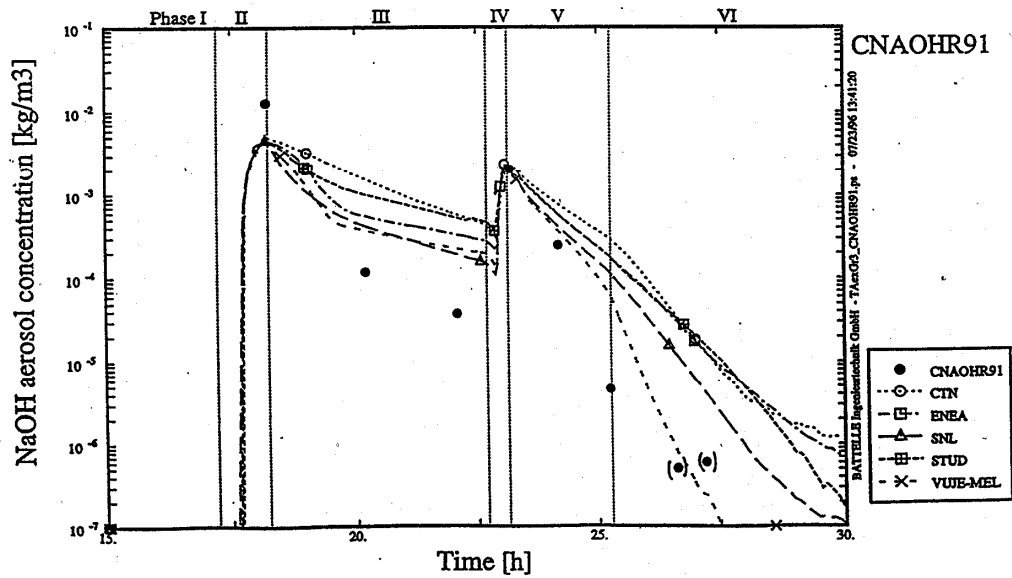


Fig. 5.3-13 ISP-37; NaOH aerosol concentration in the dome (MELCOR, part 1)

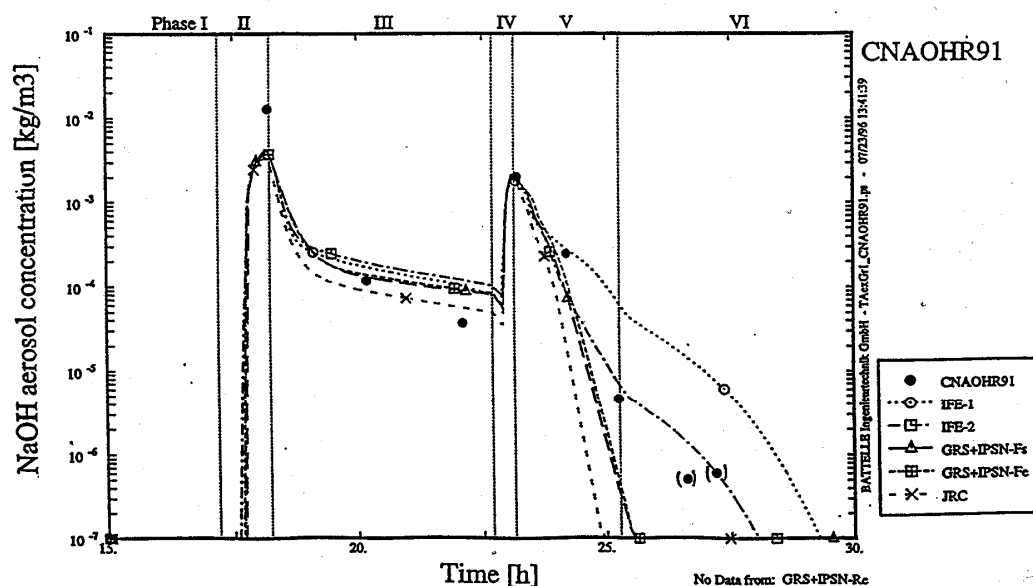


Fig. 5.3-14 ISP-37; NaOH aerosol concentration in the dome (FIPLOC)

With most codes the thermal-hydraulic behaviour (pressure, temperatures, etc.) was calculated with sufficient accuracy. But with respect to the needs of aerosol behaviour analysis the accuracies, both analytical and experimental, of specific thermal-hydraulic variables like humidity, wall condensation and heat transfer should be improved.

All codes with a tight coupling of thermal hydraulics and aerosol physics, i.e. CONTAIN, FIPLOC, and MELCOR, predicted the tendency of the aerosol concentration during the course of the experiment well. But the actually calculated NaOH concentrations showed a spread of approximately two orders of magnitude at the end of the “dry” depletion phase and about five orders of magnitude at the end of the “wet” depletion phase. Mostly the NaOH aerosol concentrations were overpredicted due to an underestimation of the droplet growth by steam condensation, e.g. because of a missing solubility model. With respect to reliable source term analyses some discrepancies are clearly too large.

In [1] the ISP-37 outcomes are summarised as follows:

Although much progress has been made in the simulation of aerosol behaviour in multi-compartment geometries the calculated local concentrations scatter widely. However, the aerosol source term to the environment is overestimated in general. The largest uncertainty concerning the aerosol results is caused by a limited number of thermal hydraulic variables like relative humidity, volume condensation rate and atmospheric flow rate. In some codes a solubility model is also missing.

By choosing a physically correct nodalization⁸ the lumped-parameter concept was found to be basically suited to predict the inhomogeneous distributions of gases and aerosols in the containment. But the user has great influence on the calculated results, both the thermal-hydraulic and the aerosol ones if specific nodalization features and different code options are selected unfavourably.

⁸ physically correct nodalisation means:

The nodalisation allows the simulation of all relevant phenomenon, probably occurring in the case investigated

References

- [1] M. Firmhaber, T.F. Kanzleiter, S. Schwarz, G. Weber International Standard Problem ISP-37 VANAM M3 - A Multi Compartment Aerosol Depletion Test with Hygroscopic Aerosol Material NEA/CSNI/ R(96)26 (Dec. 1996)
- [2] T. Kanzleiter Versuche zum Verhalten von Kernschmelzunfall-Aerosolen in einer Mehrraum-Containment-Geometrie ("VANAM-Versuche") Battelle-Institut e.V., Frankfurt am Main Abschlussbericht BleV-R67.098-01 (1995)

5.3.6 KAEVER (including ISP-44)

In the KAEVER (**K**ernschmelz-**A**erosol-**V**ersuche) project carried out from 1993 to 1997 at the Battelle Institut in Frankfurt/Main the depletion behaviour of aerosols typical for LWR core melt accidents under various thermal hydraulic conditions was measured [1]. The KAEVER tests are complementary to the large scale tests of e.g. the VANAM and the LACE series in which the number of tests was limited due to high the costs.

As test aerosols the insoluble materials Ag and SnO₂ as well as the hygroscopic materials CsI and CsOH were used. Single-component aerosols as well as mixed-component aerosols were investigated. The horizontal cylindrical test vessel made of steel had a volume of 10.6 m³. Large parts of the walls were as well thermally insulated as equipped with a wall heating (Fig. 5.3-15).

Some tests were repeated with the same aerosol and the same thermal hydraulic conditions in order to check the reproducibility of the results (e. g. tests K100/K102 and K125/K148). All these tests could be reproduced well. The differences in the results were insignificantly.

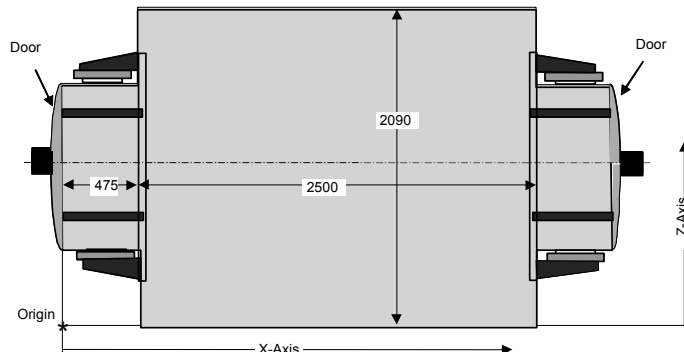


Fig. 5.3-15 Top view of the KAEVER test vessel (numbers in mm)

The thermal hydraulic conditions for the tests have been varied between rather dry conditions (r.h. $\approx 0\%$) and saturated conditions with strong volume condensation. The conditions "slightly supersaturated" and "strongly supersaturated" were achieved by two different test procedures. E. g. in the strongly supersaturated tests the aerosol was injected into the cold test vessel followed by steam. The estimated condensation rate for strongly supersaturated conditions (strong volume condensation rate) is 10^{-4} kg/(s·m³). This for slightly supersaturated conditions (weak volume condensation rate) is 10^{-5} kg/(s·m³). A total of 190 tests was performed. 33 of these were evaluated in detail (Table 5.3-8).

Table 5.3-8 Evaluated KAEVER tests

Test	Aerosol	Thermalhydraulic conditions (rh = relative humidity)	Remarks
K100	CsI	rh = 0 %	
K102	CsI	rh = 0 %	repetition of K100
K106	CsI	rh = 85 - 90 %	
K108	CsI	rh = 95, goal 100 %	
K110	CsI	rh = 95, goal 100 %	repetition of K108
K123	CsI	rh = 100 %, weak volume condensation	ISP-44
K125	Ag	rh = 100 %, weak volume condensation	
K128	Ag + CsI	rh = 0 %	
K130	Ag + CsI	rh = 100 %, weak volume condensation	
K131	Ag	rh = 85 - 90 %	
K132	Ag + CsI	rh = 85 - 90 %	
K134	Ag + CsI	rh = 85 - 90 %	repetition of K132
K138	SnO ₂	rh = 85 - 90 %	
K143	SnO ₂	rh = 100 %, weak volume condensation	
K148	Ag	rh = 100 %, weak volume condensation	repetition of K125, ISP-44
K149	Ag	rh = 85 - 90 %	repetition of K131
K150	no aerosol	rh = 100 %, weak volume condensation	fog formation test
K151	Ag	strong volume condensation, steam released into cold vessel	
K156	no aerosol	rh = 100 %, weak volume condensation	fog formation test
K159	CsI	strong volume condensation, steam released into cold vessel	
K167	CsOH	rh = 0 %	
K168	CsOH	rh = 95 %	
K171	Ag + CsOH	rh = 85 - 90 %	
K174	CsOH	strong volume condensation, steam released into cold vessel	
K175	Ag + CsI	strong volume condensation, steam released into cold vessel	
K178	Ag + CsOH	strong volume condensation, steam released into cold vessel	
K179	CsI + CsOH	rh = 100 %, weak volume condensation	
K181	CsOH	rh = 85 - 90 %	
K183	CsI + CsOH	rh = 85 - 90 %	
K186	Ag + CsOH	rh = 100 %, weak volume condensation	ISP-44
K187	Ag + CsI + CsOH	rh = 100 %, weak volume condensation	ISP-44
K188	CsOH	rh = 100 %, weak volume condensation	ISP-44

Fig. 5.3-16 gives an overview of the experimental KAEVER results. It shows the normalised⁹ aerosol depletion rates measured for different aerosol components and different thermal hydraulic conditions. The depletion rates in general increase with rising saturation ratio respectively rising volume condensation rate because of the particle growth by condensation. The influence of the hygroscopic effect can be seen clearly. CsI is weakly hygroscopic (Van't Hoff factor 1.7) and CsOH strongly (2.0). Under supersaturation conditions, with weak as well as with strong volume condensation, the depletion rate of CsOH is always the largest one.

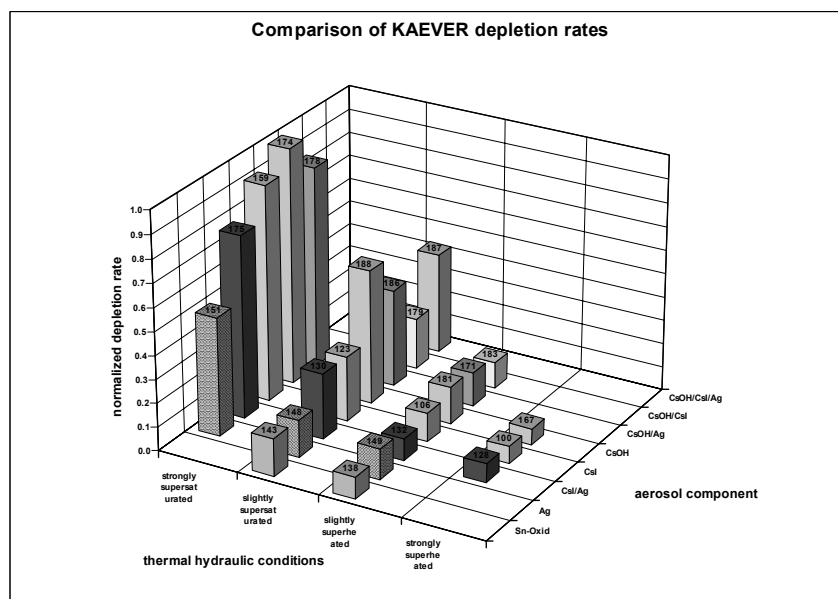


Fig. 5.3-16 Comparison of depletion rates measured in the KAEVER tests

Five KAEVER tests were selected for the International Standard Problem ISP-44 which dealt, like the earlier ISP-37, with thermal hydraulics and aerosol behaviour in a LWR containment following a severe accident with core melt down [2]. In this exercise the main emphasis was put on the depletion behaviour of different aerosol materials under thermal hydraulic conditions expected in a LWR severe accident scenario over longer periods. The KAEVER tests selected were in particular:

- K 148, test with insoluble Ag-aerosol
- K 123, test with hygroscopic CsI-aerosol
- K 188, test with strongly hygroscopic CsOH-aerosol
- K 186, test with mixed aerosol of Ag and CsOH
- K 187, test with a Ag-CsI-CsOH mixture (blind calculation)

The vessel geometry, the tests procedure and the thermal hydraulic conditions were the same in all tests. First the vessel was preconditioned by release of steam and heat until quasi-stationary conditions were obtained. In all selected tests the atmosphere was slightly supersaturated causing some condensation on the insoluble Ag-aerosol and an increasing condensation on the soluble aerosols respectively. Then the thermally generated aerosols were injected and the depletion of the aerosols in the vessel was measured without any change of the boundary conditions.

⁹ in each case related to the maximum value for aerosol concentration measured in each test

Representatives of 10 organisations from 9 countries participated in the ISP-44. The codes used were ASTEC-V0.3 (GRS-IPSN), COCOSYS V1.2 (GRS, RUB), CONTAIN 2.0 (IJS), MELCOR 1.8.3 (VEIKI), 1.8.4 (Studsvik, JRC, KAERI), 1.8.5 (NRI) and ART Mod2/REMOVAL (JAERI). Open calculations were performed on all tests except K 187, which was offered as a blind exercise.

Several discrepancies occurred concerning the test with insoluble and slightly soluble materials. Fig. 5.3-17 and Fig. 5.3- 18 show the results of test K148 with a Ag-aerosol. It has to be said that several calculations showing a good agreement with the measured aerosol concentration histories show other results which are inconsistent with the measurement. E.g. four calculations show no airborne water and in one calculation the water mass is far too high. Therefore only two out of nine calculations are in a good agreement with the experimental results.

In MELCOR calculations on the three tests with the strongly hygroscopic CsOH the droplet growth was either significantly overestimated or the solubility effect is simply ignored. The blind test K187 with a Ag/CsI/CsOH-aerosol was well calculated by four out of ten participants. The other calculations showed larger deviations from the measurement, e.g. no airborne water was calculated. Fig. 5.3-19 and Fig. 5.3-20 depict the results for test K187.

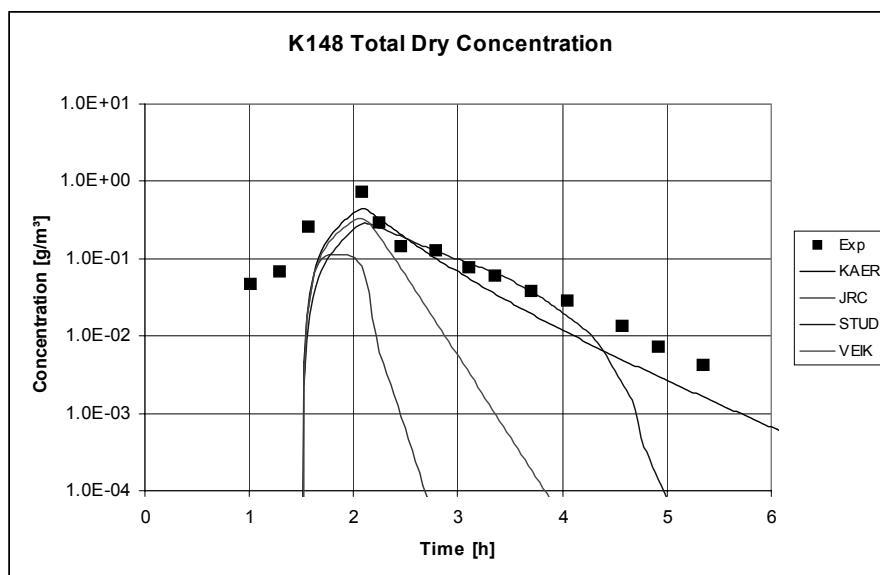


Fig. 5.3-17 KAEVER test K148, Ag-aerosol concentration (MELCOR)

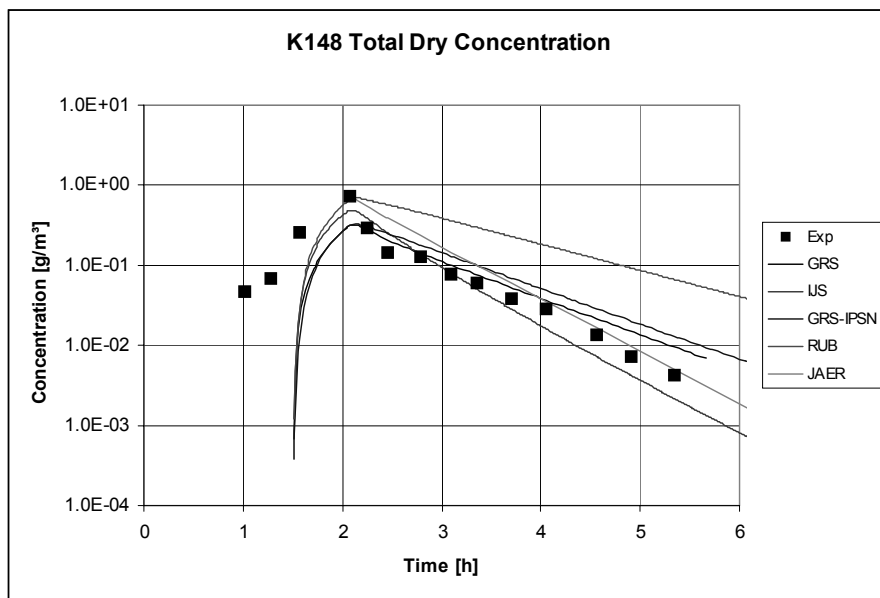


Fig. 5.3-18 KAEVER test K148, Ag-aerosol concentration (miscellaneous codes)

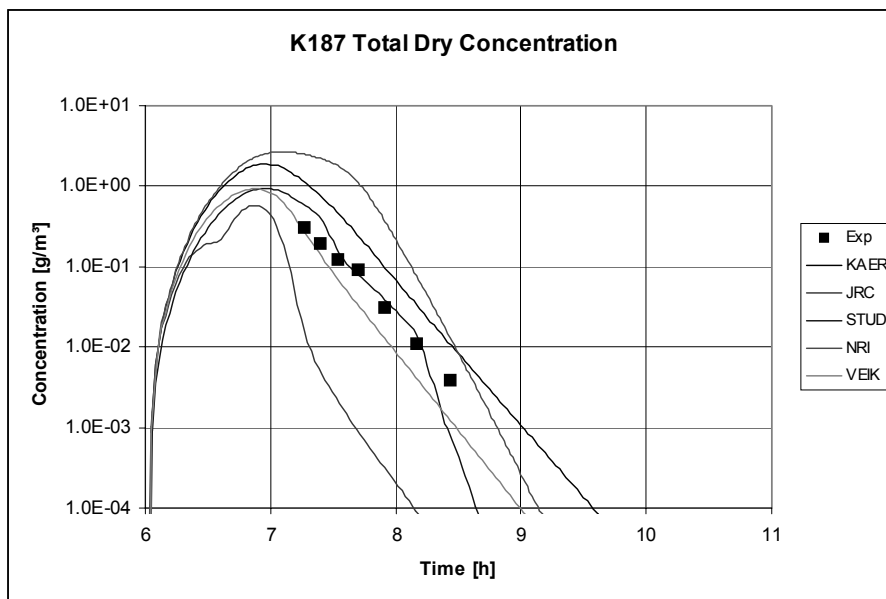


Fig. 5.3-19 KAEVER test K187, Ag/CsI/CsOH-aerosol concentration (MELCOR)

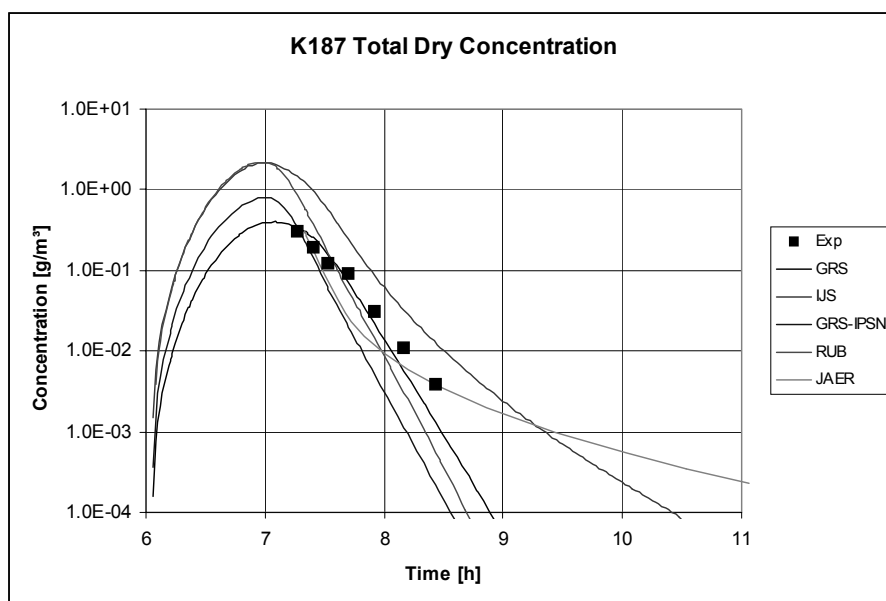


Fig. 5.3-20 KAEVER test K187, Ag/CsI/CsOH-aerosol concentration (miscellaneous codes)

In ISP-44 the agreement of the results with the measurements of these fairly simple tests was not as good as expected. In particular the aerosol condensation modeling and the accuracy of related thermal hydraulic parameters were insufficient with some codes.

- The solubility effect increases the growth of hygroscopic particles by condensation and enhances the aerosol depletion. An appropriate modeling is absolutely necessary. The solubility model in MELCOR needs some corrections.
- The Kelvin-effect may slow down the depletion of insoluble and slightly soluble aerosols in a condensing atmosphere. There are indications that the Kelvin-effect is not treated sufficiently by any codes except ASTEC and COCOSYS. The modeling of the Kelvin-effect should be checked. In some codes the numerical stability should be improved (e.g. COCOSYS).

In calculations with a correct aerosol condensation treatment the largest discrepancies in the aerosol results were caused by the uncertain thermal-hydraulic variables “relative humidity” and “volume condensation rate”.

The multi-component behaviour in the KAEVER tests was fairly easy to calculate, because the components were well mixed among all particles. Experiments with incompletely mixed aerosol components are needed to validate the multi-component capability of codes, as in an incompletely mixed aerosol the composition of components is not the same for all particles.

ISP-44 showed a large user influence on the thermal hydraulic and aerosol results. Possible measures to reduce this influence are the improvement of code input assistance, user training, further benchmarks, etc.

The KAEVER experiments calculated for ISP-44 had some measurement uncertainties (relative humidity, wet droplet size, aerosol injection rate, etc). In future tests the measurement accuracy of important parameters should be improved.

In the ISP-37 on test VANAM M3 all codes were already used except the new ones ASTEC and COCOSYS. The earlier exercise comprised the depletion of a strongly hygroscopic aerosol in a

multi-compartment geometry and was more complex than ISP-44. Among the most uncertain variables and models analysed were already “volume condensation rate”, “relative humidity”, and the solubility model. This demonstrates the necessity to perform several exercises on an important topic within a certain time.

References

- [1] G. Poss, D. Weber Versuche zum Verhalten von Kernschmelzaerosolen im LWR-Containment-KAEVER Fachbericht BF-R-67863, Battelle Ingenieurtechnik GmbH, Mai 1997
- [2] M. Firnhaber, K. Fischer, S. Schwarz, G. Weber ISP 44 – KAEVER Experiments on the Behaviour of Core-melt Aerosols in a LWR Containment NEA/CSNI/R (2003)5 (Aug. 2002)

5.3.7 AHMED

Introduction

The AHMED facility was constructed by VTT (Technical Research Centre of Finland) to study the effect of T-H on hygroscopic and inert aerosol behaviour in nuclear power plant containment during a hypothetical severe reactor accident. The objective of this work was to understand the reason for the observed large discrepancies between the results from model calculations and measurements carried out in large scale experiments. The discrepancies may be caused by inaccuracies in aerosol modelling, uncertainties in T-H conditions or measurement errors.

Facility description and instrumentation

Hygroscopic NaOH, CsOH and CsI and inert Ag aerosol behaviour at different temperatures and relative humidities (RH) was studied in a well instrumented and controlled AHMED vessel of 1.81 m³ total free volume. The relevant parameters of the vessel are presented in Table 5.3-9.

Special emphasis was placed on temperature measurements, because of homogeneous temperature field inside the vessel was necessary for the experiments. The vessel gas temperature (13 locations), inside and outside surface temperatures (14 locations) and surround temperatures as well as pressurised air and steam temperatures were measured using Pt-100 resistance type detectors (RTD). The RH was measured using three Vaisala Humicap detectors.

Table 5.3-9 System parameters

Vessel volume	1.81 m ³
Vessel radius	63.5 cm
Vessel height	142.5 cm
Sedimentation area	1.27E4 cm ²
Pressure	1 atm
Sampling rate	2.6 l/min (206 % of volume/24h)

The vessel and input line pressures and steam and air flows were also monitored continuously. Input air flow was filtered and dried. The vessel surface temperature was controlled using computer controlled heating cables. The input gas temperature was regulated using a heat exchanger.

For aerosol characterisation state-of-the-art aerosol measurement systems were used. Aerosol number and mass concentrations were measured continuously using a condensation nuclei counter (CNC) and a tapered element oscillating microbalance (TEOM) mass monitor. Before the measurement the aerosol was dried in an ejector-type diluter and in diffusion drier. Aerosol sampling into the diluter could be done from three heights through heated sampling lines.

The dry size of the particles was measured using Berner low pressure impactors (BLPI). The results were compared to measurements done with a TSI aerodynamic particle sizer (APS). A differential electrical mobility analyser (DMA) was used to check that the amount of small particles was negligible.

The particle size distribution and chemical composition in the test conditions (wet particle size) were analysed by Berner low pressure impactors (BLPI). Some size distribution measurements were also made with a PALAS PCS-2000 Optical Particle Counter.

Spherical aerosol particles were generated from water solutions of aerosol material using ultrasonic aerosol generator. Spherical Ag particles were made from $\text{AgNO}_3 + \text{H}_2\text{O}$ droplets utilising a Lindberg tube furnace at 900 °C. In order to ensure that no AgNO_3 particles were produced, the solubility of Ag particles collected on Nuclepore polycarbonate impactor foils to water and nitric acid was measured with ICP-MS. The Aerosol was always generated in the same way and it was also checked that the size distribution was same during different generation times.

Experiments

At first the behaviour of aerosol of different chemical species was studied separately in AHMED facility. Finally both Ag and CsOH aerosol particles were generated and injected into the AHMED vessel simultaneously to study the behaviour of multicomponent aerosol. The temperature in the experiments was varied between 17 °C and 51 °C and the RH between 7.3 % and 97 %. Approximate temperatures and RHs during the different experiments, mass and number concentrations as well as aerodynamic mass median diameters (AMMD) and geometric standard deviations (GSD) of the dry particle size distributions at the beginning of the experiments are presented in Table 5.3-10

Before the experiments the vessel was purged with filtered air. It was also checked that the aerosol number concentration measured with CNC was practically zero. After the aerosol generation was stopped the aerosol in the vessel was mixed with a propeller having a very small sedimentation area to ensure constant homogeneous concentration in the AHMED vessel. After the mixing the aerosol particles were settled in the calm air and the aerosol mass and number concentrations were monitored continuously over 300 minutes. From this data the decay rate of different aerosols used in the AHMED experiments can be characterised by a decay constant in a logarithmic scale.

Table 5.3-10 Experimental parameters

Material	RH [%]	T [°C]	AMMD [µm]	GSD	Mass conc. [mg/m ³]	Number conc. [1/cm ³]
NaOH	22	50	2.4	1.6	112	64 000
NaOH	34	20	2.4	1.6	200	65 000
NaOH	82	27	2.4	1.6	208	137 000
NaOH	91	17	2.4	1.6	638	400 000
NaOH	96	23	2.4	1.6	218	165 000

Material	RH [%]	T [°C]	AMMD [μm]	GSD	Mass conc. [mg/m ³]	Number conc. [1/cm ³]
CsI	27	23	2.3	1.7	102	71 820
CsI	82	24	2.3	1.7	98	94 500
CsI	96.5	27	2.3	1.7	94	92 700
CsOH	7.3	51	2.1	1.7	89	91 000
CsOH	33	19	2.1	1.7	86	48 000
CsOH	39	19	2.1	1.7	73	80 000
CsOH	96	23	2.1	1.7	64	77 000
CsOH	97	28	2.1	1.7	94	144 000
Ag	54	22	2.7	1.7	79	120 000
Ag+CsOH	91.5	24	2.1 (CsOH)	1.7	82	103 500
Ag+CsOH	91	25	2.1 (CsOH)	1.7	112	135 000
Ag+CsOH	97	24	2.1 (CsOH)	1.7	60	79 200

Results

Homogeneous temperature and RH conditions for aerosol measurements in the AHMED facility were achieved. The maximum gas temperature differences were measured to be smaller than 0.4 °C. Apart from the three sampling line connections the inside surface temperatures were 0.1 - 0.5 °C lower than the gas temperature. The slightly lower temperature is enough to cause the necessary natural convection for mixing and maintaining homogeneous aerosol concentration during the experiments [1]. Because the sampling lines were heated, the inside surface temperature at these locations was 0.5 °C higher than the gas temperature. The RHs were near each other at different locations inside the vessel and maintained nearly constant levels during experiments. During some experiments the RH changed slightly, which could also be seen on the measured wet particle size distribution.

Mass and number concentrations measured from three different heights were the same within the limits of the measurement accuracy. The total mass and number concentrations followed each others fairly well at the beginning of the experiments. Later the number concentration decayed slower than the mass concentration. This was probably due to the small particles, which settled slowly but could not be seen in the evolution of mass concentration. Mass concentration behaviour measured with TEOM and impactors also agreed fairly well. The calculated decay constants decreased as a function of time because large particles had higher sedimentation velocities.

For NaOH the ratio of aerosol mass concentration half lives at low to high RH experiments was about 4. For CsI and CsOH this ratio was about 2. This difference was due to the density effect. CsOH and CsI have higher densities than NaOH and thus during condensation their aerodynamic sizes do not increase as much as the AMMD of NaOH aerosol. The mass concentration half lives for CsOH and NaOH decreased smoothly as the RH was increased. For CsI the mass concentration behaved similarly as a function of time at RHs 27 % and 82 %. CsOH and NaOH absorb water at all RHs, but CsI starts to absorb water as the RH exceeds 91 %. The half life of silver aerosol was less than that of the other species. This was due to the

larger AMMD of the high density silver particles. However, silver behaved as a dry aerosol at all humidities. The AMMD of silver particles at high humidity was the same as in the dry conditions.

Dry size distributions measured with BLPI and APS agreed within the measurement accuracy. The wet mass size distributions measured only with BLPI showed that the AMMD of particles decreased as a function of time due to settling of larger particles. It could be seen that the hygroscopic particles reached their equilibrium size immediately after being exposed to high humidity. When there was a slight decrease in RH the AMMD of CsOH particles was also observed to decrease. The measured AMMD of CsOH particles was compared to the corresponding equilibrium values calculated from the literature data reported for the van't Hoff factor i . The equilibrium AMMD was calculated from the following equation [2]:

$$AMMD = AMMD_0 \left\{ \left(\frac{\rho_p}{\rho_{p,0}} \right)^{1/2} - \frac{iM_w}{M_s \left(\frac{1}{RH} - 1 \right)} + 1 \right\}^{1/3}$$

with

AMMD equilibrium diameter of the particle

AMMD₀ initial diameter of the dry particle

ρ_p density of the measured (wet) particle

$\rho_{p,0}$ density of the initial (dry) particle

i Van't Hoff factor

M_w molecular weight of water

M_s molecular weight of the soluble aerosol material

rh relative humidity

The Van't Hoff factor for CsOH is reported only down to 95.61 % RH [3]. Using this data, reliable values can be obtained by semi-empirical method down to 90 % [4, 5]. In Table 5.3-11 the measured and calculated AMMD values are presented. It can be seen that measured and calculated values agree within the measurement accuracy. This comparison supports both the AHMED measurements and the method to calculate equilibrium particle size.

Table 5.3-11 Measured and calculated AMMD of CsOH aerosol at different RH

	AHMED	Calculated
RH [%]	AMMD [μm]	AMMD [μm]
Dry	2.1	2.1
97.0	3.4	3.55
91.5	2.6	2.77
91.0	2.7	2.74

Conclusions

The AHMED experiments filled the gap on our knowledge of hygroscopic aerosol behaviour and the results can be used for aerosol model validation in containment codes. AHMED was the first facility where

the aerosol mass concentration could be monitored on-line and wet aerosol size distribution was measured directly in containment conditions. The behaviour of hygroscopic aerosol was observed to be very sensitive to RH at high humidity conditions. At the same RH the aerosol behaviour was not affected by changing the absolute temperature as can be expected from the available water activity data. As the steam condensation at supersaturated conditions is also well known [6], we may conclude that the data base for steam condensation on aerosol particles in containment conditions is sufficient for code validation.

References

- [1] N. Fuchs The mechanics of Aerosols. Pergamon Press, Oxford, pp. 250-257, 1964
- [2] J. Jokiniemi The effect of airborne hygroscopic matter on aerosol behaviour in severe nuclear power plant accidents Technical Research Centre of Finland, Publications 59 (Dissertation), 1990
- [3] R.A. Robinson, R.H. Stokes Electrolyte Solutions, 2nd rev. ed. Butterworth, London, 1970
- [4] H. Meissner Prediction of activity coefficients of strong electrolytes in aqueous systems ACS Series 133, pp. 495-511, 1980
- [5] J. Jokiniemi The effect of selected binary and mixed solutions on steam condensation and aerosol behaviour in containment Aerosol Sci. Technol. 13 (2), 1990
- [6] P. Wagner Condensation processes in aerosols J. Aerosol Sci. 26 S1, pp. 203-204, 1995

5.3.8 VICTORIA

5.3.8.1 Introduction

The VICTORIA facility [1] is a scale model of the ice condenser containment of Loviisa NPP with linear scale of 1:15 and volume scale of 1:3375. The height of the pressure vessel is 4.6 m and the diameter is 3.14 m.

The aim of aerosol experiments on the VICTORIA facility was to validate the containment aerosol models used in the nuclear reactor accident codes. Especially important was to ensure that containment aerosol codes were able to calculate correctly the radioactive hygroscopic and non-hygroscopic aerosol behaviour in non-homogeneous multicompartment containments.

Two research programmes has been carried out on the VICTORIA facility. In the earlier research programme (1990-1995) the thermal-hydraulic behaviour and hydrogen distribution were studied in severe accident conditions [2, 3]. During 1996-1997 VICTORIA was used in a modified geometry for aerosol experiments in a CEC Fourth Framework Programme project [4].

5.3.8.2 Facility description

Since experiments with VICTORIA facility were a part of the CEC Fourth Framework Programme project Aerosol Physics in the Containment, details of the facility and its instrumentation is included in the Asterism database.

VICTORIA containment

The dimensions of the pressure vessel were determined according to the chosen scale of the facility (1:15). The cylindrical part of the liner was built on site out of galvanised steel plate (thickness = 1 mm). A dome

was attached to the upper part of the pressure vessel. The inner diameter of the dome of the steel liner (thickness = 1.5 mm) was 2950 mm. Both the upper and inner surfaces were painted with alkyd paint. The design pressure of the vessel was 3 bar, but the pressure relief valve was set to 1 bar [5].

All the structures that are of concrete in the containment of the Loviisa NPP are made out of concrete also in the facility. All the concrete surfaces were painted with two component epox-paint, Reapox-GPL-VS. The concrete level, at + 25.4-elevation, was replaced with plywood plate, coated on both sides with phenolic resin. The upper level of this plate was at +25.8-elevation. There was two round holes ($\varnothing = 125$ mm) at the edges of the plate (90° and 270° , $r = 13.80$ m / 0.92 m), through which the aerosols and steam, injected into lower compartment, could flow into upper compartment of the containment. The upper compartment free volume was 17 m^3 and the total free volume was 22 m^3 .

The ice condensers used in the previous VICTORIA experiments were removed before the aerosol experiments. The ice condenser concrete structures, lower inlet doors and both the intermediate and top deck doors were still part of the containment. A strong convective loop between the upper and lower compartments, through the ICs, could be induced by opening the lower inlet doors of the two IC sections non-simultaneously.

The lower compartment of the VICTORIA containment could be pre-heated. The pre-heating was done by circulating hot water from central heating boiler in the piping below the lower compartment floor.

TH-measurements and control

The steam used in the experiments was generated by a small steam generator. The maximum capacity of the steam generator was 25 g/s. The injection of steam flow into the containment was adjusted by a control loop, which consists of regulator, control valve and flow meter. The injection run into the containment and the maintenance of set values were controlled by a computer.

In the experiments the piping of both the containment outer spray and the inner spray is used as a exhaust line of gases. The nozzles of the spray have been removed. The outer diameters of the pipes were 12 mm and the wall thickness 2 mm. The exhaust line was needed to equalise the overpressure caused by aerosol generation. The exhaust gases flowed through a heat exchanger and a filter in order to separate water and particles.

The outlets of the drainage piping of the sumps installed in the containment were at the bottom of the pressure vessel. The piping was made symmetrical from both of the sumps, in order to maintain uniform flow out of the lower compartment.

Gas temperature was measured at 99 locations and wall temperatures at 65 locations with T-type Thermocouples. Relative humidity (RH) was measured at 10 locations. In 8 locations the humidity was measured with a VAISALA probe HMP 135Y, that measures relative humidity in range of 0...100 % and temperature in range of 0 ... 160 °C. One probe in upper and one in lower compartment (VAISALA HMP-243) could measure relative humidities in condensing condition. The temperature range of these probes was -40 ... +180 °C. Pressure difference and water levels were measured in seven locations. The total pressure and flow rates of steam and air into the vessel were measured as well.

5.3.8.3 Aerosol generation and instrumentation

The aerosols in the experiments were generated by two aerosol generators Water-soluble aerosol, either NaOH or CsOH, was generated with two opposite jet atomisers. The dry particle AMMD was $\sim 2.3 \text{ }\mu\text{m}$,

GSD ~ 1.9 and the feed rate was close to 3 mg/s. High temperature Laminar Entrainment Flow Reactor (LEFR) was used in the generation of silver particles.

The piping from the aerosol generators (outer diameter = 23 mm, wall thickness 1.5 mm) was connected into one injection line, which was directed into the upper or lower compartment of the containment. The injection pipe was made out of acid-resistant stainless steel. The temperature of the injection line was kept at slightly over 100 °C and it was adjusted by a separate controller.

Sampling lines from the upper and lower compartments of the containment, were also made out of acid-resistant stainless steel (outer diameter 12.7 mm, wall thickness 1.65 mm). Heating cables, similar to those in the injection line, were attached onto the surfaces of the collecting lines and the temperatures were adjusted by controller of their own. The six sampling lines started from various locations inside the containment. At the inlet of each line there was a conical cover installed, in order to prevent droplets and impurities to enter the line. The samples passed through an ejector type diluter (PALAS), in which they were conditioned for the measurement devices using dried air.

The aerosol number and mass concentration was measured continuously using a Condensation Nucleus Counter (CNC) and the Tapered Element Oscillating Microbalance (TEOM) mass monitor. Particle mass and chemical composition size distributions were determined with 11-stage multijet Berner type low pressure impactors (BLPI). In order to measure the wet size distributions the impactors were placed inside the vessel. The measurement size range of impactors was 0.03 - 15 μm [6]. The elemental concentration collected on nuclepore filter substrates of each BLPI stage were analysed with Inductively Coupled Plasma-Mass Spectroscopy (ICP-MS). The dry number size distribution was measured with an Electrical Low Pressure Impactor (ELPI) and with a Differential Mobility Analyser (DMA). The size ranges of these instruments were 0.01 - 5 μm for ELPI [7] and 0.02 - 0.8 μm for DMA. Settling of particles was studied using deposition trays and deposition coupons. Coupons were acid resistant stainless steel and their size was 46 x 70 mm. Samples were analysed using ICP-MS. Also on-line Optical Particle Sizer (OPS), Aerodynamic Particle Sizer (APS) and filter samples were applied in the aerosol measurements.

5.3.8.4 *VICTORIA aerosol experiments and analysis*

VICTORIA aerosol experiments consisted of eight TH-experiments and aerosol generator tests as well as four actual aerosol behaviour experiments. Detailed information on the seven preliminary tests, numbered as 51...57, is presented in a data report [8]. Aerosol behaviour experiment number 58 and 59 belonged to CEC Fourth Framework programme project Aerosol Physics in the Containment. In both experiments aerosol was injected into the lower compartment of VICTORIA facility. The main difference between the experiments was that in experiment 58 the aerosol material was CsOH, where as in experiment 59 CsOH aerosol was mixed with silver. Information on these experiments can be found in the final report of the project [9]. Experiment number 60 was again a TH-test, in which steam and gas injection to upper compartment was tested. In aerosol behaviour experiment number 61 and 62 the particles were also injected to upper compartment of the facility. As before the main difference between the experiments was that in experiment 61 CsOH was applied as aerosol material, where as in experiment 62 the material was silver. Results from experiments 60 and 61 have been published [10]. Details of experiment 62 can be found in a data report [11].

When aerosol was fed to lower compartment particle mass and number concentrations in the upper compartment were much smaller than in the lower compartment. Aerosol mass and number concentrations in the lower compartment decreased fast due to high RH and sedimentation during the steam feed into the lower compartment. Eventually they reached values that were smaller than in the upper compartment. With hygroscopic material the average particle diameter increased during the steam feed and after that the

diameter decreased as a function of time because large particles were settling faster. The measured wet size of CsOH aerosol responded to the increasing RH as was expected.

When the aerosol was fed to the dome part of the upper compartment, the dome was in a saturated condition at a temperature of about 60 °C. A part of the aerosol particles was carried into the ice condensers and the lower compartment by a convective flow, which was driven by asymmetrical TH conditions between the two ICs. The lower part of the upper compartment, that is the volume between the ICs, remained superheated due to heat transfer through the surrounding structures, and no mixing with the saturated dome part took place. Thus, a clear difference (factor >3) could be found between the aerosol concentration decay times in these two parts of the upper compartment.

The results from experiment number 61 were compared with calculated results using FIPLOC and CONTAIN codes [12, 13]. Both the CONTAIN [14] and FIPLOC [15] calculations of the VICTORIA experiment gave fairly good overall results on thermal hydraulics. Containment pressurisation as well as temperatures and humidities in the ICs, the lower compartment and the dome part of the upper compartment were modelled accurately. The largest deviations from the measurements were found in the temperature and RH of the lower part of the upper compartment. It was evident that of a strong temperature and humidity gradient between two inter-connected volumes could not be modelled with lumped-parameter codes. Inaccuracy in modelling the convective flow pattern in the containment was another significant source of deviation in aerosol transport and deposition. The study indicated that most of the straits in containment aerosol modelling can be traced not to the aerosol model package itself, but to its physical and numerical coupling to the thermal hydraulic calculation, and parameter choices [10].

References

- [1] O. Hongisto, K. Lammila, H. Tuomisto Experiments for Hydrogen Distribution in an Ice Condenser Containment USNRC 20th Water Reactor Safety Information Meeting, October 21-23, 1992, Bethesda, Maryland, USA
- [2] O. Hongisto, H. Tuomisto Experimental Verification of the Loviisa Ice Condenser Containment Transient Operation in Reactor Accidents American Nuclear Society, Nuclear Reactor Safety Division's "Safety of Thermal Reactors", International Topical Meeting, July 21-25, 1991, Portland, Oregon, USA, 1991
- [3] P. Lundström, H. Tuomisto T. Lamberg, O. Hongisto Experimental studies of Hydrogen Behaviour in Ice Condenser Containments In: Proceedings of the OECD/NEA/CSNI Workshop on the Implementation of Hydrogen Mitigation Techniques. Winnipeg, Manitoba, 1996 May 13-15, pp. 159-179 AECL-11762, NEA/CSNI/R(96)8
- [4] V. Saldo, E. Verloo, T. Montanelli, J. Mäkinen, J. Jokiniemi, E.I. Kauppinen, H. Tuomisto, T. Routamo Aerosol physics in containment In: FISA-97 – EU research on severe accidents, Mid-term review symposium on shared-cost and concerted actions in reactor safety. Ed: Van Goethem, G., Keinhorst, G., Martin Bermejo, J. and Zurita, A. EC, Luxembourg, 17 to 19 November 1997, pp. 270-278. EUR 18258 EN
- [5] E. Heikkilä Technical description of VICTORIA Facility E.C. Report ST-APC(96)-P07 (1996)
- [6] R.E. Hillamo, E.I. Kauppinen On the performance of the Berner low pressure impactor Aerosol Sci. Technol. 14, 33-47, 1991

- [7] J. Keskinen, K. Pietarinen, M. Lehtimäki Electrical low pressure impactor J. Aerosol Sci.23, 353, 1992
- [8] J.M. Mäkynen, J.K. Jokiniemi, E.I. Kauppinen, H. Tuomisto, T. Routamo LWR Containment Aerosol Experiments at Victoria Facility - Data Report 1/96; E.C. Report ST-APC(96)-P08 (1996)
- [9] J.M. Mäkynen, J.K. Jokiniemi, E.I. Kauppinen, H. Tuomisto, T. Routamo LWR Containment Aerosol Experiments at Victoria Facility – Final Report; E.C. Report ST-APC(98)-P19 (1998)
- [10] J.M. Mäkynen, J.K. Jokiniemi, E.I. Kauppinen, A. Silde, S. Outa, T. Routamo, H. Tuomisto Experimental and Modelling Studies on Containment Aerosol Behaviour in the VICTORIA Facility, (1998)
- [11] J.M. Mäkynen, T. Routamo LWR Containment Aerosol Experiments with the VICTORIA Facility-Data report Experiment 62 (1999)
- [12] G. Weber, S. Schwarz, F. Ewig, K. Fischer FIPLOC 3.1, Benutzerhandbuch Gesellschaft für Anlagen- und Reaktorsicherheit (GRS) mbH, Januar 1998 GRS-P-2
- [13] K.K. Murata et.al.User's Manual for CONTAIN 1.1, A Computer Code for Severe Nuclear Reactor Accident Containment Analysis Revised for Revision 1.11. Nov. 1989, Revised July 1990
- [14] A. Silde Analyses of three containment accident sequences using the CONTAIN code: Source term analyses for Loviisa nuclear power plant Research Report ENE4/58/96, VTT Energy, Espoo 1996
- [15] S. Outa Modelling of Aerosol Behaviour in the Containment During Severe Reactor Accidents Master's Thesis, Helsinki University of Technology, January 1998

5.4 Aerosol Release in the Course of MCCI (ACE-C)

As part of the internationally sponsored Advanced Containment Experiments (ACE) program, seven large-scale experiments on molten core concrete interactions (MCCIs) have been performed at Argonne National Laboratory. One of the objectives of these experiments is to collect and characterise all the aerosols released from the MCCIs. Aerosols released from experiments using four types of concrete (siliceous, limestone/common sand, serpentine, and limestone/limestone) and a range of metal oxidation for both BWR and PWR reactor core material have been collected and characterised. Release fractions were determined for UO_2 , Zr, the fission products: BaO, SrO, La_2O_3 , CeO_2 , MoU_2 , Te, Ru, and control materials: Ag, In and B_4C . Release fractions of UO_2 and the fission products other than Te were small in all tests. However, release of control materials was significant [1].

Results of aerosol release calculations by six groups from six countries were compared with the releases from ACE MCCI test L6. The codes used for these calculations included: SOLGASMIX-PV, SOLGASMIX Reactor 1986, CORCON.UW, VANESA 1.01, and CORCON mod2.04/VANESA 1.01. Calculations were performed with the standard VANESA 1.01 code and with modifications to the VANESA code such as the inclusion of various zirconium-silica chemical reactors. Comparisons of results from these calculations were made with test L6 release fractions for U, Zr, Si, the fission-product elements Te, Ba, Sr, Ce, La, Mo and control materials Ag, In, and Ru. Reasonable agreement was obtained between calculations and test L6 results for the volatile elements Ag, In and Te. Calculated releases of the low volatility fission products ranged from within an order of magnitude to five orders of magnitude of test L6 values. Releases were over and underestimated by calculations. Poorest agreements were obtained for Mo and Si [2].

References

- [1] J.K. Fink, D.H. Thompson, B.W. Spencer, B.R. Sehgal Aerosols released during large-scale integral MCCI tests in the ACE program Technical Report, January 1992
- [2] J.K. Fink, M. Corradini, A. Hidaka, E. Hontanon, M.A. Mignanelli, E. Schrödl, V. Strizhov Results of aerosol code comparisons with releases from ACE MCCI tests Technical Report, January 1992

5.5 REST, REVENT, ThAI Re-Entrainment Tests

Introduction

Only a few experiments on re-entrainment from boiling sumps have been performed under LWR accident typical conditions. The most comprehensive work are the REST-tests. In the REVENT-tests especially the re-entrainment during a controlled filter venting was investigated. Finally two large-scale re-entrainment tests were carried out in the multi purpose ThAI containment facility.

REST tests

The REST tests (**Resuspension Source Term**) were carried out at the Kernforschungszentrum Karlsruhe [1]. The re-entrainment of soluble and insoluble FP surrogates was measured at four different heating levels. The superficial steam velocity lay both in the bubbly flow as well as in the low churn turbulent flow regime. The geometric sump surface was 91.6 cm². In more than 100 separate tests the following parameters were varied: heating power, concentration of soluble and insoluble materials, condensing and non-condensing atmospheres above the sump, temperature and pressure.

Fig. 5.5-1 shows the measured re-entrainment of the FP surrogates in REST tests with dry atmospheric conditions. The given superficial velocity is uncertain because the reported thermal hydraulic data for the tests are not complete. The re-entrainment of insoluble material (Fe, Zn) is an order of magnitude higher than for soluble material (CsI) because the insoluble material accumulates at the pool surface and thus in the droplets. The scatter of the measured values is wider for the insoluble material than for the soluble material.

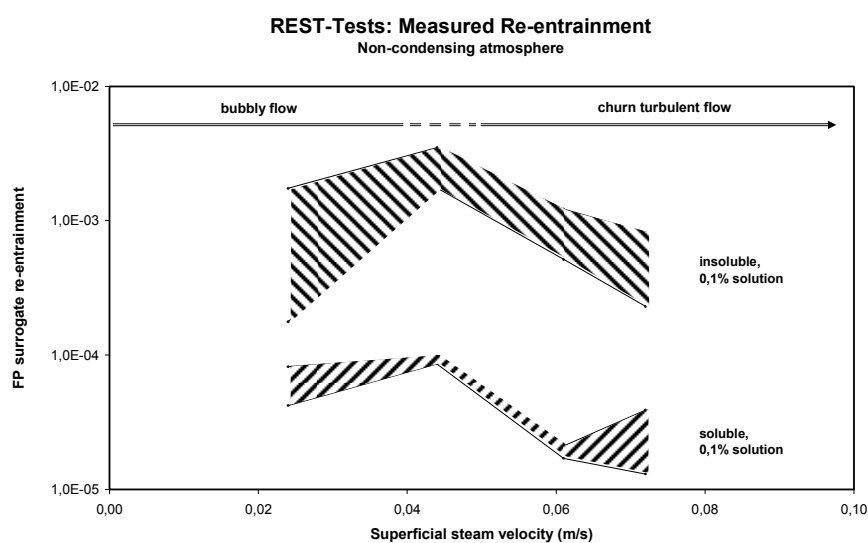


Fig. 5.5-1 Re-entrainment for insoluble and soluble material measured in the REST tests

The relative humidity in the atmosphere had a strong impact on the measured re-entrainment. The re-entrainment was significantly higher in a dry, non-condensing atmosphere, where the droplets shrank by evaporation of water and consequently sedimentation decreased. It was also observed in the REST tests that at the beginning of boiling when there are many small bubbles the re-entrainment can increase drastically (up to a factor 50) for a short time. Details of the mechanism are still not well understood and the phenomenon has not been modelled.

In the REST-study at the basis of the measured values an empirical re-entrainment correlation for rough estimations has been developed. In codes this correlation is not used because important dependencies of the re-entrainment like the superficial velocity are not considered and the correlation is valid for a limited gas flow range only.

REVENT tests

In the REVENT tests the re-entrainment of aerosols from boiling pools during a controlled filtered containment venting was measured [2]. The vessel was a 1:20 linear scaled model of a PWR containment. The pool was electrically heated (20 kW) and had a heated surface of 0.24 m². The vessel was equipped with a depressurization system for a controlled pressure relief. In the REVENT facility re-entrainment was measured under steady state conditions as well as under transient venting conditions. Soluble (Na₂SO₄, CsI, KI) and insoluble (Al₂O₃, SiC) fission product simulants were used.

For soluble material the measured re-entrainment is in the same order of magnitude as in the REST tests. For the insoluble material the re-entrainment was found to be one order of magnitude smaller than for the soluble one. This result is in contradiction to the REST tests where the re-entrainment for insoluble substances was always significantly higher than for soluble ones. By the REVENT tests it was further shown that solid airborne particles are always smaller than 3 µm. In the REVENT test a higher re-entrainment was measured at steady state conditions than at venting conditions. The reason is a pronounced volume condensation in the containment during venting, which causes droplet growth and enhances aerosol settling considerably.

ThAI tests TH14 and TH15

Two tests, TH14 and TH15, in the 60 m³ ThAI containment facility of Becker Technologies, Eschborn, have been devoted to the re-entrainment of fission products from a boiling sump [3]. The surface of the boiling sump was 0.55 m². The sump was electrically heated. In order to increase the superficial gas velocity additionally steam and/or air bubbles were released into the sump via a gas distributing system. Fission products in the sump water were simulated by soluble CsCl and KI salts.

The superficial gas velocity was varied between 0.03 m/s and 0.12 m/s. The released droplets were dried in the superheated vessel atmosphere, the residual salt particles being monitored by a Condensation Nuclei Counter to determine the number concentration, and by a Differential Mobility Analyser to obtain the size distribution of the salt particles. Additionally, filter samples have been taken to determine the aerosol mass concentration. The tests performed with a boiling sump surface area of 0.55 m² and 72 kW heating power yielded re-entrainment factors in the order of $5 \cdot 10^{-5}$, re-entrainment being defined as the mass ratio of released droplets and released steam. The re-entrainment values obtained confirm former REST laboratory-scale test data of [1]. However, as a result of the more sophisticated aerosol instrumentation applied in ThAI, the size of the released droplets and of the dried particles respectively turned out to be significantly smaller. The mass median diameter of the dried particles was about 0.1 µm. The contribution of re-entrainment to the overall source term should be re-evaluated in the light of the recent and coming experimental findings.

References

- [1] H. Bunz, M. Koyro, B. Propheter, W. Schöck, M. Wagner-Ambis Resuspension of Fission Products from Sump Water CEC, JRC, EUR 14635 EN (Nov. 1992)
- [2] M. Müller et al. REVENT Program – Aerosol Re-entrainment from Boiling Pool During Controlled Filtered Venting after a Severe Core Melt Accident NEA/CSNI/R(98)4, Session VII (Feb. 2000)
- [3] T. Kanzleiter, G. Poss, F. Funke, H.-J. Allelein ThAI Multi-Compartment Containment Test Program 14th International Conference on Nuclear Engineering (ICONE-14) July 17-20, 2006, Miami, Florida, USA

5.6 Pool Scrubbing Tests

Until mid 90's, a good number of experimental programmes had addressed the pool scrubbing issue. Table 5.6-1 and Table 5.6-2 [1] present, respectively, the main variables investigated and major specifics of the tests conducted.

Table 5.6-1 Pool scrubbing experimental programmes conducted until mid 90's

Programme	Variables investigated
UKAEA [2]	<ul style="list-style-type: none"> • Total gas flow • Steam mass fraction
GE [3]	<ul style="list-style-type: none"> • Aerosol particle size • Injector diameter • Submergence
EPRI [4-6]	<ul style="list-style-type: none"> • Total gas flow • Steam mass fraction • Submergence • Aerosol species
JAERI [7]	<ul style="list-style-type: none"> • Total gas flow • Particle size • Aerosol concentration • Submergence
POSEIDON/ POSEIDON II [8-10]	<ul style="list-style-type: none"> • Injection system • Submergence • Water temperature
ACE [11-13]	<ul style="list-style-type: none"> • Total gas flow • Steam mass fraction • Submergence • Water temperature • Water pH
LACE-España [14]	<ul style="list-style-type: none"> • Total gas flow • Steam mass fraction • Particle size
SPARTA [15]	<ul style="list-style-type: none"> • Only one test conducted
CIEMAT (RCA and GECI) [16]	<ul style="list-style-type: none"> • Total gas flow • Steam mass fraction • Particle size
EPSI [17, 18]	<ul style="list-style-type: none"> • Submergence • Pressure

Table 5.6-2 Boundary conditions of the pool scrubbing experimental programmes conducted until mid 90's

Research project	No. of tests	We	Submergence (m)	% steam	Pool conditions
UKAEA (1966)	7	$6 \cdot 10^6 - 1.8 \cdot 10^8$	0.61	4 - 75	Room
GE (1982)	18	Bubble regime	0.34 - 1.7	0	Room
EPRI (1986-91)	146	$10 - 10^4$	0.15 - 1.65	0 - 95	Room near saturation
JAERI (1987)		$1.5 \cdot 10^2 - 2 \cdot 10^3$	1, 2	0	Room
POSEIDON (1987)		$1.5 \cdot 10^4$	1, 2, 3	100	273 °C 1 - 6 MPa
ACE (1992)	4	$5 \cdot 10^4 - 1.5 \cdot 10^5$	1.4 - 4.6	1 - 40	25 - 80 °C
LACE España (1992)	11	$5 \cdot 10^3 - 1.5 \cdot 10^5$	2.5	10 - 90	110 °C 3 bar
SPARTA (1992)	1	$2 \cdot 10^4$	1.8	0	near saturation
CIEMAT (1996) (RCA and GECI)	10	$2.5 \cdot 10^4 - 2.8 \cdot 10^5$	0.25 - 2.5	0, 50, 90	80 °C near saturation
POSEIDÓN-II (1998)	17		0.3 – 4.00	0, 0.55, 0.72	85 °C

A good part of the experimental investigation were encapsulated in computer codes such as SPARC90 [19], BUSCA [20] and SUPRA [21] which were principally developed in the 80's. They contain models based on the basic knowledge gained on pool scrubbing phenomena (as summarised in the supplementary report on nuclear aerosols in reactor safety issued by NEA [22]) from the experimental programmes carried out until late 80's. Some limited model updates were done using the data made available later. Nonetheless, no further major development were made from early 90's although more detailed information were made available by the tests carried out throughout the last decade of the XX century.

Major analytical activities associated with the recent pool scrubbing research can be summarised as:

- The Source Term project of the 3rd FWP of Euratom [23]: a model for fission product scrubbing under churn turbulent flow was developed. In addition, a peer review of last versions of SPARC and BUSCA codes were assessed.
- Simplified models for scrubbing of particles during Molten Core Concrete Interaction (MCCI) with overlying water pool [24] and for BWR suppression pools [25]. Both of them were used to develop a simplified model of decontamination accounting for the uncertainties associated with both scenarios.

References

- [1] M.J. Escudero, M.J. Marcos Crespo, M. Swiderska-Kowalczyk, M. Martin Espigares, J. López Jiménez State of the Art Review on Fission Products Aerosol Pool Scrubbing under Severe Accident Conditions ST(93)-P61, Rev. 2, ITN/TS-22/DP-93, 1994
- [2] J.J. Hillary, J.C. Taylor, F. Abbey, H.R. Diffey Iodine removal by a scale model of the SGHW reactor vented steam suppression system UKAEA, TRG Report 1256 (W), August 1966
- [3] S.A. Ramsdale, G.J. Barford, S. Fishwick, H.C. Starkie Status of research and modelling of water pool scrubbing Final report, EUR 14566 EN, 1992
- [4] J.C. Cunnane, M.R. Kuhlmann, R.N. Oehlberg The scrubbing of fission product aerosols in LWR water pools under severe accident conditions - experimental results Proc. of Fission Product Behaviour and Source Term Research, 1984
- [5] D.D. Paul, L.J. Flanigan, J.C. Cunnane, R.A. Cudnik, R.P. Collier, R.N. Oehlberg Radionuclide scrubbing in water pools - gas-liquid hydrodynamics EPRI-NP-41554, Vol. 1, 1985
- [6] M.R. Kuhlmann, J.A. Gieseke, M. Merilo, R.N. Oehlberg Scrubbing of fission product aerosols in LWR water pools under severe accident conditions IAEA-SM-281/47
- [7] K. Hashimoto, K. Soda, S. Uno, H. Nakatani, H. Tateoka Effect of pool scrubbing of insoluble aerosol in two-phase flow in a pipe IAEA-SM-296/60
- [8] S. Güntay Experiment POSEIDON: Elemental iodine retention in water pools ANS 1990 Winter Meeting, Washington D.C., November 11-15, 1990, Volume 62, TANSO 062 1-722 (1990), ISSN: 0003-018X
- [9] S. Güntay Experiment POSEIDON: Pool scrubbing effect on iodine decontamination pp 937-941, ENC'90, ENS/ANS-Foratom Conference Transactions, Verlag TÜV Rheinland
- [10] A. Dehbi, D. Suckow, S. Güntay Aerosol retention in low-subcooling pools under realistic accident conditions Nuclear Engineering and Design 203, 2-3, 229-241, 2001
- [11] J.D. McCormack, D.R. Dickinson, R.T. Allemann Experimental results of ACE vent filtration pool scrubber tests AA1-AA4 and DOP1 - DOP5 ACE-TR-A1, January 1989
- [12] K. Fischer, M.R. Kuhlmann, V. Kogan Fission product pool scrubbing data and modelling assessment ACEX TR-A-01, Vol. 1, December 1996
- [13] K. Fischer, M.R. Kuhlmann, V. Kogan Fission product pool scrubbing data and modelling assessment ACEX TR-A-02, Vol. 2, June 1997
- [14] M.J. Marcos, F.J. Gomez, I. Melches, M. Martin, J. López LACE-España Experimental programme on the retention of aerosols in submerged beds Final report, CIEMAT, ITN/TS-08/DP-93, April 1993
- [15] M. Furrer, R. Passalacqua SPARTA project: scoping test results and comparison with pool scrubbing codes predictions ENEA-CRE Casaccia, January 1992

- [16] V. Peyrés, M.M. Espigares, J. Polo, M.J. Escudero, L.E. Herranz, J. López Jiménez Pool scrubbing and hydrodynamic experiments on jet injection regime CIEMAT 785
- [17] K. Hashimoto, K. Soda, S. Uno High pressure pool scrubbing experiment for a PWR severe accident ANS International Topical Meeting on Safety of Thermal Reactors, July 1991
- [18] K. Hashimoto, K. Soda, S. Uno, H. Nakatani, H. Tateoka Effect of pool scrubbing of insoluble aerosol in two-phase flow in a pipe IAEA-SM-296/60
- [19] P.C. Owczarski, K.W. Burk SPARC-90: A Code for Calculating Fission Product Capture in Suppression Pools NUREG/CR-5765, 1991
- [20] S.A. Ramsdale BUSCA-JUN90 Reference Manual, SRD-R542, 1991
- [21] A.T. Wassel, A.F. Mills, D.C. Buggy Analysis of Radionuclide Retention in Water Pools Nucl. Eng. & Des. 90, 87-104, 1985
- [22] NEA, Nuclear Aerosols in Reactor Safety: Supplementary Report, 1985
- [23] J. López Jiménez, L.E. Herranz, M.J. Escudero, M.M. Espigares, V. Peyrés, J. Polo, Ch. Kortz, M.K. Koch, U. Brockmeier, H. Unger, L.M.C. Dutton, Ch. Smedley, W. Trow, A.V. Jones, E. Bonanni, M. Calvo, A. Alonso Pool Scrubbing. ST(95)-P195, ITN/TS-12/SP-95, 1995
- [24] D.A. Powers, J.L. Sprung A Simplified Model of Aerosol Scrubbing by a Water Pool Overlying Core Debris Interacting with Concrete NUREG/CR-5901, SAND92-1422, 1993
- [25] D.A. Powers A Simplified Model of Decontamination by BWR Steam Suppression Pool NUREG/CR-6153, 1997

5.7 Resuspension Tests

The experiments performed on the topic of resuspension of aerosols are divided into two classes. The first class analyses the resuspension under a continuous airflow of at least several minutes. Such conditions are expected in the primary cooling system or at a slow depressurisation of the containment in the course of an accident scenario. The second class examines the influence of transient airflows after short time events like hydrogen deflagrations or steam explosions.

5.7.1 Continuous flow experiments

PARESS

In the PARESS (Particle Resuspension Studies) experiments Fromentin [1] analyses the resuspension under a continuous airflow in a wind channel. In a first step aerosol is injected into a sedimentation chamber, where the aerosol settles under predefined conditions onto deposition coupons. In a second step the deposition coupons are recovered and put into the wind channel. There a constant air current velocity is adjusted and the removal of aerosol mass is measured in dependence of time. Different aerosol materials are used in this study like iron oxide (Fe_2O_3), tin (Sn), and silicon (Si) or mixtures of these materials. A resuspension flux F_{res} is observed that decreases inversely proportional to time. Furthermore other influences like aging of the deposition layer, relative humidity and homogeneity of the deposition are investigated.

STORM

The experimental conditions of the STORM facility at JRC are chosen to simulate the conditions in the pressure relief lines of a PWR reactor in a station blackout scenario (de los Reyes [2]). The test section consists of a 5.0055 m long pipe with an internal diameter of 63 mm. The test SR11 is chosen as ISP40 and is performed in two phases. In the first phase the pipe is streamed by tin oxide (SnO_2) aerosol with a carrier gas of nitrogen and steam. During this period of 5 h a part of the aerosol is sedimented on the internal pipe walls. In the second phase the pipe is fed with pure nitrogen. During this phase the prior sedimented aerosol is resuspended and relocated inside the pipe or released with the carrier gas. The gas flow is increased in six consecutive steps and the resuspension rate is determined by the aerosol concentration in the carrier gas. A benchmark with different severe accident codes modelling resuspension has been performed on ISP40. Further details of the STORM experiments can be found in chapter 5.2.3.

5.7.2 *Transient flow experiments*

VANAM-M4 add-on

Subsequent to the Vanam-M4 test in the Battelle Model Containment (BMC) an add-on experiment with resuspension due to a hydrogen deflagration in a multi-compartment geometry is performed (Kanzleiter [3]). In a first step hygroscopic NaOH aerosol and insoluble SnO_2 aerosol is injected into the inner compartments of the BMC. The outer rooms are separated from the inner rooms by rupture foils. In a second step hydrogen is injected into the same compartments as the aerosol. The hydrogen is ignited in the inner rooms and the expanding atmosphere spreads out into the outer containment rooms. Although the deflagration runs very mild, the generated air currents are able to resuspend round about 1 % of the initially injected aerosol mass. It is observed that the resuspended aerosol material settles faster than the initially injected aerosol. This indicates the generation of a larger aerosol component. The observation of the particles found in filter stations with a scanning electron microscope show a wide particle spectrum with a large number of very fine particles but also some very large particles, which carry a great fraction of the aerosol mass.

AEREST

At technical university of Munich an experimental programme in the aerosol resuspension shock tube has been performed (Schneider [4]). The aerosol test section is located in a 7 m long pipe with a pressure tank on the input side. This pressure tank is discharged over a ball valve and the expanding atmosphere hits an aerosol deposition bed that is deposited on coupons with different angles of attack, which are prepared in an extra sedimentation vessel. The aerosol materials used in these experiments are silver particles of different shapes and tin oxide (TiO_2) particles. In these experiments a large scattering of the resuspended aerosol mass is observed under comparable conditions. Anyway the AEREST experiments show a large relative particle removal at high aerosol mass loads on the surface but only a minor relative particle removal at lower particle mass loads. This can be explained by a larger adhesive force of particles located directly on the surface in comparison to particles in higher positions of the particle bed.

ThAI experiments Aer-1, Aer-3, Aer-4

In the ThAI facility at Becker Technology three experiments on the topic of resuspension have been performed (Kanzleiter [5]). For that purpose a horizontal deflagration tube has been installed into the facility that was loaded with a hydrogen-air mixture. In a first phase CsI is injected into the atmosphere and settles during a period of 18 h. Then the hydrogen in the deflagration tube is ignited and the expanding atmosphere is released through a $2 \times 50 \text{ cm}^2$ large nozzle over a deposition plate, on which aerosol material has deposited during the sedimentation phase. In the three experiments Aer-1, Aer-3, and Aer-4 the

hydrogen load and thus the airflow velocities are varied. The findings are similar to that of the VANAM-M4 test with a resuspended fraction of 1 % of the initially injected aerosol mass. Also in accordance with VANAM-M4 is the higher settling velocity of the resuspended aerosol in comparison with the deposition phase.

References

- [1] A. Fromentin Particle Resuspension from a Multi-Layer Deposit by Turbulent Flow Paul Scherrer Institut, 1989 (PSI 38)
- [2] A. de los Reyes, J.A. Capitão, G.D. Santi International Standard Problem 40 - Aerosol Deposition and Resuspension OECD, 1999 (NEA/CSNI/R(99)4)
- [3] T. Kanzleiter VANAM-Mehrraum-Aerosolabbau-Versuch M4 mit Misch aerosol (lösliches und unlösliches Material) und Resuspension durch einen Wasserstoffbrand Battelle-Institut e.V., 1993 (BleV-R67.098-305)
- [4] R. Schneider Resuspension von Aerosolen durch transiente Strömungen im Containment Lehrstuhl für Thermodynamik, TU München, 2003 (150 1102)
- [5] T. Kanzleiter, G. Ahrens, K. Fischer, W. Häfner, A. Kühnel, G. Poss, F. Funke, G. Langrock, H.-J. Allelein, G. Weber, S. Schwarz Versuchsanlage und Programm zur Untersuchung offener Fragen zum Spaltproduktverhalten im Sicherheitsbehälter; ThAI Phase II Becker Technologies, Areva NP und GRS, 2006 (150 1272 – S1)

5.8 Spray Systems (French Tests)

For model development and validation purposes concerning the effects of sprays in the containment atmosphere, the Institut de Radioprotection et de Sécurité Nucléaire (IRSN) conducted two experimental programmes; CARAIDAS (an extensive analytical programme) and TOSQAN (comprising small-to-intermediate-scale tests that are still in progress). The Commissariat à l’Énergie Atomique (CEA) is carrying out some tests in the MISTRA facility where these are large-scale and complementary to those of IRSN but in which it is not foreseen to include injection of aerosols.

The CARAIDAS programme comprised analytical tests covering three effects of sprays: droplet relaxation (condensation and evaporation); aerosol capture; and iodine absorption, [1, 2]. The CARAIDAS apparatus (see Fig. 5.8-1) involved a vessel of dimensions: height of 5.7 m; internal radius of 0.6 m; total volume of nearly 1.4 m³. Single drops were generated that fell through a homogeneous air atmosphere with different humidity levels and with or without cesium-iodide aerosols or iodine vapor, respectively. The atmospheric temperature was controlled by the regulated wall temperature. Nearly 100 tests were performed showing the collection efficiency to range over more than two decades and allowing development of modelling for the ASTEC code covering droplet kinetic and thermal relaxation, gravitational coagulation, inertial capture and interception of aerosols, and iodine mass transfer and chemical transformation in the droplets, [3]. In particular, twenty-one of these tests were retained for evaluation of aerosol-capture modelling where the polydisperse ($GSD \leq 1.7$; $0.5 < AMMD < 5$ microns) CsI aerosol interacted with pure-water droplets (see Fig. 5.10-1). These aerosol-capture tests can in fact be grouped into five families: two analytical series using particles with an aerodynamic volume-median diameter (AVMD) of 2-4 µm and either large (700 µm diameter) or small (300 µm diameter) spray droplets; another two analytical series using smaller particles (AVMD between 1 and 1.5 µm) with the same large and small droplets; and a fifth series in more severe-accident representative conditions, i.e., higher pressure (0.2 - 0.4 MPa) and higher temperature (120 to 140 °C). Unfortunately, this latter series was affected by large experimental uncertainties (with

consequent dispersion of results) arising mainly from unexplained difficulties with respect to droplet collection at the containment base.

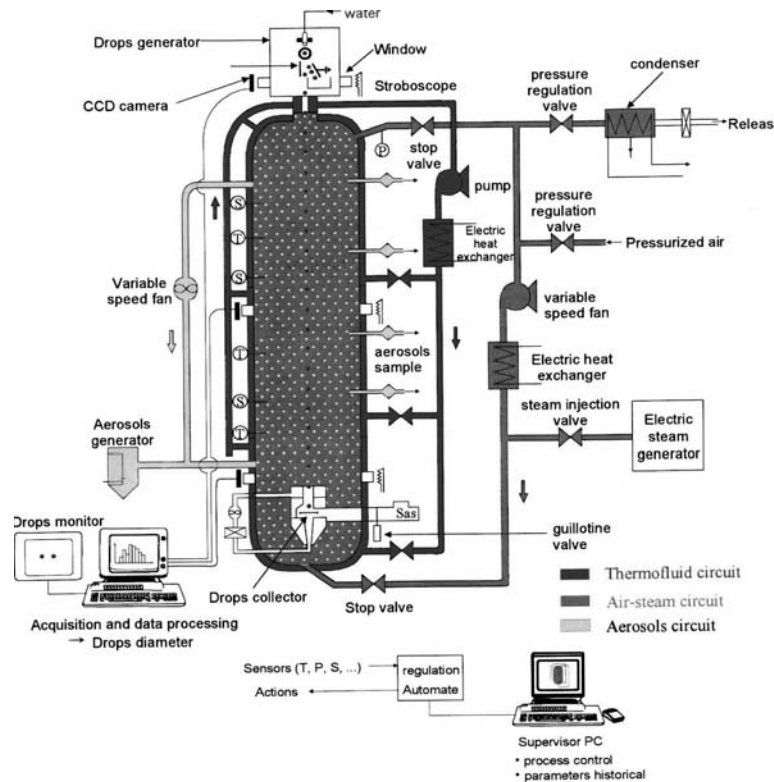


Fig. 5.8-1 Comparison of the ASTEC aerosol-capture model with the CARAIDAS data - after [1]

The TOSQAN experiments are performed in thermal-hydraulic conditions representative of containment severe-accident scenarios (wall condensation, spray, sump). The principal aim has been the measurement of steam condensation onto (or water evaporation from) spray droplets in atmospheres comprising steam and non-condensable gases while, recently, a new phase including aerosols has started. The TOSQAN facility is based on a vessel 7 m³ in volume (4.8 m high, 1.5 m wide) with thermostatically-controlled walls which is highly instrumented (gas temperature, steam concentration, droplet velocity, diameter and temperature), [4]. The main thermal-hydraulic phenomena when sprays are used the mixing induced by spray entrainment and the heat and mass transfer with respect to droplets and walls where validation of the modelling of these processes constitutes the main objective of the programme, [5, 6]. The TOSQAN spray test matrix consists of one reference test with an air-steam mixture and another with an air-steam-helium mixture. Other tests were changed the spray injection rate, the spray temperature, the superheating, the initial gas temperature, the difference between saturation temperature and injection temperature, and the gas composition. A benchmark was initiated between SARNET partners based on TOSQAN Test 101 studying droplet and wall heat and mass transfer, [7]. In this test, a cold-water spray was injected into the steam-air-filled vessel resulting in partial steam condensation and pressure reduction. This exercise involved both lumped-parameter and computational fluid dynamics (CFD) codes with a first phase that was a blind analysis and a second one (in 2005) using open results. It was seen that the calculated total pressure was very sensitive to the modelling of droplet vaporization into the gas or onto structures. Modelling of the spray injection required care and use of experimental data was necessary. A third phase with open results is in progress that includes new experimental data on spray injection. In general, calculated pressure is found to be lower than in the experiments where a possible explanation is the

droplet-wall interaction which is not taken into account in the calculations. A second TOSQAN spray benchmark is being performed based on Test 113 which concerned mixing by sprays of an initially-stratified air-helium atmosphere.

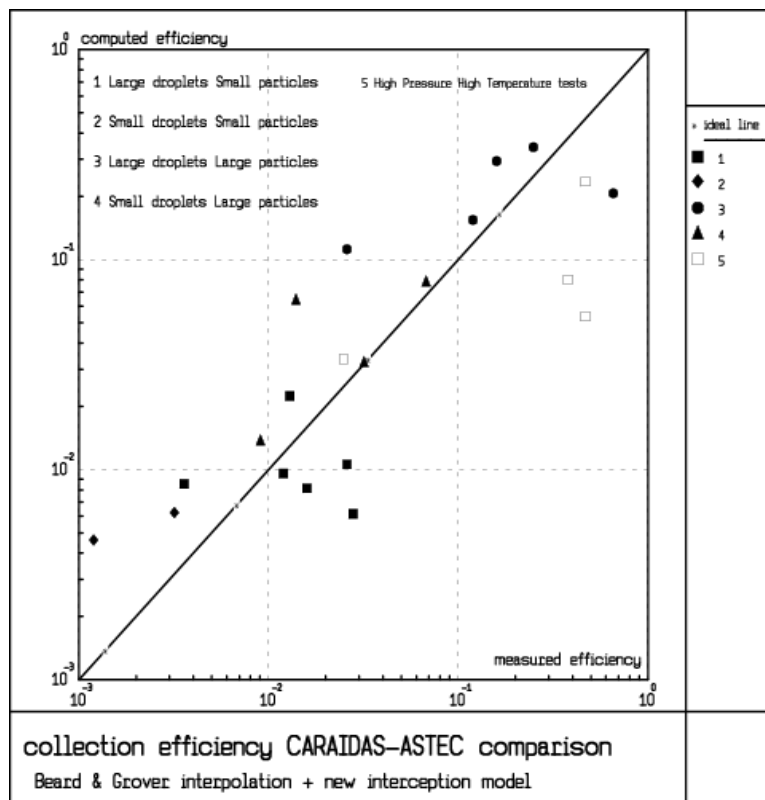


Fig. 5.8-2 Comparison of the ASTEC aerosol-capture model with the CARAIDAS data - after [3].

Tests designed for the validation of CFD codes were performed by CEA in the MISTRA facility, a much larger-scale experiment (vessel volume of 100 m³) than TOSQAN, [8, 9]. The experiments study axisymmetric and non-axisymmetric injection of steam into the containment with condensation on temperature-regulated walls investigating heat and mass (steam condensation) transfer rates as well as hydrogen distribution. Standard models for condensation used in lumped-parameter codes and multi-dimensional codes have been validated. Some results of these tests are available to the SARNET community with respect to tests M2 and M3, [10].

Finally, it is worth mentioning that many TOSQAN, MISTRA as well as ThAI results were used in ISP-47 [11]. This ISP assessed lumped-parameter and CFD codes with respect to containment thermal hydraulics involving analyses that comprised progressive modelling difficulties. The exercise highlighted the dominant impact of user effects, especially concerning nodalization, both with lumped-parameter and CFD codes. Furthermore, in spite of their higher numerical burden, CFD results were not generally better than those of lumped-parameter codes. Nevertheless, for assessing hydrogen distribution in the containment, combined use of both lumped-parameter and CFD codes was recommended it was concluded that further code development and establishment of nodalization rules and user guidelines are necessary to achieve more accurate predictive capabilities.

References

- [1] D. Ducret, Y. Billarand, D. Roblot, J. Vendel Study on collection efficiency of fission products by spray: experimental device and modelling 24th DOE/NRC Nuclear Air Cleaning and Treatment Conference, Portland, USA, 15-18 July 1996, NUREG/CP-0153.2, 1996
- [2] D. Ducret et al. Etude expérimentale et modélisation du rabattement des aérosols par des systèmes d'aspersion 14e Congrès Français sur les Aérosols, Dec. 1998, Paris, France, 1998
- [3] W. Plumecocq, V.D. Layly, A. Bentaib Modelling of the containment mitigation measures in the ASTEC code, focusing on spray and hydrogen recombiners International Topical Meeting on Nuclear Thermal-Hydraulics (NURETH-11), 3-6 October 2005, Avignon, France, 2005
- [4] P. Lemaitre, E. Porcheron, G. Grehan, L. Bouilloux Development of a global rainbow refractometry technique to measure the temperature of spray droplets in a large containment vessel Meas. Sci. Technol. 17, pp 1299-1306, 2006
- [5] J. Malet, E. Porcheron, J. Vendel Filmwise condensation applied to containment studies: conclusions of the TOSQAN air-steam condensation tests International Topical Meeting on Nuclear Reactor Thermal-Hydraulics (NURETH-11), 3-6 October 2005, Avignon, France, 2005
- [6] J. Malet, W. Plumecocq, P. Lemaitre, E. Porcheron, J. Vendel Modelling of sprays in containment applications: results of the TOSQAN spray tests International Congress on Advances in Nuclear Power Plants (ICAPP), 4-8 June 2006, Reno, NV, USA, 2006
- [7] A. Bentaïb, J. Malet, P. Lemaitre, E. Porcheron, J. Vendel, W. Plumecocq Modelling of sprays in containment applications; Results of the TOSQAN spray benchmark European Review Meeting on Severe Accident Research (ERMSAR), 14-16 November 2005, Aix-en-Provence, France, 2005
- [8] M. Caron-Charles, J.J. Quillico, J. Brinster Steam condensation experiments by the MISTRA facility for field containment code validation Proceedings of the International Conference on Nuclear Engineering (ICONE), Volume 3, pp 1041-1055, 2002
- [9] I. Tkatschenko, E. Studer, J.P. Magnaud, L. Blumenfeld, H. Simon, H. Paillère Status of the MISTRA programme for the validation of containment thermal-hydraulic codes International Topical Meeting on Nuclear Thermal-Hydraulics (NURETH-11), 3-6 October 2005, Avignon, France, 2005
- [10] A. Bentaïb, J. Vendel, H. Simon, L. Blumenfeld, I. Tkatschenko, H. Paillère Air-steam tests in the MISTRA facility: Experimental results and validation of the lumped-parameter/CFD TONUS code European Review Meeting on Severe Accident Research (ERMSAR), 14-16 November 2005, Aix-en-Provence, France, 2005
- [11] H.-J. Allelein, K. Fischer, J. Vendel, J. Malet, E. Studer, S. Schwarz, M. Houkema, H. Paillère, A. Bentaïb International Standard Problem ISP-47 on containment thermal hydraulics - final report. OECD/NEA (to appear), 2006

5.9 Containment Venting Filters

Severity of the conditions during severe accidents varies depending on the successfulness of the accident management measures attempted. However, anticipated conditions: high temperature, high pressure, high steam concentrations, hydrogen burns or detonations, high aerosol and gaseous fission product

concentration, and resulting high activity levels, are very much depending on the accident progression driven by the status of the hardware as well as the accident management efforts. Contrary to the operational or design basis accident conditions the anticipated severe accident conditions cannot be used as the design parameters for the conventional filtration systems within the practical limitations. However, as a result of the emerging new regulatory requirements for the severe accidents, which can not be 'normally' fulfilled by the conventional filtration systems new filtration concepts were developed in 1980s to backfit the current operating reactors in some countries. The main emphasis in the new regulatory requirements is to keep the pressure in the containment under the design limits in order to avoid catastrophic containment failures by relieving the pressure by venting through a containment venting filter, which should at the same time remove the aerosol particles and molecular gaseous iodine with certain efficiencies.

Some of the new developed systems by various vendors at that time were tested by an international project, Advanced Containment Experiments (ACE) Phase A [14], 1988-1992. The following section summarises the filter concepts and the results achieved from the ACE experiments. Another containment venting filter unit developed and tested in Switzerland is also introduced.

5.9.1 *International efforts for qualification of containment venting filters*

Phase A of the ACE project was comprised of two parts; the first part consists of four pool-scrubbing tests and accompanying five mono-dispersed aerosol tests. The objectives of these tests were to provide a basic database for the retention capability of the water pool before conducting the tests with various commercial containment venting filters in the second part. The filters were designed and developed by various international organizations as shown below:

- the submerged gravel scrubber from Westinghouse/USA,
- the Multi Venturi Scrubber System from ABB/Sweden,
- heat sink gravel bed from ABB Atom, Sweden,
- the sand bed filter from CEA and EdF, France,
- the submerged combined venturi filter from FRAMATOME ANP (former Siemens-KWU/Germany),
- the metal-fibre filter developed by FZK (former KfK)/ Germany
- the Soviet filter system provided by the former Soviet Union.

The filter units used in the test programme were scaled units, and the boundary conditions used were selected to demonstrate the filter efficiencies at the desired conditions. Surrogate aerosol particles, composed of CsOH, CsI and MnO, were generated using evaporation of the manganese powder by a plasma torch, evaporation of cesium with an oven and by condensation of metallic vapors in steam environment, in which hydrogen iodide (HI) was also introduced. Simultaneous chemical reactions of vaporised Mn and Cs with steam and later CsOH with HI caused the production of the desired chemical speciation. The particles generated were about 2.5 μm AMMD with geometric standard deviation of about 2. The aerosol concentration ranged from 5 to 15 g/m^3 (at standard conditions) depending on the test conducted.

Submerged gravel scrubber

A submerged gravel bed filter was a system developed by Westinghouse, USA. The filter contained a gravel bed, which was submerged in water. The gas as flowed up through the gravel bed. The water served as a sink for both the heat and aerosol removed from the gas. A schematic diagram of the filter system used is depicted in Fig. 5.9-1. Tests were conducted to investigate the effect of bed depth below the pool surface, pool temperature and inlet steam fraction Table 5.9-1 presents the boundary conditions and measured average material dependent decontamination factors.

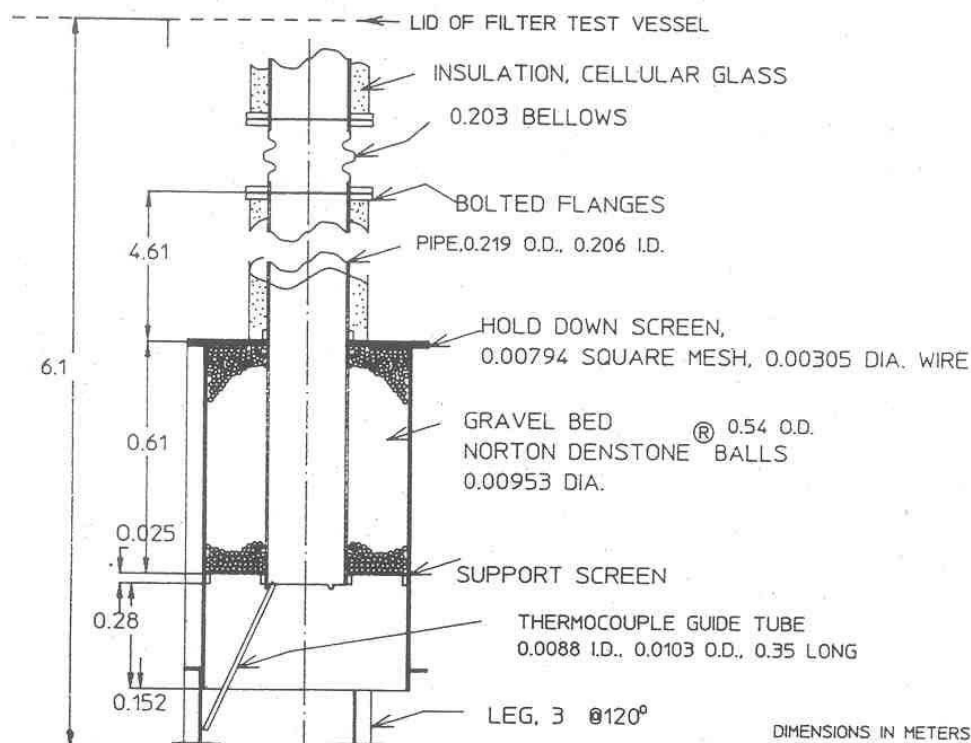


Fig. 5.9-1 Schematic Diagram of Submerged Gravel Bed Scrubber

FILTRA-MVSS

The FILTRA-MVSS (Filtered Containment Venting Multi Venturi Scrubber System) was a wet scrubber for filtered containment venting system designed and manufactured in Sweden by ABB Atom and Fläkt Industry AB. The filter contains a bank of venturis, which is located in a water pool. A schematic diagram of the filter system used is depicted in Fig. 5.9-2. A moisture separator, which contains a dry gravel bed, is attached at the exit of filter unit to reduce the content of the water droplets in the gas mixture from the venturi scrubber before the gas was discharged to the environment.

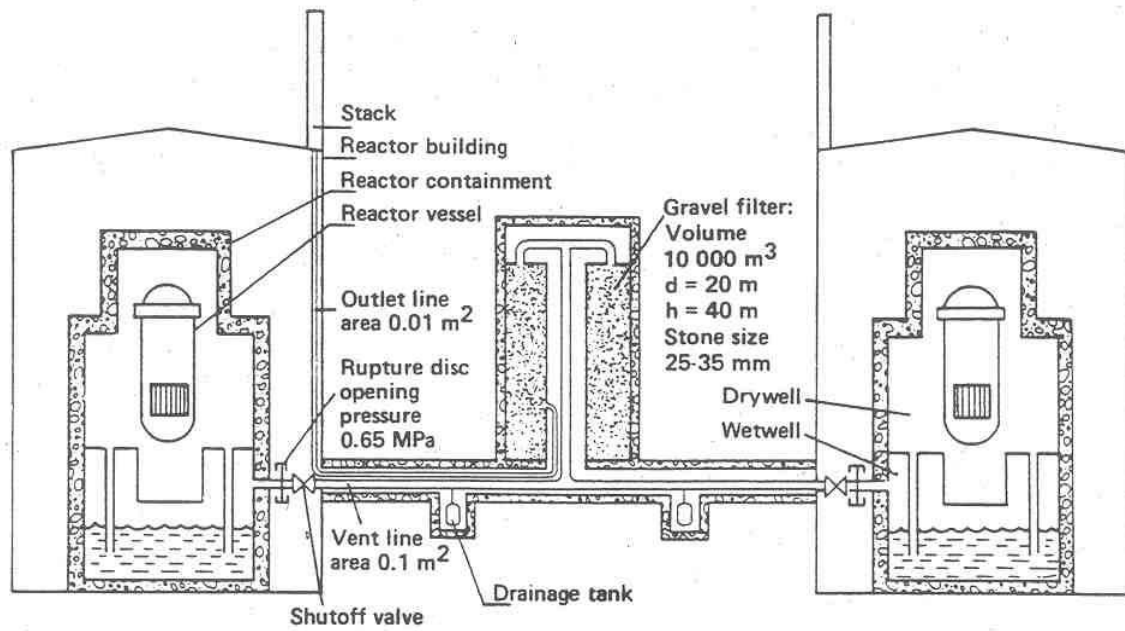


Fig. 5.9-2 FILTRA - schematic drawing

The multiple venturi part of the filter unit (without the moisture separator) was tested in the ACE-Project. Tests conducted provided aerosol removal characteristics as a function of changing the steam mass fraction in the aerosol carrier gas and also determined the level of re-entrainment of liquid from the filter test vessel pool.

Table 5.9-1 ACE project: measured key parameters and the retention factors based on the inlet and outlet concentrations

	Submerged Gravel Scrubber Westinghouse								Multi-Venturi FILTRA-MVSS ABB		Heat Sink Bed FILTRA ABB		Sand Bed CEA-EdF		Combined Venturi Siemens		Metal Fibre KJK		Russian Filter	
	AA5	AA6	AA7	AA8	AA9	AA10	AA11	AA12	AA13	AA14	AA15	AA16	AA17	AA18	AA19	AA20	AA21	AA22		
Pressure kPa	113	113	113	134	112	148	153	150	106	106	121	131	127	138	112	110	268	258		
Flow rate m ³ /s std	.0896	.09	.0867	.0867	.0897	.0897	.091	.092	.0901	.0902	.0729	.0628	.0884	.0884	.0872	.089	.0712	.0407		
Steam Fraction	.0127	.430	.426	.014	.416	.417	.012	.402	.395	.404	.392	.406	.424	.420	.0134	.434	.012	.416		
Inlet Aerosol Concent- ration g/m ³	Cs	7.4	11.0	14.6	8.2	12.1	15.8	6.88	12.08	13.2	10.1	3.43	7.2	10.0	7.6	7.2	5.0	5.7	9.0	
	Mn	12.9	23.3	23.9	11.0	14.3	7.7	10.93	15.54	15.0	13.6	20.6	10.4	17.6	17.4	9.1	10.5	2.7	4.9	
	I	0.79	1.0	0	1.04	1.17	1.49	0.86	1.29	0.79	0.71	0.69	0.86	1.1	1.1	0.51	1.2	0.49	0.34	
DF	Cs	194	66	83	1280	48	12E3	76E3	58E3	4.9	2.6	200E3	120E3	1.4E6	.9E6	>3E6	1.6E6	300E3	370E3	
	Mn	17	26	22	71	11	126	1.5E3	4.4E3	3.8	2.3	2.5E6	25E3	>1E6	>3E6	800E3	>2E6	150E3	800E3	
	I	44	68	--	1100	54	17E3	36E3	54E3	5.0	2.3	9E3	6E3	3E6	.3E6	60E3	200E3	2E6	300E3	

FILTRA

The FILTRA filter developed in Sweden utilised a gravel bed. The FILTRA system was installed in two boiling-water reactors at Barseback Nuclear Power Stations in southern Sweden. The gravel bed is designed to provide a static heat sink for condensing steam and also to serve as an expansion volume and a filter medium for removing radioactive aerosols. A schematic diagram of the filter system used is depicted in Fig. 5.9-3. The tests conducted used a similar bed, but smaller in capacity and in depth than the real FILTRA unit, provided data (Table 5.9-1) on the aerosol removal characteristics as well as the temperature and entrainment (carry-over) behaviour from the unit during passage of moist gas.

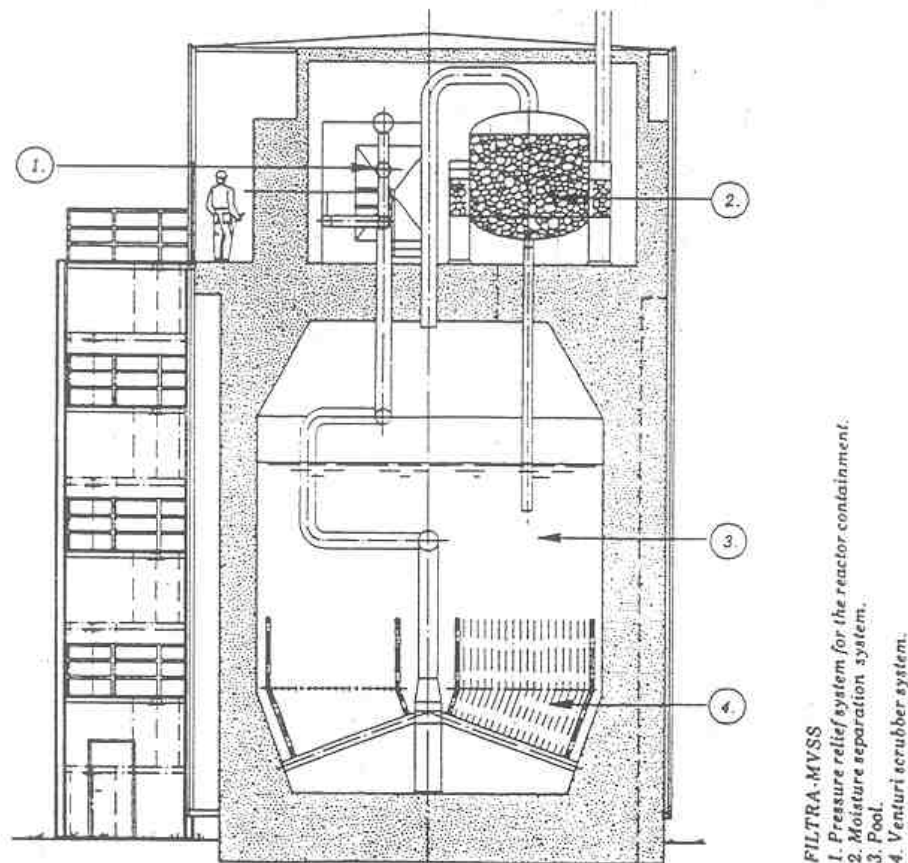


Fig. 5.9-3 FILTRA - MVSS schematic drawing

Sand bed filter

A dry sand bed filter was designed and developed by CEA and EdF in France for filtered vented containments for use at EdF's pressurised water reactors. The filter system tested at the ACE-Project used a 0.8 m deep bed of 0.6 mm grain sand and a layer of 1.5 mm gravel supporting the sand. The tests provided data (Table 5.9-1) during both condensing and non-condensing bed conditions as well as re-entrainment and temperature behaviour of the sand bed. A schematic diagram of the filter system used is depicted in Fig. 5.9-4

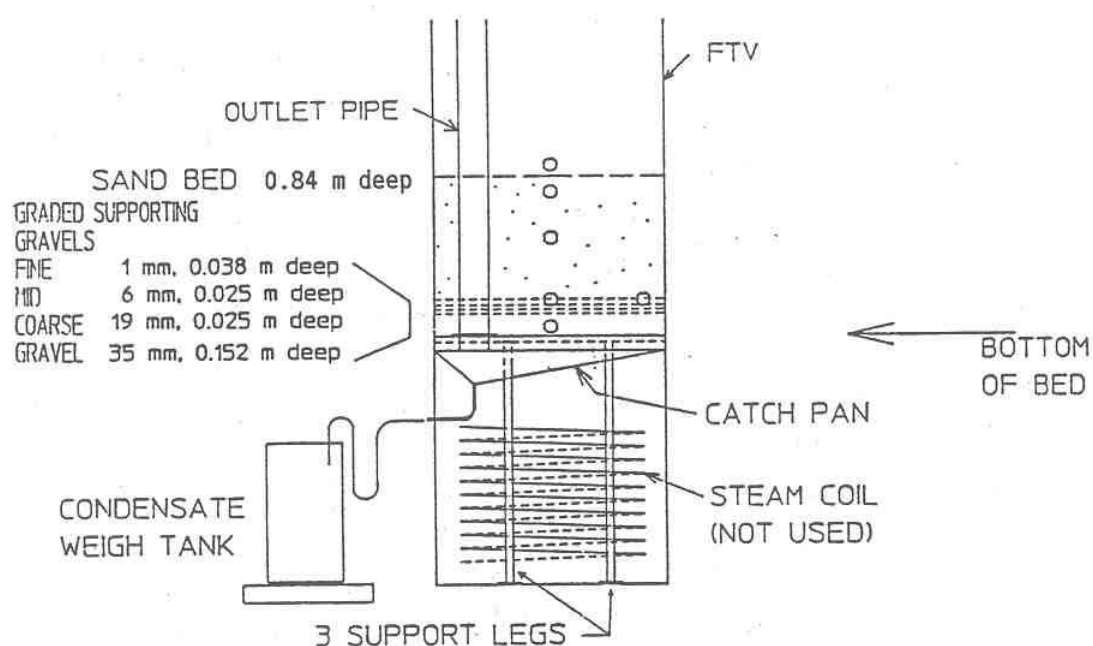


Fig. 5.9-4 Schematic layout of french sand filter

Combined venturi metal-fibre filter

A combined venturi metal-fibre filter unit, containing a venturi scrubber and a metal-fibre filter demister, which was developed by FRAMATOME ANP (former Siemens-KWU), was tested. The aerosol-laden gas flowed upward through a venturi tube and was scrubbed by water from surrounding pool, which was drawn in at the throat of the venturi and mixed with the gas. The metal fibre demister, mounted at the top of the unit, served the final filtering of the outlet gas. A schematic diagram of the filter system used is depicted in Fig. 5.9-5. Table 5.9-1 presents the boundary conditions as well as the decontamination factors measured.

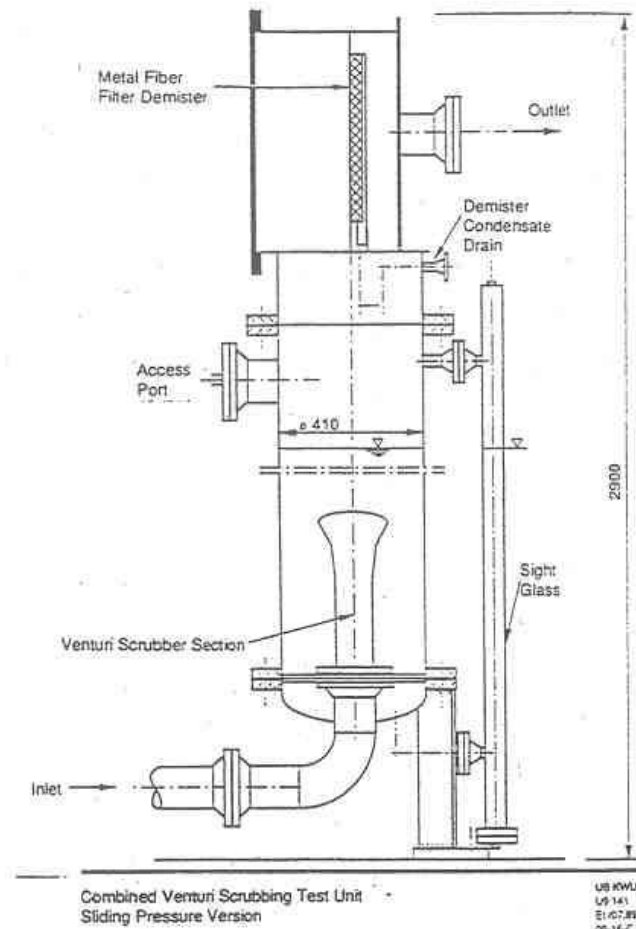


Fig. 5.9-5 Schematic diagram of combined venturi scrubber

Metal Fibre Filter

A metal fibre filter was developed by FZK (former KfK) in Germany as a possible device to remove radioactive aerosols during venting. The gas flowed horizontally through pads of stainless steel fibres of progressively smaller size. A schematic diagram of the filter system used is depicted in Fig. 5.9-6 The conducted (Table 3.4-2) demonstrated the filter efficiency at two inlet steam fractions.

Russian Filter

The filter system, developed by the former Soviet Union and tested at the ACE-Project, was consisted of two units in series. The first unit was a jet scrubber and a droplet separator above the pool to remove entrained liquid. The second unit was a dry-packed filter containing beads of an adsorbent material to remove molecular and organic species of iodine. Fig. 5.9-6 presents a schematic diagram of the filter system. The tests provided (Table 5.9-1) the aerosol removal characteristic, decontamination factor and pressure drop.

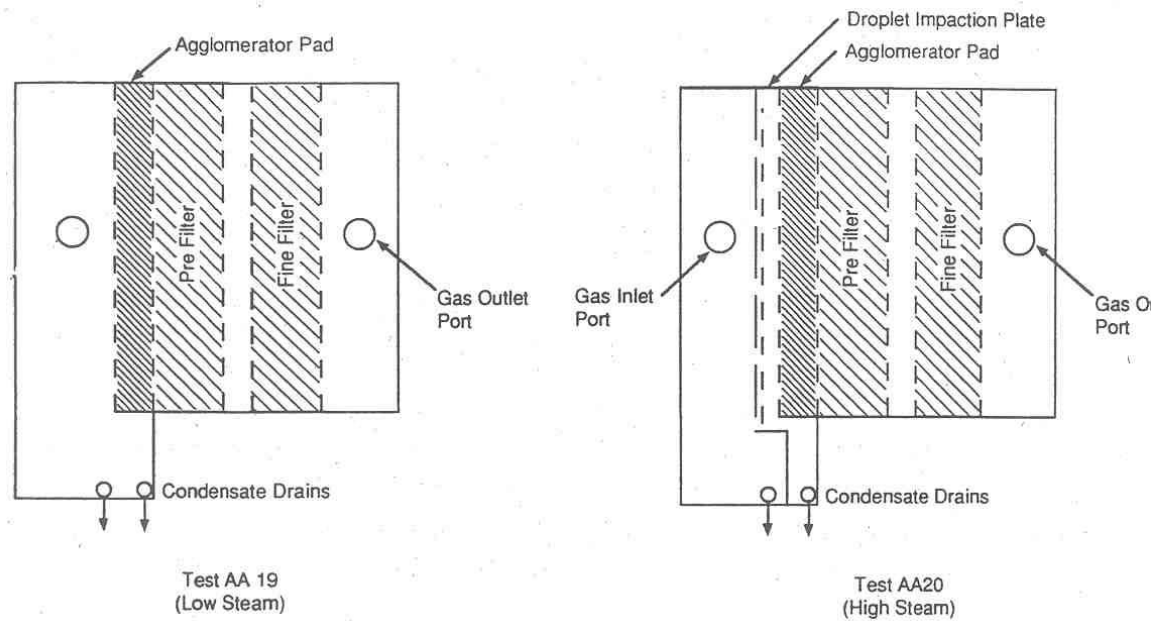


Fig. 5.9-6 Schematic diagram of metal fibre filter

5.9.2 CCI containment venting filter

CCI (former Sulzer Thermtec) in Switzerland designed and developed a wet filter system [15], composed of a specially designed orifice unit, creating small bubbles, which flow in a riser where the pool scrubbing removes the aerosol particles and gaseous species. The riser causes water and bubble circulation for an enhanced mass transfer. Upper section of the filter, containing CCI specific filter elements, removes the droplets as well as remaining aerosol particles. A schematic diagram of the filter system used is depicted in Fig. 5.9-8 Table 5.9-2 shows the results of a qualification program conducted at PSI [15]. A further qualification program on the retention efficiencies for molecular iodine and organic iodide at anticipated accident conditions was conducted in 1999 -2002 at PSI.

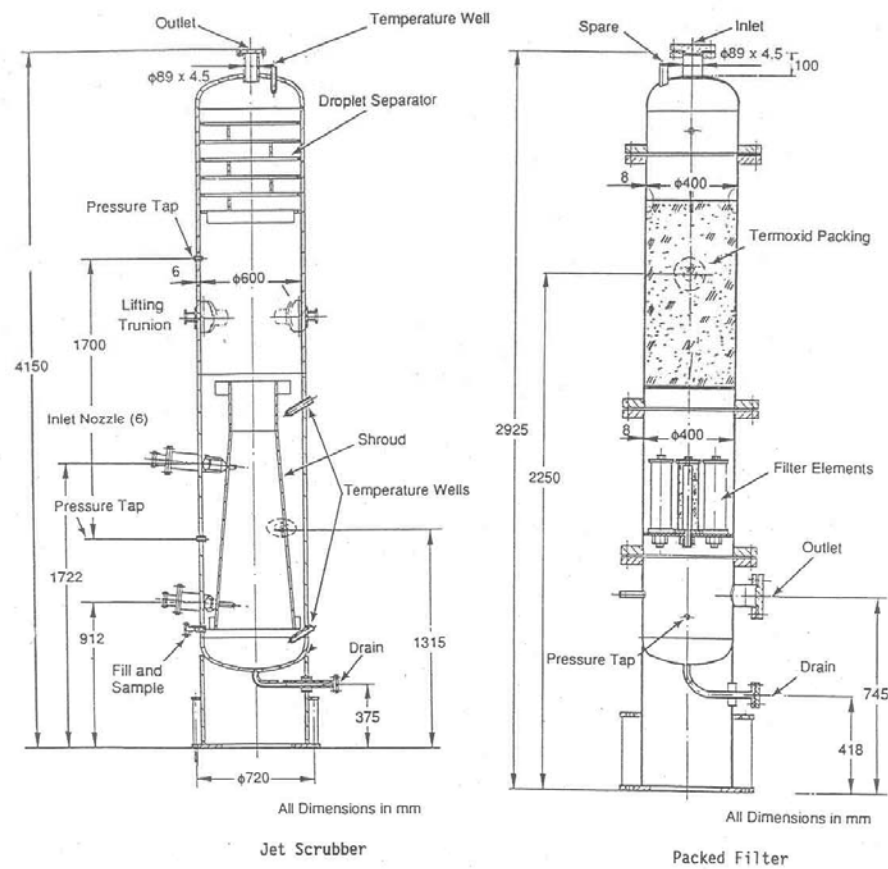


Fig. 5.9-7 Schematic diagram of jet scrubber and packed filter of the Russian filter

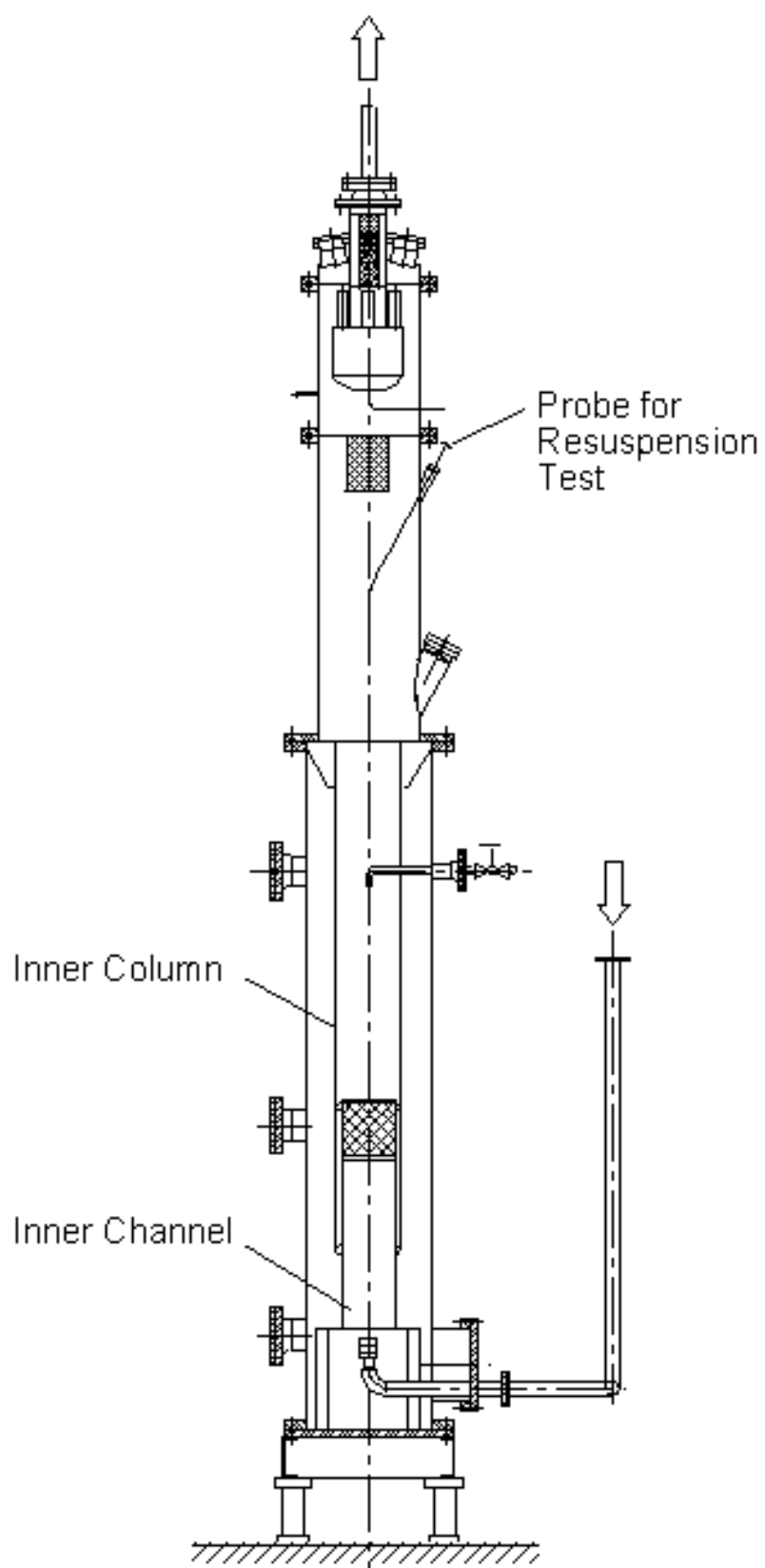


Fig. 5.9-8 Schematic diagram of CCI (former Sulzer Thermtec) containment venting filter

Table 5.9-2 Test conditions and measured decontamination factors (DF) for the CCI containment filter system

Configuration of the Filter System	‘Low Pressure’ for PWR applications	‘High Pressure’ for BWR applications	
Pressure at the inlet	3 bar	1.6 bar	5 bar
Aerosol concentration (g/m ³)	~0.2	6.4 to 15.4	1.9 to ~2.1
AMMD at the inlet (μm)	0.65	1.8	1.1
Decontamination Factor	≥ 48690	> 46300	≥ 195000

5.9.3 Removal of iodine by the containment venting filters

Gaseous iodine is scrubbed by wet scrubbers (ABBs FILTA-MVSS, Framatome ANP’s combined venturi metal-fibre and CCI’s filters), however, conditioning the filter water by use of chemicals to keep pH at a high value as well as to decompose molecular iodine or organic iodide is generally accepted procedures. No special engineering attempts were taken in the design of the gravel bed or sand bed filters, however, natural deposition processes in combination with steam condensation, which might be temporary in nature, might remove molecular iodine. The Russian system not only removes iodine by scrubbing in the filter water pool but the main removal is achieved by the dedicated iodine adsorber unit.

5.9.4 International status of use of containment venting filters

The practice of controlling pressure during a postulated severe accident in a containment of the operational nuclear power plants varies country to country due to the differences in the national regulatory practices. Therefore, the use of filters during containment venting is very plant and country specific. Most of the nuclear power plants in European countries are equipped with containment venting filters. The venting strategy is also plant and country specific. The FRAMATOME ANP’s combined venturi metal-fibre filter design, ABB’s multiple venturi and FILTRA systems, French sand bed and Swiss CCI filter are the ones currently installed in most of the units in the west, central and northern European countries.

5.10 Ongoing Tests

5.10.1 Aerosol behaviour in steam generators

5.10.1.1 Studies of vertical steam generator in the ARTIST facility

The integral tests of vertical SGs have been conducted in a representative scaled-down model of the Beznau PWR (Switzerland) SG called ARTIST facility [1]. The facility is erected and operated by PSI. The main components of the model steam generator are a bundle, a shroud, a flooding system, a full size steam separator and dryer. The bundle is consisted of 270 straight tubes, 130 bends, one break tube and two support plates. The original tube size and configuration, the distance between the tube sheet and the support plates are maintained. The bundle is attached to tube sheet. The facility is equipped with many aerosol-sampling stations. Only the bundle section of ARTIST was used in the EU-SGTR project [1] (Fig. 5.10-1). Five tests comprised the experiments performed for this project. The first three tests dealt with the aerosol retention in the break stage under dry and wet conditions. The other two tests addressed accident management (AM) issues whereby the SG bundle goes from a fully dry state to a fully flooded state. An axis-symmetric guillotine break was used and located 300 mm above the tube sheet in the middle of the bundle. The aerosol AMMD’s at the inlet were in the 2.25-3.70 μm range, while at the outlet, the AMMD’s were in the 0.49-0.84 μm range.

When the bundle is dry, and the full break flow directed into the bundle, aerosol deposition takes place all over the bundle. There is strong evidence that the aerosols disintegrate into smaller particles because of the sonic conditions at the break. This obviously promotes particle escape from the secondary and lowers the overall DF. Further investigation needs to be performed to determine the influence of the type of aerosol.

For the far-field conditions, under a flooded bundle and in the presence of steam, the DF is between 482 to 1081. A large fraction of the aerosols is scrubbed at the break level because of strong impaction of the incoming jet on the water interface and fast steam condensation. The additional water head beyond the break stage has only a secondary influence on the magnitude of decontamination. When no steam is present, the DF increases exponentially from 124 to 5739 when the water height in the bundle increases from 1.30 m to 3.6 m. The aerosol removal rate is roughly constant with height, and hence the DF is solely a function of residence time in the water pool (water height). When steam is present in the carrier gas under flooded secondary, condensation inside the tube causes aerosol deposition and produces blockages near the break, with a subsequent primary pressure rise. This has implications for real plant conditions, as aerosol deposits inside the broken tube will cause more flow to be diverted to the intact tubes, with a corresponding reduction in the source term to the secondary.

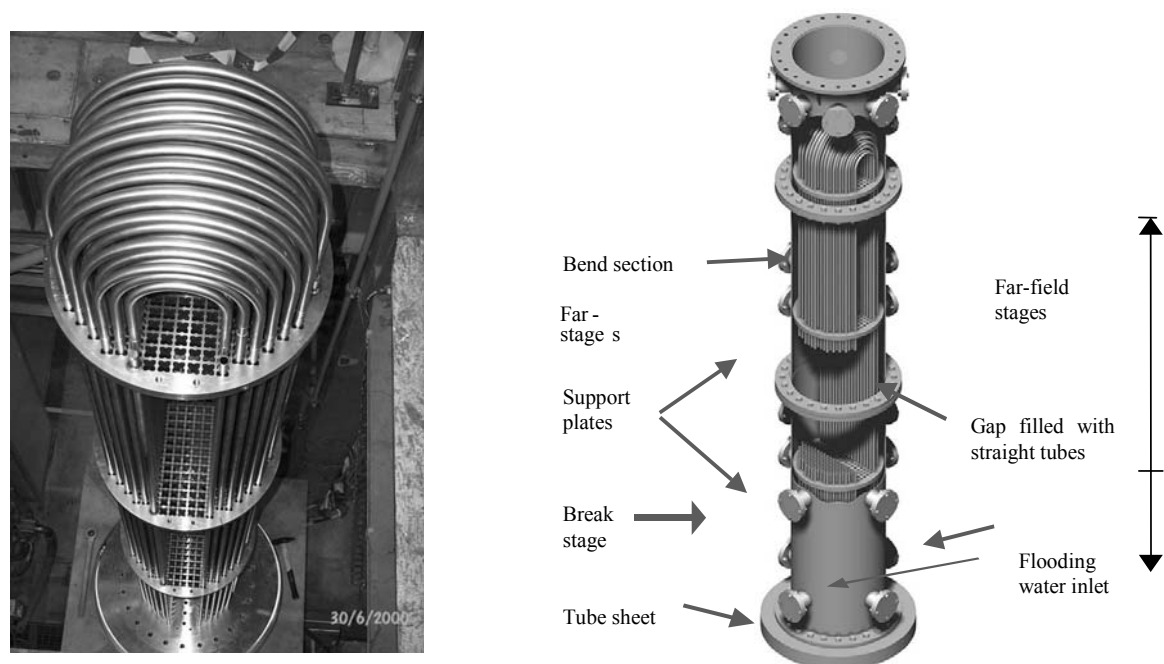


Fig. 5.10-1: Schematic and photo of the ARTIST bundle test section

The International cost share project ARTIST (2003 - 2007) addresses the specific issues associated with the aerosol behaviour in seven distinct phases:

1. *Phase I:* Aerosol retention in SG tubes under dry conditions. In this phase, in-tube aerosol deposition/resuspension is studied under high velocity conditions (up to 300 m/s). Tube length, bend curvature, and aerosol type, size and concentration are varied.

2. *Phase II*: Aerosol retention in the break vicinity under dry conditions. Aerosol deposition/resuspension at very high velocities is addressed. The break gas flow rate and break type (fish-mouth, double guillotine, vertical) are varied.
3. *Phase III*: Aerosol retention in the bundle far from the break, under dry conditions. Aerosol deposition due to thermophoresis and impaction is studied at relatively small velocities (less than 1 m/s) because the flow has evened out across the secondary side flow area. The gas flow rate and the gas-structures temperature differential are varied.
4. *Phase IV*: Aerosol retention in the separator and dryer under dry conditions. This phase studies aerosol impaction and interception due to complex 3D flows in the upper components of the SG. The gas flow rate and the gas-structures temperature difference will be varied.
5. *Phase V*: Aerosol retention in the bundle section under flooded pool conditions. This phase investigates condensation-induced aerosol scrubbing by the SG water pool as well as inertial impaction upon the structures. The break flow rate, pool submergence, carrier gas steam content and pool subcooling are varied.
6. *Phase VI*: Droplet retention in separator and dryer sections under dry conditions. This phase deals with Design Basis Accident (DBA)-type phenomena i.e. the potential for “primary bypass”, whereby a break at the top of the tube bundle sprays fine primary liquid droplets that might find their way to the environment through, for example, a stuck-open safety valve. Carrier gas flow rates and droplet sizes are varied to match prototypical Stokes numbers.
7. *Phase VII*: Integral tests. The seventh set of experiments is integral in nature and is focused on aerosol retention in the whole model SG. The conditions of the tests will be determined based on insight gained from the results of the previous phases.

ARTIST project has further demonstrated and highlighted significance of various mechanisms that might have a potential to alter the aerosol behaviour:

- a) De-agglomeration of aerosol agglomerates subjected to high shear.
- b) Effect of high turbulence on the particle agglomeration and hence the sedimentation velocity of the agglomerates.

Current ARTIST tests demonstrated that if aerosol agglomerates experience a large shear force they could display a shift in the size distribution since smaller particles are generated. As an example, the deagglomeration of aerosol agglomerates has caused a reduction in the aerodynamic mass median diameter from an initial value of 3-4 μm to about 2 μm . Further de-agglomeration did not happen. Large shear forces under the actual conditions can be generated by very high (up to sonic) velocity in the tubes or in a sonic front when the aerosol laden gas is discharged from a break into the secondary side from the primary which could be at a pressure at least 2 times higher than the secondary side. The physics of deagglomeration is not currently fully understood. The relevance of the deagglomeration to the SG tube rupture issue is that the deagglomeration can modify the aerosol input size distribution significantly as the aerosols enter into the secondary side from the break.

The ARTIST tests also demonstrated a significant amount of settled aerosol agglomerates at the floor of the 1:1 sized dryer unit but not so much on the surfaces of the dryer panels. The flow recirculation coupled with local turbulence produce a faster settling of aerosols than predicted. Research is underway to understand the mechanisms responsible for enhanced settling rates of aerosols inside cavities with

prevailing turbulent natural convection. The research makes use of Direct Numerical Simulation (DNS) coupled with Lagrangian particle tracking to determine the particle trajectories and hence their deposition rates. DNS is a rigorous methodology, which computes turbulent flow fields without introducing any modelling of turbulence. To obtain this detailed knowledge, high space and time resolutions are needed, and hence the requirements for computer power are significant.

5.10.1.2 Integral experiments of horizontal SG in the HORIZON facility

Integral experiments of horizontal SG were conducted in HORIZON facility [2] (Fig. 5.10-2), which is a scaled-down model of horizontal SGs used in VVER-440, with tube dimensions similar to real SGs. The objective of the studies was to gather data on aerosol behaviour in the primary side of the SG tubes at realistic pressure and temperature levels in different flow velocities representing either the defect or intact SG tubes. The importance of the intact tubes on the overall primary side deposition depends on the break location along the defect tubes. The data were used for the model development.

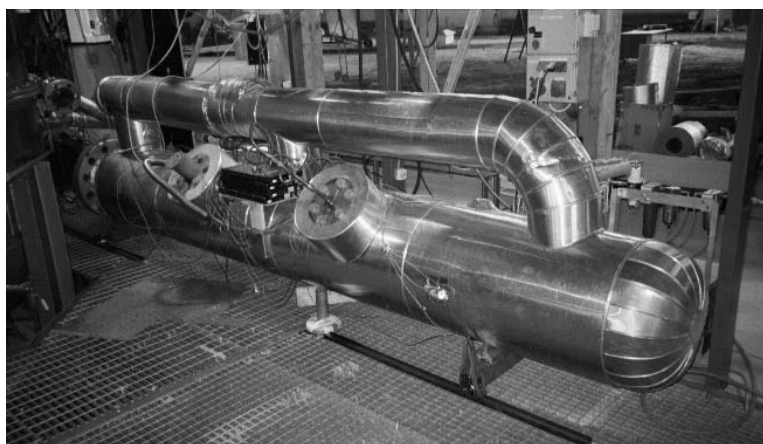


Fig. 5.10-2 Picture of the HORIZON facility

The results of aerosol deposition on the primary side of the horizontal SG were compared with the values obtained from the calculations with the existing deposition models. It appeared that the current models are adequate at low Reynolds numbers (Re) below 5000, but give too high deposition velocities at high Re above 70 000 compared to the experimental results. The turbulent impaction is considered to be the main deposition mechanism at high Re . However, the effect of resuspension, which becomes significant at high Re , is not usually taken into account in the calculations, and it should be added to the models. When looking at the amount of deposited material as a fraction of the material injected into the tubes, it is seen that in all experiments the deposited fraction per unit length has a peak at the tube bend. The effect of flooding the secondary side with water was also shown to be significant. Still, majority of the aerosol injected into the tubes is transported as aerosol out of the tubes, and therefore, the effect on environmental releases is small. More important effect of the secondary side flooding comes from the secondary side mechanisms such as pool scrubbing.

5.10.1.3 Separate effect studies of vertical SG in the PECA facility

An experimental program was carried out in the PECA rig of the Laboratory for Analysis of Safety Systems of CIEMAT [3]. The test section consisted mainly of a scaled mock-up of the tube bundle (Fig. 5.10-3) of a SG that was introduced in the 8 m³ vessel of the PECA facility. The test matrix was set up based on best estimate calculations for two real pressurised nuclear power plants [4]. The major variables to be analysed were type (guillotine and fish-mouth) and orientation of the breach and gas flow

rate. TiO_2 particles were used to keep the tests as similar as feasible to ARTIST's and, as there, there were evidences of particle fragmentation during the tests.

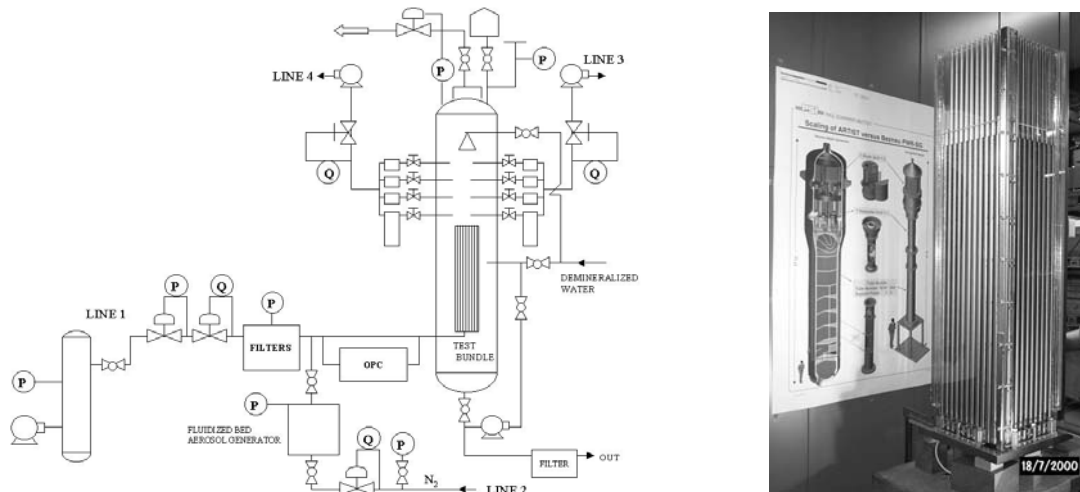


Fig. 5.10-3 Picture of the bundle used in the PECA facility

Particle retention within the breach stage of a SG was observed to be rather low (less than 20 %) under the studied conditions. This result looks consistent with those from ARTIST.

The results indicated that retention efficiency decayed with gas mass flow rate from 100 kg/h to 250 kg/h follows a very simple correlation [3].

The type of the breach and the breach orientation did not result in quantitative differences in the mass removed from the aerosol source coming into the secondary side, when gas flow rates were above 100 kg/h. Conversely, when flow rates were lower the mass retained in all the break configurations did distinguish clearly from each other. The deposition pattern within the bundle was proved to be highly dependent upon breach type. Guillotine tests showed a squared-shaped deposition profile, while in fish mouth tests a triangular-shaped one was observed. In addition, retention in guillotine type break was concentrated on the first nearest tubes, while in the fish-mouth configuration farther tubes as a whole gave a significant contribution to the total mass depleted.

5.10.1.4 Separate effect studies of horizontal SG in the PSAERO facility

The separate effect experiments of horizontal SGs were conducted in PSAERO facility [2] (Fig. 5.10-4). The separate effect experiments were designed to complement the integral experiments conducted with the HORIZON facility. In the experiments aerosol deposition and the movement of deposited particles were measured online using radiotracer technique. The objective of the experiments was to gain mechanistic understanding about aerosol behaviour in the SG tubes.

Resuspension was observed to take place simultaneously to deposition in turbulent flow. Particles most probably resuspended as large agglomerates, since the deposition velocity of resuspended particles was observed to be much higher than that of the injected aerosol. It was also evident that the resuspended agglomerates mainly moved close to the surface. The relation with the deposition and time dependence of the process requires that resuspension should thus be modelled dynamically

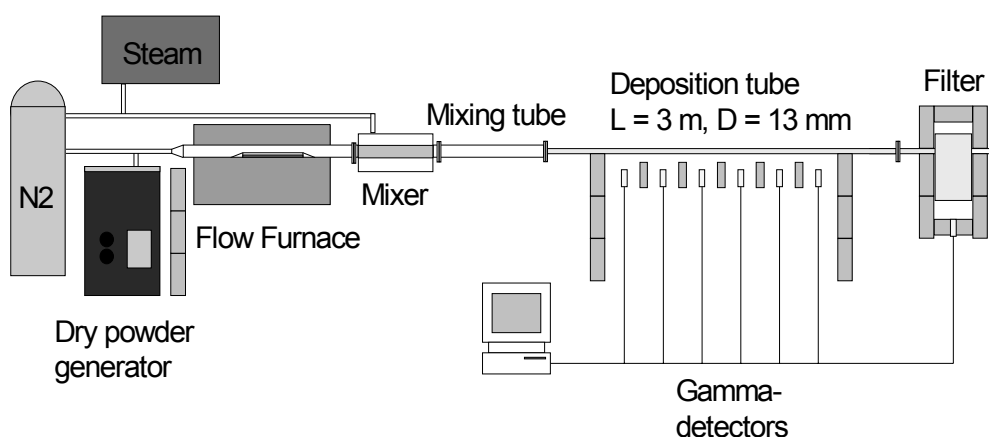


Fig. 5.10-4 A schematic picture of the PSAERO facility

The flow rate during the deposition phase had a very significant impact on the strength particles adhered to the surface. It was evident that particles deposited in a higher flow rate were much harder to resuspend than was the case with a lower flow rate. The probable reason for this was that impaction of large particles packed the deposit near the tube inlet. Therefore, resuspension was first observed close to the outlet of the tube, where the deposit was mainly formed by settling.

Particle diameter was also observed to be an important parameter in determining the adhesion of deposit. When results from these experiments were compared to previous studies, it was noted that polydisperse aerosol adheres to the surface much better than monodisperse aerosol [5]. The reason for this is that particles in the deposit layer have more contacts to other particles than is the case with monodisperse aerosol. A major problem in resuspension modelling is that the effect of particle size distribution is generally not taken into account. Parameters derived from experiments, conducted with monodisperse particles, should be used with caution in models describing the behaviour of polydisperse aerosol. As a further complication, surface roughness of the particles significantly influenced the adhesion, even if the size distribution of aerosol did not change.

The results from the experiments were adequately reproduced with a correlation model that used friction velocity as a variable. This can be understood, if it is assumed that turbulent bursts are the main mechanism for particle resuspension. The frequency of turbulent bursts in laminar sub-layer depends primarily on the friction velocity. The impaction of large particles must also have caused erosion. A significant fraction of the already deposited particles were knocked from the surface and subsequently deposited further downstream.

References

- [1] S. Güntay, D. Suckow, A. Dehbi, R. Kapulla "ARTIST: Introduction and first results" Nuclear Engineering and Design, 231(2004) 109-120
- [2] A. Auvinen^a, J.K. Jokiniemi^a, A. Lähde^a, T. Routamo^b, P. Lundström^b, H. Tuomisto^b, J. Dienstbier^c, S. Güntay^d, D. Suckow^d, A. Dehbi^d, M. Slootman^e, L. Herranz^f, V. Peyres^f, J. Polo^f, "SG tube rupture (SGTR) scenarios" Nuclear Engineering and Design 235 (2005) 457–472
 - ^a VTT Processes, Biologinkuja 7, P.O. Box 1602, VTT Espoo 02044, Finland
 - ^b Fortum Nuclear Services, Vantaa, Finland
 - ^c Nuclear Research Institute Rez plc, Czech Republic
 - ^d Paul Scherrer Institute, Villigen-PSI, Switzerland
 - ^e Nuclear Research and Consultancy Group, Arnhem, Netherlands
 - ^f Centro de Investigaciones Energeticas, Medioambientales y Tecnologicas, Madrid, Spain

- [3] L.E. Herranz, F.J.S. Velasco, C. López del Prá "Aerosol retention near the tube breach during SG tube rupture sequences" Nuclear Technology, Accepted for publication, 2005
- [4] P. Bakker, M. Sloodman, J. Dienstbier, S. Güntay, L. Herranz, J. Jokiniemi, T. Routamo, Accident Management Aspects of EU-SGTR Project Workshop on Implementation of Severe Accident Management Measures, NEA/CSNI/r(2001)20, 2001
- [5] L. Biasi, A. de los Reyes, M.W. Reeks, G.F. de Santi "Use of a simple model for the interpretation of experimental data on particle resuspension in turbulent flows" Journal of Aerosol Science 2001, 32, pp.1175-1200

5.10.2 EVAN

Within the ISTC (International Science and Technology Center) frame some Russian organisations headed by 'Saint Petersburg Research and Design Institute ATOMENERGOPROEKT' have just started with the work on a project called EVAN (Ex-Vessel Source Term Analysis [1]). Some Western partners like VTT (Finland), GRS (Germany), CEA and IRSN (France), PSI (Switzerland) and ITU of the Joint Research Center (EC) have joined the project as so-called collaborators.

Concerning aerosols there are two experimental tasks of the working programme being of particular interest:

- aerosol, transport, deposition and resuspension in the primary circuit
- release of low volatile fission products from a molten pool

In a first project phase scoping tests are planned. Concerning the aerosol behaviour in the circuit the upwards flow of liquid and solid aerosol particles (up to 10 µm) respectively will be investigated in a vertical pipe with 6 m height and 36 or 98 mm diameter. These EVAN tests are adjacent to the former STORM tests (see chapter 5.2.3) in which transport, deposition and resuspension in horizontal pipes were investigated.

In the scoping phase for the release tests low volatile compounds of the elements Mo, Ce, La, Sr and Ba will be examined. Their release from an UO₂-ZrO₂-Zr pool under oxidizing conditions at temperatures in the range of 50 - 100 K above T_{liq} will be measured. It is expected that these EVAN tests increase the knowledge based on past EC projects [2, 3]. For the future some Western partners recommend to vary the pool composition and to add in some tests the main decomposition products from molten-corium-concrete-interactions.

In parallel to the experiments analytical work is planned.

References

- [1] ISTC The 'Ex-Vessel Source Term Analysis' (EVAN) ISTC project includes theoretical and experimental research on the processes affecting the late phase fission
- [2] C.G. Benson, H. Hein, M.P. Kissane, M.K. Koch Fission Product Release from Molten Pools: Final Summary Report, CEC, 4th Framework Programme on Nuclear Fission Safety, Contract No. F14S-CT96-0021, ST: MP(99)-P031, May 1999
- [3] A.M. Beard, S. Bechta, C.G. Benson, V.T. Berlepsch, F. Funke, C.C. Kemp, M.P. Kissane, M.K. Koch, J. Kronenberg, B. Kujal, M.S. Newland, K.-G. Petzold, H. Plank, W. Plumecocq Late Phase Source Term Phenomena: Final Report, 5th EURATOM Framework Programme, Contract No. FIKS-CT-1999-00005, SAM-LPP-D032, July 2003

5.10.3 Penetration leakage tests

A series of experiments are being performed at AECL on water droplet aerosol leakage through simulated containment leak paths. The experiments are designed based on the assumption that aerosol leakage through containment leak paths such as valves and airlock-door seals will be characterised by an abrupt change in the cross-sectional flow area, where gas and aerosol flows move from a high pressure (containment) region, through small gaps resulting from seals or valves being improperly seated, to a lower pressure region. The abrupt change in flow area for a pressurised flow is expected to lead to aerosol leakage occurring under choked-flow (or sonic) conditions at the contracted portions of the leak paths.

The experiments are described in detail in Section 3.1.3. They are performed in a cubic plexi-glass chamber fitted with an aerosol characterization port. The chamber also contains two matched sampling lines fitted with filtration ports (U1 and U2). The U1 line has a high efficiency filter assembly to collect water droplets upstream of the prototypical leak path, whereas the U2 line has the filter assembly downstream of the leak path. Each line is connected to a rotameter through a valve to measure and match the flow rates through each path. Choked-flow conditions are achieved by maintaining low pressure downstream of the leak paths sufficient to ensure that the downstream-to-upstream pressure ratio is lower than 0.53. A vacuum pump is connected to the downstream port of the rotameters to maintain the low pressure.

A Cyclone Fogger (Curtis Dyna-Fog[®], Model 3000) containing a solution of an uranine (sodium fluorescein) dye in water is used for aerosol generation. The dye fluoresces at a characteristic wavelength and concentrations of the water retained on the filter assemblies and in the leak paths can be determined using fluorescence spectrophotometry. In a typical experiment, the vacuum pump is started, and the flow valves for each line are adjusted so that the rotameter reading on each line is the same. The fogger is switched on to inject aerosols into the cubic reservoir, and a phase-Doppler anemometer (PDA) is focused through the aerosol characterization port to measure the mean (average) diameter of wet aerosols. Droplet mass concentration is not measured, but can be estimated from the ratio of the aerosol injection rate and the volumetric flow rate through the filtration port. The experiments performed to date have been ambient temperatures. Filters and leak path assemblies are removed after each experiment and washed thoroughly with known quantities of distilled water, to re-dissolve the deposited uranine dye. Samples of the filter and leak path washes are then submitted for fluorescence analysis to determine the uranine concentration.

The wet aerosol experiments indicate that there is significant aerosol transport through single leak path contractions representative of airlock door seals and isolation damper valves in CANDU containment, and that leak path plugging does not occur. Further experiments are required to characterise aerosol transport through sequential expansion and contraction regions representative of the leak path from containment to the outside atmosphere during a postulated accident scenario. Additional experiments are also required to evaluate the extent of leak-path plugging at the higher aerosol mass densities (up to $1000 \text{ g}\cdot\text{m}^{-3}$) that could be anticipated during the containment over pressurization period in a CANDU accident scenario.

In connection with these investigations Japanese results [1] reported at the Cologne Workshop in 1998 should be mentioned. Their results of experiments are dealing with fission product trapping in the leakage paths of the containment. Three series of tests were conducted to study the containment integrity under accident management, the failure temperature, and the fission product retention along the leakage paths, respectively. No leakage was detected under Japanese accident management conditions of 200°C containment temperature and twice the design pressure. Beyond these conditions, a small leakage was observed at temperatures above 280°C . Fission product decontamination factors of 10 to 1000 were observed along the leakage paths depending on the type of penetration studied.

In 1998 there was agreed that knowledge of fission product retention in containment leakage is adequate for the types of paths looked at (small electrical penetrations, flanges). Additional work would be needed to assess the leakage and retention through other types of paths such as containment cracks.

Reference

- [1] A. Watanabe, T. Hashimoto, M. Osaki Fission Product Aerosol Trapping Effects in the Leakage Path of Containment Penetration under Severe Accident Conditions Workshop "Nuclear Aerosols in Reactor Safety", June 1998 NEA/CSNI/R(98)4 (February 2000)

Private communication between J. Ball and the Chairman.

5.10.4 ThAI aerosol tests

The technical-scale ThAI test facility (ThAI = Thermal hydraulics, Aerosols, Iodine) has been operated since 1998 by Becker Technologies at Eschborn, Germany, with the objective to provide an experimental data base for validation of lumped-parameter and CFD (Computational Fluid Dynamics) containment codes. Tests have been performed in the areas of containment thermal hydraulics, hydrogen distribution, combustion and mitigation, and behaviour of fission products, in particular aerosols and iodine, with respect to a potential source term [1].

Fig. 5.10-5 depicts the ThAI facility including its auxiliary rooms. Main component of the facility is the 60 m³ stainless steel vessel, 9.2 m high and 3.2 m in diameter. It can be operated up to 180 °C and 1.4 MPa overpressure, and withstand moderate hydrogen deflagrations. The vessel volume can be subdivided by removable inner structures into any multi-compartment configuration. The cylindrical part of the test vessel is equipped with three independent heating/cooling jackets for controlled wall temperature conditioning. The outer sides of the vessel and the heating/cooling jackets are thermally well isolated by rockwool. A large top flange and two man holes provide access to the interior of the vessel for modifications of internals and instrumentation. Measuring flanges on five levels at five circumferential positions allow installation of in-situ optical and conventional instrumentation, and of sampling lines. Feed systems are available for injection of steam, air, gas (e.g. helium or hydrogen), iodine, and aerosols at variable positions.

In the first ThAI test programme (2000 - 2003) exclusively thermal hydraulic tests on stratification phenomena in a multi-compartment geometry and iodine tests were carried out. In the second ThAI programme (2003 – 2006) additional tests on the aerosol issues re-entrainment from a boiling sump, resuspension by a H₂ deflagration, thermal decomposition of a CsI aerosol in a PAR (**p**assive **a**utocatalytic **h**ydrogen **r**ecombiner), and the formation of IO_x aerosol were made. They are described here briefly.

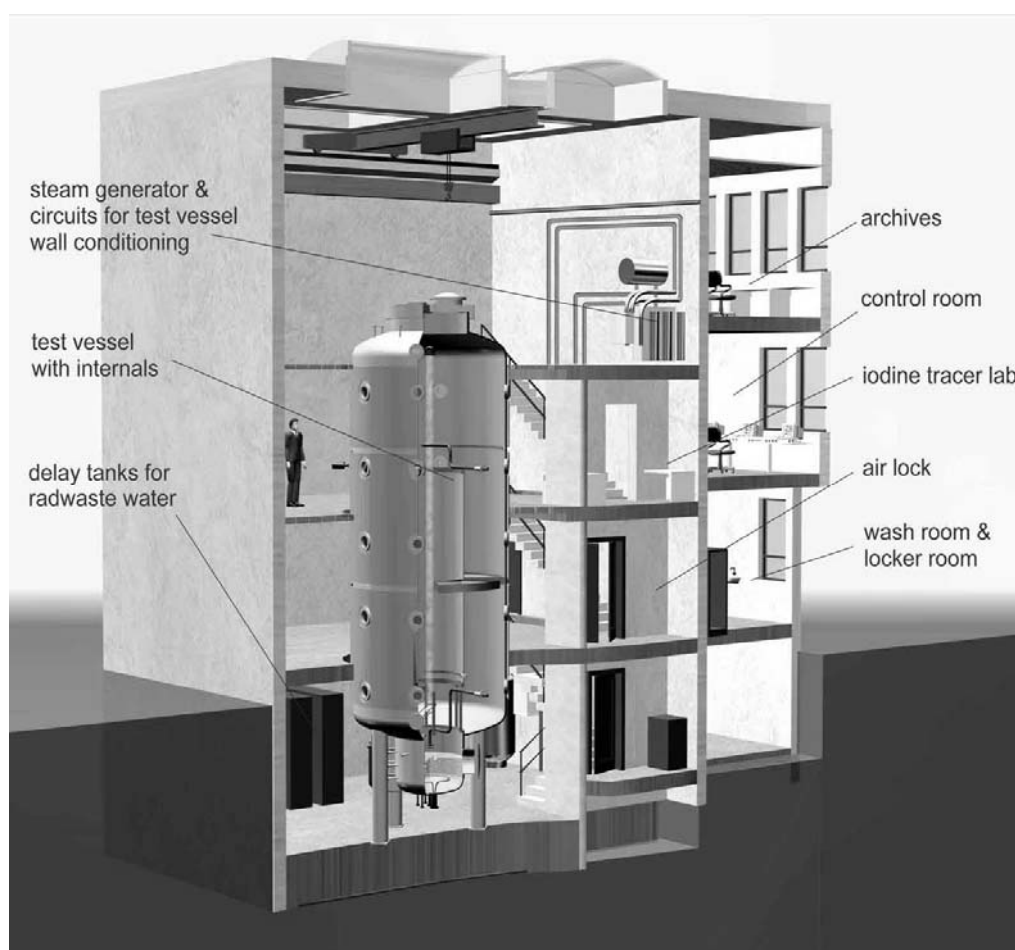


Fig. 5.10-5 ThAI facility with 60 m³ test vessel

Re-entrainment from a boiling sump

Two ThAI re-entrainment tests were made with a boiling sump surface (0.55 m²) being larger than used in earlier tests, a large gas volume above the sump (60 m³) and sophisticated aerosol instrumentation. Non-radioactive soluble CsCl and KI salts were added as fission product simulants to the boiling sump. The maximum heating power of the sump was 75 kW. In both tests the atmosphere was superheated and the released droplets dried there. The measured re-entrainment values confirm the results of the former REST tests and the KWU tests, but due to the better aerosol instrumentation the measured droplets and the dried particles respectively were significantly smaller. For the dry aerosol a mass median diameter < 0.1 µm was found. These findings may have an influence on source term estimations and should be considered.

Resuspension by a H₂-deflagration

In three ThAI tests the “dry” resuspension of deposited aerosol by a H₂ deflagration was measured. First a layer of deposited aerosol was prepared by injecting CsI aerosol followed by a settling period of 24 h. Then the 5.5 m long deflagration tube was filled with a hydrogen/air mixture and ignited. The burnt gas escaped through a slit nozzle at the bottom in horizontal direction over the aerosol deposits. Only a relatively small area was blown on by the gas with a maximum velocity between 17 and 70 m/s. However, a significant portion of the CsI was resuspended as the measured peak in the airborne aerosol concentration indicates

Just after the deflagration the measured particle size shows a large fraction of coarse particles. It has to be mentioned that gas velocities caused by faster deflagrations, local detonations and fuel-coolant interactions will be significantly higher resulting in a higher resuspended aerosol fraction. The tests are a valuable extension for the poor data base on resuspension at highly transient gas flows.

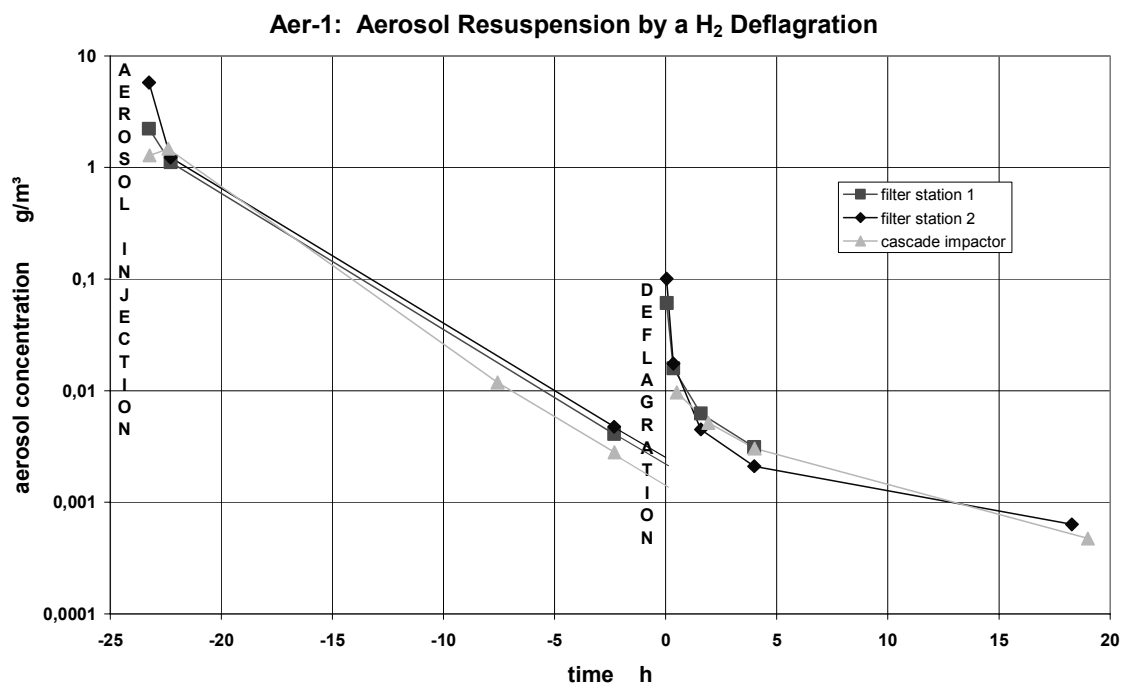


Fig. 5.10-6 Aerosol resuspension by a hydrogen deflagration in the ThAI vessel

Thermal decomposition of a CsI aerosol in a PAR

Passive autocatalytic hydrogen recombiners (PAR) are installed in LWR containments in order to reduce the hydrogen concentration in the case of a reactor accident. Laboratory-scale tests have shown that in a PAR CsI aerosol will be decomposed into gaseous molecular iodine (I₂) and CsOH aerosol at high temperatures. It is necessary to know the reaction because volatile species as I₂ or organic ones can be easily released to the environment. The volatile species do not deposit in such a degree as iodine aerosols and their retention in filters is less efficient.

Two ThAI tests were made on the interaction of a CsI aerosol with a commercially available PAR from Framatome ANP. First the CsI aerosol injection was started, then hydrogen was injected which continuously recombined in the PAR. The CsI concentration lay between 0.1 and 1.0 g/m³ and the maximum hydrogen concentration was approximately 9.0 Vol.-%. In both tests no I₂ could be detected, i.e. the CsI decomposition rate was always smaller than 3 %.

Formation of IO_x aerosol

Ozone produced under reactor accident conditions in the containment atmosphere will react with molecular iodine (I₂) forming an IO_x aerosol. Two ThAI tests were performed on the so-called iodine/ozone reaction. Surface effects have been significantly reduced compared to laboratory-scale tests.

In both tests ozone produced in a commercial apparatus was released to the vessel atmosphere containing approximately $1 \cdot 10^{-8}$ mol/l I_2 . The ozone concentrations were different in the two tests. In one test the gaseous I_2 was totally converted to IO_x (gas-to-particle conversion) while in the other test only a portion of the I_2 reacted. The measured particle size distribution of the generated fine disperse IO_x aerosol had a mean particle diameter of 0.2 μm . In these tests no so-called background aerosol simulating the nuclear aerosol was present. Such a test is planned in the next ThAI program.

The third ThAI program (2006 – 2009)

A major part of the tests planned in the German ThAI-3 program is offered to international participation in the frame of an OECD project. Among others two aerosol issues will be investigated in ThAI-3.

In continuation of the tests in ThAI-2 the formation and behaviour of an IO_x aerosol will now be measured in the presence of a simulated nuclear aerosol. The fine-disperse IO_x aerosol generated in the ThAI-2 tests remained airborne over a long period of time. It is expected that in the new tests the IO_x will be rapidly taken up by the nuclear aerosol and that the settling of the mixed aerosol with IO_x is significantly faster than for the IO_x aerosol alone.

A new issue is the wash-down of deposited aerosols from wall surfaces by condensate. Of particular interest is the distribution of the fission products between walls and sump especially with respect to decay heat effects. Decay heat released in the sump produces steam and raises the containment pressure while a decay heat release into walls and gas dries the containment atmosphere. For wash-down investigations two vertical coolers will be installed in the ThAI vessel, one with a steel surface the other with a painted surface. They will be exposed to condensing atmospheres containing soluble and insoluble aerosols as well as gaseous iodine. The time-dependent aerosol concentrations on the walls and in the sump will be measured.

Reference

- [1] T. Kanzleiter, G. Poss, F. Funke, H.-J. Allelein THAI Multi-Compartment Test Program Proceedings of ICONE14 14th International Conference on Nuclear Engineering, July 17-20, 2006, Miami, Florida, USA

5.10.5 Impact of catalytic hydrogen recombiners

Background

Passive hydrogen re-combiners have been studied for many years as a means of preventing accumulation of hydrogen in the containment of a water-cooled reactor following a design-basis or severe accident [1, 2]. Their installation is now an established and sometimes mandatory measure. Back-fitting of such devices on existing nuclear power plants has been performed or is in progress in many countries while Generation III reactor designs (AP600, EPR, etc.) are already equipped with them.

Passive autocatalytic recombiners (PAR) are usually based on palladium and/or platinum dispersed on some substrate medium. A PAR comprises a vertical conduit with the catalytically-active part near the bottom. If hydrogen is present in the containment, the hydrogen molecules making contact with the noble-metal catalyst react with the oxygen of the containment atmosphere producing steam and heat. The reaction heat provokes heating up of the catalytic elements inducing natural convection which draws more of the containment atmosphere into the PAR from below. The effect is not only to recombine hydrogen with oxygen as it passes through the catalytic elements but to mix the containment atmosphere eliminating any pockets where hydrogen concentrations may be elevated. We note also that carbon monoxide is oxidised on the catalysing surface. While the operating principle of PARs is well understood, there remains

some progress to be made before it can be said that a thorough understanding exists of the sensitivity of PARs to the conditions expected to be produced by design-basis or severe accidents. It should be noted, however, that while little information is in the public domain (e.g., see [2, 3]) much more probably remains proprietary. There are a number of companies marketing PARs, e.g., Atomic Energy of Canada Limited, AREVA/ Framatome-ANP, Nuklear Ingenieur Service mbH, Electrowatt-Ekono AG, and each design is different having its own operating characteristics.

There is a potential problem with the use of PARs in relation to aerosol particles suspended in the containment atmosphere. As these pass through the catalytic elements they will be heated up along with the gases and this will inevitably lead to partial evaporation of volatile species from the aerosols. Peak temperatures of the catalytic elements vary according to the manufacturer. In any case they are about 500 °C and higher. But the gas temperatures between the elements are significantly lower except for the boundary layer close to the elements. The level of temperature is strongly dependent from the H₂-concentration in the gas. These high temperatures might be high enough to evaporate some fission product species. These fission-product vapors may well interact chemically with each other and/or with the gases of the atmosphere (in general a combination of nitrogen, oxygen, steam, carbon monoxide and carbon dioxide), especially oxygen. There is therefore the possibility that reactions in PARs could lead to formation of more volatile forms of fission-product species aggravating the source term by converting easily-filtered aerosol material into more troublesome vapors and gases.

RECI tests

A series of experiments, known as RECI, has been performed to investigate the thermal decomposition of fission-product species in conditions related to those of a severe accident [4]. The objective of the RECI experiments was measurement of any creation of more volatile forms of iodine, viz. I₂, HOI and HI, from metal-iodide species expected in severe accidents, viz. AgI, InI, CdI₂ and CsI. Two of these species, cesium iodide or cadmium iodide, in an atmosphere of humidified air were injected as aerosols into a heated tube in tests both with and without the presence of a catalysing surface. The experiments comprised separate tests for aerosols of each of the two pure substances. The peak temperature of the heated tube was varied between 500 and 950 °C. The gas-phase iodine species were not measured in the heated tube but downstream where temperature had once again become ambient. It was found that thermal decomposition producing molecular iodine could occur even for the more stable of these species, cesium iodide, where the presence of a catalyst increased the iodide to iodine conversion by a factor of two to three. At the highest temperatures, conversion rates of more than 10 % were measured for cesium iodide. Conversion rates for cadmium iodide were significantly greater. Sensitivity to parameters such as particle size and transit time through the heated zone was checked where longer transit times and smaller particles led to higher conversion rates. A further effect of the partial evaporation of the aerosols was to produce a population of small particles as the vapor(s) re-condensed during cooling downstream of the heated tube. This new population resulting from homogeneous nucleation was significantly smaller than any of the source particles injected into the heated tube.

One of the worst actors poisoning catalysts used in PARs may be sulfur being part of the air atmosphere inside the containment and coming from cable insulation in cases of fire. Another potential effect of the molecular iodine production would be to poison the catalyst with respect to hydrogen conversion. However, in separate effect tests, this poisoning was found to be very limited [3].

Initial analysis of the RECI tests supports the idea that the maximum gas temperature (incl. boundary layer) and the kinetics of the chemical reactions downstream of the heated zone are keys to the understanding of the conversion process. In other words, if a thermodynamic approach to chemistry is assumed (i.e., equilibrium chemistry) as the flow cools then the volatile species convert back to less volatile forms and conversion is virtually zero. Furthermore, the conversion rates calculated at the peak

temperature, i.e., in the heated tube, are close to those measured at ambient temperature implying almost complete quenching of chemical reactions once they left the heated tube.

It should be understood that these experimental results are simply a confirmation of the potential for iodine species from containment aerosols to convert to more volatile species while in transit through a PAR. A number of representativity aspects prevent these results from being extrapolated to the reactor case. In the first instance, the aerosols investigated were pure substances: the consequences of using prototypical mixed-substance aerosols will necessarily alter the gas-phase chemistry produced in the PARs. In addition, the presence of mixed aerosols with refractory kernels will perhaps facilitate re-condensation of evaporated species during cooling onto existing aerosols rather than formation of new ones, i.e., heterogeneous rather than homogeneous nucleation. The gas mixture used in these tests was humidified air where, in the containment, at least during a severe accident, a less-oxidizing mixture containing a higher steam fraction as well as hydrogen will be present: it is known that reducing conditions are thermodynamically less favourable to formation of volatile iodine species. Finally, the cool-down characteristics of the flow leaving the PARs have not been reproduced in the RECI tests: this is crucial to the propensity for vapors to re-convert as they cool where more rapid cooling will not favour this re-conversion to a gas-vapor-aerosol mixture closer to that at equilibrium at ambient temperature.

ThAI tests

(see chapter 5.10.4)

Conclusions

Analytical experiments have demonstrated that there is potential for PARs to generate volatile forms of iodine, namely molecular iodine, by thermal decomposition of metal-iodide species contained in containment aerosols. It is uncertain whether such chemical transformations will be reproduced in conditions fully representative of an accident (a certain mitigation of molecular-iodine production might be expected in realistic conditions) where a new programme of experiments introducing more representativity is being planned. It has also to be recognised that iodine may not be the only fission product concerned: some formation of the highly volatile species ruthenium tetroxide is possible in the conditions expected within the PARs though no investigation of this has been performed. Nevertheless, on the basis of current knowledge, any speculation as to the consequences for the source term of PAR operation during an accident would seem unwise though, clearly, negative effects seem possible.

References

- [1] F. Fineschi, G. Koroll, J. Rohde "Mitigation of hydrogen hazards in water cooled power reactors" IAEA-TECDOC-1196 (2001)
- [2] E. Bachellerie, F. Arnould, M. Auglaire, B. de Boeck, O. Braillard, B. Eckardt, F. Ferroni, R. Moffett "Generic approach for designing and implementing a passive autocatalytic recombiner PAR-system in nuclear power plant containments" Nucl. Eng. Des. 221(1-3), 151-165 (2003)
- [3] F. Morfin, J.-C. Sabroux, A. Renouprez "Catalytic combustion of hydrogen for mitigating hydrogen risk in case of a severe accident in a nuclear power plant: study of catalysts poisoning in a representative atmosphere" Applied Catalysis B: Environmental 47, 47-58 (2004)
- [4] J.-C. Sabroux et al. "Iodine chemistry in hydrogen recombiners" EUROSAFE 2005, Brussels, November 7-8, 2005

5.10.6 Aerosol growth under saturated conditions (Canadian tests)

At present the AECL containment code SMART is still lacking the models required to simulate aerosol behaviour under conditions where fission products are released and aerosols are formed in a steam-only discharge (as opposed to a two phase jet). Although various models exist for the growth of initially dry aerosol particles by heterogeneous nucleation steam condensation or adsorption of water vapor by hygroscopic species, there does not appear to be an industry consensus regarding which of these models are the most appropriate for nuclear containments. Recent aerosol code comparison exercises have demonstrated that many aerosol codes do not model condensation (particularly solubility effects) well [see Section 5.2.5]. A significant limitation to implementing condensation models in aerosol codes is that they rely upon accurate modeling of containment thermalhydraulic parameters [see Section 3.2], and require the correct coupling (i.e. feed-back at appropriate time intervals) between thermalhydraulics and aerosol physics models. As a result, inaccurate thermalhydraulic coupling or modelling would result in large uncertainties in the condensation rates.

Given these limitations of currently available models for water aerosol production by steam condensation, a semi-empirical approach is proposed for SMART modelling of fission product release in high humidity steam environments. This approach would use existing information from large-scale experiments, augmented with new experiments, to develop a range of input parameters for the equilibrium size distribution, and the number and droplet density of water droplets aerosols formed in a steam discharge, as a function of thermalhydraulic conditions. The approach assumes that aerosol growth by steam condensation in the humid (near saturated) environment postulated in a post-accident CANDU containment will be rapid relative to aerosol depletion mechanisms, and that an equilibrium “wet aerosol” size distribution can be used as a starting point for aerosol transport and removal calculations.

Both the KAEVER and VANAM experiments were obtained under high humidity conditions that are relevant to CANDU accident conditions. Unfortunately, the published data from these experiments does not contain enough information about aerosol particle size as a function of time to be considered a sole source for validation of any single aerosol phenomenon. Consequently, the CANDU Owner’s Group is funding experiments at AECL to acquire the additional aerosol data required to characterise aerosol droplet size distribution, number density and mass density that would result from condensation of steam on fission product aerosols in a saturated steam environment. The planned experiments will be similar in nature to those performed in the KAEVER facility, using hygroscopic and non-hygroscopic simulated fission products, but with more frequent sampling of aerosol size. The experiments are to be performed in the Large Scale Containment Facility (LSCF) at Chalk River Laboratories, a 1650 m³ facility, instrumented with temperature and relative humidity probes, and with ports at three different elevations for the injection of saturated or slightly superheated steam. The facility has recently been fitted with a PDA measurement system for aerosol size and velocity.

Results observed from the KAEVER experiments indicated that aerosols of different hygroscopicity agglomerated to give particles with the same overall composition that behaved like aerosols of the most hygroscopic of the individual components. Based on these results it is anticipated that the time required for fission product/water droplets to reach equilibrium size distribution by steam condensation and adsorption of water would be short relative to the time required for their depletion by aerosol removal processes. Confirming this experimentally would mean that there is no reason to incorporate a detailed model for steam condensation into SMART.

Reference

Private communication between J. Ball and the Chairman.

6. EXAMPLES FOR VALIDATION

Here it is to remark that the assessment of the results presented in Chapter 6 reflect the opinion of the organisation providing the contribution.

6.1 Comparison of MELCOR Predictions to Experiments

It might be expected, MELCOR predictions are compared to experiment results frequently. Many of these comparisons of code predictions deal with the hydraulic and heat transfer aspects of the code predictions. Here some examples more directly pertinent to the issues of aerosol behaviour are shown.

Fig. 6.1-1 shows a comparison of the predicted releases of iodine from irradiated reactor fuel and the results of the PHÉBUS FPT-1 test [1]. The agreement between code predictions and tests observations of iodine release are considered satisfactory for the purposes of MELCOR. Fig. 6.1-2 shows a comparison of experimental results for aerosol (NaOH) depletion in the VANAM-M3 test [2] to predictions of the MELCOR code. Observed and predicted aerosol depletions are thought to be in satisfactory agreement for the purposes of the MELCOR computer code.

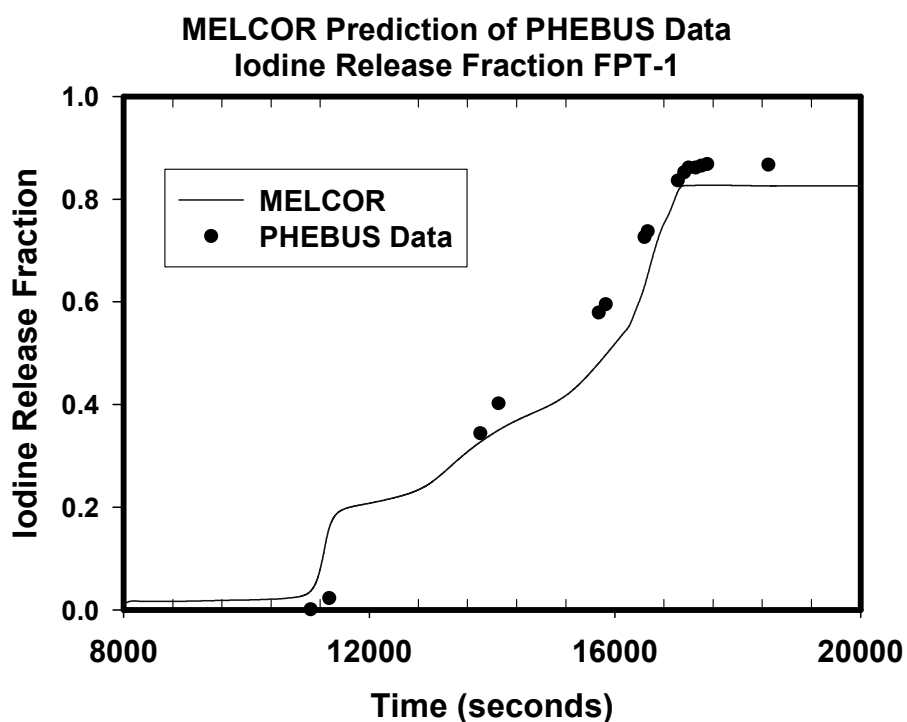


Fig. 6.1-1 Comparison of MELCOR predictions of iodine release with observations made in the PHÉBUS-FPT-1 test

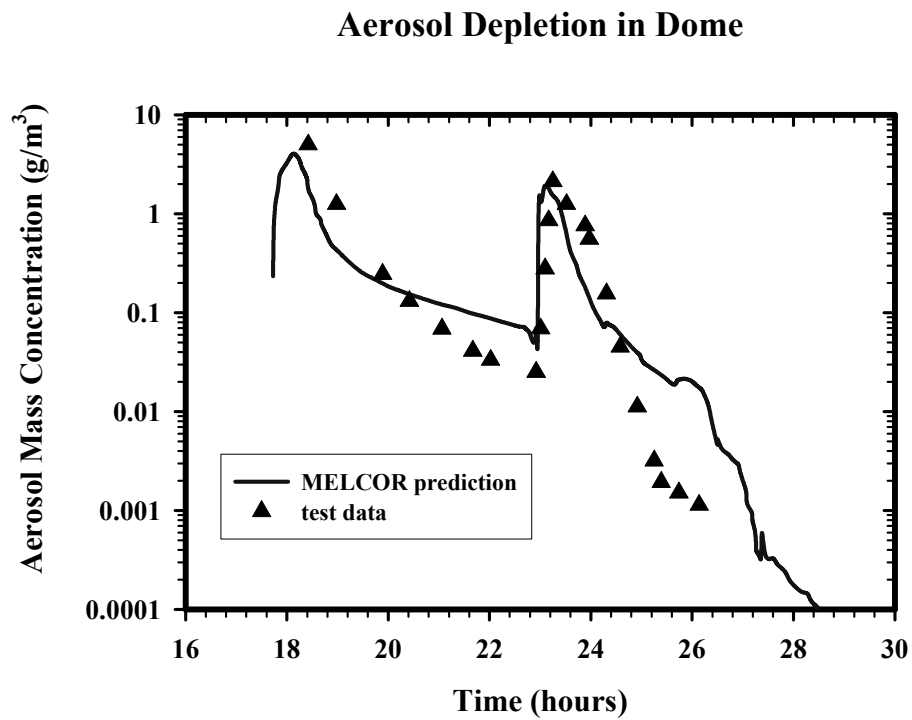


Fig. 6.1-2 Comparison of results from the VANAM-M3 test to predictions of the MELCOR computer code

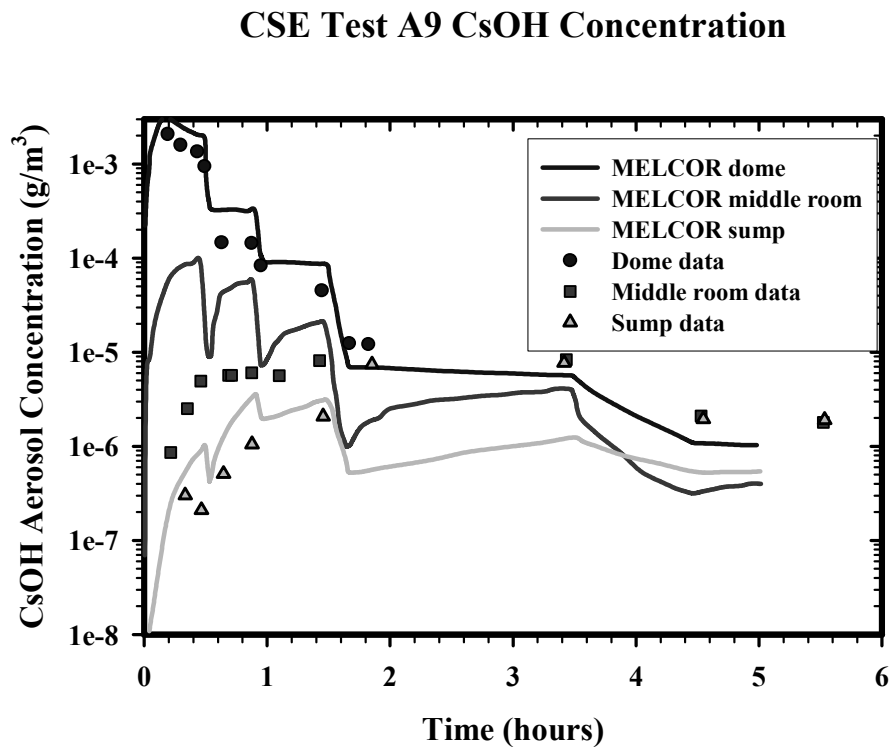


Fig. 6.1-3 Comparison of predictions obtained with the MELCOR code to results of the CSE A9 test

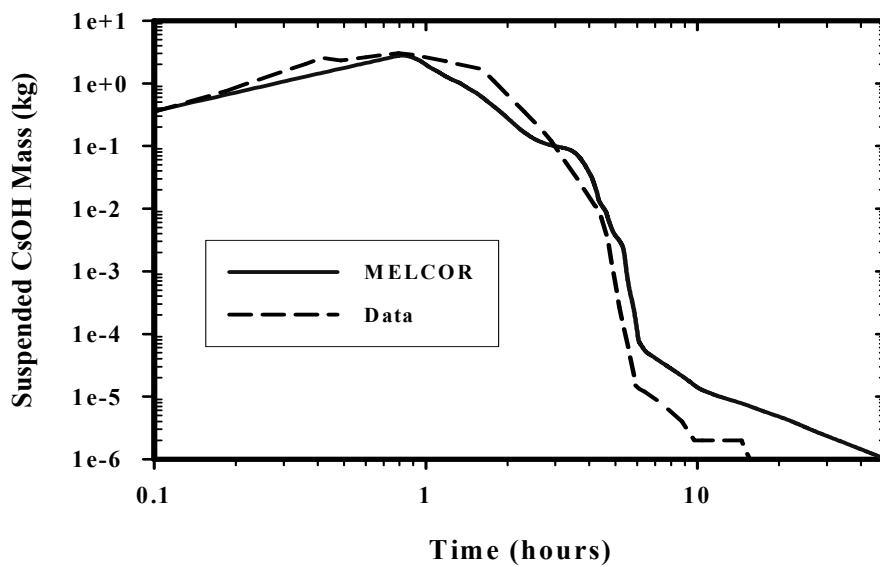
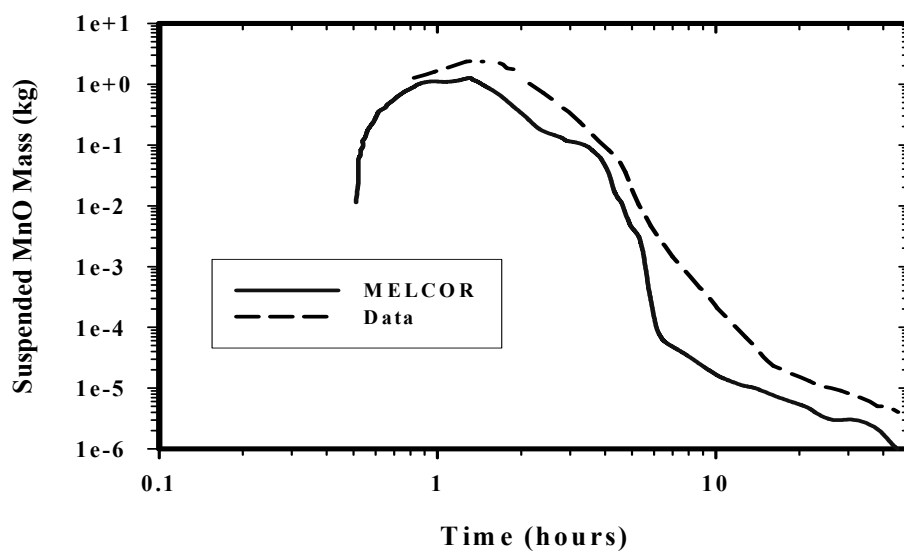
Suspended CsOH in LACE Test LA-4**MnO Aerosol in LACE Test LA-4**

Fig. 6.1-4 Comparison of MELCOR predictions to the results of the LA-4 test

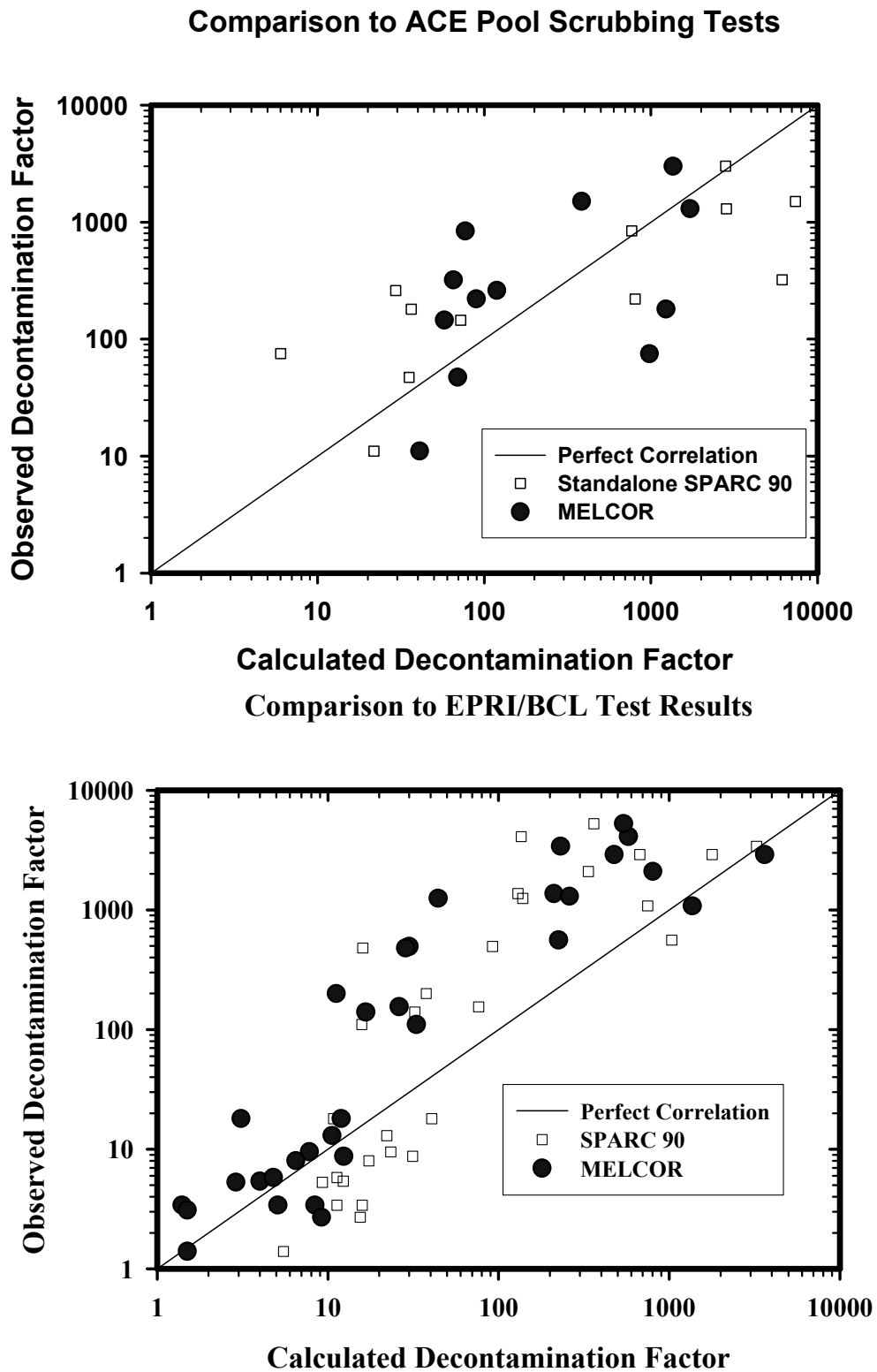


Fig. 6.1-5 Comparison of computer code predictions to suppression pool decontamination observed in various tests

A comparison of code predictions with experimental results obtained in the CSE-A9 test [3] is shown in Fig. 6.1-3. This comparison illustrates the ability of MELCOR to treat aerosol phenomena in multicompartment facilities as well as predicting decontamination by containment sprays operating in the experiment dome. Finally, comparisons of code predictions to results of the LACE LA-4 test [4] are shown in Fig. 6.1-4. In this test CsOH aerosol followed by MnO aerosol were injected into a very large containment volume. Overall agreement between predictions and test results is good. There is a tendency for MELCOR to overpredict the long term aerosol concentration and to underpredict the concentration of the second component concentration in the aerosol. These trends are observed in other code comparisons as well. A comparison of the decontamination by suppression pools predicted by MELCOR and by the standalone version SPARC90 code with decontaminations measured in the ACE tests [5] and the EPRI/BCL tests [6] are shown in Fig. 6.1-5. Were code predictions and test observations perfectly correlated, points shown in the comparisons would fall on the diagonal lines.

References:

- [1] D. Jacquemqin, S. Bourdon, A. de Bremaecker, M. Barrachin PHÉBUS P.F.: FPT1 Final Report Institut de Protection et de Surete Nucleaire, Centre d'Etudes de Cadarache, France, January 2000
- [2] M. Firnhaber et al. International Standard Problem ISP37: VANAM M3 - A Multi Compartment Aerosol Depletion Test with Hygroscopic Material OCDE/GD(97)16, December 1996
- [3] E. Lindroth Containment Systems Experiment, Part 1: Description of Experiment Facilities, BNWL-456, Battelle-Northwest Laboratory, March 1970
- [4] R.K. Hilliard Test Plan - LWR Aerosol Containment Experiment (LACE) Test LA-4-Late Containment Failure with Overlapping Aerosol Injection Periods Westinghouse Hanford Company, Richland, WA, July 1986
- [5] R.T. Allemann, J.A. Bamberger, Comparison of Code Results with ACE Pool Scrubbing Tests, ACE-TR-A13, Battelle Pacific Northwest Laboratory, Richland, WA, June 1990
- [6] J.C. Cunnane et al. The Scrubbing of Fission Product Aerosols in LWR Water Pools Under Severe Accident Conditions - Experimental Results NP-4113-SR, Electric Power Research Institute, Palo Alto, CA, 1984

6.2 CONTAIN for PHÉBUS FPT1

Introduction

The present Technical Note summarises the main results obtained by CIEMAT in the analysis and interpretation of the PHÉBUS-FPT1 experiment with the CONTAIN 2.0 code. As this note will be integrated in the State Of the Art Report (SOAR) on Nuclear Aerosols, it is focused on aerosol aspects, leaving other phenomena studied, like thermal-hydraulics and iodine chemistry, out of the scope of this document.

This technical note is based on the paper “Simulating In-Containment Aerosol Behaviour during Severe Accidents: A Validation of CONTAIN 2.0 Code Based on the PHÉBUS-FPT1 Experiment”, presented by [1] at the International Congress of Advanced Nuclear Power Plants, Seoul (Korea) 15-19 May, 2005.

Experimental description

PHÉBUS-FP is an international program set up to investigate key phenomena involved in Light Water Reactor (LWR) severe accidents, particularly those in the field of core degradation and fission products behaviour. Six integral in-pile experiments have been planned and they will be executed in a facility scaled down 1:5000 from a 900 MWe Pressurised Water Reactor (PWR). The experimental rig consists of three main sections: core, primary circuit and containment. A more exhaustive description of the program was reported by [2].

The FPT1 test [3] was aimed at investigating core degradation and release, transport and behaviour of fission products and aerosols. The specific conditions imposed in the experimental rig were: irradiated fuel (~ 23 GWd/tU), presence of a Ag-In-Cd control rod, low pressure and highly oxidizing environment in the primary circuit, a condensing and unsaturated atmosphere and a subcooled and acidic sump in the containment. From the point of view of containment phenomena, the test evolved in four main phases: bundle degradation, aerosol depletion, floor washing and iodine chemistry.

The PHÉBUS-FP containment is a 10 m^3 steel vessel (Fig. 6.2-1). Three cylindrical structures, hereafter called condensers, were attached to the ceiling in order to achieve a surface-to-volume ratio characteristic of a 900 MWe PWR. Each of them consisted of a wet upper part, where temperature was controlled below the saturation one during most of the test, and a dry part, quite overheated with respect to the atmosphere. The vessel walls were also kept at temperatures higher than the saturation temperature throughout the test. The floor of the vessel was equipped with a sump containing around 105 l of water at a temperature similar to the wet condenser ones. The injection point in the containment vessel is located at the lower region (0.8 m above the sump) and it is directed upward to the space bounded by the three condensers.

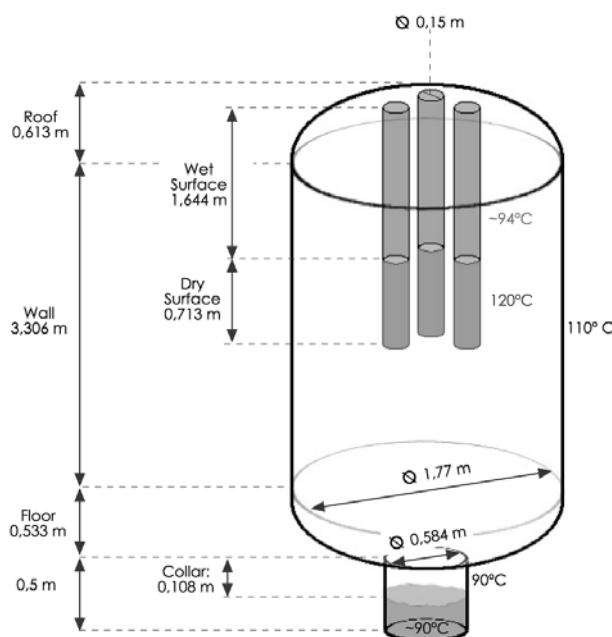


Fig. 6.2-1 Geometry and thermal conditions of containment vessel during the FPT1 test

At the beginning of the test, the vessel atmosphere was essentially nitrogen (61.4 %) and steam (35.4 %) at about 2 bar and 108 °C (the remaining 3.2 % was oxygen). Steam and hydrogen (resulting from oxidation reactions in the fuel bundle) came into the containment according to the histories presented. As can be noted, steam flow rate showed some abrupt changes but it was never zero until about 18000 s. Hydrogen

input, however, was much smaller and quite more restricted in time (it only reached a noticeable magnitude at around 11500 s).

Between 7900 s and 14500 s from the beginning of the test, the release from the control rod took place and fuel liquefaction started. As a consequence, between 11000 s and 18600 s, control rod elements as well as volatile fission products such as iodine, cesium and tellurium, arrived at the containment carried by the cooling steam and hydrogen. The aerosol input rate was far from being constant due to both bundle phenomena and/or gas flow-rate variations.

As a result of the history of steam injection through the fuel bundle as well as of the thermal boundary conditions, the atmosphere of the containment vessel was unsaturated throughout the test. In spite of this, the presence of cold surfaces on the condensers allowed to investigate aerosol dynamics in steam concentration gradients. The thermal state of the vessel became steady from 23000 s on, showing a temperature of approximately 108 °C and a relative humidity of 60 % (sump and condensers were kept constant at 90 °C and 92 °C, respectively). A more detailed description of specific thermal variables will be presented in next sections along with code predictions.

Concerning source term in the containment the main results were reported by [4].

- Fission products were conveyed to the containment by aerosol particles that were essentially composed of structural material (more than 60 % was attributed to silver, rhenium and uranium).
- Aerosols were shown to be homogeneous in composition regardless particle size.
- A total aerosol mass of about 130 g entered the containment.
- The aerosol mass distribution might be described by a log-normal function characterised by a geometric standard deviation around 2.0. Aerosol Mass Median Diameters (AMMD) of about 3.5 –4.0 µm was measured.
- Most of aerosol mass settled (~65-70 %) but a substantial fraction (25-28 %) was entrained by steam condensing on the cold surfaces (i.e., diffusiophoresis). Just a minor fraction was found on the vessel walls (Fig. 6.3-2).
- Cesium distribution in condensers and floor (~44 % and ~50 %, respectively) was noticeably different from the rest of elements.

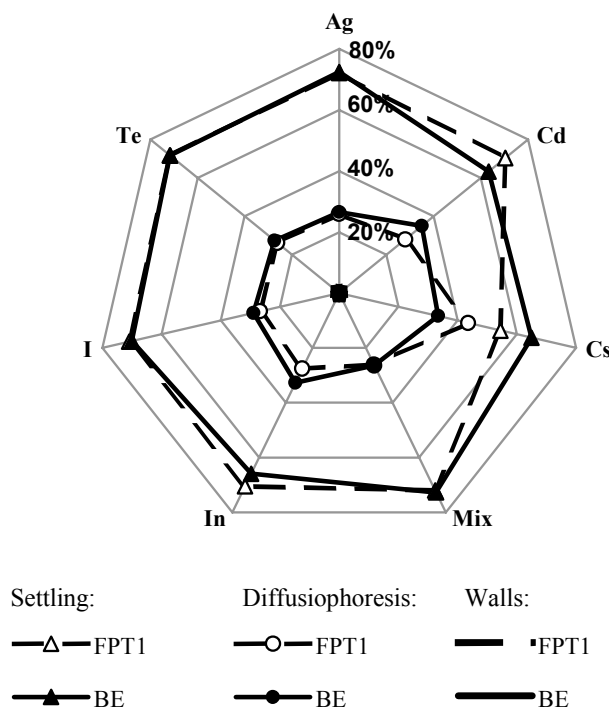


Fig. 6.2-2 Mass distribution (% of the total mass injected)

Containment modelling

The “in-containment” thermal and aerosol phenomena have been simulated with the CONTAIN 2.0 code [5] and a set of assumptions and approximations have been adopted. The conditions imposed in the experiment were not particularly challenging for CONTAIN 2.0 models, but they allowed testing them when using a rather representative aerosol source under well controlled thermal-hydraulic conditions.

A thorough description of the major approximations and hypotheses made in the simulation was reported by [1]. The PHÉBUS-FP containment vessel was modelled as a single compartment consisting of an upper and a lower cell where the sump is located. A total of 18 AISI 316L heat structures contacting vessel atmosphere have been simulated. The change in atmosphere composition was governed by three gas flows: incoming hydrogen; entering steam; and sampled gas. It has been assumed that steam and hydrogen entered the containment with the temperature measured at the closest point to the containment inlet. This temperature varied from 157 °C to 177 °C. The sump contains an initial water volume of 105 l. The role of the sump as a potential condensation site underlined the importance of capturing accurately its temperature evolution. In order to achieve it, three actions were taken through the code input deck: to impose an initial water temperature of 89.3 °C, to simulate a contacting heat structure at 90 °C and to cool the water volume at a time dependent rate.

The aerosol source in CONTAIN 2.0 is described through composition, flow rates, density and size. The particulate mass entering containment has been grouped in seven aerosol types according to their composition: Ag, Cd, I, Cs, In, Te and “Mix” (i.e., structural and bundle materials). None of the aerosols were defined as hygroscopic. Aerosol input rates were estimated from measurements of isotopes flow rates near the containment entry point. A mass-averaged density of 7.07 g/cm³ characterises all the aerosols. This estimate has been calculated from individual densities of the chemical species assumed for each element (i.e., Ag, Cd(OH)₂, In₂O₃, CsOH, SnO₂, U₃O₈, Re₂O₇, MoO₃). Aerosol particles have been

supposed to be spherical and to distribute log-normally along size domain with a mass median diameter (MMD) of $1.05\ \mu\text{m}$ and a geometric standard deviation (GSD) of 1.9 [3]. As cesium particles behaved differently than the rest, its identity was kept by defining an individual particle size based on its actual density as CsOH. So that, $\rho = 0.742\ \mu\text{m}$.

Results and discussion

CONTAIN 2.0 results were too close to data as to set meaningful quantitative comparisons. Most of the predictions have been found to be within the uncertainty range associated to measurements. All the experimental values were drawn from [3].

Fig. 6.2-2 shows a very good agreement between data and CONTAIN 2.0 predictions regarding final mass distribution. Sedimentation was estimated to be the main removal phenomenon acting on airborne particles. About 60-80 % of the injected mass was depleted by settling, and the rest (20-40 %) was swept away from the atmosphere by the condensing steam (diffusiophoresis). The amount of mass on containment walls was negligible and CONTAIN 2.0 did calculate so as well. As observed, CONTAIN 2.0 results were rather accurate and deviations never exceeded 10 %. Nonetheless, the code underestimated noticeably the cesium fraction depleted by diffusiophoresis, whereas it tended to overestimate diffusiophoresis for the rest of aerosols.

Fig. 6.2-3 shows the cesium concentration in the vessel as a function of time. Until 18000 s the disagreement between the data recorded by γ -spectrometry and by sampling prevents any statement about CONTAIN 2.0 accuracy, although from a qualitative point of view the CONTAIN 2.0 profile is rather closer to the sampling data. From 18000 s on, however, both experimental techniques approached each other and indicated that CONTAIN 2.0 removal from the atmosphere has been lower than observed. This deviation was associated to a slight under-prediction of the steam condensation rate from that time 18000 s on.

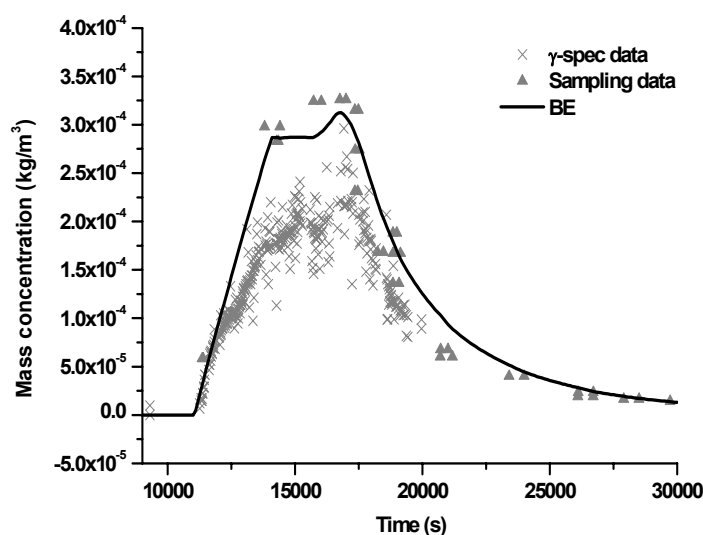


Fig. 6.2-3 Cesium concentration versus time

The case of iodine is somewhat different. The measurements from different experimental techniques looked pretty consistent all over the time (Fig. 6.2-4). CONTAIN 2.0 predicted rather accurately the

evolution during the injection period (~11000-17500 s), but, as in the case of Cs, its removal rate has been estimated to be slower than measured from that time on.

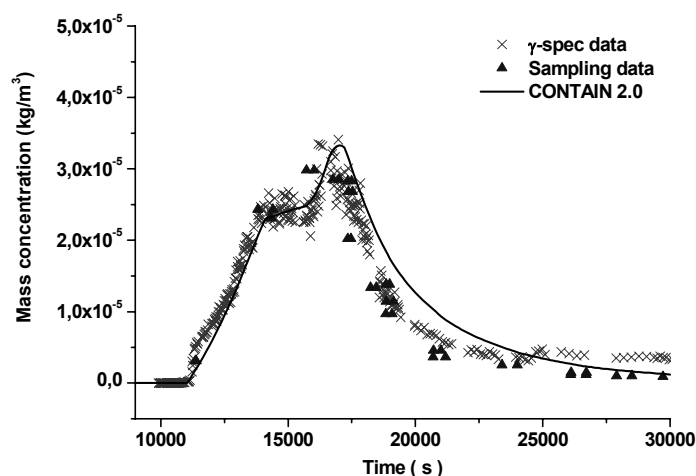


Fig. 6.2-4 Iodine concentration versus time

Finally, CONTAIN 2.0 predicted particle agglomeration along the injection phase until around 20000 s; however, no experimental data are available to compare with. In Table 6.2-1 the AMMD and GSD measured by impactors are presented together with CONTAIN 2.0 predictions. It should be observed the consistent decreasing trend predicted between 20700 and 26700 s, as well as the quantitative similarity between measurements and estimates in this same period.

Table 6.2-1 Experimental and predicted AMMD and GSD

Time	AMMD		GSD	
	FPT1	CONTAIN 2.0	FPT1	CONTAIN 2.0
20710 s	3,91 μm	4.10 μm	1.95	1.46
21002 s	3,91 μm	4.09 μm	1.95	1.45
26109 s	3,54 μm	3.76 μm	1.84	1.40
26709 s	3,54 μm	3.72 μm	1.84	1.40

Final remarks

The CONTAIN 2.0 code and the theoretical approach followed, despite its overall simple modelling, resulted in very good agreement with experimental data available and provided explanation to most of the phenomena observed in the test. In short, the main conclusions drawn from this study are the following:

- Simplified approaches of in-containment scenarios may be suitable to achieve a thorough understanding of governing thermal and aerosol phenomena when the main assumptions and approximations made are taken into account in the discussion of the results.
- CONTAIN 2.0 results indicated that airborne concentration of fission products, i.e., iodine and cesium, were well predicted. Even further, CONTAIN 2.0 results highlighted that cesium concentration evolved according to data from sampling of the atmosphere, reaching values well above the measurements coming from γ -spectroscopy.

References

- [1] L.E. Herranz, C.L. del Prá “Simulating In-Containment Aerosol Behaviour during Severe Accidents: A Validation of CONTAIN 2.0 Code Based on the PHÉBUS-FPT1 Experiment” International Congress of Advanced Nuclear Power Plants, Seoul (Korea) 15-19 May, 2005
- [2] M. Schwarz, R. Zeyen “Status of the PHÉBUS-FP Program” 5th Technical Seminar on the PHÉBUS-FP Programme, Aix-en-Provence, France, June 24-26, 2003
- [3] D. Jacquemain, S. Bordon, A. Braemaeker, M. Barrachin FPT1 Final Report (Final version)” IPSN/DRS/SA/PDF report SA1/00, IP00/479, France, December 2000
- [4] F. Arregini, D. Jacquemain, Y. Garnier “Summary of Fission Product Behaviour and Structural Material Behaviour in FPT1” 4th Technical Seminar on the PHÉBUS-FP Programme, Marseille, France, March 20-22, 2000
- [5] K.K. Murata, D.C. Williams, J. Tills, R.O. Griffith, R.G. Gido, E.L. Tadios, F.J. Davis, G.M. Martinez, K.E. Washington “Code Manual for CONTAIN 2.0: A Computer Code for Nuclear Reactor Containment Analysis” Sandia National Laboratories Albuquerque, NM 87185, December 1997

6.3 Example for Uncertainty and Sensitivity Analyses of Two Aerosol Calculations

Introduction

The main questions addressed in sensitivity and uncertainty analyses on aerosol problems are: (1) What are the uncertainties of the aerosol results like aerosol concentrations, deposited mass and the aerosol source term to the environment? (2) Which are the uncertain parameters contributing most to the uncertainties of the aerosol results?

The study described here was performed on applications of the coupled thermal hydraulic and aerosol code FIPLOC, a precursor of COCOSYS. In the first application the dry aerosol behaviour in the test VANAM M2 was investigated [1, 2]. The test was carried out in a multi-compartment geometry.

The second application was on the LACE test LA4 with a two-component aerosol under wet conditions in a single volume geometry [3].

Aerosol problem at dry conditions

VANAM M2 was performed with an insoluble SnO₂ injected into one of the nine rooms of the 640 m³ Battelle Model Containment. Only the dry part of the test without steam injection was used. The aerosol was inhomogeneously distributed by aerosol flows and depleted by natural processes. The post test FIPLOC calculation which served as a base for the study were in a good agreement with the experiment (Fig. 6.3-1).

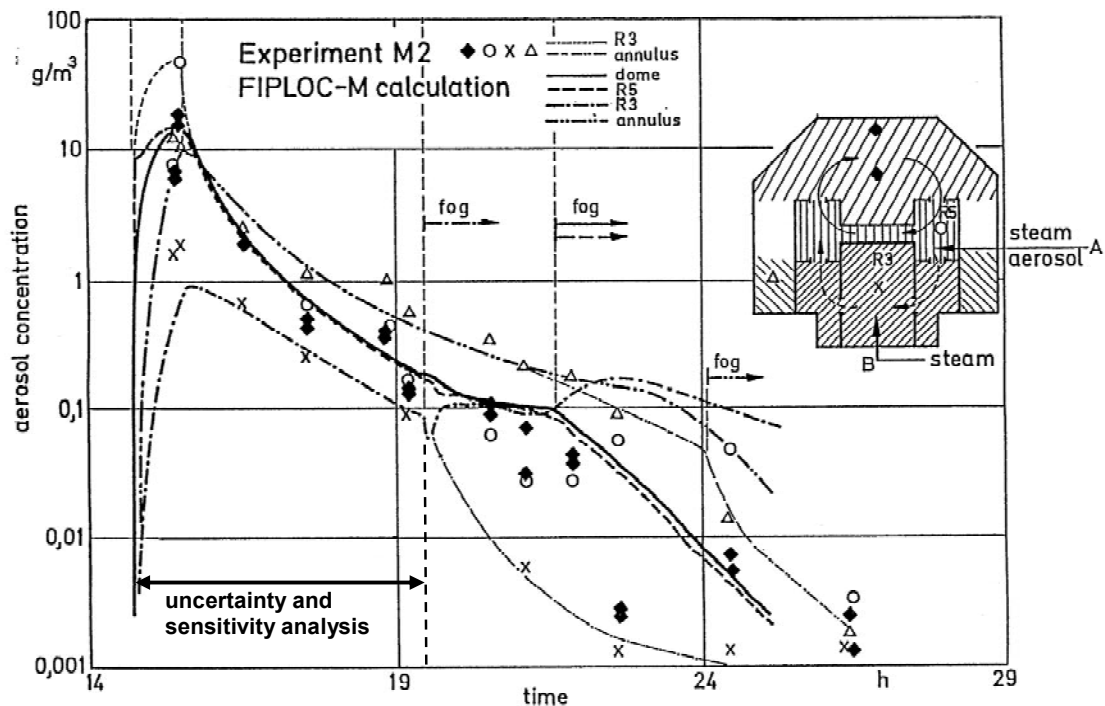


Fig. 6.3-1 Measured and calculated aerosol concentrations in the test VANAM M2 The course until 19.7 h was used for the uncertainty and sensitivity analysis

The uncertainty and sensitivity analysis was performed by use of the program package SUSA [4]. A total of 179 uncertain aerosol and thermal hydraulic parameters were identified, e.g. number of size classes, accuracy criteria, aerosol deposition areas, shape factors, aerosol source parameters, geometry parameters for junctions and zones, heat transfer coefficient, leak size, etc. The number of size classes was varied between 5 and 10. The state of the knowledge about the parameters was expressed by subjective probability distributions and the correlations between the selected parameters.

A parameter sample of size 100 was generated with randomly selected parameter values as input and the FIPLOC code was run for each. The 100 results (Fig. 6.3-2) along with the parameter form the data basis from which all subsequent uncertainty and sensitivity statements were derived.

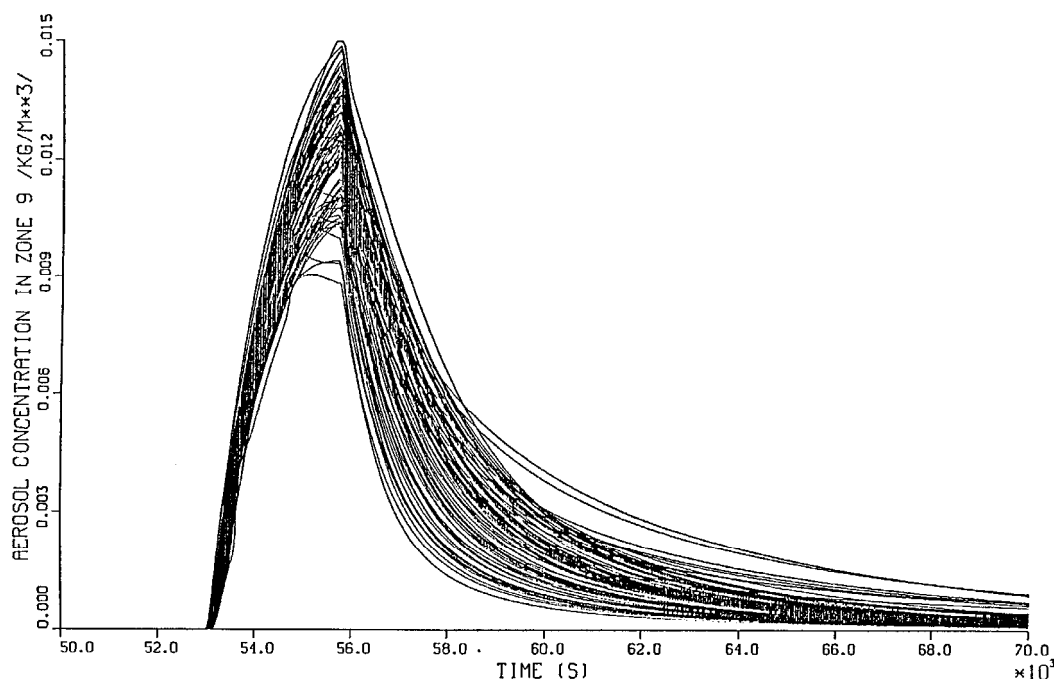


Fig. 6.3-2 Aerosol concentration in the dome compartment
100 time histories obtained with FIPLOC for randomly selected parameter vectors

At the end of the calculation 0.2 kg of the injected 8.91 kg SnO_2 are still airborne. The two side (90 %, 90 %) tolerance limits are 0.07 kg and 0.49 kg. The aerosol mass released to the environment is 0.29 kg with the tolerance limits 0.1 kg and 0.63 kg. A large amount was released early in the experiment. This is the reason why this uncertainty range is not broader than that of the total aerosol although large uncertainties of parameters for the leakage path and the gas pressure are involved.

The uncertainty of the total airborne aerosol mass depends on a few uncertain aerosol parameters:

- Dynamic and agglomeration shape factors
- Turbulence dissipation rate
- Number of size classes
- Aerosol injection rate

The uncertainty of the aerosol injection rate influences only the short term aerosol results.

The uncertainty of the released aerosol mass depends on the uncertain aerosol parameters:

- Leakage parameters (cross section area, flow resistance number)
- Dynamic and agglomeration shape factors

The results confirm the expected high ranking of the main contributors to uncertainty from aerosol modelling and reveal the importance of uncertainties in thermal hydraulics for computed aerosol behaviour.

Aerosol problem at wet conditions

The test LACE LA4 was carried out in the 852 m³ CSTF-vessel. A hygroscopic CsOH aerosol and an insoluble MnO aerosol were injected with overlapping release periods. During the whole test steam was released. Steam condensation on the hygroscopic CsOH aerosol component was higher than on the MnO aerosol which resulted in a more rapid CsOH aerosol removal. In the FIPLOC calculation used for the study the component behaviour and the hygroscopic effect were simulated. The analytical results were in a good agreement with the experimental values.

For the purpose of the uncertainty and sensitivity analysis 58 uncertain parameters were identified.

At the end of the calculation ($t = 20000$ s) $1.4 \cdot 10^{-6}$ kg/m³ of the injected CsOH are still airborne. The two side (90 %, 90 %) tolerance limits are $2.3 \cdot 10^{-9}$ kg/m³ and $3.25 \cdot 10^{-5}$ kg/m³. At the same time $1.2 \cdot 10^{-5}$ kg/m³ MnO are still airborne. The two side (90 %, 90 %) tolerance limits for the MnO concentration are $2.5 \cdot 10^{-8}$ kg/m³ and $1.02 \cdot 10^{-4}$ kg/m³.

The uncertainty of CsOH and MnO aerosol concentrations depends on a few uncertain aerosol parameters:

- Average diameter of the injected particles
- Kelvin effect regarded (yes / no)
- Numerical approach of droplet growth (steady state / dynamic)
- Feedback of hygroscopic effect on thermal hydraulics (yes / no)

The average diameter is an input parameter. Its range for variation was relatively wide (factor 10) because of a lack of experimental information. The other parameters steer model alternatives for the condensation calculation available in FIPLOC. Owing to this study recommendations for the use of the option were given.

References

- [1] J. Langhans, H.G. Friederichs, E. Hofer, B. Krzykacz, B.M. Schmitz, G. Weber Unsicherheits- und Sensitivitätsanalyse zum Aerosolmodell in FIPLOC-M, Teil 2: Nasses Aerosolverhalten im LACE-Experiment LA4 GRS-A-2217 (1994)
- [2] E. Hofer, B. Krzykacz, L. Langhans, G. Weber Uncertainties and Sensitivities in Aerosol Calculations – An Analysis of a FIPLOC-M Application to the Experiment VANAM M2 PSAM II-Conference, San Diego, 20 – 25 March 1994
- [3] J. Langhans, H.G. Friederichs, E. Hofer, B. Krzykacz, G. Weber Unsicherheits- und Sensitivitätsanalyse zum Aerosolmodell in FIPLOC-M, Teil 1: Trockenes Aerosolverhalten im VANAM-Experiment M2 GRS-A-2183 (1994)
- [4] E. Hofer Probabilistische Unsicherheitsanalyse von Ergebnissen umfangreicher Rechenmodelle GRS-A-2002, GRS Garching (1993)

7. SOURCE TERM CALCULATIONS IN PLANT APPLICATIONS

7.1 MELCOR Calculation for a US American PWR (Station Blackout Scenario)

To illustrate the effects aerosol processes have on the radioactive material available for release over the course of an accident, an example calculation of the progression of a severe accident in a pressurised water reactor is presented here. The analysis was done with the MELCOR computer code. The hypothesized accident is a Station Blackout at the Zion nuclear power plant. This nuclear facility is a four-loop pressurised water reactor in a large, dry containment. A diagram of the reactor and its containment is shown in Fig. 7.1-1. For the purposes of this illustration, attentions are focused on the behaviour of radioactive cesium released from the fuel. Times in the various figures shown here are based on the time of accident initiation. The accident progresses with the reactor coolant system pressurised at about 155 bar until core debris penetrates the reactor vessel at about 4.3 hours following accident initiation. The temperature, pressure and relative humidity of the containment over the course of the accident are shown in Fig. 7.1-2. Note that the relative humidity of the containment atmosphere is high only during the early period of the accident when coolant is being boiled from the reactor coolant system. There is a modest upward excursion in the relative humidity following vessel failure. Otherwise, the containment humidity is fairly low and water condensation on aerosol particles is not expected to be significant.

Core uncover, fuel cladding rupture and the beginning of cesium release from the fuel occur at about 3.7 hours. The inventories of cesium released from the fuel and residing in the core region, upper core internals, hot leg, and one of the steam generators are shown as functions of time in Fig. 7.1-3. Cesium is present in these various regions as vapor, aerosol and materials deposited on surfaces in the region. The abrupt drop in the cesium inventories at about 4.4 hours is caused by the depressurization of the reactor coolant system when core debris penetrates the reactor vessel and flows into the reactor cavity. Airborne cesium present as vapor or aerosol in the various volumes is vented to the containment during depressurization. The version of the MELCOR code used for these calculations does not predict resuspension of deposited particulate during the depressurization.

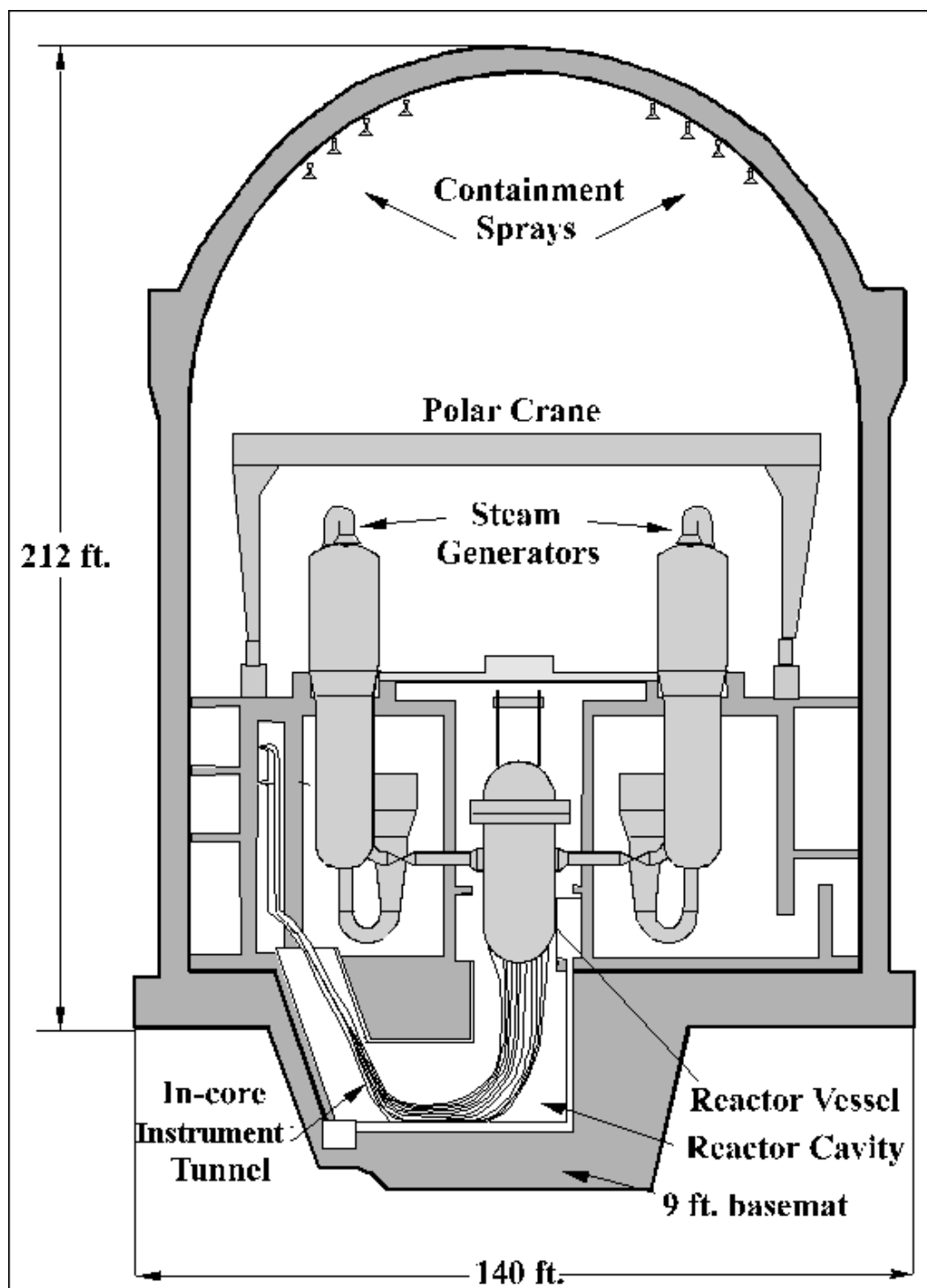


Fig. 7.1-1 Diagram of the containment for the Zion reactor. Dimensions are in English units. Conversions are: 9 ft. = 2.74 m; 140 ft. = 42.7 m; 212 ft. = 64.6 m

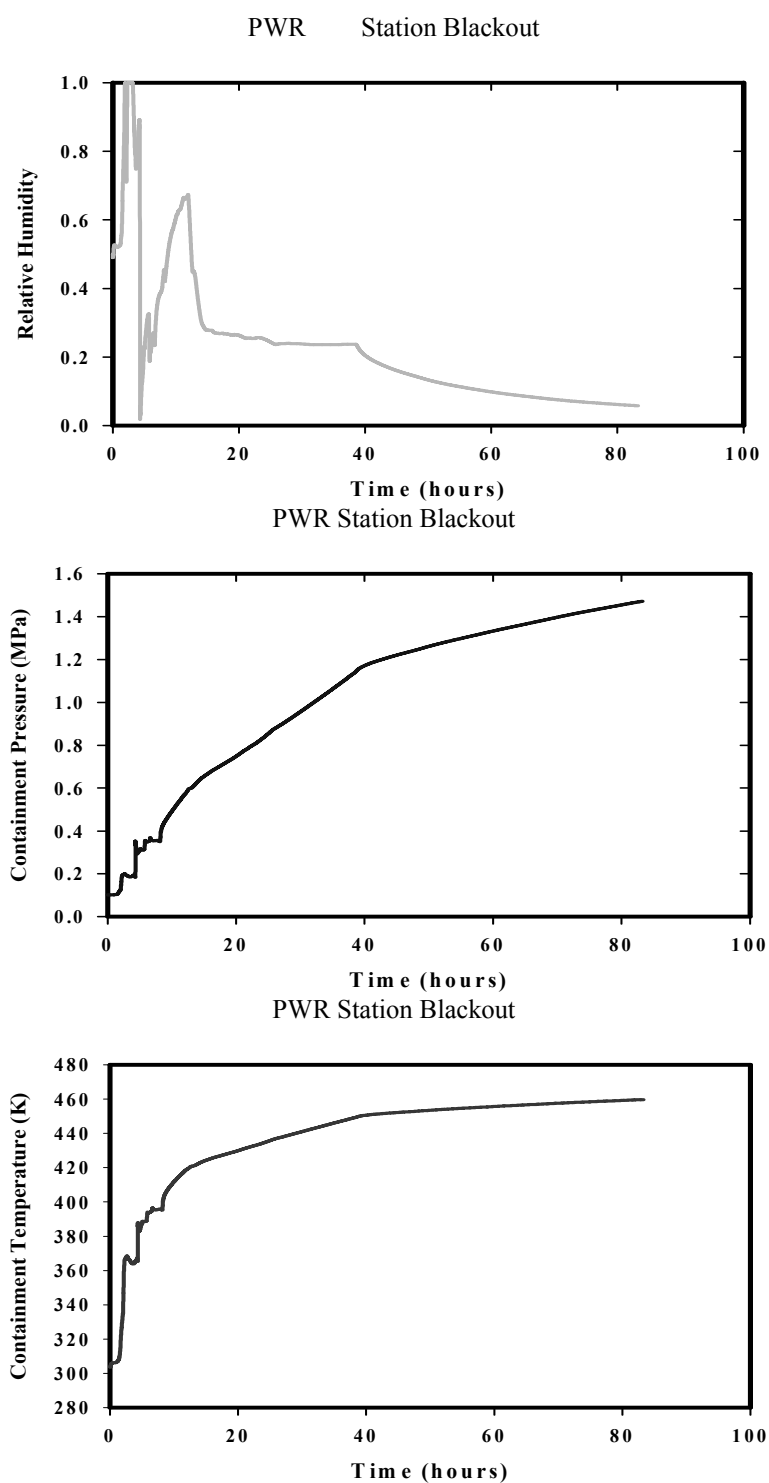


Fig. 7.1-2 Conditions in the reactor containment during a station blackout accident

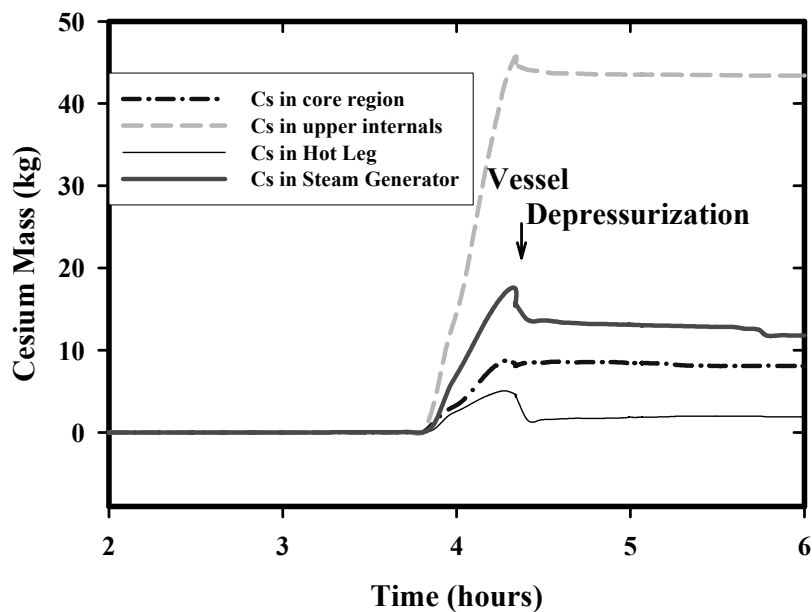


Fig. 7.1-3 Cesium within the reactor coolant system early in the accident

Comparison of the amounts of cesium present in the regions before and after depressurization provides an indication the fraction of cesium present as airborne material present as either vapors or aerosol.

Most of the cesium in the core region and in the upper internals of the reactor vessel is predicted to be deposited on surfaces. The model predicts the cesium will react to form compounds such as cesium silicate as observed on upper core internals in the accident at Three Mile Island. In contrast to this, the model predicts that much of the cesium in the hot leg remains in the gas phase.

Cesium in the reactor containment is shown in Fig. 7.1-4. Following core uncover and the onset of cesium release from the fuel, there is only a slow rise in the containment inventory of cesium. This comes from the venting of the reactor coolant system to the containment through the safety relief valves. The cesium inventory of containment rises abruptly when core debris penetrates the reactor vessel and the reactor coolant system depressurises. Depressurization is complicated by the discharge of the accumulators when system pressure falls below about 44 bar. Any cesium that remains in the reactor fuel expelled from the reactor vessel is released during core debris interactions with concrete following vessel failure. (About 10 % of the cesium inventory was found to remain in degraded reactor fuel from the Three Mile Island Accident.) There is a continuing discharge of fuel and some cesium from the vessel after depressurization as residual fuel from the peripheries of the core heats and melts.

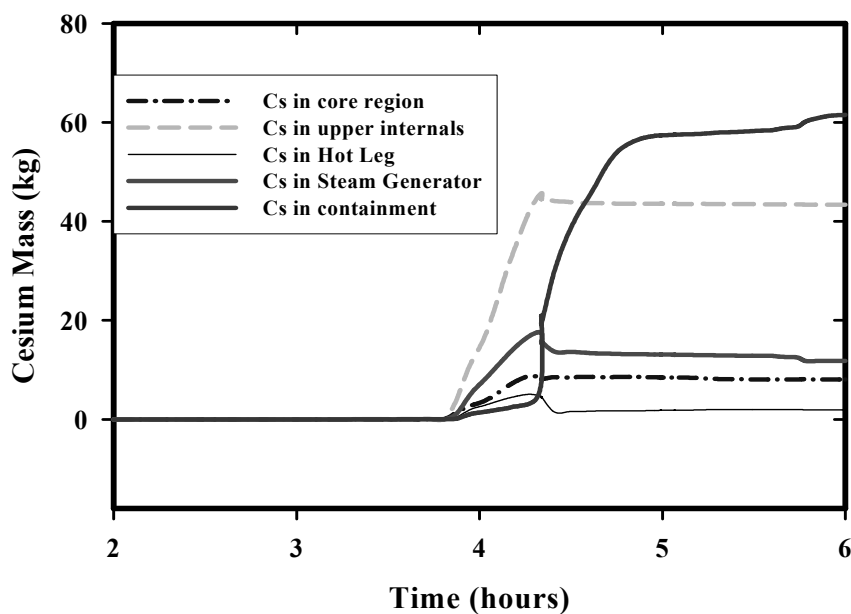


Fig. 7.1-4 Cesium in containment in comparison with cesium in reactor coolant system

Most of the very dynamic events of the accident have ended about 17 hours after accident initiation. But, as shown in Fig. 7.1-5, the cesium inventory of the containment continues to rise for about 60 hours after accident initiation. The increasing containment inventory comes from the revaporization of cesium deposited on surfaces within the reactor coolant system. Revaporization occurs because the surfaces are heated by both convection and by decay heating so that cesium compounds on the surfaces have significant vapor pressures. Convective flow through the reactor coolant system sweeps these vapors into the containment which is cool enough to condense the vapors and form aerosols. The progression of revaporization can be seen most clearly in Fig. 7.1-6 which shows the cesium inventory in one of the steam generators as a function of time. Revaporization of cesium (and other radionuclides) from surfaces in the reactor coolant system recharges the containment atmosphere with radioactive aerosol to replace, in part, material lost from the atmosphere by aerosol deposition processes. For this particular reactor and accident sequence, the deposition of aerosol from the containment atmosphere is dominated by gravitational deposition to upward facing surfaces.

Cesium in PWR Station Blackout Accident

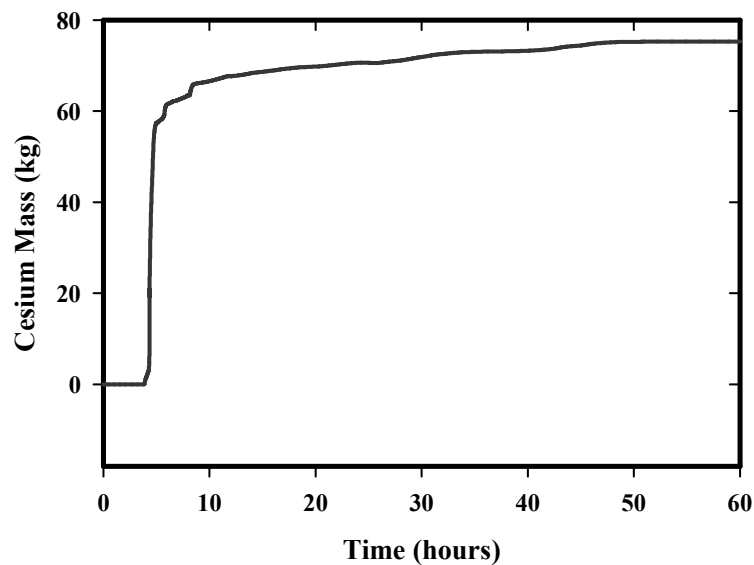


Fig. 7.1-5 Cesium in the reactor containment

Cesium Revaporization PWR Station Blackout

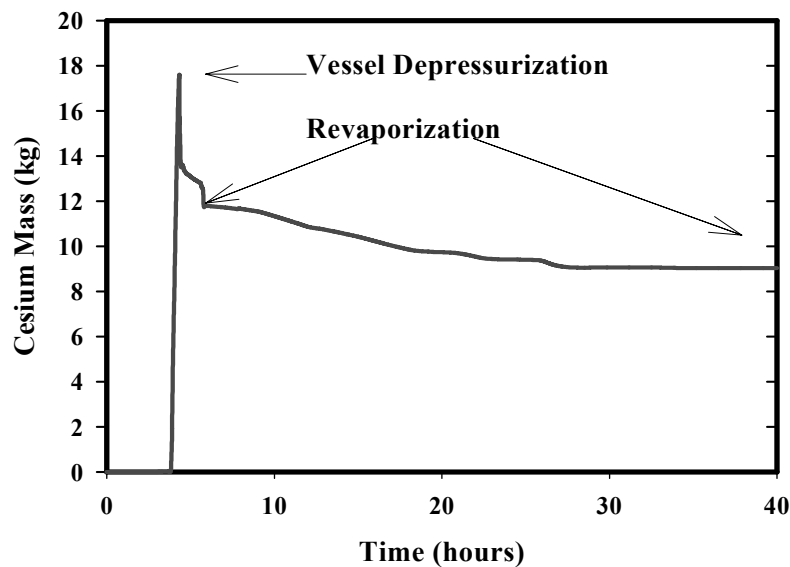


Fig. 7.1-6 Cesium revaporization from the steam generator

The aerodynamic mass median diameter of aerosol particles in the containment atmosphere is shown in Fig. 7.1-7. The aerosol in the containment has an approximately lognormal size distribution. The geometric standard deviation of the size distribution is shown in Fig. 7.1-8. The median size of the aerosol particles goes through a wild excursion following vessel rupture. Large amounts of radioactive and nonradioactive mass are injected into the atmosphere by both depressurization of the reactor vessel immediately and for a protracted period by core interactions with the limestone concrete of the reactor basemat. Mass median

particle diameters exceed $5\text{ }\mu\text{m}$ at the peak. Over the longer term, aerosols in the containment atmosphere have mass median diameters between 2 and $3\text{ }\mu\text{m}$. The geometric standard deviation of the aerosol size distribution is not so variable. Typical values are between 2.1 and 2.4 throughout the accident. Episodic excursions in these values may reflect hydrogen combustion events taking place in the atmosphere.

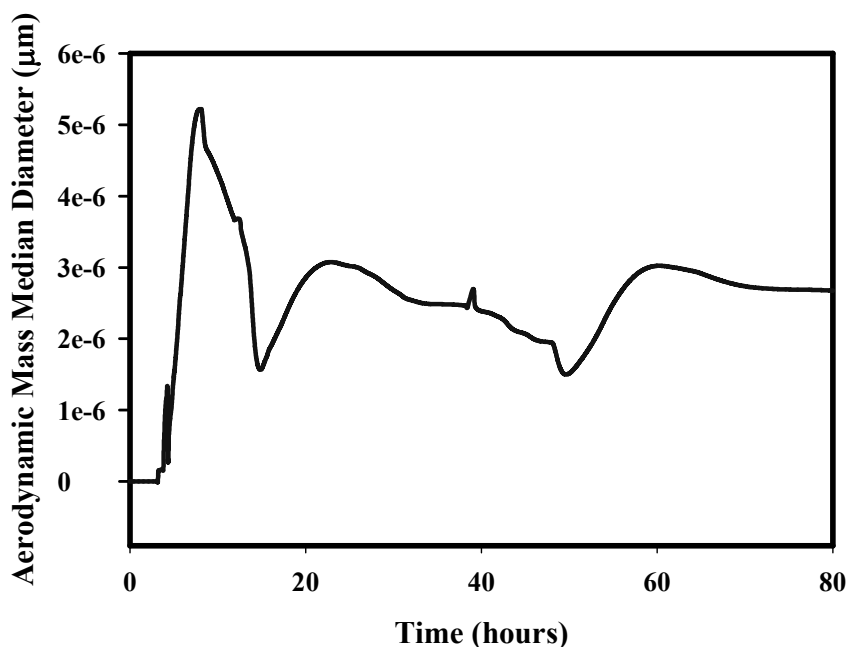


Fig. 7.1-7 Aerodynamic mass median diameter of aerosol particles in containment atmosphere

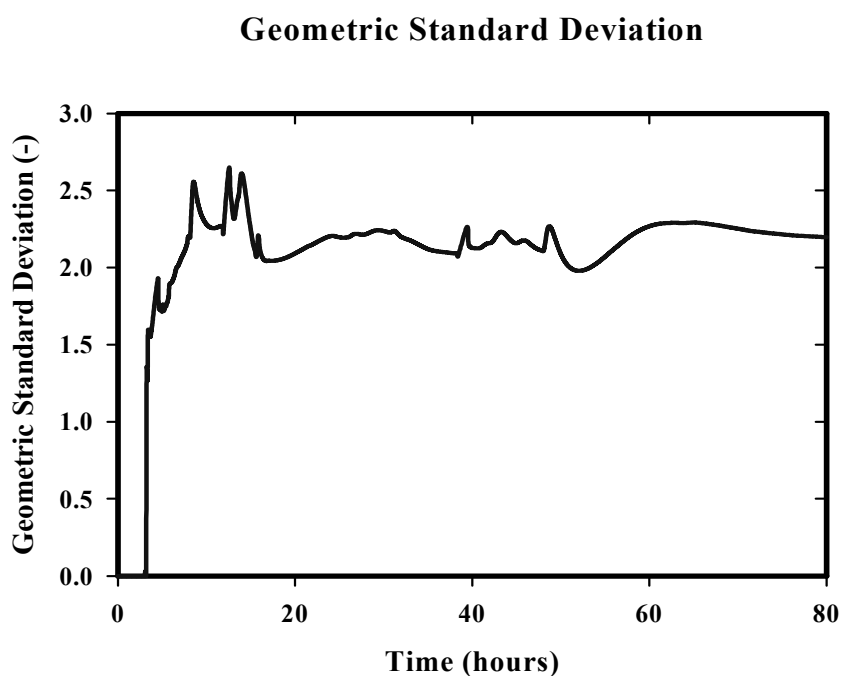


Fig. 7.1-8 Geometric standard deviation of aerosol in containment atmosphere

This example calculation for a pressurised water reactor makes it clear that there can be abundant opportunities for radionuclides released from the reactor fuel to deposit within the reactor coolant system. Revaporization of these deposited radionuclides is an important consideration in the prediction of the inventory of radionuclides available for release to the environment should there be a major loss of containment integrity. Aerosol physics is quite dynamic especially in the early stages of the accident when large amounts of particulate material are injected into the containment atmosphere. Without intervention by engineered safety features such as containment sprays, the period over which significant containment inventories of airborne, radioactive aerosol exist can be quite long - certainly in excess of 24 hours.

7.2 ASTEC Calculation for a German PWR (MB LOCA Scenario)

Introduction

The severe accident sequence of a medium break LOCA (200 cm² leak in the hot leg of the main coolant line) in a German PWR with 1300 MWe (KONVOI type) was analysed with ASTEC V1.2 rev1. The plant application sequence from the opening of the leak until vessel rupture, corium slump into the cavity and MCCI was investigated. FP, aerosol and iodine transport phenomena in the circuit to the leak until the release into the containment and the transportation within the containment have been considered.

Input model for a German PWR 1300 MWe

The investigations have been carried out for a typical German PWR with 1300 MWe. The 4 loop plant with U-tube steam generators has been modelled with one single loop containing the pressuriser and the break and one triple loop. The break is situated between the reactor pressure vessel and the surge line connection (Fig. 7.2-1).

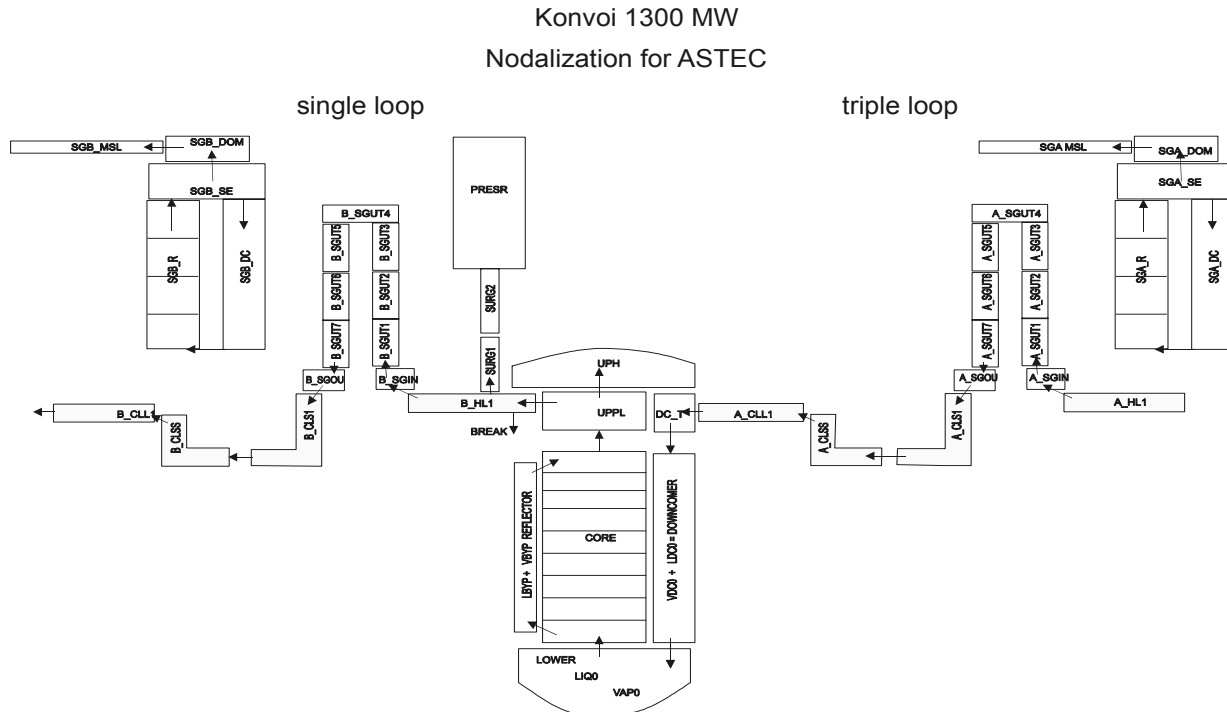


Fig. 7.2-1 ASTEC V1.21 nodalisation scheme of primary circuit with break in hot leg

The containment (Fig. 7.2-2) is subdivided into two nearly symmetrical parts. Exceptions concern the central situated compartments for sump, cavity, reactor well and dome. They are not further subdivided. Smaller rooms and for example staircases are combined and added to the adjacent rooms. The equipment compartments in the lower part of the containment are modelled by eleven volumes and the operational compartments in the upper part by nine volumes.

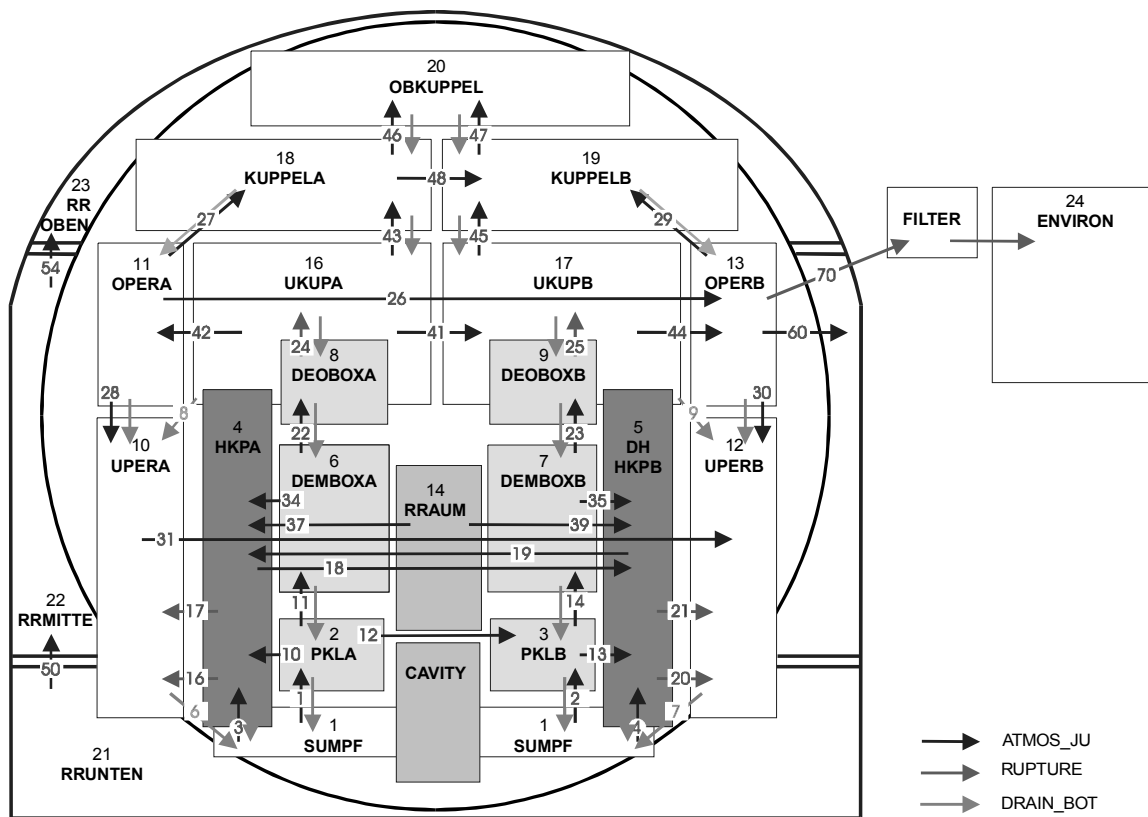


Fig. 7.2-2 ASTEC V1.21 containment nodalisation

The annulus is divided into 3 volumes. A virtual volume with time independent and constant boundary conditions represents the environment. Existing connections between the compartments within the containment are combined considering the selected arrangement of the volumes.

In the course of the accident the free convective flow area between the equipment compartments and the operational compartments is determined by the failure of a discrete number of rupture diaphragms in the steam generator towers (red arrows). For the connections in the missile protection wall equipped with burst devices a sequential failure was modelled.

There is no containment spray installed in this type of PWR. The condensate discharge from the different compartments into the sump is modelled by a special type of connection. Initial conditions for all compartments of the containment are: 30 °C for gas and wall temperatures, a relative humidity of 50 % and a total pressure of 1 bar. The catalytic recombination of hydrogen is performed by the use of 18 catalytic boxes. The carrier gas, generally a steam-hydrogen mixture, transports released species through the reactor coolant system. The transportation of the fission products is calculated with the ASTEC module SOPHAEROS. The purpose of the SOPHAEROS code is the numerical simulation of FP transport and deposition in light-water reactor circuits during a severe accident involving significant core degradation due to loss of primary coolant. The transportation path in the case of the 200 cm² leak in the cold leg leads

through the upper plenum (UPPL), a vertical volume situated above the core (see Fig. 1) and in the single loop via the hot leg (B_HL1) to the leak.

Description of the severe accident sequence

With the opening of the 200 cm² leak in the hot leg at the beginning of the accident a fast depressurisation occurs and the water level in the core decreases. Water and steam are released into the containment. The emergency feeding systems inject water into the loops until the water supply is empty. Switch over to sump suction is assumed to fail and core heat up begins. The steam generators are in hot standby. At 5612 s core degradation with fission product release starts. The fuel cladding begins to burst; relocation and melting occur, and at 6721 s the first lateral corium slump takes place. A pool of molten material is built up in the vessel lower head and the temperature escalation beyond 1200 °C causes a failure of the vessel wall at 20868 s. The following molten corium concrete interaction (MCCI) is investigated until the end of calculation at 50000 s. For MCCI no aerosol release is calculated as at present there is no reliable model for aerosol release from molten corium pools mixed with concrete available in ASTEC.

Containment thermal hydraulics during MBLOCA

In the beginning of the accident the containment pressure raises up to 2.9 bar due to the blow down via the break (Fig. 7.2-3) and drops with the feeding of the emergency systems. During dry out and core degradation phase the pressure rises up to 2.5 bar. The temperatures in this phase are in the range of 100 °C to 150 °C (Fig. 7.2-4) except for the break room where high temperature peaks can be observed. The corresponding humidity is shown in Fig. 7.2-5. The relative humidity in the compartments of the containment is high during the phase of accident, where a large amount of coolant is injected. After this period the humidity decreases. Only some compartments, e.g. PKLA (see Fig. 7.2-5), show a level of humidity that reaches 80 % which possibly could lead to hygroscopic effects on aerosol particles. But in this calculation hygroscopic effect were not taken into account.

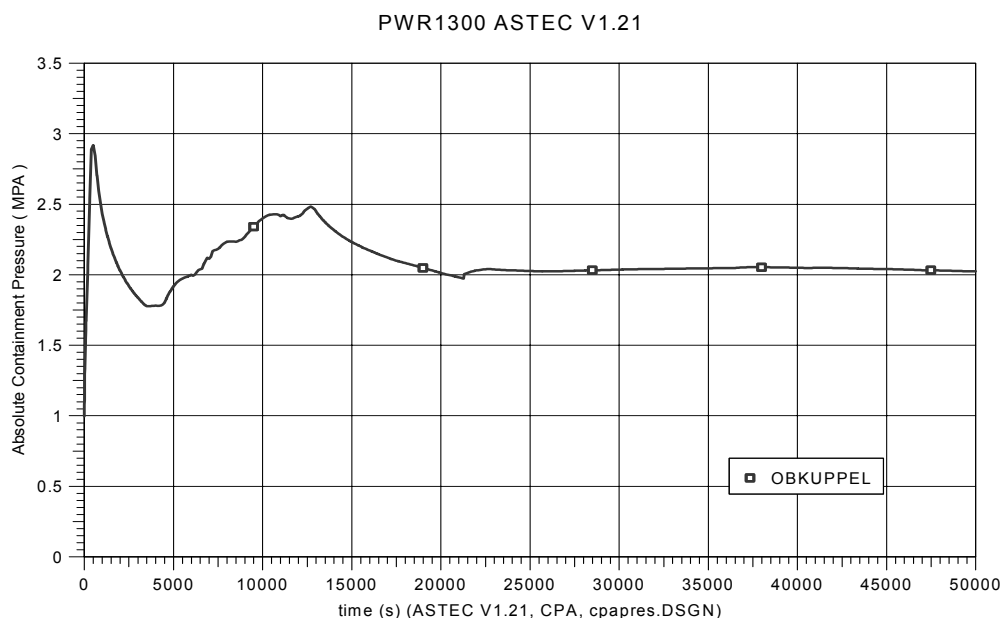


Fig. 7.2-3 Pressure in the containment

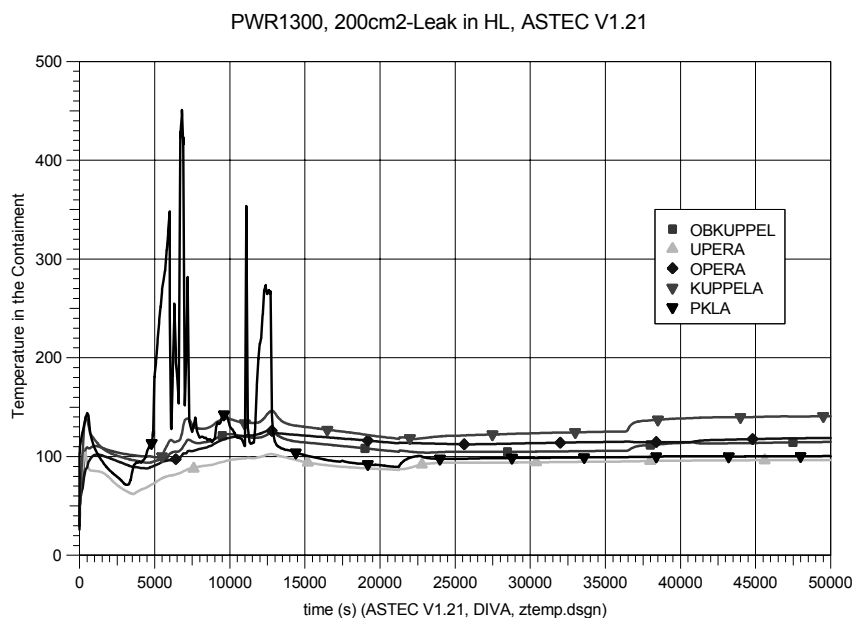


Fig. 7.2-4 Temperature distribution between the break room (PKLA) and the dome (OBKUPPEL)

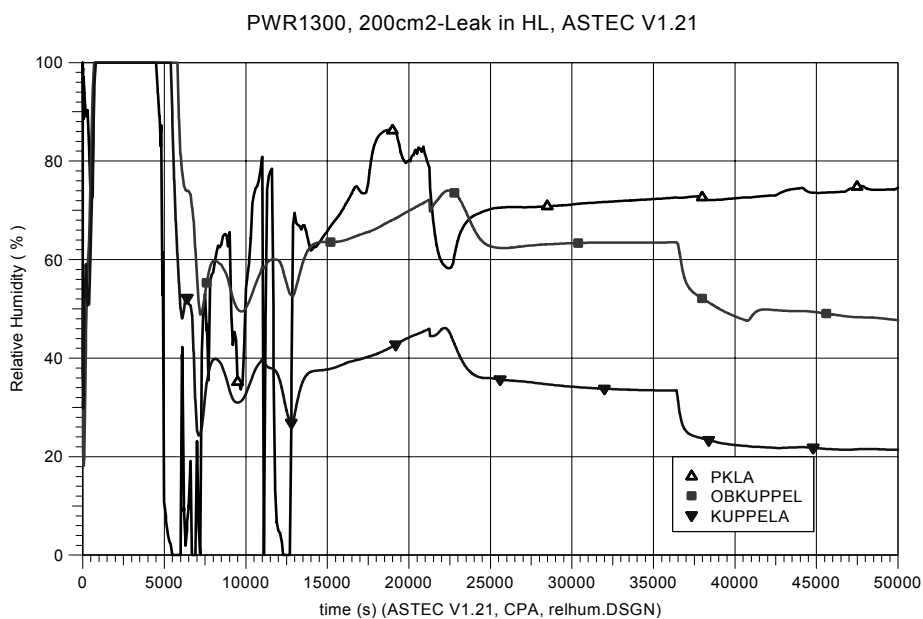


Fig. 7.2-5 Relative humidity between the break room (PKLA) and the dome (OBKUPPEL)

Aerosol distribution in the loop

During the core degradation a total aerosol mass of 1280 kg is generated. Fig. 7.2-6 shows the evolution of the aerosol deposition. At the late phase of the core degradation shortly after 17200 s the deposited aerosol mass concentration in the upper plenum (UPPL) suddenly turns to very low values typical for a mechanical resuspension process. A sudden release of steam from the core caused by a large slump of corium at this time point leads to a significant increase in the carrier gas velocity in the upper plenum. The wall temperature in the upper plenum increases at the same time to about 670 °C which is

about the boiling point of Cs. Under these conditions a part of the deposited aerosol is mechanically resuspended and the other part is revaporated.

Fig. 7.2-7 and Fig. 7.2-8 show the particle size distribution of the aerosol in the upper plenum and the hot leg volume with the break shortly before and after resuspension / revaporisation. At about 17200 s the aerosol deposited in the upper plenum is resuspended and transported via the hot leg to the containment. The resuspended aerosol contains a large fraction of coarse particles.

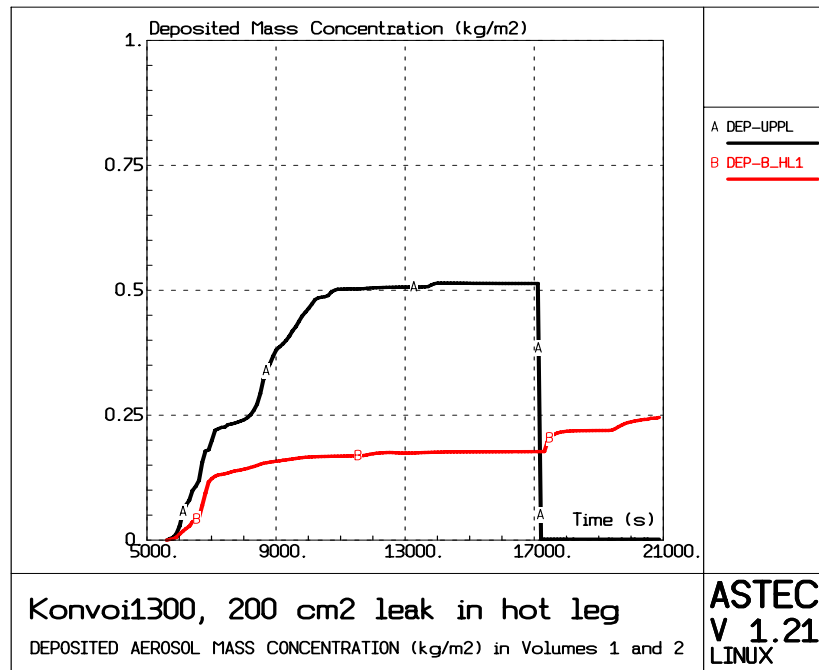


Fig. 7.2-6 Evolution of deposited aerosol mass concentration in volumes 1 and 2

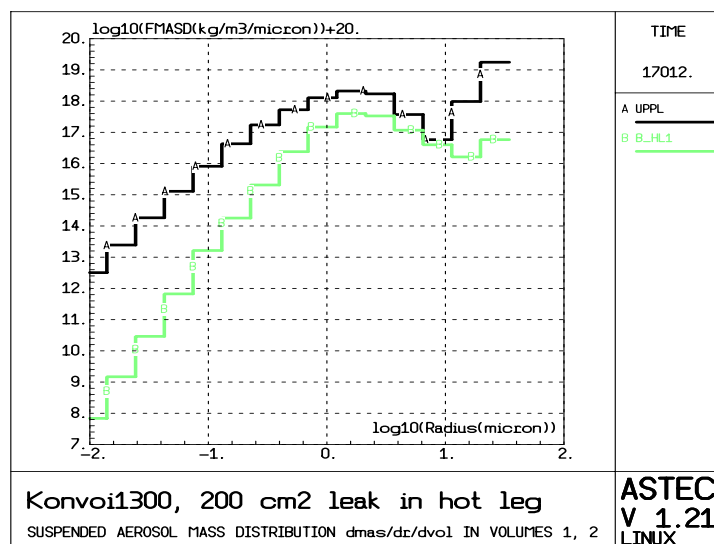


Fig. 7.2-7 Particle size distribution in the upper plenum and the hot leg (break position) at 17012 s

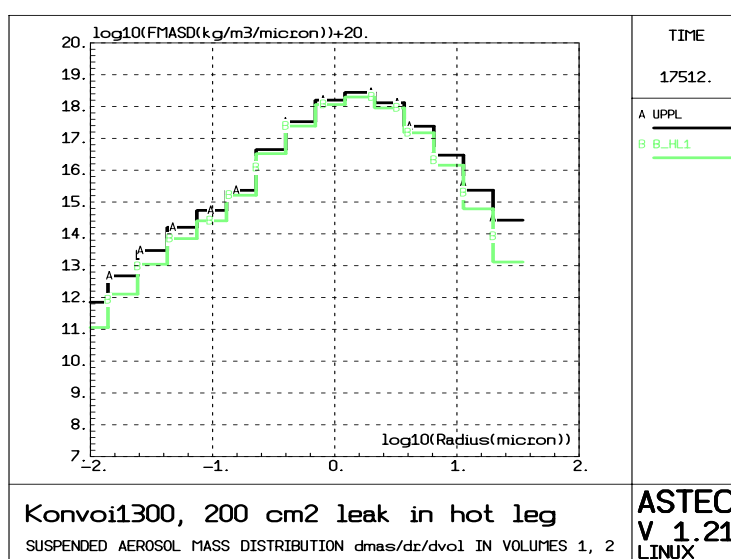


Fig. 7.2-8 Particle size distribution in the upper plenum and the hot leg (break position) at 17512 s

At 17512 s the aerosol size distributions in the upper plenum respectively in hot leg become quite similar indicating the end of the short resuspension period. The slight differences remaining between the particle size distributions after the resuspension are due to different geometries in the two volumes.

The sudden aerosol release by resuspension / revaporization increases the aerosol concentration in the break room and other volumes in the containment.

Fig. 7.2-9 shows that thermophoresis (THERMOPH) is the most effective mechanism for aerosol retention in the upper plenum. Only at about 6000 s there is also some retention of particles deposited by inertia effects from turbulent gas flows (TURBINER). In the adjacent horizontal pipe volume B_HL1 additionally a small contribution to the particle deposition by impaction in bends and settling is calculated.

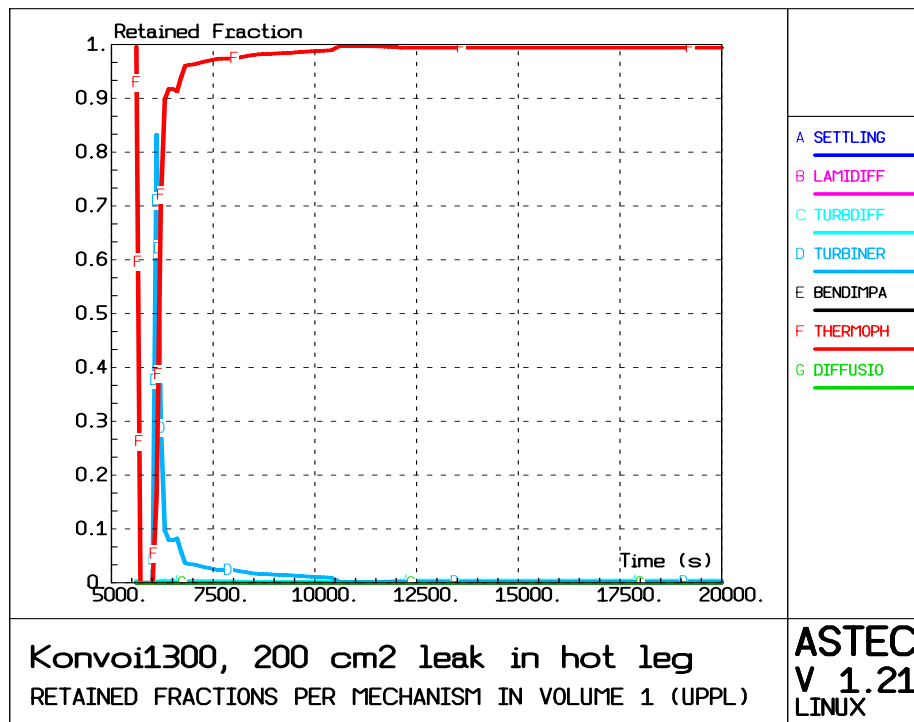


Fig. 7.2-9 Retained aerosol fractions according to different deposition mechanisms in UPPL

Aerosol in containment

From the total aerosol mass generated during the in-vessel phase a large amount of 817 kg reaches the containment because the leak is located in the hot leg close to the upper plenum. The steep incline and the depletion of aerosol concentration in the different containment compartments are shown in Fig. 7.2-10. The black curve is the aerosol concentration in the break room. The concentration peaks are caused by the material release during the corium slumping. Due to the rupture of the burst devices shortly after break opening (see 7.2.2) the released aerosol is rapidly distributed in the containment by atmospheric flows. However differences between the local concentrations persist during the whole sequence.

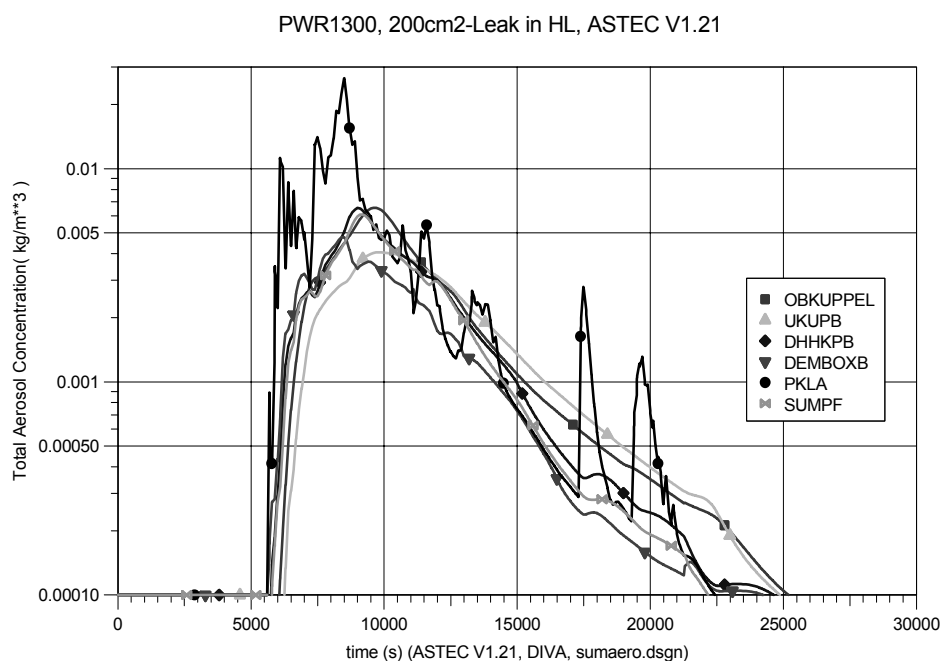


Fig. 7.2-10 Total aerosol concentration in different compartments

Fig.7.2-11 displays the mass median diameter (MMD) of the aerosol in the break room PKLA. The MMD peak values are due to the aerosol releases during slumping. The MMD increases slightly by agglomeration till 20000 s and decreases due to the enhanced deposition of the larger particles afterwards.

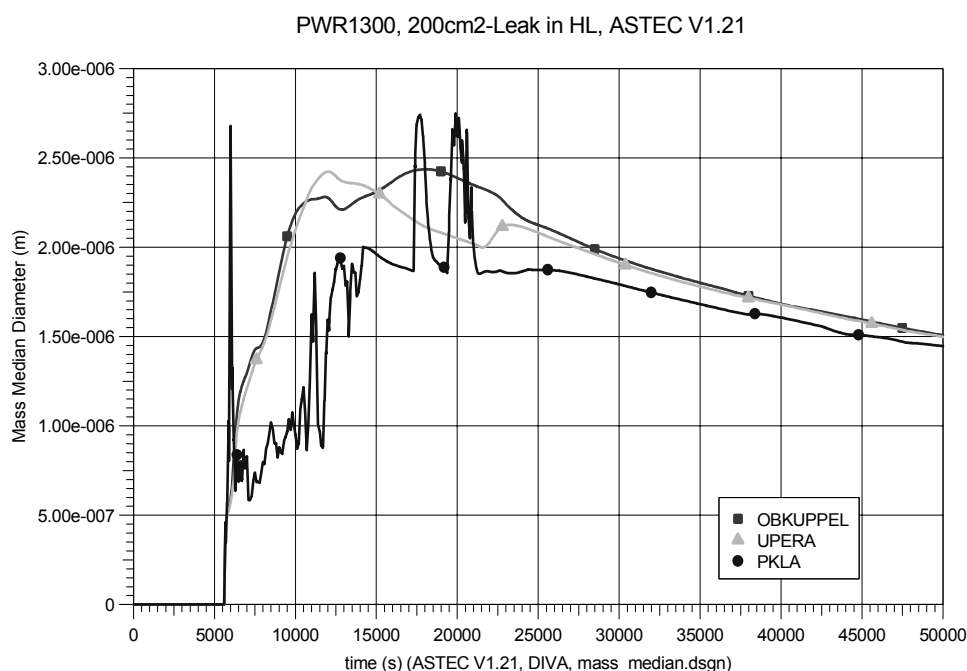


Fig.7.2-11 Mass median diameter in different compartments

Fig. 7.2-12 shows the particle size distribution in the break room before (17026 s) and after (17512 s) arrival of the aerosol released by resuspension / revaporization in the upper plenum.

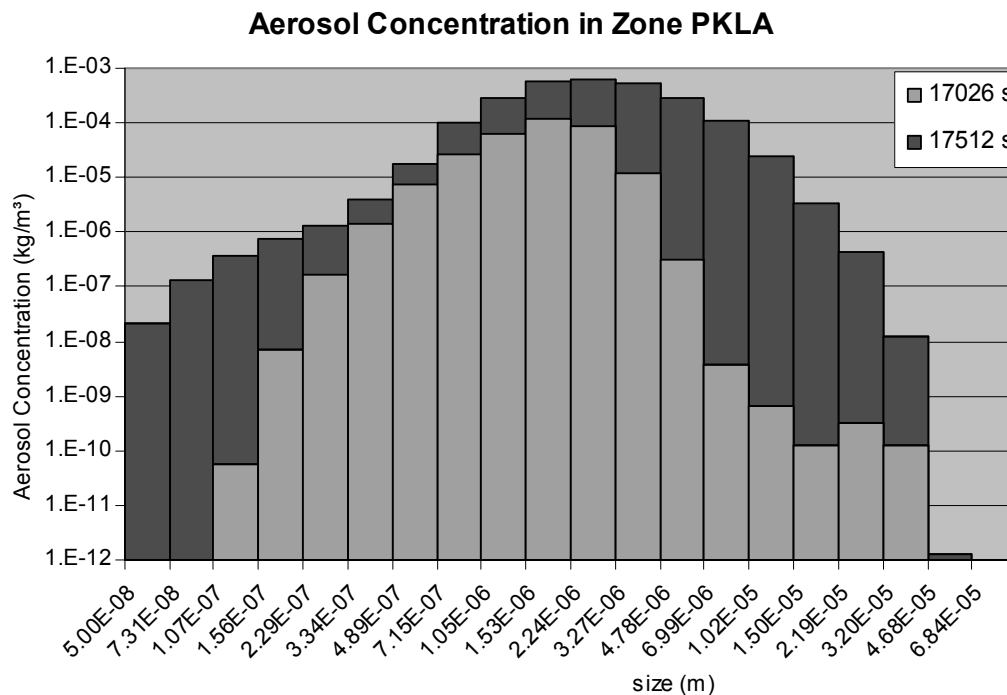
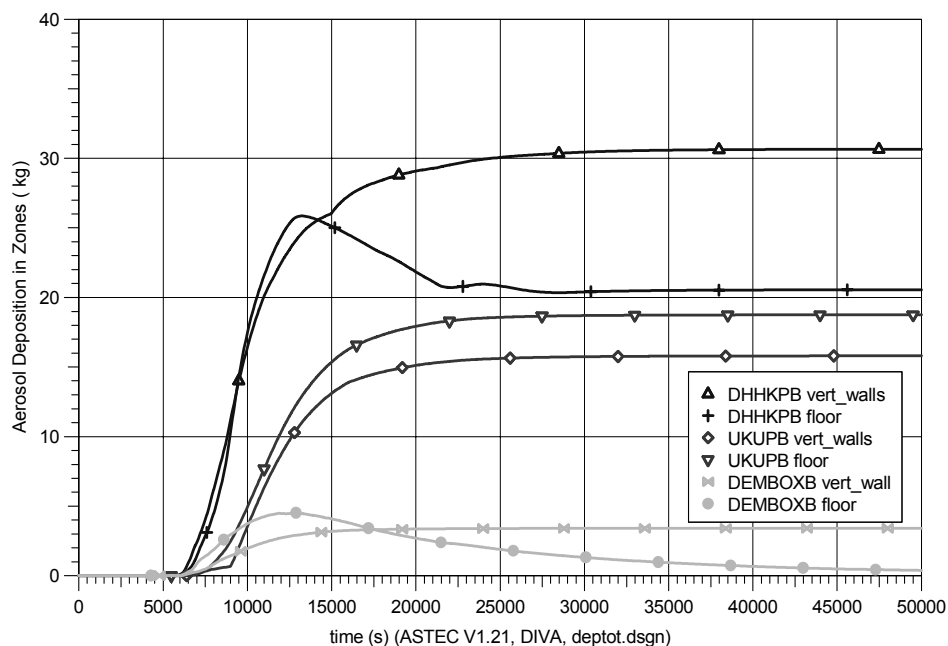
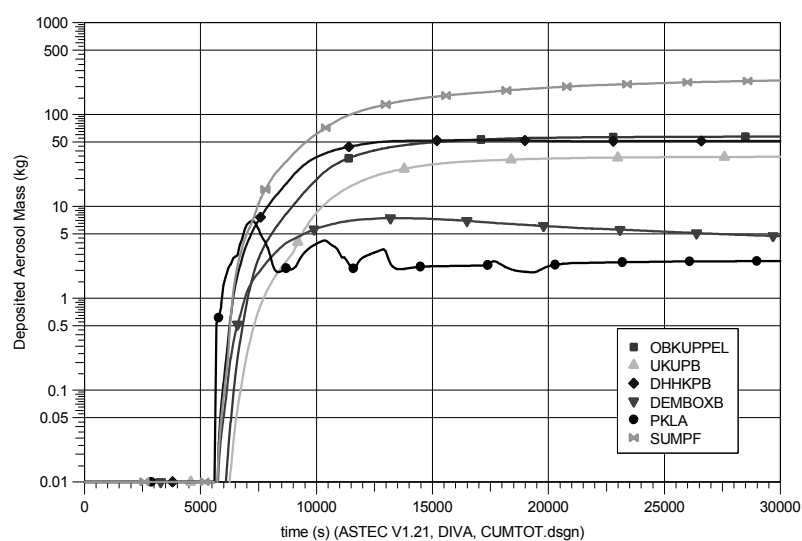


Fig. 7.2-12 Aerosol size distribution in the compartment PKLA at 17026 and 17512 s

Fig. 7.2-13 depicts in more detail the deposited aerosol mass in three different compartments. Since volumes and deposition areas are different the deposited masses cannot be compared directly. The high amount of aerosol on the walls is deposited by diffusiophoresis as consequence of the significant wall condensation. In two compartments (DHHKPB and DEMBOXB) the deposited aerosol mass is reduced by wash down with draining condensate after 12000 s. Most of this aerosol mass is transported into the sump.

In Fig. 7.2-14 the deposited aerosol mass is shown for different volumes including the sump. The highest amount of aerosols is continuously built up in the sump caused by aerosol wash down. At the end of the calculation about one fourth of the containment aerosol has been washed down into the sump.

PWR1300, 200cm²-Leak in HL, ASTEC V1.21**Fig. 7.2-13** Aerosol deposition in different zones on floor and vertical wallsPWR1300, 200cm²-Leak in HL, ASTEC V1.21**Fig. 7.2-14** Deposited Aerosol mass in different compartments

Conclusions

Generation and behaviour of the nuclear aerosol in the primary circuit and the containment during a core melt accident in a German PWR was analysed consistently with ASTEC. In this integral multi-compartment calculation all relevant interrelations between aerosol and other phenomena like thermal-hydraulics were considered. It is shown that aerosol processes in the primary circuit like resuspension and revaporization influence the local aerosol concentrations in the containment directly. This calculation indicates a rather homogeneous distribution of the suspended aerosol in the containment.

7.3 Aerosol-Related Uncertainties in the Prediction of Severe Accident Source Terms

In the 1990s two research projects supported by the EU examined the impact of various phenomenological uncertainties on the prediction of plant severe accident source terms. In the STU project, reported in the archival literature in [1], experts from a consortium of utilities, engineering consultancies and research organisations investigated 13 processes probably occurring in severe accidents, selected on the grounds of relevance to typical sequences and their impact on off-site risk. Eight European reference plants were examined with respect to 23 sequences taken from recent PSA studies, with selection criteria taking into account phenomenology, absolute frequency and contribution to risk. Basing their views on literature surveys and in-house plant analysis, the experts considered severe accident processes both from the point of view of their uncertainty, ranging from high, meaning too difficult to model or poorly understood, to low, signifying modelled in a detailed way with adequate validation, and from the point of view of their sensitivity. Processes judged to be highly sensitive were (naturally) those expected to have a significant impact on the source term. In turn, a significant impact was taken to mean one where the predicted source term to the environment or containment exceeded a threshold fraction of the core inventory and the variation traceable to the phenomenological uncertainty under study exceeded half an order of magnitude for the volatile elements (noble gases, Cs, I, Te) or an order of magnitude for the less volatile elements such as Ru, Ce and Pu. This set of criteria was intended to be a generally applicable surrogate for the category “large release” in use in several European countries.

The processes and their significance ratings are to be found in [1]. Processes of relevance to NARSOAR are summarised in Table 7.3-1 below. Significance varies with the sequence examined, and a practical grouping of the sequences was arrived at by the experts on the basis of containment failure (early or late), with or without natural and engineered retention mechanisms, and a separate category for bypass sequences.

Table 7.3-1 Sensitivity of the source term to the environment, by aerosol-related processes and sequence category. Bold type indicates the strongest sensitivity

	Containment sequences			Bypass sequences	
	Early containment failure		Late failure		
	no retention	retention	retention	no retention	retention
Vapor and aerosol transport and retention in the primary circuit	Volatiles			Volatiles	Iodine only
Behaviour of non-fission product materials			Iodine only		
Low-volatile releases from in-vessel pools	Involatiles			Involatiles	
Low-volatile releases from MCCI	Involatiles				Te only
Aerosol behaviour in the containment					
Late revaporisation				Volatiles	
Pool scrubbing		Volatiles & involatiles			Volatiles & involatiles
Release route and failure mode effects		Volatiles & involatiles	Volatiles & involatiles		Volatiles & involatiles

The absence of a phenomenon from a particular cell in the table does not indicate that it is not important for the source term, but rather that the present status of its modelling is such that residual uncertainties do not have a significant impact on the uncertainty of the release to the environment. In practice the modelling considered when assessing the uncertainty of a process was that of the versions of MAAP and MELCOR current at the time, although more specialised codes were also considered or applied in specific cases. Sensitivities were judged from the results of PSA2 studies on plants including BWRs, 3-and 4-loop PWRs, KONVOI and the VVER-440/213 PWR.

Some of the conclusions reached within this project merit re-examination within the NARSOAR writing group or more widely within the CSNI structure. Examples are the safety importance of the late release of involatiles from in-vessel pools (and by analogy, from deposits within the core and the above-core structure), the importance of pool scrubbing for bypass sequences, and the low safety importance ascribed to uncertainties in the behaviour of aerosols within the containment.

In a follow-up study (OPTSAM, 2000-2002), a similar group of European experts made an extensive study of severe accident management measures (both engineered safety features and operating procedures) for a range of plant types in current operation in Europe and for risk-dominant accident sequences. The full results of OPTSAM have not yet been published, and the information provided here is based on the project summary report [2]. It was concluded that none of the measures examined would worsen the source term to the environment.

For example, operation of recombiners, where installed, would always be beneficial. The obvious caveat is that the validity of this conclusion is limited by the validation status of the models implemented in the codes used in the sequence calculations (MAAP and MELCOR) and the former status of knowledge. As example for the increased of knowledge the present RECI findings (see chapter 5.10.5) are mentioned here.

References

- [1] M.L. Ang, E. Grindon, L.M.C. Dutton, P. Garcia-Sedano, C.S. Santamaria, B. Centner, M. Auglaire, T. Routamo, S. Outa, J. Jokiniemi, V. Gustavsson, H. Wennerstrom, L. Spanier, M. Gren, M.-H. Boschiero, J.-L. Droulas, H.-G. Friedrichs, M. Sonnenkalb A risk-based evaluation of the impact of key uncertainties on the prediction of severe accident source terms - STU. Nuclear Engineering and Design 209 (2001) 183-192
- [2] M.L. Ang, E. Grindon, C.S. Santamaria, B. Centner, M. Auglaire, T. Routamo, F. Bertels, V. Gustavsson, L. Spanier, M. Sonnenkalb, J.-L. Droulas, J. Duspiva, G. Horvath Optimisation of severe accident management strategies of the control of radiological releases - results of study for eleven reference plants (OPTSAM). Final Summary Report, 2002

8. IDENTIFIED OPEN ISSUES (INCLUDING RECOMMENDATIONS)

8.1 Introductory Remarks

Safety-related issues for current and near-future generations of LWRs have been reviewed several times within the OECD framework. A relatively recent list of identified issues and research recommendations is to be found in the proceedings of the OECD Workshop “Nuclear Aerosols in Reactor Safety” in Cologne, June 1998 [1]. These are addressed point-by-point in Appendix 5 while, here, updated identified issues and recommendations are presented; some unavoidable duplication exists between this section and Appendix 5.

Concerning the **reactor circuit** the 1998 workshop identified as issues:

- uncertainties in calculated thermal-hydraulics as they impact vapor and aerosol transport;
- deposition in singularities such as valves and bends;
- thermal-hydraulics and deposition in flow across steam generator tube bundles;
- modelling and assessment of the safety relevance of resuspension and revaporisation of circuit deposits.

Concerning the **reactor containment** the 1998 workshop singled out:

- validation of models for aerosol removal by sprays;
- possible further removal mechanisms such as turbulent impaction and charge effects (suggested by Phébus FP results at that time);
- potential impact of hydrogen recombiners on aerosol depletion rates as well as chemical effects;
- effect of hydrogen burns on aerosol composition and atmospheric chemistry including the production of volatile forms of iodine;
- uneven level of detail in pool scrubbing models may not satisfy safety tolerances for all conditions;
- re-entrainment from boiling pools, possibly important for off-site releases.

In addition to investigation of the issues listed the Workshop also recommended:

- holding a meeting on the use of severe accident codes in plant calculations for source term estimation, including codes used by utilities within the following two years;
- in view of the intensive research into nuclear aerosols then prevailing, the writing of a SOAR on aerosol behaviour in the primary circuit and containment.

Following the mandate from the CSNI this last recommendation has finally been fulfilled in the present report. It takes into account the outcomes of the major experimental and analytical programmes that have been completed or are still in progress, and has identified the issues with associated recommendations which are contained in the sections which follow.

8.2 Generic Issues

8.2.1 *Code-users' workshop on plant analysis*

Circuit thermal-hydraulics are important for vapor and aerosol transport in the circuit. Extensive code comparisons in the EC projects EVITA [3] and under continuation in the EC network SARNET [4] have identified significant thermal-hydraulic differences in supposedly similar plant calculations and helped increase understanding of their causes. To fully explain differences in the results from different codes and users requires a deep understanding of the modelling and numerical approaches within each code and of the choices made by the user. Such evaluations are time consuming but necessary and should be continued in future with more involvement of utilities and vendors. Chapters 6 and 7 of this report are intended to reinforce the international discussions on this topic.

More generally, the CSNI workshop recommended in 1998 that a meeting on the use of severe-accident codes in plant calculations for source term estimation, including codes used by utilities, be held. More than eight years after formulation of this recommendation it has still not been acted upon. There remains a need to harmonise user practices with respect to plant analyses in order to reduce divergence in results. The objective would ideally be to produce online "best practice" guidelines for the major codes.

8.2.2 *Shape factors*

The models describing aerosol dynamics have been traditionally developed for spherical, fully dense particles. Dynamic and agglomeration (collision) shape factors are introduced into the aerosol physics equations to describe the dynamics of non-spherical particles.

Real particles of a nuclear aerosol in the primary system or the containment are seldom either fully dense or spherical. So-called primary particles may agglomerate to form fractal structures but vapors condensing on them can change their shapes. Only at a very high humidity or with steam condensation in the bulk do the particles become spherical (droplets). Some evidence exists that particles in accident conditions (i.e., prototypical multi-component source, different vapors having condensed at different temperatures, etc.) would not form the branching structures familiar from carbonaceous smoke; however, information is particularly sparse for aerosols in the containment (see Appendix 1). Information that is contradictory to this can be found but arises from less-representative experiments (see Appendix 2).

The importance of shape factors is demonstrated, for example, in a comprehensive uncertainty and sensitivity analyses for a coupled thermal hydraulic and aerosol calculation of the dry aerosol test VANAM-M2 [2]. The main contributors to the uncertainty of the calculated aerosol concentrations were the dynamic and agglomeration shape factors in addition to, e.g., the turbulent dissipation rate and the number of particle size classes.

A comprehensive theory of aerosol shape factors does not exist. The theory of dynamic shape factors, which can be checked in a measurable way, is more advanced than the theory of agglomeration shape factors. Understanding of dynamic shape factors is based on experiments with aerosols formed from pure vapors. In reactor accidents multi-component aerosols formed from complex vapors are expected. A fitting ("back calculation") of shape factors is not recommended.

The influence of shape factors may be larger in accident scenarios involving large parts of the containment with a rather low humidity. Some parametric source term calculations for such scenarios could be performed but the difficulty is knowing what constitutes "reasonable" variation of the shape factors. Only if the impact of shape factors on the overall results is significant are further investigations justified from the point of reactor safety. The real requirement is further characterization of representative particles

where, as a minimum, measurement of two diameters such as aerodynamic diameter and volume-equivalent diameter provides access to the dynamic shape factor.

8.2.3 *Computational fluid dynamics codes*

CFD treatment of flow phenomena in the reactor coolant circuit and the containment is becoming more common and CFD methods are growing in power. Although the entire plant is presently not simulated with CFD tools - mainly because of the immense effort required for grid preparation, the incompleteness of the codes with regards to reactor-safety-specific models and tremendous calculation times - selected components under well-defined boundary conditions are becoming amenable to CFD analyses. The first applications for full containments have just been published. Today's CFD methods have the capability to describe effects that are difficult or impossible to predict reliably with the classical lumped-parameter approach, e.g., local inhomogeneous gas distributions in rather small volumes or hydrogen combustion processes. Because of the more detailed knowledge of the flow field, certain aspects of the study of fission-product transport should also be improved. CFD codes have for example been applied to simulate aerosol transport in small scales such as the PHÉBUS FP circuit and containment (but without any possibility to compare the code calculations with local measurements absent from these integral tests).

Even if transport and depletion of aerosols are described reasonably by experienced users using adequate options of lumped parameter codes (where these propose comprehensive and well-validated modelling with regard to this issue), there seems to be serious limitations of this approach for so-called complex structures such as exist in parts of the circuit, both sides of heat exchangers and paths resulting in containment leakages.

At present there are efforts being made towards using CFD codes to simulate particle transport and deposition in steady conditions in complex reactor structures (as part of the simulation or as a post-test exercise). Broadly, Lagrangian treatment of deposition with industrial CFD codes may provide reliable predictions in laminar flow regimes. In turbulent regimes, uncertainties are introduced by the limitations inherent in the flow-field turbulence modelling. In any case, it is advisable to resort to the best (and most computationally intensive) turbulence models, such as the Reynolds Stress Model. In addition, modelling turbulence-particles interactions in the framework of CFD requires using data either from experiments or Direct Numerical Simulation computations, both of which are rather difficult and scarce for complex geometries. Thus more work needs to be done before CFD treatment of particle behaviour in complex turbulent flows becomes satisfactorily accurate.

Finally, it is indispensable to compare the benefit with regard to reactor safety to the effort needed to obtain reliable results using CFD. The scientific aspect needs no discussion.

8.3 *Reactor Coolant System Issues*

8.3.1 *Mechanical resuspension*

The safety impact of aerosol resuspension in the primary circuit is both design- and scenario-dependent, and must be evaluated case by case. It does not appear that existing resuspension models are adequate for this purpose. Resuspension was the focus of ISP-40 and studies of the phenomenon have continued both in general and with a nuclear safety objective. The majority of the nuclear safety studies use simulants. Some limited information on circuit resuspension is also available from the PHÉBUS-FP programme in which the deposits are representative in character. Theoretical and experimental investigations both in pipe geometries and in tube bundle geometries have demonstrated that the resuspended mass for a given geometry and given flow conditions is sensitive to the deposit's mass loading, particle size distribution, chemical composition and structure, this last parameter being in turn a function of the conditions under

which the deposit was laid down, whether by settling, thermophoresis, turbulent impaction etc. or a combination of such mechanisms. Current deposition models do not however predict the deposit structure, e.g., its porosity. For the purposes of resuspension modelling this is a deficiency which requires attention.

Resuspension models exist which are able to take account of the porosity of the deposit, but they are not yet fully developed or validated. Unlike the resuspension models implemented in current safety codes such models also aim to predict the size distribution of the resuspended clusters, a parameter important for the prediction of its subsequent transport and deposition. The further development of such models deserves encouragement.

Up to now all the work on resuspension has focused on the resuspension due to an increase in flow. Shocks and vibrations, especially in conjunction with flow increases can exacerbate resuspension in ways that are not well understood. These phenomena are expected to be prevalent in reactor accident scenarios, and one needs therefore to address them individually as well as in combination with flow acceleration.

Little experimental or theoretical work has been done on the resuspension of wet deposits or of deposits which have become wet and have then dried in situ. It is recommended that scoping analyses be performed to assess the potential impact on source terms of the differing resuspension behaviour of dry and wetted aerosols.

Finally, it has to be said that the consequences for a severe accident of a light-water reactor due to resuspension from the RCS varies depending on the scenario, i.e., bypass or non-bypass sequences. Resuspension occurs due to the steam spike generated by the core collapsing into remaining water in the reactor vessel, an event occurring close in time to the peak release of fission products. Hence, for non-bypass sequences, the influence of this resuspension on the potential source term may well be insignificant within a few hours. However, improvement of resuspension modelling with respect to bypass sequences is clearly very desirable.

8.3.2 *Deposition in singularities and complex structures*

No significant advances appear to have been made since 1998 in the experimental investigation or the modelling of deposition in singularities such as changes in cross section or bends. Some code improvements have been made by including the best-available models from published literature.

Regarding deposition in complex structures, progress has been made with respect to the secondary side of steam generators (SGs). While the last decade has seen considerable efforts to understand degradation processes that can lead to SG tube cracking, wall thinning and potentially rupture as well as to develop improved modes of operation and preventative and corrective measures, the SG tube leakage incidents that occurred rather frequently in the past prove that such events cannot be completely ruled out. Steam generator tube rupture (SGTR) accidents are, however, design basis accidents so measures are in place to cope with them: for the 11 known incidents the plants concerned coped.

A leakage of radionuclides from the primary circuit into the secondary side negates the purpose of the containment. Under certain conditions high release of radionuclides to the environment is possible during postulated severe accidents. Risk assessment studies generally consider two types of severe accidents:

- an operational event or design basis fault that causes a SGTR which then results in core damage;
- a core damage sequence which might impose pressure and temperature conditions that could lead to SGTR.

Most probabilistic risk assessments (PRAs) and severe-accident codes assume that a significant fraction of fission products flowing through a non-isolated break in a SG escapes to the environment. For example, in NUREG 1150, the median estimate (based on expert opinion) of the fraction of the core inventory of iodine released to the environment was 27 %, and the 95th percentile estimate was 80 %.

SGTR was the first European project (2000-2002) to improve understanding in a systematic way of possible retention mechanisms in tubes and in the complex structures of the secondary side of a SG. In particular, the PSAERO and HORIZON experiments from Finland were conducted to study in-tube retention whereas retention in the SG bundle has been investigated in PECA-SGTR and the ongoing ARTIST experiments (respectively in Spain and Switzerland) – see §5.10.1. In addition, certain modelling efforts to develop a correlation for the retention in the bundle were initiated.

Thorough interpretation of the data from the above experiments is incomplete and modelling efforts continue. It is expected that the main issues regarding SGTR will be answered after termination of these activities.

8.3.3 Particle break-up in highly turbulent flows

Highly turbulent flow inside a tube may induce break-up of particles due to (i) impaction on the walls, (ii) strong shear in the flow or (iii) the vena contracta and shock wave at the tube exit. This phenomenon was observed, e.g., in Phase I of the ARTIST tests as well as in supplementary experiments [5]. Two types of aerosol materials were used in ARTIST Phase I: TiO₂ particles that were loosely-packed (low-coordination) agglomerates comprising primary particles of approximately 20-40 nm in diameter or spherical SiO₂ particles. TiO₂ agglomerates had an AMMD of approximately 2-5 µm at the tube inlet but were reduced to sub-micron-sized particles at the tube exit; the SiO₂ particles did not break up in the tests. Clearly, these results indicate a possibility of particle break-up during SGTR sequences. However, to determine whether aerosol particles may break up in severe accidents would require more information on the structure and the nature of the bonding forces between primary particles for severe accident aerosols as well as for the TiO₂ agglomerates used in ARTIST Phase I. In Phébus tests, which produced more prototypical aerosols, SEM micrographs showed fairly compact, sintered agglomerate structures unlike the ARTIST TiO₂ particles. Consequently, intra-particle forces can be expected to be higher in reality than in these TiO₂ agglomerates. Nevertheless, the issue is of some importance since the generation of submicron particles from supramicron ones leads to less-efficient retention of the aerosols concerned. In the first instance, accident sequences other than SGTR inducing highly-turbulent flows need to be identified; comparison of plant calculations without and with (assumed) break-up for SGTR and the other pertinent sequences would then allow evaluation of the risk relevance of the break-up phenomenon. If the risk impact is significant then, in the absence of appropriate data for severe accident aerosols, data for prototypical particles are needed in highly-turbulent accident-relevant conditions.

8.3.4 Influence of chemistry

The fundamental importance of chemistry is well established given its direct influence on many phenomena of high significance to prediction of source terms arising from potential severe accidents (e.g., nucleation/condensation, chemisorption, revaporization, etc.). Probably most critical in terms of safety consequences is the decisive impact of chemistry for a given FP on the split between the gas/vapor fraction and condensed phases (aerosol and condensates). Broadly, a lower-volatility species for a given FP presents a lower hazard due to its greater propensity to be trapped on a surface (structure or filter) rather than be released into the environment.

As described earlier in this report, nuclear-safety codes model chemical reactions using the thermodynamic equilibrium approach where codes use empirical or estimated thermodynamic data for each chemical

species covered. The uncertainties associated with these data vary greatly and are often large especially with respect to estimated data. Furthermore, divergence between data series originating from different sources can be considerable. It can be said that, for many species and some very important systems, uncertainties associated with the data can only be reduced by further analytical experiments. While there seems to be little prospect presently of new experimental work producing better data, it is recommended (as is being done for the ASTEC code) that the thermochemical data used by codes are thoroughly verified and completed with identification of key sources of uncertainty.

Beyond the thermodynamic approach to chemistry, commonly accepted to be valid at high temperature (i.e., roughly, in the reactor vessel and the hot leg), at intermediate and lower temperatures some reaction rates become comparable to or slower than convection rates. The ensuing non-equilibrium state as the flow progresses downstream will not be predicted by the equilibrium approach. While the importance of this modelling deficiency for severe accidents may be high, it has to be recognised that sufficient rate data will never be available for development of comprehensive kinetic models. So, while the thermodynamic approach is pragmatic, it probably encounters significant limitations when addressing accident scenarios involving secondary-side or cold-leg conditions and is inappropriate in the containment. In this context it becomes important to do three things:

- assess the value of the simplified approach of stopping chemical reactions in the RCS below a user-supplied cut-off temperature (ASTEC/Sophaeros and VICTORIA codes) where PHÉBUS FP results with respect to iodine in the RCS should prove to be very useful;
- follow closely experiments, e.g., the French CHIP programme, investigating reaction rates for some of the iodine system;
- assess whether important FP species other than molecular iodine, reaching the containment in the vapor phase, require kinetic modelling at the circuit breach. This is an especially important issue with respect to hot-leg and high-pressure sequences where vapor fractions at the RCS breach will be significant and quenching of reactions may occur leaving highly volatile species in the gas phase (e.g., ruthenium tetroxide, hydrogen iodide).

Lastly, the effects of radiolysis in the RCS are unknown. It may well produce significant quantities of radical and exotic species unpredicted by thermodynamic and/or kinetic models alone. Radiolysis may have little impact in the core region (temperatures being so high that only simple atomic and radical species exist), but may be important in cooler regions of the RCS involving significant deposits (high local dose rate) such as in a cold-leg sequence. In terms of direct consequences for aerosols, one effect will be reduction of the threshold super-saturation at which vapors nucleate since a high density of electrically-charged condensation nuclei will form. In terms of consequences for the source term, the meagre state of knowledge renders even qualitative evaluation difficult.

8.3.5 *Revaporisation of deposits*

Studies on revaporisation with Phébus FP and simulant samples were undertaken in the EC 4th Framework Programme projects RVP and REVAP-ASSESS. Based on these studies and the evaluation of PHEBUS FP results themselves the knowledge of revaporization has significantly increased. It has been shown to significantly influence transport of volatile fission products compounds in the RCS to the containment during core degradation. In addition, plant calculations indicate that revaporisation can be a potential long-term source of fission products to the containment. Currently further studies of revaporisation with samples from PHEBUS FP experiments are on-going. In addition, release of volatile fission product compounds due reactions on the primary circuit surfaces is carried out in EXSI project within the SAFIR2010 programme. Lastly, in the frame of SARNET programme, one technical circle is dedicated to

sharing information on revaporisation. Only after termination of these evaluations can it be decided what additional work might be necessary.

Experimental work on revaporization remains scarce; further theoretical and experimental developments are necessary to understand the revaporization process. In addition, the safety relevance ought to be further demonstrated by assessing, conceivably, the impact of a weak source of fission products from the reactor coolant system for some hours after the main release-from-core phase.

8.4 Containment Issues

8.4.1 *Charge effects*

Small deposits of aerosols on the outer walls of the 10 m³ containment vessel in the PHÉBUS test FPT0 could not be explained by electrophoretic effects as shown in an IRSN study (and while this study was made available to the PHEBUS partners it did not lead to further studies). However, even if charge effects on aerosol deposition are not seen to be significant in test facilities (with or without a radiation field) there is no firm evidence that this effect would be negligible in an accident. At present there is no consensus among experts on whether further investigations of charging effects are necessary or not.

8.4.2 *Mixed aerosols in condensing atmospheric conditions*

Although there has been considerable progress in modelling aerosol deposition as a function of relative humidity, a comparison of the adequacy of code results from ISP 37 and ISP 44 indicate that there is still some work to be done to ensure satisfactory coupling between thermal hydraulic and aerosol models so that these capture correctly aerosol behaviour in most environments. An additional uncertainty in modelling aerosol behaviour in the containment in highly humid conditions arises from determining the hygroscopicity associated with a mixture of aerosols of different compositions. Both the PHÉBUS tests and the KAEVER experiments suggest that an average aerosol particle composition and size might be attained in containment. There is still an uncertainty related to the density of multi-component aerosols. Uncertainty analyses (see Chapter 6.4) based on experiments with well-defined material do not show that the density is of central importance. However, this has to be confirmed for accident conditions with a wide variety of aerosol components. The KAEVER experiments further suggest that this average particle would behave like the most hygroscopic of its individual components. Confirmation of these findings, in a large-or intermediate-scale experiment performed under saturated conditions might significantly simplify modelling aerosol behaviour in wet conditions.

The impact of steam condensation on aerosols is accelerated depletion of suspended material in the containment and so is beneficial in terms of an accident. In this respect, to implement new models for steam condensation on aerosols in the Canadian code SMART and to ensure adequate coupling between thermal hydraulic input (GOTHIC) and aerosol modelling, additional data relevant to this design are required (notably from experiments using a CANDU-representative aerosol composition where, unlike for PWRs, control-rod material is not expected to be a major component). Some CANDU relevant data are available from experiments in the KAEVER, AHMED and VANAM facilities, however additional data under higher bulk-condensation rates is required. Large-scale experiments (1650 m³) are planned at AECL, funded by the CANDU Owner's Group, to characterize aerosol formation in a condensing steam environment to obtain the additional data needed for Canadian model development.

8.4.3 *Mechanical resuspension*

Compared with deposits in the primary system, deposits in the containment are likely to feature significantly lower surface loadings and be widely distributed over walls and floors. Depending on the specific reactor, the accident scenario and the deposit location, the particles may undergo exposure to both

wet and dry atmospheres, as well as flows of surface water. Resuspension of the deposits is possible as a consequence of a sudden breach of containment and/or a hydrogen burn. Subsequently a portion of their radiological burden may thus be transferred to other parts of the plant or to the environment.

A limited number of specific investigations on resuspension in the containment have been performed. These have been confined to dry deposits and indicate that resuspension is quite easily induced in simulated containment deposits by sudden increases of flow. In particular an experimental study concluded that the flow disturbance created by hydrogen burns efficiently resuspends containment deposits.

Therefore, in addition to probabilistic studies to evaluate the safety significance of containment resuspension, it is recommended that experimental studies be performed on the resuspension behaviour of real or simulated deposits at containment-typical loadings, particularly under flow disturbances, as a function both of the composition of the deposit and of the deposit history (dry, wet, wet then dried in situ etc.). New experimental investigations are being performed on resuspension under flow conditions caused by real hydrogen deflagrative combustion in the ThAI facility.

8.4.4 *Re-entrainment from pools*

Re-entrainment of particulate fission products will occur at several water and core melt pools during a severe accident. The release rates of radiological materials are relatively small but the sources are persistent. A significant contribution to the source term by re-entrainment is possible in the late accident phase. However, reliable analytical investigations including risk relevant aspects do not exist yet. Few codes are able to simulate, with some restrictions, the FP release from boiling or flashing sumps.

Re-entrainment models need further improvements especially in the bubbly flow regime and in the transition regime to churn turbulent conditions. The size distribution of the entrained droplets should be described.

Up till now the main experimental investigations have been either small scale (e.g., the KWU tests and the REST tests) or medium scale (e.g., the REVENT tests). Large-scale tests were performed in the ThAI facility recently in order to improve the model RECOM which will be integrated into COCOSYS. The ThAI results show in particular that the size of the released aerosol particles is significantly smaller than those reported for earlier tests.

Up to now all re-entrainment tests including ThAI have been made with relatively ideal systems with different concentrations of soluble and insoluble materials but without surfactants and impurities. Therefore, tests in realistic conditions are still necessary.

After improvement and validation of re-entrainment models for realistic conditions is achieved reliable accident calculations to quantify the effect of re-entrainment from boiling pools on the source term will be possible. In the light of these results it may be desirable to investigate measures reducing the release of fission products by re-entrainment.

8.4.5 *Pool scrubbing*

Some BWR and PWR severe accident scenarios involve transport paths of radioactive aerosols which include passages through fixed pools of water where particles (and vapors) can be retained. Therefore, this phenomenon, known as pool scrubbing, has the potential to reduce the source term. The extent of this mitigating effect would be a function of prevailing conditions, such as aerosol characteristics, water depth, pool sub-cooling and gas hydrodynamics, as well as the longer-term evolution of the radioactive material retained in the water.

By the mid-1990s, a good number of experimental programmes had addressed the pool scrubbing issue and a set of computer codes (i.e., SPARC90, BUSCA and SUPRA) were developed and partially validated. However, these tools have not been updated with respect to additional experiments carried out in the last decade of the 20th century. Most of the earlier available data concerned essentially gas jet injection and hot pools. The most recent investigations have demonstrated that decontamination by bubble formation and equilibration in a water pool can be significant, both in BWR and PWR risk-relevant sequences.

Hydrodynamic models in different codes are remarkably different both in their approach and in the results they provide (i.e., bubble size and shape); several hydrodynamic phenomena are not modelled in codes or are dealt with using highly-specific empirical correlations (i.e., jet injection, primary bubble rupture, churn-turbulent flow and bubble oscillations and deformations) and these are probably important to accurate prediction of aerosol retention in risk-relevant scenarios. We add that particle size heavily influences the pool decontamination capability so uncertainties in this parameter also have to be considered.

Pool scrubbing has been considered to be well investigated since results provided by stand alone models or modules of integral codes provide satisfactory integral retention with respect to regulatory requirements. However, there are insufficient available data for systematic validation under all relevant conditions. Aspects hardly explored to date include: removal of aerosols during the formation of bubbles or globules and the subsequent hydrodynamic processes (i.e., bubble disintegration and coalescence) and the effects of submerged structures interfacing with the incoming gas flow and of contaminants (surfactants) in the aqueous bulk.

8.4.6 *Removal by sprays*

This issue has been extensively investigated by the French organisations CEA and IRSN using specific apparatuses and the CARAIDAS, MISTRA and TOSQAN test facilities. The data should be made accessible to the nuclear community, at least the OECD partners. Validated modelling based on these experimental investigations has been implemented in the codes ASTEC and TONUS. The ASTEC model can be found in the open literature. Further work on containment sprays is low priority for countries that have access to this data but in other countries and for certain advanced designs it remains important to establish effective removal by spray systems and both experimental and analytical efforts continue.

8.4.7 *Influence of recombiners*

Phenomenological experiments have demonstrated that there is potential for PARs to generate volatile forms of iodine, namely molecular iodine, by thermal decomposition of metal-iodide species that would be present in containment aerosols. It is likely that such chemical conversions will be reproduced in accident-representative conditions but initial (limited) results from relevant experiments indicate high mitigation of this molecular-iodine production. It has also to be recognised that iodine may not be the only fission product concerned, e.g., some formation of the highly volatile species ruthenium tetroxide might be possible in the conditions expected within PARs though no investigation of this has been performed. Furthermore, scoping calculations have shown that such a conversion process even when very limited might make a non-negligible contribution to the gas-phase iodine in the containment atmosphere. Further experimental investigations in realistic conditions (mixed-aerosol and mixed-atmosphere composition) are necessary.

8.4.8 *Hydrogen-burn effects on suspended aerosols*

Heat release by hydrogen burns may have a strong effect on aerosol characteristics as a result of the thermal-hydraulic transient and could possibly liberate volatile forms of iodine. Experiments in the ThAI

facility demonstrate that there is a clear effect of hydrogen-combustion-induced flows on resuspension of already deposited CsI aerosol. Initial source-term calculations for plant conditions show an increase of airborne aerosol of up to one order of magnitude. Assuming a small leak in the containment of 0.01 m², the released aerosol mass increases by a factor of 4, in the case of a global containment failure, by a factor of 10. These findings have to be expanded to consider other types of relevant aerosol species and other plant applications. However, chemical effects on iodine-containing aerosols have not been studied; information from the ongoing investigation of the impact of recombiners on aerosols may be relevant.

8.4.9 Release from MCCI pool

The behaviour of aerosols formed following releases from a molten corium concrete pool was notably investigated in the late 1980s and early 1990s in the frame of the ACE phase C tests and the BETA tests (from which the ISP 30 should especially be mentioned). In parallel, models such as VANESA were developed along with approaches using thermodynamic equilibrium codes such as SOLGASMIX or ChemSage to calculate release of fission products. Summarizing the results of these efforts it can be said that uncertainties remained high and the predictive capability remained poor.

Some investigations of molten-corium concrete interactions were started again some years ago, e.g., within the OECD Melt Coolability and Concrete Interaction project, but there is no work related to aerosols. In addition there have been two projects (LPP and MP within recent EC Framework Programmes) in which the release from molten corium pools was investigated for in-vessel pool conditions, i.e., without concrete.

As far as an accident is concerned, from the experimental data it can be said that MCCI is likely to add a large amount of non-active aerosol material (constituents of concrete and structural materials) to the containment atmosphere in the size range of the existing aerosols. This will promote agglomeration and diversification of the aerosol composition and increase settling of the already-suspended aerosols.

In terms of modelling needs with respect to aerosols, it can be assumed that transport, deposition and resuspension of aerosols caused by MCCI can be adequately treated by the same aerosol modelling elaborated for aerosols coming directly from the RCS. The uncertainty arises with respect to the release and formation mechanisms of such MCCI aerosols where these were describe in §3.9. The relevant parameters are:

- a) the type of concrete, e.g., calcareous or siliceous;
- b) the progress of the concrete erosion process in time being responsible for
 - the temperature of the magma
 - the generation rates for vapors and gases, e.g., CO, CO₂, H₂ and H₂O, leading to sparging;
- c) aerosol nucleation due to vapors from the free upper surface of the magma and within gas bubbles leaving the pool
- d) mechanical aerosol production when bubbles burst at the pool surface.

In this context with, in particular, no significant activity in this area at present, the following steps seem necessary in the near future:

- recalculation of the older tests mentioned above using current models (for processes b) and c), in order to check progress in relation to, e.g., the thermodynamic aspects; if these models perform satisfactorily then more reliable estimates of quantities of aerosols produced in an accident can be produced;

- synthesis of the information on the characteristics of MCCI-generated aerosols; conventional (non-nuclear) knowledge of concrete aerosols may of use;
- review of the applicability of the EC projects MP and LPP where some of these tests included a significant silica component.

8.4.10 Penetration through leak paths

From the review of available databases, models in the open literature and ongoing research within SARNET on dry aerosol transport in cracks, the recommendation can be made that both separate-effect and integral tests should be performed:

- separate-effect tests should provide a detailed characterization of the mechanisms involved and they would contribute to model development and to detailed validation;
- integral tests should focus on measuring overall process variables, e.g., the mass retained, and would provide a database for checking overall model performance.

Investigations regarding the influence of boundary conditions should focus in particular on the hydraulic diameter and curvature of the path, the fluid composition and pressure drop, wall temperature, and aerosol size, obviously as close as feasible to actual scenarios. Concerning particle size, great emphasis should be placed on submicron particles, around 0.1 to 0.3 μm , as they would largely contribute to the release.

Although there are some deposition models that have been developed for dry aerosol retention in leak paths, these may not be applicable to wet aerosol behaviour since aerosol characteristics such as particle shape, and deposit characteristics (fluid rather than solid) could cause somewhat different behaviour. Wet aerosols (droplets containing suspended or dissolved fission products) are more prevalent than dry aerosols in most postulated design-basis CANDU accident scenarios.

The wet aerosol experiments performed at AECL indicate that there is significant aerosol transport through single leak path contractions representative of airlock door seals and isolation damper valves in CANDU containment. Taking into consideration the Japanese findings mentioned in chapter 5.10.3 recommendations regarding this process are:

- Further experiments are required to characterise aerosol transport through sequential expansion and contraction regions representative of the leak path from containment to the outside atmosphere during a postulated accident scenario;
- Additional experiments are also required to evaluate the extent of leak-path plugging at higher aerosol mass densities that could be anticipated during the containment over-pressurization period in a CANDU accident scenario.

8.4.11 Fire aerosols

Fires in a nuclear power plant can threaten the safety of the plant and initiate a severe accident. Cable fires are of most concern compared to other possible fires.

Cable fires can produce an enormous amount of aerosol which is quite corrosive. Fire aerosols can cause: (1) equipment damage, (2) aerosol filter plugging, and (3) contamination of passive autocatalytic recombiners (PARs). In case of core degradation the fire aerosol will interact with the nuclear aerosol. The depletion behaviour of the nuclear aerosol will be changed. Organic components of the fire aerosol will react with certain iodine species, e. g. to form organic iodides.

Only little is known on the amount of aerosols produced from fires and their properties (particle size distribution, shape factors). There is a need for further experimental investigation of fire aerosols especially from cable fires. This could be done in a future step of the OECD PRISME and/or the Sandia CAROLFIRE projects. The aerosol production rate, the particle size distribution and the shape factors are of main concern. Existing multi-component aerosol models should be extended in order to simulate the interaction of fire aerosols with a present nuclear aerosol. Of special interest is the mixing process of probably branched-chain fire aerosols with core-generated aerosols affecting their depletion behaviour.

8.5 Concluding Remarks

At the time when the previous state of the art report on circuit aerosols was written (1994) the plant analysis codes, as distinct from the special-purpose research tools, were relatively crude, and their experimental support only partial and largely confined to tests using simulant materials. Since that time substantial progress has been made. While still using lumped-parameter descriptions of the thermal-hydraulics, systems codes now include more complete calculation of gas-phase chemistry and chemical interactions with particles and surfaces in the primary circuit, and a better treatment of coupling between aerosol dynamics and thermal-hydraulics in the containment.

The limited accuracy and resolution of the calculated thermal-hydraulics are now constraining the reliability of aerosol predictions in some special cases. Models are available for the aerosol physics in a number of components such as suppression pools in BWRs and the complex structures on the secondary side of the steam generator in PWRs, as well as for retention in engineered safety features.

The experimental database supporting such codes and models has benefited from more accurate and extensive instrumentation covering a wider range of phenomena, e.g., able to measure airborne water in containment experiments. More experimentation on specific phenomena, e.g., resuspension, revaporisation, trapping in complex structures, etc., has been performed where some of this is ongoing. Large-scale and small-scale containment aerosol experiments have been performed and some have been analysed in international programmes, notably the KAEVER tests. Most significant on the experimental side is perhaps the availability of integral experiments on fission-product release and transport using a degrading-fuel and control-rod bundle as the source, viz. the PHÉBUS FP programme. The PHÉBUS FP tests have had a strong impact on our understanding of nuclear aerosols, particularly in the circuit, where now for certain scenarios we are better informed, for instance, with respect to particle sizes, shapes and compositions whereas in the past all these quantities could only be estimated. PHÉBUS has also been able to provide information helpful to modellers on specific phenomena, e.g., revaporisation.

A large number of PSA2 plant studies has been performed around the world, frequently involving aspects of aerosol behaviour, but rather few of them have been published or even summarised in the open literature. The aerosol community is, therefore, not always fully briefed on the risk-relevance of the numerous phenomena and processes currently under study.

Although large strides have been made in our understanding and application of the physics and chemistry of nuclear aerosols, their study is by no means over. Aerosol-related experimental programmes such as ARTIST and ThAI are either still in progress or their analysis is incomplete. The PHÉBUS FP series of integral experiments is now terminated but post-test analyses are not complete, and the code-based interpretation of the results continues. Conclusions drawn from the PHÉBUS FP results are at this stage necessarily provisional. The experiments did not attempt to cover the full range of conditions encountered in plant severe-accident scenarios and it remains a challenge to extrapolate from the limited aerosol data available to, e.g., aerosol emissions and transport in high-pressure scenarios.

It is expected that increasingly stringent safety standards in combination with new generations of power reactors will continue to produce aerosol-related safety questions and that to meet the ongoing challenge both experimental expertise and analytical tools supported by the know-how to use them intelligently will need to be maintained. The aerosol-related computational and modelling development now underway to tackle industrial problems and major environmental issues such as climate change is producing a body of knowledge which should be integrated with that built up within the nuclear-safety community. The CSNI structure appears well suited to developing structures and mechanisms for stimulating such cross-fertilisation.

The question of risk importance deserves a more concerted effort, in aerosol physics as in other relevant fields. This report has included some examples of plant analyses coupled with sensitivity studies to reveal the impact of aerosol-related processes and parameters, but this only scratches the surface. A rational assessment of risk importance requires the investigation of more designs and their accident scenarios with associated probabilities, and of sensitivity to models as well as to parameters.

References

- [1] H.-J. Allelein Third OECD specialist meeting on nuclear aerosols in reactor safety GRS-166, NEA/CSNI/R(98)4, ISBN 3-931995-31-3, June 1998
- [2] J. Langhans, H.G. Friederichs, E. Hofer, B. Krzykacz, G. Weber Unsicherheits-und Sensitivitätsanalyse zum Aerosolmodell in FIPLOC-M, Teil 1: Trockenes Aerosolverhalten im VANAM-Experiment M2 GRS-A-2183 (1994)
- [3] H.-J. Allelein et al. EVITA - European validation of the integral code ASTEC Final report of the project FIKS-CT-1999-00010 (5th FwP), 1999
- [4] H.-J. Allelein, K. Neu, J.P. Van Dorsselaere European validation of the integral code ASTEC (EVITA) - First experience in validation and plant sequence calculations, Nuclear Engineering and Design, August 2004
- [5] Y. Ammar (2008). Agglomeration and break-up of aerosols in turbulent flows. Ph.D. thesis, University of Newcastle, UK.

LIST OF APPENDICES

Appendix 1:

On the characteristics of aerosols arising during a severe accident of a water-cooled reactor

Appendix 2:

Aerosol Shape Factors

Appendix 3:

Spray Modelling Developed from Recent Analytical Work

Appendix 4:

Complete filter contribution of Guntay

Appendix 5:

Point-by-Point of Issues Identified at the 1998 Aerosol Workshop

9. APPENDIX 1: Characteristics of Aerosols under LWR Severe Accident Conditions

9.1 Context

The behaviour of an aerosol particle can depend strongly not just on classic properties such as aerodynamic size but on properties that are microscopic involving internal structure and composition (where these are not necessarily independent parameters)¹⁰. A concern is that the role of structure and composition is particularly pertinent to situations of strong differential forces on the particle such as during impact with a surface or in flows involving intense shear. Particle deposition can be highly sensitive in the former situation by leading to, e.g., capture of the particle on the surface or its break-up and re-entrainment in the form of a number of fragments. With respect to the latter situation, evidence of particles breaking up due to intense shear has recently been observed in high-velocity flow tests of the ARTIST programme [1]. This is not an isolated example of this behaviour, e.g., see [2, 3]. Evidently, particle break up may have significant safety implications where it is a question of easily-trapped supra-micron particles fragmenting to produce sub-micron ones for which trapping is less efficient¹¹.

In this report, information on aerosol characteristics from prototypical experiments (i.e., those producing aerosols from over-heated irradiated fuel) is reviewed in order to identify common features and typical variations. For completeness, both aerosols in the reactor coolant system (RCS), i.e., relevant to an experiment such as ARTIST, and the containment are dealt with though, it must be said, information on these latter particles turns out to be quite limited. Subsequent effort will need to be devoted to detailed consideration of whether interparticle bonding forces within prototypical and non-prototypical agglomerated particles are comparable. This aspect could be resolved relatively simply by calculating Van der Waal's forces between primary particles, e.g., [4], and estimating the bond structure (the so-called internal co-ordination) of the agglomerates from images of prototypical particles and the non-prototypical ones used in experiments. However, given the complex composition of core-melt-produced aerosols (see below), major difficulties arise from the heterogeneity of primary-particle composition and, potentially, chemical reactions at points of contact.

9.2 Review of Available Information

A search for literature providing information on aerosols produced in prototypical, severe-accident conditions shows public-domain information to be rather meagre. Three principal sources have been found for particles relevant to the RCS and only one (PHÉBUS PF) with respect to the containment.

¹⁰ It should be understood that we are dealing here with the general, realistic case of agglomerated, compound particles as opposed to uniform, single-substance ones.

¹¹ Another implication that arises concerns experiments: given that particle composition and structure can have safety implications, an experiment not using prototypical particles and involving high impact velocities and/or intense shear may not produce aerosol behaviour representative of what would happen in an accident. This report can also serve as an initial step in the process of assessing the use of non-prototypical particles in nominally representative experiments performed in severe-accident conditions.

9.2.1 *Aerosols in the RCS*

The information reviewed excludes experiments with significant non-prototypical features, these being typically a flawed source (e.g., low temperature, incomplete or uncertain inventory) and injection of only inert gas. The following experiments constitute the best information available where the focus here is not on particles close to their point of formation (for which, in any case, there is virtually no information) but more in relation to hot leg conditions, i.e., after some amount of conditioning (cooling, further condensation of vapors, agglomeration) where particle evolution is less rapid.

9.2.1.1 *AECL*

Mulpuru [5] performed small-scale experiments on Zircaloy-clad CANDU fuel samples heating them to and holding them at 1860 K in a flowing steam-rich atmosphere at ambient pressure. CANDU fuel has a typical end-of-life burn-up $\leq 8 \text{ GWd/tU}$. Apart from the cladding, no structural materials relevant to LWRs were present in the furnace. Thermal-hydraulic boundary conditions are not well-known between the specimen and the exit of the furnace tube where temperature (of the gas, presumably) dropped to 380 K and, schematically, is indicated to have remained at this level up to and including the aerosol sampling zone. In this zone aerosols were collected during four distinct phases: during heat up then during three one-hour periods at the hold temperature of 1860 K. The four sequential systems comprised thin platinum wires for individual SEM¹² (size) and WDX¹³ (elemental composition) analysis with the outflow from these proceeding downstream to a common filter.

The experimenters conclude that spherical particles of around 0.1 to 0.3 μm formed (though their composition was not established) then these agglomerated giving rise to a mixture of compact particles between 0.1 and 3.0 μm in size at the point of measurement. The composition of the particles was found to be dominated by Cs, Sn and U: while the Cs and Sn mass contributions remained constant and very similar in mass, U was relatively minor in the first hour at 1860 K evolving to be the main contributor in the third (very approximately: 42 % U, 26 % Sn, 33 % Cs). Neither break down of composition by particle size nor statistical size information was measured.

9.2.1.2 *PBF-SFD*

Information is available from analyses of aerosols produced during the most prototypical test of the large-scale PBF programme, test SFD 1-4, [6, 7]. The test comprised a bundle of 28 Zircaloy-clad fuel rods (of which 26 with an average burn-up of 36 GWd/tU) with 4 stainless-steel-clad Ag-In-Cd control rods. The presence of 4 control rods leads, according to the authors own figures, to a higher-than-normal proportion of control-rod alloy, e.g., a ratio of 3.5 higher than was the case for the TMI-2 core. The Zircaloy content was also somewhat high, around 6 kg as opposed to nearly 15 kg of UO_2 . With pressure fixed at 6.9 MPa and the bundle immersed in water, a flow of water at 0.6 g.s^{-1} was injected while bundle nuclear power was increased. Nowhere is it stated that the initial or injected water was borated and it must be presumed that it was not. During a one-hour transient, dry out and extensive degradation occurred with peak temperature thought to have reached nearly 3100 K. Vapors and aerosols were transported along a line initially heated to 800 K descending to $\sim 600 \text{ K}$ in the aerosol sampling zone (no steam condensation).

SEM was used on deposits on a specific deposition structure over a 2 m distance starting about 0.3 m above the bundle. This analysis, concerning only (seemingly) individual particles, gives no statistics on the size distribution and, being post-test, can be misleading given that particles may have agglomerated upon deposition. The SEM analyses showed some very large particles, 25-250 μm , on horizontal surfaces. More

¹² Scanning electron microscopy.

¹³ Wavelength dispersive X-ray.

interestingly, while impactors were not used (and, consequently, no possibility of quantitative information on composition as a function of aerosol size), large variation in deposit composition is seen at the same axial location depending on whether the deposition surface was vertical (in the direction of the flow) or horizontal. In terms of the structural elements and volatile fission products at the 0.6 m elevation, Table 9.2-1 provides the details. It can be inferred that, over the duration of the test in this zone, significant variation in aerosol composition occurred where larger particles (favouring settling and inertial deposition due to changes of geometry) contained a very high cadmium fraction whereas smaller particles were far more heterogeneous in composition. Since thermophoretic deposition is relatively insensitive to size if particles are not very small, and since gas-to-coupon temperature difference is seen to be between 20 and 70 °C at this elevation during the period of release (Figure 38 of [6]), it can be argued that the vertical-surface deposit occurred mainly due to thermophoresis and that its composition can be considered representative of that of the overall suspended aerosol at this location.

Further interesting measurements for purposes here were six isokinetic, sequential, filtered samples located about 13 m from the bundle outlet. These were used to follow the evolution of the aerosol composition and to examine particle size (SEM). Based on these analyses the authors state that particle geometrical-mean diameter varied over the range 0.29-0.56 µm (elimination of the first filter due to it being early with respect to the main transient gives the range 0.32-0.56 µm) while standard deviation fluctuated between 1.6 and 2.06. In the images of filter deposits needle-like forms are seen. Turning to composition, if the first filter sample is eliminated and “below detection limit” is taken as zero, for the structural components and volatile fission products we have in terms of percentages the values given in Table 9.2-1.

Lastly, it should be noted that no data are provided on uranium release; though a very low release in fractional terms such a release is potentially very significant in terms of absolute mass. It might be concluded that the release was below detection limits since the range of analysis techniques applied-which included alpha analysis - ought to have measured any significant U in deposits (though the authors do not state this explicitly). Furthermore, the test conditions at high temperature comprising the low water-injection rate and the metal-rich bundle led to full reduction of the steam during most of the transient as measured downstream of the bundle (§5.2.1 of [6]). This total starvation, probably occurring from the hottest point in the bundle upwards, would have been unfavourable to uranium release from the bundle.

Table 9.2-1 Aerosol composition (%) in terms of the measured elements (NB: data for In are not shown due to being below detection limits¹⁴)

location	position/time	Ag	Cd	Sn	Zr	volatile FPs
0.6 m	vertical surface	0.2	8.3	44.2	13.3	34.0
	horizontal surface	0.5	75.1	0.3	0.2	24.0
13 m	2040 s (filter 2)	1.9	6.2	75.9	3.9	12.0
	2100 s (filter 3)	1.4	27.9	39.5	2.6	28.6
	2385 s (filter 4)	1.6	24.2	36.3	0	37.9
	2850 s (filter 5)	1.2	13.3	39.9	0	45.6
	3060 s (filter 6)	3.9	12.5	29.7	2.4	51.5

¹⁴ Compilation of this table relies on Table VI of [5] which provides the volatile-FP content. Data in that table have been taken as mass percentages since molar percentages would imply even higher contributions of volatile FPs given that the other principal contributions arise from Cd and Sn.

9.2.1.3 PHÉBUS FP

For the PHÉBUS tests a great deal of information is available on aerosols that can either be inferred from deposits or arises from direct measurements. However, at the present time, only two tests are considered “open” (allowing results to be freely discussed): tests FPT0 and FPT1, [8, 9]. Furthermore, though two other tests, FPT2 and FPT3, are of great interest here due to the presence of boron (boric acid in the injected steam for FPT2, boron carbide in the control rod of the bundle for FPT3), the final, self-consistent data have not yet been issued for these tests and partial results would have to be treated with caution. Hence, presentation of results from the FPT1 test will be the focus here. It is worth noting that FPT1 complements the PBF-SFD1-4 test rather well by being at low pressure (<0.3 MPa) and comprising highly oxidizing conditions apart from a very brief phase where molar hydrogen concentration peaked at about 50 %.

For purposes here, FPT1 (and FPT0) can be described as comparable to PBF-SFD 1-4 with a slightly smaller bundle in terms of the number of fuel rods where these were of lower burn-up, viz. 23 GWd/tU (trace irradiated for FPT0). A single steel-clad Ag-In-Cd control rod was placed centrally in the bundle. There were about 3.5 kg of Zircaloy for just over 10 kg of UO_2 : this is a somewhat lower Zrly- UO_2 ratio than in SFD 1-4. Steam was injected at a rate typically around 1.9 g.s^{-1} – whence the oxidizing in conditions with respect to SFD 1-4. The line between the bundle and the first release measurement station was maintained at around 970 K (i.e., higher than in PBF).

For a representative view of the suspended aerosols relevant to the hot leg of a PWR we need to look at deposits or samples not too close to the bundle in a zone where vapors have stabilised at near-equilibrium values. This is characteristic of the upper part of the so-called vertical hot line and downstream of this location. Data on deposits (predominantly thermophoresis) in the vertical hot line do not provide a complete coverage of elements (e.g., data for uranium, known to be a major contributor, appears to be lacking). However, it is clear that the volatile FPs Cs and Te are significant contributors as is Ag. Note that Cd is predominantly in the vapor phase at the hot-line temperature and so is negligible in deposits until lower temperatures are reached. More quantitative data are available from aerosol sampling performed downstream using filters and impactors both in a zone at 700 °C and another at 150 °C. Table 9.2-2 summarises data on aerosol composition where it worth noting that different phases of the bundle transient have been covered, viz. the bundle oxidation runaway, the stabilization period, the second arc oxidation phase, the advanced degradation phase.

Concerning particle size, impactors were used to take samples at both 700 °C and 150 °C. These samples are, of course, punctual and may only be indicative of a particular phase of the transient. The results indicate an aerosol population at 150 °C that is fairly lognormal with an AMMD around $3 \mu\text{m}$ with a standard deviation of about 2. The population at 700 °C is less clearly lognormal and somewhat smaller in mean size. However, these results must be treated with some caution as the impactor plates were heavily overloaded and sampling flow was not steady: the impactors were not always functioning in their range of calibration. Furthermore, in the opinion of the author, this size information is incompatible with the absence of enhanced deposition by impaction in bends indicating particles with a rather smaller mean size. SEM analyses of the impactor plates for FPT0 and FPT1 as well as of filter samples show particles to comprise agglomerates of particles in the size range $0.1\text{--}0.5 \mu\text{m}$ – see Fig. 9.2-1.

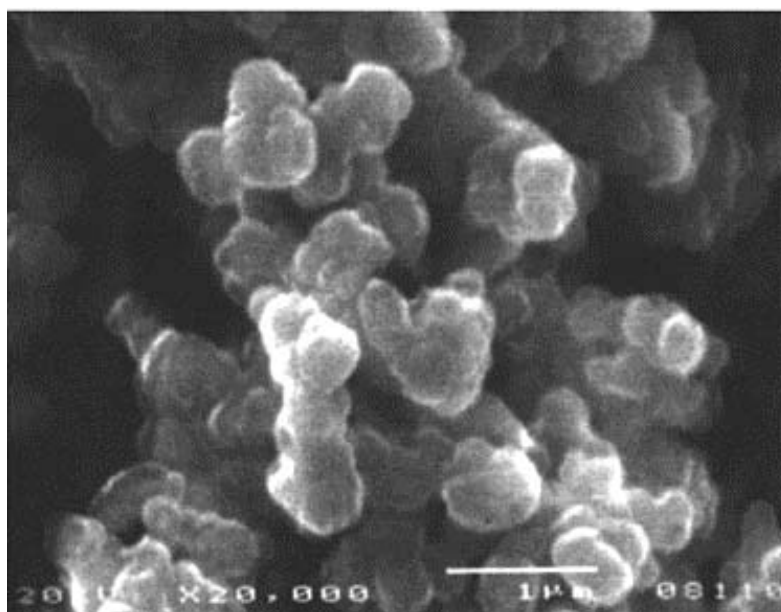


Fig. 9.2-1 SEM images of aerosols from an impactor plate in the circuit of the PHÉBUS FPT0 test showing an agglomerated structure of particles typically in the range 0.1 - 0.5 μm (Fig. 20 of [8])

Finally, there is some information on aerosol structure pertaining to the sample shown in Table 9.2-2, taken at the 700 °C location late in the transient. This concerns an XPS¹⁵ sputtering analysis of the deposit on the filter concerned and so cannot be interpreted as statistically significant. Nevertheless, a depth profile is seen with an indium-rich surface layer (also carbon- and oxygen-rich, both results to be treated with caution since the former is very probably contamination while the latter is probably partly the result of post-test oxidation) from which Cs and Sn are notably absent. Progressing deeper, Cs and Sn appear below the surface while concentrations of uranium (thought to be probably U_3O_8 , i.e., UO_2 oxidised post-test¹⁶) and rhenium increase monotonically. Ag, Cl, O (once below the surface) and Ni (from the Inconel filter) concentrations appear relatively uniform as a function of depth. It is also interesting to note that these results with respect to Cs are corroborated by progressive-dissolution analyses (water, alkali, acid, strong acid). The most striking results of these analyses concern the very limited water-solubility of Cs and Rb in two samples widely separated in time taken at 700 °C. It was found necessary to apply strong acid in order to dissolve the remaining 70 % of these two FPs after only 30 % dissolved in water, alkali and acid washes. Either they migrated chemically into a protective aerosol substrate after condensing on its surface (probably non-uniformly) or they were “encased” by another/other species condensing subsequently. Te and Mo, both elements that may have been chemically associated with Cs and Rb in the vapor phase, are similarly insoluble with respect to the early sample but mostly soluble in weak acid in the late sample. W (released from thermocouples), Sn and Cd display similar behaviour in both samples. Low-temperature samples do not show this behaviour where Cs and Rb both exhibit high solubility in water. A precautionary note must be raised with respect to these results since not only is post-test oxidation of the sample apparent (as already said) but the potential migration behaviour of Cs and Rb may not have occurred on the time scale of their transport to the sampling point but over a much longer period; the relevance of migration to consideration of the nature of aerosols as they reach the break in the primary circuit is debatable.

¹⁵ X-ray photoelectron spectroscopy

¹⁶ Note that evidence of post-test oxidation of samples was also seen in FPT0 where indium in aerosol samples was found in the form In_2O_3 .

Table 9.2-2 FPT1 aerosol composition (%) in terms of the measured elements (NB: data adjusted by subtracting Re, W and any other non-prototypical contributions)¹⁷

location	position/time	Ag	In	Cd	Sn	U	Mo	Cs	others
13 m	700 °C (17034 s)	29	0	0	14	18	16	9	13
25 m	150 °C (11051 s)	32	22	9	18	0	4	9	6
	150 °C (13810 s)	30	8	3	8	6	17	24	3
	150 °C (16473 s)	52	3	0	3	27	5	3	6
	150 °C (17034 s)	46	10	4	6	13	8	6	8

To summarise what can be concluded from the above information, and to some extent paraphrase the experimenters' (executive summary of Jacquemain et al.), condensed material was transported in the hot leg and cold leg as mixed aerosols the bulk of which were dominated by control rod (mainly Ag), structural (mainly Re, Sn) and fuel material (U).

Low-volatility FPs were probably associated with this core of low-volatility materials upon which more volatile compounds (control rod In, Sn from clad, Cs) condensed. For Cs and Rb, diffusion and chemical reaction with the low-volatility substrate probably occurred. Aerosol composition depended on the stage of degradation (i.e., conditioning release) where highest aerosol concentrations occurred during bundle oxidation when Ag, In, Cd and Sn were dominant. This subsequently became Ag, Re, Cs and Mo then Ag, Re and U during the final degradation phase with formation of a molten pool. Impactor data show the composition to be fairly independent of particle size (though, in the opinion of the author, this result must be treated with caution – see above remarks related to aerosol size).

9.2.1.4 Other sources of information

A piece of information from the European 4th Framework project OPSA is worthy of note here. One phase of this project involved realistic tests investigating the consequences of air ingress for an unirradiated 9-rod fuel bundle where aerosol measurements were included, [10]. The absence of fission products limits the value of the results in the present context but one fact is intriguing: the smallest particles measured were uranium-rich, about 0.1-0.5 µm in size and fairly compact (rectangular). This is entirely consistent with expertations for uranium dioxide and size distributions measured in former Japanese tests.

Finally, it is noted that there is a significant amount of information on fuel particles produced during the Chernobyl accident. This source of data can be discounted in the present context since the aerosols differ significantly from those produced by a LOCA. The vast majority of such aerosols represent whole-fuel micro-fragments produced by the initial shattering of the fuel resulting from the explosion; subsequent emissions produced aerosols via the evaporation-condensation-agglomeration route characteristic of

¹⁷ Compilation of this table used Figure 5.2-79 of [9] which provides results of ICPMS/OES analyses of filter and impactor samples. SEM/EDX analyses are also available for three of the five samples showing significant differences, e.g., greater Cd content, different (either higher or lower) Sn content and some Zr in the sample at 700°C.

LOCAs but the conditions (graphite fire, formation and prolonged ageing in highly oxidizing conditions, high dilution in the gas phase) mean that these cannot be considered relevant here.

9.2.2 *Aerosols in the containment*

The identification of typical features for aerosols in the containment is more problematic than for aerosols in the RCS. Not only does a wide diversity of accident sequences exist with varying pre-conditioning of the source in the RCS before release to the containment, but also information for (more or less) prototypical particles is dependent on just one experimental programme, i.e., PHÉBUS PF. In addition, the timescale of evolution of aerosols in the containment - about one day - leaves room for transformations due to radiolysis, oxidation, formation of (bi) carbonates, etc. to occur; this area is virtually unstudied beyond some of the consequences for iodine species.

Further complications arise in the containment from the (potential) occurrence of major secondary sources of aerosol material, i.e., other than the direct source generated by a degrading core. These are, in particular, pressurised ejection of molten corium (high-pressure sequences), hydrogen deflagrations and molten-core-concrete interaction (MCCI). Only the latter of these, MCCI, will be covered here since information on aerosols from this source is relatively adequate.

9.2.2.1 *PHÉBUS FP*

Information from the PHÉBUS FP programme is derived mainly from the following two references on the two open tests of this programme: FPT0 [8] and FPT1 [9]. We recall that FPT1 is the more representative of the two tests since FPT0 used only trace-irradiated fuel.

Firstly, with respect to aerosol composition, it must be noted that the relative humidity in these tests was never more than about 60 % in FPT0 and 85 % (at the end of the aerosol production phase) in FPT1 so any steam condensation on aerosols would have required a hygroscopic effect. Given that analyses do not predict formation of strongly hygroscopic substances prior to release into the containment, e.g., [11], a hygroscopic effect is difficult to justify except, possibly, for a short time and to a limited extent in the FPT1 test in relation to the presence of cesium iodide. Hence, with negligible water contribution, aerosol composition was identical to the average composition of aerosols leaving the circuit (c.f. Table 9.2-2 for FPT1 at the 25 m location), viz., in decreasing order: silver, tin, indium, uranium and cadmium for the structural elements where the tin, indium and uranium contributions are similar. Of the fission products, molybdenum and cesium were significant contributors (data from FPT1, c.f. Table 9.2-2).

The aerosol size distributions were fairly lognormal with an average size (AMMD) in FPT0 of 2.4 μm at the end of the 5-hour bundle-degradation phase growing to 3.5 μm before stabilizing at 3.35 μm ; aerosol size in FPT1 was slightly larger at between 3.5 and 4.0 μm . Geometric-mean diameter (d_{50}) of particles in FPT1 was seen to be between 0.5 and 0.65 μm ; a SEM image of a deposit is shown in Fig. 9.2-2. In both tests the geometric standard deviation of the lognormal distribution was fairly constant at a value of around 2.0. There was clear evidence that aerosol composition varied very little as a function of particle size except for the late settling phase of the FPT1 test: during this period, the smallest particles were found to be cesium-rich. In terms of chemical speciation, X-ray techniques were used on some deposits and there also exist many data on the solubilities of the different elements in numerous deposits giving a clue as to the potential forms of some of the elements. However, post-test oxidation of samples cannot be excluded since storage times were long (months) and the value of speculating on potential speciation on the basis of the available information is debatable. Nevertheless, there is clear evidence that some elements reached higher states of oxidation in the containment when compared to their chemical form in the circuit.

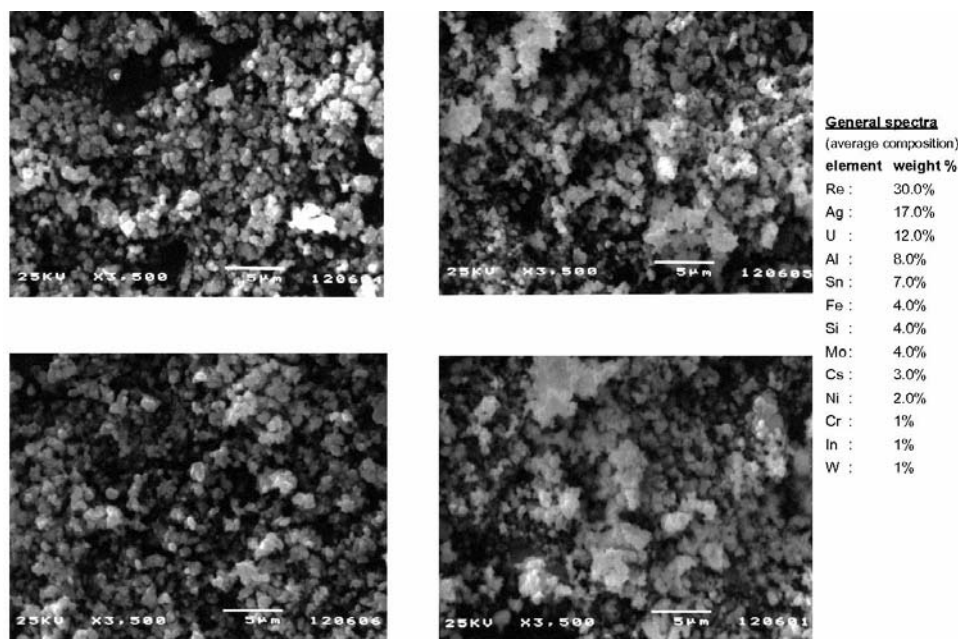


Fig. 9.2-2 SEM images of a filter deposit in the containment of the PHÉBUS FPT1 test showing a fairly uniform structure of typically submicron particles (Fig. A9-8 of [8])

9.2.2.2 MCCI aerosols

The composition of aerosols arising from interaction of molten corium with concrete is different from that of aerosols generated by a degrading core. The seven large-scale experiments of the international Advanced Containment Experiments (ACE) programme on melt behaviour and aerosol release during MCCI addressed four types of concrete (siliceous, limestone/sand, serpentine and limestone) and a range of metal oxidations for both boiling-water and pressurised-water reactor core debris, [12]. The released aerosols contained mainly constituents of the concrete. In the tests with metal and limestone/sand siliceous concrete, silicon compounds comprised 50 % or more of the aerosol mass. Releases of tellurium and neutron-absorber materials - silver, indium and boron (from boron carbide) - were high. Releases of uranium and low-volatility fission-product elements were small in all tests. During ablation of the concrete, aerosol composition remained fairly stable and particles were compact but varied considerable in size the majority being typically micron-sized (geometric diameter) but with some considerably larger sizes.

It is worth noting that experiments at a smaller scale that preceded the ACE programme, [13], indicated smaller aerosols (sub-micron AMMD) and a larger contribution to aerosol composition from uranium mainly in the larger particles. The large-scale SURC tests at Sandia NL also addressed aerosol release (as well as thermal-hydraulic phenomena in the cavity) associated with prototypical core-melt materials in various types of concrete crucible, [14], but for this programme and others few results are readily available. Nonetheless, in summary, it can be said that MCCI is likely to add a large amount of non-active aerosol material to the containment atmosphere in the size range of the existing aerosols thus promoting agglomeration and diversification of the aerosol composition.

9.2.2.3 Other sources of information

As for RCS aerosols, it is worth noting that information from the Chernobyl accident is not relevant here (see §2.1.4).

9.3 Discussion

9.3.1 Uranium contribution

The Mulpuru et al. experiments [5] are interesting in that they show a progression of the uranium content which can only be due to the progressive oxidation of the UO_2 ; however, its dominant contribution at the later times is not confirmed by the PHÉBUS results though, here too, a progressive contribution is observed. While the fractional uranium release is very low its dominance in the total inventory makes this release a major contributor to total aerosol in later stages of the transient unless conditions remain reducing (c.f. the contrast with the PBF-SFD 1-4 results).

9.3.2 Tin contribution

The tin contribution (as oxide from Zircaloy oxidation) to aerosol mass is always present. It is not very significant in PHÉBUS FPT0 (results not shown here) and FPT1 outside the two main oxidation phases in the bundle, i.e., the relatively short (with respect to the total transient) oxidation runaway and the much later and gentler secondary oxidation phase. In the reactor case, this variability would be smoothed out (see 'Variability' below). Tin comprises a very significant contribution in the other experiments, probably too significant in PBF-SFD 1-4 due to the high Zircaloy fraction in the bundle. In summary, tin has a reliable presence whatever the conditions. It must be noted that this observation applies to Zircaloy 4 whereas newer cladding materials and VVER cladding have a lower or zero tin content.

9.3.3 Silver contribution

The silver contribution to aerosol mass in PHÉBUS FPT0 (results not shown here) and FPT1 is much higher than in PBF-SFD 1-4 despite there being proportionally less silver in the PHÉBUS bundle. It might be thought that this can be accounted for by purely an over-pressure effect in PHÉBUS where the lower system pressure led to mechanical formation of droplets when the control rod burst. However, Ag is found in all samples spread over time so clearly it is evaporating as degradation progresses. Perhaps it is important that the control rod in PHÉBUS was centrally placed and experienced the highest bundle temperatures. Or that the transient in PBF was more than twice as fast as that of FPT1 and more rapid relocation of the molten Ag-In alloy occurred (Cd being rapidly released). In the end it may not matter much in the RCS because it seems that either Cd and/or Ag contributes in a major way and both exist predominantly in the metallic phase in the aerosols; in the containment it is a different matter since silver and not cadmium has a major impact on the behaviour of iodine, [8].

9.3.4 Cadmium contribution

Cadmium is seen to be a very significant fraction of the PBF-SFD 1-4 aerosols whereas in PHÉBUS its contribution is minor, sometimes negligible. A major influence in this difference is, of course, the different temperature of the line between the bundle and the measurement point. Up to the first measurement station in PHÉBUS, Point C, temperatures have not dropped below about 1000 K and the cadmium is very largely in the vapor phase as Cd(g) . In PBF-SFD 1-4 the temperature of the equivalent line descends very quickly to 800 K then to around 600 K and the cadmium in this case condenses contributing to the aerosol population.

9.3.5 Indium contribution

It is seen in PHÉBUS FPT0 (results not shown) and FPT1 that indium contributes significantly to the overall aerosol composition whereas in PBF-SFD 1-4 its contribution is not mentioned. This contrast is consistent with thermodynamic calculations indicating that PHÉBUS FPT0 and FPT1 conditions (predominantly near-pure steam for most of the transient) are close to optimal for the volatilization of

indium via the formation of $\text{In}_2\text{O}(\text{g})$ and $\text{InOH}(\text{g})$, [15]. In reducing conditions, such as those of PBF-SFD 1-4, the dominant evaporating species is the much less volatile metal, $\text{In}(\text{g})$.

9.3.6 *Fission product contribution*

Total aerosol mass is seen in the tests reviewed to be typically between 10 and 40 % FPs (though, in the LWR context here, it must be recalled that the AECL tests give too much weight to FPs by not including structural components other than cladding).

9.3.7 *Size, shape and structure*

There is some evidence that particles are compact, i.e., somewhat spherical, unlike the branched structures that one finds for soot, for example. As for size, it is difficult on the basis of the information reviewed to conclude on a typical size; perhaps a near-lognormal distribution with an AMMD not exceeding $1\text{ }\mu\text{m}$ and a standard deviation of around 2 would seem reasonable in the hot leg. The aerosols comprise agglomerates of particles typically in the range $0.1\text{--}0.5\text{ }\mu\text{m}$. This particle size is much too large to represent true primary particles since these are typically $\leq 10\text{ nm}$. It is likely these particles represent clusters of primary particles upon which different vapors may have condensed. It is worth noting that these clusters are themselves probably very resistant to break-up and, hence, constitute the smallest possible size of aerosol fragments post-break-up. Such a phenomenon has been observed for titanium dioxide particles where agglomerates of $0.1\text{ }\mu\text{m}$ -sized clusters of 3 nm -sized primary particles could be broken apart by impact at high velocity onto a surface but the clusters themselves proved resistant to break-up at impact speeds up to 120 m.s^{-1} , [15]¹⁸, see Fig. 9.3-1.

It is worth noting that the information available for containment aerosols does not take into account potential effects from hot-leg sequences. As has been seen in the PHÉBUS FP tests, many fission-products species have significant fractions in the vapor-phase at temperatures above 900 K . This means that, for a hot-leg sequence, such vapors would be released into the containment and either nucleate creating a population of small particles rich in FPs and/or condense onto existing aerosols (conforming to the assumptions of current analyses). Small particles are also expected due to the radiolytic conversion of gaseous I_2 into IO_x aerosol. But it is known from probabilistic risk assessments that small breaks are more likely and in such cases nucleation takes place in the reactor coolant system. As has been noted in the past, [16], the former situation creates a bimodal source to the containment where, according to models, agglomeration between the two populations can be weak. It is important to take into account here, therefore, the potential for a small-sized aerosol rich in volatile fission products (notably I and Cs) to exist in the containment and be relatively resistant to agglomeration and deposition - its importance with respect to accident management is also clear.

¹⁸ This interesting piece of work measured break-up of primary-particle agglomerates as a function of impact velocity and attempted to discover a relationship with the primary-particle bonding force (with qualitative success). The technique developed is ideal for the problem of particle representativity in high-flow-velocity experiments if only representative particles were available for comparison with those used in such out-of-pile tests: their break-up behaviour upon impact could be used as a measure of representativity.

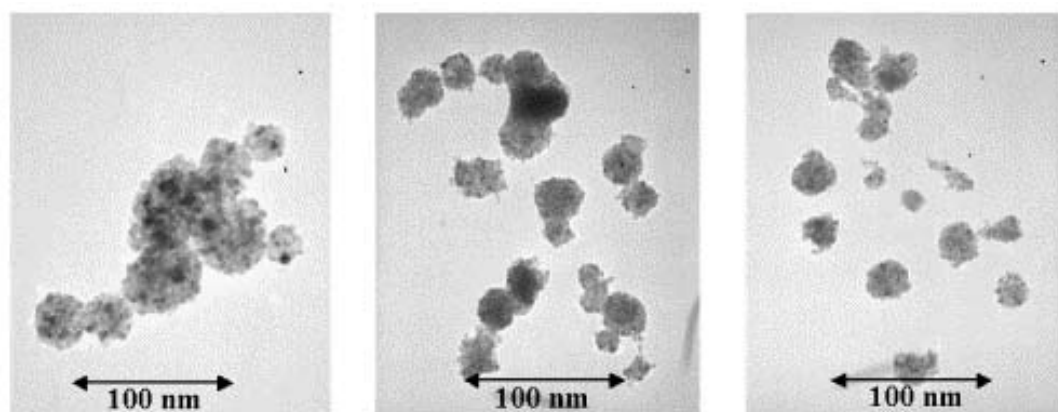


Fig. 9.3-1 TEM images of agglomerates of titanium dioxide nanoparticles: before impact (left); after impact at a velocity of 45 m.s⁻¹ (centre) and 71 m.s⁻¹ (right). The primary clusters resist fragmentation (Fig. 3(c) of [15])

9.3.8 Variability

Variability of aerosols as a function of time is to a large extent dependent on scale being very evident in the smallest-scale tests ([5]) where conditions are virtually homogeneous for the whole fuel sample. The more heterogeneous conditions (extent of oxidation, fuel burn-up, temperature field, etc.) inherent at core scale would lead to significant smoothing of the different releases as seen in the primary circuit, and, hence, give rise to a more uniform particle composition over the majority of the release-from-core phase. What would have more impact is the accident scenario, i.e., a high-pressure sequence relative to a low-pressure one may well lead to more variation in the aerosol composition than is seen over the duration of a single, given sequence. It should be taken into account that current emergency action guidelines intend to transfer high pressure cases into low pressure ones. This may be particularly true of control-rod and uranium contributions to overall aerosol mass where both of these may be expected to decrease at high pressure: no bursting behaviour and lower Cd volatility for the former and greater dissolution by Zrly and less oxidation and volatilization for the latter.

A final consideration is that of the multi-component nature of the aerosols: how uniform a composition do they have? Does composition vary not only with size, but for a given size are there particles of significantly different composition? Concerning composition as a function of size, results from VERCORS tests without control-rod materials provide information on aerosols that have formed close to their point of release: a bimodal population is observed with smaller, sub-micron particles rich in volatile FPs and larger micron-sized particles rich in less volatile FPs such as Ba, [18]. However, the possibility of agglomeration was perhaps limited in these tests. PHÉBUS FP implies a significantly homogeneous composition in the primary circuit and, more especially, in the containment. This is an aspect that probably merits further investigation with respect to primary circuit aerosols and containment aerosols in the event of a hot let break (see the discussion of the potential bimodal distribution in §3.8).

9.3.9 Other considerations

There is a potentially significant contribution to the aerosol during an accident arising from the presence of large quantities of boron. This has not been covered in the experiments reviewed above but useful data will be forthcoming from the PHÉBUS FPT2 and FPT3 tests. Boron is present as boron carbide in BWRs, French 1300 and 1450 MWe PWRs and VVER 1000 s; the quantities involved are significant, around 330 kg of B₄C in the French PWRs, [19], and around 270 kg in a VVER 1000, [20]. In a BWR, this amount may exceed one tonne, [21]. As for the borated coolant, it has been estimated that, at the time core uncover starts, typically about 46 kg of boron (as boric acid) will be present in the water, [21]. While

these quantities are significantly less than the approximately 3 tonnes of Ag-In-Cd alloy in a typical PWR, the boron as boric acid (as added to the coolant or as a reaction product of steam and boron carbide) is very volatile: boron cannot be neglected as a potentially significant contributor to aerosol mass. It is also noted that borated species such as CsBO_2 have a hygroscopic potential comparable to that of CsI .

9.4 Conclusion

Literature on aerosols produced from overheated uranium fuel has been reviewed and discussed.

The typical aerosol composition for PWRs is seen to be a mixture of metals (Ag and/or Cd, 15-40 %) with a similar metal-oxide content (tin oxide and, potentially, uranium dioxide and zirconium dioxide) and FPs covering a diversity of compounds (from metal to oxides to salts (e.g., RbI) to ternary compounds). It would appear that a particle composed of one third metal, one third metal oxide and one third a mixture of mainly FP species (salts, ternaries, oxides, hydroxides) would not be out of place in any of the potential LWR accident sequences. Secondary sources of aerosol material in the containment can add significant masses of aerosol to those of the primary source where, in the case of MCCI, significant diversification of composition occurs due to agglomeration with the largely concrete-derived contribution. It must be noted that it has not been possible to take account of boron (from boron carbide in BWR control blades and some French PWRs and VVER 1000 control rods or boric acid in the coolant) in this assessment.

Relative compact particles without branching chain-like structures are observed in PHÉBUS, especially in the circuit. If steam condensation on particles occurs (in the cold-leg in a cold leg sequence, or in the containment) then, due to the surface tension effect, compaction will occur to the limit of the particle becoming a spherical droplet.

On size and structure, information is less reliable but it would seem realistic for aerosols in the hot leg to comprise a near-lognormal population of particles with AMMD around $1\ \mu\text{m}$ or less and standard deviation around 2. The larger particles would consist for the most part of agglomerates of compact clusters as small as $0.1\ \mu\text{m}$. The evidence from PHÉBUS implies the thesis of an “onion-skin” type of structure where the kernel of the particle is rich in highly refractory materials. Vapors of more volatile species containing cesium and rubidium that have condensed on these refractory kernels may migrate into and interact chemically with the substrate. In the containment, particles are typically larger representing the particles formed in the primary circuit and agglomerates of these. A smaller population of FP-rich particles may form at the breach, i.e., creating a bimodal aerosol population in the containment, in the event of a hot-leg sequence, which have a relatively low probability. The IO_x formed due to the molecular iodine-ozone reaction contribute to the part of fine dispersed aerosols.

References

- [1] S. Güntay, D. Suckow, A. Dehbi, R. Kapulla ARTIST: introduction and first results Nucl. Eng. Des. 231 Issue 1, 109-121, 2004
- [2] O. Brandt, A.M. Rajathurai, P. Roth First observations on break-up of particle agglomerates in shock waves Experiments in Fluids 5 (2), 86-94, 1987
- [3] J.J.F. Strecker, P. Roth Particle breakup in shock waves studied by single particle light scattering Particle and Particle Systems Characterization 11(3), 222-226, 1994
- [4] H.C. Hamacker The London - Van der Waals attraction between spherical particles Physica 4, 1058 - 1072, 1937
- [5] S.R. Mulpuru, M.D. Pellow, D.S. Cox et al. Characteristics of radioactive aerosols generated from a hot nuclear fuel sample J. Aerosol Sci. 23 suppl. 1, S827-S830, 1992

- [6] D.A. Petti, Z.R. Martinson, R.R. Hobbins, C.M. Allison, E.R. Carlson, D.L. Hagrman et al. Power Burst Facility (PBF) severe fuel damage test 1-4 test results report NUREG/CR-5163 (EGG-2542), April 1989
- [7] D.A. Petti, R.R. Hobbins, D.L. Hagrman The composition of aerosols generated during a severe reactor accident: experimental results from the Power Burst Facility severe fuel damage test 1-4 Nuclear Technology 105, 334-345, 1994
- [8] B. Clément, N. Hanniet-Girault, G. Repetto, D. Jacquemain, A.V. Jones, M.P. Kissane, P. von der Hardt (2003). LWR severe accident simulation : synthesis of the results and interpretation of the first PHÉBUS FP experiment FPT0. Nucl. Eng. Des. 226, 5-82, 2003
- [9] D. Jacquemain, S. Bourdon, A. De Bremaecker, M. Barrachin FPT1 final report - IRSN report IPSN PH-PF IP/00/479, Dec. 2000
- [10] Pintér Csordás, L. Matus et al. Investigation of aerosols released at high temperature from nuclear reactor core models J. Nucl. Mat. 282, 205-215, 2000
- [11] M.P. Kissane, I. Drosik Interpretation of fission-product behaviour in the PHÉBUS FPT0 and FPT1 tests Nucl. Eng. Des. 236 (11), 1210-1223, 2006
- [12] J.K. Fink, D.H. Thompson, B.W. Spencer, B.R. Sehgal Aerosol and melt chemistry in the ACE molten core-concrete interaction experiments. High Temperature and Materials Science 33(1), 51-76, 1995
- [13] B.W. Spencer, D.H. Thompson, J.K. Fink, W.H. Gunther, B.R. Sehgal Results of fission product release from intermediate-scale MCCI tests Proc. Int' Conf. on Thermal Reactor Safety, Avignon, France, 2-7 Oct. 1988.
- [14] S.B. Burson, D. Bradley, J. Brockmann, E. Copus, D. Powers, G. Greene, C. Alexander United States Nuclear Regulatory Commission Research Program on molten core debris interactions in the reactor cavity Nucl. Eng. Des. 115(2-3), 305-313
- [15] P. Taylor Calculations on the volatility of control-rod elements in various atmospheres at 1200 to 2500 K IPSN Note Technique SEMAR 98/160, 1998
- [16] S. Froeschke, S. Kohler, A.P. Weber, G. Kasper Impact fragmentation of nanoparticle agglomerates J. Aerosol Sci. 34 Issue 3, 275-287, 2003
- [17] CSNI, report by a group of experts Physical and chemical characteristics of aerosols in the containment. OECD/NEA/CSNI/R(93)7, 1993
- [18] J.P. Leveque, D. Boulaud Fission product aerosols in the programmes HEVA and VERCORS J. Aerosol Sci. 25 Suppl. 1, 87-88, 1994
- [19] B. Adroguer et al. COLOSS Final Extended Report: Part 2; Synthesis on plant calculations SAM-COLOSS-P080, IRSN/DRS/SEMAR 03/30, June 2003
- [20] L. Belovsky Heat release from B4C oxidation in steam and air Proceedings IAEA-TCM, Dimitrovgrad, Russia, October 1995
- [21] M.P. Kissane, B.R. Bowsher, Y. Drossinos, D.A. Powers Final report of the PHÉBUS-FP boric acid task force IPSN Note Technique SEMAR 94/1007, 1994

10. APPENDIX 2: Aerosol Shape Factors

10.1 Fundamentals

The equations of aerosol physics are derived traditionally in terms of spherical, fully dense particles. Real aerosol particles are seldom either fully dense or spherical. The equations of aerosol physics are most directly applicable to liquid droplets. Some types of aerosol generated in reactor accidents can be, indeed, liquid droplets (see discussion of Direct Containment Heating, chapter 3.8). Usually vapors produced in reactor accidents condense to form solid particles. This is because of the supersaturation needed to drive particle nucleation (even particle nucleation on another aerosol particle) and the speed with which vapor pass through sharp thermal gradients around degrading core materials. The nucleated particles following some growth as a result of vapor condensation form what are called “primary particles” and these primary particles do agglomerate quickly but seldom is the initial agglomeration to form a compact structure. Today, it widely thought that primary particles agglomerate to form fractal structure where the number of primary particles, N_{pr} , is related to the diameter of the conglomerate by:

$$N_{pr} = k \left(\frac{D}{d_{primary}} \right)^f$$

where:

- k = first order lacunarity constant 1
- f = fractal dimension
- D = some measure of the effective particle diameter
- $D_{primary}$ = primary particle diameter

Of course, for a close packed structure, the value of “ f ” would be very close to 3. For aerosol particles, it is not uncommon to find values of the fractal dimension between 1.4 and 2.5. Consequently, the particles are far from fully dense.

Experiments by [1] at the Oak Ridge National Laboratory showed that many aerosols pertinent to the issues of reactor safety (but not all) developed approximately spherical envelopes in environments of very high humidity. Some example results of tests by Adams are shown in Fig. 10.1-1 for U_3O_8 aerosols. It is thought that surface forces produced when water vapor condensed in the concave interstices of particle agglomerates (reverse Kelvin effect) drew elements of these agglomerates into approximately spherical forms to minimise energy. These ‘spheroidized’ were still far from fully dense.

The spheroidization of particles at high humidity is an issue that affects aerosols in the reactor containment. It is not evident that such effects will be important for aerosols in the reactor coolant system. It is, then, likely that aerosols in the reactor coolant system could exhibit very substantial deviations from the conditions assumed in the derivation of aerosol equation of fully dense spheres.

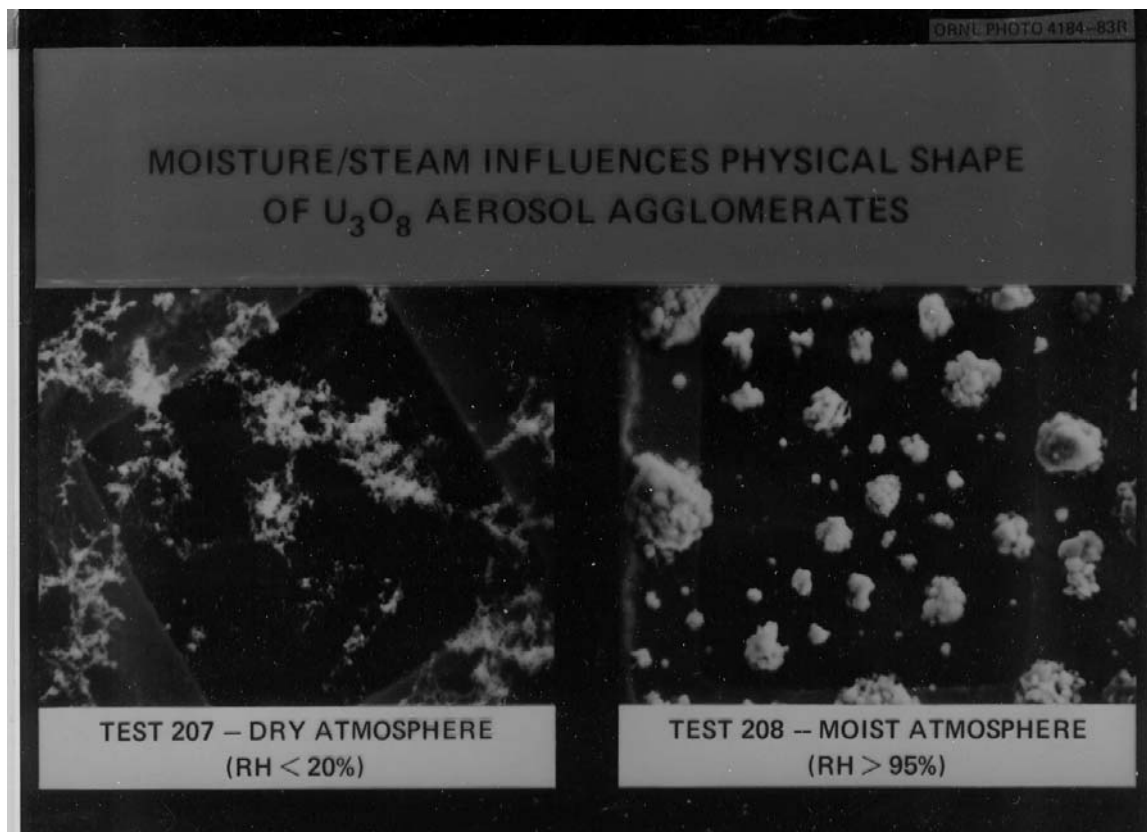


Fig. 10.1-1 Example of test results obtained by Adams et al. showing spheroidization of uranium oxide aerosols at high relative humidity

10.2 Dynamic and Collision Shape Factors

To correct the aerosol physics equations for the properties of real aerosols, shape factors are introduced. Commonly, a shape factor to account for the real drag on aerosol particles, the dynamic shape factor, and a shape factor to account for the collision cross section of real particles are introduced. These shape factors are usually referenced to the volume-equivalent spherical particle that would have the diameter D_v . In terms of the number of primary particles that make up an agglomerate, the volume-equivalent spherical particle has a diameter given by:

$$D_v = N_{pr}^{1/3} d_{pr}$$

where d_{pr} is the diameter of a primary particle that is considered fully dense and spherical. The dynamic and collision shape factors are defined, then, by:

$$\chi = \frac{\rho D_v^2}{\rho_o D_{ac}^2} \frac{C(D_v)}{C(D_{ac})}$$

$$\gamma = \frac{D_c}{D_v}$$

where:

ρ = density of material making up aerosol

$\rho_o = 1 \text{ g/cm}^3$

D_{ae} = aerodynamic equivalent spherical diameter

D_c = collision equivalent spherical diameter

D_v = volume equivalent spherical diameter

$C(D_x)$ = slip correction factor for a sphere of diameter D_x for $x = ae, c, v$

[2] has reviewed information available on dynamic and collision shape factors in reactor containment atmospheres. He concludes that in humid environments where spheroidization occurs, dynamic and collision shape factors are equal and can vary between 1 and about 4. [3] provides a useful account of dynamic shape factors for non-nuclear circumstances. Some efforts were made in the past to “back calculate” effective shape factors from comparison of measurements of aerosol sedimentation and calculations. This, of course, is an ill-advised approach and certainly will not yield results transferable to reactor accidents. [3] proposed a packing fraction model of aerosol shape factors in containments:

$$\chi = \gamma = \alpha^{1/3}$$

$$\alpha = \frac{\varepsilon \rho + (1 - \varepsilon) \rho_\varepsilon}{\rho}$$

$$\varepsilon = \min \left(1, \left(\frac{d_{pr}}{D_v} \right)^{3(3-f)/f} \right)$$

where ρ_ε is the density of gas or liquid that fills the interstices of the particle agglomerate and f is the fractal dimension of the agglomerate. Shape factors calculated with this expression are shown in Fig. 10.2-1 for particles with interstices filled with water, interstices with only 10 % water and with only gas. The expression approximates well known shape factors for dimers of primary particles.

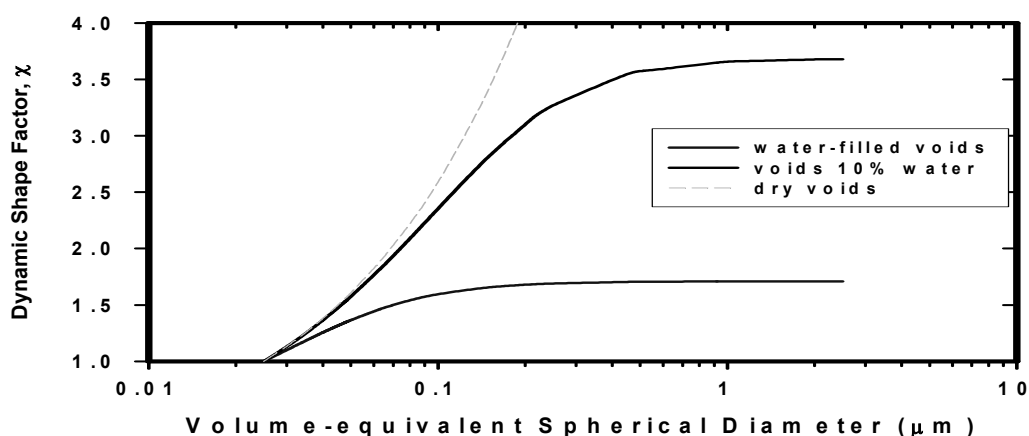


Fig. 10.2-1 Prediction of the dynamic shape factors for spheroidized particles

Shape factors of aerosol particles in the reactor coolant system pose more of a problem. Dynamic shape factors can be measured in principle and, consequently, the understanding of the dynamic shape factor is more advanced. [4, 5] have examined the shape factors of aerosols formed from pertinent materials using high temperature processes. Kops used exploding wires to produce aerosols of iron oxide and uranium oxide. Allen *et al.* used laser evaporation to form aerosols of mixed oxide reactor fuel. Both studies showed that primary particles agglomerated initially to form chains. As the chains grew, they developed branches. Once the agglomerates contained more than 2000 to 20,000 primary particles, they folded into irregular masses. Sketches of aerosol particles near the transition and having the same aerodynamic diameter are shown in Fig. 10.2-2.

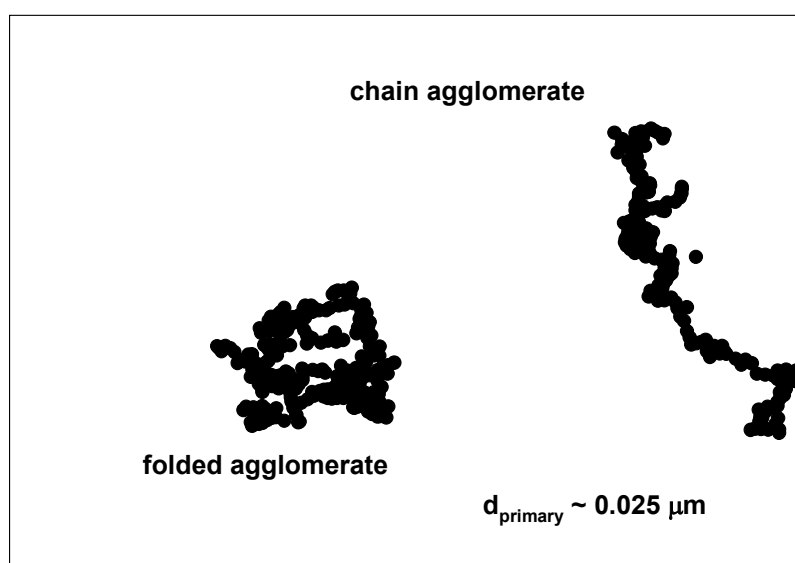


Fig. 10.2-2 Sketches of branched chain and folded agglomerates

The investigators observed that the aerodynamic-equivalent diameters of the branched chain agglomerates varied with the number of primary particles present to the 1/6th power:

$$D_{ae} = k_1 N_{pr}^{1/6} d_{pr} \sqrt{\frac{\rho}{\rho_o}}$$

The dynamic shape factor for the branched chains is then given by:

$$\chi = \frac{N_{pr}^{1/3}}{k_1^2} \frac{C(N_{pr}^{1/3} d_{pr})}{C(D_{ae})}$$

That is, the shape factor grows reasonably rapidly with particle size. Indeed, Kops et al. mention dynamic shape factors as large as 35.

On the other hand, the folded agglomerates had aerodynamic diameters that varied with the 1/3rd power of the number of primary particles present:

$$D_{ac} = k_2 N_{pr}^{1/3} d_{pr} \sqrt{\frac{\rho}{\rho_o}}$$

The aerosol material density was assumed to be 5 g/cm³ and the fractal dimension was taken to be 1.78 for these predictions. Primary particle diameter was taken to be 0.025 µm.

Both particles had the same aerodynamic diameter. The structure of the folded agglomerate collapsed on deposition so it appears more densely packed than when it was airborne.

Then, the dynamic shape factor is only very weakly dependent on particle size:

$$\chi = \frac{1}{k_2^2} \frac{C(N_{pr}^{1/3} d_{pr})}{C(D_{ac})}$$

Both Allen *et al.* and Kops *et al.* suggest that shape factors for folded agglomerates (sometimes called ‘dust bunnies’) decrease slowly with increasing size.

Proportionality factors in these expressions for the aerodynamic diameter are very uncertain. The proportionality factor for chain agglomerates can be chosen so that predicted shape factors agree well with the known shape factors of rigid chains of 1 to 6 monomers shown in Table 10.2-1.

Table 10.2-1 Dynamic shape factors for rigid chains of monomers

Number of Monomers	χ	Number of Monomers	χ
1	1.00	5	1.45
2	1.12	6	1.57
3	1.27	7	1.73
4	1.32	8	2.04

The proportionality factor for the aerodynamic diameter of folded agglomerates should depend on the fractal dimensionality of the agglomerates:

$$k_2 = \left(\frac{C(D)}{N_{critical}^{(3-f)/3f} C(D_{ac})} \right)^{1/2}$$

where $N_{critical}$ is the number of primary particles present in an agglomerate when it begins to transform from a branched chain to fold agglomerate (~5000).

Shape factors predicted for primary particles 0.025 µm in diameter and a fractal dimension of 1.78 are shown in Fig. 10.2-3. As expected, smaller particles that are chains have shape factors that are strongly dependent on particle size. Larger particles that are folded agglomerates have shape factors nearly invariant with particle size but dependent on the fractal dimensionality of the agglomerate.

The fractal dimension, f , of agglomerates has been studied both theoretically and experimentally. Under conditions of Brownian diffusion of monomers to a stationary agglomerate, there is reasonable consensus that the fractal dimensionality of the agglomerate is about 1.78 [6]. Fractal dimension decreases when coagulation of agglomerates as well as monomers is considered. Fractal dimensions on the order of 1.4 are found for conditions of Brownian diffusion [7].

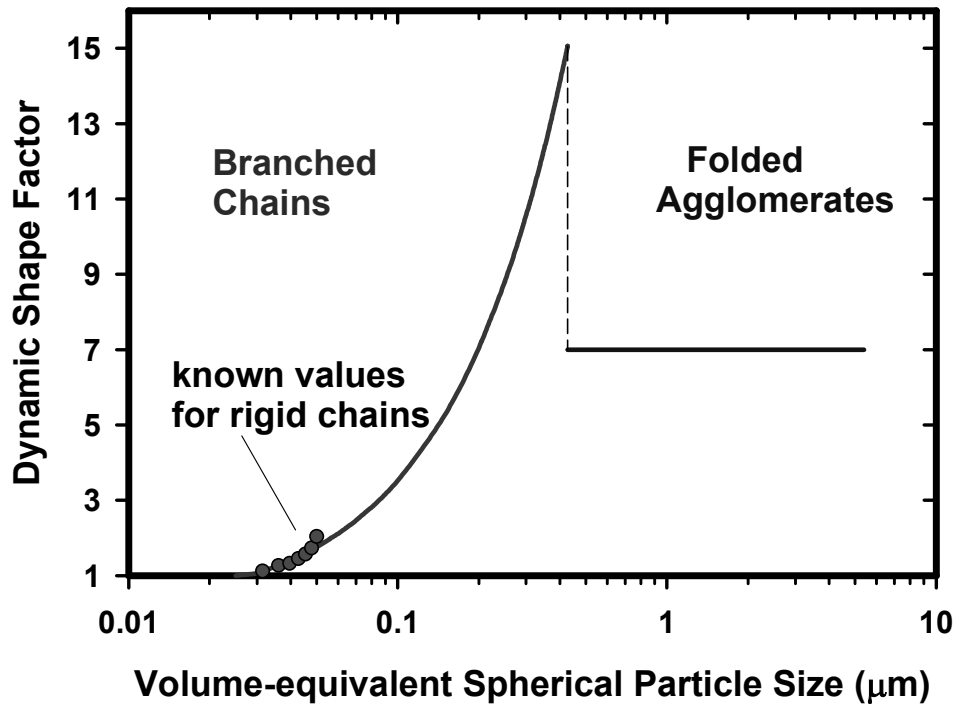


Fig. 10.2-3 Shape factors for branched chains and folded agglomerates
($D_{\text{primary}} = 0.025 \mu\text{m}$; Fractal dimension = 1.78)

Fractal dimensions of agglomerates will be affected by the continued heating under reactor accident conditions. Primary particles are quite reactive since such a large fraction of their constituents are surface species with unsatisfied bonding. [8] have addressed the issue of sintering in aerosol agglomerates and have advanced a model based on the proportionality of the shrinkage rate with surface area. Based on this model, the rate of change of the fractal dimension of a folded agglomerate composed of N_{pr} primary particles is given by:

$$\ln N_{\text{pr}} \frac{d\left(\frac{1}{f}\right)}{dt} = \frac{1}{D} \frac{dD}{dt}$$

The rate of change of the particle diameter might be taken from a model of initial stage sintering such as that of [9]. Such a model is dependent on the grain boundary diffusion coefficients which are not likely to be known for materials of interest in the analysis of reactor accidents:

$$\frac{dD(t)}{dt} = -0.31 D(0) \frac{1}{t^{0.69}} \left[\frac{800 b \gamma a^3 D_{\text{gb}}}{7 \pi k T d_{\text{pr}}^4} \right]^{0.31}$$

where:

b = grain boundary thickness

γ = surface energy

a^3 = vacancy volume

D_{gb} = grain boundary diffusion coefficient

The theory of collision shape factors is less developed than that of dynamic shape factors. Certainly a lower bound estimate of the collision shape factor can be obtained by ignoring the chain branching [10]:

$$\gamma = \frac{1}{\sqrt{2\pi}} \frac{\sqrt{[(1+N_{pr})\pi^2 + 4(3\sqrt{3}-4)(N-1)]}}{N_{pr}^{1/3}}$$

For folded agglomerates, the estimated collision shape factor will again depend on the fractal dimension:

$$\gamma = N_{pr}^{(3-f)/3f}$$

There are few data available to judge the adequacy of these estimates of the collision shape factor.

References

- [1] R. Adams "Behaviour of U_3O_8 , Fe_2O_3 , and Concrete Aerosols in a Condensing Steam Environment" Proc. Int'l. Mtg. On LWR Severe Accident Evaluation, Cambridge, MA, August 28 – September 1, 1983
- [2] J.E. Brockmann "Range of Possible Dynamic and Collision Shape Factors", Appendix F, R.J. Lipinski et al., Uncertainty in Radionuclide Release under Specific LWR Accident Conditions, Volume II TMLB' Analyses SAND84-0410 Vol.2, Sandia National Laboratories, Albuquerque, NM, February 1985
- [3] W. Stoeber "Dynamic Shape factors of Nonspherical Aerosol Particles", Chapter 14, Assessment of Airborne Particles, T.T. Mercer, P.E. Morrow, and W. Stoeber, editors, Charles C. Thomas Publisher, 1972
- [4] D.A. Powers, K.E. Washington, S.B. Burson, J.L. Sprung A Simplified Model of Aerosol Removal by Natural Processes in Reactor Containments NUREG/CR-6189, Sandia National Laboratories, Albuquerque, NM, July 1996
- [5] J. Kops, G.Dibbets, L. Hermans, J.F. Van De Vate J. Aerosol Science, 6 (1975) 329
- [6] M.D. Allen, O.R. Moss J.K. Braint J. Aerosol Science, 10 (1978) 43
- [7] S. Tang, J.M. Preece, C.M. McFarlane, Z. Shang J. Colloid and Interface Science, 221 (2000) 114
- [8] P. Meakin Phys. Rev. A, 29 (1984) 997
- [9] W. Koch, S.K. Friedlander J. Colloid and Interface Science, 140 (1990) 419
- [10] D.L. Johnson, I.B. Cutler J. Amer. Ceramic Soc., 46 (1963) 541
- [11] A.D. Maynard, A.T. Zimmer Aerosol Science and Technology, 37 (2003) 804

11. APPENDIX 3: Spray Modelling Developed from Recent Analytical Work

This Appendix presents a thorough description of the mechanistic approach to modelling of sprays and their effects that has been developed and validated over the last few years for the ASTEC code, [1]. Note that the nomenclature of the equations is provided at the end rather than in the text.

11.1 Relaxation of Droplets

The mass, velocity and temperature evolution of a droplet during its fall is obtained by solving a set of equations for mass, momentum and energy balance (the z axis is oriented downwards):

$$\frac{dm_w}{dz} = \pi d_w Sh_g \bar{D}_s \bar{c}_g M_w B_M / v_w, \quad (1)$$

$$\frac{d}{dz}(m_w v_w) = m_w g / v_w - \frac{\pi d_w^2}{8} C_D \rho_g v_w, \quad (2)$$

$$\frac{d}{dz}(m_w H_w) = \pi d_w \lambda_g Nu_g (T_g - T_w) / v_w + \frac{dm_w}{dz} H_s \quad (3)$$

Equations (1), (2), (3) are solved on a fixed mesh using an implicit numerical scheme. The mesh size follows a geometrical progression, small meshes being necessary within the first two metres below the spray nozzles where transfers are very fast. The solution provides the evolution of the droplet size, velocity and temperature versus height in the containment.

The physical modelling is contained in the Nusselt number, Nu_g , Sherwood number, Sh_g , and drag coefficient, C_D . The Nusselt and Sherwood numbers were deduced by [2] from steady evaporation in dry air of droplets having diameters in the range 600 to 1100 microns who proposed the following correlations:

$$Sh_g = 2 + 0.6 Re_w^{1/2} Sc_g^{1/3}, \quad (4)$$

$$Nu_g = 2 + 0.6 Re_w^{1/2} Pr_g^{1/3} \quad (5)$$

The drag coefficient is obtained from the Oseen formulation [3] for hard spheres:

$$\text{for } Re_w < 3 \quad C_D = 24 / Re_w \quad (\text{Stokes flow}), \quad (6)$$

$$\text{for } 3 < Re_w < 905 \quad C_D = \frac{24}{Re_w} \left(1 + \frac{Re_w^{2/3}}{6} \right) \quad (\text{intermediate flow}), \quad (7)$$

$$\text{for } Re_w > 905 \quad C_D = 0.44 \quad (\text{potential flow}) \quad (8)$$

When using the above correlations, the “one-third” law must be followed, i.e., the relevant physical parameters (steam-air diffusion coefficient, thermal conductivity, average molar concentration, fluid density) are calculated at the following temperature:

$$\bar{T} = \frac{1}{3} T_g + \frac{2}{3} T_w \quad (9)$$

except for the Reynolds number which is calculated at the gas temperature.
(It should be mentioned that alternatives to the correlations based on [2] are available today.)

11.2 Droplet Coalescence

The droplet size distribution produced by the spray nozzle typically used in PWRs is well represented by a log-normal distribution function, [4]:

$$f(r) = \frac{n_0}{\sqrt{2\pi} (\ln \sigma) r} \exp\left(-\frac{\ln^2(r/r_g)}{2 (\ln \sigma)^2}\right) \quad (m^{-4}) \quad (10)$$

The droplet size distribution just below the injection nozzles changes with the height in the containment due to heat, momentum and mass transfer with the surrounding gas, and gravitational coagulation. Neither the complex phenomena linked to the droplet trajectories and collisions at the spray ring outlet nor the interactions with the vertical walls are considered. The uncertainties due to these phenomena are assumed to be contained in the mass-median diameter and standard deviation of the distribution. Nevertheless, the model allows evaluation of the sensitivity to these parameters.

Droplet-droplet interactions are rather important since containments typically have multiple spray heads aimed in a variety of directions to minimise the unsprayed region.

Regarding the modelling of droplet coalescence, it is more convenient to express the droplet distribution function in term of volume since the coalescence allows volume conservation. The distribution function $f(x)$, where x is the volume of the droplets in a given size class, is described on a fixed axial mesh with a geometrical progression. The size nodes are distributed on a constant logarithmic scale. This allows limitation of the number of classes taken into account with accurate description in the small size classes where the peak of the distribution is located.

The variation of the distribution function due to the coalescence is obtained, in each axial mesh, by the resolution of the system of n equations of the following form:

$$\frac{\partial f(x_j, t)}{\partial t} = \frac{1}{2} \int_0^{x_j} \Phi(y, x_j - y, t) f(y, t) f(x_j - y, t) dy - f(x_j, t) \int_0^\infty \Phi(x_j, y, t) f(y, t) dy \quad (11)$$

where n is the number of nodes of the distribution. The physical model is contained in the expression of the droplet collision kernel $\Phi(x_i, x_j, t)$:

$$\Phi(x_i, x_j, t) = \varepsilon \pi (r_i + r_j)^2 (v_j - v_i) \quad (m^3.s^{-1}) \quad (12)$$

where v_j and r_j are respectively the velocity and the radius of a droplet in size class j . The collision efficiency is:

$$\mathcal{E} = r_i^2 / (r_j + r_i)^2 \quad \text{with } r_i > r_j \quad (13)$$

In Equation (11), the first integral describes the rate of appearance of droplets in the class j due to coalescence of smaller droplets and the second integral describes their rate of disappearance from this size class. We assume a linear variation of the distribution function in a given interval between two nodes:

$$\forall x \in [x_j, x_{j+1}], \quad f(x, t) = F_j(t) \frac{x_{j+1} - x}{x_{j+1} - x_j} + F_{j+1}(t) \frac{x - x_j}{x_{j+1} - x_j} \quad (14)$$

where $F_j(t)$ is the value of the distribution function at node j . With this assumption, the distribution function can be expressed from the node values and from an interpolation function $g_j(x)$ as follows:

$$\forall x \in [x_1, x_N], \quad f(x, t) = \sum_{j=1}^N F_j(t) g_j(x) \quad (15)$$

where $g_j(x)$ is a triangular type function.

The discrete formulation of the set of equations (11) is then:

$$\frac{dF_j(t)}{dt} = \frac{1}{2} \sum_{i=1}^N \sum_{k=1}^N F_i(t) F_k(t) J_{ikj}(t) - F_j(t) \sum_{i=1}^N F_i(t) I_{ij}(t) \quad (16)$$

with (overlapping integrals):

$$I_{ij}(t) = \int_0^\infty \Phi(x_j, y, t) g_i(y) dy \quad (\text{m}^6 \cdot \text{s}^{-1}) \quad (17)$$

$$J_{ikj}(t) = \int_0^{x_j} \Phi(y, x_j - y, t) g_i(y) g_k(x_j - y) dy \quad (\text{m}^6 \cdot \text{s}^{-1}) \quad (18)$$

The difficulty in the resolution of this system arises from the calculation of the sink integrals $I_{ij}(t)$ and source integrals $J_{ikj}(t)$. In order to calculate the first kind of overlapping integral, we assume a linear variation of the collision kernel between two nodes. The computation of the source integrals (18) is more difficult and can be avoided in the following way: the most important thing being to ensure conservation of the mass during the coalescence process, which implies a relation between the sources and sink integrals, a mathematical formulation of this relation can be found:

$$J_{ikj}(t) = I_{ik}(t) \Gamma_{ikj} \quad (19)$$

where Γ_{ikj} is a function of the nodes x_i , x_k and x_j of the distribution.

11.3 Coupling of Droplet Relaxation and Coalescence

The main difficulty in describing the downward evolution of the droplet size distribution is to take into account at the same time the droplet relaxation and coalescence. Here, the term “relaxation” designates the heat, mass and momentum transfer with the containment atmosphere until the equilibrium size and temperature, and terminal velocity of an individual droplet are reached. In the containment, and for a saturated atmosphere (when the spray is fully established), we can distinguish three zones: a zone just

below the spray nozzles where droplet relaxation is taking place while their coalescence is weak, a lower zone where droplet coalescence at terminal velocity is dominant (located approximately two meters below spray nozzles), and an intermediate zone where there is no conservation of the number flux of droplets (relaxation) and no conservation of the volume flux of droplets (coalescence). This is no longer valid if the atmosphere is superheated (generally at the start of the spray) or if conditions are not homogeneous. It is then necessary to solve the problem continuously along the total droplet fall height whatever the gas conditions. In our model, the equation of conservation of the population of droplets, as expressed at the node values, is given by an equation of the form:

$$\frac{d}{dz} (F_j(z) v_j(z) \Delta x_j) = \underbrace{\frac{d^C F_j(t)}{dt} \Delta x_j}_{coalescence} + \underbrace{\frac{d^R F_j(t)}{dt} \Delta x_j}_{relaxation} \quad (m^{-3}.s^{-1}) \quad (20)$$

where $F_j(z)$ is the node value of the distribution function at elevation z at node j and $v_j(z)$ is the velocity of the droplet of the class j at elevation z . The rigorous method of resolution would comprise solving simultaneously the relaxation and coalescence of droplets for each mesh. This would need an implicit scheme for both relaxation and coalescence mechanisms and would consume too much CPU time. Moreover, it is well known that numerical stability is better reached by using a moving grid for the size distribution when one wants to compute the relaxation process. A method was proposed, [5], that allows conservation of the droplet number flux in the relaxation zone (zone located just below the spray nozzles), conservation of the mass flux in the coalescence zone (lower part of the containment), and good agreement in the intermediate zone. The method consists of solving firstly the droplet relaxation for each size node without considering the interaction between droplets (no coagulation) from the different classes. The displaced grid obtained in this way at the end of the step is used to compute the coagulation term. Finally, when recovering the new distribution on the fixed grid, a normalisation factor (always very close to one, even in the intermediate zone) is applied to ensure volume flux conservation in the coagulation term. Frontiers between vertically-connected volumes are part of the meshing. This allows droplets moving from one volume to another to be treated, the numerical scheme being stable enough to advance the solution with slightly changing atmosphere conditions.

The evolution of the droplet distribution function as a function of fall height in a saturated atmosphere (log-normal distribution at injection with 500 μm mass-median diameter and 1.5 standard deviation) is shown in Fig. 11.3-1. We note an increase of the concentration of droplets at 5 m, where terminal velocity is reached, and later on a decrease of the concentration due to coalescence.

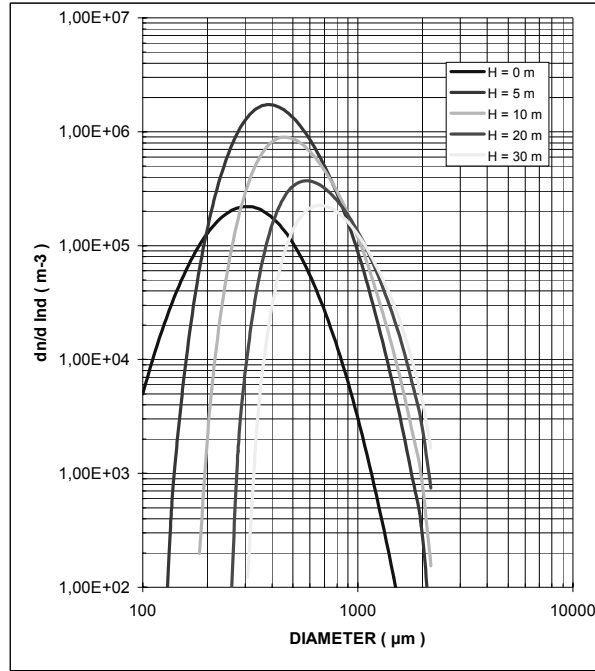


Fig. 11.3-1 Evolution of the droplet distribution function versus height in the containment in a saturated atmosphere under the influence of droplet relaxation and coalescence

11.4 Evolution of the Atmosphere Conditions

In the context of a multi-compartment description of the containment as used in ASTEC, the atmosphere composition and temperature are assumed to be homogeneous inside each compartment. The time evolution of the thermal-hydraulic conditions in a compartment (pressure, temperature and relative humidity) due to the spray is obtained from a mass and energy balance. This balance corresponds to the mass and enthalpy removed by spray droplets during their fall inside the considered compartment. They are determined from the evolution of the droplet distribution function between the top and the bottom of the compartment as follows:

$$\frac{dU}{dt} = - \frac{1}{\Delta Z} \Delta \left(\int f(r) m_w(r) H_w(r) v_w(r) dr \right), \quad (21)$$

$$\frac{d\rho_s}{dt} = - \frac{1}{\Delta Z} \Delta \left(\int f(r) m_w(r) v_w(r) dr \right), \quad (22)$$

$$\frac{d\rho_a}{dt} = 0, \quad (23)$$

and the set of equations of state:

$$U = \rho_s H_s(P_s, T_g) + \rho_a H_a(P_a, T_g) - P_{tot}, \quad (24)$$

$$\rho_s = \rho_s(P_s, T_g) \quad (25)$$

Equations (21) and (22) express the variation of the energy and steam density depending on the differences between the outgoing and entering enthalpy and mass fluxes, where $f(r)$ is the size distribution function of the spray, respectively at the bottom and top of the compartment. The solution of the set of equations (1), (2), (3), (20), (21), (22) and (23) coupled with the equations (24) and (25) for each size node provides the evolution of P_s , P_g , T_g versus time. Although the atmosphere conditions are assumed to be stationary during droplet fall, the transfer rates are quite sensitive to them and an implicit scheme is necessary in order to avoid numerical instabilities.

Resulting mass and energy sink rates are returned to other ASTEC models handling the overall mass and energy balances including transfers between compartments and transfers to the walls and sumps. Note that the gas transfer between compartments depends on pressure/temperature differences and does not take into account the force exerted by the spray droplets: this is a limitation linked to the multi-compartment description.

11.5 Aerosol Removal Modelling

By definition, the collection efficiency of aerosol particles by a droplet is equal to the number of particles captured by this droplet divided by the number of particles present in the volume swept during its fall. It results from several mechanisms which are mainly related to the flow motion around the droplet, to the steam mass transfer (evaporation or condensation) and to the particle concentration gradient near the droplet surface (diffusion). The collection efficiency has then the following general expression:

$$\varepsilon(i, \Phi, d_p, v(z, \Phi)) \quad (26)$$

in which i refers to the considered compartment (atmosphere conditions and composition), Φ is the droplet diameter, d_p is the particle diameter, and $v(z, \Phi)$ is the velocity of a droplet of size Φ at the axial location z .

The mass concentration in a given size class in this compartment changes according to the equation:

$$\frac{d(d C_m)}{d t} = - \frac{S}{V} \left(\int \frac{\pi \Phi^2}{4} \left(\int F(z, \Phi) v(z, \Phi) \varepsilon(i, \Phi, d_p, v(z, \Phi)) dz \right) d\Phi \right) dC_m \quad (27)$$

This equation allows calculation of the removal rate of aerosol particles having a radius between r_p and $r_p + dr_p$. The removal rate is returned to the overall mass balance equation in ASTEC which describes all other aerosol transport mechanisms: agglomeration, sedimentation, deposition on walls, convective transfer between compartments and particle growth due to heterogeneous nucleation.

11.5.1 Inertial capture

Aerosol particles tend to be driven away from a droplet (assumed to have a spherical shape) by the flow around it. However, if their inertia is large enough, they have trajectories which depart from the streamlines and, depending on their upstream position with respect to the flow axis, can drive them to collide with the droplet. This mechanism is called inertial capture. It can significantly enhance collision efficiency.

In order to calculate the collection efficiency, one must solve equations for a velocity field by a numerical simulation, and with the conditions that the particle is launched far upstream at a distance y from the droplet axis and with no velocity relative to the flow. Due to axial symmetry, this problem is two dimensional. Depending on y , a trajectory may result or not in capture. Starting from a low value, y is increased until there is no more capture for $y = y_c$.

The collection efficiency is defined by:

$$\varepsilon_p(\text{Re}, K) = y_c^2 \quad (28)$$

where K is the Stokes number characterizing the non-dimensional stopping distance of the particle and Re is the droplet Reynolds number. The dependency of ε_p in equation (28) is contained in the equations describing the flow field and the particle trajectories. The size of the particles does not appear since, in the numerical simulations, only point particles are considered.

[6] performed numerical simulations of particle trajectories for various particle sizes and droplet Reynolds numbers. They used computations of the flow field previously performed by [7]. Their results were correlated in the following way for values of K greater than the critical Stokes number:

$$y_c = \frac{2}{\pi} \tan^{-1}(H) \quad (29)$$

$$\begin{aligned} \text{with : } H &= B_0 + B_1 Z + B_2 Z^2 + B_3 Z^3, \\ F &= \ln(\text{Re}), G = A_0 + A_1 F + A_2 F^2, K_0 = \exp(G), A_0 = -0.0658, \\ A_1 &= -0.3254, A_2 = 0.0193, Z = \ln(K/K_0), B_0 = 0.1465 \\ B_1 &= 1.302 \quad B_2 = -0.607 \quad B_3 = 0.293 \end{aligned}$$

y_c goes to zero at the critical value of K : $K_{\text{cr}} \sim 0.9 K_0$. The values of the coefficients A_0, A_1, A_2 have been modified with respect to those in the paper by Beard and Grover in order to have a better fit with the numerical simulation results for low values of y_c , rather than for high values. This choice was made for two reasons: firstly, in the CARAIDAS experiments, the sizes of the droplets and aerosol particles are such that y_c is in most cases much less than 1, and rather close to 0.1. The second reason is linked to reactor accident simulations: at the beginning of spray activation, approximately during the first ten minutes, the largest particles, having a collision efficiency close to 1, are removed. The decay rate of the aerosol concentration is then depending on the collision efficiency of the remaining smaller particles.

11.5.2 Interception

The size of the aerosol particles (interception effect) cannot be taken into account in the numerical simulations of the inertial deposition mechanism. Owing to the fact that this effect appears to be non-negligible only for low values of y_c , many authors, [8, 9, 10], have i.e., for particles which follow the streamlines. It can then be shown that the collection efficiency is linked to variation of the stream function near the sphere surface. The non-dimensional particle size a (ratio of the particle diameter to the droplet diameter) is usually quite small, typically less than 10^{-2} , so that there is a large difference between values for potential and viscous flows. Consequently, an interpolation for any Reynolds number from viscous flow to potential flow using these two formulas does not make sense.

A new model has been developed with the aim at taking into account the case of particles having a small but non-zero inertia and a finite size. This model comprises providing an approximate analytical solution of the velocity-field equations for small values of K . The analytical solution allows inclusion of the interception effect (boundary condition on the sphere). Owing to the small values of y_c for such particles, approximate expressions of the streamline equations and flow velocity field close to the sphere were used: it was assumed that the particles depart from the streamlines only in the vicinity of the sphere surface. The following expression is then obtained:

$$\varepsilon_i = \frac{4}{3} f'(1) a + \frac{4 \alpha K}{\sqrt{3}}, \quad (30)$$

where

$$\alpha = \frac{1}{20} \left(1 - \frac{2}{3} f'(1) + 4 f'(1)^2 \right) \text{ and}$$

$$2f'(1) = \text{Re}^{0.434} - 0.7856 \text{Re}^{0.307} - \frac{3}{2} \text{Re}^{0.4} + 1.2855 \text{Re}^{0.312}$$

One should recall that this expression is valid only for small values of K and y_c . For values of K larger than the critical Stokes number and y_c larger than 0.2, the Beard and Grover formulation (Equation 29) can be used with confidence. In order to have continuity between these two formulations, a simple transition is used:

$$\varepsilon_m = 1 - (1 - \varepsilon_i)(1 - \varepsilon_p) \quad \varepsilon_i : (\text{formula 30}), \quad \varepsilon_p : \text{Beard \& Grover} \quad (31)$$

11.5.3 Brownian diffusion

This collection mechanism is important with respect to particles that are transported by the flow close to the droplet surface and then can reach it by Brownian motion. A formulation due to [11] is implemented in ASTEC. According to this, the collection efficiency is:

$$\varepsilon_B = \frac{8}{\sqrt{\pi}} \sqrt{\frac{D_B}{U_\infty \Phi}} \quad (32)$$

D_B is the usual Brownian diffusion coefficient given by the Stokes-Einstein formulation.

Han et al. [11] derived the above formulation by solving the diffusion-convection equation with an approximate description of the flow field, assumed to be potential, near the sphere. So, to be rigorous, it is not suitable for low values of the Reynolds number. Anyway, this mechanism is weak, except for very small particles.

11.5.4 Phoretic capture

This mechanism is due to the phoretic motion of particles under the action of a strong temperature gradient between the atmosphere and the droplets (thermophoresis), or to their convective motion due to fast steam condensation, this convective motion being reduced by an inverse phoretic motion occurring at the same time (diffusiophoresis). It may be efficient in the upper part of the containment, where droplets have not reached thermal equilibrium. In terms of a mass transfer coefficient analogous to a velocity, the collection efficiency is expressed as, [5]:

$$\varepsilon_{ph} = \frac{4 V_{ph}}{U_\infty} \quad (33)$$

since V_{ph} is a deposition velocity averaged over the droplet surface, as in the following correlations:

In the case of thermophoresis, this is given by:

$$V_{ph} = -K_{TA} \frac{\eta}{T} \nabla T \quad (34)$$

K_{TA} is a factor depending on the ratio of the atmosphere thermal conductivity to particles thermal conductivity, and on the ratio of the molecular mean free path to the particles radius, derived by [12]. The temperature gradient ∇T between the gas and the droplet is derived by using the heat transfer coefficient.

In the case of steam condensation, this is given by the [13] theory:

$$V_{ph} = \frac{X_s \sqrt{M_s}}{X_s \sqrt{M_s} + (1 - X_s) \sqrt{M_a}} \frac{\dot{m}_s}{\pi \Phi^2 \rho_s} \quad (35)$$

The second term on the right hand side of the equation is the Stefan flow velocity, [14]. The condensation rate is derived from the mass transfer coefficient. The first term in the right hand side of the equation reveals the drift velocity with respect to the Stefan flow (diffusiophoresis).

The removal rate in a compartment and for a particular aerosol size class, which is returned to the aerosol mass balance equation in ASTEC, is calculated as shown by formula (27), which requires knowledge of the elementary collision efficiency. The latter is expressed as:

$$\varepsilon = 1 - (1 - \varepsilon_m)(1 - \varepsilon_{ph}) + \varepsilon_B \quad (36)$$

11.6 Gaseous Iodine Removal by Sprays

It is well known that gaseous iodine, particularly its molecular form I_2 , may be present in the containment atmosphere during a severe accident. The suppression of this form of iodine by spray water is an important issue because about 10 % of it would not be trapped by sand filters in the case of emergency containment depressurization. Moreover, in the long term, it can be transformed into methyl iodide by interaction with the painted surfaces, and the latter would be trapped neither by the sand filters nor in the extraction line.

The interaction of gaseous iodine with a droplet involves mass transfer in the gas phase, interfacial transfer, mass transfer in the liquid phase and chemical reactions and speciation within the droplet. These mechanisms depend mainly on the flow around the droplet, on the convective flow inside the droplet, on its temperature, and on the droplet pH. Moreover, the capture efficiency is very dependent on the iodine concentration in the gas phase. It is not possible to describe rigorously all these mechanisms unless one uses an internal meshing of the droplet, which is not compatible for a severe-accident code application. Therefore, a simple model has been proposed for the molecular iodine removal (CH_3I is not considered) which is, however, able to give predictions in satisfactory agreement with the experimental data, namely those of the CSE programme, [15].

In this scheme, the capture process involves the following steps:

$$\text{gas phase transfer:} \quad J = k_g(C_g - C_{ig}) \quad (37)$$

$$\text{interfacial equilibrium:} \quad C_{iw} = p(T)C_{ig} \quad (38)$$

$$\text{liquid phase transfer:} \quad J = k_w(C_{iw} - C_w), \quad (39)$$

and chemical reactions in the bulk liquid:



The underlying assumption (and main simplification) in this scheme is that the mass transfer in the liquid phase takes place in a very narrow area near the droplet surface and that everywhere else the concentrations of different species are rapidly homogenised. Other assumptions are that thermodynamic interfacial equilibrium is reached instantaneously, the water pH is maintained constant and the transfer is quasi-stationary. Furthermore radiolytical reactions are not taken into consideration. In the case of condensation on or evaporation from the droplet, an additional term in the mass transfer coefficient is considered in a form due to the Stefan flow.

Nomenclature

a	non-dimensional particle diameter	M_s	steam molar mass
B_M	Spalding number: $B_M = \frac{X_{s\infty} - X_{sw}}{1 - X_{sw}}$	M_w	water molar mass
C_D	drag coefficient	n	number of recombiners in a zone
\bar{c}_g	average steam-air mixture molar conc.	n_0	number concentration of droplets
C_g	I_2 bulk concentration in the gas	Nu_g	Nusselt number of the gas
C_w	I_2 bulk concentration in the liquid	p	thermodynamic partition coefficient
C_{ig}	I_2 concentration in the gas at droplet surface	P_{tot}	total pressure of the zone
C_{iw}	I_2 concentration in the liquid at droplet surface	P_a	partial pressure of air
C_m	mass concentration of aerosols	P_s	partial pressure of steam
D_B	Brownian diffusion coefficient	Pr_g	Prandtl number of the gas
\bar{D}_s	average steam-air diffusion coefficient	r_g	geometric radius
d_p	particle diameter	r_p	particle radius
d_w	droplet diameter	Re_w	droplet Reynolds number
e	efficiency of the recombiner	S	cross section area covered by the spray
g	acceleration due to gravity	Sc_g	Schmidt number of the gas
H_a	specific enthalpy of air	Sh_g	Sherwood number of the gas
H_s	specific enthalpy of steam	t	time
H_w	specific enthalpy of water	T_w	droplet temperature
J	I_2 mass transfer coefficient	T_g	gas temperature
K	Stokes number	T_0	reference temperature
K_0	efficiency of the recombiner in case of non stoichiometric conditions	U	internal energy per unit volume
K_{eff}	efficiency of the recombiner linked to the length of the chimney	U_∞	upstream fluid velocity
k_g	mass transfer coefficient in the gas	V	volume of the compartment
k_w	mass transfer coefficient in the liquid	V_{ph}	phoretic velocity
K_1	coefficient used in the recombination law	v_w	droplet velocity
K_2	coefficient used in the recombination law	x_1	exponent used in the recombination law
\dot{m}_s	steam condensation mass flow rate	x_2	exponent used in the recombination law
m_w	droplet mass	x_{crit}	critical mole fraction ratio
m_{H_2}	hydrogen mass	$X_{s\infty}$	molar fraction of steam in the bulk fluid
M_a	incondensable molar mass	X_{sw}	molar fraction of steam at droplet surface
		y	non dimensional distance from flow axis
		y_c	critical impact parameter
		z	height
		Δz	compartment height
		Φ	droplet diameter
		ε	collection efficiency of aerosols
		λ_g	steam-air mixture thermal conductivity
		η	fluid viscosity

References

- [1] W. Plumecocq, V.D. Layly, A. Bentaib Modelling of the containment mitigation measures in the ASTEC code, focusing on spray and hydrogen recombiners International Topical Meeting on Nuclear Thermal-Hydraulics (NURETH-11), 3-6 October 2005, Avignon, France, 2005
- [2] W.E. Ranz, W.R. Marshall Evaporation from drops J. Chemical Engineering Progress, 48, n°3 141-146, n°4 173-180, 1952
- [3] W.C. Hinds Aerosol Technology Wiley Interscience Publication, 1982
- [4] D.A. Powers, S.B. Burson A Simplified Model of Aerosol Removal by Containment Spray NUREG/CR 5966, 1993
- [5] W. Plumecocq Etude de l'interaction d'un système d'aspersion liquide avec l'atmosphère environnante PhD thesis, Université de Provence, Marseille, France, 1997
- [6] K. Beard, S. Grover Numerical collision efficiencies for small raindrops colliding with micron size particles Journal of the Atmospheric Sciences, 31, 1974
- [7] B.P. Le Clair et al. A numerical study of the drag on a sphere at low and intermediate Reynolds numbers Journal of the Atmospheric Sciences, 27, 1970
- [8] N.A. Fuchs The Mechanics of Aerosols Dover Publications New York (1989 edition), 1964
- [9] C.N. Davies Aerosol Science, Academic Press, 1966
- [10] G.M. Hidy, J.R. Brock The dynamics of aerocolloidal systems 1, Pergamon Press, New York, 1970
- [11] R.J. Han, O.R. Moss, B.A. Wong Derivation and application of an analytical solution to the mass transfer equation to the case of forced convective flow around a cylindrical and a spherical particle with fluid surface properties Journal of Aerosol Science, 27 n° 2, 1996
- [12] L. Talbot et al. Thermophoresis of particles in a heated boundary layer Journal of Fluid Mechanics, 101 (4), 1980
- [13] L. Waldmann, K.H. Schmitt Thermophoresis and Diffusiophoresis of Aerosols, Chap. 6 of Aerosol Science, Edited by C.N. Davies, Academic Press, New York, 1966
- [14] J.G. Collier, J.R. Thome Convective boiling and condensation 3rd edn. Oxford Clarendon Press, 1994
- [15] A.K. Postma, L.F. Coleman Effect of continuous spray operation on the removal of aerosols and gases in the Containment Systems Experiment, BNWL 1485, 1970

12. APPENDIX 4: Overview of Filtration Devices

Ref. [1] provides a detailed account of history of aerosol filtration and gas adsorption development. This section briefly summarises the historical development.

12.1 Nuclear Aerosol Filtration

Filtration of airborne aerosol particles is relatively new and goes back to the Second World War. In the early days of World War II, the British troops realised that the German mask canisters were equipped with better filter papers and delivered them to the U.S. Army Chemical Warfare Service Laboratories (CWS) in Edgewood, Maryland [2]. The German filter paper was made of fine asbestos dispersed in esparto grass and had unusually high particle retention characteristics, acceptable resistance to airflow, good dust storage, and resistance to plugging from oil-type screening smokes (a deficiency of the resin-wool filters then used by the British forces).

After some more research and development Americans could generate filter papers made up of northern spruce sulphite and sulphate pulp (approximately 76 %), cotton waste (approximately 15 %), and Bolivian Blue crocidolite asbestos (approximately 14 %) with an penetration efficiency of 0.025-0.04 % based on a methylene blue stain-intensity test procedure [3].

Desire to have more efficient filters solicited the assistance of a number of university and industrial scientists in the USA in search for better smoke filters. This effort resulted in important U.S. advances in the theory and technology of aerosol filtration. Up to this time, aerosol filtration theory had developed almost exclusively as an offshoot of water filtration knowledge. To meet then-current military requirements, however, researchers such as Irving Langmuir [4] examined the physical basis for particle retention on fibres or small granules. Langmuir concluded that the principal mechanisms involved were: (1) interception, which affected suspended particles of sizes substantially greater than $1.0\ \mu\text{m}$ in diameter when moving through a devious flow path in a bed of porous material; and (2) diffusion, which affected suspended particles with diameters substantially smaller than $1.0\ \mu\text{m}$. His analysis, later modified by Ramskill and Anderson [5] to include inertia, indicated that the combined effects of these forces on a particle would be minimal when the particle was $0.3\ \mu\text{m}$ in diameter. Langmuir advised testing gas mask filters with smoke of this particle size to determine their minimum retention efficiency and indicated that, when particles with diameters greater or smaller than $0.3\ \mu\text{m}$ were present during field use of the gas mask, they would be removed at higher efficiencies than the test particles.

After the war, Victor LaMer [6] of Columbia University performed many experiments to further examine Langmuir's theory of a minimum filterable particle size, concluding that efficiency declined as particle size decreased below $0.3\ \mu\text{m}$. Subsequent studies showed that other forces should also be taken into account (particle inertia, flow rate, naturally occurring electrostatic charges on particles and filter media) to determine particle size dependent collection efficiency. Methods to generate test aerosols and standardised testing procedures were developed for rating ultra-high-efficiency (i.e., absolute) filters [7].

12.1.1 Development of the high-efficiency particulate air (HEPA) filter

The need for high efficiency particulate air (HEPA) filter stamp from requirements for protection of operational headquarters against chemical warfare agents and where wearing of an individual gas mask

was impractical. A mechanical blower and air purifier known as a “collective protector” filter unit containing the same filter paper used for the gas mask canister smoke filter but refabricated into a filter constructed of deep pleats separated by a spacer panel and sealed into a rigid rectangular frame using rubber cement. The spaces between the teeth of the comb-shaped separators provided air passages to the depths of the pleats and were inserted front and back in alternate folds to direct contaminated air in and clean air out (Fig. 12.1-1 adapted from Ref. 1).

These units were called collective protector filters and were used also in the Manhattan Project and later by the U.S. Atomic Energy Commission (AEC) after some adaptation to confine airborne radioactive particles in the exhaust ventilation systems of experimental reactors, as well as for most other areas of nuclear research. In this application, they were known as AEC filters or simply nuclear filters.

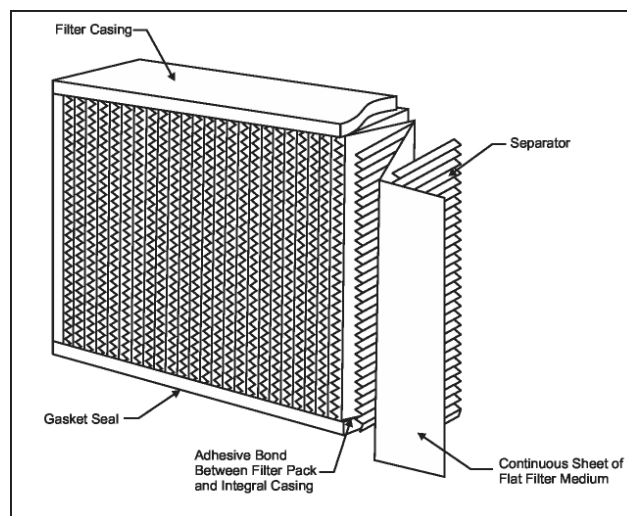


Fig. 12.1-1 A typical HEPA filter design

In recognition of their unusually high retention efficiency for very small particles, these collective protector filters were also known as absolute, super-interception, and super-efficiency filters. The most widely used name, however, was HEPA filters, an acronym coined by Humphrey Gilbert, a former Manhattan Project safety engineer, from the title of a 1961 AEC report called High-Efficiency Particulate Air Filter Units, Inspection, Handling, Installation [8]. A HEPA filter was defined as a throwaway, extended-medium, dry-type filter with: (1) a minimum particle removal efficiency of 99.95 % (later raised to 99.97 %) for a 0.3- μm monodisperse particle cloud; (2) a maximum resistance (when clean) of 1 inches water gauge (in.wg) when operated at rated airflow capacity; and (3) a rigid frame [now called “casing” in American Society of Mechanical Engineers (ASME) AG-1, Code [9] on Nuclear Air and Gas Treatment] extending the full depth of the medium. HEPA filters have proven to be extraordinarily effective, reliable, and economical devices for removing radioactive and nonradioactive submicrometer-sized particles at a high rate of collection efficiency.

The first nuclear reactor fitted with effluent high-efficiency air filters is believed to have been the graphite-moderated, air-cooled unit at Oak Ridge National Laboratory (ORNL) in Oak Ridge, Tennessee. The initiating event was the discovery in 1948 of radioactive particles up to 600 μm in size on the ground around the reactor stack. A reinforced concrete filter house was constructed to prevent further emissions [10].

Along the years the filter materials have been further developed to address fire issues, higher loading and retention, the HEPA filters were further improved in the USA and Europe for higher flow rates, resistance

to wetting and radiation. Further design improvements have been made to facilitate easy inspection and to address emerging stringent new standards and quality control for filters especially in nuclear service use.

12.1.2 Challenges for test procedures

The wide diversity of aerosols generated in the nuclear industry raises an important question regarding the relevance of the qualification test procedures utilised. For example, the aerosols predicted to be present inside the confinement vessel of a power reactor following a loss-of-coolant accident (LOCA) are certain to be very different from the test aerosols. The filter efficiencies observed during the standardised qualification tests performed may not necessarily produce the same results that will be obtained during an accident. Filtration efficiencies during an accident may be better or worse, depending on the characteristics of the aerosol challenge. However, passing a standardised qualification test gives reasonable assurance that the filters have been produced from high-quality components and carefully assembled to exacting standards. Therefore, the standard qualification test results should be viewed as an index of merit (an indication of quality) rather than a quantitative description of filter efficiency under unknown or ill-defined operating conditions.

12.1.3 Demonstrated safety by the use of HEPA filters

The value and effectiveness of correctly designed and installed nuclear-grade aerosol filtration systems are illustrated by the very different events that took place at the Three Mile Island-2 (TMI-2) and Chernobyl reactors. During the March 1979 accident at TMI-2 involving substantial core damage causing release of fission products and aerosols, it was determined after the accident that two filter systems in the auxiliary building prevented essentially the release of all of the particulate material and the bulk of the radioiodine to the environment [11]. Consequently, release of radioactive particles to the environment was negligible. The outcome was very different, however, during the April 1986 accident involving core disruption and subsequent fire at Chernobyl Unit 4, where engineered safeguards did not include complete confinement with air filtration systems. The widespread apprehension caused by that accident is likely to produce a demand for still higher collection efficiency and greater filter resistance to internal disruptive events (fires, explosions) and to external natural disasters (earthquakes, tornadoes).

12.1.4 Deep-bed sand and glass fibre filters

Although HEPA filters came to dominate aerosol confinement for most nuclear applications from the beginning there were other filter innovations of note. When a high-activity level due to radioactive particles emitted from the chemical processing ventilation stacks was detected at the Hanford, Washington, site in 1948 a filter based on the chemical engineering practice on deep beds of graded granular was used for the first time for the nuclear application. The sand filter construction closely followed the deep-bed, graded-granule techniques. These filters had collection efficiencies for particles greater than 0.5 μm that compared favourably with the best fibrous filters then available.

Rapidly emerging glass fibre technology during the 1940s and 1950s shifted attention to the use of very deep beds (23 cm or more) of curly glass fibres in combination with HEPA-quality final filters as a satisfactory substitute for sand filters when treating gaseous effluents from chemical operations [12].

There has been interest in sand filters for emergency confinement venting for light water reactors. An installed Swedish confinement venting system known as FILTRA features large concrete silos filled with crushed rock. These silos were designed to condense and filter steam blown from the confinement and to retain at least 99.9 % of the core inventory [13]. Later designs for confinement venting utilised wet systems to remove gaseous radioiodine.

12.1.5 Brief history of gas adsorption

In a nuclear accident, especially involving core damage substantial amounts gaseous fission products may be released directly from the degrading core and may additionally be produced, in the case of iodine, as a result of chemical reactions.

Wet scrubbing and adsorption are the main filtration mechanisms adopted for the nuclear applications since the late 1940s using the practices developed for the chemical and process industry as well as the technologies developed for the military applications for removing a wide range of toxic substances from breathing air. Along the years not only the filtration aspects of gaseous fission products were emphasised but also utilization of chemical means for long term retention have been given importance.

Adsorbents of various types, both impregnated and unimpregnated, have become widely used since the First World War (WWI). Activated carbon derived from nutshells was used in the early days. Later, the activated carbon used in the service gas mask was derived from coal and impregnated with metals that catalyse reactions with gas warfare agents. The theoretical basis for adsorption processes was greatly advanced by the need to develop gas mask applications during WWI, and Langmuir [1] made an early theoretical analysis of physical adsorption. Thus, there was a considerable body of knowledge available on the application of adsorbents, especially for activated carbon, when the nuclear industry developed a need for this technology.

Iodine releases to the atmosphere in the event of a reactor accident became a major concern as the nuclear industry began its rapid expansion during the early 1960s, and attention focused on iodine removal during normal and abnormal conditions at ambient and elevated temperatures. At ORNL, studies [1] were conducted on activated carbon beds for the hold-up of radioactive fission gases generated during the operation of nuclear reactors and during nuclear fuel reprocessing. The principal area of interest was delaying release until short-half-life isotopes decayed to levels that were acceptable for release. This approach utilised conventional theoretical plate equations.

Iodine in its many chemical forms is probably among the most extensively studied fission products produced in the nuclear industry. The generation, release mechanism, properties, forms, trapping and retention behaviour, and health effects of iodine-131 have been the subject of numerous studies, but a comprehensive understanding of the significance of its release to the environment and integration of the chemical technology into protection technology may remain incomplete in some aspects. The technology associated with the removal and retention of all iodine isotopes is similar to that for iodine-131, but interest in removal efficiency has shifted somewhat toward the importance of long-term retention with the increasing half-life of the iodine isotope.

Control of iodine emissions from chemical processing of spent nuclear fuel was initially done by liquid scrubbing using caustic solutions, and sometimes with the addition of sulphate salts, but retention efficiency by scrubbing seldom exceeded 90 %. To improve iodine retention efficiency for dissolver offgas cleaning, activated carbon beds were added to the caustic scrubber at DOE's Idaho Chemical Plant in 1958 [1]. The use of Silver-plated Fiberfrax fibres and silver-plated copper filaments were also investigated [1] to reach higher removal efficiency of iodine for use as a combined particulate filter and iodine retention device.

The application of adsorbents for noble gas retention was developed at ORNL [1]. The concept involves self regeneration of the adsorbent due to decay of the noble gases to solid daughter products as they pass through very deep adsorbent beds that require a long time for passage and results in the successive extinction of noble gas radioisotopes (i.e., those with the shortest half-lives disappear first). This technology is generally used to decontaminate all noble gas isotopes (except krypton-85 because of its

relatively long half-life - nearly 11 years). The process is particularly well suited to treat BWR offgas streams and was applied first at the nuclear power plant Gundremmingen (KRB) site in Germany [1]. The first BWR installation in the United States was the Interim Offgas System at the Vermont Yankee Plant [1]. It was succeeded by the Advanced Offgas System at the same site. Earlier technology involved ambient temperature systems. Cooled or refrigerated systems were later designed by the General Electric Company.

Volatile metal compounds such as ruthenium and technetium can be removed from gas streams by adsorption, but a solid-surface-supported chemical reaction is often necessary for good retention. Removal technologies for carbon-14 and tritium also involve the use of adsorbents, either as collecting agents or as catalysts for conversion to other, more easily removed compounds.

12.2 Type of Filters in Use

The requirements for the design of a filter system in removing the fission products depend on the thermal hydraulic conditions (temperature, pressure, humidity level or steam condensation, flow rate through the filter system) and concentration of the fission products in gaseous and aerosol form. The severity of the conditions imposed by the normal operational conditions or accidents (design basis or severe accidents involving core damage) produce the challenge for the design of the systems.

12.3 Normal Operation and Design Basis Accidents

During operational conditions many containments are kept subatmospheric in order to avoid any accidental release of even small activity into the environment. Ventilations systems, depending on the design and regulatory requirements, may contain parallel trains of filtration systems. A typical train contains the following sequential components: (1) a moisture separator to remove entrained water droplets, (2) a heater to control relative humidity (RH) when the RH of the air entering the carbon adsorber exceeds nominally 70 %, (3) prefilters, (4) HEPA filters, (5) a charcoal adsorber, (6) HEPA filters downstream of the adsorbers, and (7) a fan. Fig. 12.3-1, adopted from Ref. 1, displays a typical filtration unit. Ducts, valves, and dampers are also included for system isolation and flow control, as well as related instrumentation. When the moisture and dust loads are low for all credible operating modes, the prefilter and moisture separator may not be required. The carbon or charcoal adsorbers may be impregnated or unimpregnated.

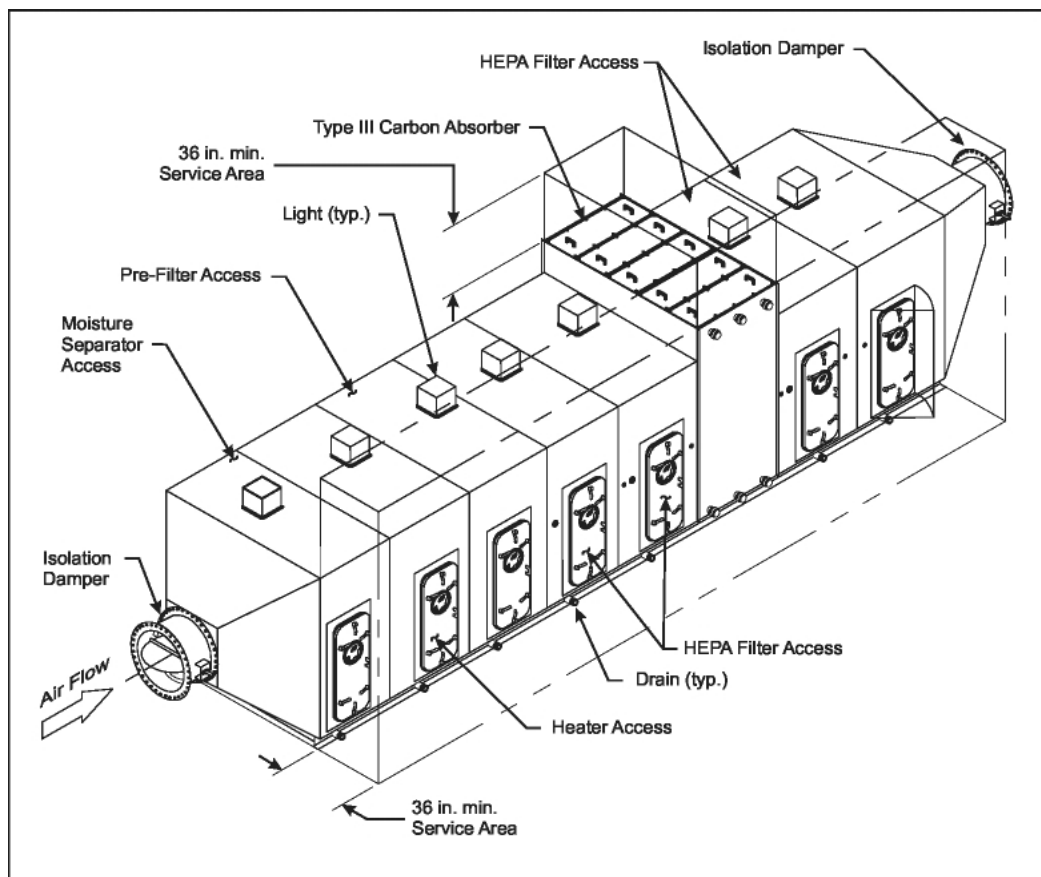


Fig. 12.3-1 A typical air cleaning system

The source of activity in the containment is due to release of dissolved activity (e.g., iodine) in the primary coolant water with a leak from the circuit. The source of the activity in the circuit could be due to leaking fuel elements or due to iodine spiking. The maximum permissible activity level in the circuit and in the containment is defined by regulations. Most currently operating reactors keep coolant concentrations of radionuclides orders of magnitude below the technical specifications or regulatory limits.

By definition design basis accidents (DBA) involving loss of coolant foresee failure of certain number of fuel cladding, which then causes the release of noble gases and volatile fission products (iodine, cesium), into the primary coolant water. The release of the primary coolant water into the containment causes the activity release into the containment. If the accident is a containment by-pass accident then the activity is released directly either into the auxiliary/reactor building (V-sequence) or through the broken steam generator tube(s) (SGTR) into the steam generator secondary side and after some scrubbing in the secondary water, eventually directly into the environment. Loss of coolant accidents due to SGTR with few tube failure normally do not cause any fuel cladding failure but a certain fraction of the dissolved activity in the primary circuit at the time of the accident may be released into the environment in form of gas, and/or through droplet or water flow depending on the location of the broken tube(s).

Containment or auxiliary (reactor) building filtration systems are designed to avoid any substantial release of activity transported by aerosol particles and gaseous iodine. Of course the main assumption at the background of this statement is that the containments are isolated and there are no uncontrolled leak paths.

12.4 Brief Review on Mechanisms of Filtration

Particle removal from a gas depends upon it making contact with, and adhering to, either a liquid or solid surface. These surfaces can consist of such elements as fibres, sand grains, pieces of gravel, or water droplets, to mention a few. It is the nature of these surfaces that characterises the collection device. As a result of the filter test program in the ACE international project a review report was prepared [16] to provide the main mechanisms and the formulation of each mechanism based on the available literature information. The following sections briefly summaries the work published in [16]. Since the limited release of this report in 1992 there has been no further progress made in the theoretical area for modelling or understanding the mechanisms.

The mechanisms, which will bring an aerosol particle into contact with a collection surface and which will remove them from a gas bubble are in detail introduced in the previous chapters of the SOAR. The ones, especially important for the filtration, are repeated very briefly below:

I Interception

Deposition by interception occurs when a particle follows a streamline that comes within one particle radius of the collection body. This capture, which is illustrated in Fig. 12.4-1, occurs because of the finite size of the aerosol particle.

II Inertial impaction

Deposition by inertial impaction occurs when a particle, due to its inertia, is unable to follow a curving streamline. It will then cross other streamlines and impact on the collecting body as illustrated in Fig. 12.4-2.

III Brownian diffusion

Deposition by Brownian diffusion occurs when a particle, due to collisions with gas molecules, deviates from the path of a streamline, which would not normally result in deposition, and impacts on the collection surface as illustrated in Fig. 12.4-3.

IV Sedimentation

Deposition by sedimentation occurs when gravity acting on the aerosol particle causes it to impact on the collection surface.

V Thermophoresis

Deposition by thermophoresis occurs when the collection surface is at a substantially lower temperature than the aerosol carrier gas. The particle moves in a direction down the temperature gradient in the gas because it is being hit by more energetic molecules on the hot than the cold side.

VI Condensation

Deposition by condensation on a collection surface results from two independent mechanisms, diffusiophoresis and Stefan flow. Diffusiophoresis refers to the motion of an aerosol particle in a concentration gradient in a direction from the heavier towards the lighter molecules. Stefan flow refers to the convective flow of condensing gas towards the cold surface. This flow carries the aerosol particles along by Stokes drag. For example, if there is a mixture of two gases, which have the same molecular weight, and one of them is condensing on a surface, there would be no diffusiophoresis. The aerosol particles would, however, be carried to the surface by Stefan flow alone.

VII Pool scrubbing

The mechanisms, except the interception, listed above occur within the bubble boundary and under the effect of gas circulation or no circulation conditions in the bubble.

The relative importance of these mechanisms depends upon the aerosol characteristics, conditions of the aerosol transport, and the system boundary conditions. For each mechanism it is possible to define single collection body efficiency, η_o , as the ratio of the cross section area bounded by the limiting streamlines far upstream of the collection body, to the projected area of the collection body normal to the flow far upstream. In Fig. 12.4-4, this is defined as y/r for an infinite cylinder, and $(y/r)^2$ for a sphere. Clearly, the overall efficiency for an assemblage of bodies is a function of the single body efficiency.

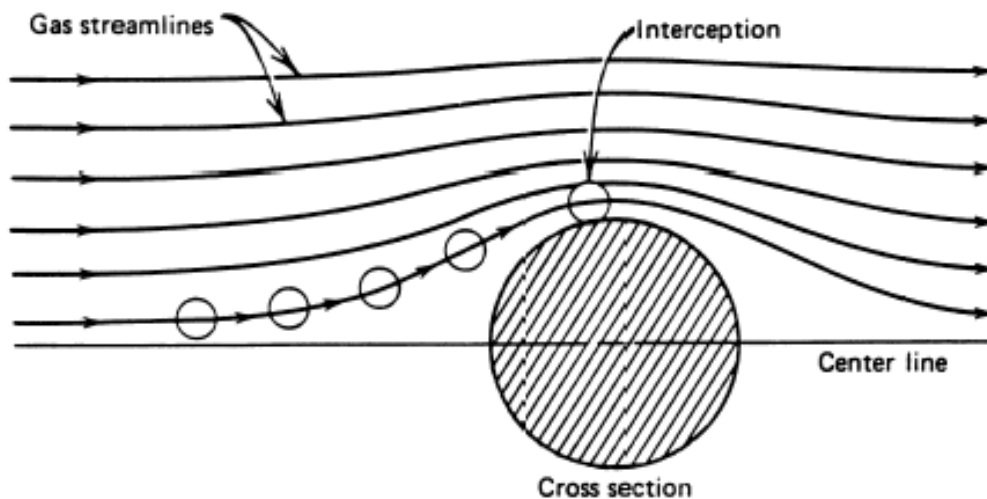


Fig. 12.4-1 Single body collection by impaction [10]

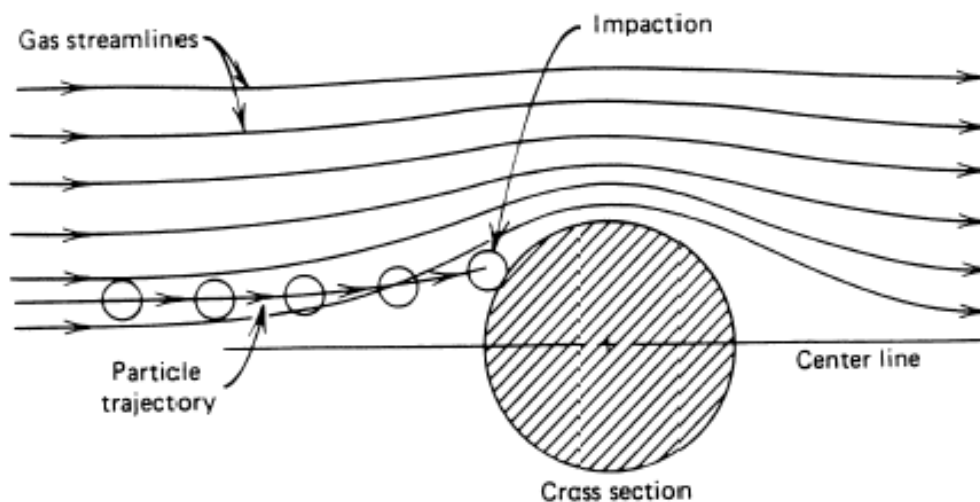


Fig. 12.4-2 Single body collection by impaction [10]

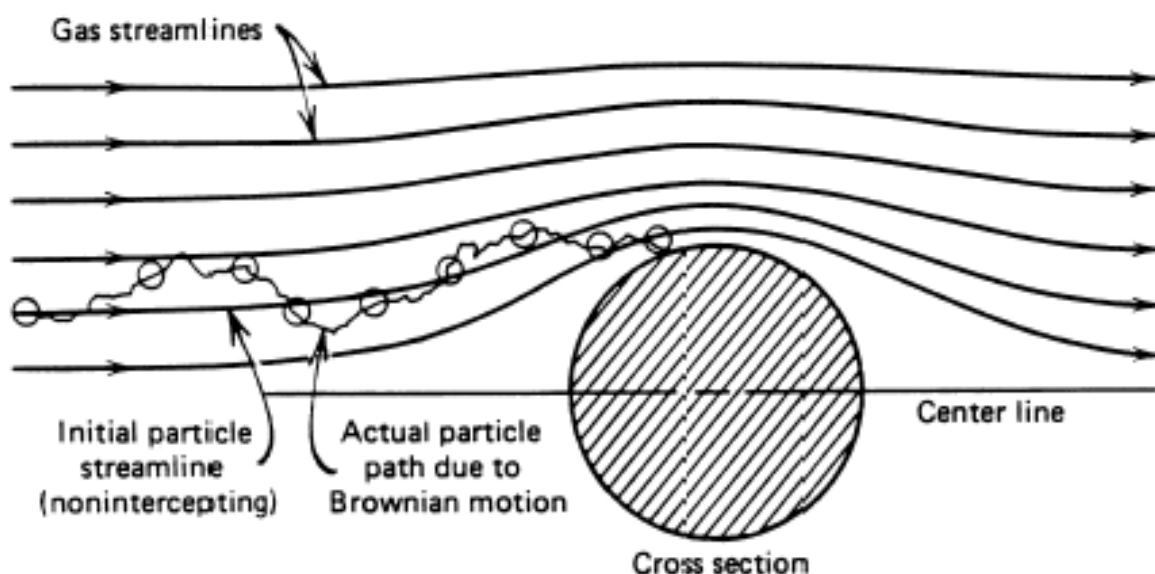


Fig. 12.4-3 Single body collection by diffusion [23]

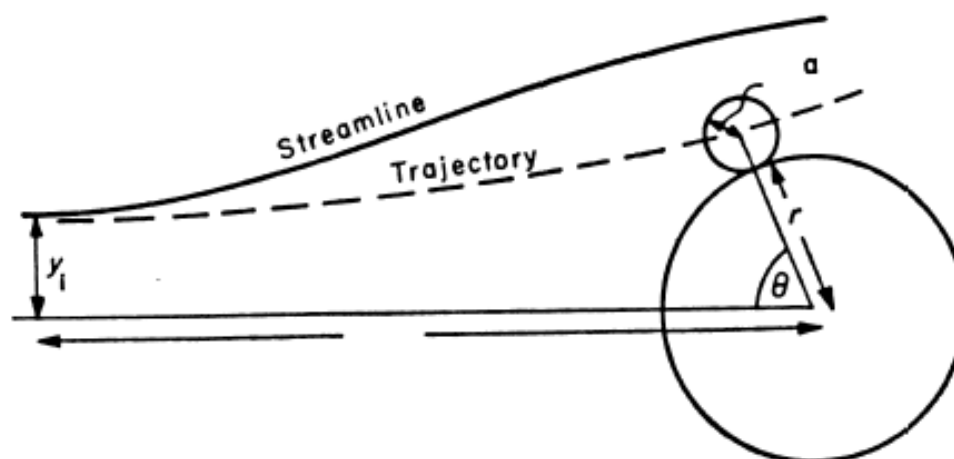


Fig. 12.4-4 Illustration of the collision efficiency

12.5 Characterisation of Filter Performance

There are several parameters currently in use to describe the effectiveness of a filtration device. These are, however, all based on the mass of material injected to a device, m_{in} , and the mass of material exhausted, m_{out} . In the nuclear industry the most commonly used parameter is the Decontamination Factor, DF, which is defined as the ratio of the injected to exhausted mass:

$$DF \equiv \frac{m_{in}}{m_{out}}$$

Intimately related to the DF is the penetration, Pt, which is defined as the ratio:

$$P_t \equiv \frac{m_{out}}{m_{in}}$$

This is just the inverse of the DF. The collection efficiency, η , is defined the ratio of the collected to the injected mass. This can be written in terms of the injected and exhausted masses as:

$$\eta \equiv 1 - \frac{m_{out}}{m_{in}}$$

For most filtration devices, the efficiency of collection depends strongly on the particle size. Hence it is useful to introduce the concept of a "fractional efficiency" where the definitions above apply for particular particle size ranges. This definition introduces a difficulty for processes where the particles change size within the filtration device. For example, hygroscopic particles can grow substantially [17] in wet scrubbers. In this situation, the amount of exhausted mass in a particular size range must be based on the inlet size distribution. Unfortunately, this is impossible to do experimentally, where only inlet and outlet size distributions are measured, but the inlet and outlet particle concentrations in each size range cannot be related. The only ways to determine this information are to either use aerosols, which do not grow, or less ambiguously, inject only monodisperse aerosols.

The penetration can be quantified on the basis of a one dimensional filtration model as illustrated in Fig. 12.5-1.

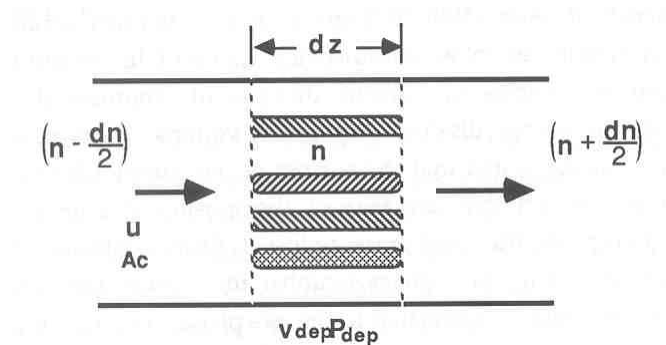


Fig. 12.5-1 Scheme of a one-dimensional filtration model

If the flow of aerosols through a control volume of length dz is considered and additionally a deposition velocity v_{dep} and a deposition area of $P_{dep}dz$ are postulated, a mass conservation equation for aerosols can be written as:

$$\begin{aligned} \text{Aerosols in} & - \text{Aerosols out} & = & \text{Aerosols deposited} \\ \left(n - \frac{dn}{2}\right) u_g A_c & - \left(n + \frac{dn}{2}\right) u_g A_c & = & n v_{dep} P_{dep} dz \\ - \frac{dn}{n} & = & \frac{v_{dep} P_{dep}}{Q_g} dz \end{aligned}$$

and after the integration as:

$$P_t \equiv \frac{1}{DF} \equiv 1 - \eta = \frac{n_{out}}{n_{in}} = \exp \left(- \frac{v_{dep} A_{dep}}{Q_g} \right)$$

$$= \exp \left(- \frac{v_{dep} A_{dep} \tau}{V_g} \right)$$

These expressions for overall penetration or efficiency apply to all the filters considered subsequently.

12.6 Cut Diameter Method

Lapple and Kamack [18], and Semrau *et al.* [19-21] have suggested that there is a unique power law relationship between efficiency and pressure drop across any scrubber. According to Semrau *et al.*, venturi scrubber energy consumption determines collection efficiency. Calvert [22] found that the aerosol capture efficiencies of various designs of commercial wet scrubbers depend on the energy dissipation per unit volume of gas in each system. Jepson [24] has suggested that the success of the energy dissipation correlation is due to the fact that the area of the gas-liquid interface is proportional to the two-phase frictional pressure loss. Calvert established that the "50 % cut diameter", d_{50} , of a given scrubber for a given lognormal particle size distribution could be correlated to the gas-phase pressure drop or power input to the scrubber. As can be seen from Fig. 12.6-1, the higher the energy dissipation per unit volume of gas, the smaller the 50 % cut diameter for any given class of filter.

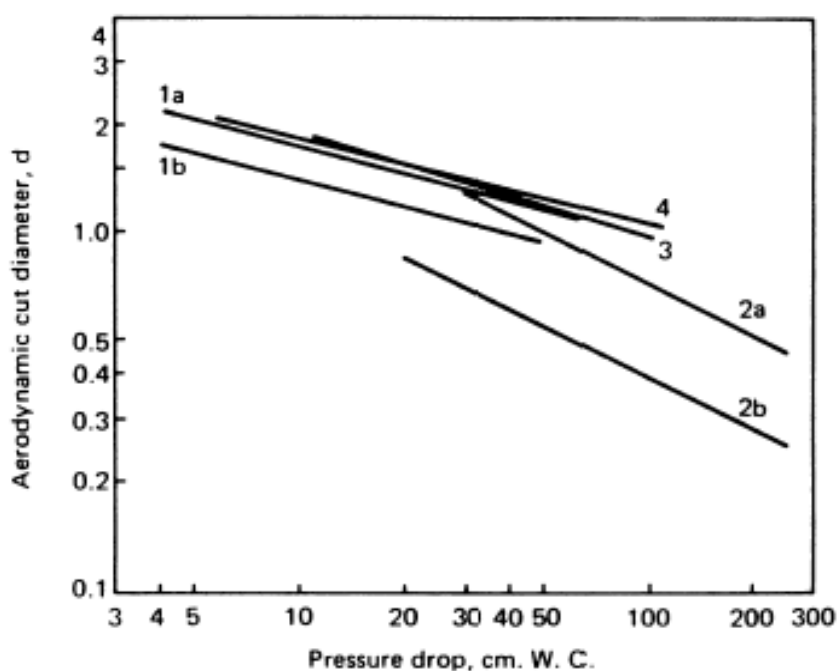


Fig. 12.6-1 Representative cut diameters as a function of pressure drop for several scrubbers

Calvert developed an approximate graphical method [25] to compare various designs of wet scrubbers on the basis of d_{50} vs. gas pressure drop. Calvert's correlation assumes that impaction is the main mechanisms of aerosol capture and that the aerosol size distribution is lognormal. Most scrubbers that collect particles by inertial impaction obey [25]

$$P_t = \exp \left\{ -A d_{pa}^B \right\}$$

where B usually has the value, two. Integration of this expression over several lognormal particle size distributions yields the graphical relationships shown in Fig. 12.6-2. The overall penetration, P_t , for the entire size distribution is plotted against the ratio of the 50 % cut diameter, d_{50} , to the mass median diameter d_{pg} , with σ , the geometric standard deviation, as a parameter. Fig. 12.6-2 can be used in conjunction with Figure 15 to select a scrubber with a required efficiency.

Hilliard et al. [26] used Calvert's method to correlate the 50 % cut diameter with the gas pressure drop (Pool depth) of a submerged gravel scrubber. Morewitz [27] showed that both suppression pools and the submerged gravel scrubber appear to have cut diameter vs. pressure drop characteristics for insoluble aerosols similar to either a gas atomised scrubber [22] or a washed, high void fraction bed of 100 μm diameter packed fibres. He noted that the 50 % cut diameters decrease with increasing pool depth and that soluble particles at a given depth have smaller cut diameters than insoluble ones. This latter effect is probably due to increase in size of soluble particles as they pick up water vapor.

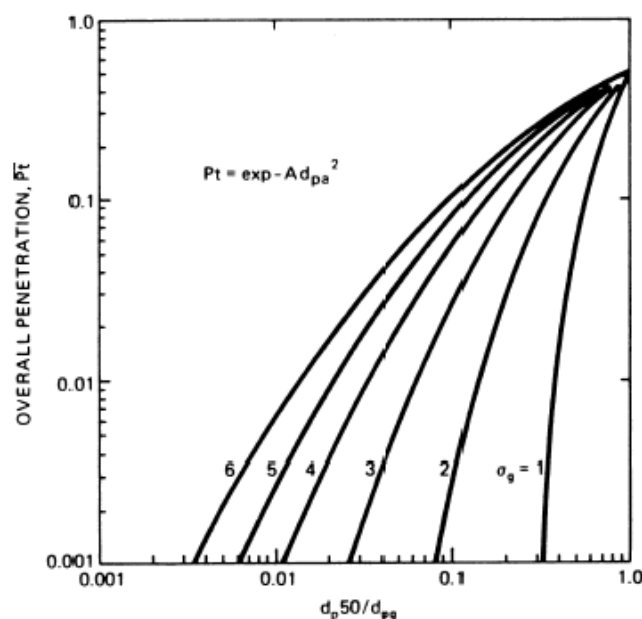


Fig. 12.6-2 Overall penetration as a function of cut diameter and particle parameters

12.7 Fibrous Filter

Filter media for gas filtration consist of an assemblage of fibres, which are woven or loosely packed. The major performance criteria are collection efficiency, pressure loss, and lifetime. For filtered vented containment application the most important is collection efficiency, since the driving pressure is from the containment pressurization, and most probably there will be only one nonrepetitive use.

The particle collection efficiency is usually calculated by considering the particle removal by one fibre, and then summing over all fibres [23, 28, 29]. Applying Equation for overall penetration or efficiency (introduced in the previous section) to this geometry, the efficiency of a filter at the beginning of use, i.e. before a layer of particles has formed is given by:

$$\eta = 1 - \exp \left\{ \frac{-4(1-\epsilon)H}{\pi \epsilon d_f} \eta_0 \right\}$$

where η_0 is the single fibre collection efficiency modified for the effects of neighbouring fibres. This equation is not controversial, however, the entire crux in determining the overall filter efficiency boils down to the determination of the single fibres collection efficiency. The differences between most authors boil down to how to account for the effects of neighbouring fibres, and how to account for the coupled deposition mechanisms for the polydisperse particles.

Kirsch and Stechkina [28] suggest that convective diffusion, η_D , and interception, η_I be accounted for additively and that deviations from superposition be accommodated through the use of an interaction term η_{DI} as follows:

$$\eta_f = \eta_D + \eta_I + \eta_{DI}$$

where

$$\eta_0 = \eta_f \psi$$

from theoretical arguments it is possible to write

$$\eta_I = (2K_H)^{-1} [(1+I)^{-1} - (1+I) + 2(1+I) \ln(1+I) + 2.86Kn(2+I)I(1+I)^{-1}]$$

$$\eta_D = 2.7Pe^{-2/3} [1 + 0.39K_H^{1/3}Pe^{1/3}Kn] + 0.624Pe^{-1}$$

and

$$\eta_{DI} = 1.24 K_H^{-1/2} Pe^{-1/2} I^{2/3}$$

where the hydrodynamic factor for cylindrical arrays is given by

$$K_H = 0.5 \ln(1-\epsilon) - 0.52 + 0.64(1-\epsilon) + 1.43 \epsilon Kn$$

Kirsch and Stechkina [28] recommend the following relationships to determine the effects of the filter inhomogeneity:

$$\psi = \frac{\{0.64(1-\epsilon) - 0.5 \ln(1-\epsilon) - 0.52\} D_0^*}{4\pi}$$

where ψ is the dimensionless drag force on the filter for $Kn = 0$. It should be pointed out that these relationships apply to clean filters only, and that the actual efficiency of the filter improves as the particulates clog the filter.

Another theoretical approach for the prediction of filter behaviour is to calculate particle trajectories through regular cylindrical arrays representing filter fibres [30]. These methods have the advantage of being able to directly couple the various deposition mechanisms, however they cannot handle mats of randomly distributed fibres. Thus these models are at best qualitative tools to understand the mechanisms of filtration, however, for application to real systems it is necessary to obtain actual measurements of filter performance.

12.8 Granular Beds

Dry granular beds have been used for filtration of particulates for over a century [31], but only in 80's have mechanistic models for their filtration efficiency been developed. These are based on the single grain capture efficiency, extended to a bed of particular size. The particle collection efficiency is usually calculated by considering the particle removal by one grain, and then summing over all grains. The penetration of a granular bed filter obtained from Equation for overall penetration or efficiency is given by:

$$P_t = \exp \left\{ - \frac{3 \alpha H}{2 d_g} \eta_g \right\}$$

where η_g is the single grain-capture efficiency, which is analogous to the single fibre-capture efficiency used for fibrous filters. The problem of a granular bed filter reduces to finding appropriate expressions for η_g .

Goren and co-workers [32,33] have performed experiments and developed correlations, which permit the calculation of aerosol, capture efficiencies in granular beds. These correlations cover a wide range of aerosol size, grain size, gas velocity, and depth of filter bed. Goren [32, 33] mentions the following expressions for the individual deposition efficiencies.

Brownian diffusion,

$$\eta_D = 3.97 \frac{A_h^{1/3}}{Pe^{2/3}}$$

Sedimentation,

$$\eta_G = Gv = \frac{\rho_p d_p C_p g}{18 \mu U_o}$$

Interception,

$$\eta_I = 1.5 A I^2$$

Impaction,

$$\eta_{Im} = \frac{1}{1 + 1.67 (A St)^{-3.55}}$$

Since the flow around the grains are not well approximated by Stokes flow it is necessary to introduce a hydrodynamic factor into the collection efficiencies to accommodate this shortcoming. Michaels and Goren [33] modified Happel's [34] expression, which was derived by using a cell model in low Reynolds number flow, for high Reynolds number to get

$$A = \frac{(6 - \alpha^{5/3})}{(6 - 9\alpha^{1/3} + 9\alpha^{5/3} - 6\alpha^2)} + 1.14 \frac{Re^{1/2}}{(1 - \alpha)^{3/2}}$$

which should be applicable to the entire range of Reynolds numbers. For the ranges of parameters tested, if the superficial gas velocity is greater than approximately 10 cm/s, the flow is in the impaction-dominated regime and only that efficiency needs to be used. For superficial gas velocities ranging from 0.1 to 8 cm/s, both sedimentation and Brownian diffusion dominate. To handle the coupled mechanisms, rather than just adding them, the following approach is suggested based on the results of numerical analyses.

If

$$\beta = \left(\frac{2A}{Pe^2 Gv^3} \right)^{1/3}$$

and

$$\gamma = Pe Gv I$$

are defined then the capture efficiency for combined sedimentation, diffusion and interception can be written as

$$\eta_g = Gv \left\{ 1 + 1.9\beta + 0.75\beta^3\gamma^2 - \frac{1.9\beta}{(1 + 1.9\beta + 0.75\beta^3\gamma^2)} \right\}$$

Results of this expression as applied to experiments performed on glass spheres are shown in Fig. 12.8-1 and Fig. 12.8-2 for two different sphere sizes. The agreement is satisfactory however, looking at data points for particular particle sizes indicate that there are systematic deviations between correlation and experiments.

For the case when impaction dominates, the comparison between calculation and experiments is shown in Fig. 12.8-3 for two different aerosol materials. The DOP aerosols are liquid, whereas the KHP (potassium biphthalate) was solid. The levelling off of the efficiency for the KHP aerosols at high effective Stokes numbers was attributed to rebounding.

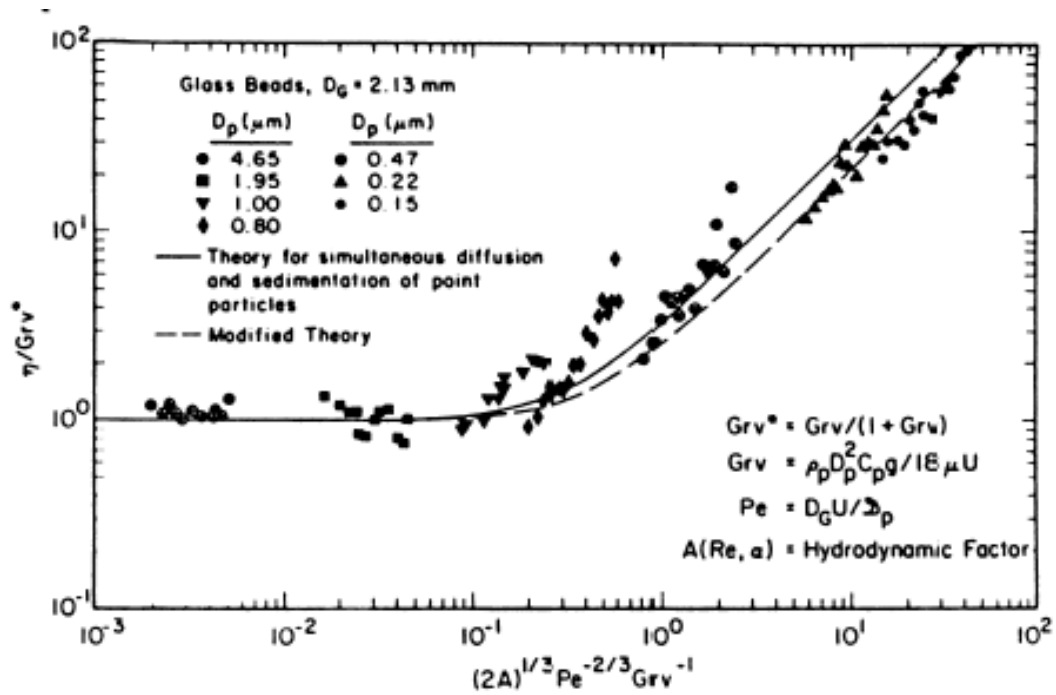


Fig. 12.8-1 Single grain efficiencies for beds of 2.13 mm glass beads

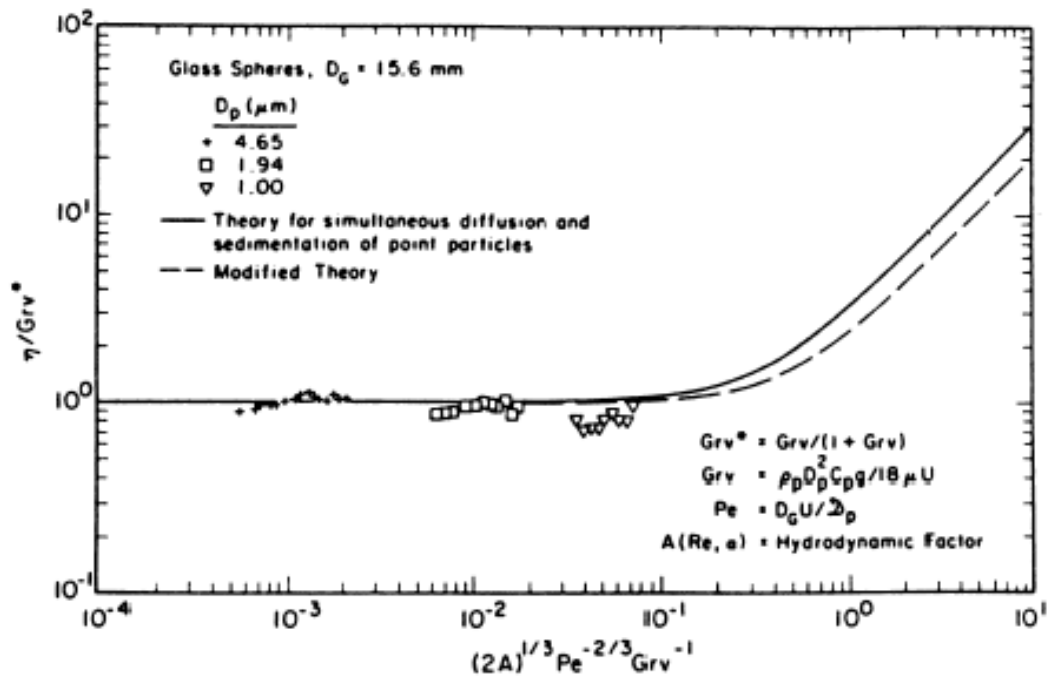


Fig. 12.8-2 Single grain efficiencies for beds of 15.6 mm glass beads

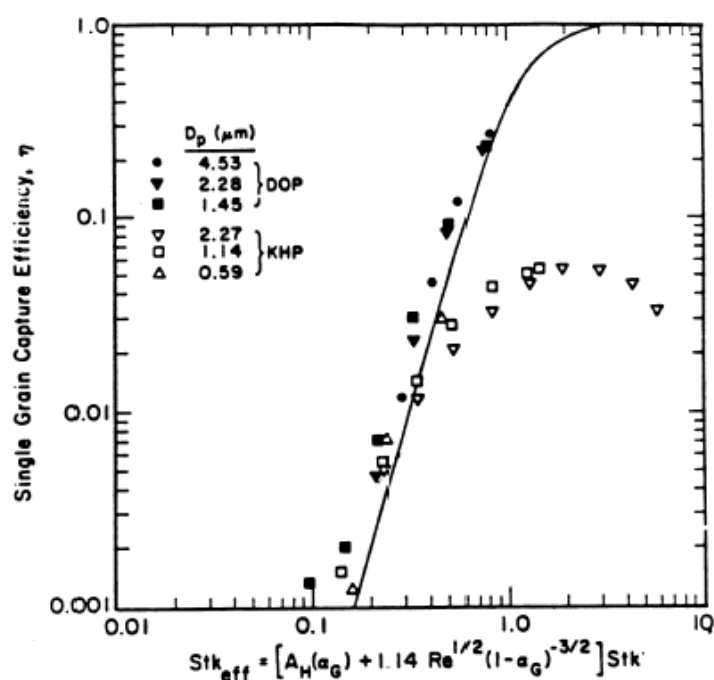


Fig. 12.8-3 Single grain efficiencies in the impaction dominated regime

12.9 Sand Beds

The experiments on which Goren's expressions are based were performed with grains (spherical glass beads) that were 2 mm in diameter or larger. Sher [35] applied the expression for efficiency in the impaction dominated regime to French sand bed filtration experiments reported by Guieu et al. [36]. The results are shown in Fig. 12.9-1. The effective Stokes numbers of these experiments fall into the lower range of Goren's experiments where the single grain efficiency levels off and becomes independent of the effective Stokes number. To match this data, Sher added an arbitrary factor of 0.0017 to the Goren impaction correlation to get:

$$\eta_g = \eta_{Im} = \frac{1}{1 + 1.67 (A St)^{-3.55}} + 0.0017$$

This curve is shown in Figure as the "Modified Goren Correlation". Since at these low Stokes numbers the efficiency is constant it appears that another deposition mechanism besides impaction must dominate.

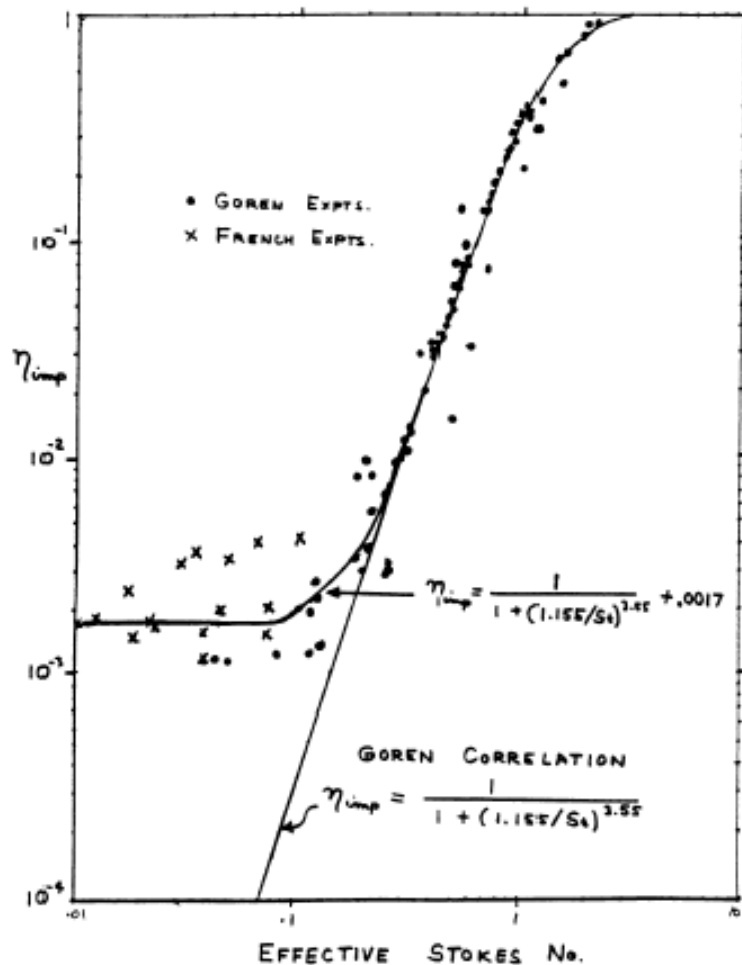


Fig. 12.9-1 Application of impact correlation to sand bed data

12.10 Gravel Beds

Ström et al. [37] performed experiments on particle retention in a bed of crushed rock with a stone size ranging from 25 to 30 mm. These are bigger than the gravel tested by Goren, which did not exceed 19 mm in equivalent spherical diameter. The velocities that these experiments were performed at were 5, 10, and 20 cm/s, while Goren's tests were performed at 0.2 to 8 cm/s. For the analysis of their data, Ström et al. used the following single grain efficiencies:

Impaction:

$$\eta_{Im} = 0.68 St / \epsilon$$

Diffusion:

$$\eta_D = 4 Sh / Pe$$

Sedimentation:

$$\eta_G = 0.76 B m_p g / U_o$$

The overall single grain efficiency was then assumed to be simply the sum of the separate effects,

$$\eta_g = \eta_{lm} + \eta_D + \eta_G$$

When this expression was applied to the experimental data for dry gravel, the results were very good as can be seen in Fig. 12.10-1. The deviation between the experiments and calculations was usually less than a factor of two in the range of 0.3 to 3 μm , mass equivalent diameter. No theory was presented for the cases involving condensing steam.

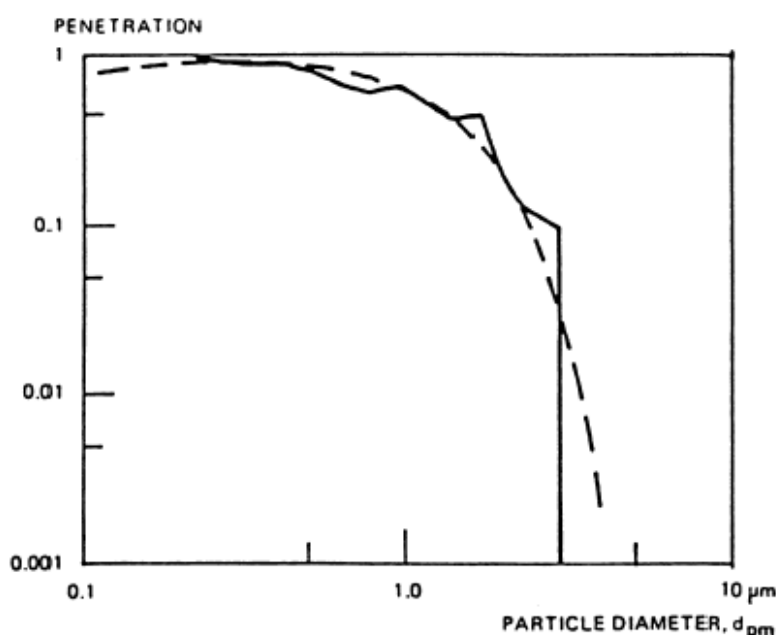


Fig. 12.10-1 Observed (-), and calculated (- - -) penetration for a dry 6 m gravel bed [37]

Goren also analysed the results of his gravel bed experiments [32] with the equations which are applicable to the sedimentation and diffusion dominated regimes. The main question in such an analysis is what "effective" grain or packing size should be used. For calculating pressure drop, common practice is to use the combination $d'_G \phi_s$ where ϕ_s is called the sphericity, and is defined as the ratio of the surface area of a volume equivalent sphere to the actual surface area of the grain. The Sauter mean diameter d'_G is calculated from:

$$d'_G = \frac{\sum (6 V_i / \pi)}{\sum (6 V_i / \pi)^{2/3}}$$

The parameter, $d'_G \Phi_s$ is usually obtained by fitting measured pressure drops to the Ergun equation [38] given by:

$$\frac{\Delta p d'_G \Phi_s \epsilon^3}{\rho U^2 H (1-\epsilon)} = \frac{150 (1-\epsilon) \mu}{\rho U d'_G \Phi_s} + 1.79$$

Pressure drops for beds of spherical glass beads are in excellent agreement with this equation with the sphericity equal to one. The overall penetration through a gravel bed with depth, H , is

$$P_t = \exp \left\{ - \frac{3 \alpha H}{2 d'_g \Phi_F} \eta_g \right\}$$

where Φ_F is defined as the ratio of the projected surface area of a volume equivalent sphere, to the actual projected surface area of the grain. Mann and Goren [32] propose that in the absence of other information, the relationship:

$$\Phi_F = 1.17 \Phi_s$$

be used. The single grain collection efficiency is obtained from the Ergun equation. Fig. 12.10-2 shows the agreement between these expressions and the experiments for a gravel bed of size 10 mm. Since the equivalent sphericities in these expressions were chosen to fit this data, the agreement is not surprising.

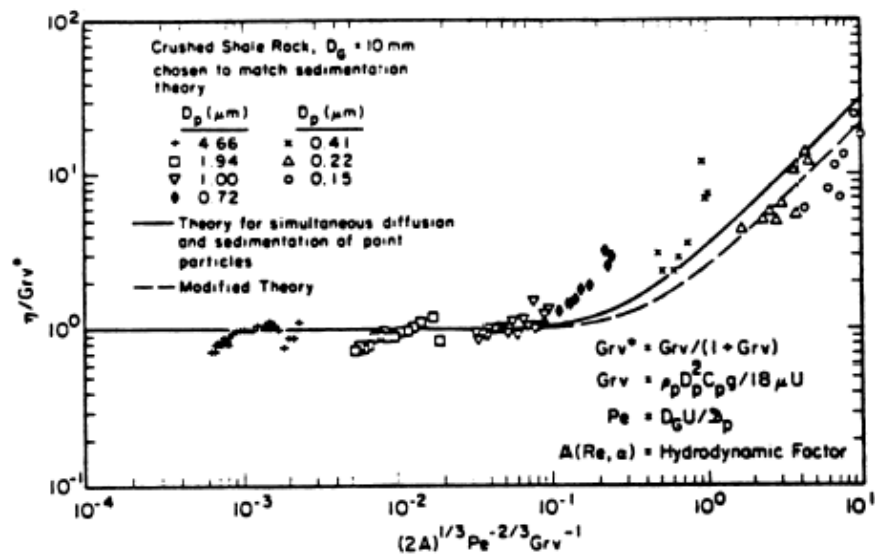


Fig. 12.10-2 Single grain collection efficiencies for crushed rock [39]

12.11 Venturi Scrubbers

Venturi scrubbers differ from the previously described devices in that the deposition bodies are composed of liquid droplets and are not rigidly fixed in place. The key issue of particulate scrubbing is that the aerosols must be brought into contact with the liquid droplets. In fibrous filters and sand beds, since the collected particles remain in place, they are susceptible to plugging. When the scrubbing takes place by water droplets, the material, which is collected, can usually flow away, or be collected in large water tanks.

After the aerosol particles have been collected by water droplets it is necessary to collect these in turn. In submerged venturi scrubbers this is accomplished by submerging the whole unit in water, and taking advantage of pool scrubbing to capture the large water droplets. A further advantage of the venturi scrubber is that the droplets are also useful for gas absorption.

To achieve efficient separation of aerosols from gases, it is helpful to have a high relative velocity between collectors and aerosols, and to have a high collection area. In venturi scrubbers this is achieved by injecting water into a high velocity gas stream. This provides a high relative velocity, which is useful for increasing the impaction efficiency, but more important it causes a break-up of the liquid droplets resulting in very large surface areas.

There are several reasons why venturis are well suited for venting containments during severe accidents. In particular, they are very efficient at removing submicron particles, and because water droplets are used for collection bodies, they are useful for cooling and absorbing hot gases.

A typical schematic geometry for a venturi scrubber is shown in Fig. 2.1-1. The gas has its maximum velocity in the throat, where the cross sectional area is the smallest. This is the best location to inject water since it has the highest relative velocity, which would break the water into the smallest droplets. The gas decelerates in the expansion region since the cross sectional area increases.

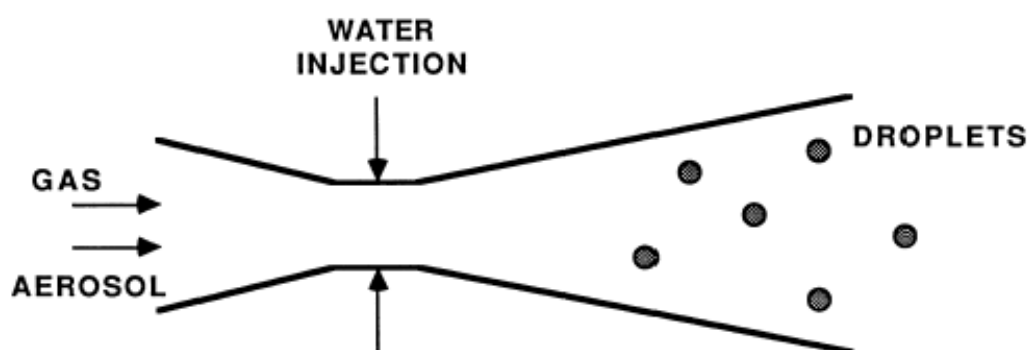


Fig. 12.11-1 Schematic diagram of a venturi scrubber

The general expression for penetration in any filtration device is from the expression for the penetration:

$$P_t = \exp \left\{ - \frac{v_d A_d \tau}{V_0} \right\}$$

For a venturi scrubber, this can be written as [39]

$$P_t = \exp \left\{ - \frac{V^*}{V_g} \right\} = \exp \left\{ - \frac{V^* Q_L}{V_L Q_g} \right\}$$

where V^* refers to the gas volume swept clean of aerosol particles. This is obtained by integrating over the residence time in the venturi

$$V^* = \int_0^{\tau} \eta_d |u_d - u_g| A_d dt$$

where u_d is the droplet capture efficiency. An expression proposed by Calvert [40], which is often used is

$$\eta_d = \frac{K^2}{(K + 0.7)^2}$$

where K is defined as

$$K = \frac{2 \tau_p |u_d - u_g|}{d_d}$$

and τ_p is the particle relaxation time [41]:

$$\tau_p = \frac{C \rho_p d_p^2}{18 \mu}$$

It is at this point necessary to evaluate the relative velocity between the gas and the water droplets. This can be done by solving the one dimensional momentum equation, where the droplet acceleration is caused by the interfacial drag. The gas flow is obtained from the steady continuity equation. The droplet momentum equation is

$$\frac{d u_d}{d z} = \frac{3}{4} \frac{\rho_g C_d}{\rho_d d_d} \frac{|u_g - u_d|}{u_d} (u_g - u_d)$$

where the drag coefficient, C_d , is given by an expression such as [39]

$$C_d = 0.22 + \frac{24}{Re} (1 + Re^{0.5})$$

Once a droplet size has been determined, either from a critical Weber number criterion, or a correlation such as [25] for the Sauter mean drop diameter

$$d_d = \frac{585}{|u_g - u_d|} \sqrt{\frac{\sigma}{\rho_d}} + 597 \left(\frac{\mu}{\sqrt{\sigma \rho_d}} \right)^{0.45} \left(1000 \frac{Q_L}{Q_g} \right)^{1.5}$$

it is possible to integrate the momentum equation numerically. In this empirical correlation the units of the variables are: velocity (cm/s), surface tension (dyn/cm), density (gm/cm³), viscosity (poise), and the calculated diameter (μ m).

Typical results for such an analysis are given in Fig. 12.11-2. For this [39] sample calculation the droplet size was 50 μ m, and the particle aerodynamic diameter was 1 μ m.

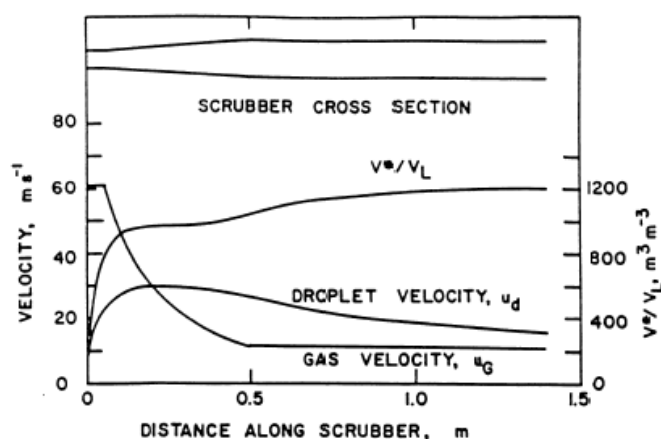


Fig. 12.11-2 Predicted venturi scrubber behaviour

The horizontal axis is the distance from the throat entrance, where the water was injected at zero axial velocity. The droplets accelerate quickly due to the drag, whereas the gas is decelerating because of the area variation. After a distance of approximately 0.2 m downstream of the throat, the water droplets are moving faster than the gas. The particle collection only occurs when there is a net relative velocity between the droplets and the gas, hence the gas volume that is swept clean of particles levels off at the point where the droplet and gas velocities are equal. It is interesting to note for this case that each droplet cleans out a gas volume equal to about 1200 times its own volume.

A comparison of a similar calculation with experiment is shown in Fig. 12.11-3, obtained from [42]. It can be seen that the results are quite encouraging.

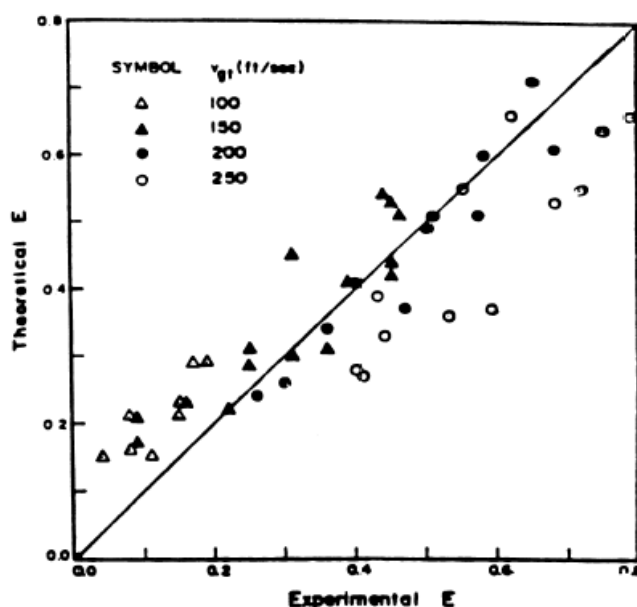


Fig. 12.11-3 Comparison of calculated collection efficiency predictions with data of Calvert et al. [43]

12.12 Water Pools

The chapter on pool scrubbing provides the mechanism of aerosol retention and no further specifics associated with the filters are provided here.

References

- [1] DOE handbook, nuclear air cleaning handbook, DOE Technical Standards, DOE-HDBK-1169-2003, November 2003
- [2] H. Gilbert "The High-Efficiency Filter in Nuclear Air Cleaning" 19th US Department of Energy / US Nuclear Regulatory Commission Nuclear Air Cleaning Conference, Seattle, WA, CONF-860820, National Technical Information Service, Springfield, VA, pp. 933-946, August 1986
- [3] G.D. Knight "Development of Type 6 Filter Material" Massachusetts Institute of Technology Memorandum Report No. 142, Project Dlg-4, Chemical Warfare Service Development Laboratory, Massachusetts Institute of Technology, Cambridge, MA, 1942
- [4] I. Langmuir Report on Smokes and Filters, OSRD 865, Office of Scientific Research and Development, Office of Technical Services, Washington, DC, 1942
- [5] E.A. Ramskill, W.L. Anderson "The Inertial Mechanism in the Mechanical Filtration of Aerosols" Journal of Colloid. Science, Vol. 6, p. 416, 1951
- [6] V.K. LaMer "Atomic Energy Commission Report NYO-512" Technical Information Service, Oak Ridge, TN, 1951
- [7] V.K. LaMer, D. Sinclair Portable Optical Instrument for the Measurement of the Particle Size in Smokes, the 'OWL', an Improved Homogeneous Aerosol Generator, OSRD 1668, Office of Technical Services, Springfield, VA, August 1943
- [8] H. Gilbert High-Efficiency Particulate Air Filter Units, Inspection, Handling, Installation AEC Report TID-7023, National Technical Information Service, Springfield, VA, 1961
- [9] ASME (American Society of Mechanical Engineers), Code on Nuclear Air and Gas Treatment, ASME AG-1, New York, NY, 2003
- [10] W.G. Stockdale, J.C. Suddath, W.K. Eister "Control of Radioactive Air Contamination at Oak Ridge National Laboratory" Paper 11, 3rd Atomic Energy Commission Air Cleaning Conference, pp. 55-57, Los Alamos, NM, 1950
- [11] R.R. Bellamy "Investigations into the Air Cleaning Aspects of the Three Mile Island Incident" 16th DOE Nuclear Air Cleaning Conference, San Diego, CA, National Technical Information Service, Springfield, VA, pp. 1427-1441, October 1980
- [12] A.S. Blasewitz "Dissolver Offgas Filtration," Second Atomic Energy Commission Air Cleaning Seminar AEC Report WASH-149, National Technical Information Service, Springfield, VA, 1954
- [13] L. Lindau, K. Ellison "Filtered Containment Venting in Sweden" 20th Department of Energy/Nuclear Regulatory Commission Nuclear Air Cleaning Conference, Boston, MA, National Technical Information Service, Springfield, VA, pp. 695-708, August 1988
- [14] M. Merilo, I.B. Wall "Containment Filtration Systems Tests, Summary Report" Electric Power Research Institute, ACE Phase A, TR-A22, February 1992
- [15] S. Guntay, D. Suckow, H. Leute, H. Knuchel, H. Schütt, P. Winkler "SULZER Containment Venting Filter Verification Experiments" PSI-Report No: 96-04/380, 1996

- [16] M. Merilo, H.A. Morewitz Engineering Models for Filtration Systems, ACE-TR-A6, May 1991
- [17] M.S. Hoseyni, A.T. Wassel "Growth of Aerosol Particles in a Steam Environment and its Effect on Removal" Nuclear Eng. & Des., Vol. 97, 103 - 109, (1986)
- [18] C.E. Lapple, H.J. Kamack "Performance of Wet Dust Scrubbers" Chem. Engng. Prog. Vol. 51, 110-121, (1955)
- [19] K.T. Semrau "Correlation of Dust Scrubber Efficiency" J. Air Pollut. Control Ass. 10, 200-207 (1960)
- [20] K.T. Semrau "Practical Process Design of Particulate Scrubbers" Chem. Engng 84, 87-91 (1977)
- [21] K.T. Semrau, C.L. Witham, W.W. Kerlin "Energy Utilization by Wet Scrubbers", NTIS, Springfield, VA, Report EPA-600/2-77-234 (1977)
- [22] S. Calvert "How to Choose a Particulate Scrubber" Chem. Eng., Aug. 29, 54 - 68, (1977)
- [23] W.C. Hinds "Aerosol Technology: Properties, Behaviour, and Measurement of Airborne Particles" John Wiley & Sons (1982)
- [24] J.C. Jepson "Mass Transfer in Two-Phase Flow in Horizontal Pipelines" AIChE J. Vol. 16, 705, (1970)
- [25] S. Calvert "Scrubbing", Air Pollution, Ed. A. C. Stern, 257 - 291, Academic Press, (1977)
- [26] R.K. Hilliard, J.D. McCormack, A.K. Postma "Submerged Gravel Scrubber Demonstration as a Passive Air Cleaner for Containment Venting and Purging with Sodium Aerosols -- CSTF Tests AC7 - AC10" Hanford Engr. Development Lab. Report: HEDL-TME 81-30 (1981)
- [27] H.A. Morewitz "The Attenuation of Aerosols Bubbling Through Water Pools" H. M., Associates Ltd. Report: HMA-2-83 (1983)
- [28] A.A. Hirsch, I.B. Stechkina "The Theory of Aerosol Filtration With Fibrous Filters" in Fundamentals of Aerosol Science, D. T. Shaw, ed., Wiley, New York, 165 - 256, (1978)
- [29] G.M. Hidy "Aerosols, An Industrial and Environmental Science" Academic Press, Orlando, (1984)
- [30] N. Rao, M. Faghri "Computer Modeling of Aerosol Filtration by Fibrous Filters" Aerosol Sci. Technol. Vol. 8, 133 - 156, (1988)
- [31] R.A. Juvinall, R.W. Kessie, M.J. Steindler "Sand-Bed Filtration of Aerosols: A Review of Published Information on their Use in Industrial and Atomic Energy Facilities" Argonne National Lab. Report: ANL-7683 (1970)
- [32] L. Mann, S. Goren "Aerosol Capture in Granular Beds in the Sedimentation and Diffusion Dominated Regimes" Aerosol Sci. Technol. Vol. 3, 195 - 213, (1984)
- [33] C. Michaels, S.L. Goren "Aerosol Capture in Particle Laden Granular Beds in the Impaction Dominated Regime" Aerosol Sci. and Technol. 7 31-46 (1987)
- [34] J. Happel, A.I.Ch.E. J. Vol. 4, 197 -201, (1958)

- [35] R. Sher An unpublished work, conducted for the ACE International Project, 1990
- [36] B.S. Guieu, A. Couvrat-Desvergnès, M. Berlin, J. Dufresne "Filtered Venting System for Reactor Containment Building Operating Conditions and Research and Development Work" IAEA International Symposium on Severe Accidents in Nuclear Power Plants, Sorrento, Italy, March 21-25 (1988)
- [37] L. Ström, J. Chyssler, G. Gebert "Particle Retention in a Bed of Crushed Rock, Under Conditions of condensing Steam" J. Aeros. Science, Vol. 14, No. 3, p. 225, (1983) and Studsvik Report No. NW-82/313, (1982)
- [38] S. Ergun "Fluid Flow through Packed Columns" Chem. Eng. Prog. 48, 89-94 (1952)
- [39] D.W. Cooper, D. Leith "Venturi Scrubber Optimization Revisited" Aerosol Sci. and Technol., 63-70 (1984)
- [40] S. Calvert "Venturi and Other Atomizing Scrubbers Efficiency and Pressure Drop" AIChE J., 16, No. 3, 392-396 (1970).
- [41] N.A. Fuchs "The Mechanics of Aerosols" The MacMillan Co., New York, NY (1964)
- [42] K.C. Goel, K.G.T. Hollands "A General Method for Predicting Particulate Collection Efficiency of Venturi Scrubbers" Ind. Engr. Chem. Fund., 16, No. 2, 186-193 (1977)
- [43] S. Calvert, D. Lundgren, D.S. Mehta "Venturi Scrubber Performance" J. Air Pollut. Control Assoc., 22, 529-532 (1972)

Nomenclature

Latin Symbols

A	Constant
A_h	Hydrodynamic factor which depends on the Reynolds number
A_c	Cross sectional flow area
A_d	Cross-sectional area of droplet
B	Particle mobility
C_p	Cunningham slip correction factor
C_d	Drag coefficient
D_F	Decontamination factor
D^*_0	Dimensionless drag force, $D / v_{if}\mu_g$
D	Drag force
d_d	Droplet diameter
d_f	Fiber diameter
d_g	Grain diameter
d'_G	Sauter mean diameter of grain
d_p	Physical diameter of aerosol particle
d_{pa}	Aerodynamic mass mean diameter
d_{p50}	50 % cut diameter, aerodynamic
DOP	Test aerosol, dioctyl phthalate
g	Acceleration of gravity
H	Filter thickness
I	Interception parameter, d_p/d_f

K_H	Hydrodynamic factor
K_n	Knudsen Number
M_{in}	Mass injected to filtration system
M_{out}	Mass exhausted from filtration system
m_p	Particle mass
n	Aerosol concentration
P_t	Penetration
Pe	Peclet Number
Q_g	Volumetric flow rate of gas
Q_L	Volumetric flow rate of liquid
Re	Reynolds number
Sh	Sherwood number
St	Stokes number
U_o	Superficial gas velocity
U_d	Droplet velocity
u_g	Gas velocity
v_f	Face velocity
v_{dep}	Deposition velocity
V_g	Gas volume in filter
V_i	Single grain volume
z	Axial distance along venturi from the water injection point

Greek Symbols

α	Volumetric solids fraction
ΔP	Pressure drop
ε	Volumetric void fraction of fibrous or granular bed
η	Overall collection efficiency
η_0	Single fibre collection efficiency including influence of neighbouring fibres
η_D	Single fibre collection efficiency for convective diffusion
η_d	Individual droplet collection efficiency
η_{DI}	Single fibre collection efficiency for interaction between diffusion and interception
η_f	Single fibre collection efficiency
η_g	Single grain collection efficiency
η_I	Single fibre collection efficiency for interception
μ	Gas viscosity
ρ_d	Droplet density
ρ_g	Gas density
ρ_p	Particle density
ρ	Surface tension
τ	Residence time
τ_p	Particle relaxation time
ψ	Filter inhomogeneity factor

13. APPENDIX 5: Point-by-Point Review of Issues Identified at the 1998 Aerosol Workshop

In the proceedings of the OECD Workshop “Nuclear Aerosols in Reactor Safety” in Cologne, June 1998, remaining issues identified during the discussions and general recommendations are summarised on pages 4 and 5 [1]. These issues and recommendations are repeated and discussed here from the current point of view in order to increase the pertinence of the present SOAR rendering the understanding of the progress described in this SOAR easier.

Circuit behaviour

Ci 1 Circuit thermal-hydraulics are important for vapor and aerosol transport in the circuit. As an example, three independent calculations for a station blackout sequence differed considerably in the predict fission product retentions because of difference in predicted recirculation patterns and local temperatures. It is necessary to improve confidence in predictions for flow paths, velocities and temperatures in the circuit under severe accident conditions.

Response to Ci 1

This is an observation with general importance for severe accident calculations and in no way limited to aerosol analyses. Code comparisons in the EC project EVITA [2,3] and continuing in the EC network SARNET [4] have led to a significant increase in understanding differences between calculations even when performed with the same code but by different users.

For understanding differences resulting from the use of different codes (and moreover different users) one needs a thorough understanding of the modelling and numerical approaches inside the code. Such evaluations are time consuming but are, nevertheless, necessary and should be continued in future with greater involvement of utilities and vendors (see Cologne recommendation R 1). Chapters 6 and 7 of this report intend to reinforce the international discussions on this topic.

Ci 2 There is still a need to investigate aerosol deposition in singularities such as valves and beds.

Ci 3 An important removal mechanism in sequences with steam generator tube rupture is flow across tube bundles. It is planned to perform scale experiments to investigate this and other potential removal mechanisms.

Response to Ci 3

The international ARTIST programme performed at PSI in Switzerland has addressed this issue. After termination of interpretation of ARTIST results this issue will have progressed and might be closed.

Ci 4 The ISP-40 exercise results indicate that resuspension is not sufficiently understood for plant applications. PHEBUS data indicate that reactor aerosols are rather easily resuspended. Measurements of parameters such as surface roughness, bed porosity, chemistry on the surface and stickiness of the particles are needed to support the modelling development. There is a need for specific experiments related to clearly defined accident sequences, if it is required to quantify circuit retention.

Response to Ci 2 and Ci 4

Since 1998 there has been little significant progress made with respect to deposition and resuspension. Even if some efforts to increase the capabilities of SOPHAEROS (see chapter 4.1.2) have been made, the fundamental lack of experiments mentioned at the Cologne workshop 1998 is still a problem; furthermore, it now seems that the experiments performed in the frame of EVAN (see chapter 5.10.2) provide incomplete information and just for straight pipes.

Ci 5 Experimental work on revaporisation is scarce; theoretical and experimental development are both necessary to understand the revaporisation process.

Response to Ci 5

Studies on revaporisation with Phébus FP and simulant samples were undertaken in the EC 4th Framework Programme projects RVP and REVAP-ASSESS. Based on these studies and the evaluation of PHEBUS FP results themselves the knowledge of revaporization has significantly increased. It has been shown to significantly influence transport of volatile fission products compounds in the RCS to the containment during core degradation. In addition, plant calculations indicate that revaporisation can be a potential long-term source of fission products to the containment. Currently further studies of revaporisation with samples from PHEBUS FP experiments are on-going. In addition, release of volatile fission product compounds due reactions on the primary circuit surfaces is carried out in EXSI project within the SAFIR2010 programme. Lastly, in the frame of SARNET programme, one technical circle is dedicated to sharing information on revaporisation. Only after terminations of these evaluations can it be decided what additional work might be necessary.

Experimental work on revaporization remains scarce; further theoretical and experimental developments are necessary to understand the revaporization process. In addition, the safety relevance ought to be further demonstrated by assessing, conceivably, the impact of a weak source of fission products from the reactor coolant system for some hours after the main release-from-core phase.

Containment behaviour

Co 1 Both detailed and integral tests are necessary to support the modelling of the removal of aerosols by sprays. Particle size and density, as well as spray droplet size, are important parameters. Removal by interacting droplets may be significant and is being investigated.

Response to Co 1

This issue has been extensively investigated by the French organisations CEA and IRSN using specific apparatuses and the CARAIDAS, MISTRA and TOSQAN test facilities. The data should be made accessible to the nuclear community, at least the OECD partners. Validated modelling based on these experimental investigations has been implemented in the codes ASTEC and TONUS. In the context of containment sprays, further work is no longer a priority.

Co 2 There are indications from PHEBUS that further mechanisms may play a role in aerosol removal in plants. These include turbulent impaction and charge effects and should be further investigated to scope their potential impact.

Response to Co 2

From the substantial examinations performed for the aerosol deposition in the PHEBUS FP 'quasi'-containment, especially for test FPT1, it cannot be concluded that turbulent impaction has a major

influence compared to other deposition mechanisms. The mechanism is in any case included in current containment codes. Concerning charge effects, small deposits of aerosols on the outer walls of the 10 m³ containment vessel in the PHÉBUS test FPT0 could not be explained by electrophoretic effects as shown in an IRSN study (and while this study was made available to the PHÉBUS partners it did not lead to further studies). However, even if charge effects on aerosol deposition are not seen to be significant in test facilities (with or without a radiation field) there is no firm evidence that this effect would be negligible in an accident. At present there is no consensus among experts on whether further investigations of charging effects are necessary or not.

Co 3 The possible impact of hydrogen recombiners on aerosol depletion rates due to affecting local thermal-hydraulic conditions and to chemical effects have to be investigated.

Response to Co 3

With respect to this issue experimental work has been carried out in France (RECI) and Germany (ThAI). The direct impact of recombiners on thermal-hydraulics may have a limited influence on the overall aerosol depletion, whereas the chemical effect might be significant. The decomposition of metal-iodide aerosol inside a recombiner forming molecular iodine may have an important impact on the source term. This process has to be examined further in order to generate an adequate amount of reliable data and allow complete understanding for modelling. The quantitative impact on the source term remains uncertain.

Co 4 Pool scrubbing modelling is uneven in its level of detail (i.e., hydrodynamic models). The resulting uncertainties require review in terms of performance requirements and tolerance for uncertainty in plant applications. Coupling to containment codes is recommended.

Response to Co 4

Since 1998 some progress has been made on this issue in the context of the ARTIST programme but it is still largely open.

Co 5 Modelling of re-entrainment from boiling pools (a weak, but persistent late-phase source of fission products) performs well for ideal systems, but currently lacks consideration of non-ideal effects arising from suspended materials, solutes and surfactants. It has to be examined, if re-entrainment from boiling pools may have a significant effect of offsite releases.

Response to Co 5

Investigations with respect to the aerosol re-entrainment from a boiling water pool are ongoing in the German ThAI facility; in parallel analytical work is performed. It is part of this activity to examine whether re-entrainment may have a significant effect on offsite release (as recommended in 1998).

Co 6 Heat release by hydrogen burns may have a strong effect on aerosol characteristics, as a result of the thermal-hydraulic transient and can possibly liberate volatile forms of iodine. Experimental evidence and thermodynamic analysis are inconclusive as to the magnitude of the effect.

Response to Co 6

Experiments in the ThAI facility demonstrate that there is a clear effect of hydrogen-combustion-induced flows on resuspension of already deposited CsI aerosol. Initial source-term calculations for plant conditions show an increase of airborne aerosol of up to one order of magnitude. Assuming a small leak in the containment of 0.01 m² the released aerosol mass increases by a factor of 4, in the case of a global containment failure by a factor of 10. These findings have to be expanded to other types of relevant aerosol

species and other plant applications. However, chemical effects on iodine-containing aerosols have not been studied; information from the ongoing investigation of the impact of recombiners on aerosols may be relevant.

Recommendations

R 1 A meeting in the use of severe accident codes in plant calculations for source term estimation, including codes used by utilities, is recommended within the next two years.

Response to R 1

Ten years after formulation of this recommendation it has still not put into practice. As already stated above (see the response to Ci 1), there is a need to harmonise user practices with respect to plant analyses in order to reduce divergence in results. The objective would ideally be to produce an online “best practice” guide for the major codes.

R 2 Important experimental and analytical work is in progress on aerosol behaviour in the primary circuit; a SOAR could be productively undertaken in this area, within two years.

R 3 In light of substantial recent work completed on aerosol behaviour in the containment, the writing of a SOAR on containment aspects of severe accident aerosols behaviour is recommended.

Response to R 2 and R 3

These recommendations are fulfilled with this report.

References

- [1] H.-J. Allelein Third OECD specialist meeting on nuclear aerosols in reactor safety GRS-166, NEA/CSNI/R(98)4, ISBN 3-931995-31-3, June 1998
- [2] H.-J. Allelein et al. EVITA - European validation of the integral code ASTEC Final report of the project FIKS-CT-1999-00010, EC 5th Framework Programme (1999)
- [3] H.-J. Allelein, K. Neu, J.P. Van Dorsselaere European validation of the integral code ASTEC (EVITA) - First experience in validation and plant sequence calculations, Nuclear Engineering and Design 235(2-4), 285-308 (2005).
- [4] J.P. Van Dorsselaere, H.-J. Allelein, K. Neu Progress and perspectives of ASTEC application for severe accidents in the network SARNET, EUROSAFE, 2006.